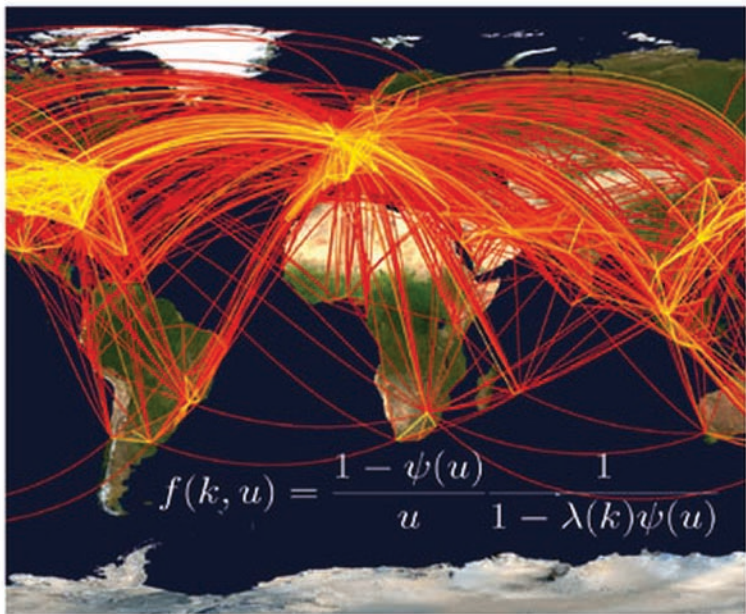


Edited by
R. Klages, G. Radons, and I. M. Sokolov

WILEY-VCH

Anomalous Transport

Foundations and Applications



Anomalous Transport

Foundations and Applications

Edited by

Rainer Klages, Günter Radons, and Igor M. Sokolov



WILEY-VCH Verlag GmbH & Co. KGaA

Anomalous Transport

Edited by

*Rainer Klages, Günter Radons, and
Igor M. Sokolov*

Related Titles

Chakrabarti, B. K., Chakraborti, A., Chatterjee, A. (eds.)

Econophysics and Sociophysics Trends and Perspectives

2006

ISBN: 978-3-527-40670-8

Rice, S. A. (ed.)

Advances in Chemical Physics

**Volume 133: Fractals, Diffusion and Relaxation
in Disordered Complex Systems**

2006

ISBN: 978-0-470-04607-4

Radons, G., Neugebauer, R. (eds.)

Nonlinear Dynamics of Production Systems

2004

ISBN: 978-3-527-40430-8

Bornholdt, S., Schuster, H. G. (eds.)

Handbook of Graphs and Networks

From the Genome to the Internet

2003

ISBN: 978-3-527-40336-3

Anomalous Transport

Foundations and Applications

Edited by

Rainer Klages, Günter Radons, and Igor M. Sokolov



WILEY-VCH Verlag GmbH & Co. KGaA

The Editors

Dr. habil. Rainer Klages

Queen Mary, University of London
School of Mathematical Sciences
London, United Kingdom
r.klages@qmul.ac.uk

All books published by Wiley-VCH are carefully produced. Nevertheless, authors, editors, and publisher do not warrant the information contained in these books, including this book, to be free of errors. Readers are advised to keep in mind that statements, data, illustrations, procedural details or other items may inadvertently be inaccurate.

Prof. Dr. Günter Radons

Chemnitz University of Technology
Institute of Physics
Chemnitz, Germany
radons@physik.tuchemnitz.de

Library of Congress Card No.: applied for

British Library Cataloguing-in-Publication Data

A catalogue record for this book is available from the British Library.

Prof. Dr. Igor M. Sokolov

Humboldt-Universität zu Berlin
Institut für Physik
Berlin, Germany
Igor.sokolov@physik.hu-berlin.de

Bibliographic information published by the Deutsche Nationalbibliothek

Die Deutsche Nationalbibliothek lists this publication in the Deutsche Nationalbibliografie; detailed bibliographic data are available on the Internet at <<http://dnb.d-nb.de>>.

Cover

***Dr. Dirk Brockmann*, MPI Göttingen**

The worldwide air traffic network, which leads to anomalous transport in human travel. Such anomalous processes can be modelled by the continuous time random walk theory of which the Montroll-Weiss equation displayed in the picture is the key ingredient.

© 2008 WILEY-VCH Verlag GmbH & Co. KGaA,
Weinheim

All rights reserved (including those of translation into other languages). No part of this book may be reproduced in any form – by photoprinting, microfilm, or any other means – nor transmitted or translated into a machine language without written permission from the publishers.
Registered names, trademarks, etc. used in this book, even when not specifically marked as such, are not to be considered unprotected by law.

Backcover Picture

***Dr. Nickolay Korabel*, Bar-Ilan University**

Anomalous probability distribution function (oscillatory structure) for the positions of a subdiffusively spreading ensemble of particles generated by an intermittent map and three fit functions (other lines).

Composition Uwe Krieg, Berlin
Printing betz-druck GmbH, Darmstadt
Bookbinding Litges & Dopf GmbH, Heppenheim

Printed in the Federal Republic of Germany
Printed on acid-free paper

ISBN: 978-3-527-40722-4

Contents

Preface XV

List of Contributors XIX

1	In Memoriam: Radu Balescu	1
	<i>Boris Weyssow, Angelo Vulpiani, Francesco Mainardi, Raul Sánchez, and Diego del-Castillo-Negrete</i>	
1.1	Radu Balescu's Abstract for the Conference on Anomalous Transport in Bad Honnef	2
1.2	The Scientific Career of Radu Balescu by Boris Weyssow	3
1.3	My Memory of Radu Balescu by Angelo Vulpiani	5
1.4	My Memory of Radu Balescu by Francesco Mainardi	6
1.5	In Memoriam: Radu Balescu by Raul Sánchez	8
1.6	Remembering Radu Balescu by Diego del-Castillo-Negrete	10
	References	11

Part I Fractional Calculus and Stochastic Theory 13

Introduction to Part I 15

2	Threefold Introduction to Fractional Derivatives	17
	<i>Rudolf Hilfer</i>	
2.1	Historical Introduction to Fractional Derivatives	17
2.1.1	Leibniz	17
2.1.2	Euler	18
2.1.3	Paradoxa and Problems	18
2.1.4	Liouville	20
2.1.5	Fourier	21
2.1.6	Grünwald	21
2.1.7	Riemann	21
2.2	Mathematical Introduction to Fractional Derivatives	22

2.2.1	Fractional Integrals	22
2.2.2	Fractional Derivatives	31
2.2.3	Eigenfunctions	44
2.3	Physical Introduction to Fractional Derivatives	46
2.3.1	Basic Questions	46
2.3.2	Fractional Space	46
2.3.3	Fractional Time	48
2.3.4	Identification of α from Models	53
	Appendix A: Tables	59
	Appendix B: Function Spaces	61
	Appendix C: Distributions	65
	References	69
3	Random Processes with Infinite Moments	75
	<i>Michael F. Shlesinger</i>	
3.1	St. Petersburg Paradox	75
3.2	Holtsmark Distribution	76
3.3	Activated Hopping	77
3.4	Deterministic Examples of Long Tail Distributions	78
3.5	Random Walks and Master Equations	80
3.6	Random Walks and Upper Critical Dimensions	82
3.7	Weierstrass Random Walk	83
3.8	Fractal Time Random Walk	85
3.9	Coupled Memory Random Walks: Diffusion or Telegraph Equation	86
3.10	Random Walks: Coupled Memory Lévy Walks: Turbulent and Relativistic	89
	References	91
4	Continuous Time Random Walk, Mittag-Leffler Waiting Time and Fractional Diffusion: Mathematical Aspects	93
	<i>Rudolf Gorenflo and Francesco Mainardi</i>	
4.1	Introduction	93
4.2	An Outline of the Gnedenko–Kovalenko Theory of Thinning	95
4.3	The Continuous Time Random Walk (CTRW)	98
4.4	Manipulations: Rescaling and Respeeding	101
4.5	Power Laws and Asymptotic Universality of the Mittag-Leffler Waiting-Time Density	103
4.6	Passage to the Diffusion Limit in Space	104
4.7	The Time-Fractional Drift Process	110
4.8	Conclusions	113
	Appendix A: The Time-Fractional Derivatives	117

Appendix B: The Space-Fractional Derivatives 119

Appendix C: The Mittag-Leffler Function 123

References 125

5 Introduction to the Theory of Lévy Flights 129

Alexei V. Chechkin, Ralf Metzler, Joseph Klafter, and Vsevolod Yu. Gonchar

- 5.1 Lévy Stable Distributions 130
- 5.2 Underlying Random Walk Processes 133
- 5.3 Space Fractional Fokker–Planck Equation 135
- 5.4 Free Lévy Flights in the Semi-Infinite Domain 137
 - 5.4.1 First Passage Time and Leapover Properties 137
 - 5.4.2 Lévy Flights and the Method of Images 140
- 5.5 Lévy Flights in External Fields 141
 - 5.5.1 Reminder: Stationary Solution of the Fokker–Planck Equation, $\alpha = 2$ 141
 - 5.5.2 Lévy Flights in an Harmonic Potential 141
 - 5.5.3 Lévy Flights in a Quartic Potential, $1 \leq \alpha < 2$ 142
 - 5.5.4 Lévy Flights in a More General Potential Well 144
 - 5.5.5 Kramers Problem for Lévy Flights 145
 - 5.6 Lévy Flights in Phase Space 147
 - 5.6.1 Langevin Description 147
 - 5.6.2 Velocity-Fractional Klein–Kramers Equation 148
 - 5.6.3 Space-Homogeneous Relaxation in Absence of External Field 148
 - 5.6.4 Space-Inhomogeneous Relaxation in the Absence of an External Field 149
 - 5.6.5 Relaxation of the Linear Oscillator [84] 149
 - 5.6.6 Relaxation in a Magnetized Plasma 150
 - 5.6.7 Damped Lévy Flights [89] 152
- 5.7 Power-Law Truncated Lévy Flights 153
- 5.8 Summary 158
- 5.9 References 159

6 Fractional Diffusion Models of Anomalous Transport 163

Diego del-Castillo-Negrete

- 6.1 Introduction 163
- 6.2 Anomalous Transport 165
 - 6.2.1 Anomalous Transport of Tracers in Flows with Coherent Structures 165
 - 6.2.2 Continuous Time Random Walk Model and Fractional Diffusion 170
- 6.3 Fractional Diffusion 172

6.3.1	Fractional Derivatives	173
6.3.2	Fractional Diffusion Equation: Green's Function and Self-Similar Scaling	177
6.3.3	Interplay of Regular and Fractional Diffusion	179
6.3.4	Fractional Diffusion Equation for Truncated Lévy Processes	181
6.3.5	Nonlocality and Uphill Transport	185
6.3.6	Fractional Diffusion Models of Turbulent Transport	190
6.4	Fractional Diffusion in Finite-Size Domains	193
6.4.1	Finite-Size Domain Model	194
6.4.2	Finite-Difference Numerical Integration Method	195
6.4.3	Examples	200
6.5	Summary and Conclusions	208
	References	211
7	Anomalous Kinetics Leads to Weak Ergodicity Breaking	213
	<i>Eli Barkai</i>	
7.1	Introduction	213
7.2	Normal Occupation Time Statistics	215
7.2.1	Ergodicity for Bounded Normal Diffusion	219
7.2.2	Occupation Times for Nonrecurrent Diffusion	220
7.2.3	Occupation Times for Unbounded Normal Diffusion	220
7.3	Anomalous Diffusion	221
7.3.1	Derivation of Fractional Equation for Occupation Times	222
7.3.2	Weak Ergodicity Breaking	225
7.3.3	Example: Anomalous Diffusion in an Interval	227
7.4	Deterministic Weak Ergodicity Breaking	228
7.5	Discussion	234
	Appendix A	237
	References	239
Part II	Dynamical Systems and Deterministic Transport	241
	Introduction to Part II	243
8	Deterministic (Anomalous) Transport	245
	<i>Roberto Artuso and Giampaolo Cristadoro</i>	
8.1	Introduction	245
8.2	Transport and Thermodynamic Formalism	246
8.3	The Periodic Orbits Approach	249
8.4	One-Dimensional Transport: Kneading Determinant	253
8.5	An Anomalous Example	256
8.6	Probabilistic Approximations	263

8.7	Conclusions	265
	References	266
9	Anomalous Transport in Hamiltonian Systems	269
	<i>Eduardo G. Altmann and Holger Kantz</i>	
9.1	Introduction	269
9.2	Continuous Time Random Walk Model	270
9.3	Origin of Long-Time Tails in Hamiltonian System	272
9.3.1	Phase Space of Hamiltonian Systems	272
9.3.2	Main Properties of Hamiltonian Chaos	273
9.3.3	Connection to CTRW	276
9.4	Paradigmatic Fluid Model	278
9.4.1	Incompressible Fluid Flows as Hamiltonian Systems	278
9.4.2	Specific Model	279
9.4.3	Transport Properties of Passive Tracers	281
9.4.4	Effect of Noise Perturbation	282
9.5	Discussion	288
	References	289
10	Anomalous Heat Conduction	293
	<i>Stefano Lepri, Roberto Livi, and Antonio Politi</i>	
10.1	Introduction	293
10.2	An Historical Perspective	294
10.2.1	Fourier and the Problem of Heat Transport in the Earth	294
10.2.2	From the Old Kinetic Theory to Boltzmann	295
10.2.3	The Harmonic Pathology and the Phonons	297
10.2.4	The Fermi–Past–Ulam (FPU) Numerical Experiment	298
10.3	Harmonic Systems	301
10.3.1	Homogeneous Chain	301
10.3.2	Disordered Chain	304
10.4	Anomalous Transport in Anharmonic Chains with Momentum-Conserving Potentials	310
10.4.1	Early Studies	310
10.4.2	Green–Kubo Formalism	311
10.4.3	The Quasi-Integrable Limit	312
10.4.4	The Strong-Chaos Regime	312
10.4.5	Integrable Nonlinear Systems	314
10.4.6	Universality	315
10.4.7	Anomalous Diffusion	317
	References	320

Part III Anomalous Transport in Disordered Systems 323**Introduction to Part III 325**

- 11 Anomalous Relaxation in Complex Systems: From Stretched to Compressed Exponentials 327**
Jean-Philippe Bouchaud
- 11.1 Introduction 327
11.2 Stretched Exponential Relaxations 328
11.2.1 Trapping-Induced Subdiffusion 328
11.2.2 Two-Step Relaxation 332
11.2.3 Superposition of Relaxation Times and Stretched Exponentials 335
11.3 Models of Compressed Exponentials 338
11.3.1 Superdiffusion and Lévy Flights 338
11.3.2 Rearrangement-Induced Stress Fields in Elastic Media 340
11.4 Conclusion 343
References 344
- 12 Anomalous Transport in Glass-Forming Liquids 347**
Walter Kob, Gustavo A. Appignanesi, J. Ariel Rodríguez Fris, and Ruben A. Montani
- 12.1 Introduction 347
12.2 Model 352
12.3 Results 353
12.4 Summary 364
References 365
- 13 Subdiffusion-Limited Reactions 367**
Santos Bravo Yuste, Katja Lindenberg, and Juan Jesús Ruiz-Lorenzo
- 13.1 Introduction 367
13.2 Subdiffusion Contexts and Modeling Approaches 369
13.3 Target and Trapping Problem 373
13.3.1 Target Problem 374
13.3.2 Trapping Problem 376
13.4 Two Basic Reactions 378
13.4.1 Annihilation and Coalescence Reactions 378
13.4.2 Annihilation of Two Species, $A + B \rightarrow 0$ 380
13.5 Reactions with Nonhomogeneous Distribution of Reactants 381
13.5.1 Reaction–Subdiffusion Equations 382
13.5.2 Reaction Fronts 385
13.6 Reactants with Different (Sub)diffusion Exponents 387
13.7 Finale 392
References 393

14	Anomalous Transport on Disordered Fractals	397
<i>Karl Heinz Hoffmann and Janett Prehl</i>		
14.1	Motivation	397
14.2	Anomalous Diffusion on Regular Sierpinski Carpets	398
14.2.1	Regular Sierpinski Carpets	399
14.2.2	Random Walks on Fractals	401
14.2.3	Resistance Scaling Method	403
14.2.4	Master Equation Approach	405
14.2.5	Diffusion Simulation	406
14.3	Anomalous Diffusion on Disordered Sierpinski Carpets	407
14.3.1	Disordered Sierpinski Carpets	408
14.3.2	Modeling Carpets and Calculating Diffusion Exponents	409
14.3.3	Results and Discussion	412
14.4	Fractional Differential Equation	416
14.4.1	Sierpinski Gasket	418
14.4.2	Koch Curve	421
14.5	Summary	424
	References	426
Part IV	Applications to Complex Systems and Experimental Results	429
Introduction to Part IV 431		
15	Superstatistics: Theoretical Concepts and Physical Applications	433
<i>Christian Beck</i>		
15.1	Introduction	433
15.2	The Basic Idea	434
15.3	Typical Distributions $f(\beta)$	435
15.4	Asymptotic Behavior for Large Energies	437
15.5	Anomalous Diffusion in Superstatistical Systems	439
15.6	From Time Series to Superstatistics	442
15.7	Overview of Applications	445
15.8	Lagrangian Turbulence	446
15.9	Defect Turbulence	448
15.10	Statistics of Cosmic Rays	450
15.11	Statistics of Train Delays	453
15.12	Conclusion and Outlook	455
	References	456

16	Money Circulation Science – Fractional Dynamics in Human Mobility	459
	<i>Dirk Brockmann</i>	
16.1	Dispersal Ecology	460
16.2	Diffusive Dispersal and Reaction Kinetics	460
16.2.1	SIS Dynamics	461
16.2.2	A Word of Caution	461
16.3	Long Distance Dispersal and Lévy Flights	462
16.3.1	Lévy Flights	463
16.4	Human Travel in the 21st Century	464
16.5	Money as a Proxy for Human Travel	466
16.5.1	The Lack of Scale in Money Movements	466
16.6	Is That All?	469
16.7	Scaling Analysis	470
16.8	Scale Free Waiting Times	471
16.9	Ambivalent Processes	473
16.9.1	Scaling Relation	474
16.9.2	The Limiting Function for Ambivalent Processes	476
	References	481
17	Anomalous Molecular Displacement Laws in Porous Media and Polymers Probed by Nuclear Magnetic Resonance Techniques	485
	<i>Rainer Kimmich, Nail Fatkullin, Markus Kehr, and Yujie Li</i>	
17.1	General Introduction	485
17.2	From Nano- to Milliseconds: Segment Diffusion in Polymer Melts	487
17.2.1	Evaluation Theory for the Field-Cycling NMR Relaxometry Technique	488
17.2.2	Results for Polymer Melts	491
17.2.3	Discussion of the Results for Polymer Melts	492
17.3	From 100 Microseconds to Seconds	495
17.3.1	The Measuring Principles of Field-Gradient NMR Diffusometry	495
17.3.2	Sub- and Superdiffusive Transport in Porous Glasses	499
17.3.3	Discussion of the Results for Porous Glasses	504
17.4	The Time Scale Beyond Seconds	505
17.4.1	NMR Microscopy Diffusometry Techniques	505
17.4.2	Diffusion of Solvents in Swollen Polymers	509
17.4.3	Diffusion on Random-Site Percolation Clusters	512
17.4.4	Discussion of the Results for Percolation Clusters	514
17.5	General Discussion and Outlook	515
	References	517

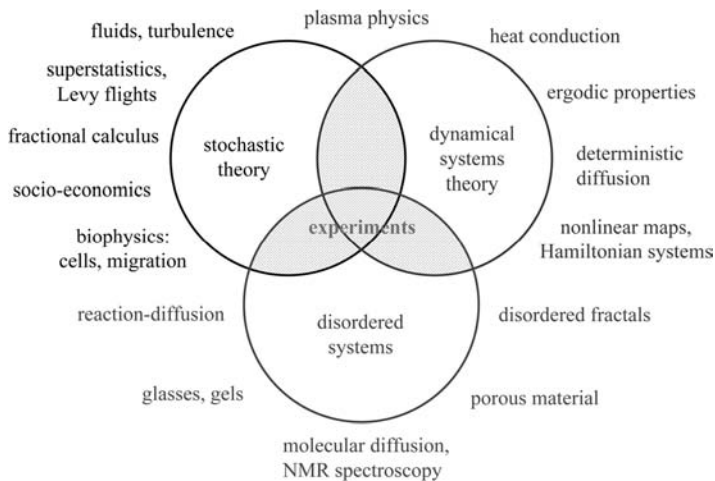
18	Anomalous Molecular Dynamics in Confined Spaces	519
	<i>Rustem Valiullin and Jörg Kärger</i>	
18.1	Introduction	519
18.2	The Materials Under Study	520
18.2.1	Zeolites	520
18.2.2	Mesoporous Glass and Silica	521
18.3	NMR Fundamentals	522
18.3.1	The Phenomenon and Measurement of Concentration	522
18.3.2	Diffusion Measurement	524
18.4	Diffusion in Channel Micropores	526
18.4.1	Single-File Diffusion	526
18.4.2	Molecular Transport in Intersecting Channels	527
18.5	Molecular Dynamics in Mesopores	530
18.5.1	Dynamics in Random Pore Spaces	530
18.5.2	Molecular Dynamics in Channel Pores	535
18.6	Conclusions	539
	References	540
19	Paradigm Shift of the Molecular Dynamics Concept in the Cell Membrane: High-Speed Single-Molecule Tracking Revealed the Partitioning of the Cell Membrane	545
	<i>Akihiro Kusumi, Yasuhiro Umemura, Nobuhiro Morone, and Takahiro Fujiwara</i>	
19.1	Introduction	545
19.2	Thirty-Year Old Enigma about the Diffusion Rate of Membrane Molecules in the Plasma Membrane	549
19.3	Macroscopic Diffusion Coefficients for Transmembrane Proteins are Suppressed by the Presence of the Membrane Skeleton	551
19.4	Single-Molecule Tracking Revealed That Transmembrane Proteins Undergo Hop Diffusion	552
19.5	Corralling Effects of the Membrane Skeleton for Transmembrane Proteins (the Membrane-Skeleton Fence Model)	558
19.6	Phospholipids Also Undergo Hop Diffusion in the Plasma Membrane	561
19.7	The Biological Significance of Oligomerization-Induced Trapping Based on the Membrane-Skeleton Fences and Pickets	568
19.8	A Paradigm Shift of the Plasma Membrane Structure Concept is Necessary: From the Simple Two-dimensional Continuum Fluid Model to the Compartmentalized Fluid Model	570
	References	571

Preface

Anomalous transport refers to nonequilibrium processes that cannot be described by using standard methods of statistical physics. This novel class of transport phenomena has recently been observed in a wide variety of complex systems such as amorphous semiconductors, plasmas, glassy materials, nanopores, biological cells and epidemic spreading. The coherent description of anomalous transport in such a broad range of systems poses a fundamental challenge to the theoretical modeling and to the mathematical language in which these models are formulated. It asks for a synergy of many different disciplines, from the mathematical theory of dynamical systems over the theory of stochastic processes to the statistical physics of disordered systems.

This book gives a comprehensive introduction to the newly emerging field of anomalous transport. It discusses particularly the important examples of anomalous particle transport in high-energy plasmas and in turbulence, ageing in glassy materials, anomalous diffusion in porous media, anomalous heat conduction and chemical reaction-diffusion as well as anomalous correlations in polymer melts. Anomalous dynamics is also observed in biological and socio-economic processes for which we include anomalous diffusion in the cell membrane and in human travel as examples. The theoretical description of such different phenomena leads, in turn, to the prediction of novel physical and mathematical properties such as sub- and superdiffusion, probability distributions with infinite moments, weak ergodicity breaking, anomalous relaxation in complex systems or subdiffusion limited reactions, topics that are all explored in this book. Anomalous transport thus nicely exemplifies the saying, freely after Tolstoi, that “all simple systems are simple in the very same manner, whereas any complex system exhibits its very own type of complexity”.

The individual chapters of this multi-author monograph are written by mathematicians, theoretical physicists and experimentalists who are all internationally recognized experts in their fields. The aim of the editors was to bring together the disciplines of *stochastic theory*, *dynamical systems theory* and *disordered systems*, as sketched in the figure shown below. These three fields



form rapidly growing research areas in themselves, which so far have developed quite independently from each other. However, in all these branches anomalous transport is moving more and more into the center of the activities. The book invites the reader to look beyond the scope of any of these three special disciplines. We editors hope that it will be thought-provoking by motivating researchers to establish cross-disciplinary connections between these neighbouring research areas. We would be particularly happy if it fosters further fruitful interactions between theory and experiment.

In contrast to original research articles and conference proceedings all book chapters are written in an introductory manner, which aims at making them accessible to graduate-level students. However, bringing together reviews from authors with so diverse scientific backgrounds, this book may also form a very useful reference for researchers already working in this field. All book chapters can in principle be read independently from each other, but the non-expert reader may strongly benefit from following the path we have suggested by our ordering of the single reviews. Since each contribution was written by different authors, the style and the type of the presentation varies from chapter to chapter. The reader may also find certain central aspects presented from different viewpoints, which in our eyes leads to a deeper understanding of the subject. We believe that altogether the book gives the reader a sensible account of what the main problems and methods in this newly emerging area of research are.

The idea for this monograph originated from the international WE Heraeus Seminar *Anomalous transport: experimental results and theoretical challenges*, organized by the three editors of this book, which took place in Bad Honnef, Germany, in July 2006. The photograph displayed after the introduction shows all participants of this meeting, including many of this book's authors. Triggered by the enthusiasm of all participants for the conference topic, this

book project got started. Unfortunately, one of the keynote speakers of this conference passed away right before the event took place. The first chapter of this book is therefore dedicated to Prof. Radu Balescu, one of the founders of the theory of nonequilibrium transport in plasmas, who before his death developed a very strong interest in anomalous dynamical processes.

The remainder of the book is organized into four main parts leading from mathematical foundations of anomalous transport over theoretical physical formulations to experimental results and applications. *Part I* introduces to *Fractional calculus and stochastic theory*. It starts with a two-fold opening: The first chapter provides the formal access road to the main topic of the book by introducing to fractional calculus, a mathematical technique that elegantly enables to deal with dynamical correlations in stochastic processes. The second chapter summarizes the physically intuitive side of the problem by sketching historical developments of anomalous transport and demonstrating basic ideas in form of simple examples. These two introductory chapters are followed by expositions elaborating on important mathematical and physical aspects of anomalous transport from the point of view of stochastic processes, which are in particular continuous time random walk theory, Lévy flights, numerical solutions of fractional diffusion equations and weak forms of ergodicity breaking.

Part II highlights *Dynamical systems and deterministic transport*. Its three chapters introduce to basic models generating anomalous deterministic transport such as intermittent one-dimensional maps, low-dimensional Hamiltonian systems exhibiting a mixed phase space and chains of (non)linear oscillators. These simple systems enable one to understand the microscopic origin of anomalous transport in terms of nonlinearities in the microscopic equations of motion. This leads to stickiness of trajectories to regular orbits or specific eigenmodes of dynamical systems by producing anomalous deterministic diffusion and anomalous heat conduction.

Part III focuses on *Anomalous transport in disordered systems*. Disorder is an appropriate characterization of many systems ranging from glasses or porous materials to biological systems such as actin networks or living cells. In this part some of the rare exact results for these systems are presented. Paradigmatic examples for anomalous behavior, such as structural glasses and random fractal structures, are considered in detail. The extension of anomalous transport in these contexts to reacting species introduces new aspects and poses new challenges, which are also elaborated in this part of the book.

The final *Part IV* reports *Applications to complex systems and experimental results*. It features a superstatistical Langevin-type theory, which identifies anomalous dynamics in experimental data of turbulence, cosmic rays and train delays. Anomalous transport by human dispersal, which is intimately related to epidemic spreading, is described subsequently. An important tool for experimentally observing anomalous molecular diffusion in porous struc-



tures as well as in polymer melts are NMR techniques, which is the subject of the following two chapters. The book concludes with new insights into the anomalous properties of the plasma membrane of biological cells, which are obtained by high-speed single-molecule tracking techniques.

We are extremely grateful to the Heraeus foundation for the financial support of the conference in Bad Honnef, which motivated us to edit this book. Particularly, we thank Dr. Ernst Dreisigacker for his advice and Jutta Lang for her help in successfully organizing this event. Thanks also go to Vera Palmer and to Ulrike Werner from Wiley-VCH publishers for their kind and efficient assistance in editing this book. R.K. acknowledges financial support by a grant from the British EPSRC under EP/E00492X/1, I.M.S. is grateful to the SFB555 – Complex Nonlinear Processes for support. We finally wish to thank our colleagues for the time and efforts they have invested in writing the individual chapters, thus making their joint expertise available in form of this multi-author monograph.

*London,
Chemnitz,
Berlin,
Winter 2007/2008*

*Rainer Klages
Günter Radons
Igor M. Sokolov*

List of Contributors

Eduardo G. Altmann

Max Planck Institute for the
Physics of Complex Systems
Noethnitzer Strasse 38
01187 Dresden
Germany
edugalt@pks.mpg.de

Gustavo A. Appignanesi

Laboratorio de Fisicoquimica
Departamento de Quimica
Universidad Nacional del Sur
Av. Alem 1253
8000 Bahia Blanca
Argentina

Roberto Artuso

Universita degli studi dell'Insubria
Dipartimento di Fisica e Matematica
Via Valleggio 11
22100 Como
Italy
roberto.artuso@uninsubria.it

Eli Barkai

Bar-Ilan University
Department of Physics
Ramat Gan 52900
Israel
barkaie@mail.biu.ac.il

Christian Beck

Queen Mary, University of London
School of Mathematical Sciences
Mile End Road
London E1 4NS
UK
c.beck@qmul.ac.uk

Jean-Phillipe Bouchaud

Centre d'Etudes de Saclay (CEA)
Service de Physique de l'Etat Condense
(SPEC)
Orme des Meurisiers
91191 Gif-sur-Yvette Cedex
France
Jean-Philippe.Bouchaud@cea.fr

Dirk Brockmann

Northwestern University
Department of Engineering Sciences and
Applied Mathematics
2145 Sheridan Road
Evanston, IL 60208
USA
brockmann@northwestern.edu

Alexei V. Chechkin

Institute for Theoretical Physics
NSC KIPT
Akademicheskaya St. 1
61108 Kharkov
Ukraine
achechkin@kipt.kharkov.ua

Giampaolo Cristadoro

Universita degli studi dell'Insubria
Dipartimento di Fisica e Matematica
Via Valleggio 11
22100 Como
Italy
giampaolo.cristadoro@uninsubria.it

Diego del-Castillo-Negrete

Fusion Energy Division
Oak Ridge National Laboratory
P.O. Box 2008
MS 6169, Oak Ridge
TN 37831-6169
USA
delcastillod@ornl.gov

Nail Fatkullin

Kazan State University
Department of Physics
Kazan 420008, Tatarstan
Russia

Takahiro Fujiwara

Membrane Mechanisms Project
International Cooperative Research
Project (ICORP)-Japan
Science and Technology Agency (JST)
Institute for Integrated Cell-Material
Sciences (iCeMS)
Kyoto University
Kyoto 606-8507
Japan
fujiwara@frontier.kyoto-u.ac.jp

Vsevolod Yu. Gonchar

Institute for Theoretical Physics
NSC KIPT
Akademicheskaya St. 1
61108 Kharkov
Ukraine

Rudolf Gorenflo

Free University of Berlin
Department of Mathematics and
Computer Science
Arnimallee 3
14195 Berlin
Germany
gorenflo@mi.fu-berlin.de

Rudolf Hilfer

Universität Stuttgart
Institut für Computerphysik
Pfaffenwaldring 27
70569 Stuttgart
Germany
and
Institut für Physik
Universität Mainz
Staudinger Weg 7
55099 Mainz
Germany
hilfer@ica1.uni-stuttgart.de

Karl Heinz Hoffmann

Chemnitz University of Technology
Institute of Physics
09107 Chemnitz
Germany
hoffmann@physik.tu-chemnitz.de

Jörg Käger

University of Leipzig
Department of Interface Physics
Linnestr. 5
04103 Leipzig
Germany
kaerger@physik.uni-leipzig.de

Holger Kantz

Max Planck Institute for the
Physics of Complex Systems
Noethnitzer Strasse 38
01187 Dresden
Germany
kantz@mpipks-dresden.mpg.de

Markus Kehr

Universität Ulm
Sektion Kernresonanzspektroskopie
89069 Ulm
Germany

Rainer Kimmich

Universität Ulm
Sektion Kernresonanzspektroskopie
89069 Ulm
Germany
rainer.kimmich@uni-ulm.de

Joseph Klafter

Tel Aviv University
School of Chemistry
69978 Tel Aviv
Israel
klafter@post.tau.ac.il

Rainer Klages

Queen Mary, University of London
School of Mathematical Sciences
Mile End Road
London E1 4NS
UK
r.klages@qmul.ac.uk

Walter Kob

Universite Montpellier 2
Laboratoire des Colloides
Verres et Nanomateriaux
UMR 5587, cc69
34095 Montpellier Cedex 05
France
kob@lcvn.univ-montp2.fr

Akihiro Kusumi

Membrane Mechanisms Project
International Cooperative Research
Project (ICORP)-Japan
Science and Technology Agency (JST)
Institute for Integrated Cell-Material
Sciences (iCeMS)
Kyoto University
Kyoto 606-8507
Japan
akusumi@frontier.kyoto-u.ac.jp

Stefano Lepri

Istituto dei Sistemi Complessi
Consiglio Nazionale delle Ricerche
via Madonna del Piano 10
50019 Sesto Fiorentino
Italy
stefano.lepri@isc.cnr.it

Katja Lindenberg

University of California - San Diego
Department of Chemistry
and Biochemistry
La Jolla, CA 92093-0340
USA
klindenberg@ucsd.edu

Roberto Livi

Università di Firenze
Dipartimento di Fisica – CSDC
Via Sansone, 1
50019 Sesto Fiorentino
Italy
and
INFN Sez. Firenze
Via Sansone, 1
50019 Sesto Fiorentino
Italy
livi@fi.infn.it

Yujie Li

Universität Ulm
Sektion Kernresonanzspektroskopie
89069 Ulm
Germany

Francesco Mainardi

University of Bologna
Department of Physics and INFN
Via Irnerio 46
40126 Bologna
Italy
mainardi@bo.infn.it

Ralf Metzler

Technical University of Munich
Theoretische Physik T30g
Physics Department
James Franck Straße
85747 Garching
Germany
metz@ph.tum.de

Ruben A. Montani

Universidad Nacional del Sur
Laboratorio de Fisicoquímica
Departamento de Química
Av. Alem 1253
8000 Bahía Blanca
Argentina

Nobuhiro Morone

National Institute of Neuroscience
National Center of Neurology and
Psychiatry
Department of Ultrastructural Research
Tokyo 187-8502
Japan
morone@ncnp.go.jp

Antonio Politi

Istituto dei Sistemi Complessi
Consiglio Nazionale delle Ricerche
via Madonna del Piano 10
50019 Sesto Fiorentino
Italy
antonio.politi@isc.cnr.it

Janett Prehl

Chemnitz University of Technology
Institute of Physics
09107 Chemnitz
Germany
janett.prehl@physik.tu-chemnitz.de

Günter Radons

Chemnitz University of Technology
Institute of Physics
09107 Chemnitz
Germany
guenter.radons@physik.tu-chemnitz.de

J. Ariel Rodríguez Fris

Universidad Nacional del Sur
Laboratorio de Fisicoquímica
Departamento de Química
Av. Alem 1253
8000 Bahía Blanca
Argentina

Juan Jesús Ruiz-Lorenzo

Universidad de Extremadura
Departamento de Física
Avda. Elvas s/n
06071 Badajoz
Spain
ruiz@unex.es

Raul Sanchez

Fusion Energy Division
Oak Ridge National Laboratory
Oak Ridge, TN 37831
USA
sanchezferlr@ornl.gov

Michael F. Shlesinger

Office of Naval Research/Code 30
875 N. Randolph St.
Arlington VA 22203-1995
USA
mike.shlesinger@navy.mil

Igor M. Sokolov

Humboldt Universität zu Berlin
Institute of Physics
Newtonstr. 15
12489 Berlin
Germany
igor.sokolov@physik.hu-berlin.de

Yasuhiro Umemura

Membrane Mechanisms Project
International Cooperative Research
Project (ICORP)-Japan
Science and Technology Agency (JST)
Institute for Integrated Cell-Material
Sciences (iCeMS)
Kyoto University
Kyoto 606-8507
Japan
yumemura@frontier.kyoto-u.ac.jp

Rustem Valiullin

University of Leipzig
Department of Interface Physics
Linnestr. 5
04103 Leipzig
Germany
Valiulli@rz.uni-leipzig.de

Angelo Vulpiani

Università degli studi La Sapienza
P.le A. Moro 2
00185 Roma
Italy
Angelo.Vulpiani@roma1.infn.it

Boris Weyssow

Research Unit Statistical and
Plasma Physics
Université Libre de Bruxelles, CP 231
EURATOM – Belgian State
Association for Fusion
Boulevard du Triomphe
1050 Bruxelles
Belgium
bweyssow@ulb.ac.be

Santos Bravo Yuste

Universidad de Extremadura
Departamento de Física
Avda. Elvas s/n
06071 Badajoz
Spain
santos@unex.es

1

In Memoriam: Radu Balescu

Boris Weyssow, Angelo Vulpiani, Francesco Mainardi, Raul Sánchez, and Diego del-Castillo-Negrete

This chapter is dedicated to Professor Radu Balescu, who very unexpectedly passed away on June 1, 2006, during a trip to Romania at the age of 73 years. Radu Balescu was invited as one of the keynote speakers to the conference on *anomalous transport: experimental results and theoretical challenges* in Bad Honnef, Germany, which took place about 1 month later in July 2006. This conference



Figure 1.1 Professor Radu Balescu († June 1, 2006); photo by Jacques Misguich, July 2005, Provence.

initiated the writing of the present book. Being a world class leader in the theory of nonequilibrium transport in plasmas, before his death Radu Balescu developed a very strong interest in anomalous dynamical processes. We start this chapter by including the abstract of the talk that Radu Balescu was intending to give in Bad Honnef.

Radu Balescu was planning to meet several colleagues at this conference for the very first time, with whom before he had intensive e-mail correspondences on topics of anomalous transport. These colleagues, as well as other conference participants who earlier had the privilege to meet Radu Balescu, have been invited to contribute to this book with their own obituaries. Their memories are added after a short summary of the scientific career of Radu Balescu, written by one of his closest collaborators.

1.1

Radu Balescu's Abstract for the Conference on Anomalous Transport in Bad Honnef

Statistical Mechanics and Strange Transport

Radu Balescu

*Association Euratom- Etat Belge pour la Fusion
Université Libre de Bruxelles
CP 231 Campus Plaine ULB, Bd du Triomphe
B-1050 Bruxelles, Belgium*

In recent years continuous time random walk (CTRW)s (CTRW) and fractional differential equations (FDE) have proved to be extremely successful modeling techniques for describing a wide range of applications for which standard diffusive transport is found experimentally to be inadequate. Yet there does not exist a complete justification of these concepts based on first principles of mechanics. A tractable starting point is provided by a "semidynamical" approach, based on a V-Langevin equation: an equation of motion of Newtonian (or Hamiltonian) type for a tracer particle moving in the presence of a random potential. Associated with it there is a "hybrid kinetic equation" (HKE) for the (stochastic) distribution function $f(x, t)$ of the positions. By standard methods of statistical mechanics an equation of evolution of the ensemble average of this function, called the "density profile" $n(x, t) = \langle f(x, t) \rangle$, is derived. The latter is, however, not closed because of its nonlocal character: on its right-hand side appears, under an ensemble average, the density profile evaluated at the fluctuating position of the particle, together with other fluctuating quantities. The usual "local approximation" provides a good description

of normal diffusive processes, but is inadequate for strange transport (sub- or supradiffusive).

Recently, Sánchez et al.¹ used an elegant method for overcoming the non-locality difficulty, based on functional integration techniques applied to the fluctuating particle trajectories (supposed to be self-similar) in order to derive a closed nonlocal equation for the density profile. Under special assumptions this equation can be reduced to a FDE.

In the present work we use a quite different approach, based on an analysis of the various types of propagators appearing in the treatment of the HKE. We introduce a nonlocal extension of an approximation similar to the Corrsin factorization assumption of turbulence theory. The result is a non-Markovian and nonlocal, formally linear equation, in which the rate of change of the density profile $n(x, t)$ at point x and time t is related to the values of this function at neighboring points $x + r$ and at past times $t - T$. Its structure is similar, but not identical (because of different approximations), to the equation of Sánchez et al. On the other hand, it can be shown that there exists an “equivalent” CTRW. The transition probability in the Montroll–Shlesinger equation describing the latter is related to the Eulerian velocity autocorrelation and to the ensemble-averaged propagator of the HKE $\langle G(x, t|x', t') \rangle$. Under certain special assumptions on the form of the latter two quantities (such as self-similar power-law forms), the equation for the density profile can be reduced to a fractional differential equation.

When viewed from a more general point of view, the equation of evolution for $n(x, t)$ is readily transformed into an equation for the average propagator $\langle G(x, t|x', t') \rangle$. The latter provides, as usual, the solution of the Dirichlet problem of the former equation for an arbitrary initial condition $n(x, 0)$. Besides its non-Markovian and nonlocal character, this equation appears to be explicitly nonlinear. Thus, not surprisingly, even in this simplest “nonlocal Corrsin-like” approach, one is faced with the complexity of a nonlinear process. A self-consistent theory of strange transport should therefore involve adequate approximation methods (such as renormalization techniques) for treating this equation.

1.2

The Scientific Career of Radu Balescu by Boris Weyssow

Professor Emeritus Radu Balescu unexpectedly passed away on June 1, 2006, during a trip in Romania at the age of 73 years. Professor at the Université Libre de Bruxelles, Member of the Royal Academy of Science, Humanities and Fine Arts of Belgium, Honorary Member of the Romanian Academy, Radu

¹) see Ref. [1], the editors.

Balescu was at a very young age recognized internationally as a leader in the development of the Statistical Physics of charged particles (the well-known Balescu–Lenard collision operator) and of the theory of transport in magnetically confined plasmas.

Professor Radu Balescu was born in 1932 in Bucharest, Romania, from a Belgian mother, and acquired Belgian nationality in 1959. He studied at the Université Libre de Bruxelles and from 1957 until 1961 was the assistant of Professor Illya Prigogine (Nobel Laureate in 1977). Professor Radu Balescu made original contributions in the kinetic theory of plasmas and published his first book *Statistical Mechanics of Charged Particles* (Interscience, 465 pp) in 1963 followed in 1975 by a comprehensive treatise of statistical mechanics, *Equilibrium and Nonequilibrium Statistical Mechanics* (Wiley, 742 pp). The main purpose of this book was to achieve a presentation that would be as unified as possible with a very wide coverage of nonequilibrium theory, not treated in standard textbooks of that time. It also introduced for the first time in a textbook some new concepts, such as the renormalization group theory of critical phenomena, which turned out to be very successful in forthcoming years. This book is still very widely cited in the literature. Both this book and the previous one have been translated into Russian by leading Russian theorists.

Until becoming Emeritus in 1997, he had been Ordinary Professor at the University of Brussels. He has lectured or has been visiting Professor all over Europe, in Kyoto, Austin, and Mexico. Professor Radu Balescu was involved in the European fusion program for more than 30 years as a scientist and as the head of research unit of the ULB group in the Euratom-Belgian State Association.

In 1988, Professor Balescu published a magnum opus *Transport Processes in Plasmas: Volume 1: Classical Transport; Volume 2: Neoclassical Transport* (North-Holland, 803 pp). This set of two volumes presents a comprehensive review of the classical and the neoclassical theories of transport in plasmas, especially in the regime relevant to thermonuclear fusion. This is one of the first fully consistent presentations of the theory. It starts from first principles (Hamiltonian mechanics), going through kinetic theory, and ending in the explicit calculation of the transport coefficients and the discussion of the thermodynamic aspects of the transport. The second volume describes the nontrivial influence of the toroidal geometry (existing in magnetically confined plasmas) on the transport. Again, the main aim here was a unified presentation of the theory. It should be emphasized that these volumes encompass not only the work of many authors but that they are original in their conception and include many hundreds of pages of new consistent calculations and results. They are considered by many theorists as the current bible for plasma transport processes and has already been translated into Chinese.

A third volume on transport was about to be finished at that time. However Professor Balescu found that some elements of the mathematical theory of stochastic processes and of turbulence were not advanced enough to be published as chapters of a book. It is in 2005 that *Aspects of Anomalous Transport in Plasmas* was finally published by IOP publishing. The final version contains several chapters on the kinetic theory of turbulence (quasilinear theory, renormalization, DIA) but also includes a thorough discussion on random processes with applications to fusion experiments. This book also extends *Statistical Dynamics: Matter out of Equilibrium* published in 1997 by Imperial College Press which is a survey of nonequilibrium statistical mechanics, from Hamiltonian systems to complex systems and summarizes the first considerations of the author on CTRW and percolation processes.

This survey of Professor Balescu's work amply demonstrates the breadth and the depth of his contribution, not only to theoretical basic plasma and fusion physics, but also to statistical physics in general. It encompasses the conceptual roots of the disciplines and addresses the most challenging present-day problems. The excellence of his contributions has early been recognized by the most prestigious Belgian Scientific prize: "Le Prix Francqui" in 1970. He was a member or foreign member of several academies. He was awarded the first von Engel Prize of the International Conference on Phenomena in Ionised Gases in 1999 and the first Hannes Alfvén Prize of the Plasma Physics Division of the European Physical Society in 2000.

Radu Balescu was not only a recognized scientist but also a very appreciated teacher. All along his career, he spread his love of physics amongst his students with brilliance and enthusiasm. Radu Balescu will also be remembered as a true and respected humanist. He was constantly guided by exceptional honesty and integrity in his scientific career, in the management of his group and in his relationship with colleagues.

1.3

My Memory of Radu Balescu by Angelo Vulpiani

I had the opportunity, and privilege, to know Radu Balescu and to collaborate with him. I guess it is not necessary to spend time to remind of his long career, his seminal contributions to statistical physics and plasma physics (one can just mention the celebrated Lenard–Balescu equation and its basic role in the statistical kinetic theory of charged particles), and the important awards, as the Hannes Alfvén Price. For a discussion of his late contributions to anomalous transport, see [2].

In autumn 1984, I was in the CEA Plasma Physics Center of Fontenay-aux-Roses (then the Center moved to Cadarache) working on the diffusion of

particle-guiding centers across a strong magnetic field, caused by a turbulent electrostatic field. The research was a project with Marco Pettini and Jacques Misguich and was mainly based on some ideas by Radu Balescu. As a consequence of funny interactions with the CEA bureaucracy, Marco Pettini and I went to Bruxelles where we had the opportunity to use a free good computer, and overall get to know Radu.

My knowledge of plasma physics was (and still is) rather elementary; fortunately our research was basically a statistical mechanics problem. So Marco and I had not particular difficulties in the computational and theoretical aspects, but we had very vague ideas of the real physical relevance of our results. We thought that the agreement between the numerical results and the theoretical prediction for the diffusion coefficient was very bad (their ratio was between 1.5 and 4), so we informed Radu that the computation based on his theory was not so good. Immediately Radu realized how naive we were. With tolerance and irony he explained to us that plasma physics is a very intricate field, where it is not enough to solve equations, but overall it is necessary to be aware of the role of the assumptions and approximations. Then he concluded by saying that, since in that issue the ratio between theory and experiment was typically between 10 and 100, the result was really nice [3,4]. At the first glance I thought he was joking, but Radu invited us for dinner to celebrate.

At that time when I was a young assistant professor, Radu was already a well-known scientist, although he was still associate professor (sic!). In spite of the clear difference of our positions in the international scientific ranking, Radu treated me as a young colleague. I remember him in his small office, in a forest of partial differential equations, special functions and asymptotic expansions, spending the major part of his time writing a magnum opus on transport processes in plasma physics [5]. However, everybody could enter and discuss science with him. Radu Balescu was a master of statistical mechanics with a deep physical insight. He will certainly be missed, but his scientific legacy will continue to be influential.

1.4

My Memory of Radu Balescu by Francesco Mainardi

My first acquaintance with Radu Balescu was in the late 1990s through his book *Statistical Mechanics – Matter out of Equilibrium* (Imperial College Press, 1997). I found his treatment of statistical mechanics very innovative compared to those in the classical books and I much appreciated his chapter on non-Gaussian stable probability distributions and generalized master equations. A few years earlier, these topics had reawakened in me the interest toward the potential of fractional calculus in statistical physics, in particular to explore

the phenomena of anomalous diffusion and transport. So, during a visit at the Université Libre de Bruxelles (ULB), I had the opportunity to meet Radu Balescu in his office and to express to him my appreciation and interest for his approach to statistical mechanics. I also pointed out where in that book possible connections with fractional calculus could be envisaged. Unfortunately, this brief colloquium did not have any immediate consequence, since it was forgotten by himself, as it was recognized later.

It was a (nice) surprise for me when on November 1, 2005, I received the following kind letter from him:

Dear Professor Mainardi,

Please let me introduce myself. I am Radu Balescu, professor emeritus at the Université Libre de Bruxelles. I have worked throughout my career on nonequilibrium statistical mechanics, and in particular on its application to plasma physics. I wrote (among others) two books which may be of interest to you: "Statistical Mechanics – Matter out of Equilibrium" (Imperial College Press, 1997) and "Aspects of Anomalous Transport in Plasmas" (Taylor and Francis, 2005). They contain sections on strange (= anomalous) transport, a subject that fascinated me for a long time.

Recently I discovered your works on fractional differential equations – in particular the one in Fractional Calc. Appl. Anal. 2001 – (see [6]) which I found wonderful, by their content and the clarity of the exposition. I regretted strongly that I did not know them before the completion of my latest book. I should greatly appreciate your sending me your latest works in this area.

I am attaching a text containing my latest work in this domain. It is a "long version", not intended for publication as such. It contains many details (it was the basis of some seminars I delivered here). I should sincerely appreciate your having a look at it and letting me know your comments and suggestions.

With best regards, Radu Balescu

From then on, a kind exchange of e-mails was carried out with information about the conferences appointed in the near past and future, related in some way to the applications of fractional calculus in statistical physics, that is the Workshop *In Search of a Theory of Complexity* organized by A. Allegrini, P. Grigolini and B.J. West at Denton (TX), August 2005 and the Workshop *Anomalous Transport: Experimental Results and Theoretical Challenges* organized by R. Klages, G. Radons and I.M. Sokolov at Bad Honnef (Germany), July 2006.

For the former workshop, which was attended by myself but not by him, the organizers invited him to submit his contribution to the special issue of *Chaos*

Solitons and Fractals. For the latter workshop, both of us agreed to participate: in our intentions this event would have provided the occasion for our meeting and exchange of ideas on topics of common interest. Unfortunately, just a few weeks before the workshop in Bad Honnef, exactly on June 2, I received a circular mail from Professor Jacques Misguich (being entered in the mailing list of Radu) with the bad news of Balescu's death on June 1, 2006, in Romania.

Consequently, his interesting contribution for the Denton special issue appeared posthumous [7]: the Guest Editors dedicated that issue to his memory, see [8]. The abstract of his invited lecture at Bad Honnef has been included by the Editors in the present book. The last version of his lecture notes on anomalous transport, based on the applications of fractional calculus (the object of our exchange of e-mails), was submitted by his colleagues to the Physics section of the *Cornell University Archives* in April 2007, see [9]. Both posthumous contributions appeared with the same title "V-Langevin Equations, Continuous Time Random Walks and Fractional Diffusion," but they were edited with different purposes: the former as a research paper, the latter as a didactic review paper. They provide the last messages to the scientific community from a great man, who had spent his life for research and teaching with enthusiasm. Personally, I have lost with him a great pen pal but overall a possible mentor and collaborator.

1.5

In Memoriam: Radu Balescu by Raul Sánchez

The unexpected passing away of Radu Balescu saddened deeply his numerous friends and colleagues. Our group had the privilege of interacting with him frequently during the last 2 years of his life. In what follows, I will recall some of my personal memories about him, rather than regarding discussing his great scientific achievements, which are well known.

I first heard Radu Balescu's name when I was in my fourth year in college, pursuing my Physics degree. That year, I had to take a rather hard course on Statistical Mechanics, and I remember being forever grateful to Professor Radu Balescu for the great book he had written on this topic [10], which helped me get through the course successfully and even learn some Physics along the way. At the time, I knew nothing about him and his many important contributions to the field of Plasma Physics. Little did I suspect that I was to end up, a few years later, working in that very same beautiful but extremely hard part of Physics myself. As I was becoming acquainted with this new phase of my career, his books paid again another great service to me: I pretty much learnt neoclassical transport in toroidally confined plasmas by using, side by side, Hirshman & Sigmar's famous review article [11] together with Radu Balescu's two-volume book on the subject [5].

Therefore, having used extensively his books for many years, I held a deep respect for Radu Balescu's scientific achievements and pedagogical abilities as I advanced in my scientific career. I had never met him personally; else he would have almost surely ignored my existence. But precisely for that reason I became extremely excited when one spring morning of 2004 (I was visiting Ben Carreras at Oak Ridge National Laboratory at the time), Boudewijn van Milligen wrote us from CIEMAT (Madrid, Spain) to tell Ben and me that Radu Balescu himself had e-mailed him to congratulate us for our very recent paper [12]. The paper dealt with some initial exploration of the use of ideas based on the Continuous-Time Random Walk (CTRW) concept to advance the understanding of radial turbulent transport in magnetically confined plasmas. We knew that Radu Balescu was himself a CTRW aficionado, since he had published an earlier paper on CTRWs and magnetic turbulent transport [13], but his great interest in our findings came to us as a very pleasant surprise.

This confluence of common interests triggered a very intense collaboration between Radu Balescu and us during the last 2 years of his life. We started exchanging numerous e-mails with notes, drafts of papers, calculations, comments, questions, doubts, criticisms, and what not. We discussed details of what, to the best of my knowledge, was the last physics problem Radu Balescu attacked: the derivation of superdiffusive fractional differential equations (FDEs) from what he called the V-Langevin kinetic equation [14]. Fractional equations are differential equations that contain the rather esoteric fractional derivatives and which have become quite fashionable lately. They appear as the natural fluid limit (at very long times and long distances) of CTRWs. Thus, if CTRWs or FDEs are to provide a reasonable description of turbulent transport, they should be derivable, at least in some limit, from more standard continuous equations. The V-Langevin equation, which is simply the continuity equation for the density of particles which are advected by a flow (V) with prescribed statistical and correlation properties, provides one such starting point for the derivation. Both Radu and we attempted to complete it frantically. Radu did not work together with our team (composed of Ben, Boudewijn, David Newman from the University of Alaska, Vickie Lynch from Oak Ridge, and myself), but in parallel. The path we chose to attack the derivation was quite different from the one Radu chose to pursue. But Radu kept our progress under close scrutiny as much as we kept his. In the end we completed the derivation, not without Radu pointing out several shortcomings and improving it through his comments [1]. Radu also completed his own derivation, but we never got to see it. He died in Romania a few weeks before we were to meet in person at Bad Honnef, for the first time, to discuss the details of his approach and compare it with ours. But even when we never got to see each other in person, we got to meet his real persona during this time of intense collaboration. And he turned out to be much more than the very

bright and technically gifted scientist we expected him to be. We met a man with the greatest scientific honesty and as critical with our ideas as he was with his own. Regretfully, this kind of “symmetry” is not commonly found in the competitive arena that scientific research has become. It is just one of the reasons for which, without a doubt, I can say that he will be missed.

1.6

Remembering Radu Balescu by Diego del-Castillo-Negrete

Radu Balescu once wrote: “I have been ‘in love’ with the statistical mechanics of plasma physics over my whole scientific career” [5]. Out of this love, important contributions to the study of anomalous transport in plasmas in general, and magnetically confined fusion plasmas in particular, were born. Of special value are Balescu’s seminal contributions on the application of non-Gaussian stochastic processes to the description of anomalous transport. These works set the path of a very promising and elegant research direction that was sadly interrupted by Radu’s unexpected death. Understanding anomalous transport is one of the main roadblocks to achieve controlled nuclear fusion in magnetically confined plasmas. Radu Balescu’s original and unique perspective on this subject will prove to be very valuable in the years to come.

It is a great honor to share in this brief note my personal acquaintance with Radu during the last years of his life. Although at a long distance, this interaction was extremely valuable to me. As many scientists of my generation, I first learned about Radu Balescu from his books on statistical mechanics and plasma transport. However, my first contact with Radu at a more personal level came at the end of 2004 when I sent him a brief e-mail along with a paper that I had published in August of that year. The work focused on anomalous, superdiffusive transport in plasma turbulence. In particular, it discussed how the CTRW (Continuous Time Random Walk) formalism was a natural framework to describe this problem, and showed that the probability distribution function of particle displacements can be obtained from the propagator of a space–time fractional diffusion equation. Radu’s response was prompt and enthusiastic; he was “...happy to see that the CTRW philosophy continues its development!”

Radu’s interest on the application to the CTRW model to study transport in plasmas goes back to 1995 when he proposed for the first time the application of this formalism to study anomalous transport in magnetized plasmas [13]. However, despite the close connection between the CTRW and fractional diffusion, Radu was at the beginning skeptical about the value of fractional diffusion. This explains why fractional diffusion did not play a prominent role in his book on anomalous transport [14].

However, this situation changed rapidly during 2005. In an e-mail exchange on February of that year he wrote, "... I became convinced (for the first time) of the usefulness of fractional calculus. All the papers I read previously about the subject left me with an impression of a heavy and untransparent formalism, which did not give me an impetus for further study. After reading your paper I clearly understand that fractional calculus is, indeed, an indispensable tool for a fine analysis of the CTRW." Over the next few months Radu became increasingly interested in the fractional diffusion approach to plasma turbulence, and we had the opportunity to discuss the topic in considerable detail. During this time, I was thankful to Radu's kindness, enthusiasm, and support.

In August 2005 Radu circulated a set of notes entitled "V-Langevin Equations leading to superdiffusion." Although with his characteristic modesty Radu referred to them as preliminary, the notes contained not only a valuable summary of fractional calculus, but also a very interesting discussion on the connection between particle dynamics with random velocity (V-Langevin equation), the CTRW model, and fractional diffusion. Elaborating on these notes, Radu prepared an extended manuscript including review material, and a short research paper, both entitled "V-Langevin Equations, Continuous Time Random Walks and Fractional Diffusion." At this point Radu was fully engaged in the study of fractional diffusion. The year was 2006 and I had received an invitation to participate in the summer workshop on "Anomalous Transport: Experimental Results and Theoretical Challenges" in Bad Honnef, Germany. I was delighted to accept the invitation that would give me the opportunity to meet Radu in person, and to learn more about his most recent ideas. Sadly, he unexpectedly passed away before the meeting on June 1 during a trip to Romania. His last two papers were published early this year [7,9]. Radu left us with great memories, and long-lasting contributions to statistical mechanics and plasma physics that will inspire many generations to come.

References

- 1 R. Sánchez, B.A. Carreras, D.E. Newman, V.E. Lynch, and B.Ph. van Milligen, "Renormalization of tracer turbulence leading to fractional differential equations", *Phys. Rev. E* **74**, 016305 (2006).
- 2 R. Sánchez, B.A. Carreras, and B. Ph. van Millegen, "Radu Balescu and the search for a stochastic description of turbulent transport in plasma", *Phys. Ann. Univ. Cracovia* **17**, 27 (2007) (special issue *In Memoriam of Radu C. Balescu (1932–2006)*).
- 3 M. De Leener, J. Orban, M. Pettini, A. Vulpiani, J.H. Misguich, and R. Balescu, in *Proceedings of the Congrès Société Francaise de Physique*, Nice, 1985, *Bull. Soc. Franc. Phys.* **57**, 56 (1985).
- 4 M. Pettini, A. Vulpiani, J.H. Misguich, M. de Leener, J. Orban, and R. Balescu, "Chaotic diffusion across a magnetic field in a model of electrostatic turbulent plasma", *Phys. Rev. A* **38**, 344 (1988).
- 5 R. Balescu, *Transport Processes in Plasma: Vol. 1: Classical Transport. Vol. 2: Neoclassical Transport* (North-Holland, Amsterdam, 1988).

- 6 F. Mainardi, Yu. Luchko, and G. Pagnini, "The fundamental solution of the space-time fractional diffusion equation", *Fract. Calc. Appl. Anal.* **4**, 153 (2001). [E-print <http://arxiv.org/abs/cond-mat/0702419>]
- 7 R. Balescu, "V-Langevin equations, continuous time random walks and fractional diffusion", *Chaos, Solitons and Fractals* **34**, 62 (2007).
- 8 P. Allegrini, P. Grigolini, and B.J. West, "Preface", *Chaos, Solitons & Fractals* **34**, 1 (2007).
- 9 R. Balescu, "V-Langevin equations, continuous time random walks and fractional diffusion", E-print <http://arxiv.org/abs/0704.2517> [physics.plasma-ph], 19 April 2007, p. 69.
- 10 R. Balescu, *Equilibrium and Nonequilibrium Statistical Mechanics* (Wiley, New York, 1975).
- 11 S.P. Hirshman and D.J. Sigmar, "Neoclassical transport of impurities in tokamak plasmas", *Nucl. Fusion* **21**, 1079 (1981).
- 12 B. Ph. van Milligen, R. Sánchez, and B.A. Carreras, "Probabilistic finite-size transport models for fusion: anomalous transport and scaling laws", *Phys. Plasmas* **11**, 2272 (2004).
- 13 R. Balescu, "Anomalous transport in turbulent plasmas and continuous time random walks", *Phys. Rev. E* **51**, 4807 (1995).
- 14 R. Balescu, *Aspects of Anomalous Transport in Plasmas* (IOP, Bristol, 2005).

Part I Fractional Calculus and Stochastic Theory

Introduction to Part I

The opening Part I of this book is devoted to *Fractional calculus and stochastic theory*. It presents in detail the theoretical and mathematical foundations of the formalism describing anomalous transport, such as fractional differentials and fractional differential equations, and gives a modern outline of random walk approaches to anomalous transport. These tools can be applied to a wide variety of complex systems, as is demonstrated in the remainder of the book. However, we emphasize that it is not mandatory to fully familiarize with all these techniques to understand the later more applied chapters.

This first part starts with a *Threefold introduction to fractional derivatives* by Rudolf Hilfer, which gives a thorough, intuitive and at the same time quite rigorous introduction to this indispensable instrument of theoretically analysing and describing anomalous diffusion as considered within the framework of random walk models. It is followed by Michael Schlesinger's *Anomalous processes with infinite moments* giving a general, easy-to-read and motivating account on the historical development of probabilistic models underlying anomalous diffusion and on most of the further problems discussed in the first part of the book. The part proceeds with *Continuous time random walks, Mittag-Leffler waiting time and fractional diffusion: mathematical aspects* by Rudolf Gorenflo and Francesco Mainardi, which contains a precise and rigorous discussion of one of the models mentioned above, namely of the continuous time random walk (CTRW). The following chapter, *Introduction to the theory of Lévy flights* by Alexei Chechkin, Ralf Metzler, Joseph Klafter and Vsevolod Gonchar does the same for another model discussed by Michael Shlesinger, which are Lévy flights. *Fractional diffusion models of anomalous transport* by Diego del-Castillo-Negrete shows the path from mathematical descriptions to applications of the corresponding models, particularly to problems in hydrodynamics and in plasma physics. It combines CTRW theory with Lévy flights, which are both important ingredients of a general theory of anomalous transport. This chapter also contains a profound mathematical part, which is presented from a somewhat different point of view than the previous contributions. Part I concludes with *Anomalous kinetics leads to weak ergodicity breaking* by Eli Barkai

discussing a question that was hardly mentioned in the previous chapters, where the theory was based on ensemble averages. Being a non-Markovian process with diverging characteristic time scales, CTRW theory refers to a situation where ensemble averages and the correspondingly taken time averages do not coincide, a behavior denoted as “weak ergodicity breaking”. Eli Barkai’s contribution deals with these subtle problems, which have important implications both for the theoretical description and for the interpretation of experimental results of anomalous transport.

2

Threefold Introduction to Fractional Derivatives

Rudolf Hilfer

2.1

Historical Introduction to Fractional Derivatives

2.1.1

Leibniz

Already at the beginning of calculus one of its founding fathers, namely G.W. Leibniz, investigated fractional derivatives [72, 73]. Differentiation, denoted as d^α ($\alpha \in \mathbb{N}$), obeys Leibniz' product rule

$$d^\alpha(fg) = 1 d^\alpha f d^0 g + \frac{\alpha}{1} d^{\alpha-1} f d^1 g + \frac{\alpha(\alpha-1)}{1 \cdot 2} d^{\alpha-2} f d^2 g + \dots \quad (2.1)$$

for integer α , and Leibniz was intrigued by the analogy with the binomial theorem

$$p^\alpha(f+g) = 1 p^\alpha f p^0 g + \frac{\alpha}{1} p^{\alpha-1} f p^1 g + \frac{\alpha(\alpha-1)}{1 \cdot 2} p^{\alpha-2} f p^2 g + \dots, \quad (2.2)$$

where he uses the notation $p^\alpha f$ instead of f^α to emphasize the formal operational analogy.

Moving from integer to noninteger powers $\alpha \in \mathbb{R}$ Leibniz suggests that “on peut exprimer par une serie infinie une grandeur comme” $d^\alpha h$ (with $h = fg$). As his first step he tests the idea of such a generalized differential quantity $d^\alpha h$ against the rules of his calculus. In his calculus the differential relation $dh = hdx$ implies $dx = dh/h$ and $dh/dx = h$. One has, therefore, also $d^2h = hdx^2$ and generally $d^\alpha h = hdx^\alpha$. Regarding $d^\alpha h = hdx^\alpha$ with noninteger α as a fractional differential relation subject to the rules of his calculus, however, leads to a paradox. Explicitly, he finds (for $\alpha = 1/2$)

$$\frac{d^\alpha h}{dx^\alpha} = \frac{d^\alpha h}{(dh/h)^\alpha} \neq h, \quad (2.3)$$

where $dx = dh/h$ was used. Many decades had to pass before Leibniz' paradox was fully resolved.

2.1.2

Euler

Derivatives of noninteger (fractional) order motivated Euler to introduce the Gamma function [25]. Euler knew that he needed to generalize (or interpolate, as he calls it) the product $1 \cdot 2 \cdot \dots \cdot n = n!$ to noninteger values of n , and he proposed an integral

$$\prod_{k=1}^n k = n! = \int_0^1 (-\log x)^n \, dx \quad (2.4)$$

for this purpose. In §27–29 of [25] he immediately applies this formula to partially resolve Leibniz' paradox, and in §28 he gives the basic fractional derivative (reproduced here in modern notation with $\Gamma(n+1) = n!$)

$$\frac{d^\alpha x^\beta}{dx^\alpha} = \frac{\Gamma(\beta+1)}{\Gamma(\beta-\alpha+1)} x^{\beta-\alpha} \quad (2.5)$$

valid for integer and for noninteger α, β .

2.1.3

Paradoxa and Problems

Generalizing Eq. (2.5) to all functions that can be expanded into a power series might seem a natural step, but this “natural” definition of fractional derivatives does not really resolve Leibniz’ paradox. Leibniz had implicitly assumed the rule

$$\frac{d^\alpha e^{\lambda x}}{dx^\alpha} = \lambda^\alpha e^{\lambda x} \quad (2.6)$$

by demanding $d^\alpha h = h dx^\alpha$ for integer α . One might therefore take Eq. (2.6) instead of Eq. (2.5) as an equally “natural” starting point (this was later done by Liouville in [76, p. 3, eq. (1)]), and define fractional derivatives as

$$\frac{d^\alpha f}{dx^\alpha} = \sum_k c_k \lambda_k^\alpha e^{\lambda_k x} \quad (2.7)$$

for functions represented as exponential series $f(x) \sim \sum_k c_k \exp(\lambda_k x)$. Regarding the integral (a Laplace integral)

$$x^{-\beta} = \frac{1}{\Gamma(\beta)} \int_0^\infty e^{-yx} y^{\beta-1} \, dy \quad (2.8)$$

as a sum of exponentials, Liouville [76, p. 7] then applied Eq. (2.6) inside the integral to find

$$\frac{d^\alpha x^{-\beta}}{dx^\alpha} = \frac{1}{\Gamma(\beta)} \int_0^\infty e^{-yx} (-y)^\alpha y^{\beta-1} \, dy = \frac{(-1)^\alpha \Gamma(\beta+\alpha)}{\Gamma(\beta) x^{\beta+\alpha}}, \quad (2.9)$$

where the last equality follows by substituting $yx = z$ in the integral. If this equation is formally generalized to $-\beta$, disregarding existence of the integral, one finds

$$\frac{d^\alpha x^\beta}{dx^\alpha} = \frac{(-1)^\alpha \Gamma(-\beta + \alpha)}{\Gamma(-\beta)} x^{\beta - \alpha} \quad (2.10)$$

a formula similar to, but not exactly equal to Eq. (2.5). Although Eq. (2.10) agrees with Eq. (2.5) for integer α it differs for noninteger α . More precisely, if $\alpha = 1/2$ and $\beta = -1/2$, then

$$\frac{\Gamma(3/2)}{\Gamma(0)} x^{-1} = 0 \neq \frac{i}{x\sqrt{\pi}} = \frac{(-1)^{1/2}\Gamma(1)}{\Gamma(1/2)} x^{-1} \quad (2.11)$$

revealing again an inconsistency between Eq. (2.5) and Eq. (2.10) (resp. (2.9)).

Another way to see this inconsistency is to expand the exponential function into a power series, and to apply Euler's rule, Eq. (2.5), to it. One finds (with obvious notation)

$$\begin{aligned} \left(\frac{d^\alpha}{dx^\alpha} \right)_{(2.5)} \exp(x) &= \left(\frac{d^\alpha}{dx^\alpha} \right)_{(2.5)} \sum_{k=0}^{\infty} \frac{x^k}{k!} = \sum_{k=0}^{\infty} \frac{x^{k-\alpha}}{\Gamma(k-\alpha+1)} \\ &\neq \left(\frac{d^\alpha}{dx^\alpha} \right)_{(2.6)} \exp(x) = \exp(x) \end{aligned} \quad (2.12)$$

and this shows that Euler's rule (2.5) is inconsistent with the Leibniz/Liouville rule (2.6). Similarly, Liouville found inconsistencies [75, p. 95/96] when calculating the fractional derivative of $\exp(\lambda x) + \exp(-\lambda x)$ based on definition (2.7).

A resolution of Leibniz' paradox emerges when Eqs. (2.5) and (2.6) are compared for $\alpha = -1$, and interpreted as integrals. Such an interpretation was already suggested by Leibniz himself [73]. More specifically, one has

$$\frac{d^{-1}e^x}{dx^{-1}} = e^x = \int_{-\infty}^x e^t dt \neq \int_0^x e^t dt = e^x - 1 = \frac{d^{-1}}{dx^{-1}} \sum_{k=0}^{\infty} \frac{x^k}{k!} \quad (2.13)$$

showing that Euler's fractional derivatives on the right-hand side differs from Liouville's and Leibniz' idea on the left. Similarly, Eq. (2.5) corresponds to

$$\frac{d^{-1}x^\beta}{dx^{-1}} = \frac{x^{\beta+1}}{\beta+1} = \int_0^x y^\beta dy. \quad (2.14)$$

On the other hand, Eq. (2.9) corresponds to

$$\frac{d^{-1}x^{-\beta}}{dx^{-1}} = \frac{x^{1-\beta}}{1-\beta} = - \int_x^\infty y^{-\beta} dy = \int_\infty^x y^{-\beta} dy. \quad (2.15)$$

This shows that Euler's and Liouville's definitions differ with respect to their limits of integration.

2.1.4

Liouville

It has already been mentioned that Liouville defined fractional derivatives using Eq. (2.7) (see [76, p. 3, eq. (1)]) as

$$\frac{d^\alpha f}{dx^\alpha} = \sum_k c_k \lambda_k^\alpha e^{\lambda_k x} \quad (2.7)$$

for functions represented as a sum of exponentials

$$f(x) \sim \sum_k c_k \exp(\lambda_k x). \quad (2.16)$$

Liouville seems not to have recognized the necessity of limits of integration. From his definition(2.7) he derives numerous integral and series representations. In particular, he finds the fractional integral of order $\alpha > 0$ as

$$\int^\alpha f(x) dx^\alpha = \frac{1}{(-1)^\alpha \Gamma(\alpha)} \int_0^\infty f(x+y) y^{\alpha-1} dy \quad (2.17)$$

(see formula [A] on page 8 of [76]). Liouville then gives formula [B] for fractional differentiation on page 10 of [76] as

$$\frac{d^\alpha f}{dx^\alpha} = \frac{1}{(-1)^{n-\alpha} \Gamma(n-\alpha)} \int_0^\infty \frac{d^n f(x+y)}{dx^n} y^{n-\alpha-1} dy, \quad (2.18)$$

where $n - 1 < \alpha < n$. Liouville restricts the discussion to functions represented by exponential series with $\lambda_k > 0$ so that $f(-\infty) = 0$. Liouville also expands the coefficients λ_k^α in (2.7) into binomial series

$$\lambda_k^\alpha = \lim_{h \rightarrow 0} \frac{1}{h^\alpha} (1 - e^{-h\lambda_k})^\alpha, \quad \lambda_k > 0 \quad (2.19a)$$

$$= (-1)^\alpha \lim_{h \rightarrow 0} \frac{1}{h^\alpha} (1 - e^{h\lambda_k})^\alpha, \quad \lambda_k < 0 \quad (2.19b)$$

and inserts the expansion into his definition (2.7) to arrive at formulas that contain the representation of integer order derivatives as limits of difference quotients (see [75, p. 106ff]). The results may be written as

$$\frac{d^\alpha f}{dx^\alpha} = \lim_{h \rightarrow 0} \left\{ \frac{1}{h^\alpha} \sum_{m=0}^{\infty} \left[(-1)^m \binom{\alpha}{m} f(x-mh) \right] \right\} \quad (2.20a)$$

$$= (-1)^\alpha \lim_{h \rightarrow 0} \left\{ \frac{1}{h^\alpha} \sum_{m=0}^{\infty} \left[(-1)^m \binom{\alpha}{m} f(x+mh) \right] \right\}, \quad (2.20b)$$

where the binomial coefficient $\binom{\alpha}{m}$ is $\Gamma(\alpha - 1)\Gamma(m - 1)/\Gamma(\alpha + m - 1)$. Later, this idea was taken up by Grünwald [34], who defined fractional derivatives as limits of generalized difference quotients.

2.1.5

Fourier

Fourier [29] suggested to define fractional derivatives by generalizing the formula for trigonometric functions,

$$\frac{d^\alpha}{dx^\alpha} \cos(x) = \cos\left(x + \frac{\alpha\pi}{2}\right) \quad (2.21)$$

from $\alpha \in \mathbb{N}$ to $\alpha \in \mathbb{R}$. Again, this is not unique because the generalization

$$\frac{d^\alpha}{dx^\alpha} \cos(x) = (-1)^\alpha \cos\left(x - \frac{\alpha\pi}{2}\right) \quad (2.22)$$

is also possible.

2.1.6

Grünwald

Grünwald wanted to free the definition of fractional derivatives from a special form of the function. He emphasized that fractional derivatives are integroderivatives, and established for the first time general fractional derivative operators. His calculus is based on limits of difference quotients. He studies the difference quotients [34, p. 444]

$$F[u, x, \alpha, h]_f = \sum_{k=0}^n (-1)^k \binom{\alpha}{k} \frac{f(x - kh)}{h^\alpha} \quad (2.23)$$

with $n = (x - u)/h$ and calls

$$D^\alpha[f(x)]_{x=u}^{x=x} = \lim_{h \rightarrow 0} F[u, x, \alpha, h]_f \quad (2.24)$$

the α th differential quotient taken over the straight line from u to x [34, p. 452]. The title of his work emphasizes the need to introduce limits of integration into the concept of differentiation. His ideas were soon elaborated upon by Letnikov (see [99]) and applied to differential equations by Most [89].

2.1.7

Riemann

Riemann, like Grünwald, attempts to define fractional differentiation for general classes of functions. Riemann defines the n th differential quotient of a function $f(x)$ as the coefficient of h^n in the expansion of $f(x + h)$ into integer

powers of h [96, p. 354]. He then generalizes this definition to noninteger powers and demands that

$$f(x+h) = \sum_{n=-\infty}^{n=\infty} c_{n+\alpha} (\partial_x^{n+\alpha} f)(x) h^{n+\alpha} \quad (2.25)$$

holds for $n \in \mathbb{N}, \alpha \in \mathbb{R}$. The factor $c_{n+\alpha}$ is determined such that $\partial^\beta(\partial^\gamma f) = \partial^{\beta+\gamma} f$ holds, and found to be $1/\Gamma(n + \alpha + 1)$. Riemann then derives the integral representation [96, p. 363] for negative α ,

$$\partial^\alpha f = \frac{1}{\Gamma(-\alpha)} \int_k^x (x-t)^{-\alpha-1} f(t) dt + \sum_{n=1}^{\infty} K_n \frac{x^{-\alpha-n}}{\Gamma(-n-\alpha+1)}, \quad (2.26)$$

where k, K_n are finite constants. He then extends the result to nonnegative α by writing “für einen Wert von α aber, der ≥ 0 ist, bezeichnet $\partial^\alpha f$ dasjenige, was aus $\partial^{\alpha-m} f$ (wo $m > \alpha$) durch m -malige Differentiation nach x hervorgeht, . . .” [96, p. 341]. The combination of Liouville’s and Grünwald’s pioneering work with this idea has become the definition of the Riemann–Liouville fractional derivatives (see Section 2.2.2.1).

2.2

Mathematical Introduction to Fractional Derivatives

The brief historical introduction has shown that fractional derivatives may be defined in numerous ways. A natural and frequently used approach starts from repeated integration and extends it to fractional integrals. Fractional derivatives are then defined either by continuation of fractional integrals to negative order (following Leibniz’ ideas [73]), or by integer order derivatives of fractional integrals (as suggested by Riemann [96]).

2.2.1

Fractional Integrals

2.2.1.1 Iterated Integrals

Consider a locally integrable¹ real-valued function $f : G \rightarrow \mathbb{R}$ whose domain of definition $G = [a, b] \subseteq \mathbb{R}$ is an interval with $-\infty \leq a < b \leq \infty$. Integrating

1) A function $f : G \rightarrow \mathbb{R}$ is called locally integrable if it is integrable on all compact subsets $K \subset G$ (see Eq. (B.9)).

n times gives the fundamental formula

$$\begin{aligned} (\mathbb{I}_{a+}^n f)(x) &= \int_a^x \int_a^{x_1} \cdots \int_a^{x_{n-1}} f(x_n) dx_n \cdots dx_2 dx_1 \\ &= \frac{1}{(n-1)!} \int_a^x (x-y)^{n-1} f(y) dy, \end{aligned} \quad (2.27)$$

where $a < x < b$ and $n \in \mathbb{N}$. This formula may be proved by induction. It reduces n -fold integration to a single convolution integral (Faltung). The subscript $a+$ indicates that the integration has a as its lower limit. An analogous formula holds with lower limit x and upper limit a . In that case the subscript $a-$ will be used.

2.2.1.2 Riemann–Liouville Fractional Integrals

Equation (2.27) for n -fold integration can be generalized to noninteger values of n using the relation $(n-1)! = \prod_{k=1}^{n-1} k = \Gamma(n)$ where

$$\Gamma(z) = \int_0^1 (-\log x)^{z-1} dx \quad (2.28)$$

is Euler's Γ -function defined for all $z \in \mathbb{C}$.

Definition 2.1 Let $-\infty \leq a < x < b \leq \infty$. The *Riemann–Liouville fractional integral of order $\alpha > 0$ with lower limit a* is defined for locally integrable functions $f : [a, b] \rightarrow \mathbb{R}$ as

$$(\mathbb{I}_{a+}^\alpha f)(x) = \frac{1}{\Gamma(\alpha)} \int_a^x (x-y)^{\alpha-1} f(y) dy \quad (2.29a)$$

for $x > a$. The *Riemann–Liouville fractional integral of order $\alpha > 0$ with upper limit b* is defined as

$$(\mathbb{I}_{b-}^\alpha f)(x) = \frac{1}{\Gamma(\alpha)} \int_x^b (y-x)^{\alpha-1} f(y) dy \quad (2.29b)$$

for $x < b$. For $\alpha = 0$

$$(\mathbb{I}_{a+}^0 f)(x) = (\mathbb{I}_{b-}^0 f)(x) = f(x) \quad (2.30)$$

completes the definition. The definition may be generalized to $\alpha \in \mathbb{C}$ with $\operatorname{Re} \alpha > 0$.

Formula (2.29a) appears in [96, p. 363] with $a > -\infty$ and in [76, p. 8] with $a = -\infty$. The notation is not standardized. Leibniz, Lagrange, and Liouville used the symbol \int^α [22, 73, 76], Grünwald wrote $\int^\alpha [\cdots dx^\alpha]_{x=a}^{x=x}$, while Riemann used $\partial_x^{-\alpha}$ [96] and Most wrote $d_a^{-\alpha}/dx^{-\alpha}$ [89]. The notation in (2.29) is that of [52, 54, 98, 99]. Modern authors also use f_α [37], I^α [97], ${}_a I_x^\alpha$ [94], I_x^α [23], ${}_a D_x^{-\alpha}$ [85, 91, 102], or $d^{-\alpha}/d(x-a)^{-\alpha}$ [92] instead of I_{a+}^α .

The fractional integral operators $I_{a+}^\alpha, I_{b-}^\alpha$ are commonly called Riemann–Liouville fractional integrals [94, 98, 99] although sometimes this name is reserved for the case $a = 0$ [85]. Their domain of definition is typically chosen as $D(I_{a+}^\alpha) = L^1([a, b])$ or $D(I_{a+}^\alpha) = L_{loc}^1([a, b])$ [94, 98, 99]. For the definition of Lebesgue spaces see Appendix B. If $f \in L^1([a, b])$ then $(I_{a+}^\alpha f) \in L^1([a, b])$ and $(I_{a+}^\alpha f)(x)$ is finite for almost all x . If $f \in L^p([a, b])$ with $1 \leq p \leq \infty$ and $\alpha > 1/p$ then $(I_{a+}^\alpha f)(x)$ is finite for all $x \in [a, b]$. Analogous statements hold for $(I_{b-}^\alpha f)(x)$ [98].

A short table of Riemann–Liouville fractional integrals is given in Appendix A. For a more extensive list of fractional integrals see [24].

2.2.1.3 Weyl Fractional Integrals

Examples (2.5) and (2.6) or (A.2) and (A.3) show that Definition 2.1 is well suited for fractional integration of power series, but not for functions defined by Fourier series. In fact, if $f(x)$ is a periodic function with period 2π , and³

$$f(x) \sim \sum_{k=-\infty}^{\infty} c_k e^{ikx} \quad (2.31)$$

then the Riemann–Liouville fractional $(I_{a+}^\alpha f)$ will in general not be periodic. For this reason an alternative definition of fractional integrals was investigated by Weyl [124].

Functions on the unit circle $\mathbb{G} = \mathbb{R}/2\pi\mathbb{Z}$ correspond to 2π -periodic functions on the real line. Let $f(x)$ be periodic with period 2π and such that the integral of f over the interval $[0, 2\pi]$ vanishes, so that $c_0 = 0$ in Eq. (2.31). Then the integral of f is itself a periodic function, and the constant of integration can be chosen such that the integral over $[0, 2\pi]$ vanishes again. Repeating the integration n times one finds using (2.6) and the integral representation

- 2) Some authors [23, 26, 85, 91, 92, 97] employ the derivative symbol D also for integrals, resp. I for derivatives, to emphasize the similarity between fractional integration and differentiation. If this is done, the choice of Riesz and Feller, namely I , seems superior in the sense that fractional derivatives, similar to integrals, are nonlocal operators, while integer derivatives are local operators.
- 3) The notation \sim indicates that the sum does not need to converge, and, if it converges, does not need to converge to $f(x)$.

$c_k = (1/2\pi) \int_0^{2\pi} e^{-iks} f(s) ds$ of Fourier coefficients

$$\sum_{k=-\infty}^{\infty} c_k \frac{e^{ikx}}{(ik)^n} = \frac{1}{2\pi} \int_0^{2\pi} f(y) \sum_{\substack{k=-\infty \\ k \neq 0}}^{\infty} \frac{e^{ik(x-y)}}{(ik)^n} dy \quad (2.32)$$

with $c_0 = 0$. Recall the convolution formula [132, p. 36]

$$(f * g)(t) = \frac{1}{2\pi} \int_0^{2\pi} f(t-s)g(s) ds = \sum_{k=-\infty}^{\infty} f_k g_k e^{ikt} \quad (2.33)$$

for two periodic functions $f(t) \sim \sum_{k=-\infty}^{\infty} f_k e^{ikt}$ and $g(t) \sim \sum_{k=-\infty}^{\infty} g_k e^{ikt}$. Using Eq. (2.33) and generalizing (2.32) to noninteger n suggests the following definition [94, 99].

Definition 2.2 Let $f \in L^p(\mathbb{R}/2\pi\mathbb{Z}), 1 \leq p < \infty$, be periodic with period 2π and such that its integral over a period vanishes. The *Weyl fractional integral of order α* is defined as

$$(I_{\pm}^{\alpha} f)(x) = (\Psi_{\pm}^{\alpha} * f)(x) = \frac{1}{2\pi} \int_0^{2\pi} \Psi_{\pm}^{\alpha}(x-y) f(y) dy, \quad (2.34)$$

where

$$\Psi_{\pm}^{\alpha}(x) = \sum_{\substack{k=-\infty \\ k \neq 0}}^{\infty} \frac{e^{ikx}}{(\pm ik)^{\alpha}} \quad (2.35)$$

for $0 < \alpha < 1$.

It can be shown that the series for $\Psi_{\pm}^{\alpha}(x)$ converges and that the Weyl definition coincides with the Riemann–Liouville definition [133]

$$(I_{+}^{\alpha} f)(x) = \frac{1}{\Gamma(\alpha)} \int_{-\infty}^x (x-y)^{\alpha-1} f(y) dy, \quad (2.36a)$$

respectively,

$$(I_{-}^{\alpha} f)(x) = \frac{1}{\Gamma(\alpha)} \int_x^{\infty} (y-x)^{\alpha-1} f(y) dy \quad (2.36b)$$

for 2π periodic functions whose integral over a period vanishes. This is Eq. (2.29) with $a = -\infty$ resp. $b = \infty$. For this reason the Riemann–Liouville

fractional integrals with limits $\pm\infty$, $I_+^\alpha f = I_{(-\infty)+}^\alpha f$, and $I_-^\alpha f = I_{\infty-}^\alpha f$ are often called *Weyl fractional integrals* [24, 85, 94, 99].

The Weyl fractional integral may be rewritten as a convolution

$$(I_\pm^\alpha f)(x) = (K_\pm^\alpha * f)(x), \quad (2.37)$$

where the convolution product for functions on \mathbb{R} is defined as⁴

$$(K * f)(x) := \int_{-\infty}^{\infty} K(x-y)f(y) dy \quad (2.38)$$

and the convolution kernels are defined as

$$K_\pm^\alpha(x) := \Theta(\pm x) \frac{(\pm x)^{\alpha-1}}{\Gamma(\alpha)} \quad (2.39)$$

for $\alpha > 0$. Here

$$\Theta(x) = \begin{cases} 1, & x > 0 \\ 0, & x \leq 0 \end{cases} \quad (2.40)$$

is the Heaviside unit step function, and $x^\alpha = \exp \alpha \log x$ with the convention that $\log x$ is real for $x > 0$. For $\alpha = 0$ the kernel

$$K_+^0(x) = K_-^0(x) = \delta(x) \quad (2.41)$$

is the Dirac δ -function defined in (C.2) in Appendix C. Note that $K_\pm^\alpha \in L^1_{loc}(\mathbb{R})$ for $\alpha > 0$.

2.2.1.4 Riesz Fractional Integrals

Riemann–Liouville and Weyl fractional integrals have upper or lower limits of integration, and are sometimes called left-sided resp. right-sided integrals. A more symmetric definition was advanced in [97].

Definition 2.3 Let $f \in L^1_{loc}(\mathbb{R})$ be locally integrable. The *Riesz fractional integral* or *Riesz potential* of order $\alpha > 0$ is defined as the linear combination [99]

$$\begin{aligned} (I^\alpha f)(x) &= \frac{(I_+^\alpha f)(x) + (I_-^\alpha f)(x)}{2 \cos(\alpha\pi/2)} \\ &= \frac{1}{2\Gamma(\alpha) \cos(\alpha\pi/2)} \int_{-\infty}^{\infty} \frac{f(y)}{|x-y|^{1-\alpha}} dy \end{aligned} \quad (2.42)$$

⁴If $K, f \in L^1(\mathbb{R})$ then $(K * f)(t)$ exists for almost all $t \in \mathbb{R}$ and $f \in L^1(\mathbb{R})$. If $K \in L^p(\mathbb{R}), f \in L^q(\mathbb{R})$ with $1 < p, q < \infty$ and $1/p + 1/q = 1$, then $K * f \in C_0(\mathbb{R})$, the space of continuous functions vanishing at infinity.

of right- and left-sided Weyl fractional integrals. The *conjugate Riesz potential* is defined by

$$\begin{aligned} (\tilde{I}^\alpha f)(x) &= \frac{(I_+^\alpha f)(x) - (I_-^\alpha f)(x)}{2 \sin(\alpha\pi/2)} \\ &= \frac{1}{2\Gamma(\alpha) \sin(\alpha\pi/2)} \int_{-\infty}^{\infty} \frac{\operatorname{sgn}(x-y)f(y)}{|x-y|^{1-\alpha}} dy. \end{aligned} \quad (2.43)$$

Of course, $\alpha \neq 2k+1, k \in \mathbb{Z}$, in (2.42) and $\alpha \neq 2k, k \in \mathbb{Z}$, in (2.43). The definition is again completed with

$$(I^0 f)(x) = (\tilde{I}^0 f)(x) = f(x) \quad (2.44)$$

for $\alpha = 0$.

Riesz fractional integration may be written as a convolution

$$(I^\alpha f)(x) = (K^\alpha * f)(x) \quad (2.45a)$$

$$(\tilde{I}^\alpha f)(x) = (\tilde{K}^\alpha * f)(x) \quad (2.45b)$$

with the (one-dimensional) Riesz kernels

$$K^\alpha(x) = \frac{K_+^\alpha(x) + K_-^\alpha(x)}{2 \cos(\alpha\pi/2)} = \frac{|x|^{\alpha-1}}{2 \cos(\alpha\pi/2)\Gamma(\alpha)} \quad (2.46)$$

for $\alpha \neq 2k+1, k \in \mathbb{Z}$, and

$$\tilde{K}^\alpha(x) = \frac{K_+^\alpha(x) - K_-^\alpha(x)}{2 \sin(\alpha\pi/2)} = \frac{|x|^{\alpha-1} \operatorname{sgn}(x)}{2 \sin(\alpha\pi/2)\Gamma(\alpha)} \quad (2.47)$$

for $\alpha \neq 2k, k \in \mathbb{Z}$. Subsequently, Feller introduced the generalized Riesz–Feller kernels [26]

$$K^{\alpha,\beta}(x) = \frac{|x|^{\alpha-1} \sin[\alpha(\pi/2 + \beta \operatorname{sgn} x)]}{2 \sin(\alpha\pi/2)\Gamma(\alpha)} \quad (2.48)$$

with parameter $\beta \in \mathbb{R}$. The corresponding generalized *Riesz–Feller fractional integral of order α and type β* is defined as

$$(I^{\alpha,\beta} f)(x) = (K^{\alpha,\beta} * f)(x). \quad (2.49)$$

This formula interpolates continuously from the Weyl integral $I_-^\alpha = I^{\alpha,-\pi/2}$ for $\beta = -\pi/2$ through the Riesz integral $I^\alpha = I^{\alpha,0}$ for $\beta = 0$ to the Weyl integral $I_+^\alpha = I^{\alpha,\pi/2}$ for $\beta = \pi/2$. Due to their symmetry Riesz–Feller fractional integrals are readily generalized to higher dimensions.

2.2.1.5 Fractional Integrals of Distributions

Fractional integration can be extended to distributions using the convolution formula (2.37) above. Distributions are generalized functions [31, 105]. They are defined as linear functionals on a space X of conveniently chosen “test functions.” For every locally integrable function $f \in L^1_{\text{loc}}(\mathbb{R})$ there exists a distribution $F_f : X \rightarrow \mathbb{C}$ defined by

$$F_f(\varphi) = \langle f, \varphi \rangle = \int_{-\infty}^{\infty} f(x)\varphi(x) \, dx, \quad (2.50)$$

where $\varphi \in X$ is a test function from a suitable space X of test functions. By abuse of notation one often writes f for the associated distribution F_f . Distributions that correspond to functions via (2.50) are called *regular distributions*. Examples for regular distributions are the convolution kernels $K_{\pm}^{\alpha} \in L^1_{\text{loc}}(\mathbb{R})$ defined in (2.39). They are locally integrable functions on \mathbb{R} when $\alpha > 0$. Distributions that are not regular are sometimes called *singular*. An important example for a singular distribution is the Dirac δ -function, $\delta : X \rightarrow \mathbb{C}$, defined as

$$\int \delta(x)\varphi(x) \, dx = \varphi(0) \quad (2.51)$$

for every test function $\varphi \in X$. The test function space X is usually chosen as a subspace of $C^{\infty}(\mathbb{R})$, the space of infinitely differentiable functions. A brief introduction to distributions is given in Appendix C.

In order to generalize (2.37) to distributions one must define the convolution of two distributions. To do so one multiplies Eq. (2.38) on both sides with a smooth test function $\varphi \in C_c^{\infty}(\mathbb{R})$ of compact support. Integrating gives

$$\begin{aligned} \langle K * f, \varphi \rangle &= \int_{-\infty}^{\infty} \int_{-\infty}^{\infty} K(x-y)f(y)\varphi(x) \, dy \, dx \\ &= \int_{-\infty}^{\infty} \int_{-\infty}^{\infty} K(x)f(y)\varphi(x+y) \, dy \, dx \\ &= \langle K(x), \langle f(y), \varphi(x+y) \rangle \rangle, \end{aligned} \quad (2.52)$$

where the notation $\langle f(y), \varphi(x+y) \rangle$ means that the functional F_f is applied to the function $\varphi(x+\cdot)$ for fixed x . Explicitly, for fixed x

$$F_f(\varphi_x) = \langle f(y), \varphi_x(y) \rangle = \langle f(y), \varphi(x+y) \rangle = \int_{-\infty}^{\infty} f(y)\varphi(x+y) \, dx, \quad (2.53)$$

where $\varphi_x(\cdot) = \varphi(x + \cdot)$. Equation (2.52) can be used as a definition for the convolution of distributions provided that the right-hand side has meaning. This is not always the case as the counterexample $K = f = 1$ shows. In general, the convolution product is not associative (see Eq. (2.113)). However, associative and commutative convolution algebras exist [21]. Equation (2.52) is always meaningful when $\text{supp } K$ or $\text{supp } f$ is compact [63]. Another case is when K and f have support in \mathbb{R}_+ . This will be assumed in the following.

Definition 2.4 Let f be a distribution $f \in C_0^\infty(\mathbb{R})'$ with $\text{supp } f \subset \mathbb{R}_+$. Then its fractional integral is the distribution $I_{0+}^\alpha f$ defined as

$$\langle I_{0+}^\alpha f, \varphi \rangle = \langle I_+^\alpha f, \varphi \rangle = \langle K_+^\alpha * f, \varphi \rangle \quad (2.54)$$

for $\text{Re } \alpha > 0$. It has support in \mathbb{R}_+ .

If $f \in C_0^\infty(\mathbb{R})'$ with $\text{supp } f \subset \mathbb{R}_+$ then also $I_{0+}^\alpha f \in C_0^\infty(\mathbb{R})'$ with $\text{supp } I_{0+}^\alpha f \subset \mathbb{R}_+$.

2.2.1.6 Integral Transforms

The Fourier transformation is defined as

$$\mathcal{F}\{f\}(k) = \int_{-\infty}^{\infty} e^{-ikx} f(x) dx \quad (2.55)$$

for functions $f \in L^1(\mathbb{R})$. Then

$$\mathcal{F}\{I_\pm^\alpha f\}(k) = (\pm ik)^{-\alpha} \mathcal{F}\{f\}(k) \quad (2.56)$$

holds for $0 < \alpha < 1$ by virtue of the convolution theorem. The equation cannot be extended directly to $\alpha \geq 1$ because the Fourier integral on the left-hand side may not exist. Consider, e.g., $\alpha = 1$ and $f \in C_c^\infty(\mathbb{R})$. Then $(I_+^1 f)(x) \rightarrow \text{const}$ as $x \rightarrow \infty$ and $\mathcal{F}\{I_+^1 f\}$ does not exist [94]. Equation (2.56) can be extended to all α with $\text{Re } \alpha > 0$ for functions in the so-called Lizorkin space [99, p. 148] defined as the space of functions $f \in \mathcal{S}(\mathbb{R})$ such that $(D^m \mathcal{F}\{f\})(0) = 0$ for all $m \in \mathbb{N}_0$.

For the Riesz potentials one has

$$\mathcal{F}\{I^\alpha f\}(k) = |k|^{-\alpha} \mathcal{F}\{f\}(k) \quad (2.57a)$$

$$\mathcal{F}\{\tilde{I}^\alpha f\}(k) = (-i \operatorname{sgn} k) |k|^{-\alpha} \mathcal{F}\{f\}(k) \quad (2.57b)$$

for functions in Lizorkin space.

The Laplace transform is defined as

$$\mathcal{L}\{f\}(u) = \int_0^\infty e^{-ux} f(x) dx \quad (2.58)$$

for locally integrable functions $f : \mathbb{R}_+ \rightarrow \mathbb{C}$. Now

$$\mathcal{L}\{I_{0+}^\alpha f\}(u) = u^{-\alpha} \mathcal{L}\{f\}(u) \quad (2.59)$$

by the convolution theorem for Laplace transforms. The Laplace transform of $I_{0-}^\alpha f$ leads to a more complicated operator.

2.2.1.7 Fractional Integration by Parts

If $f(x) \in L^p([a, b]), g \in L^q([a, b])$ with $1/p + 1/q \leq 1 + \alpha, p, q \geq 1$ and $p \neq 1, q \neq 1$ for $1/p + 1/q = 1 + \alpha$, then the formula

$$\int_a^b f(x)(I_{a+}^\alpha g)(x) dx = \int_a^b g(x)(I_{b-}^\alpha f)(x) dx \quad (2.60)$$

holds. The formula is known as fractional integration by parts [99]. For $f(x) \in L^p(\mathbb{R}), g \in L^q(\mathbb{R})$ with $p > 1, q > 1$ and $1/p + 1/q = 1 + \alpha$, the analogous formula

$$\int_{-\infty}^\infty f(x)(I_{+}^\alpha g)(x) dx = \int_{-\infty}^\infty g(x)(I_{-}^\alpha f)(x) dx \quad (2.61)$$

holds for Weyl fractional integrals.

These formulae provide a second method of generalizing fractional integration to distributions. Equation (2.60) may be read

$$\langle I_{a+}^\alpha f, \varphi \rangle = \langle f, I_{b-}^\alpha \varphi \rangle \quad (2.62)$$

for a distribution f and a test function φ . It shows that right- and left-sided fractional integrals are adjoint operators. The formula may be viewed as a definition of the fractional integral $I_{a+}^\alpha f$ of a distribution provided that the operator I_{b-}^α maps the test function space into itself.

2.2.1.8 Hardy–Littlewood Theorem

The mapping properties of convolutions can be studied with the help of Young's inequality. Let p, q, r obey $1 \leq p, q, r \leq \infty$ and $1/p + 1/q = 1 + 1/r$. If $K \in L^p(\mathbb{R})$ and $f \in L^q(\mathbb{R})$ then $K * f \in L^r(\mathbb{R})$ and Young's inequality $\|K * f\|_r \leq \|K\|_p \|f\|_q$ holds. It follows that $\|K * f\|_q \leq C \|f\|_p$ if

$1 \leq p \leq q \leq \infty$ and $K \in L^r(\mathbb{R})$ with $1/r = 1 + (1/q) - (1/p)$. The Hardy–Littlewood theorem states that these estimates remain valid for K_{\pm}^{α} although these kernels do not belong to any $L^p(\mathbb{R})$ -space [37, 38]. The theorem was generalized to higher dimensions by Sobolev in 1938, and is also known as the Hardy–Littlewood–Sobolev inequality (see [37, 38, 63, 113]).

Theorem 2.5 Let $0 < \alpha < 1$, $1 < p < 1/\alpha$, $-\infty \leq a < b \leq \infty$. Then $I_{a+}^{\alpha}, I_{b-}^{\alpha}$ are bounded linear operators from $L^p([a, b])$ to $L^q([a, b])$ with $1/q = (1/p) - \alpha$, i.e., there exists a constant $C(p, q)$ independent of f such that $\|I_{a+}^{\alpha} f\|_q \leq C \|f\|_p$.

2.2.1.9 Additivity

The basic composition law for fractional integrals follows from

$$\begin{aligned} (K_{+}^{\alpha} * K_{+}^{\beta})(x) &= \int_0^x K_{+}^{\alpha}(x-y) K_{+}^{\beta}(y) dy = \int_0^x \frac{(x-y)^{\alpha-1}}{\Gamma(\alpha)} \frac{y^{\beta-1}}{\Gamma(\beta)} dy \\ &= \frac{x^{\alpha-1}}{\Gamma(\alpha)} \frac{x^{\beta-1}}{\Gamma(\beta)} \int_0^1 (1-z)^{\alpha-1} z^{\beta-1} x dz \\ &= \frac{x^{\alpha+\beta-1}}{\Gamma(\alpha+\beta)} = K_{+}^{\alpha+\beta}(x), \end{aligned} \quad (2.63)$$

where Euler's Beta-function

$$\frac{\Gamma(\alpha)\Gamma(\beta)}{\Gamma(\alpha+\beta)} = \int_0^1 (1-z)^{\alpha-1} z^{\beta-1} x dz = B(\alpha, \beta) \quad (2.64)$$

was used. This implies the semigroup law for exponents

$$I_{a+}^{\alpha} I_{a+}^{\beta} = I_{a+}^{\alpha+\beta} \quad (2.65)$$

also called additivity law. It holds for Riemann–Liouville, Weyl, and Riesz–Feller fractional integrals of functions.

2.2.2

Fractional Derivatives

2.2.2.1 Riemann–Liouville Fractional Derivatives

Riemann [96, p. 341] suggested to define fractional derivatives as integer order derivatives of fractional integrals.

Definition 2.6 Let $-\infty \leq a < x < b \leq \infty$. The *Riemann–Liouville fractional derivative of order $0 < \alpha < 1$ with lower limit a* (resp. upper limit b) is defined for

functions such that $f \in L^1([a, b])$ and $f * K^{1-\alpha} \in W^{1,1}([a, b])$ as

$$(D_{a\pm}^\alpha f)(x) = \pm \frac{d}{dx} (I_{a\pm}^{1-\alpha} f)(x) \quad (2.66)$$

and $(D_{a\pm}^0 f)(x) = f(x)$ for $\alpha = 0$. For $\alpha > 1$ the definition is extended for functions $f \in L^1([a, b])$ with $f * K^{n-\alpha} \in W^{n,1}([a, b])$ as

$$(D_{a\pm}^\alpha f)(x) = (\pm 1)^n \frac{d^n}{dx^n} (I_{a\pm}^{n-\alpha} f)(x), \quad (2.67)$$

where⁵ $n = [\text{Re } \alpha] + 1$ is the smallest integer larger than α .

Here $W^{k,p}(G) = \{f \in L^p(G) : D^k f \in L^p(G)\}$ denotes a Sobolev space defined in (B.17). For $k = p = 1$ the space $W^{1,1}([a, b]) = AC^0([a, b])$ coincides with the space of absolutely continuous functions.

The notation for fractional derivatives is not standardized.⁶ Leibniz and Euler used d^α [25, 72, 73] Riemann wrote ∂_x^α [96], Liouville preferred d^α/dx^α [76], Grünwald used $\{d^\alpha f/dx^\alpha\}_{x=a}^{x=x}$ or $D^\alpha[f]_{x=a}^{x=x}$ [34], Marchaud wrote $D_a^{(\alpha)}$, and Hardy–Littlewood used an index f^α [37]. The notation in (2.67) follows [52, 54, 98, 99]. Modern authors also use $I^{-\alpha}$ [97], $I_x^{-\alpha}$ [23], ${}_a D_x^\alpha$ [85, 94, 102], d^α/dx^α [102, 129], $d^\alpha/d(x-a)^\alpha$ [92] instead of D_{a+}^α .

Let $f(x)$ be absolutely continuous on the finite interval $[a, b]$. Then, its derivative f' exists almost everywhere on $[a, b]$ with $f' \in L^1([a, b])$, and the function f can be written as

$$f(x) = \int_a^x f'(y) dy + f(a) = (I_{a+}^1 f')(x) + f(a). \quad (2.68)$$

Substituting this into $I_{a+}^\alpha f$ gives

$$(I_{a+}^\alpha f)(x) = (I_{a+}^1 I_{a+}^\alpha f')(x) + \frac{f(a)}{\Gamma(\alpha+1)} (x-a)^\alpha, \quad (2.69)$$

where commutativity of I_{a+}^1 and I_{a+}^α was used. It follows that

$$(D I_{a+}^\alpha f)(x) - (I_{a+}^\alpha D f)(x) = \frac{f(a)}{\Gamma(\alpha)} (x-a)^{\alpha-1} \quad (2.70)$$

for $0 < \alpha < 1$. Above, the notations

$$(D f)(x) = \frac{df(x)}{dx} = f'(x) \quad (2.71)$$

were used for the first-order derivative.

5) $[x]$ is the largest integer smaller than x .

6) see footnote 2.

This observation suggests to introduce a modified Riemann–Liouville fractional derivative through

$$(\tilde{D}_{a+}^{\alpha} f)(x) := I_{a+}^{n-\alpha} f^{(n)}(x) = \frac{1}{\Gamma(n-\alpha)} \int_a^x \frac{f^{(n)}(y)}{(x-y)^{\alpha-n+1}} dy, \quad (2.72)$$

where $n = [\operatorname{Re} \alpha] + 1$. Note that f must be differentiable at least n times. Formula (2.72) is due to Liouville [76, p. 10] (see Eq. (2.18)), but nowadays sometimes named after Caputo [17].

The relation between (2.72) and (2.67) is given by

Theorem 2.7 *For $f \in AC^{n-1}([a, b])$ with $n = [\operatorname{Re} \alpha] + 1$ the Riemann–Liouville fractional derivative $(D_{a+}^{\alpha} f)(x)$ exists almost everywhere for $\operatorname{Re} \alpha \geq 0$. It can be written as*

$$(D_{a+}^{\alpha} f)(x) = (\tilde{D}_{a+}^{\alpha} f)(x) + \sum_{k=0}^{n-1} \frac{(x-a)^{k-\alpha}}{\Gamma(k-\alpha+1)} f^{(k)}(a) \quad (2.73)$$

in terms of the Liouville(–Caputo) derivative defined in (2.72).

The Riemann–Liouville fractional derivative is the left inverse of Riemann–Liouville fractional integrals. More specifically, [99, p. 44]

Theorem 2.8 *Let $f \in L^1([a, b])$. Then*

$$D_{a+}^{\alpha} I_{a+}^{\alpha} f(x) = f(x) \quad (2.74)$$

holds for all α with $\operatorname{Re} \alpha \geq 0$.

For the right inverses of fractional integrals one finds

Theorem 2.9 *Let $f \in L^1([a, b])$ and $\operatorname{Re} \alpha > 0$. If in addition $I_{a+}^{n-\alpha} f \in AC^n([a, b])$ where $n = [\operatorname{Re} \alpha] + 1$, then*

$$I_{a+}^{\alpha} D_{a+}^{\alpha} f(x) = f(x) - \sum_{k=0}^{n-1} \frac{(x-a)^{\alpha-k-1}}{\Gamma(\alpha-k)} \left(D^{n-k-1} I_{a+}^{n-\alpha} f \right) (a) \quad (2.75)$$

holds. For $0 < \operatorname{Re} \alpha < 1$ this becomes

$$I_{a+}^{\alpha} D_{a+}^{\alpha} f(x) = f(x) - \frac{(I_{a+}^{1-\alpha} f)(a)}{\Gamma(\alpha)} (x-a)^{\alpha-1}. \quad (2.76)$$

The last theorem implies that for $f \in L^1([a, b])$ and $\operatorname{Re} \alpha > 0$ with $n = [\operatorname{Re} \alpha] + 1$ the equality

$$I_{a+}^{\alpha} D_{a+}^{\alpha} f(x) = f(x) \quad (2.77)$$

holds only if

$$I_{a+}^{n-\alpha} f \in AC^n([a, b]) \quad (2.78a)$$

and

$$\left(D^k I_{a+}^{n-\alpha} f \right) (a) = 0 \quad (2.78b)$$

for all $k = 0, 1, 2, \dots, n - 1$. Note that the existence of $g(x) = D_{a+}^\alpha f(x)$ in Eq. (2.77) does not imply that $f(x)$ can be written as $(I_{a+}^\alpha g)(x)$ for some integrable function g [99]. This holds only if both conditions (2.78) are satisfied. As an example where one of them fails, consider the function $f(x) = (x - a)^{\alpha-1}$ for $0 < \alpha < 1$. Then $D_{a+}^\alpha (x - a)^{\alpha-1} = 0$ exists. Now $D^0 I_{a+}^{1-\alpha} (x - a)^{\alpha-1} \neq 0$ so that (2.78b) fails. There does not exist an integrable g such that $I_{a+}^\alpha g = (x - a)^{\alpha-1}$. In fact, g corresponds to the δ -distribution $\delta(x - a)$.

2.2.2.2 General Types of Fractional Derivatives

Riemann–Liouville fractional derivatives have been generalized in [52, p. 433] to fractional derivatives of different types.

Definition 2.10 The *generalized Riemann–Liouville of order $0 < \alpha < 1$ and type $0 \leq \beta \leq 1$ with lower (resp. upper) limit a* is defined as

$$(D_{a\pm}^{\alpha,\beta} f)(x) = \left(\pm I_{a\pm}^{\beta(1-\alpha)} \frac{d}{dx} \left(I_{a\pm}^{(1-\beta)(1-\alpha)} f \right) \right) (x) \quad (2.79)$$

for functions such that the expression on the right-hand side exists.

The type β of a fractional derivative allows us to interpolate continuously from $D_{a\pm}^\alpha = D_{a\pm}^{\alpha,0}$ to $\tilde{D}_{a\pm}^\alpha = D_{a\pm}^{\alpha,1}$. A relation between fractional derivatives of the same order but different types was given in [52, p. 434].

2.2.2.3 Marchaud–Hadamard Fractional Derivatives

Marchaud's approach [78] is based on Hadamard's finite parts of divergent integrals [36]. The strategy is to define fractional derivatives as analytic continuation of fractional integrals to negative orders (see [99, p. 225]).

Definition 2.11 Let $-\infty < a < b < \infty$ and $0 < \alpha < 1$. The *Marchaud fractional derivative of order α with lower limit a* is defined as

$$(M_{a+}^\alpha f)(x) = \frac{f(x)}{\Gamma(1-\alpha)(x-a)^\alpha} + \frac{\alpha}{\Gamma(1-\alpha)} \int_a^x \frac{f(x)-f(y)}{(x-y)^{\alpha+1}} dy \quad (2.80)$$

and the *Marchaud fractional derivative of order α with upper limit b* is defined as

$$(M_{b-}^{\alpha} f)(x) = \frac{f(x)}{\Gamma(1-\alpha)(b-x)^{\alpha}} + \frac{\alpha}{\Gamma(1-\alpha)} \int_x^b \frac{f(x)-f(y)}{(x-y)^{\alpha+1}} dy. \quad (2.81)$$

For $a = -\infty$ (resp. $b = \infty$) the definition is

$$(M_{\pm}^{\alpha} f)(x) = \frac{\alpha}{\Gamma(1-\alpha)} \int_0^{\infty} \frac{f(x)-f(x \mp y)}{y^{\alpha+1}} dy. \quad (2.82)$$

The definition is completed with $M^0 f = f$ for all variants.

The idea of Marchaud's method is to extend the Riemann–Liouville integral from $\alpha > 0$ to $\alpha < 0$, and to define

$$(I_{+}^{-\alpha} f)(x) = \frac{1}{\Gamma(-\alpha)} \int_0^{\infty} y^{-\alpha-1} f(x-y) dy. \quad (2.83)$$

where $\alpha > 0$. However, this is not possible because the integral in (2.83) diverges. The idea is to subtract the divergent part of the integral,

$$\int_{\varepsilon}^{\infty} y^{-\alpha-1} f(x) dy = \frac{f(x)}{\alpha \varepsilon^{\alpha}} \quad (2.84)$$

obtained by setting $f(x-y) \approx f(x)$ for $y \approx 0$. Subtracting (2.83) from (2.84) for $0 < \alpha < 1$ suggests the definition

$$(M_{+}^{\alpha} f)(x) = \lim_{\varepsilon \rightarrow 0+} \frac{1}{\Gamma(-\alpha)} \int_{\varepsilon}^{\infty} \frac{f(x)-f(x-y)}{y^{\alpha+1}} dy. \quad (2.85)$$

Formal integration by parts leads to $(I_{+}^{1-\alpha} f')(x)$, showing that this definition contains the Riemann–Liouville definition.

The definition may be extended to $\alpha > 1$ in two ways. The first consists in applying (2.85) to the n th derivative $d^n f / dx^n$ for $n < \alpha < n+1$. The second possibility is to regard $f(x-y) - f(x)$ as a first-order difference, and to generalize to n th-order differences. The n th-order difference is

$$(\Delta_y^n f)(x) = (\mathbb{1} - T_y)^n f(x) = \sum_{k=0}^n (-1)^k \binom{n}{k} f(x-ky), \quad (2.86)$$

where $(\mathbb{1} f)(x) = f(x)$ is the identity operator and

$$(T_h f)(x) = f(x-h) \quad (2.87)$$

is the translation operator. The Marchaud fractional derivative can then be extended to $0 < \alpha < n$ through [94, 98]

$$(M_{+}^{\alpha} f)(x) = \lim_{\varepsilon \rightarrow 0+} \frac{1}{C_{\alpha,n}} \int_{-\varepsilon}^{\infty} \frac{\Delta_y^n f(x)}{y^{\alpha+1}} dy, \quad (2.88)$$

where

$$C_{\alpha,n} = \int_0^{\infty} \frac{(1 - e^{-y})^n}{y^{\alpha+1}} dy, \quad (2.89)$$

where the limit may be taken in the sense of pointwise or norm convergence.

The Marchaud derivatives M_{\pm}^{α} are defined for a wider class of functions than Weyl derivatives D_{\pm}^{α} . As an example consider the function $f(x) = \text{const.}$

Let f be such that there exists a function $g \in L^1([a, b])$ with $f = I_{a+}^{\alpha} g$. Then the Riemann–Liouville derivative and the Marchaud derivative coincide almost everywhere, i.e., $(M_{a+}^{\alpha} f)(x) = (D_{a+}^{\alpha} f)(x)$ for almost all x [99, p. 228].

2.2.2.4 Weyl Fractional Derivatives

There are two kinds of Weyl fractional derivatives for periodic functions. The *Weyl–Liouville fractional derivative* is defined as [99, p. 351], [94]

$$(D_{\pm}^{\alpha} f)(x) = \pm \frac{d}{dx} (I_{\pm}^{1-\alpha} f)(x) \quad (2.90)$$

for $0 < \alpha < 1$ where the Weyl integral $\pm I_{\pm}^{\alpha} f$ was defined in (2.34). The *Weyl–Marchaud fractional derivative* is defined as [99, p. 352], [94]

$$(W_{\pm}^{\alpha} f)(x) = \frac{1}{2\pi} \int_0^{2\pi} [f(x-y) - f(x)] (D^1 \Psi_{\pm}^{1-\alpha})(y) dy \quad (2.91)$$

for $0 < \alpha < 1$ where $\Psi_{\pm}(x)$ is defined in Eq. (2.35). The Weyl derivatives are defined for periodic functions of with zero mean in $C^{\beta}(\mathbb{R}/2\pi\mathbb{Z})$ where $\beta > \alpha$. In this space $(D_{\pm}^{\alpha} f)(x) = (W_{\pm}^{\alpha} f)(x)$, i.e., the Weyl–Liouville and Weyl–Marchaud form coincide [99]. As for fractional integrals, it can be shown that the Weyl–Liouville derivative ($0 < \alpha < 1$)

$$(D_{+}^{\alpha} f)(x) = \frac{1}{\Gamma(1-\alpha)} \int_{-\infty}^x \frac{f(y)}{(x-y)^{\alpha}} dy \quad (2.92)$$

coincides with the Riemann–Liouville derivative with lower limit $-\infty$. In addition one has the equivalence $D_{+}^{\alpha} f = W_{+}^{\alpha} f$ with the Marchaud–Hadamard fractional derivative in a suitable sense [99, p. 357].

2.2.2.5 Riesz Fractional Derivatives

To define the Riesz fractional derivative as integer derivatives of Riesz potentials consider the Fourier transforms

$$\mathcal{F}\left\{\mathrm{DI}^{1-\alpha} f\right\}(k)=(\mathrm{i} k)|k|^{\alpha-1} \mathcal{F}\{f\}(k)=(\mathrm{i} \operatorname{sgn} k)|k|^{\alpha} \mathcal{F}\{f\}(k) \quad(2.93)$$

$$\mathcal{F}\left\{\mathrm{DI}^{\widetilde{1-\alpha}} f\right\}(k)=(\mathrm{i} k)(-\mathrm{i} \operatorname{sgn} k)|k|^{\alpha-1} \mathcal{F}\{f\}(k)=|k|^{\alpha} \mathcal{F}\{f\}(k) \quad(2.94)$$

for $0<\alpha<1$. Comparing this to Eq. (2.57) suggests to consider

$$\frac{\mathrm{d}}{\mathrm{d} x}\left(\widetilde{\mathrm{I}^{1-\alpha}} f\right)(x)=\lim _{h \rightarrow 0} \frac{1}{h}\left[\left(\widetilde{\mathrm{I}^{1-\alpha}} f\right)(x+h)-\left(\widetilde{\mathrm{I}^{1-\alpha}} f\right)(x)\right] \quad(2.95)$$

as a candidate for the Riesz fractional derivative.

Following [94] the *strong Riesz fractional derivative of order α* $\mathrm{R}^{\alpha} f$ of a function $f \in L^p(\mathbb{R})$, $1 \leq p<\infty$, is defined through the limit

$$\lim _{h \rightarrow 0}\left\|\frac{1}{h}\left(f * K_h^{1-\alpha}\right)-\mathrm{R}^{\alpha} f\right\|_p=0 \quad(2.96)$$

whenever it exists. The convolution kernel defined as

$$K_h^{1-\alpha}=\frac{1}{2 \Gamma(1-\alpha) \sin (\alpha \pi / 2)}\left[\frac{\operatorname{sgn}(x+h)}{|x+h|^{\alpha}}-\frac{\operatorname{sgn} x}{|x|^{\alpha}}\right] \quad(2.97)$$

is obtained from Eq. (2.95). Indeed, this definition is equivalent to Eq. (2.94). A function $f \in L^p(\mathbb{R})$ where $1 \leq p \leq 2$ has a strong Riesz derivative of order α if and only if there exists a function $g \in L^p(\mathbb{R})$ such that $|k|^{\alpha} \mathcal{F}\{f\}(k)=\mathcal{F}\{g\}(k)$. Then $\mathrm{R}^{\alpha} f=g$.

2.2.2.6 Grünwald–Letnikov Fractional Derivatives

The basic idea of the Grünwald approach is to generalize finite difference quotients to noninteger order, and then take the limit to obtain a differential quotient. The first-order derivative is the limit

$$\frac{\mathrm{d}}{\mathrm{d} x} f(x)=(\mathrm{D} f)(x)=\lim _{h \rightarrow 0} \frac{f(x)-f(x-h)}{h}=\lim _{h \rightarrow 0} \frac{[\mathbb{1}-\mathsf{T}(h)]}{h} f(x) \quad(2.98)$$

of a difference quotient. In the last equality $(\mathbb{1} f)(x)=f(x)$ is the identity operator, and

$$[\mathsf{T}(h) f](x)=f(x-h) \quad(2.99)$$

is the translation operator. Repeated application of T gives

$$[\mathsf{T}(h)^n f](x)=f(x-n h), \quad(2.100)$$

where $n \in \mathbb{N}$. The second-order derivative can then be written as

$$\begin{aligned} \frac{d^2}{dx^2} f(x) = (D^2 f)(x) &= \lim_{h \rightarrow 0} \frac{f(x) - 2f(x-h) + f(x-2h)}{h^2} \\ &= \lim_{h \rightarrow 0} \left\{ \frac{[1 - T(h)]}{h} \right\}^2 f(x) \end{aligned} \quad (2.101)$$

and the n th derivative as

$$\begin{aligned} \frac{d^n}{dx^n} f(x) = (D^n f)(x) &= \lim_{h \rightarrow 0} \frac{1}{h^n} \sum_{k=0}^n (-1)^k \binom{n}{k} f(x-kh) \\ &= \lim_{h \rightarrow 0} \left\{ \frac{[1 - T(h)]}{h} \right\}^n f(x), \end{aligned} \quad (2.102)$$

which exhibits the similarity with the binomial formula. The generalization to noninteger n gives rise to fractional difference quotients defined through

$$(\Delta_h^\alpha f)(x) = \sum_{k=0}^{\infty} (-1)^k \binom{\alpha}{k} f(x-kh) \quad (2.103)$$

for $\alpha > 0$. These are generally divergent for $\alpha < 0$. For example, if $f(x) = 1$, then

$$\sum_{k=0}^N (-1)^k \binom{\alpha}{k} = \frac{1}{\Gamma(1-\alpha)} \frac{\Gamma(N+1-\alpha)}{\Gamma(N+1)} \quad (2.104)$$

diverges as $N \rightarrow \infty$ if $\alpha < 0$. Fractional difference quotients were studied in [68]. Note that fractional differences obey [99]

$$(\Delta_h^\alpha (\Delta_h^\beta f))(x) = (\Delta_h^{\alpha+\beta} f)(x) \quad (2.105)$$

Definition 2.12 The *Grünwald–Letnikov fractional derivative of order $\alpha > 0$* is defined as the limit

$$(G_\pm^\alpha f)(x) = \lim_{h \rightarrow 0^+} \frac{1}{h^\alpha} (\Delta_{\pm h}^\alpha f)(x) \quad (2.106)$$

of fractional difference quotients whenever the limit exists. The Grünwald–Letnikov fractional derivative is called *pointwise* or *strong* depending on whether the limit is taken pointwise or in the norm of a suitable Banach space.

For a definition of Banach spaces and their norms see, e.g., [128].

The Grünwald–Letnikov fractional derivative has been studied for periodic functions in $L^p(\mathbb{R}/2\pi\mathbb{Z})$ with $1 \leq p < \infty$ in [94, 99]. It has the following properties.

Theorem 2.13 Let $f \in L^p(\mathbb{R}/2\pi\mathbb{Z})$, $1 \leq p < \infty$ and $\alpha > 0$. Then the following statements are equivalent:

1. $G_+^\alpha f \in L^p(\mathbb{R}/2\pi\mathbb{Z})$.
2. There exists a function $g \in L^p(\mathbb{R}/2\pi\mathbb{Z})$ such that $(ik)^\alpha \mathcal{F}\{f(x)\}(k) = \mathcal{F}\{g(x)\}(k)$ where $k \in \mathbb{Z}$.
3. There exists a function $g \in L^p(\mathbb{R}/2\pi\mathbb{Z})$ such that $f(x) - \mathcal{F}\{f(x)\}(0) = (I_+^\alpha g)(x)$ holds for almost all x .

Theorem 2.14 Let $f \in L^p(\mathbb{R}/2\pi\mathbb{Z})$, $1 \leq p < \infty$ and $\alpha, \beta > 0$. Then

1. $G_+^\alpha f \in L^p(\mathbb{R}/2\pi\mathbb{Z})$ implies $G_+^\beta f \in L^p(\mathbb{R}/2\pi\mathbb{Z})$ for every $0 < \beta < \alpha$.
2. $G_+^\alpha G_+^\beta f = G_+^{\alpha+\beta} f$.
3. $G_+^\alpha (I_+^\alpha f) = f(x) - \mathcal{F}\{f\}(0)$.

2.2.2.7 Fractional Derivatives of Distributions

The basic idea for defining fractional differentiation of distributions is to extend the definition of fractional integration (2.54) to negative α . However, for $\operatorname{Re} \alpha < 0$ the distribution K_+^α becomes singular because $x^{\alpha-1}$ is not locally integrable in this case. The extension of K_+^α to $\operatorname{Re} \alpha < 0$ requires regularization [31, 63, 128]. It turns out that the regularization exists and is essentially unique as long as $(-\alpha) \notin \mathbb{N}_0$.

Definition 2.15 Let f be a distribution $f \in C_0^\infty(\mathbb{R})'$ with $\operatorname{supp} f \subset \mathbb{R}_+$. Then the *fractional derivative of order α with lower limit 0* is the distribution $D_{0+}^\alpha f$ defined as

$$\langle D_{0+}^\alpha f, \varphi \rangle = \langle D_+^\alpha f, \varphi \rangle = \langle K_+^{-\alpha} * f, \varphi \rangle, \quad (2.107)$$

where $\alpha \in \mathbb{C}$ and

$$K_+^\alpha(x) = \begin{cases} \Theta(x) \frac{x^{\alpha-1}}{\Gamma(\alpha)}, & \operatorname{Re} \alpha > 0 \\ \frac{d^N}{dx^N} \left[\Theta(x) \frac{x^{\alpha+N-1}}{\Gamma(\alpha+N)} \right], & \operatorname{Re} \alpha + N > 0, N \in \mathbb{N} \end{cases} \quad (2.108)$$

is the kernel distribution. For $\alpha = 0$ one finds $K_+^0(x) = (d/dx)\Theta(x) = \delta(x)$ and $D_{0+}^0 = \mathbb{1}$ as the identity operator. For the $\alpha = -k$, $k \in \mathbb{N}$, one finds

$$K_+^{-k}(x) = \delta^{(k)}(x), \quad (2.109)$$

where $\delta^{(k)}$ is the k th derivative of the δ distribution.

The kernel distribution in (2.108) is

$$K_+^{-\alpha}(x) = \frac{d}{dx} \left[\Theta(x) \frac{x^{-\alpha}}{\Gamma(1-\alpha)} \right] = \frac{d}{dx} K_+^{1-\alpha}(x) \quad (2.110)$$

for $0 < \alpha < 1$. Its regularized action is

$$\langle K_+^{-\alpha}(x), \varphi(x) \rangle = \left\langle \frac{d}{dx} K_+^{1-\alpha}(x), \varphi(x) \right\rangle = - \left\langle K_+^{1-\alpha}(x), \varphi(x)' \right\rangle \quad (2.111a)$$

$$= -\frac{1}{\Gamma(1-\alpha)} \lim_{\varepsilon \rightarrow 0} \int_{\varepsilon}^{\infty} x^{-\alpha} \varphi(x)' dx \quad (2.111b)$$

$$= -\lim_{\varepsilon \rightarrow 0} \left\{ \left. \frac{\varphi(x) + C}{\Gamma(\alpha)x^\alpha} \right|_{\varepsilon}^{\infty} - \int_{\varepsilon}^{\infty} \frac{\varphi(x) + C}{\Gamma(-\alpha)x^{1+\alpha}} dx \right\} \quad (2.111c)$$

$$= \int_0^{\infty} \frac{\varphi(x) - \varphi(0)}{\Gamma(-\alpha)x^{1+\alpha}} dx, \quad (2.111d)$$

where $\varphi(\infty) < \infty$ was assumed in the last step and the arbitrary constant was chosen as $C = -\varphi(0)$. This choice regularizes the divergent first term in (2.111c). If this rule is used for the distributional convolution

$$(K_+^{-\alpha} * f)(x) = \frac{1}{\Gamma(-\alpha)} \int_0^{\infty} \frac{f(x) - f(x-y)}{y^{\alpha+1}} dy = (M_+^\alpha f)(x) \quad (2.112)$$

then the Marchaud–Hadamard form is recovered with $0 < \alpha < 1$.

It is now possible to show that the convolution of distributions is in general not associative. A counterexample is

$$(1 * \delta') * \Theta = 1' * \Theta = 0 * \Theta = 0 \neq 1 = 1 * \delta = 1 * \Theta' = 1 * (\delta' * \Theta), \quad (2.113)$$

where Θ is the Heaviside step function.

$D_{0+}^\alpha f$ has support in \mathbb{R}_+ . The distributions in $f \in C_0^\infty(\mathbb{R})'$ with $\text{supp } f \subset \mathbb{R}_+$ form a convolution algebra [21] and one finds [31, 99]

Theorem 2.16 *If $f \in C_0^\infty(\mathbb{R})'$ with $\text{supp } f \subset \mathbb{R}_+$, then also $I_{0+}^\alpha f \in C_0^\infty(\mathbb{R})'$ with $I_{0+}^\alpha \text{supp } f \subset \mathbb{R}_+$. Moreover, for all $\alpha, \beta \in \mathbb{C}$*

$$D_{0+}^\alpha D_{0+}^\beta f = D_{0+}^{\alpha+\beta} f \quad (2.114)$$

with $D_{0+}^\alpha f = I_{0+}^{-\alpha} f$ for $\text{Re } \alpha < 0$. For each $f \in C_0^\infty(\mathbb{R})'$ with $\text{supp } f \subset \mathbb{R}_+$ there exists a unique distribution $g \in C_0^\infty(\mathbb{R})'$ with $\text{supp } g \subset \mathbb{R}_+$ such that $f = I_{0+}^\alpha g$.

Note that

$$D_{0+}^\alpha f = D_{0+}^\alpha (\mathbb{1} f) = (K_+^{-\alpha} * K_+^0) * f = (D_{0+}^\alpha \delta) * f = \delta^{(\alpha)} * f \quad (2.115)$$

for all $\alpha \in \mathbb{C}$. Also, the differentiation rule

$$D_{0+}^\alpha K_+^\beta = K_+^{\beta-\alpha} \quad (2.116)$$

holds for all $\alpha, \beta \in \mathbb{C}$. It contains

$$D K_+^\beta = K_+^{\beta-1} \quad (2.117)$$

for all $\beta \in \mathbb{C}$ as a special case.

2.2.2.8 Fractional Derivatives at Their Lower Limit

All fractional derivatives defined above are nonlocal operators. A local fractional derivative operator was introduced in [40, 41, 52].

Definition 2.17 For $-\infty < a < \infty$ the *Riemann–Liouville fractional derivative of order $0 < \alpha < 1$ at the lower limit a* is defined by

$$\left. \frac{d^\alpha f}{dx} \right|_{x=a} = f^{(\alpha)}(a) = \lim_{x \rightarrow a^\pm} (D_{a\pm}^\alpha f)(x), \quad (2.118)$$

whenever the two limits exist and are equal. If $f^{(\alpha)}(a)$ exists the function f is called fractionally differentiable at the limit a .

These operators are useful for the analysis of singularities. They were applied in [40–42, 44, 52] to the analysis of singularities in the theory of critical phenomena and to the generalization of Ehrenfests classification of phase transitions. There is a close relationship to the theory of regularly varying functions [107] as evidenced by the following result [52].

Theorem 2.18 Let the function $f : [0, \infty[\rightarrow \mathbb{R}$ be monotonically increasing with $f(x) \geq 0$ and $f(0) = 0$, and such that $(D_{0+}^{\alpha,\lambda} f)(x)$ with $0 < \alpha < 1$ and $0 \leq \lambda \leq 1$ is also monotonically increasing on a neighborhood $[0, \delta]$ for small $\delta > 0$. Let $0 \leq \beta < \lambda(1 - \alpha) + \alpha$, and let $C \geq 0$ be a constant and $\Lambda(x)$ a slowly varying function for $x \rightarrow 0$. Then

$$\lim_{x \rightarrow 0} \frac{f(x)}{x^\beta \Lambda(x)} = C \quad (2.119)$$

holds if and only if

$$\lim_{x \rightarrow 0} \frac{(D_{0+}^{\alpha,\lambda} f)(x)}{x^{\beta-\alpha} \Lambda(x)} = C \frac{\Gamma(\beta+1)}{\Gamma(\beta-\alpha+1)} \quad (2.120)$$

holds.

A function f is called slowly varying at infinity if $\lim_{x \rightarrow \infty} f(bx)/f(x) = 1$ for all $b > 0$. A function $f(x)$ is called slowly varying at $a \in \mathbb{R}$ if $f(1/(x-a))$ is slowly varying at infinity.

2.2.2.9 Fractional Powers of Operators

The spectral decomposition of self-adjoint operators is a familiar mathematical tool from quantum mechanics [116]. Let A denote a self-adjoint operator with domain $D(A)$ and spectral family E_λ on a Hilbert space X with scalar product (\cdot, \cdot) . Then

$$(Au, v) = \int_{\sigma(A)} \lambda d(E_\lambda u, v) \quad (2.121)$$

holds for all $u, v \in D(A)$. Here $\sigma(A)$ is the spectrum of A . It is then straightforward to define the fractional power $A^\alpha u$ by

$$(A^\alpha u, u) = \int_{\sigma(A)} \lambda^\alpha d(E_\lambda u, u) \quad (2.122)$$

on the domain

$$D(A^\alpha) = \{u \in X : \int_{\sigma(A)} \lambda^\alpha d(E_\lambda u, u) < \infty\}. \quad (2.123)$$

Similarly, for any measurable function $g : \sigma(A) \rightarrow \mathbb{C}$ the operator $g(A)$ is defined with an integrand $g(\lambda)$ in Eq. (2.122). This yields an operator calculus that allows one to perform calculations with functions instead of operators.

Fractional powers of the Laplacian as the generator of the diffusion semigroup were introduced by Bochner [13] and Feller [26] based on Riesz' fractional potentials. The fractional diffusion equation

$$\frac{\partial f}{\partial t} = -(-\Delta)^{\alpha/2} f \quad (2.124)$$

was related by Feller to the Lévy stable laws [74] using one-dimensional fractional integrals $I^{-\alpha, \beta}$ of order $-\alpha$ and type β [26]⁷. For $\alpha = 2$ Eq. (2.124) reduces to the diffusion equation. This type of fractional diffusion will be referred to as *fractional diffusion of Bochner–Lévy type* (see Section 2.3.4 for more discussion). Later, these ideas were extended to fractional powers of closed⁸ semigroup generators [4, 5, 69, 70]. If $(-A)$ is the infinitesimal generator of a

7) Fellers motivation to introduce the type β was this relation.

8) An operator $A : B \rightarrow B$ on a Banach space B is called *closed* if the set of pairs (x, Ax) with $x \in D(A)$ is closed in $B \times B$.

semigroup $T(t)$ (see Section 2.3.3.2 for definitions of $T(t)$ and A) on a Banach space B , then its fractional power is defined as

$$(-A)^\alpha f = \lim_{\varepsilon \rightarrow 0+} \frac{1}{-\Gamma(-\alpha)} \int_{\varepsilon}^{\infty} t^{-\alpha-1} [\mathbb{1} - T(t)] f dt \quad (2.125)$$

for every $f \in B$ for which the limit exists in the norm of B [93, 120, 121, 123]. This approach is clearly inspired by the Marchaud form (2.82). Alternatively, one may use the Grünwald approach to define fractional powers of semigroup generators [99, 122].

2.2.2.10 Pseudodifferential Operators

The calculus of pseudodifferential operators represents another generalization of the operator calculus in Hilbert spaces. It has its roots in Hadamard's ideas [36], Riesz' potentials [97], Feller's suggestion [26] and Calderon–Zygmund singular integrals [16]. Later it was generalized and became a tool for treating elliptic partial differential operators with nonconstant coefficients.

Definition 2.19 A (Kohn–Nirenberg) *pseudodifferential operator of order $\alpha \in \mathbb{R}$* $\sigma(x, D) : \mathcal{S}(\mathbb{R}^d) \rightarrow \mathcal{S}(\mathbb{R}^d)$ is defined as

$$\sigma(x, D)f(x) = \frac{1}{(2\pi)^d} \int_{\mathbb{R}^d} e^{ixk} \sigma(x, k) \mathcal{F}\{f\}(k) dk \quad (2.126)$$

and the function $\sigma(x, k)$ is called its *symbol*. The symbol is in the Kohn–Nirenberg symbol class S^α if it is in $C^\infty(\mathbb{R}^{2d})$, and there exists a compact set $K \subset \mathbb{R}^d$ such that $\text{supp } \sigma \subset K \times \mathbb{R}^d$, and for any pair of multiindices β, γ there is a constant $C_{\beta, \gamma}$ such that

$$D_k^\beta D_x^\gamma \sigma(x, k) \leq C_{\beta, \gamma} (1 + |k|)^{\alpha - |\beta|}. \quad (2.127)$$

The Hörmander symbol class $S_{\rho, \delta}^\alpha$ is obtained by replacing the exponent $\alpha - |\beta|$ on the right-hand side with $\alpha - \rho|\beta| + \delta|\gamma|$ where $0 \leq \rho, \delta \leq 1$.

Pseudodifferential operators provide a unified approach to differential and integral or convolution operators that are “nearly” translation invariant. They have a close relation with Weyl quantization in physics [28, 116]. However, they will not be discussed further because the traditional symbol classes do not contain the usual fractional derivative operators. Fractional Riesz derivatives are not pseudodifferential operators in the sense above. Their symbols do not fall into any of the standard Kohn–Nirenberg or Hörmander symbol classes due to the lack of differentiability at the origin.

2.2.3

Eigenfunctions

The eigenfunctions of Riemann–Liouville fractional derivatives are defined as the solutions of the fractional differential equation

$$(D_{0+}^{\alpha} f)(x) = \lambda f(x), \quad (2.128)$$

where λ is the eigenvalue. They are readily identified using Eq. (A.6) as

$$f(x) = x^{1-\alpha} E_{\alpha,\alpha}(\lambda x^{\alpha}), \quad (2.129)$$

where

$$E_{\alpha,\beta} = \sum_{k=0}^{\infty} \frac{x^k}{\Gamma(\alpha k + \beta)} \quad (2.130)$$

is the generalized Mittag-Leffler function [125, 126]. More generally the eigenvalue equation for fractional derivatives of order α and type β reads

$$(D_{0+}^{\alpha,\beta} f)(x) = \lambda f(x), \quad (2.131)$$

and it is solved by [54, eq. 124]

$$f(x) = x^{(1-\beta)(1-\alpha)} E_{\alpha,\alpha+\beta(1-\alpha)}(\lambda x^{\alpha}), \quad (2.132)$$

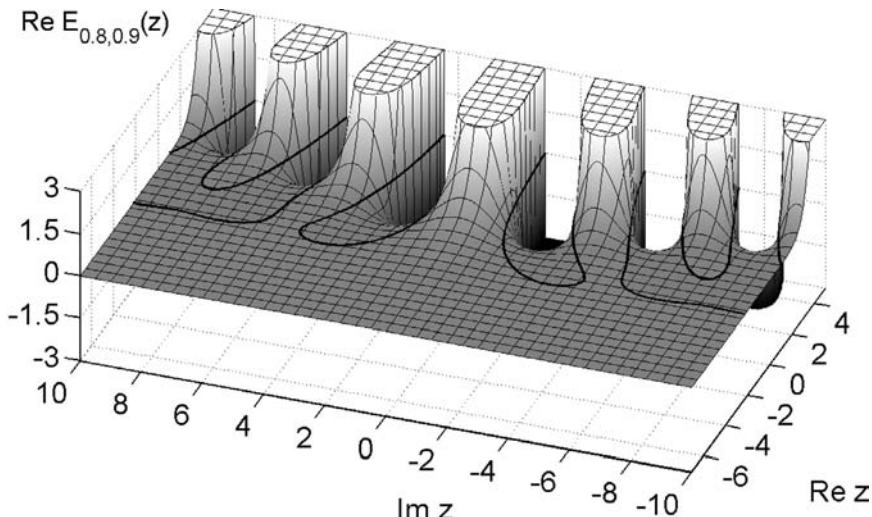


Figure 2.1 Truncated real part of the generalized Mittag-Leffler function $-3 \leq \operatorname{Re} E_{0.8,0.9}(z) \leq 3$ for $z \in \mathbb{C}$ with $-7 \leq \operatorname{Re} z \leq 5$ and $-10 \leq \operatorname{Im} z \leq 10$. The solid line is defined by $\operatorname{Re} E_{0.8,0.9}(z) = 0$.

where the case $\beta = 0$ corresponds to (2.128). A second important special case is the equation

$$(D_{0+}^{\alpha,1} f)(x) = \lambda f(x), \quad (2.133)$$

with $D_{0+}^{\alpha,1} = \tilde{D}_{0+}^{\alpha}$. In this case the eigenfunction is

$$f(x) = E_{\alpha}(\lambda x^{\alpha}) \quad (2.134)$$

where $E_{\alpha}(x) = E_{\alpha,1}(x)$ is the Mittag-Leffler function [86]. The Mittag-Leffler function plays a central role in fractional calculus. It has only recently been calculated numerically in the full complex plane [62, 108]. Figures 2.1 and 2.2 illustrate $E_{0.8,0.9}(z)$ for a rectangular region in the complex plane (see [108]).

The solid line in Figure 2.1 is defined by $\operatorname{Re} E_{0.8,0.9}(z) = 0$, and in Figure 2.2 by $\operatorname{Im} E_{0.8,0.9}(z) = 0$.

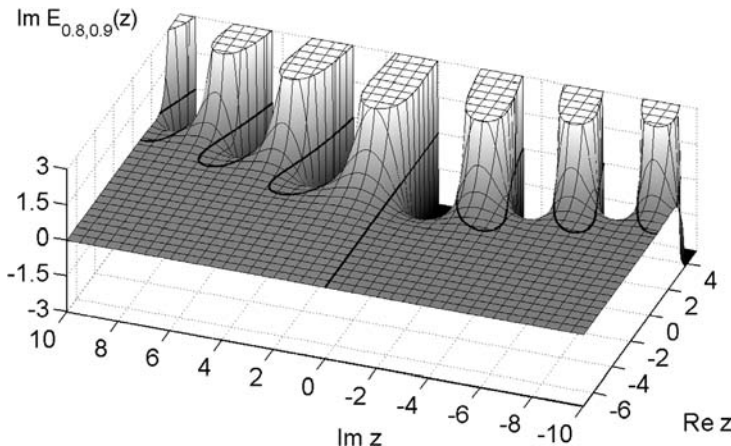


Figure 2.2 Same as Figure 2.1 for the imaginary part of $E_{0.8,0.9}(z)$. The solid line is $\operatorname{Im} E_{0.8,0.9}(z) = 0$.

Note that some authors are avoiding the operator $D_{0+}^{\alpha,1}$ in fractional differential equations (see, e.g., [7, 82, 84, 101, 111, 112] or chapters in this volume). In their notation the eigenvalue equation (2.133) becomes (cf. [112, eq. (22)])

$$\frac{d}{dx} f(x) = \lambda D_{0+}^{1-\alpha} f(x) \quad (2.135)$$

containing two derivative operators instead of one.

2.3

Physical Introduction to Fractional Derivatives

2.3.1

Basic Questions

An introduction to fractional derivatives would be incomplete without an introduction to applications. In the past fractional calculus has been used predominantly as a convenient calculational tool [26, 76, 89]. A well-known example is Riesz' interpolation method for solving the wave equation [20]. In recent times, however, fractional differential equations appear as “generalizations” of more or less fundamental equations of physics [3, 12, 18, 23, 43, 46, 52, 54–56, 58, 60, 90, 91, 102, 104, 119, 129]. The idea is that physical phenomena can be described by fractional differential equations. This practice raises at least two fundamental questions:

1. Are mathematical models with fractional derivatives consistent with the fundamental laws and fundamental symmetries of nature?
2. How can the fractional order α of differentiation be observed or how does a fractional derivative emerge from concrete models?

Both questions will be addressed here. The answer to the first question is provided by the theory of fractional time evolutions [43, 47], and the answer to the second question by anomalous subdiffusion [46, 60].

2.3.2

Fractional Space

Fractional derivatives are nonlocal operators. Nevertheless, numerous authors have proposed fractional differential equations involving fractional spatial derivatives. Particularly popular are fractional powers of the Laplace operator due to the well-known work of Riesz, Feller and Bochner [13, 27, 97]. The nonlocality of fractional spatial derivatives raises serious (largely) unresolved physical problems.

As an illustration of the problem with spatial fractional derivatives consider the one-dimensional potential equation for functions $f \in C^2(\mathbb{R})$,

$$\frac{d^2}{dx^2} f(x) = 0, \quad x \in \mathbb{G} \tag{2.136}$$

on the open interval $\mathbb{G} =]a, b[$ with boundary conditions $f(a) = 0, f(b) = 0$ with $a < b$. A solution of this boundary value problem is $f(x) = 0$ with $x \in \mathbb{G}$. This trivial solution remains unchanged as long as the boundary values $f(a) = f(b) = 0$ remain unperturbed. All functions $f \in C^2(\mathbb{R})$ that vanish on $[a, b]$ are solutions of the boundary value problem. In particular, the boundary

specification

$$f(x) = 0, \quad \text{for } x \in \mathbb{R} \setminus G \quad (2.137)$$

and the perturbed boundary specification

$$f(x) = g(x), \quad \text{for } x \in \mathbb{R} \setminus G \quad (2.138)$$

with $g \geq 0$ and $\text{supp } g \cap [a, b] = \emptyset$ have the same trivial solution $f = 0$ in G . The reason is that d^2/dx^2 is a local operator.

Consider now a fractional generalization of (2.136) that arises for example as the stationary limit of (Bochner–Lévy) fractional diffusion equations with a fractional Laplace operator [13]. Such a one-dimensional fractional Laplace equation reads

$$R^\alpha f(x) = 0, \quad (2.139)$$

where R^α is a Riesz fractional derivative of order $0 < \alpha < 1$. For the boundary specification (2.137) it has the same trivial solution $f(x) = 0$ for all $x \in G$. But this solution no longer applies for the perturbed boundary specification (2.138). In fact, assuming (2.138) for $x \in \mathbb{R} \setminus G$ and $f(x) = 0$ for $x \in G$ now yields $(R^\alpha f)(x) \neq 0$ for all $x \in G$. The exterior $\mathbb{R} \setminus G$ of the domain G cannot be isolated from the interior of G using classical boundary conditions. The reason is that R^α is a nonlocal operator.

Locality in space is a basic and firmly established principle of physics (see, e.g., [35, 115]). Of course, one could argue that relativistic effects are negligible, and that fractional spatial derivatives might arise as an approximate phenomenological model describing an underlying physical reality that obeys spatial locality. However, spatial fractional derivatives not only imply action at a distance, but, as seen above, they also imply that the exterior domain cannot be decoupled from the interior by conventional walls or boundary conditions. This has far-reaching consequences for theory and experiment. In theory it invalidates all arguments based on surface to volume ratios becoming negligible in the large volume limit. This includes many concepts and results in thermodynamics and statistical physics that depend on the lower dimensionality of the boundary. Experimentally it becomes difficult to isolate a system from its environment. Fractional diffusion would never come to rest inside a vessel with thin rigid walls unless the equilibrium concentration prevails also outside the vessel. A fractionally viscous fluid at rest inside a container with thin rigid walls would have to start to move when the same fluid starts flowing outside the vessel. It seems therefore difficult to reconcile nonlocality in space with theory and experiment.

2.3.3

Fractional Time

2.3.3.1 Basic Questions

Nonlocality in time, unlike space, does not violate basic principles of physics, as long as it respects causality [43, 47–49, 54]. In fact, causal nonlocality in time is a common nonequilibrium phenomenon known as history dependence, hysteresis, and memory.

Theoretical physics postulates time translation invariance as a fundamental symmetry of nature. As a consequence, energy conservation is fundamental, and the infinitesimal generator of time translations is a first-order time derivative. Replacing integer order time derivatives with fractional time derivatives raises at least three basic questions:

1. What replaces time translations as the physical time evolution?
2. Is the nonlocality of fractional time derivatives consistent with the laws of nature?
3. Is the asymmetry of fractional time derivatives consistent with the laws of nature?

These questions as well as ergodicity breaking, stationarity, long time limits, and temporal coarse grainig were discussed first within ergodic theory [47–49] and later from a general perspective in [54].

The third question requires special remarks because irreversibility is a long-standing and controversial subject [71]. The problem of irreversibility may be formulated briefly in two ways.

Definition 2.20 (The normal irreversibility problem) Assume that time is reversible. Explain how and why time irreversible equations arise in physics.

Definition 2.21 (The reversed irreversibility problem) Assume that time is irreversible. Explain how and why time reversible equations arise in physics.

While the normal problem has occupied physicists and mathematicians for more than a century, the reversed problem was apparently first formulated in [59]. Surprisingly, the reversed irreversibility problem has a clear and quantitative solution within the theory of fractional time. The solution is based on the simple postulate that every time evolution of a physical system is irreversible. It is not possible to repeat an experiment in the past [59]. This empirical fact seems to reflect a fundamental law of nature that rivals the law of energy conservation.

The mathematical concepts corresponding to irreversible time evolutions are operator semigroups and abstract Cauchy problems [15, 93]. The following brief introduction to fractional time evolutions (Sections 2.3.3.2–2.3.3.8) is in large parts identical to the brief exposition in [59]. For more details see [54].

2.3.3.2 Time Evolution

A physical time evolution $\{T(\Delta t) : 0 \leq \Delta t < \infty\}$ is defined as a one-parameter family (with time parameter Δt) of bounded linear time evolution operators $T(\Delta t)$ on a Banach space B . The parameter Δt represents time durations. The one-parameter family fulfills the conditions

$$[T(\Delta t_1)T(\Delta t_2)f](t_0) = [T(\Delta t_1 + \Delta t_2)f](t_0) \quad (2.140)$$

$$[T(0)f](t_0) = f(t_0) \quad (2.141)$$

for all $\Delta t_1, \Delta t_2 \geq 0$, $t_0 \in \mathbb{R}$ and $f \in B$. The elements $f \in B$ represent time-dependent physical observables, i.e., functions on the time axis \mathbb{R} . Note that the argument $\Delta t \geq 0$ of $T(\Delta t)$ has the meaning of a time duration, while $t \in \mathbb{R}$ in $f(t)$ means a time instant. Equations (2.140) and (2.141) define a semigroup. The inverse elements $T(-\Delta t)$ are absent. This reflects the fundamental difference between past and future.

The linear operator A defined as

$$Af = \text{s-lim}_{\Delta t \rightarrow 0+} \frac{T(\Delta t)f - f}{\Delta t} \quad (2.142)$$

with domain

$$D(A) = \left\{ f \in B : \text{s-lim}_{\Delta t \rightarrow 0+} \frac{T(\Delta t)f - f}{\Delta t} \text{ exists} \right\} \quad (2.143)$$

is called the infinitesimal generator of the semigroup. Here $\text{s-lim } f = g$ is the strong limit and means $\lim \|f - g\| = 0$ in the norm of B as usual.

2.3.3.3 Continuity

Physical time evolution is continuous. This requirement is represented mathematically by the assumption that

$$\text{s-lim}_{\Delta t \rightarrow 0} T(\Delta t)f = f \quad (2.144)$$

holds for all $f \in B$, where s-lim is again the strong limit. Semigroups of operators satisfying this condition are called strongly continuous or C^0 -semigroups [15, 93]. Strong continuity is weaker than uniform continuity and has become recognized as an important continuity concept that covers most applications [2].

2.3.3.4 Homogeneity

Homogeneity of time means two different requirements: Firstly, it requires that observations are independent of a particular instant or position in

time. Secondly, it requires arbitrary divisibility of time durations and self-consistency for the transition between time scales.

Independence of physical processes from their position on the time axis requires that physical experiments are reproducible if they are *ceteris paribus* shifted in time. The first requirement that the start of an experiment can be shifted is expressed mathematically as the requirement of invariance under time translations. As a consequence one demands commutativity of the time evolution with time translations in the form

$$[T(\tau)T(\Delta t)f](t_0) = [T(\Delta t)T(\tau)f](t_0) = [T(\Delta t)f](t_0 - \tau) \quad (2.145)$$

for all $\Delta t \geq 0$ and $t_0, \tau \in \mathbb{R}$. Here the translation operator $T(t)$ is defined by

$$T(\tau)f(t_0) = f(t_0 - \tau). \quad (2.146)$$

Note that $\tau \in \mathbb{R}$ is a time shift, not a duration. It can also be negative. Physical experiments in the past have the same outcome as in the present or in the future. Outcomes of past experiments can be studied in the present with the help of documents (e.g., a video recording), irrespective of the fact that the experiment cannot be repeated in the past.

The second requirement of homogeneity is homogeneous divisibility. The semigroup property (2.140) implies that for $\Delta t > 0$

$$T(\Delta t) \cdots T(\Delta t) = [T(\Delta t)]^n = T(n\Delta t) \quad (2.147)$$

holds. Homogeneous divisibility of a physical time evolution requires that there exist rescaling factors D_n for Δt such that with $\Delta t = \overline{\Delta t}/D_n$ the limit

$$\lim_{n \rightarrow \infty} T(n\overline{\Delta t}/D_n) = \overline{T}(\overline{\Delta t}) \quad (2.148)$$

exists and defines a time evolution $\overline{T}(\overline{\Delta t})$. The limit $n \rightarrow \infty$ at constant $\overline{\Delta t}$ requires two simultaneous limits $D_n \rightarrow \infty, \Delta t \rightarrow 0$, and it corresponds to the passage from a microscopic time scale Δt to a macroscopic time scale $\overline{\Delta t}$.

2.3.3.5 Causality

Causality of the physical time evolution requires that the values of the image function $g(t) = (T(\Delta t)f)(t)$ depend only upon values $f(s)$ of the original function with time instants $s < t$.

2.3.3.6 Fractional Time Evolution

The requirement (2.145) of homogeneity implies that the operators $T(\Delta t)$ are convolution operators [114,128]. Let T be a bounded linear operator on $L^1(\mathbb{R})$ that commutes with time translations, i.e., that fulfills Eq. (2.145). Then there

exists a finite Borel measure μ such that

$$(Tf)(s) = (\mu * f)(s) = \int f(s - x)\mu(dx) \quad (2.149)$$

holds [128], [114, p. 26]. Applying this theorem to physical time evolution operators $T(\Delta t)$ yields a convolution semigroup $\mu_{\Delta t}$ of measures $T(\Delta t)f(t) = (\mu_{\Delta t} * f)(t)$,

$$\mu_{\Delta t_1} * \mu_{\Delta t_2} = \mu_{\Delta t_1 + \Delta t_2} \quad (2.150)$$

with $\Delta t_1, \Delta t_2 \geq 0$. For $\Delta t = 0$ the measure μ_0 is the Dirac measure concentrated at 0.

The requirement of causality implies that the support $\text{supp } \mu_{\Delta t} \subset \mathbb{R}_+ = [0, \infty)$ of the semigroup is contained in the positive half-axis.

The convolution semigroups with support in the positive half-axis $[0, \infty)$ can be characterized completely by Bernstein functions [10]. An arbitrarily often differentiable function $b : (0, \infty) \rightarrow \mathbb{R}$ with continuous extension to $[0, \infty)$ is called Bernstein function if for all $x \in (0, \infty)$

$$b(x) \geq 0 \quad (2.151)$$

$$(-1)^n \frac{d^n b(x)}{dx^n} \leq 0 \quad (2.152)$$

holds for all $n \in \mathbb{N}$. Bernstein functions are positive, monotonically increasing and concave.

The characterization is given by the following theorem [10, p. 68]. There exists a one-to-one mapping between the convolution semigroups $\{\mu_t : t \geq 0\}$ with support on $[0, \infty)$ and the set of Bernstein functions $b : (0, \infty) \rightarrow \mathbb{R}$ [10]. This mapping is given by

$$\int_0^\infty e^{-ux} \mu_{\Delta t}(dx) = e^{-\Delta t b(u)} \quad (2.153)$$

with $\Delta t > 0$ and $u > 0$.

The requirement of homogeneous divisibility further restricts the set of admissible Bernstein functions. It leaves only those measures μ that can appear as limits

$$\lim_{n \rightarrow \infty, \Delta t \rightarrow 0} \underbrace{\mu_{\Delta t} * \cdots * \mu_{\Delta t}}_{n \text{ factors}} = \lim_{n \rightarrow \infty} \mu_{n\Delta t / D_n} = \overline{\mu}_{\overline{\Delta t}}. \quad (2.154)$$

Such limit measures $\overline{\mu}$ exist if and only if $b(x) = x^\alpha$ with $0 < \alpha \leq 1$ and $D_n \sim n^{1/\alpha}$ holds [11, 32, 54].

The remaining measures define the class of fractional time evolutions $T_\alpha(\Delta t)$ that depend only on one parameter, the fractional order α . These

remaining fractional measures have a density and they can be written as [43, 47–49, 54]

$$T_\alpha(\Delta t)f(t_0) = \int_0^\infty f(t_0 - s)h_\alpha\left(\frac{s}{\Delta t}\right)\frac{ds}{\Delta t}, \quad (2.155)$$

where $\Delta t \geq 0$ and $0 < \alpha \leq 1$. The density functions $h_\alpha(x)$ are the one-sided stable probability densities [43, 47–49, 54]. They have a Mellin transform [45, 103, 131]

$$\mathcal{M}\{h_\alpha(x)\}(s) = \int_0^\infty x^{s-1}h_\alpha(x)dx = \frac{1}{\alpha} \frac{\Gamma((1-s)/\alpha)}{\Gamma(1-s)} \quad (2.156)$$

allowing us to identify

$$h_\alpha(x) = \frac{1}{\alpha x} H_{11}^{10} \left(\begin{array}{c|cc} 1 & (0, 1) \\ x & (0, 1/\alpha) \end{array} \right) \quad (2.157)$$

in terms of H -functions [30, 45, 95, 103].

2.3.3.7 Infinitesimal Generator

The infinitesimal generators of the fractional semigroups $T_\alpha(\Delta t)$

$$A_\alpha f(t) = -(M_+^\alpha f)(t) = -\frac{1}{\Gamma(-\alpha)} \int_0^\infty \frac{f(t-s) - f(t)}{s^{\alpha+1}} ds \quad (2.158)$$

are fractional time derivatives of Marchaud–Hadamard type [51, 98]. This fundamental and general result provides the basis for generalizing physical equations of motion by replacing the integer order time derivative with a fractional time derivative as the generator of time evolution [43, 54].

For $\alpha = 1$ one finds $h_1(x) = \delta(x - 1)$ from Eq. (2.158), and the fractional semigroup $T_{\alpha=1}(\Delta t)$ reduces to the conventional translation semigroup $T_1(\Delta t)f(t_0) = f(t_0 - \Delta t)$. The special case $\alpha = 1$ occurs more frequently in the limit (2.154) than the cases $\alpha < 1$ in the sense that it has a larger domain of attraction. The fact that the semigroup $T_1(\Delta t)$ can often be extended to a group on all of \mathbb{R} provides an explanation for the seemingly fundamental reversibility of mechanical laws and equations. This solves the “reversed irreversibility problem.”

2.3.3.8 Remarks

Homogeneous divisibility formalizes the fact that a verbal statement in the present tense presupposes always a certain time scale for the duration of an

instant. In this sense the present should not be thought of as a point, but as a short time interval [48, 54, 59].

Fractional time evolutions seem to be related to the subjective human experience of time. In physics the time duration is measured by comparison with a periodic reference (clock) process. Contrary to this, the subjective human experience of time amounts to the comparison with an hour glass, i.e., with a nonperiodic reference. It seems that a time duration is experienced as “long” if it is comparable to the time interval that has passed since birth. This phenomenon seems to be reflected in fractional stationary states defined as solutions of the stationarity condition $T_\alpha(\Delta t)f(t) = f(t)$. Fractional stationarity requires a generalization of concepts such as “stationarity” or “equilibrium.” This outlook could be of interest for nonequilibrium and biological systems [43, 47–49, 54].

Finally, also the special case $\alpha \rightarrow 0$ challenges philosophical remarks [59]. In the limit $\alpha \rightarrow 0$ the time evolution operator degenerates into the identity. This could be expressed verbally by saying that for $\alpha = 0$ “becoming” and “being” coincide. In this sense the paradoxical limit $\alpha \rightarrow 0$ is reminiscent of the eternity concept known from philosophy.

2.3.4

Identification of α from Models

Consider now the second basic question of Section 2.3.1: How can the fractional order α be observed in experiment or identified from concrete models. To the best knowledge of this author there exist two examples where this is possible. Both are related to diffusion processes. There does not seem to exist an example of a rigorous identification of α from Hamiltonian models, although it has been suggested that such a relation might exist (see [129]).

2.3.4.1 Bochner–Lévy Fractional Diffusion

The term fractional diffusion can refer either to diffusion with a fractional Laplace operator or to diffusion equations with a fractional time derivative. Fractional diffusion (or Fokker–Planck) equations with a fractional Laplacian may be called *Bochner–Lévy diffusion*. The identification of the fractional order α in Bochner–Lévy diffusion equations has been known for more than five decades [13, 14, 26]. For a lucid account see also [27]. The fractional order α in this case is the index of the underlying stable process [13, 27]. With few exceptions [77] these developments in the nation of mathematics did, for many years, not find much attention or application in the nation of physics although eminent mathematical physicists such as Mark Kac were thoroughly familiar

with Bochner–Lévy diffusion [65].⁹ A possible reason might be the unresolved problem of locality discussed above. Bochner himself writes, “Whether this (equation) might have physical interpretation, is not known to us” [13, p. 370].

2.3.4.2 Montroll–Weiss Fractional Diffusion

Diffusion equations with a fractional time derivative will be called *Montroll–Weiss diffusion* although fractional time derivatives do not appear in the original paper [87] and the connection was not discovered until 30 years later [46, 60]. As shown in Section 2.3.3, the locality problem does not arise. Montroll–Weiss diffusion is expected to be consistent with all fundamental laws of physics. The fact that the relation between Montroll–Weiss theory and fractional time derivatives was first established in [46, 60] seems to be widely unknown at present, perhaps because this fact is never mentioned in widely read reviews [82] and popular introductions to the subject [112].¹⁰

There exist several versions of diffusion equations with fractional time derivatives, and they differ physically or mathematically from each other [54, 82, 104, 127, 130]. Of interest here will be the fractional diffusion equation for $f : \mathbb{R}^d \times \mathbb{R}_+ \rightarrow \mathbb{R}$,

$$D_{0+}^{\alpha,1} f(\mathbf{r}, t) = C \Delta f(\mathbf{r}, t) \quad (2.159)$$

with a fractional time derivative of order α and type 1. The Laplace operator is Δ and the fractional diffusion constant is C . The function $f(\mathbf{r}, t)$ is assumed to obey the initial condition $f(\mathbf{r}, 0+) = f_0 \delta(\mathbf{r})$. Equation (2.159) was introduced in integral form in [104], but the connection with [87] was not given.

An alternative to Eq. (2.159), introduced in [53, 54], is

$$D_{0+}^{\alpha,0} f(\mathbf{r}, t) = C \Delta f(\mathbf{r}, t) \quad (2.160)$$

with a Riemann–Liouville fractional time derivative D_{0+}^α of type 0. This equation does not describe diffusion of Montroll–Weiss type [53]. It has therefore been called “inconsistent” in [81, p. 3566]. As emphasized in [53] the choice of D_{0+}^α in (2.159) is physically and mathematically consistent, but corresponds to a modified initial condition, namely $I_{0+}^{1-\alpha} f(\mathbf{r}, 0+) = f_0 \delta(\mathbf{r})$. Similarly, fractional diffusion equations with time derivative $D_{0+}^{\alpha,\beta}$ of order α and type β have been investigated in [54]. For $\alpha = 1$ they all reduce to the diffusion equation.

Before discussing how α arises from an underlying continuous time random walk it is of interest to give an overall comparison of ordinary diffusion with

9) Also, Hermann Weyl, who pioneered fractional as well as functional calculus and worked on the foundations of physics, seems not to have applied fractional derivatives to problems in physics.

10) Note that, contrary to [112, p. 51], fractional derivatives are never mentioned in [6].

$\alpha = 1$ and fractional diffusion of the form (2.159) with $\alpha \neq 1$. This is conveniently done using the following table published in [46]. The first column gives the results for $\alpha = 1$, the second for $0 < \alpha < 1$ and the third for the limit $\alpha \rightarrow 0$. The first row compares the infinitesimal generators of time evolution A_α . The second row gives the fundamental solution $f(\mathbf{k}, u)$ in Fourier–Laplace space. The third row gives $f(\mathbf{k}, t)$ and the fourth $f(\mathbf{r}, t)$. In the fifth and sixth rows the asymptotic behavior is collected for $r^2/t^\alpha \rightarrow 0$ and $r^2/t^\alpha \rightarrow \infty$.

Table 2.1 Comparison of fractional diffusion with ordinary diffusion.

$\alpha = 1$	$0 < \alpha < 1$	$\alpha \rightarrow 0$
A_α	$\frac{d}{dt}$	$\tilde{D}_{0+}^\alpha \rightarrow \mathbb{1}$
$f(\mathbf{k}, u)$	$\frac{f_0}{u + C\mathbf{k}^2}$	$\frac{f_0 u^{\alpha-1}}{u^\alpha + C\mathbf{k}^2} \rightarrow \frac{f_0}{u(1 + C\mathbf{k}^2)}$
$f(\mathbf{k}, t)$	$f_0 e^{-Ct\mathbf{k}^2}$	$f_0 E_\alpha(-Ct\mathbf{k}^2) \rightarrow \frac{f_0}{1 + C\mathbf{k}^2}$
$f(\mathbf{r}, t)$	$\frac{f_0 e^{-\mathbf{r}^2/4Ct}}{(4\pi Ct)^{-d/2}}$	$\frac{f_0}{(\mathbf{r}^2\pi)^{d/2}} H_\alpha^d\left(\frac{\mathbf{r}^2}{4Ct^\alpha}\right) \frac{f_0 \mathbf{r} ^{1-\frac{d}{2}}}{\sqrt{C}(2\pi)^d} K_{\frac{d-2}{d}}\left(\frac{ \mathbf{r} }{\sqrt{C}}\right)$
$\frac{\mathbf{r}^2}{t^\alpha} \rightarrow 0$	$t^{-d/2}$	$\frac{ \mathbf{r} ^{2-d}}{t^\alpha} \quad \mathbf{r} ^{(2/d)-(d/2)}$
$\frac{\mathbf{r}^2}{t^\alpha} \rightarrow \infty$	$\exp\left[-\frac{\mathbf{r}^2}{4Ct}\right]$	$\exp\left[-c_\alpha\left(\frac{\mathbf{r}^2}{4Ct^\alpha}\right)^{\frac{1}{2-\alpha}}\right] \quad \exp\left(-\frac{ \mathbf{r} }{\sqrt{C}}\right)$

In the table $E_{\alpha,\beta}(x)$ denotes the generalized Mittag-Leffler function from Eq. (2.130), $K_\nu(x)$ is the modified Bessel function [1], $d > 2$, $c_\alpha = (2 - \alpha)\alpha^{\alpha/(2-\alpha)}$ and the shorthand

$$H_\alpha^d(x) = H_{12}^{20} \left(x \left| \begin{array}{l} (1, \alpha) \\ (d/2, 1), (1, 1) \end{array} \right. \right) \quad (2.161)$$

was used for the H -function H_{12}^{20} . For information on H -functions see [30, 54, 79, 95].

The results in the table show that the normal diffusion ($\alpha = 1$) is slowed down for $0 < \alpha < 1$ and comes to a complete halt for $\alpha \rightarrow 0$. For more discussion of the solution see [46].

2.3.4.3 Continuous Time Random Walks

The fractional diffusion equation (2.159) can be related rigorously to the microscopic model of Montroll–Weiss continuous time random walks (CTRWs) [64, 87] in the same way as ordinary diffusion is related to random walks [27]. The fractional order α can be identified and has a physical meaning related to waiting times in the Montroll–Weiss model. The relation between fractional time derivatives and CTRWs was first exposed in [46, 60]. The relation was established in two steps. First, it was shown in [60] that Montroll–Weiss continuous time random walks with a Mittag-Leffler waiting time density are rigorously equivalent to a fractional master equation. Then, in [46] this underlying random walk model was connected to the fractional diffusion equation (2.159) in the usual asymptotic sense [109] of long times and large distances.¹¹ For additional results see also [50, 53, 54, 57]

The basic integral equation for separable continuous time random walks describes a random walker in continuous time without correlation between its spatial and temporal behavior. It reads [39, 64, 87, 88, 118]

$$f(\mathbf{r}, t) = \delta_{\mathbf{r}, 0}\Phi(t) + \int_0^t \psi(t - t') \sum_{\mathbf{r}'} \lambda(\mathbf{r} - \mathbf{r}') f(\mathbf{r}', t') dt', \quad (2.162)$$

where $f(\mathbf{r}, t)$ denotes the probability density of finding the walker at position $\mathbf{r} \in \mathbb{R}^d$ after time t if it started from $\mathbf{r} = \mathbf{0}$ at time $t = 0$. The function $\lambda(\mathbf{r})$ is the probability for a displacement by \mathbf{r} in each step, and $\psi(t)$ gives the probability density of waiting time intervals between steps. The transition probabilities obey $\sum_{\mathbf{r}} \lambda(\mathbf{r}) = 1$, and $\Phi(t) = 1 - \int_0^t \psi(t') dt'$ is the survival probability at the initial site.

The fractional master equation introduced in [60] with initial condition $f(\mathbf{r}, 0) = \delta_{\mathbf{r}, 0}$ reads

$$\mathcal{D}_{0+}^{\alpha, 1} f(\mathbf{r}, t) = \sum_{\mathbf{r}'} w(\mathbf{r} - \mathbf{r}') f(\mathbf{r}', t) \quad (2.163)$$

with fractional transition rates $w(\mathbf{r})$ obeying $\sum_{\mathbf{r}} w(\mathbf{r}) = 0$. Note that Eq. (2.162) contains a free function $\psi(t)$ that has no counterpart in Eq. (2.163). The rigorous relation between Eq. (2.162) and Eq. (2.163), first established in [60], is given by the relation

$$\lambda(\mathbf{k}) = 1 + \tau^\alpha w(\mathbf{k}) \quad (2.164)$$

11) This is emphasized in eqs. (1.8) and (2.1) in [46] that are, of course, asymptotic.

for the Fourier-transformed transition rates $w(\mathbf{r})$ and probabilities $\lambda(\mathbf{r})$, and the choice

$$\psi(t) = \frac{t^{\alpha-1}}{\tau^\alpha} E_{\alpha,\alpha} \left(-\left(\frac{t}{\tau}\right)^\alpha \right) \quad (2.165)$$

for the waiting time density, where $\tau > 0$ is a characteristic time constant. With $E_{\alpha,\alpha}(0) = 1$ it follows that

$$\psi(t) \sim t^{\alpha-1} \quad (2.166)$$

for $t \rightarrow 0$. From $E_{\alpha,\alpha}(x) \sim x^{-2}$ for $x \rightarrow \infty$ one finds

$$\psi(t) \sim t^{-\alpha-1} \quad (2.167)$$

for $t \rightarrow \infty$. For $\alpha = 1$ the waiting time density becomes the exponential distribution, and for $\alpha \rightarrow 0$ it approaches $1/t$.

It had been observed already in the early 1970s that continuous time random walks are equivalent to generalized master equations [9, 66]. Similarly, the Fourier–Laplace formula

$$f(\mathbf{k}, u) = u^{\alpha-1} / (u^\alpha + C\mathbf{k}^2) \quad (2.168)$$

for the solution of CTRWs with algebraic tails of the form (2.167) was well known (see [117, eq. (21), p. 402] [110, eq. (23), p. 505] [67, eq. (29), p. 3083]). Comparison with row 2 of the table makes the connection between the fractional diffusion equation (2.159) and the CTRW equation (2.162) evident. However, this connection with fractional calculus was not made before the appearance of [46, 60]. In particular, there is no mention of fractional derivatives or fractional calculus in [6].

The rigorous relation between fractional diffusion and CTRWs, established in [46, 60] and elaborated in [50, 53, 54, 57], has become a fruitful starting point for subsequent investigations, particularly into fractional Fokker–Planck equations with drift [19, 33, 51, 61, 80–83, 100, 111, 112, 130].

Acknowledgments

The author thanks Th. Müller and S. Candelaresi for reading the manuscript.

Appendix A: Tables

Let $\alpha \in \mathbb{C}, x > a$

$$f(x) \quad (I_{a+}^{\alpha} f)(x)$$

$$f(\lambda x) \quad \lambda^{-\alpha} (I_{\lambda a+}^{\alpha} f)(\lambda x), \lambda > 0 \quad (\text{A.1})$$

$$(x-a)^{\beta} \quad \frac{\Gamma(\beta+1)}{\Gamma(\alpha+\beta+1)} (x-a)^{\alpha+\beta} \quad (\text{A.2})$$

$$\operatorname{Re} \beta > 0$$

$$e^{\lambda x} \quad e^{\lambda a} (x-a)^{\alpha} E_{1,\alpha+1}(\lambda(x-a)) \quad (\text{A.3})$$

$$\lambda \in \mathbb{R}$$

$$(x-a)^{\beta-1} e^{\lambda x} \quad \frac{\Gamma(\beta)e^{\lambda a}}{\Gamma(\alpha+\beta)} (x-a)^{\alpha+\beta-1} {}_1F_1(\beta; \alpha+\beta; \lambda(x-a))$$

$$\operatorname{Re} \beta > 0 \quad (\text{A.4})$$

$$(x-a)^{\beta-1} \log(x-a) \quad \frac{\Gamma(\beta)(x-a)^{\alpha+\beta-1}}{\Gamma(\alpha+\beta)} [\psi(\beta - \psi(\alpha+\beta)) + \log(x-a)]$$

$$(\text{A.5})$$

$$(x-a)^{\beta-1} E_{\gamma,\beta}((x-a)^{\gamma}) \quad (x-a)^{\alpha+\beta-1} E_{\gamma,\alpha+\beta}((x-a)^{\gamma}) \quad (\text{A.6})$$

$$\operatorname{Re} \beta > 0, \operatorname{Re} \gamma > 0.$$

Appendix B: Function Spaces

The set \mathbb{G} denotes an interval, a domain in \mathbb{R}^d , or a measure space $(\mathbb{G}, \mathcal{A}, \mu)$ [8] depending on the context. \mathbb{K} stands for \mathbb{R} or \mathbb{C} . $\gamma = (\gamma_1, \dots, \gamma_d) \in \mathbb{N}_0^d$ is a multiindex and $|\gamma| = \sum_{i=1}^d \gamma_i$. For the definition of Hilbert and Banach spaces the reader may consult, e.g., [128]. The following notation is used for various spaces of continuous functions:

$$C^0(\mathbb{G}) := \{f : \mathbb{G} \rightarrow \mathbb{K} \mid f \text{ is continuous}\} \quad (\text{B.1})$$

$$C^k(\mathbb{G}) := \{f \in C^0(\mathbb{G}) \mid f \text{ is } k \text{ times continuously differentiable}\} \quad (\text{B.2})$$

$$C_0^k(\mathbb{G}) := \{f \in C^k(\mathbb{G}) \mid f \text{ vanishes at the boundary } \partial\mathbb{G}\} \quad (\text{B.3})$$

$$C_b^k(\mathbb{G}) := \{f \in C^k(\mathbb{G}) \mid f \text{ is bounded}\} \quad (\text{B.4})$$

$$C_c^k(\mathbb{G}) := \{f \in C^k(\mathbb{G}) \mid f \text{ has compact support}\} \quad (\text{B.5})$$

$$C_{ub}^k(\mathbb{G}) := \{f \in C^k(\mathbb{G}) \mid f \text{ is bounded and uniformly continuous}\} \quad (\text{B.6})$$

$$\text{AC}^k([a, b]) := \{f \in C^k([a, b]) \mid f^{(k)} \text{ is absolutely continuous}\}. \quad (\text{B.7})$$

For compact \mathbb{G} the norm on these spaces is

$$\|f\|_\infty := \sup_{x \in \mathbb{G}} |f(x)|. \quad (\text{B.8})$$

The Lebesgue spaces over $(\mathbb{G}, \mathcal{A}, \mu)$ are defined as

$$L_{\text{loc}}^p(\mathbb{G}, \mu) := \{f : \mathbb{G} \rightarrow \mathbb{K} \mid f^p \text{ is integrable on every compact } K \subset \mathbb{G}\} \quad (\text{B.9})$$

$$L^p(\mathbb{G}, \mu) := \{f : \mathbb{G} \rightarrow \mathbb{K} \mid f^p \text{ is integrable}\} \quad (\text{B.10})$$

with norm

$$\|f\|_p := \left(\int_{\mathbb{G}} |f(s)|^p d\mu(s) \right)^{1/p}. \quad (\text{B.11})$$

For $p = \infty$

$$L^\infty(\mathbb{G}, \mu) := \{f : \mathbb{G} \rightarrow \mathbb{K} \mid f \text{ is measurable and } \|f\|_\infty < \infty\}, \quad (\text{B.12})$$

where

$$\|f\|_\infty := \sup \{|z| : z \in f_{\text{ess}}(\mathbb{G})\} \quad (\text{B.13})$$

and

$$f_{\text{ess}}(\mathbb{G}) := \{z \in \mathbb{C} : \mu(\{x \in \mathbb{G} : |f(x) - z| < \varepsilon\}) \neq 0 \text{ for all } \varepsilon > 0\} \quad (\text{B.14})$$

is the *essential range* of f .

The Hölder spaces $C^\alpha(\mathbb{G})$ with $0 < \alpha < 1$ are defined as

$$C^\alpha(\mathbb{G}) := \{f : \mathbb{G} \rightarrow \mathbb{K} \mid \exists c \geq 0 \text{ s.t. } |f(x) - f(y)| \leq c|x - y|^\alpha, \forall x, y \in \mathbb{G}\} \quad (\text{B.15})$$

with norm

$$\|f\|_\alpha := \|f\|_\infty + c_\alpha, \quad (\text{B.16})$$

where c_α is the smallest constant c in (B.15). For $\alpha > 1$ the Hölder space $C^\alpha(\mathbb{G})$ contains only the constant functions and therefore α is chosen as $0 < \alpha < 1$. The spaces $C^{k,\alpha}(\mathbb{G})$, $k \in \mathbb{N}$, consist of those functions $f \in C^k(\mathbb{G})$ whose partial derivatives of order k all belong to $C^\alpha(\mathbb{G})$.

The Sobolev spaces are defined by

$$W^{k,p}(\mathbb{G}) = \left\{ f \in L^p(\mathbb{G}) : \begin{array}{l} f \text{ is } k \text{ times differentiable in the} \\ \text{sense of distributions and } D^\gamma f \in L^p(\mathbb{G}) \text{ for all } \gamma \in \mathbb{N}_0^d \text{ with } |\gamma| \leq k \end{array} \right\}, \quad (\text{B.17})$$

where the derivative $D^\gamma = \partial_1^{\gamma_1} \cdots \partial_d^{\gamma_d}$ with multiindex $\gamma = (\gamma_1, \dots, \gamma_d) \in \mathbb{N}_0^d$ is understood in the sense of distributions. A distribution f is in $W^{k,p}(\mathbb{G})$ if and only if for each $\gamma \in \mathbb{N}_0^d$ with $|\gamma| \leq k$ there exists $f_\gamma \in L^p(\mathbb{G})$ such that

$$\int_{\mathbb{G}} \phi f_\gamma dx = (-1)^{|\gamma|} \int_{\mathbb{G}} (D^\gamma \phi) f dx \quad (\text{B.18})$$

for all test functions ϕ . In the special case $d = 1$ one has $f \in W^{k,p}(\mathbb{G})$ if and only if $f \in C^{k-1}(\mathbb{G})$, $f^{(k-1)} \in AC(\mathbb{G})$, and $f^{(j)} \in L^p(\mathbb{G})$ for $j = 0, 1, \dots, k$. The Sobolev spaces are equipped with the norm

$$\|f\|_{W^{k,p}(\mathbb{G})} = \sum_{|\gamma| \leq m} \|D^\gamma f\|_p \quad (\text{B.19})$$

(see [2]). A function is called *rapidly decreasing* if it is infinitely many times differentiable, i.e., $f \in C^\infty(\mathbb{R}^d)$ and

$$\lim_{|x| \rightarrow \infty} |x|^n D^\gamma f(x) = 0 \quad (\text{B.20})$$

for all $n \in \mathbb{N}$ and $\gamma \in \mathbb{N}^d$. The test function space

$$\mathcal{S}(\mathbb{R}^d) := \{f \in C^\infty(\mathbb{R}^d) \mid f \text{ is rapidly decreasing}\} \quad (\text{B.21})$$

is called *Schwartz space*.

Appendix C: Distributions

Distributions are generalized functions [31]. They were invented to overcome the differentiability requirements for functions in analysis and mathematical physics [63, 105]. Distribution theory has also a physical origin. A physical observable f can never be measured at a point $x \in \mathbb{R}^d$ because every measurement apparatus averages over a small volume around x [115]. This “smearing out” can be modeled as an integration with smooth “test functions” having compact support.

Let X denote the space of admissible test functions. Commonly used test function spaces are $C^\infty(\mathbb{R}^d)$, the space of infinitely often differentiable functions, $C_c^\infty(\mathbb{R}^d)$, the space of smooth functions with compact support (see (B.5)), $C_0^\infty(\mathbb{R}^d)$, the space of smooth functions vanishing at infinity (see (B.3)), or the so-called Schwartz space $\mathcal{S}(\mathbb{R}^d)$ of smooth functions decreasing rapidly at infinity (see (B.21)).

A distribution $F : X \rightarrow \mathbb{K}$ is a linear and continuous mapping that maps $\varphi \in X$ to a real ($\mathbb{K} = \mathbb{R}$) or complex ($\mathbb{K} = \mathbb{C}$) number.¹² There exists a canonical correspondence between functions and distributions. More precisely, for every locally integrable function $f \in L_{\text{loc}}^1(\mathbb{R}^d)$ there exists a distribution $F_f = \langle f, \cdot \rangle$ (often also denoted with the same symbol f) defined by

$$F_f(\varphi) = \langle f, \varphi \rangle = \int_{\mathbb{R}^d} f(x)\varphi(x) \, dx \quad (\text{C.1})$$

for every test function $\varphi \in X$. Distributions that can be written in this way are called *regular distributions*. Distributions that are not regular are sometimes called *singular*. The mapping $f \rightarrow \langle f, \cdot \rangle$ that assigns to a locally integrable f its associated distribution is injective and continuous. The set of distributions is again a vector space, namely the dual space of the vector space of test functions, and it is denoted as X' where X is the test function space.

¹²) For vector-valued distributions see [106]

Important examples for singular distributions are the Dirac δ -function and its derivatives. They are defined by the rules

$$\int \delta(x)\varphi(x) dx = \varphi(0) \quad (\text{C.2})$$

$$\int \delta^{(n)}(x)\varphi(x) dx = (-1)^n \left. \frac{d^n \varphi}{dx^n} \right|_{x=0} \quad (\text{C.3})$$

for every test function $\varphi \in X$ and $n \in \mathbb{N}$. Clearly, $\delta(x)$ is not a function, because if it were a function, then $\int \delta(x)\varphi(x) dx = 0$ would have to hold. Another example for a singular distribution is the finite part or principal value $\mathcal{P}\{1/x\}$ of $1/x$. It is defined by

$$\left\langle \mathcal{P}\left\{\frac{1}{x}\right\}, \varphi \right\rangle = \lim_{\varepsilon \rightarrow 0^+} \int_{|x| \geq \varepsilon} \frac{\varphi(x)}{x} dx \quad (\text{C.4})$$

for $\varphi \in C_c^\infty(\mathbb{R})$. It is a singular distribution on \mathbb{R} , but regular on $\mathbb{R} \setminus \{0\}$ where it coincides with the function $1/x$.

Equation (C.2) illustrates how distributions circumvent the limitations of differentiation for ordinary functions. The basic idea is the formula for partial integration

$$\int_G \partial_i f(x)\varphi(x) dx = - \int_G f(x)\partial_i \varphi(x) dx \quad (\text{C.5})$$

valid for $f \in C_c^1(G)$, $\varphi \in C^1(G)$, $i = 1, \dots, d$, and $G \subset \mathbb{R}^d$ an open set. The formula is proved by extending $f\varphi$ as 0 to all of \mathbb{R}^d and using Leibniz' product rule. Rewriting the formula as

$$\langle \partial_i f, \varphi \rangle = -\langle f, \partial_i \varphi \rangle \quad (\text{C.6})$$

suggests to view $\partial_i f$ again as a linear continuous mapping (integral) on a space X of test functions $\varphi \in X$. Then the formula is a rule for differentiating f given that φ is differentiable.

Distributions on the test function space $\mathcal{S}(\mathbb{R}^d)$ are called *tempered distributions*. The space of tempered distributions is the dual space $\mathcal{S}(\mathbb{R}^d)'$. Tempered distributions generalize locally integrable functions growing at most polynomially for $|x| \rightarrow \infty$. All distributions with compact support are tempered. Square integrable functions are tempered distributions. The derivative of a tempered distribution is again a tempered distribution. $\mathcal{S}(\mathbb{R}^d)$ is dense in $L^p(\mathbb{R}^d)$ for all $1 \leq p < \infty$ but not in $L^\infty(\mathbb{R}^d)$. The Fourier transform and its inverse are continuous maps of the Schwartz space onto itself. A distribution f belongs to $\mathcal{S}(\mathbb{R}^d)'$ if and only if it is the derivative of a continuous function with slow growth, i.e., it is of the form $f = D^\gamma[(1 + |x|^2)^{k/2}g(x)]$ where

$k \in \mathbb{N}$, $\gamma \in \mathbb{N}^d$ and g is a bounded continuous function on \mathbb{R}^d . Note that the exponential function is not a tempered distribution.

A distribution $f \in \mathcal{S}(\mathbb{R}^d)'$ is said to have *compact support* if there exists a compact subset $K \subset \mathbb{R}^d$ such that $\langle f, \varphi \rangle = 0$ for all test functions with $\text{supp } \varphi \cap K = \emptyset$. The Dirac δ -function is an example. Other examples are Radon measures on a compact set K . They can be described as linear functionals on $C^0(K)$. If the set K is sufficiently regular (e.g., if it is the closure of a region with piecewise smooth boundary), then every distribution with compact support in K can be written in the form

$$f = \sum_{|\gamma| \leq N} D^\gamma f_\gamma, \quad (\text{C.7})$$

where $\gamma = (\gamma_1, \dots, \gamma_d)$, $\gamma_j \geq 0$ is a multiindex, $|\gamma| = \sum \gamma_i$ and f_γ are continuous functions of compact support. Here $N \geq 0$ and the partial derivatives in D^γ are distributional derivatives defined above. A special case are distributions with support in a single point taken as $\{0\}$. Any such distributions can be written in the form

$$f = \sum_{|\gamma| \leq N} c_\gamma D^\gamma \delta, \quad (\text{C.8})$$

where δ is the Dirac δ -function and c_γ are constants.

The multiplication of a distribution f with a smooth function g is defined by the formula $\langle gf, \varphi \rangle = \langle f, g\varphi \rangle$ where $g \in C^\infty(\mathbb{G})$. A combination of multiplication by a smooth function and differentiation allows one to define differential operators

$$A = \sum_{|\gamma| \leq m} a_\gamma(x) D^\gamma \quad (\text{C.9})$$

with smooth $a_\gamma(x) \in C^\infty(\mathbb{G})$. They are well defined for all distributions in $C_c^\infty(\mathbb{G})'$.

A distribution is called homogeneous of degree $\alpha \in \mathbb{C}$ if

$$f(\lambda x) = \lambda^\alpha f(x) \quad (\text{C.10})$$

for all $\lambda > 0$. Here $\lambda^\alpha = \exp(\alpha \log \lambda)$ is the standard definition. The Dirac δ -distribution is homogeneous of degree $-d$. For regular distributions the definition coincides with homogeneity of functions $f \in L^1_{\text{loc}}(\mathbb{R}^d)$. The convolution kernels K_\pm^α from Eq. (2.39) are homogeneous of degree $\alpha - 1$. Homogeneous distributions remain homogeneous under differentiation. A homogeneous locally integrable function g on $\mathbb{R}^d \setminus \{0\}$ of degree α can be extended to homogeneous distributions f on all of \mathbb{R}^d . The degree of homogeneity of f must again be α . As long as $\alpha \neq -d, -d - 1, -d - 2, \dots$ the integral

$$\langle g_\beta, \varphi \rangle = \int g\left(\frac{x}{|x|}\right) |x|^\beta d^d x, \quad (\text{C.11})$$

which converges absolutely for $\operatorname{Re} \beta > -d$ can be used to define $f = g_\alpha$ by analytic continuation from the region $\operatorname{Re} \beta > -d$ to the point α . For $\alpha = -d, -d-1, \dots$, however, this is not always possible. An example is the function $1/|x|$ on $\mathbb{R} \setminus \{0\}$. It cannot be extended to a homogeneous distribution of degree -1 on all of \mathbb{R} .

For $f \in L^1_{\text{loc}}(\mathbb{G}_1)$ and $g \in L^1_{\text{loc}}(\mathbb{G}_2)$ their tensor product is the function $(f \otimes g)(x, y) = f(x)g(y)$ defined on $\mathbb{G}_1 \times \mathbb{G}_2$. The function $f \otimes g$ gives a functional

$$\langle f \otimes g, \varphi(x, y) \rangle = \langle f(x), \langle g(y), \varphi(x, y) \rangle \rangle \quad (\text{C.12})$$

for $\varphi \in C_c^\infty(\mathbb{G}_1 \times \mathbb{G}_2)$. For two distributions this formula defines their tensor product. An example is a measure $\mu(x) \otimes \delta(y)$ concentrated on the surface $y = 0$ in $\mathbb{G}_1 \otimes \mathbb{G}_2$ where $\mu(x)$ is a measure on \mathbb{G}_1 . The convolution of distributions defined in the main text (see Eq. (2.52)) can then be defined by the formula

$$\langle f * g, \varphi \rangle = \langle (f \otimes g)(x, y), \varphi(x + y) \rangle, \quad (\text{C.13})$$

whenever one of the distributions f or g has compact support.

References

- 1 M. Abramowitz and I.A. Stegun (eds.). *Pocketbook of Mathematical Functions (abridged edition of Handbook of Mathematical Functions)*. Verlag Harri Deutsch, Thun, Frankfurt, 1984.
- 2 W. Arendt, C.K. Batty, M. Hieber, and F. Neubrander. *Vector-Values Laplace Transforms and Cauchy Problems*. Birkhäuser, Basel, 2001.
- 3 R.L. Bagley and P.J. Torvik. A theoretical basis for the application of fractional calculus to viscoelasticity. *J. Rheol.*, 27:201, 1983.
- 4 A.V. Balakrishnan. An operational calculus for infinitesimal generators of semigroups. *Trans. Am. Math. Soc.*, 91:330, 1959.
- 5 A.V. Balakrishnan. Fractional powers of closed operators and the semigroups generated by them. *Pacific J. Math.*, 10:419, 1960.
- 6 V. Balakrishnan. Anomalous diffusion in one dimension. *Physica A*, 132A:569, 1985.
- 7 E. Barkai. Fractional Fokker–Planck equation, solution and application. *Phys. Rev. E*, 63:046118–1, 2001.
- 8 H. Bauer. *Maß- und Integrationstheorie*. Walter de Gruyter, Berlin, 1992.
- 9 D. Bedeaux, K. Lakatos-Lindenberg, and K.E. Shuler. On the relation between master equations and random walks and their solutions. *J. Math. Phys.*, 12:2116, 1971.
- 10 C. Berg and G. Forst. *Potential Theory on Locally Compact Abelian Groups*. Springer, Berlin, 1975.
- 11 H. Bergström. *Limit Theorems for Convolutions*. Wiley, New York, 1963.
- 12 H. Beyer and S. Kempfle. Definition of physically consistent damping laws with fractional derivatives. *Z. Angew. Math. Mech.*, 75:623, 1995.
- 13 S. Bochner. Diffusion equation and stochastic processes. *Proc. Natl Acad. Sci. USA*, 35:368, 1949.
- 14 S. Bochner. *Harmonic Analysis and the Theory of Probability*. University of California Press, Berkeley, CA, 1955.
- 15 R.L. Butzer and H. Berens. *Semigroups of Operators and Approximation*, volume 145 of *Die Grundlehren der mathematischen Wissenschaften in Einzeldarstellungen*. Springer, Berlin, 1967.
- 16 A. Calderon and A. Zygmund. Singular integral operators and differential equations. *Am. J. Math.*, 79:901, 1957.
- 17 M. Caputo. *Elasticità e Dissipazione*. Zanichelli, Bologna, 1969.
- 18 M. Caputo and F. Mainardi. Linear models of dissipation in anelastic solids. *Pure Appl. Geophys.*, 91:134, 1971.
- 19 A. Compte. Stochastic foundations of fractional dynamics. *Phys. Rev. E*, 53:4191, 1996.
- 20 E. Copson. *Partial Differential Equations*. Cambridge University Press, Cambridge, 1975.
- 21 R. Dautray and J.L. Lions. *Mathematical Analysis and Numerical Methods for Science and Technology*, volume 2. Springer, Berlin, 2000.
- 22 M. de la Grange. Sur une nouvelle espece de calcul relatif à la differentiation et à la integration des quantités variables. *Nouveaux Mémoires de l'Academie Royale des Sciences et Belles-Lettres*, 1772:185, 1772.
- 23 J. Douglas. Polymer science applications of path-integration, integral equations and fractional calculus. In R. Hilfer, editor, *Applications of Fractional Calculus in Physics*, World Scientific, Singapore, 2000, p. 240.
- 24 A. Erdelyi (et al.). *Tables of Integral Transforms*, volume 2. McGraw-Hill, New York, 1954.
- 25 L. Euler. De progressionibus transcendentibus seu quarum termini generales algebraice dari nequeunt. *Commentarii academiae scientiarum Petropolitanae*, 5:36–57, 1738.
- 26 W. Feller. On a generalization of Marcel Riesz' potentials and the semi-groups generated by them. *Lund Univ. Mat. Sem. Medd.*, Suppl. dedie a Marcel Riesz:73, 1952.
- 27 W. Feller. *An Introduction to Probability Theory and Its Applications*, volume 2. Wiley, New York, 1971.

- 28** G.B. Folland. *Harmonic Analysis in Phase Space*. Princeton University Press, Princeton, 1989.
- 29** J. Fourier. Theorie analytique de la chaleur. In M. Darboux, editor, *Oeuvre de Fourier*, volume 1. Gauthier-Villars, Paris, 1822, p. 1.
- 30** C. Fox. The G and H functions as symmetrical Fourier kernels. *Trans. Am. Math. Soc.*, 98:395, 1961.
- 31** I.M. Gel'fand and G.E. Shilov. *Generalized Functions*, volume 1. Academic Press, New York, 1964.
- 32** B.V. Gnedenko and A.N. Kolmogorov. *Limit Distributions for Sums of Independent Random Variables*. Addison-Wesley, Cambridge, 1954.
- 33** R. Gorenflo, F. Mainardi, D. Moretti, G. Pagnini, and P. Paradisi. Discrete random walk models for space-time fractional diffusion. *Chem. Phys.*, 284:521, 2002.
- 34** A. K. Grünwald. Über "begrenzte" Derivationen und deren Anwendung. *Z. f. Math. Phys.*, 12:441, 1867.
- 35** R. Haag. *Local Quantum Physics*. Springer, Berlin, 1992.
- 36** J. Hadamard. *Le probleme de Cauchy et les equations aux derivees partielles lineaires hyperboliques*. Hermann, Paris, 1932.
- 37** G.H. Hardy and J.E. Littlewood. Some properties of fractional integrals: I. *Math. Zeitschr.*, XXVII:565, 1928.
- 38** G.H. Hardy and J.E. Littlewood. Some properties of fractional integrals: II. *Math. Zeitschr.*, XXXIV:403, 1932.
- 39** J.W. Haus and K. Kehr. Diffusion in regular and disordered lattices. *Phys. Rep.*, 150:263, 1987.
- 40** R. Hilfer. Thermodynamic scaling derived via analytic continuation from the classification of Ehrenfest. *Physica Scripta*, 44:321, 1991.
- 41** R. Hilfer. Multiscaling and the classification of continuous phase transitions. *Phys. Rev. Lett.*, 68:190, 1992.
- 42** R. Hilfer. Scaling theory and the classification of phase transitions. *Mod. Phys. Lett. B*, 6:773, 1992.
- 43** R. Hilfer. Classification theory for anequilibrium phase transitions. *Phys. Rev. E*, 48:2466, 1993.
- 44** R. Hilfer. Classification theory for phase transitions. *Int. J. Mod. Phys. B*, 7:4371, 1993.
- 45** R. Hilfer. Absence of hyperscaling violations for phase transitions with positive specific heat exponent. *Z. Physik B*, 96:63, 1994.
- 46** R. Hilfer. Exact solutions for a class of fractal time random walks. *Fractals*, 3(1):211, 1995.
- 47** R. Hilfer. An extension of the dynamical foundation for the statistical equilibrium concept. *Physica A*, 221:89, 1995.
- 48** R. Hilfer. Foundations of fractional dynamics. *Fractals*, 3:549, 1995.
- 49** R. Hilfer. Fractional dynamics, irreversibility and ergodicity breaking. *Chaos, Solitons & Fractals*, 5:1475, 1995.
- 50** R. Hilfer. On fractional diffusion and its relation with continuous time random walks. In A. Pekalski, R. Kutner, and K. Szajd-Weron, editors, *Anomalous Diffusion: From Basis to Applications*, Springer, Berlin, 1999, p. 77.
- 51** R. Hilfer. *Applications of Fractional Calculus in Physics*. World Scientific, Singapore, 2000.
- 52** R. Hilfer. Fractional calculus and regular variation in thermodynamics. In R. Hilfer, editor, *Applications of Fractional Calculus in Physics*, World Scientific, Singapore, 2000, p. 429.
- 53** R. Hilfer. Fractional diffusion based on Riemann–Liouville fractional derivatives. *J. Phys. Chem. B*, 104:3914, 2000.
- 54** R. Hilfer. Fractional time evolution. In R. Hilfer, editor, *Applications of Fractional Calculus in Physics*, World Scientific, Singapore, 2000, p. 87.
- 55** R. Hilfer. Experimental evidence for fractional time evolution in glass forming materials. *Chem. Phys.*, 284:399, 2002.
- 56** R. Hilfer. Fitting the excess wing in the dielectric α -relaxation of propylene carbonate. *J. Phys.: Condens. Matter*, 14:2297, 2002.

- 57** R. Hilfer. On fractional diffusion and continuous time random walks. *Physica A*, 329:35, 2003.
- 58** R. Hilfer. On fractional relaxation. *Frac-tals*, 11:251, 2003.
- 59** R. Hilfer. Remarks on fractional time. In L. Castell and O. Ischebeck, editors, *Time, Quantum and Information*, Springer, Berlin, 2003, p. 235.
- 60** R. Hilfer and L. Anton. Fractional master equations and fractal time random walks. *Phys. Rev. E*, 51:R848, 1995.
- 61** R. Hilfer, R. Metzler, A. Blumen, and J. Klafter(eds). Strange kinetics. *Chem. Phys.*, 284, 2002.
- 62** R. Hilfer and H.J. Seybold. Computation of the generalized Mittag-Leffler function and its inverse in the complex plane. *Integr. Transf. Spec. Funct.*, 17:637, 2006.
- 63** L. Hörmander. *The Analysis of Linear Partial Differential Operators*, volume 1. Springer, Berlin, 1990.
- 64** B.D. Hughes. *Random Walks and Random Environments*, volume 1. Clarendon Press, Oxford, 1995.
- 65** M. Kac. *Probability and Related Topics in Physical Sciences*. Interscience, New York, 1959.
- 66** V.M. Kenkre, E.W. Montroll, and M.F. Shlesinger. Generalized master equations for continuous time random walks. *J. Stat. Phys.*, 9:45, 1973.
- 67** J. Klafter, A. Blumen, and M.F. Shlesinger. Stochastic pathway to anomalous diffusion. *Phys. Rev. A*, 35:3081, 1987.
- 68** K. Knopp. Mehrfach monotone zahlenfolgen. *Math. Zeitschr.*, 22:75, 1925.
- 69** H. Komatsu. Fractional powers of operators. *Pacific J. Math.*, 19:285, 1966.
- 70** H. Komatsu. Fractional powers of operators II: interpolation spaces. *Pacific J. Math.*, 21:89, 1967.
- 71** J.L. Lebowitz. Macroscopic laws, microscopic dynamics, time's arrow and Boltzmann's entropy. *Physica A*, 194:1, 1993.
- 72** G.W. Leibniz. Symbolismus memorabilis calculi Algebraici et infinitesimalis, in comparatione potentiarum et differentiarum; et de Lege Homogeneorum Transcendentali. *Miscellaneo Berolinensis ad incrementum scientiarum, ex scriptis Societate Regiae Scientiarum exhibitis*, I:160, 1710.
- 73** G.W. Leibniz. Brief von Leibniz an de l'Hospital vom 30.9.1695. In C.I. Gerhardt, editor, *G.W. Leibniz Mathematische Schriften, Band II, Briefwechsel zwischen Leibniz, Hugens van Zulichem und dem Marquis de l'Hospital*, Georg Olms Verlagsbuchhandlung, Hildesheim, 1962, p. 297.
- 74** P. Lévy. *Theorie de l'addition des variables aleatoires*. Gauthier-Villars, Paris, 1937.
- 75** J. Liouville. Mémoire sur le calcul des differentielles a indices quelconques. *J. l'Ecole Polytech.*, XIII:71, 1832.
- 76** J. Liouville. Mémoire sur quelques questions de geometrie et de mecanique, et sur un nouveau genre de calcul pour resoudre ces questions. *J. l'Ecole Polytech.*, XIII:1, 1832.
- 77** B.B. Mandelbrot. *The Fractal Geometry of Nature*. Freeman, San Francisco, 1982.
- 78** A. Marchaud. Sur les derivess et sur les differences des fonctions de variables reelles. *J. Math. Pures Appl.*, 6:337, 1927.
- 79** A.M. Mathai and R.K. Saxena. *The H-function with Applications in Statistics and Other Disciplines*. Wiley, New Delhi, 1978.
- 80** M. Meerschaert, D. Benson, H.P. Scheffler, and P. Becker-Kern. Governing equations and solutions of anomalous random walk limits. *Phys. Rev. E*, 66:060102, 2002.
- 81** R. Metzler, E. Barkai, and J. Klafter. Anomalous diffusion and relaxation close to equilibrium: a fractional Fokker-Planck equation approach. *Phys. Rev. Lett.*, 82:3563, 1999.
- 82** R. Metzler and J. Klafter. The random walk's guide to anomalous diffusion: a fractional dynamics approach. *Phys. Rep.*, 339:1, 2000.
- 83** R. Metzler, J. Klafter, and I. Sokolov. Anomalous transport in external fields: continuous time random walks and fractional diffusion equations extended. *Phys. Rev. E*, 58:1621, 1998.
- 84** R. Metzler and T. Nonnenmacher. Space- and time-fractional diffusion and wave equations, fractional Fokker-Planck equations, and physical motivation. *Chem. Phys.*, 284:67, 2002.

- 85** K.S. Miller and B. Ross. *An Introduction to the Fractional Calculus and Fractional Differential Equations*. Wiley, New York, 1993.
- 86** G. Mittag-Leffler. Sur la representation analytique d'une branche uniforme d'une fonction monogene. *Acta Math.*, 29:101, 1905.
- 87** E.W. Montroll and G.H. Weiss. Random walks on lattices: II. *J. Math. Phys.*, 6:167, 1965.
- 88** E.W. Montroll and B.J. West. On an enriched collection of stochastic processes. In E.W. Montroll and J.L. Lebowitz, editors, *Fluctuation Phenomena*, North-Holland, Amsterdam, 1979, p. 61.
- 89** R. Most. Ueber die Anwendung der Differentialquotienten mit allgemeinem Index zum Integrieren von Differentialgleichungen. *Z. f. Math. Phys.*, 16:190, 1871.
- 90** R.R. Nigmatullin. The realization of the generalized transfer equation in a medium with fractal geometry. *Phys. Stat. Sol. b*, 133:425, 1986.
- 91** T. F. Nonnenmacher and R. Metzler. Applications of fractional calculus techniques to problems in biophysics. In R. Hilfer, editor, *Applications of Fractional Calculus in Physics*, World Scientific, Singapore, 2000, p. 377.
- 92** K.B. Oldham and J.S. Spanier. *The Fractional Calculus*. Academic Press, New York, 1974.
- 93** A. Pazy. *Semigroups of Linear Operators and Applications to Partial Differential Equations*. Springer, Berlin, 1983.
- 94** P.L. Butzer and U. Westphal. Introduction to fractional calculus. In R. Hilfer, editor, *Applications of Fractional Calculus in Physics*, World Scientific, Singapore, 2000, p. 1.
- 95** A.P. Prudnikov, Yu.A. Brychkov, and O.I. Marichev. *Integrals and Series*, volume 3. Gordon and Breach, New York, 1990.
- 96** B. Riemann. Versuch einer allgemeinen auffassung der integration und differentiation, (Januar 1847). In H. Weber, editor, *Bernhard Riemann's gesammelte mathematische Werke und wissenschaftlicher Nachlass*, Dover, New York, 1953, p. 353.
- 97** M. Riesz. L'integrale de Riemann-Liouville et le probleme de Cauchy. *Acta Math.*, 81:1, 1949.
- 98** B. Rubin. *Fractional Integrals and Potentials*. Longman, Harlow, 1996.
- 99** S. Samko, A. Kilbas, and O. Marichev. *Fractional Integrals and Derivatives*. Gordon and Breach, Berlin, 1993.
- 100** E. Scalas, R. Gorenflo, and F. Mainardi. Uncoupled continuous time random walks: solution and limiting behaviour of the master equation. *Phys. Rev. E*, 69:011107, 2004.
- 101** H. Scher, G. Margolin, and B. Berkowitz. Towards a unified framework for anomalous transport in porous media. *Chem. Phys.*, 284:349, 2002.
- 102** H. Schiessel, C. Friedrich, and A. Blumen. Applications to problems in polymer physics and rheology. In R. Hilfer, editor, *Applications of Fractional Calculus in Physics*, World Scientific, Singapore, 2000, p. 330.
- 103** W.R. Schneider. Stable distributions: Fox function representation and generalization. In S. Albeverio, G. Casati, and D. Merlini, editors, *Stochastic Processes in Classical and Quantum Systems*, Springer, Berlin, 1986, p. 497.
- 104** W.R. Schneider and W. Wyss. Fractional diffusion and wave equations. *J. Math. Phys.*, 30:134, 1989.
- 105** L. Schwartz. *Theorie des Distributions*. Hermann, Paris, 1950.
- 106** L. Schwartz. Theorie des distributions a valeur vectorielles I. *Ann. Inst. Fourier*, 7:1, 1957.
- 107** E. Seneta. *Regularly Varying Functions*. Springer, Berlin, 1976.
- 108** H.J. Seybold and R. Hilfer. Numerical results for the generalized Mittag-Leffler function. *Fract. Calculus Appl. Anal.*, 8:127, 2005.
- 109** M.F. Shlesinger. Asymptotic solutions of continuous time random walks. *J. Stat. Phys.*, 10:421, 1974.
- 110** M.F. Shlesinger, J. Klafter, and Y.M. Wong. Random walks with infinite spatial and temporal moments. *J. Stat. Phys.*, 27:499, 1982.
- 111** I. Sokolov. Thermodynamics and fractional Fokker-Planck equations. *Phys. Rev. E*, 63:056111, 2001.

- 112** I. Sokolov, J. Klafter, and A. Blumen. Fractional kinetics. *Phys. Today*, Nov.:48, 2002.
- 113** E. Stein and G. Weiss. Fractional integrals on n -dimensional Euclidean space. *J. Math. Mech.*, 7:503, 1958.
- 114** E. Stein and G. Weiss. *Introduction to Fourier Analysis on Euclidean Spaces*. Princeton University Press, Princeton, 1971.
- 115** R.F. Streater and A.S. Wightman. *PCT, Spin and Statistics, and All That*. Benjamin, Reading, MA, 1964.
- 116** W. Thirring. *Lehrbuch der Mathematischen Physik 3: Quantenmechanik von Atomen und Molekülen*. Springer, Wien, 1979.
- 117** J.K.E. Tunaley. Asymptotic solutions of the continuous time random walk model of diffusion. *J. Stat. Phys.*, 11:397, 1974.
- 118** G.H. Weiss and R.J. Rubin. Random walks: theory and selected applications. *Adv. Chem. Phys.*, 52:363, 1983.
- 119** B.J. West and P. Grigolini. Fractional differences, derivatives and fractal time series. In R. Hilfer, editor, *Applications of Fractional Calculus in Physics*, World Scientific, Singapore, 2000, p. 171.
- 120** U. Westphal. Ein Kalkül für gebrochene Potenzen infinitesimaler Erzeuger von Halbgruppen und Gruppen von Operatoren. Teil I: Halbgruppenerzeuger. *Compositio Math.*, 22:67, 1970.
- 121** U. Westphal. Ein Kalkül für gebrochene Potenzen infinitesimaler Erzeuger von Halbgruppen und Gruppen von Operatoren. Teil II: Gruppenerzeuger. *Compositio Math.*, 22:104, 1970.
- 122** U. Westphal. An approach to fractional powers of operators via fractional differences. *Proc. London Math. Soc.*, 29:557, 1974.
- 123** U. Westphal. Fractional powers of infinitesimal generators of semigroups. In R. Hilfer, editor, *Applications of Fractional Calculus in Physics*, World Scientific, Singapore, 2000, p. 131.
- 124** H. Weyl. Bemerkungen zum Begriff des Differentialquotienten gebrochener Ordnung. *Vierteljahrsschrift der Naturforsch. Ges. Zürich*, 62:296, 1917.
- 125** A. Wiman. Über den Fundamentalsatz in der Theorie der Funktionen $E_\alpha(x)$. *Acta Math.*, 29:191, 1905.
- 126** A. Wiman. Über die Nullstellen der Funktionen $E_\alpha(x)$. *Acta Math.*, 29:217, 1905.
- 127** W. Wyss. The fractional diffusion equation. *J. Math. Phys.*, 27:2782, 1986.
- 128** K. Yosida. *Functional Analysis*. Springer, Berlin, 1965.
- 129** G. Zaslavsky. Fractional kinetics of Hamiltonian chaotic systems. In R. Hilfer, editor, *Applications of Fractional Calculus in Physics*, World Scientific, Singapore, 2000, p. 202.
- 130** G. Zaslavsky. Chaos, fractional kinetics, and anomalous transport. *Phys. Rep.*, 371:461, 2002.
- 131** V.M. Zolotarev. Mellin-Stieltjes transforms in probability theory. *Theor. Prob. Appl.*, II:433, 1957.
- 132** A. Zygmund. *Trigonometric Series*, volume 1. Cambridge University Press, Cambridge, 1959.
- 133** A. Zygmund. *Trigonometric Series*, volume 2. Cambridge University Press, Cambridge, 1959.

3

Random Processes with Infinite Moments

Michael F. Shlesinger

3.1

St. Petersburg Paradox

Right at the beginnings of probability theory a random process with infinite moments was encountered. The problem, posed by Nikolaus Bernoulli, appeared in the 1708 probability book of Pierre Remond de Montmort *Essay d'analyse sur les jeux de hazard* (*Essay on the analysis of games of chance*). The problem was deceptively simple. It was to determine the fair ante in a game of chance. The game was to flip a coin until a head appeared. This had a probability of $1/2$ to occur on the first flip, and the payoff would be one coin. The sequence TH has probability $1/4$ and a payoff of two coins. The sequence T \cdots T H with N tails prior to the first head has probability $(1/2)^{N+1}$ and a payoff of 2^N . Typically, one sets the ante to be the mean (i.e., the expected value) of the probability distribution for winning. The expected winnings are

$$\sum_{N=0}^{\infty} 2^N \left(\frac{1}{2}\right)^{N+1} = \frac{1}{2} + \frac{1}{2} + \dots = \infty. \quad (3.1)$$

The banker wants the player to ante an infinite number of coins because this is his expected loss. The player counters that to win an infinite amount he must flip the coin an infinite number of times, a physical impossibility. Besides the player's median winnings are only one coin and with probability $3/4$ he would win two or less coins, with probability $7/8$ he would win four or less coins, etc. The problem is that one is trying to determine the characteristic size of a distribution that does not possess one. There is nothing wrong mathematically with the distribution for winning coins, it is normalized to one, and it shows a scaling of winning an order of magnitude more (in base 2) with an order of magnitude less probability (in base 2). To possess scaling, a characteristic size should not appear, so infinite moments are to be expected. Although other distributions with infinite moments eventually appeared, such as the Cauchy distribution, the formal analysis of probability distributions with infinite moments had to wait for the works of Paul Lévy [1]. In the 1930s he determined

the Fourier transform representation of such probabilities for the sum of identically distributed random variables with the scaling property that their sum has the same distribution as the individual terms in the sum, up to a scale factor.

3.2

Holtsmark Distribution

Holtsmark [2], in his 1919 paper “The broadening of spectral lines” was concerned with the spectroscopy of ions in a plasma, especially the electric field Stark effect. Here we present a simplified version of Holtsmark’s calculation by only considering the nearest neighbor effect. The force $F(r)$ between two charged particles separated by a distance r varies as r^{-2} . The probability that the nearest neighbor of a charged particle is a distance r away is the probability that the largest sphere containing no other particles is of radius r . If this empty volume V follows a Poisson distribution $g(V) = V_0^{-1} \exp(-V/V_0)$, then the nearest-neighbor probability $g(r)$ of a separation r is given by, in 3D,

$$g(V) dV = \frac{4\pi r^2}{V_0} \exp\left(-\frac{4\pi r^3}{3V_0}\right) dr. \quad (3.2)$$

This will induce a distribution $W(F)$ of force F given by $W(F)dF = g(V)dV$ with $F(r) = q^2/r^2$ and $dF/dr = -2q^2/r^3$. Thus,

$$\begin{aligned} W(|F|) &= g(V) \frac{dV}{dF} = \frac{1}{V_0} \exp\left(-\frac{4\pi q^2}{3V_0 F}\right) \frac{dV}{dr} \frac{dr}{dF} \\ &= \frac{1}{V_0} \exp\left(-\frac{4\pi q^2}{3V_0 F}\right) \frac{q^5}{F^{5/2}} \end{aligned} \quad (3.3)$$

which has an infinite second moment. This $F^{-5/2}$ behavior is due to the nearest-neighbor effect but this is the dominant term when one accounts for all particles. In the complete analysis the probability density function $W(F)$ is more complicated and given by an integral [2, 3],

$$W(|F|) = \frac{1}{2\pi^2 |F^2|} \int_0^\infty x \sin x \exp\left(-\frac{\text{const. } x^{3/2}}{|F^{3/2}|}\right) dx$$

Chandrasekar [3] investigated the equivalent calculation for the gravitation force distribution between randomly distributed stars. A related analysis was applied to studying the fluctuations in the transition energy of a single molecule embedded in a solid [4].

3.3

Activated Hopping

Even a process as familiar as activated hopping can produce a probability density with an infinite moment when some disorder is considered. Start with the Arrhenius law to define a time scale τ ,

$$\tau = \tau_0 \exp(\Delta/kT), \quad (3.4)$$

where Δ is the free energy barrier, T is the temperature, and the prefactor τ_0 is a constant. A probability density $h(\Delta)$ of activation energies Δ induces a probability density $\psi(\tau)$ of trapping times τ . Note that $h(\Delta)$ has units of inverse energy and $\psi(\tau)$ has units of inverse time. These probability densities are connected by

$$\psi(\tau)d\tau = h(\Delta)d\Delta. \quad (3.5)$$

Choosing $h(\Delta) = (1/\Delta_0) \exp(-\Delta/\Delta_0)$ with Δ_0 being the mean barrier height, and employing Eq. (3.4) to write Δ as a function of τ , gives the equality

$$\exp(-\Delta/\Delta_0) = (\tau/\tau_0)^{-kT/\Delta_0}$$

which together with $d\tau/d\Delta = \tau/kT$ yields [5]

$$\psi(\tau) = \beta \frac{\tau_0^\beta}{\tau^{1+\beta}} \text{ for } \tau > \tau_0, \quad (3.6)$$

where $\beta = kT/\Delta_0$. When $\beta < 1$ we get anomalous diffusion because the first moment, the mean waiting time $\langle t \rangle = \int_0^\infty t\psi(t)dt$, is infinite.

The artifact of having a minimum time can be overcome by treating τ_0 as a random variable, as well. Consider the question of how to determine the probability distribution function for the product of two random variables. Let X , Y , and Z be random variables with probability distributions $f(x)$, $g(y)$, and $p(z)$, respectively.

Let $Z = XY$

Then

$$p(z) = \int_{-\infty}^{\infty} f\left(\frac{z}{y}\right) g(y) \frac{dy}{y}. \quad (3.7)$$

As we will show, the $1/y$ term comes from the Jacobian $J = \partial(x, y)/\partial(z, y)$ of the transformation from (x, y) to (z, y) . The joint probabilities are related by

$$P(z, y) dz dy = F(x, y) dx dy,$$

where

$$F(x, y) = f\left(\frac{x}{y}\right) g(y) \quad \text{and} \quad p(z) = \int_{-\infty}^{\infty} P(z, y) dy.$$

Thus, $P(z, y) = F(x, y) J$ with

$$J = \begin{vmatrix} \partial x / \partial z & \partial x / \partial y \\ \partial y / \partial z & \partial y / \partial y \end{vmatrix} = \begin{vmatrix} 1/y & -z/y^2 \\ 0 & 1 \end{vmatrix} = 1/y.$$

Integrating $P(z, y)$ over y gives Eq. (3.7).

In our case, the random variables τ, τ_0 , and Δ are related by $\tau = \tau_0 \exp(\Delta/kT)$.

Set $X = \tau_0$ and $Y = \exp(\Delta/kT)$. Note when Δ is zero that $Y = 1$, so Eq. (3.7) becomes

$$p(z) = \int_1^\infty f(z/y) g(y) \frac{dy}{y}$$

Choosing $f(t) = (2/\sqrt{\pi}) \exp(-t^2)$ so there is more weight toward smaller attempt times t , and keeping Eq. (3.6) for the Y distribution yields [5]

$$p(\tau) = \frac{2\beta}{\sqrt{\pi}} \int_1^\infty \exp(-\tau^2/y^2) \frac{dy}{y^{2+\beta}}. \quad (3.8)$$

Let $u = 1/y^2$ and $du = -2/y^3 dy$; then

$$\begin{aligned} p(\tau) &= \frac{\beta}{\sqrt{\pi}} \int_0^1 \exp(-u\tau^2) y^3 \frac{du}{y^{2+\beta}} \\ &= \frac{\beta}{\sqrt{\pi}} \int_0^1 \exp(-u\tau^2) \frac{du}{u^{(1-\beta)/2}}. \end{aligned} \quad (3.9)$$

Writing $q = u\tau^2$ yields

$$p(\tau) = \frac{1}{\sqrt{\pi}} \frac{\beta}{\tau^{1+\beta}} \int_0^{\tau^2} \exp(-q) q^{(\beta-1)/2} dq \quad (3.10)$$

with the integral going to a constant as $\tau \rightarrow \infty$. Thus, $p(\tau)$, at long times behaves as $1/\tau^{1+\beta}$ the same as if the prefactor was fixed and not random.

While Eqs. (3.6) and (3.10) have the same long-time asymptotic behavior, their short-time behavior is quite different. From Eq. (3.10) $p(\tau) \approx (\beta/\sqrt{\pi}) \exp(-\tau^2)$ for small times, while Eq. (3.6) has a minimum time τ_0 .

3.4

Deterministic Examples of Long Tail Distributions

Even a seemingly deterministic example can produce probability densities with infinite moments. Consider a long corridor of length L and width d

and a ball rolling down the corridor at an angle experiencing elastic collisions with the walls. If the ball enters at an angle θ , then it will move a distance $x(\theta) = d / \tan(\theta)$ before hitting the wall. There will be $n = L/x = (L/d) \tan(\theta)$ collisions before the ball exits the corridor. A uniform distribution of angles $f(\theta) = 2/\pi$ produces a distribution $p(n)$ of the number n of collisions with

$$p(n) dn = f(\theta) d\theta = \frac{2}{\pi} d\theta \quad (3.11a)$$

and

$$\frac{dn}{d\theta} = \frac{L}{d} \frac{1}{\cos^2(\theta)}. \quad (3.11b)$$

Using

$$n^2 = \left(\frac{L}{d}\right)^2 \tan^2(\theta) = \left(\frac{L}{d}\right)^2 \frac{1 - \cos^2(\theta)}{\cos^2(\theta)}$$

and solving for $\cos^2(\theta)$ as a function of n , we arrive at

$$p(n) = \frac{\pi}{2} \frac{\left(\frac{L}{d}\right)}{n^2 + \left(\frac{L}{d}\right)^2} \quad (3.12)$$

the Cauchy distribution with a long tail and an infinite second moment.

Each hit of the ball along the corridor can be tracked with a mapping. If one wall is curved creating a neck, then the ball can experience many bounces when traversing the confined space. This is reminiscent of a trajectory near a tangent bifurcation in a dynamical mapping [6,7]. Mappings of the form

$$x_{t+1} = x_t + ax^z \quad (3.13)$$

have been studied by Geisel and Thomae [8], in the continuum limit, with the solution for a starting (injection) point x_0 , to reach position L at time t ,

$$L = x(t) = \left[x_0^{1-z} - a(z-1)t \right]^{-1/(z-1)} \quad (3.14a)$$

or equivalently setting $t = T(x_0)$ and $x = L$,

$$T(x_0) = \left(x_0^{1-z} - L^{1-z} \right) / a(1-z). \quad (3.14b)$$

Geisel and Thomae [8] have used this approach to convert this deterministic process into a random process by allowing for a random distribution $f(x_0)$ of

starting points x_0 . They calculate the probability density to spend a time T to traverse from x_0 to L ,

$$\psi(T) dT = f(x_0) dx_0$$

with a uniform distribution of starting points producing a power-law density,

$$\psi(T) \propto \frac{1}{T^{z/(z-1)}} \quad (3.15)$$

at asymptotically long times T .

Hamiltonian systems can also display seemingly stochastic behavior. Orbits with slightly different starting points in phase space stick around nested quasiperiodic islands for widely different times. The histogram, for an ensemble of initial conditions, produces algebraic first passage time distributions to leave the quasiperiodic region [9,10].

3.5

Random Walks and Master Equations

The master equation (see Eq. (3.16)) that is being considered looks like a rate equation, but it is directly written for probabilities instead of for moments of probabilities:

$$\begin{aligned} \frac{\partial P(x,t)}{\partial t} &= \sum_{x'} \int_0^t \phi(t') p(x') P(x-x',t-t') dt' \\ &\quad - \int_0^t \phi(t') P(x,t-t') dt'. \end{aligned} \quad (3.16)$$

The quantity $p(x)$ is the probability for a jump of displacement x , and $\phi(t)$ has units of $1/t^2$. The meaning of $\phi(t)$ will become clear after we relate it to a probability waiting time density. Performing the Laplace (over time) and Fourier (over space) transforms give the master equation in the form

$$s\tilde{P}^*(k,s) - \tilde{P}(k,t=0) = \phi^*(s)\tilde{p}(k)\tilde{P}^*(k,s) - \phi^*(s)\tilde{P}^*(k,s)$$

and solving for the transformed probability gives

$$\tilde{P}^*(k,s) = \frac{1}{s + \phi^*(s) - \phi^*(s)\tilde{p}(k)}. \quad (3.17)$$

Next, let us consider a random walk on a lattice where the walker waits for a random time, governed by a probability density $\psi(t)$ for the waiting time

between jumps [11]. The probability density $Q(x, t)$ to just arrive at a site x at time t is given by

$$Q(x, t) = \sum_{x'} \int_0^t Q(x - x', t - t') p(x') \psi(t') dt' + \delta_{x,0} \delta(t) \quad (3.18)$$

and the probability $P(x, t)$ to be at that site includes reaching the site at an earlier time $t - \tau$ and then not jumping away at least for a time τ

$$P(x, t) = \int_0^t Q(x, t - \tau) \left(1 - \int_0^\tau \psi(t') dt' \right) d\tau. \quad (3.19)$$

In Laplace–Fourier space,

$$\begin{aligned} \tilde{P}^*(k, s) &= \tilde{Q}^*(k, s) \frac{1 - \psi^*(s)}{s} \\ &= \frac{1}{1 - \tilde{p}(k) \psi^*(s)} \frac{1 - \psi^*(s)}{s} \end{aligned}$$

If we set

$$\phi^*(s) = s\psi^*(s) / (1 - \psi^*(s)) \quad (3.20)$$

then

$$\begin{aligned} \tilde{P}^*(k, s) &= \frac{1}{1 - \tilde{p}(k) \phi^*(s) / (s + \phi^*(s))} \frac{1}{s + \phi^*(s)} \\ &= \frac{1}{s + \phi^*(s) - \tilde{p}(k) \phi^*(s)} \end{aligned}$$

and this is the same solution as in Eq. (3.17). This shows how to relate the memory in the random walk semi-Markov equation to the memory in the master equation such that both provide an equivalent description of the random process [12]. Markov means that the present jump only depends on where the jump originates, and not directly on previous jumps. Semi-Markov just means that the waiting time probability is taken into account and time only moves forward. For long tail temporal memories, such that moments of the memory diverge, some rewrite the master equation with a Riemann–Liouville fractional derivative, instead of the memory term, i.e., in the continuum limit one has

$$\frac{\partial^\alpha P(x, t)}{\partial t^\alpha} = D \nabla^2 P(x, t)$$

We will discuss in Section 3.7 the case when the space derivatives are infinite, (the Lévy flight case) with the equation symbolically written as

$$\frac{\partial P(x,t)}{\partial t} = D \nabla^\beta P(x,t)$$

But we will not treat the case with separate α and β derivatives. Instead we will work with a coupled space-time memory formalism that we have called Lévy walks because this approach introduces a velocity to the random walk segments. The Lévy flight only addresses the end points of jumps and does not account for the time spent in the flight or points crossed. The time factor will become important when the flight time becomes a random variable with infinite moments. The term Lévy walk implies that all points on the flight are accounted for as well as the time of flight, see Figure 3.1.

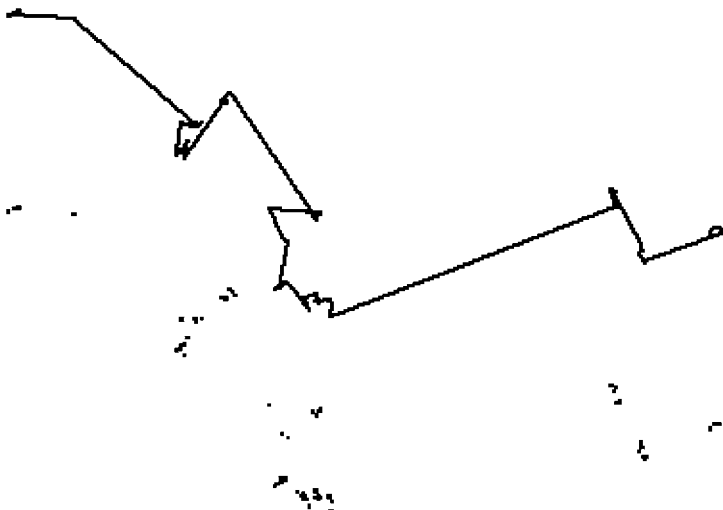


Figure 3.1 A section of a fractal space random walk. The solid line is the actual random walk and the dots below are sets of points visited displaced vertically to illustrate their fractal structure. The Lévy flight is represented by the dots. The Lévy walk is the solid line with an associated velocity.

3.6

Random Walks and Upper Critical Dimensions

Consider a random walk, starting at the origin, on a 1D periodic lattice with steps occurring at a discrete fixed interval. The probability to be at site x at the

n th step is given by

$$P_{n+1}(x) = \sum_{x'} P_n(x - x') p(x'), \quad (3.21)$$

which takes the form in Fourier space of

$$\tilde{P}_n(k) = [\tilde{p}(k)]^n, \quad (3.22)$$

where for small values of k and a symmetric random walk we have

$$\tilde{p}(k) \approx 1 - \frac{1}{2} k^2 \langle x^2 \rangle + o(k^4)$$

letting us approximate Eq. (3.22) as

$$\tilde{P}_n(k) \approx \exp\left(-\frac{n}{2} \langle x^2 \rangle k^2\right) \quad (3.23a)$$

or in real space

$$P_n(x) = \frac{1}{2\pi} \int_{-\pi}^{\pi} \exp\left(-\frac{n}{2} \langle x^2 \rangle k^2\right) \exp(-ikx) dk. \quad (3.23b)$$

We can extend the limits of the integral to $+$ and $-$ infinity because for large n the integrand has a sharp peak around $k = 0$ producing Gaussian behavior

$$P_n(x) \approx \frac{1}{\sqrt{2\pi \langle x^2 \rangle n}} \exp\left(-\frac{x^2}{2 \langle x^2 \rangle n}\right). \quad (3.24)$$

This analysis appears to dictate Gaussian behavior as the Taylor expansion of $\tilde{p}(k)$ provides the k^2 term making 2 the upper critical spatial dimension of the random walk. One way around this result is to consider random processes with $\langle x^2 \rangle$ being infinite. We provide an example in the next section.

3.7

Weierstrass Random Walk

Consider a random walk that can jump an order of magnitude further (in base b) with an order of magnitude less probability (in base w), i.e.,

$$p(x) = \frac{w-1}{w} \sum_{j=0}^{\infty} w^{-j} [\delta_{x,b^j} + \delta_{x,b^{-j}}], \quad (3.25)$$

whose Fourier transform is the famous Weierstrass function,

$$\tilde{p}(k) = \frac{w-1}{w} \sum_{j=0}^{\infty} w^{-j} \cos(kb^j). \quad (3.26)$$

Expanding the cosine in a Taylor series we can see that the coefficient of the k^2 term is $\sum_{j=0}^{\infty} (b^2/w)^j$ and this term is infinite when $b^2 > w$. This coefficient is the mean square displacement for the random walk per jump. Weierstrass introduced this function as an example of a continuous, but everywhere non-differentiable function when $b > w$. We introduced this function [13] because it produced a fractal set of points visited (clusters of size w within a cluster of w clusters, etc., with each subcluster a scale factor b smaller than the cluster size) and it provides an example of a random process with an infinite second moment $\langle x^2 \rangle = \infty$. We can still expand $\tilde{p}(k)$ in a series of powers, except that one of the powers will be a noninteger. The trick to accomplish this is to write the cosine term as its own inverse Mellin transform

$$\cos(k) = \frac{1}{2\pi i} \oint \Gamma(s) \cos\left(\frac{\pi s}{2}\right) |k|^{-s} ds$$

and substitute this expression into Eq. (3.26). One then switches the sum with the contour integral and then performs the summation in Eq. (3.26) to arrive at

$$\tilde{p}(k) = \frac{1}{2\pi i} \frac{w-1}{w} \oint \frac{|k|^{-s} \Gamma(s) \cos(\pi s/2)}{1 - w^{-1} b^{-s}} ds, \quad (3.27)$$

whose integrand has simple poles at $s = 0$ and the positive and negative even integers from the cosine–gamma function combination and from the denominator simple poles at $s = -\ln w / \ln b \pm 2\pi i n$ for integer n . If $b^2 > w$ then the small k expansion follows from contributions from the pole at $s = 0$ and the one at $s = -\ln w / \ln b$ and at $s = -2$ yielding

$$\begin{aligned} \tilde{p}(k) &\approx 1 - |k|^\beta + o(k^2) \\ &\approx \exp(-|k|^\beta), \end{aligned} \quad (3.28)$$

where $\beta = \ln w / \ln b$.

This result sheds light on Lévy's results for what he called stable distributions. He asked the basic question of when can the probability $P(x, n)$ for the position of a random walk after n jumps be the same probability function as after a single jump, up to scale factors. Consider a two-step random walker being at position $X = X_1 + X_2$ where the first jump had displacement X_1 and the second jump displacement X_2 . This can be described in terms of probabilities as

$$P(x, n=2) = \int_{x'} p(x - x', n=1) p(x', n=1) dx'. \quad (3.29)$$

If the small p 's describing single jumps are non-Gaussian probabilities with finite second moments, then the large P governing the position after n jumps

will converge to a Gaussian, i.e., P and p need not be the same function. Lévy asked the question of when they are the same function. Assuming that p and P have the same form and Fourier transforming Eq. (3.29) we have the relationship for a general n -step random walk

$$\tilde{P}(k, n) = [\tilde{P}(k, n=1)]^n \quad (3.30a)$$

with a solution in the form

$$\tilde{P}(k, n) = \exp(-n|k|^\beta). \quad (3.30b)$$

The P 's for a single jump or for n jumps are the same, except for the scale factor n . The exponent β is equal to or less than 2 because if it were greater than 2 the k^2 term would dominate the k^β term for small k and Gaussian behavior would be asymptotically approached.

3.8

Fractal Time Random Walk

In Section 3.5 we treated continuous-time random walks with a random waiting time between jumps. Here we consider explicitly the case when the mean waiting time is infinite. If this is a waiting time between jumps of a trapped particle then one expects subdiffusive behavior. On the other hand, if this is a waiting time for being stuck in a momentum state, then one can expect supradiffusive behavior.

When all of the moments of the waiting time distribution exist, then

$$\psi^*(s) \equiv \int_0^\infty \psi(t) \exp(-st) = \sum_{j=0}^\infty (-1)^j s^j \langle t^j \rangle, \quad (3.31)$$

where

$$\langle t^j \rangle \equiv \int_0^\infty t^j \psi(t) dt.$$

For small s (long times) the expansion of $\psi^*(s)$ behaves as $1 - s\langle t \rangle + O(s^2)$. As with the Weierstrass random walk, we consider a probability density with scaling properties and therefore no characteristic average waiting time $\langle t \rangle$, i.e., we consider

$$\psi(t) = \frac{1-q}{q} \sum_{j=0}^\infty q^j \lambda^j \exp(-\lambda^j t) \quad (\lambda < q < 1). \quad (3.32)$$

When $q > \lambda$ then the first moment is infinite,

$$\langle t \rangle = \frac{1-q}{q} \sum_{j=1}^{\infty} \left(\frac{q}{\lambda}\right)^j = \infty. \quad (3.33)$$

Rather than going through the Mellin transform analysis, we will note the following scaling behavior:

$$\psi^*(s) = q\psi^*\left(\frac{s}{\lambda}\right) + \frac{\lambda(1-q)}{s+\lambda}, \quad (3.34)$$

which has a solution with dominant terms going as

$$\psi^*(s) \propto 1 - s^\alpha + O(s) \quad \left(\alpha = \frac{\ln q}{\ln \lambda} \right)$$

which implies at long times

$$\psi(t) \propto t^{-1-\alpha}. \quad (3.35)$$

If $\alpha > 1$, the first moment exists and the s term dominates the s^α term, so as expected the upper critical dimension of time is 1.

The behavior of

$$\frac{1}{1 - \psi^*(s)} \approx \begin{cases} s^{-\alpha}, & \langle t \rangle = \infty \\ (s \langle t \rangle)^{-1}, & \langle t \rangle < \infty \end{cases} \quad (3.36)$$

produces the number of jumps $N(t)$ at long times behaving as

$$N(t) \propto \begin{cases} t^\alpha, & \langle t \rangle = \infty \\ t, & \langle t \rangle < \infty \end{cases} \quad (3.37)$$

3.9

Coupled Memory Random Walks: Diffusion or Telegraph Equation

One obvious point to stress in a discrete random walk of jumps of unit length is that the walker cannot go further than N units away in N unit steps. In the continuum limit leading to the diffusion equation, with D a constant, this condition of a front beyond which the probability is zero is absent. At any time t , even at an infinitesimally small time, there will be a positive probability (Eq. (3.24)) for a diffusing particle to be arbitrarily far away from its starting point. For example, the Gaussian solution would overestimate the spread of pollution over a short time. A diffusion front can be obtained in a random walk with a coupled space-time memory such that if the particle possesses a velocity V , then $P(x, t)$ will equal zero if $x > Vt$.

Let us return to the continuous-time random walk and introduce the coupled memory [14]

$$\Psi(x, t) \equiv p(x|t) \psi(t) \quad (3.38)$$

for the probability density of a single jump of displacement x taking a time t . This is given as the product of the conditional probability that the jump is of displacement x given that it is of duration t times the probability that the jump is of duration t . The solution to the random walk retains the same form of Eq. (3.8) except that the term $\psi^*(s) \tilde{p}(k)$ is replaced by $\tilde{\Psi}^*(k, s)$, a coupled memory.

Again, let us look at a simple case, with $p(x)$ allowing only nearest-neighbor jumps with equal probability and

$$p(x|t) = \delta(|x| - Vt), \quad (3.39)$$

where V , the particle velocity, is introduced into the problem. The delta function provides the Galilean kinematic relationship $x = Vt$. Our discussion will have much in common with the discussion of the telegrapher's equation in Ref. [15], Weiss' excellent book on random walks. For this random walk

$$\Psi(x, t) = \delta(|x| - Vt) \lambda \exp(-\lambda t). \quad (3.40)$$

Transforming to k -space gives $\lambda \cos(kVt) \exp(-\lambda t)$ and then taking the Laplace transform of Eq. (3.40) gives for the coupled memory

$$\tilde{\Psi}^*(k, s) = \frac{\lambda(s + \lambda)}{(s + \lambda)^2 + (kV)^2}. \quad (3.41)$$

Using this result, the equation for $\tilde{P}^*(k, s)$ becomes

$$\tilde{P}^*(k, s) = \frac{1}{(s + \lambda)} \frac{(s + \lambda)^2 + (kV)^2}{s^2 + s\lambda + (kV)^2}. \quad (3.42)$$

If one takes the very long time, long-distance limit ($k, s \rightarrow 0$) $\tilde{P}^*(k, s)$ becomes more familiar as

$$\tilde{P}^*(k, s) \approx \lambda / (s\lambda + (kV)^2), \quad (3.43)$$

which transforms back into a Gaussian,

$$P(x, t) \approx (4\pi Dt)^{-1/2} \exp\left(-\frac{x^2}{4Dt}\right) \quad (3.44)$$

with the diffusion constant $D = V^2/\lambda$.

We can also see this by rewriting Eq. (3.42) as

$$(s\lambda + (kV)^2) \tilde{P}^*(k, s) = \lambda \quad (3.45)$$

and inverse Laplace and Fourier transforming to arrive at, term by term:

$$\frac{\partial P(x, t)}{\partial t} = \frac{V^2}{\lambda} \frac{\partial^2 P(x, t)}{\partial x^2}. \quad (3.46)$$

Using the same procedure with Eq. (3.42) with the more accurate approximation for s and k going to zero, we have

$$\left[2s^2\lambda + s\lambda^2 + \lambda (kV)^2 \right] \tilde{P}^*(k, s) = \lambda^2 \quad (3.47)$$

and using Laplace and Fourier inverse transform we arrive at the telegrapher's equation

$$\frac{\partial^2 P(x, t)}{\partial t^2} + \frac{\lambda}{2} \frac{\partial P(x, t)}{\partial t} = V^2 \frac{\partial^2 P(x, t)}{\partial x^2}. \quad (3.48)$$

This equation describes diffusion, but with a moving front with $P(x, t) = 0$ if $|x| > Vt$. In this sense the diffusion equation is nonphysical as it allow a finite probability to be at large x at small times t . In addition the diffusion equation does not have a well-defined velocity. The Wiener measure was invented to handle the Brownian trajectory which is nondifferentiable. The telegrapher's equation does not suffer from these shortcomings. In his 1900's thesis, Louis Bachelier treated bond prices as a random walk with price changes occurring at finite velocity. He arrived at a diffusion equation, but was criticized because the velocity is not defined for the diffusion equation. He should have really arrived at the telegrapher's equation instead of the diffusion equation.

In more detail, let us transform Eq. (3.42) exactly back to x -space to calculate [15]

$$P^*(x, s) = \frac{1}{(s + \lambda)} \cdot \frac{\left[(s + \lambda)^2 \right] \exp \left(- \left| \frac{x}{V} \right| \sqrt{s^2 + \lambda s} \right) + (s^2 + \lambda s) \exp \left(- \left| \frac{x}{V} \right| \sqrt{s^2 + \lambda s} \right)}{2\sqrt{s^2 + \lambda s}}. \quad (3.49)$$

Let us again take the small s limit,

$$\lim_{s \rightarrow 0} P^*(x, s) \approx \frac{\lambda \exp \left(- \left| \frac{x}{V} \right| \sqrt{s^2 + \lambda s} \right)}{2\sqrt{s^2 + \lambda s}}. \quad (3.50)$$

Writing $\sqrt{s^2 + \lambda s} = \sqrt{(s + \lambda/2)^2 - \lambda^2/4}$ and using the identity

$$L^{-1} \frac{\left\{ \exp -k\sqrt{s^2 - a^2} \right\}}{\sqrt{s^2 - a^2}} = I_0 \left(a\sqrt{t^2 - k^2} \right) \Theta(t - |k|), \quad (3.51)$$

where the theta step function is 1 if $t > |k|$ and zero otherwise, we arrive at

$$P(x, t) \approx \exp\left(-\frac{\lambda t}{2}\right) I_0\left(\frac{\lambda}{2} \left(\sqrt{t^2 - \frac{x^2}{V^2}}\right)\right) \Theta(Vt - |x|). \quad (3.52)$$

This is where the diffusion front at $x = Vt$ enters the equation through the step function. For Vt greater than the absolute value of x , the probability function becomes, at longer times, more diffusive-like inside of the diffusion front. This can be checked by writing for very large t that $I_0(z) \approx \exp(z)/\sqrt{2\pi z}$ where in our case

$$\begin{aligned} z &= (\lambda t/2) \sqrt{1 - \frac{x^2}{V^2 t^2}} \approx \frac{\lambda t}{2} \left(1 - \frac{x^2}{2V^2 t^2}\right) \\ P(x, t) &\approx \frac{1}{\sqrt{\pi \lambda t}} \exp\left(-\left(\frac{x^2}{4V^2 t/\lambda}\right)\right) \Theta(x - Vt). \end{aligned}$$

3.10

Random Walks: Coupled Memory Lévy Walks: Turbulent and Relativistic

Consider the constant velocity random walk with the probability of completing a flight of length x given that the flight was of duration t ,

$$p(x|t) = \delta(t - x/V) \quad (3.53)$$

and let $\psi(t)$ be the probability density that the flight time is t choosing

$$\psi(t) \propto t^{-1-\alpha}. \quad (3.54)$$

Then the coupled memory random walk calculation yields the result [10]

$$\langle x^2(t) \rangle \propto \begin{cases} t^2 & 0 < \alpha < 1 \\ t^2/\ln t & \alpha = 1 \\ t^{3-\alpha} & 1 < \alpha < 2 \\ t \ln t & \alpha = 2 \\ t & \alpha > 2. \end{cases} \quad (3.55)$$

The first case with the t^2 has the mean time $\langle t \rangle$ for a flight being infinite, the second case has $\langle t \rangle$ diverging logarithmically, the third case has $\langle t \rangle$ finite, but $\langle t^2 \rangle$ infinite, the fourth case has $\langle t^2 \rangle$ diverging logarithmically, and the last case has $\langle t^2 \rangle$ finite. This last case is the particle bouncing around randomly with finite length segments and the behavior is governed by the telegrapher's equation, as discussed in the last section.

Other kinematics are possible besides the constant velocity ballistic motion [16–18]. For inertial range turbulent flow for a passive scalar particle of mass m moving with velocity V over a distance R , the average dissipation ε is independent of the scale R , that is

$$\varepsilon = \frac{\text{energy}}{\text{time}} = \frac{\frac{1}{2}mV^2}{R/V}. \quad (3.56)$$

For scale independence we need

$$V(R) \propto R^{1/3}. \quad (3.57)$$

The energy, in Fourier space $E(k)$, varies as $k^{-5/3}$, as $E(R)$ varies as $V(R)^2$, which is proportional to $R^{2/3}$. This is known as Kolmogorov scaling. For turbulent diffusion we choose

$$p(R|t) = \delta(R - V(R)t)$$

and the same asymptotic algebraic form for $\psi(t)$ as in Eq. (3.54) and calculate [16]

$$\langle R^2(t) \rangle \propto \begin{cases} t^3 & \alpha < 1/3 \\ t^{2+\frac{3}{2}(1-\alpha)} & 1/3 < \alpha < 5/3 \\ t & \alpha > 5/3. \end{cases} \quad (3.58)$$

Longer flights correspond to larger vortices with more energy and hence larger velocities. But when the mean square time spent in a flight is finite the Brownian motion linear growth of the mean square displacement is recovered.

A relativistic turbulent diffusion law can be found [18] by replacing $(1/2)Mv^2$ with its relativistic generalization, so

$$\varepsilon = (\gamma - 1) m_0 c^2 V / R, \quad (3.59)$$

where $\gamma = (1 - V^2/c^2)^{-1/2}$. For $V \ll c$, $\gamma - 1 \approx \frac{1}{2} \left(\frac{V}{c} \right)^2$ and Eq. (3.59) reduces to the classical turbulent diffusion result with the mean square displacement growing at t^3 when $\alpha < 1/3$. At long times, longer flights with their associated higher velocities are encountered so $\gamma - 1$ is approximated by γ . Squaring Eq. (3.59) and solving for $V(R)$ we obtain

$$V^2(R) \approx \frac{R^2}{1 + R^2/c^2} \quad (3.60)$$

so

$$R^2 \approx V^2 t^2 \approx \frac{R^2}{1 + R^2/c^2} t^2 \approx c^2 t^2 \quad (3.61)$$

and this result will describe the asymptotic mean square displacement when $\alpha < 1/3$.

For relativistic flights accelerating in a gravitational field we have the term

$$p(x|t) = \delta \left(x - \frac{c^2}{g} \left\{ \left[1 + \left(g \frac{t}{c} \right)^2 - 1 \right] \right\} \right), \quad (3.62)$$

which yields $\langle x^2(t) \rangle \approx \frac{1}{4}g^2 t^4 \rightarrow c^2 t^2$ with the initial ballistic acceleration going over to the relativistic t^2 result at long times.

References

- 1 P. Lévy, *Théorie de l'addition des variables aléatoires* (Gauthier-Villars, Paris, 1937).
- 2 J. Holtsmark, "Über die Verbreiterung von Spektrallinien" Ann. Physik **58** 577–630 (1919).
- 3 S. Chandrasekar, "Stochastic problems in physics and astronomy" Rev. Mod. Phys **15** 1–89 (1943).
- 4 G. Zumofen and J. Klafter, "Spectral random walk of a single molecule" Chem. Phys. Lett. **219** 303–309 (1994).
- 5 J. T. Bendler, J. J. Fontanella, and M. F. Shlesinger, "Anomalous diffusion producing normal relaxation and transport" J. Phys.: Condens. Matter **19** 065121/1–7 (2007).
- 6 Y. Pomeau and P. Manneville, "Intermittent transition to turbulence in dissipative dynamical systems" Commun. Math. Phys. **74** 189–197 (1980).
- 7 J. E. Hirsch, B. A. Huberman, and D. J. Scalapino, "Theory of intermittency" Phys. Rev. A **25** 519–532 (1982).
- 8 T. Geisel and S. Thomae, "Anomalous diffusion in intermittent chaotic systems" Phys. Rev. Lett. **52** 1936–1939 (1984).
- 9 M. Shlesinger, G. Zaslavsky, and J. Klafter, "Strange kinetics" Nature **363** 31–37 (1993).
- 10 J. Klafter, M. Shlesinger, G. Zumofen, "Beyond Brownian motion" Phys. Today **49** 33–39 (1996).
- 11 E. W. Montroll and G. H. Weiss, "Random walks on lattices: II" J. Math. Phys. **6** 167–181 (1965).
- 12 V. M. Kenkre, E. W. Montroll, and M. F. Shlesinger, "Generalized master equations for continuous-time random walks" J. Stat. Phys. **9** 45–50 (1973).
- 13 B. D. Hughes, E. W. Montroll, and M. F. Shlesinger, "Random walks with self-similar clusters" Proc. Natl Acad. Sci. **78** 3287–3291 (1981).
- 14 M. F. Shlesinger, J. Klafter, and Y. M. Wong, "Random walks with infinite temporal and spatial moments" J. Stat. Phys. **27** 499–512 (1982).
- 15 G. H. Weiss, *Aspects and Applications of the Random Walk* (North-Holland, Amsterdam, 1994).
- 16 M. F. Shlesinger, J. Klafter, and B. J. West, "Lévy dynamics of enhanced diffusion: application to turbulence" Phys. Rev. Lett. **58** 1100–1103 (1987).
- 17 M. F. Shlesinger, "Supra-diffusion," in *Processes with Long-Range Correlations* eds. G. Rangarajan and M. Ding (Springer, Berlin, 1995), pp. 139–147.
- 18 M. F. Shlesinger, J. Klafter, and G. Zumofen, "Lévy flights: chaotic, turbulent and relativistic" Fractals **3** 491–498 (1995).

4

Continuous Time Random Walk, Mittag-Leffler Waiting Time and Fractional Diffusion: Mathematical Aspects

Rudolf Gorenflo and Francesco Mainardi

4.1

Introduction

The purpose of this paper is to outline the fundamental role the Mittag-Leffler function in renewal processes that are relevant in the theories of anomalous diffusion. As a matter of fact the interest in this function in statistical physics and probability theory has recently increased as is shown by the large number of papers published since 1990 of which a brief (incomplete) bibliography includes [2, 3, 16, 21, 22, 27–31, 36, 41, 44, 47, 51, 60, 62, 67].

In this paper, we develop a theory for long-time behavior of a renewal process with a generic power-law waiting-time distribution of order β , $0 < \beta \leq 1$ (thereby for easy readability dispensing with decoration by a slowly varying function). To bring the distant future into near sight we change the unit of time from 1 to $1/\tau$, $0 < \tau \ll 1$.

For the random waiting times T this means replacing T by τT . Then, having many events in a moderate span of time we compensate this compression by respeeding the whole process, actually slowing it down so that again we have a moderate number of events in a moderate span of time. We will relate the rescaling factor τ and the respeeding factor a in such a way that in the limit $\tau \rightarrow 0$ we have a reasonable process, namely one whose waiting-time distribution is the Mittag-Leffler waiting-time distribution whose density is

$$\phi^{\text{ML}}(t) = -\frac{d}{dt}E_\beta(-t^\beta), \quad 0 < \beta \leq 1, \quad (4.1)$$

with the Mittag-Leffler function

$$E_\beta(z) := \sum_{n=0}^{\infty} \frac{z^n}{\Gamma(\beta n + 1)}, \quad z \in \mathbf{C}, \quad \beta > 0. \quad (4.2)$$

We will call the renewal process with waiting-time density $\phi^{\text{ML}}(t)$ the *Mittag-Leffler (renewal) process*. This process can be seen as a fractional generalization of the Poisson process, see [40].

Our method is, in some sense, analogous to the one applied in the 60s of the past century by Gnedenko and Kovalenko [15] in their analysis of *thinning* (or *rarefaction*) of a renewal process. They found, under certain power-law assumptions, in the infinite thinning limit, for the waiting-time density the Laplace transform $1/(1+s^\beta)$ but did not identify it as a Mittag-Leffler type function. In Section 4.2, we provide, in our notation, an outline of the thinning theory for renewal processes essentially following Gnedenko and Kovalenko. Their method has inspired us for the treatment of our problems.

As we consider our renewal process formally as a continuous time random walk (CTRW) with constant nonrandom jumps 1 in space (for the counting function $N(t)$), in Section 4.3 we embed *ab initio* our theory into that of the CTRW, thus being in the position to treat the theory of a CTRW as limiting case of a CTRW with power-law waiting-time distribution. In this context the pioneering paper by Balakrishnan [1] in 1985 deserves to be mentioned. Balakrishnan already found the importance of the Laplace transform $1/(1+s^\beta)$ for processes that in our time are called time-fractional CTRW and time-fractional diffusion, but he did not identify it as the Laplace transform of $\phi^{\text{ML}}(t)$. Then, in 1995 Hilfer and Anton [29], (see also [27,28]), showed that this waiting-time density is characteristic for the time-fractional CTRW and can be expressed in terms of the Mittag-Leffler function in two parameters, that is

$$\phi^{\text{ML}}(t) = t^{\beta-1} E_{\beta,\beta}(-t^\beta), \quad 0 < \beta \leq 1, \quad (4.3)$$

with the generalized Mittag-Leffler function

$$E_{\beta,\gamma}(z) := \sum_{n=0}^{\infty} \frac{z^n}{\Gamma(\beta n + \gamma)}, \quad z \in \mathbf{C}, \quad \beta > 0, \quad \gamma \in \mathbf{R}. \quad (4.4)$$

The form (4.3) is equivalent to the form (4.1) that we prefer as it exhibits visibly as well the cumulative probability function, the *survival probability*, $E_\beta(-t^\beta)$.

We explain in Section 4.4 two manipulations, *rescaling* and *respeeding* and use these in Section 4.5 to deduce the asymptotic universality of the Mittag-Leffler waiting-time density under a power-law assumption for the original waiting time. Then, in Section 4.6, assuming a suitable power law also for the spatial jumps we show that by a rescaling of the jump widths by a positive factor h (that means a change of the unit of space from 1 to $1/h$ to bring into near sight the far-away space) another respeeding is effected, now an acceleration, that in the limit $h \rightarrow 0$ (under a proper relation between h and τ) leads to space-time fractional diffusion.

In Section 4.7, we pass to a properly scaled limit for the counting function $N(t)$ of a renewal process (again under power-law assumption) and obtain the time-fractional drift process (viewing $N(t)$ as a spatial variable).

We will extensively work with the transforms of Fourier and Laplace, so easing calculations and proofs of *convergence in distribution* (also called “weak convergence”) for our passages to the limit.

Essentially, we treat in this paper three topics. First, in Section 4.2, the thinning of a pure renewal process. Second, in Sections 4.3–4.6, under power-law assumption for the waiting time, the asymptotic relevance of the Mittag-Leffler law, and then the general CTRW with special attention to space and time transition limits to fractional diffusion. As a third topic, in Section 4.7, we investigate the long-time behavior of the Mittag-Leffler renewal process.

Essential properties of the derivative of fractional order in time and in space are given in Appendix A and Appendix B, respectively. Finally, in Appendix C we give details on the two special functions of the Mittag-Leffler type that play a fundamental role in this paper, the Mittag-Leffler survival probability and the Mittag-Leffler waiting-time density.

4.2

An Outline of the Gnedenko–Kovalenko Theory of Thinning

The *thinning* theory for a renewal process has been considered in detail by Gnedenko and Kovalenko [15]. We must note that other authors, like Szántai [63, 64] speak of *rarefaction* in place of thinning. Let us sketch here the essentials of this theory: in the interest of transparency and easy readability we avoid the possible decoration of the relevant power law by multiplying it with a *slowly varying function*. As usual we call a (measurable) positive function $a(y)$ *slowly varying at zero* if $a(cy)/a(y) \rightarrow 1$ with $y \rightarrow 0^+$ for every $c > 0$, and *slowly varying at infinity* if $a(cy)/a(y) \rightarrow 1$ with $y \rightarrow +\infty$ for every $c > 0$. A standard example of a slowly varying function at zero and at infinity is $|\log y|^\gamma$, with $\gamma \in \mathbf{R}$.

Denoting by t_n , $n = 1, 2, 3, \dots$, the time instants of events of a renewal process, assuming $0 = t_0 < t_1 < t_2 < t_3 < \dots$, with independent identically distributed (iid) waiting times $T_1 = t_1$, $T_k = t_k - t_{k-1}$ for $k \geq 2$, (generically denoted by T), *thinning* (or *rarefaction*) means that for each positive index k a decision is made: the event happening in the instant t_k is deleted with probability p or it is maintained with probability $q = 1 - p$, $0 < q < 1$. This procedure produces a *thinned* or *rarefied* renewal process with fewer events (very few events if q is near zero, the case of particular interest) in a moderate span of time.

To compensate for this loss we change the unit of time so that we still have not very few but still a moderate number of events in a moderate span of time. Such change of the unit of time is equivalent to rescaling the waiting time, multiplying it with a positive factor τ so that we have waiting times

$\tau T_1, \tau T_2, \tau T_3, \dots$, and instants $\tau t_1, \tau t_2, \tau t_3, \dots$, in the rescaled process. Our intention is, vaguely speaking, to dispose on τ in relation to the rarefaction parameter q in such a way that for q near zero in some sense the “average” number of events per unit of time remains unchanged. In an asymptotic sense we will make these considerations precise.

Denoting by $F(t) = P(T \leq t)$ the probability distribution function of the (original) waiting time T , by $f(t)$ its density ($f(t)$ is a generalized function generating a probability measure) so that $F(t) = \int_0^t f(t') dt'$, and analogously by $F_k(t)$ and $f_k(t)$ the distribution and density, respectively, of the sum of k waiting times, we have recursively

$$f_1(t) = f(t), \quad f_k(t) = \int_0^t f_{k-1}(t-t') dF(t'), \text{ for } k \geq 2. \quad (4.5)$$

Observing that after a maintained event the next one of the original process is kept with probability q but dropped in favor of the second-next with probability $p q$ and, generally, $n - 1$ events are dropped in favor of the n th-next with probability $p^{n-1} q$, we get for the waiting-time density of the thinned process formula

$$g_q(t) = \sum_{n=1}^{\infty} q p^{n-1} f_n(t). \quad (4.6)$$

With the modified waiting time τT we have

$$P(\tau T \leq t) = P(T \leq t/\tau) = F(t/\tau), \quad (4.7)$$

hence the density $f(t/\tau)/\tau$, and analogously for the density of the sum of n waiting times $f_n(t/\tau)/\tau$. The density of the waiting time of the rescaled (and thinned) process now turns out to be

$$g_{q,\tau}(t) = \sum_{n=1}^{\infty} q p^{n-1} f_n(t/\tau)/\tau. \quad (4.8)$$

In the Laplace domain we have $\tilde{f}_n(s) = (\tilde{f}(s))^n$; hence by using $p = 1 - q$

$$\tilde{g}_q(s) = \sum_{n=1}^{\infty} q p^{n-1} (\tilde{f}(s))^n = \frac{q \tilde{f}(s)}{1 - (1-q) \tilde{f}(s)}, \quad (4.9)$$

from which by Laplace inversion we can, in principle, construct the waiting-time density of the thinned process. By rescaling we get

$$\tilde{g}_{q,\tau}(s) = \sum_{n=1}^{\infty} q p^{n-1} (\tilde{f}(\tau s))^n = \frac{q \tilde{f}(\tau s)}{1 - (1-q) \tilde{f}(\tau s)}. \quad (4.10)$$

Being interested in stronger and stronger thinning (*infinite thinning*) let us now consider a scale of processes with the parameters τ (of *rescaling*) and q (of *thinning*), with q tending to zero *under a scaling relation* $q = q(\tau)$ yet to be specified.

We have essentially two cases for the waiting-time distribution: its expected value is finite or infinite. In the first case we put

$$\lambda = \int_0^\infty t' f(t') dt' < \infty. \quad (4.11a)$$

In the second case we assume a queue of power-law type (dispensing with a possible decoration by a function slowly varying at infinity)

$$\Psi(t) := \int_t^\infty f(t') dt' \sim \frac{c}{\beta} t^{-\beta}, \quad t \rightarrow \infty \quad \text{if } 0 < \beta < 1. \quad (4.11b)$$

Then, by the Tauberian theory (see [12, 68]) the above conditions mean in the Laplace domain

$$\tilde{f}(s) = 1 - \lambda s^\beta + o(s^\beta), \quad \text{for } s \rightarrow 0^+, \quad (4.12)$$

with a positive coefficient λ and $0 < \beta \leq 1$. The case $\beta = 1$ obviously corresponds to the situation with finite first moment (4.11a), whereas the case $0 < \beta < 1$ is related to a power-law queue with $c = \lambda \Gamma(\beta + 1) \sin(\beta\pi)/\pi$.

Now, passing to the limit of $q \rightarrow 0$ of infinite thinning under the scaling relation

$$q = \lambda \tau^\beta, \quad 0 < \beta \leq 1, \quad (4.13)$$

between the positive parameters q and τ , the Laplace transform of the rescaled density $\widetilde{g}_{q,\tau}(s)$ in (4.10) of the thinned process tends for fixed s to

$$\widetilde{g}(s) = \frac{1}{1 + s^\beta}, \quad (4.14)$$

which corresponds to the Mittag-Leffler density

$$g(t) = -\frac{d}{dt} E_\beta(-t^\beta) = \phi^{\text{ML}}(t). \quad (4.15)$$

Let us remark that Gnedenko and Kovalenko obtained (4.14) as the Laplace transform of the limiting density but did not identify it as the Laplace transform of a Mittag-Leffler type function. Observe that in the special case $\lambda < \infty$ we have $\beta = 1$, hence as the limiting process the Poisson process, as formerly shown in 1956 by Rényi [54].

4.3

The Continuous Time Random Walk (CTRW)

The name *continuous time random walk* (CTRW) became popular in physics after Montroll, Weiss, and Scher (just to cite the pioneers) in the 1960s and 1970s published a celebrated series of papers on random walks for modeling diffusion processes on lattices, see e.g., [48, 49], and the book by Weiss [66] with references therein. CTRWs are rather good and general phenomenological models for diffusion, including processes of anomalous transport, that can be understood in the framework of the classical renewal theory, as stated for example in the book by Cox [7]. In fact a CTRW can be considered as a compound renewal process (a simple renewal process with reward) or a random walk *subordinated* to a simple renewal process.

A spatially one-dimensional CTRW is generated by a sequence of *iid* positive random waiting times T_1, T_2, T_3, \dots , each having the same probability density function $\phi(t)$, $t > 0$, and a sequence of *iid* random jumps X_1, X_2, X_3, \dots , in \mathbf{R} , each having the same probability density $w(x)$, $x \in \mathbf{R}$.

Let us remark that, for ease of language, we use the word density also for generalized functions in the sense of Gel'fand and Shilov [13], which can be interpreted as probability measures. Usually the *probability density function* is abbreviated by PDF. We recall that $\phi(t) \geq 0$ with $\int_0^\infty \phi(t) dt = 1$ and $w(x) \geq 0$ with $\int_{-\infty}^{+\infty} w(x) dx = 1$.

Setting $t_0 = 0$, $t_n = T_1 + T_2 + \dots + T_n$ for $n \in \mathbf{N}$, the wandering particle makes a jump of length X_n in instant t_n so that its position is $x_0 = 0$ for $0 \leq t < T_1 = t_1$, and $x_n = X_1 + X_2 + \dots + X_n$, for $t_n \leq t < t_{n+1}$. We require the distribution of the waiting times and that of the jumps to be independent of each other. So, we have a compound renewal process (a renewal process with reward), compare [7].

By natural probabilistic arguments we arrive at the *integral equation* for the probability density $p(x, t)$ (a density with respect to the variable x) of the particle being in point x at instant t , see e.g., [21, 23, 44, 58–60],

$$p(x, t) = \delta(x) \Psi(t) + \int_0^t \phi(t-t') \left[\int_{-\infty}^{+\infty} w(x-x') p(x', t') dx' \right] dt', \quad (4.16)$$

in which the *survival probability*

$$\Psi(t) = \int_t^\infty \phi(t') dt' \quad (4.17)$$

denotes the probability that at instant t the particle is still sitting in its starting position $x = 0$. Clearly, (4.16) satisfies the initial condition $p(x, 0^+) = \delta(x)$.

Note that the *special choice*

$$w(x) = \delta(x-1) \quad (4.18)$$

gives the *pure renewal process*, with position $x(t) = N(t)$, denoting the *counting function*, and with jumps all of length 1 in positive direction happening at the renewal instants.

For many purposes the integral equation (4.16) of CTRW can be easily treated by using the Fourier and Laplace transforms. Writing these as

$$\mathcal{F}\{g(x);\kappa\} = \hat{g}(\kappa) := \int_{-\infty}^{+\infty} e^{+i\kappa x} g(x) dx, \quad (4.19)$$

$$\mathcal{L}\{f(t);s\} = \tilde{f}(s) := \int_0^{\infty} e^{-st} f(t) dt, \quad (4.20)$$

then in the Fourier–Laplace domain, Eq. (4.16) reads

$$\hat{p}(\kappa, s) = \frac{1 - \tilde{\phi}(s)}{s} + \tilde{\phi}(s) \hat{w}(\kappa) \hat{p}(\kappa, s). \quad (4.21)$$

Introducing formally in the Laplace domain the auxiliary function

$$\tilde{H}(s) = \frac{1 - \tilde{\phi}(s)}{s \tilde{\phi}(s)} = \frac{\tilde{\Psi}(s)}{\tilde{\phi}(s)}, \quad \text{hence} \quad \tilde{\phi}(s) = \frac{1}{1 + s\tilde{H}(s)}, \quad (4.22)$$

and assuming that its Laplace inverse $H(t)$ exists, we get, following [44], in the Fourier–Laplace domain the equation

$$\tilde{H}(s) [s\hat{p}(\kappa, s) - 1] = [\hat{w}(\kappa) - 1] \hat{p}(\kappa, s), \quad (4.23)$$

and in the space–time domain the generalized Kolmogorov–Feller equation

$$\int_0^t H(t-t') \frac{\partial}{\partial t'} p(x, t') dt' = -p(x, t) + \int_{-\infty}^{+\infty} w(x-x') p(x', t) dx', \quad (4.24)$$

with $p(x, 0) = \delta(x)$.

If the Laplace inverse $H(t)$ of the formally introduced function $\tilde{H}(s)$ does not exist, we can formally set $\tilde{K}(s) = 1/\tilde{H}(s)$ and multiply (4.23) with $\tilde{K}(s)$. Then, if $K(t)$ exists, we get in place of (4.24) the alternative form of the generalized Kolmogorov–Feller equation

$$\frac{\partial}{\partial t} p(x, t) = \int_0^t K(t-t') \left[-p(x, t') + \int_{-\infty}^{+\infty} w(x-x') p(x', t') dx' \right] dt', \quad (4.25a)$$

with $p(x, 0) = \delta(x)$.

Special choices of the memory function $H(t)$ are (i) and (ii), see Eqs. (4.26) and (4.30):

$$(i) \quad H(t) = \delta(t) \quad \text{corresponding to} \quad \tilde{H}(s) = 1, \quad (4.26)$$

giving the *exponential waiting time* with

$$\tilde{\phi}(s) = \frac{1}{1+s}, \quad \phi(t) = \Psi(t) = e^{-t}. \quad (4.27)$$

In this case we obtain in the Fourier–Laplace domain

$$s\hat{\tilde{p}}(\kappa, s) - 1 = [\hat{w}(\kappa) - 1] \hat{\tilde{p}}(\kappa, s), \quad (4.28)$$

and in the space–time domain the *classical Kolmogorov–Feller equation*

$$\frac{\partial}{\partial t} p(x, t) = -p(x, t) + \int_{-\infty}^{+\infty} w(x - x') p(x', t) dx', \quad p(x, 0) = \delta(x). \quad (4.29)$$

$$(ii) \quad H(t) = \frac{t^{-\beta}}{\Gamma(1-\beta)}, \quad 0 < \beta < 1, \text{ corresponding to } \tilde{H}(s) = s^{\beta-1}, \quad (4.30)$$

giving the *Mittag-Leffler waiting time* with

$$\tilde{\phi}(s) = \frac{1}{1+s^\beta}, \quad \phi(t) = -\frac{d}{dt} E_\beta(-t^\beta) = \phi^{\text{ML}}(t), \quad \Psi(t) = E_\beta(-t^\beta). \quad (4.31)$$

In this case we obtain in the Fourier–Laplace domain

$$s^{\beta-1} [s\hat{\tilde{p}}(\kappa, s) - 1] = [\hat{w}(\kappa) - 1] \hat{\tilde{p}}(\kappa, s), \quad (4.32)$$

and in the space–time domain the *time-fractional Kolmogorov–Feller equation*

$${}_t D_*^\beta p(x, t) = -p(x, t) + \int_{-\infty}^{+\infty} w(x - x') p(x', t) dx', \quad p(x, 0^+) = \delta(x), \quad (4.33)$$

where ${}_t D_*^\beta$ denotes the fractional derivative of order β in the Caputo sense, see Appendix A, compare with [29].

The time-fractional Kolmogorov–Feller equation can also be expressed via the Riemann–Liouville fractional derivative ${}_t D^{1-\beta}$, see again Appendix A, that is

$$\frac{\partial}{\partial t} p(x, t) = {}_t D^{1-\beta} \left[-p(x, t) + \int_{-\infty}^{+\infty} w(x - x') p(x', t) dx' \right], \quad (4.34)$$

with $p(x, 0^+) = \delta(x)$. The equivalence of the two forms (4.33) and (4.34) is easily proved in the Fourier–Laplace domain by multiplying both sides of Eq. (4.32) with the factor $s^{1-\beta}$.

We note that the choice (i) may be considered as a limit of the choice (ii) as $\beta = 1$. In fact, in this limit we find $\tilde{H}(s) \equiv 1$ so $H(t) = t^{-1}/\Gamma(0) \equiv \delta(t)$ (according to a formal representation of the Dirac generalized function

[13]), so that Eqs. (4.23) and (4.24) reduce to (4.28) and (4.29), respectively. In this case the order of the Caputo derivative reduces to 1 and that of the R–L derivative to 0, whereas the Mittag-Leffler waiting time law reduces to the exponential.

In the sequel we will formally unite the choices (*i*) and (*ii*) by defining what we call the Mittag-Leffler memory function

$$H^{\text{ML}}(t) = \begin{cases} \frac{t^{-\beta}}{\Gamma(1-\beta)}, & \text{if } 0 < \beta < 1, \\ \delta(t), & \text{if } \beta = 1, \end{cases} \quad (4.35)$$

whose Laplace transform is

$$\tilde{H}^{\text{ML}}(s) = s^{\beta-1}, \quad 0 < \beta \leq 1. \quad (4.36)$$

Thus we will consider the whole range $0 < \beta \leq 1$ by extending the Mittag-Leffler waiting-time law in (4.31) to include the exponential law (4.27).

Remark Equation (4.24) may be clearly supplemented by an arbitrary initial probability density $p(x,0) = f(x)$. The corresponding replacement of $\delta(x)$ by $f(x)$ in (4.16) then requires in (4.21) multiplication of the term $(1 - \tilde{\phi}(s))/s$ by $\widehat{f}(\kappa)$ and in (4.23) replacement of the LHS by $\tilde{H}(s) [s\widehat{p}(\kappa,s) - \widehat{f}(\kappa)]$. With $p(x,0) = \delta(x)$ we obtain the fundamental solution of (4.24) in $p(x,t)$.

4.4

Manipulations: Rescaling and Respeeding

We now consider two types of manipulations on the CTRW by acting on its governing equation (4.24) in its Fourier–Laplace representation (4.23).

- (A) *rescaling the waiting time*, and hence the whole time axis;
- (B) *respeeding the process*.

(A) means change of the unit of time (measurement). We replace the random waiting time T by a waiting time τT , with the positive *rescaling factor* τ . Our idea is to take $0 < \tau \ll 1$ in order to bring into near sight the distant future. In a moderate span of time we will have a large number of jump events. For $\tau > 0$ we get the rescaled waiting-time density

$$\phi_\tau(t) = \phi(t/\tau)/\tau, \quad \text{hence} \quad \tilde{\phi}_\tau(s) = \tilde{\phi}(\tau s). \quad (4.37)$$

By decorating also the density p with an index τ we obtain the rescaled integral equation of the CTRW in the Fourier–Laplace domain as

$$\tilde{H}_\tau(s) [\widehat{s\tilde{p}}_\tau(\kappa,s) - 1] = [\widehat{w}(\kappa) - 1] \widehat{\tilde{p}}_\tau(\kappa,s), \quad (4.38)$$

where, in analogy to (4.22),

$$\tilde{H}_\tau(s) = \frac{1 - \tilde{\phi}(\tau s)}{s \tilde{\phi}(\tau s)}. \quad (4.39)$$

(B) means multiplying the quantity representing $\frac{\partial}{\partial t} p(x, t)$ by a factor $1/a$, where $a > 0$ is the *respeeding factor*: $0 < a < 1$ means *deceleration*. $a > 1$ means *acceleration*, . In the Fourier–Laplace representation this means multiplying the RHS of Eq. (4.23) by the factor a since the expression $[s \hat{p}(\kappa, s) - 1]$ corresponds to $\frac{\partial}{\partial t} p(x, t)$.

We now chose to consider the procedures of rescaling and respeeding in their combination so that the equation in the transformed domain of the rescaled and respeeded process has the form

$$\tilde{H}_\tau(s) [s \hat{p}_{\tau,a}(\kappa, s) - 1] = a [\hat{w}(\kappa) - 1] \hat{p}_{\tau,a}(\kappa, s). \quad (4.40)$$

Clearly, the two manipulations can be discussed separately: the choice $\{\tau > 0, a = 1\}$ means *pure rescaling*, the choice $\{\tau = 1, a > 0\}$ means *pure respeeding* of the original process. In the special case $\tau = 1$ we only respeed the original system; if $0 < \tau \ll 1$ we can counteract the compression effected by rescaling to obtain again a moderate number of events in a moderate span of time by respeeding (decelerating) with $0 < a \ll 1$. These vague notions will become clear as soon as we consider power-law waiting times.

Defining now

$$\tilde{H}_{\tau,a}(s) := \frac{\tilde{H}_\tau(s)}{a} = \frac{1 - \tilde{\phi}(\tau s)}{as \tilde{\phi}(\tau s)}, \quad (4.41)$$

we finally get, in analogy to (4.23), the equation

$$\tilde{H}_{\tau,a}(s) [s \hat{p}_{\tau,a}(\kappa, s) - 1] = [\hat{w}(\kappa) - 1] \hat{p}_{\tau,a}(\kappa, s). \quad (4.42)$$

What is the combined effect of rescaling and respeeding on the waiting-time density?

In analogy to (4.22) and taking account of (4.41) we find

$$\tilde{\phi}_{\tau,a}(s) = \frac{1}{1 + s \tilde{H}_{\tau,a}(s)} = \frac{1}{1 + s \frac{1 - \tilde{\phi}(\tau s)}{as \tilde{\phi}(\tau s)}}, \quad (4.43)$$

and so, for the deformation of the waiting-time density, the *essential formula*

$$\tilde{\phi}_{\tau,a}(s) = \frac{a \tilde{\phi}(\tau s)}{1 - (1 - a) \tilde{\phi}(\tau s)}. \quad (4.44)$$

Remark The formula (4.44) has the same structure as the thinning formula (4.10) by identification of a with q . In both the problems, we have a rescaled process defined by a time scale τ , and we send the relevant factors τ , a , and q to zero under a proper relationship. However in the thinning theory the relevant independent parameter going to 0 is that of thinning (actually respeeding) whereas in the present problem it is the rescaling parameter τ .

4.5

Power Laws and Asymptotic Universality of the Mittag-Leffler Waiting-Time Density

We have essentially two different situations for the waiting-time distribution according to its first moment (the expectation value) being finite or infinite. In other words, we assume for the waiting time PDF $\phi(t)$ either

$$\rho := \int_0^\infty t' \phi(t') dt' < \infty, \quad \text{labeled as } \beta = 1, \quad (4.45)$$

or

$$\phi(t) \sim c t^{-(\beta+1)} \text{ for } t \rightarrow \infty \quad \text{hence} \quad \Psi(t) \sim \frac{c}{\beta} t^{-\beta}, \quad 0 < \beta < 1, \quad c > 0. \quad (4.46)$$

For convenience we have dispensed in (4.46) with decorating by a slowly varying function at infinity the asymptotic power law. Then, by the standard Tauberian theory (see [12, 68]), the above conditions (4.45) and (4.46) mean in the Laplace domain the (comprehensive) asymptotic form

$$\tilde{\phi}(s) = 1 - \lambda s^\beta + o(s^\beta) \quad \text{for } s \rightarrow 0^+, \quad 0 < \beta \leq 1, \quad (4.47)$$

where we have

$$\lambda = \rho, \quad \text{if } \beta = 1; \quad \lambda = c\Gamma(-\beta) = \frac{c}{\Gamma(\beta+1)} \frac{\pi}{\sin(\beta\pi)}, \quad \text{if } 0 < \beta < 1. \quad (4.48)$$

Then, fixing s as required by the continuity theorem of probability theory for Laplace transforms, taking

$$a = \lambda \tau^\beta, \quad (4.49)$$

and sending τ to zero, we obtain in the limit the Mittag-Leffler waiting-time law. In fact, Eqs. (4.44) and (4.47) imply as $\tau \rightarrow 0$ with $0 < \beta \leq 1$,

$$\tilde{\phi}_{\tau, \lambda \tau^\beta}(s) = \frac{\lambda \tau^\beta [1 - \lambda \tau^\beta s^\beta + o(\tau^\beta s^\beta)]}{1 - (1 - \lambda \tau^\beta) [1 - \lambda \tau^\beta s^\beta + o(\tau^\beta s^\beta)]} \rightarrow \frac{1}{1 + s^\beta}, \quad (4.50)$$

the Laplace transform of $\phi^{\text{ML}}(t)$, see (4.1) and Appendix C. This formula expresses the *asymptotic universality of the Mittag-Leffler waiting-time law* that includes the exponential law for $\beta = 1$. It can easily be generalized to the case of

power laws decorated with slowly varying functions, thereby using the generalized Tauberian theory by Karamata (see again [12, 68]).

Comment The formula (4.50) says that our general power-law waiting time density is gradually deformed into the Mittag-Leffler waiting-time density as τ tends to zero.

Remark Let us stress here the distinguished character of the Mittag-Leffler waiting-time density $\phi^{\text{ML}}(t) = -\frac{d}{dt}E_\beta(-t^\beta)$ defined in (4.1). Considering its Laplace transform

$$\tilde{\phi}^{\text{ML}}(s) = \frac{1}{1+s^\beta}, \quad 0 < \beta \leq 1, \quad (4.51)$$

we can easily prove the identity

$$\tilde{\phi}_{\tau,a}^{\text{ML}}(s) = \tilde{\phi}^{\text{ML}}(\tau s/a^{1/\beta}) \quad \text{for all } \tau > 0, \quad a > 0. \quad (4.52)$$

Note that Eq. (4.52) states the *self-similarity* of the combined operation *rescaling–respeeding* for the Mittag-Leffler waiting-time density. In fact, (4.52) implies $\phi_{\tau,a}^{\text{ML}}(t) = \phi^{\text{ML}}(t/c)/c$ with $c = \tau/a^{1/\beta}$, which means replacing the random waiting time T^{ML} by $c T^{\text{ML}}$. As a consequence, choosing $a = \tau^\beta$ we have

$$\tilde{\phi}_{\tau,\tau^\beta}^{\text{ML}}(s) = \tilde{\phi}^{\text{ML}}(s) \quad \text{for all } \tau > 0. \quad (4.53)$$

Hence the Mittag-Leffler waiting-time density is invariant against combined rescaling with τ and respeeding with $a = \tau^\beta$.

Observing (4.50) we can say that $\phi^{\text{ML}}(t)$ is a $\tau \rightarrow 0$ attractor for any power-law waiting time (4.46) under simultaneous rescaling with τ and respeeding with $a = \lambda \tau^\beta$.

Remark In other words, this attraction property of the Mittag-Leffler probability distribution with respect to power-law waiting times (with $0 < \beta \leq 1$) is a kind of analogy to the attraction of sums of power-law jump distributions by stable distributions.

4.6

Passage to the Diffusion Limit in Space

We have again two different situations for the jump-width distribution but according to its second moment being finite or infinite. In other words we

assume for the jump-width probability density $w(x)$ (assumed for simplicity to be symmetric: $w(x) = w(-x)$) either

$$\sigma^2 := \int_{-\infty}^{+\infty} x^2 w(x) dx < \infty, \quad \text{labeled as } \alpha = 2, \quad (4.54)$$

or

$$w(x) \sim b |x|^{-(\alpha+1)} \quad \text{for } |x| \rightarrow \infty, \quad 0 < \alpha < 2, \quad b > 0. \quad (4.55)$$

Then we have the asymptotic relation, compare, e.g., with [16, 20–22],

$$\hat{w}(\kappa) = 1 - \mu |\kappa|^\alpha + o(|\kappa|^\alpha) \quad \text{for } \kappa \rightarrow 0, \quad (4.56)$$

where

$$\mu = \frac{\sigma^2}{2} \quad \text{if } \alpha = 2, \quad \mu = \frac{b \pi}{\Gamma(\alpha + 1) \sin(\alpha \pi / 2)} \quad \text{if } 0 < \alpha < 2. \quad (4.57)$$

The above asymptotic relations are known in the framework of the attraction properties of the stable densities. We note that the classical book by Gnedenko and Kolmogorov [14] has unfortunately the wrong constant μ for $0 < \alpha < 2$. As before we dispense with the possible decoration of the relevant power law by a slowly varying function.

By another respeeding, in fact an acceleration, we can pass over to space-time fractional diffusion processes. For this we have *three choices*:

- (a) *diffusion limit in space only, for general waiting time,*
- (b) *diffusion limit in space only, for ML waiting time,*
- (c) *joint limit in time and space (with power laws in both) with scaling relation.*

Note that (b) is just a special case of (a) but of particular relevance (as we shall see).

In all the three cases we rescale the jump density by a factor $h > 0$, replacing the random jumps X by hX . This means changing the unit of measurement in space from 1 to $1/h$, with $0 < h \ll 1$, so bringing into near sight the far-away space. We get the rescaled jump density as $w_h(x) = w(x/h)/h$, corresponding to $\hat{w}_h(\kappa) = \hat{w}(h\kappa)$.

Choice (a): diffusion limit in space only, with a general waiting-time law.

Starting from Eq. (4.23), the Laplace–Fourier representation of the CTRW equation, without special assumption on the waiting-time density, we fix the Fourier variable κ and accelerate the spatially rescaled process by the respeeding factor $1/(\mu h^\alpha)$, arriving at the equation (using q_h as new dependent variable)

$$\tilde{H}(s) \left[s \hat{q}_h(\kappa, s) - 1 \right] = \frac{\hat{w}(h\kappa) - 1}{\mu h^\alpha} \hat{q}_h(\kappa, s). \quad (4.58)$$

Then, fixing κ as required by the continuity theorem of probability theory for Fourier transforms, and sending h to zero we get, noting that $[\widehat{w}(h\kappa) - 1]/(\mu h^\alpha) \rightarrow -|\kappa|^\alpha$, and writing u in place of q_0 ,

$$\widetilde{H}(s) \left[s\widehat{\bar{u}}(\kappa, s) - 1 \right] = -|\kappa|^\alpha \widehat{\bar{u}}(\kappa, s), \quad (4.59)$$

where we still have, consistently with (4.22),

$$\widetilde{H}(s) = \frac{1 - \widetilde{\phi}(s)}{s \widetilde{\phi}(s)} = \frac{\widetilde{\Psi}(s)}{\widetilde{\phi}(s)}, \quad (4.60)$$

being $\phi(t)$ the original waiting-time density. In physical space–time we have the integro-pseudodifferential equation

$$\int_0^t H(t-t') \frac{\partial}{\partial t'} u(x, t') dt' = {}_x D_0^\alpha u(x, t), \quad 0 < \alpha \leq 2, \quad (4.61)$$

with $-|\kappa|^\alpha$ as the symbol of the Riesz pseudodifferential operator ${}_x D_0^\alpha$ usually referred to as the Riesz fractional derivative of order α , see Appendix B.

Comment By this rescaling and acceleration the jumps become smaller and smaller, their number in a given span of time larger and larger, and the waiting times between jumps smaller and smaller. In the limit there are no waiting times anymore, the original waiting-time density $\phi(t)$ is now only spiritual, but still determines via $H(t)$ the memory of the process. Equation (4.61) offers a great variety of diffusion processes with memory depending on the choice of the function $H(t)$.

Choice (b): diffusion limit in space only, with a Mittag-Leffler waiting-time law.
We now choose in Eq. (4.61) the Mittag-Leffler memory function (4.35), namely

$$H(t) = H^{\text{ML}}(t), \quad \text{hence} \quad \widetilde{H}(s) = 1/s^{(1-\beta)}, \quad (4.62)$$

corresponding to the Mittag-Leffler waiting-time law

$$\phi^{\text{ML}}(t) = -\frac{d}{dt} E_\beta(-t^\beta), \quad 0 < \beta \leq 1, \quad (4.63)$$

consistently with the time-fractional Kolmogorov–Feller equation (4.33), that includes for $\beta = 1$ the classical Kolmogorov–Feller equation (4.29). As a consequence of our spatial diffusion limit, compare with [23, 44], we so arrive immediately at the *space–time fractional diffusion equation*

$${}_t D_*^\beta u(x, t) = {}_x D_0^\alpha u(x, t), \quad 0 < \alpha \leq 2, \quad 0 < \beta \leq 1. \quad (4.64)$$

Choice (c): Diffusion limit combined in time and space.

Assuming the behavior for the waiting-time density as in Eqs. (4.45) and (4.46), and for the jump-width density as in Eqs. (4.54) and (4.55), rescaling as described the waiting times and the jumps by factors τ and h , starting from (4.40), decelerating by a factor $\lambda \tau^\beta$ in time, then accelerating for space by a factor $1/(\mu h^\alpha)$, we obtain (compare to Section 4.4, case (B)), fixing s and κ and setting, for convenience

$$a(\tau, h) = \frac{\lambda \tau^\beta}{\mu h^\alpha}, \quad (4.65)$$

$$\tilde{H}_\tau(s) \left[s \tilde{\hat{p}}_{\tau,a(\tau,h)}(\kappa, s) - 1 \right] = a(\tau, h) [\tilde{w}_h(\kappa) - 1] \tilde{\hat{p}}_{\tau,a(\tau,h)}(\kappa, s), \quad (4.66)$$

with $\tilde{w}_h(\kappa) = \tilde{w}(h\kappa)$ and

$$\tilde{H}_\tau(s) = \frac{1 - \tilde{\phi}(\tau s)}{s \tilde{\phi}(\tau s)} \sim \lambda \tau^\beta s^{\beta-1}. \quad (4.67)$$

Fixing $a(\tau, h)$ to the constant value 1, which means introducing the relationship of *well-scaledness*

$$a(\tau, h) = \frac{\lambda \tau^\beta}{\mu h^\alpha} \equiv 1, \quad (4.68)$$

between the rescaling of time and space, we get

$$\tilde{H}_\tau(s) \sim \lambda \tau^\beta s^{\beta-1}, \quad \text{for } \tau \rightarrow 0. \quad (4.69)$$

Because of

$$\frac{\tilde{w}(h\kappa) - 1}{\mu h^\alpha} \rightarrow -|\kappa|^\alpha, \quad \text{for } h \rightarrow 0, \quad (4.70)$$

we finally get the limiting equation

$$s^{\beta-1} \left[s \tilde{\hat{u}}(\kappa, s) - 1 \right] = -|\kappa|^\alpha \tilde{\hat{u}}(\kappa, s), \quad (4.71)$$

corresponding to Eq. (4.64), the space–time fractional diffusion equation.

Comments on some mathematical and physical aspects:

1. The Mittag-Leffler waiting time (choice (b)), obeying the asymptotics (4.46) with $\lambda = 1$ leads from (4.61) directly to the space–time fractional diffusion equation (4.64), without requirement of rescaling and deceleration in time, and with these procedures we arrive likewise at (4.64). This strange fact is caused by the invariance of the Mittag-Leffler density to the combined effects of rescaling by τ and deceleration by τ^β , expressed in Eq. (4.53).

2. Going again through our preceding deductions, we observe that the combined (well-scaled) passage of τ and h , under the relation (4.68), toward zero can be split in two distinct ways into two separate passages. *First way:* keep h fixed letting τ tend to zero, then in the resulting model send also h to zero. *Second way:* interchange the order played by h and τ in the first way. Under our power law assumptions we can transform (4.24), the basic integral equation of CTRW, into Eq. (4.33) (time-fractional CTRW) by rescaling–respeeding manipulation only in the time variable, and then by rescaling in space followed by an acceleration into (4.64), the space–time fractional diffusion equation. Or we can transform (4.24) by rescaling in space followed by an acceleration into Eq. (4.61) (general space fractional diffusion with memory), and then by rescaling–respeeding in the time variable arrive at (4.64).
3. Where have the waiting times gone in the space–time fractional diffusion equation (4.64)? We can answer this question by interpreting Eq. (4.66) under the scaling relation (4.68) as the Fourier–Laplace representation

$$\tilde{H}_\tau(s) \left[s \hat{\tilde{p}}_{\tau,1}(\kappa, s) - 1 \right] = [\tilde{w}_h(\kappa) - 1] \hat{\tilde{p}}_{\tau,1}(\kappa, s), \quad (4.72)$$

of our original CTRW (4.16), whose Fourier–Laplace representation (4.23) coincides with (4.72) if we delete all decorations with indices there. Thus Eq. (4.72) represents the same physical process as (4.16) but expressed in terms of new units $1/\tau$ and $1/h$ of time and space, respectively. However, the respeeding factor $a(\tau, h)$ being fixed to 1, there is no change of physical speed. When these new units are made smaller and smaller, moderate spans of time and space become numerically smaller and smaller, shrinking toward zero as τ and h tend to zero, and likewise the waiting times and the jump widths shrink to zero. The distant future and the far-away space come numerically into near sight. As long as τ and h are positive, we always have the same physical process, only measured in other units. The finally resulting space–time fractional diffusion process (4.64) remembers the power laws for waiting times and jumps in form of the orders β and α of fractional differentiation.

4. An objection could be raised against the somewhat mystical actions of respeeding. Namely, if the respeeding factor a in Eq. (4.40) differs from 1, the underlying renewal process and consequently the whole CTRW are distorted. However, for the CTRW we carry out the actions of deceleration and acceleration in either order in succession or simultaneously in combination, and by our special choice of these factors they cancel each other in effect, so that there remains no physical distortion. This is particularly obvious in our choice (c), see the above comment (γ).
5. Let us finally point out an advantage of splitting the passages $\tau \rightarrow 0$ and $h \rightarrow 0$. Whereas by the combined passage as in choice (c), if done in the

well-scaled way (4.68), the mystical concept of respeeding can be avoided, there arises the question of correct use of the continuity theorems of probability. There is one continuity theorem for the Laplace transform, one for the Fourier transform, see [12]. Possible doubts whether their simultaneous use is legitimate vanish by applying them in succession, as in our two splitting methods.

Discussion on the involved stochastic processes:

In our investigations we have met four types of spatially one-dimensional stochastic processes for the sojourn probability density $p(x, t)$ or $u(x, t)$. For the reader's convenience let us give a list of these processes in physical coordinates, referring to the preceding text for details, and remind briefly how they can be connected by appropriate scaling and passages to the limit. Let us note that in all these processes the initial condition $\delta(x)$ for $p(x, 0^+)$ or $u(x, 0^+)$ can be replaced by a more general PDF $f(x)$.

(I) The integral equation for the CTRW is, see (4.16) and (4.17),

$$p(x, t) = p(x, 0^+) \Psi(t) + \int_0^t \phi(t - t') \left[\int_{-\infty}^{+\infty} w(x - x') p(x', t') dx' \right] dt' \quad (4.73)$$

is equivalent, by the introduction of the memory function $H(t)$, see (4.22), to the generalized Kolmogorov–Feller equation, see (4.24),

$$\int_0^t H(t - t') \frac{\partial}{\partial t'} p(x, t') dt' = -p(x, t) + \int_{-\infty}^{+\infty} w(x - x') p(x', t) dx'. \quad (4.74)$$

(II) The time-fractional Kolmogorov–Feller equation, see (4.33),

$${}_t D_*^\beta p(x, t) = -p(x, t) + \int_{-\infty}^{+\infty} w(x - x') p(x', t) dx', \quad 0 < \beta \leq 1. \quad (4.75)$$

(III) The integro-pseudodifferential equation of space fractional diffusion with general memory, see (4.61),

$$\int_0^t H(t - t') \frac{\partial}{\partial t'} u(x, t') dt' = {}_x D_0^\alpha u(x, t), \quad 0 < \alpha \leq 2. \quad (4.76)$$

(IV) The space–time fractional diffusion equation, see (4.64),

$${}_t D_*^\beta u(x, t) = {}_x D_0^\alpha u(x, t) \quad 0 < \beta \leq 1, \quad 0 < \alpha \leq 2. \quad (4.77)$$

We now sketch shortly how these four evolution equations are connected in our theory. Eq. (I) goes over in Eq. (II), likewise Eq. (III) in Eq. (IV) by the special choice $H(t) = H^{\text{ML}}(t)$ for the memory function, see (4.35). Under our power-law assumption for the waiting time, see (4.45) and (4.46), these transitions can be achieved asymptotically by manipulation via rescaling and respeeding of the underlying renewal process.

Under our power-law assumption for the jumps, see (4.54) and (4.55), the transition from Eq. (I) to Eq. (III) and from (II) to (IV) can be achieved asymptotically by passage to the diffusion limit only in space.

Under our power-law assumption for time *and* space there is a direct way from Eq. (I) to Eq. (IV), namely *the well-scaled passage to the diffusion limit*, for which the condition (4.68) is relevant.

4.7

The Time-Fractional Drift Process

It is instructive to study the spatial transition to the diffusion limit for the *Mittag-Leffler renewal process*. As said in Section 4.3 this renewal process, viewed as a CTRW by treating its counting function N as a spatial variable x , is obtained by choosing $w(x) = \delta(x - 1)$ as the jump width density, see Eq. (4.18). Its waiting-time density is, see (4.1), (4.31),

$$\phi(t) = \phi^{\text{ML}}(t) = -\frac{d}{dt}E_\beta(-t^\beta), \quad 0 < \beta \leq 1. \quad (4.78)$$

We have $\tilde{H}(s) = s^{\beta-1}$, $\widehat{w}(\kappa) = e^{i\kappa}$, hence

$$s^{\beta-1} \left[s\widehat{p}(\kappa, s) - 1 \right] = (e^{i\kappa} - 1) \widehat{p}(\kappa, s). \quad (4.79)$$

Rescaling in space by a factor h and accelerating (because of $w(\kappa) = e^{i\kappa} = 1 + i\kappa + o(\kappa)$ for $\kappa \rightarrow 0$) this pure renewal process by the factor $1/h$ we get a process

$$s^{\beta-1} \left[s\widehat{q}_h(\kappa, s) - 1 \right] = \frac{1}{h} (e^{ih\kappa} - 1) \widehat{q}_h(\kappa, s), \quad (4.80)$$

which as $h \rightarrow 0$ and κ fixed gives

$$s^{\beta-1} \left[s\widehat{u}(\kappa, s) - 1 \right] = i\kappa \widehat{u}(\kappa, s), \quad (4.81)$$

which implies

$$\widehat{u}(\kappa, s) = \frac{s^{\beta-1}}{s^\beta - i\kappa}. \quad (4.82)$$

We note that Eq. (4.81) corresponds to the time-fractional drift equation

$${}_t D_*^\beta u(x, t) = -\frac{\partial}{\partial x} u(x, t), \quad u(x, 0) = \delta(x), \quad x \in \mathbf{R}^+, t \in \mathbf{R}^+. \quad (4.83)$$

By using the known scaling rules for the Fourier and Laplace transforms,

$$f(ax) \xleftrightarrow{\mathcal{F}} a^{-1} \hat{f}(k/a), \quad a > 0, \quad f(bt) \xleftrightarrow{\mathcal{L}} b^{-1} \tilde{f}(s/b), \quad b > 0, \quad (4.84)$$

we infer directly from (4.82) (thus without inverting the two transforms) the following *scaling property* of the (fundamental) solution

$$u(ax, bt) = b^{-\beta} u(ax/b^\beta, t). \quad (4.85)$$

Consequently, introducing the *self-similarity variable* x/t^β , we can write

$$u(x, t) = t^{-\beta} U(x/t^\beta), \quad (4.86)$$

where $U(x) \equiv u(x, 1)$.

To determine the solution in the space-time domain we can follow two alternative strategies related to the different order in carrying out the inversion of the Fourier–Laplace transforms in (4.82). Indeed we can

- (S1) Invert the Fourier transform getting $\tilde{u}(x, s)$, and then invert this Laplace transform,
- (S2) Invert the Laplace transform getting $\hat{u}(k, t)$, and then invert this Fourier transform.

Strategy (S1): Recalling the Fourier transform pair,

$$a e^{-xb} \Theta(x) \xleftrightarrow{\mathcal{F}} \frac{a}{b - ik}, \quad b > 0, \quad (4.87)$$

where $\Theta(x)$ denotes the unit step Heaviside function, we get

$$\tilde{u}(x, s) = s^{\beta-1} e^{-xs^\beta} \Theta(x). \quad (4.88)$$

In view of the fact that $\exp(-s^\beta)$ is the Laplace transform of the extremal unilateral stable density of order β , $L_\beta^{-\beta}(t)$ (see for notation Appendix B), we recognize that the solution in the space-time domain can be expressed in terms of a R–L fractional integral (see Appendix A) of such density, namely

$$u(x, t) = \frac{1}{x^{1/\beta}} {}_t J^{1-\beta} \left[L_\beta^{-\beta} (t/x^{1/\beta}) \right]. \quad (4.89)$$

Working in the Laplace domain we can note that the fundamental solution of our fractional drift equation (4.83) is simply related to that of the time-fractional diffusion wave equation

$${}_t D_*^{2\beta} u(x, t) = \frac{\partial^2}{\partial x^2} u(x, t), \quad 0 < \beta \leq 1, \quad x \in \mathbf{R}, t \in \mathbf{R}^+, \quad (4.90)$$

equipped with the initial conditions $u(x, 0^+) = \delta(x)$ if $0 < \beta \leq 1$ and $\frac{\partial}{\partial t} u(x, 0^+) = 0$ if $1/2 < \beta \leq 1$. In fact, the solution of (4.90) turns out the half of the solution (4.89) of our time-fractional drift equation (4.83), extended in a symmetric way to all of \mathbf{R} , as can be seen by factorizing Eq. (4.90) as

$$\left({}_t D_*^{2\beta} - \frac{\partial^2}{\partial x^2} \right) u(x, t) = \left({}_t D_*^\beta - \frac{\partial}{\partial x} \right) \left({}_t D_*^\beta + \frac{\partial}{\partial x} \right) u(x, t) = 0. \quad (4.91)$$

Indeed Eq. (4.90) was solved by using the Laplace transform strategy by Mainardi in the 1990s, see e.g., [37, 38, 43] where the reader can find mathematical details of the proof and instructive plots of the fundamental solution. Then, based on Mainardi's analysis, we can state that the required solution of Eq. (4.83) reads

$$u(x, t) = t^{-\beta} M_\beta(x/t^\beta) \Theta(x), \quad (4.92)$$

where M denotes the function of Wright type defined in the complex plane

$$M_\beta(z) = \sum_{n=0}^{\infty} \frac{(-z)^n}{n! \Gamma[-\beta n + (1-\beta)]} = \frac{1}{\pi} \sum_{n=1}^{\infty} \frac{(-z)^{n-1}}{(n-1)!} \Gamma(\beta n) \sin(\pi \beta n). \quad (4.93)$$

The M function is a special case of the Wright function defined by the series representation, valid in the whole complex plane,

$$\Phi_{\lambda, \mu}(z) := \sum_{n=0}^{\infty} \frac{z^n}{n! \Gamma(\lambda n + \mu)}, \quad \lambda > -1, \quad \mu \in \mathbf{C}, \quad z \in \mathbf{C}. \quad (4.94)$$

Indeed, we recognize

$$M_\beta(z) = \Phi_{-\beta, 1-\beta}(-z), \quad 0 < \beta < 1. \quad (4.95)$$

Originally, Wright introduced and investigated this function with the restriction $\lambda \geq 0$ in a series of notes starting from 1933 in the framework of the asymptotic theory of partitions. Only later in 1940, he considered the case $-1 < \lambda < 0$. We note that in the handbook of the Bateman Project [10] (see Vol. 3, Ch. 18), presumably for a misprint, λ is restricted to be nonnegative. For further mathematical details on the M -Wright function we recommend [17, 18, 24].

For our time-fractional drift equation (4.83) we note the particular case $\beta = 1/2$ for which we obtain

$$\beta = 1/2 : \quad u(x, t) = \frac{1}{\sqrt{\pi t}} \exp \left[-x^2/(4t) \right], \quad x \geq 0, \quad t \geq 0. \quad (4.96)$$

In the limiting case $\beta = 1$ we recover the rightward pure drift,

$$\beta = 1 : \quad u(x, t) = \frac{1}{t} \delta(x/t - 1) = \delta(x - t), \quad x \geq 0, \quad t \geq 0. \quad (4.97)$$

In view of the fact that M -Wright function of order β is related to the extremal unilateral stable density of order β , see [42], we conclude by displaying the alternative form of the solution of the time-fractional drift equation

$$u(x, t) = \frac{t}{\beta x^{1+1/\beta}} L_\beta^{-\beta} \left(t/x^{1/\beta} \right), \quad (4.98)$$

which, compared with (4.89), shows the effect of the fractional integral on the (extremal unilateral) stable density function $L_\beta^{-\beta}$.

Strategy (S2): Recalling the Laplace transform pair, see e.g., [10, 19],

$$E_\beta(ct^\beta) \xleftrightarrow{\mathcal{L}} \frac{s^{\beta-1}}{s^\beta - c}, \quad \operatorname{Re}(s) > |c|^{1/\beta}, \quad (4.99)$$

we get

$$\hat{u}(\kappa, t) = E_\beta(i\kappa t^\beta), \quad (4.100)$$

from which

$$u(x, t) = \frac{1}{2\pi} VP \int_{-\infty}^{+\infty} e^{-i\kappa x} E_\beta(i\kappa t^\beta) d\kappa, \quad (4.101)$$

where VP denotes the Cauchy principal value. Because, see [10], Vol. 3, Chapter XVIII on Miscellaneous Functions, Section 18.1 Eq. (7),

$$E_\beta(iy) \sim \frac{i}{\Gamma(1-\beta)y} \quad \text{for } y \rightarrow \pm\infty \quad \text{if } 0 < \beta < 1, \quad (4.102)$$

we see that $E_\beta(iy)$ does not tend to zero fast enough for the integral (4.101) to exist as a regular improper Riemann integral. But there should be no problem for existence as a Cauchy principal value integral. It can be shown that the present strategy based on Fourier integral (4.101) provides the result (4.92).

Remark Not wanting to overload our paper we have deliberately avoided the concept of *subordination* in fractional diffusion. But, referring to [25], let us say that if in (4.98) we replace x by t_* we get the *subordinator*, i.e. the probability law for generating the operational time t_* from the physical time t , see Eq. (5.20) in [25], and, in other notation, [46]. Because of its relation (4.100) via Fourier transform to the Mittag-Leffler function with imaginary argument, the probability law governing the process (4.98) sometimes is called the *Mittag-Leffler distribution*, see e.g., [46]. Although so named it must not be confused with our *Mittag-Leffler waiting-time distribution* whose density is given by (4.1).

4.8 Conclusions

The basic role of the Mittag-Leffler waiting time probability density in time-fractional continuous time random walk (CTRW) has become well known by

the fundamental paper of 1995 by Hilfer and Anton [29]. Earlier in the theory of thinning (rarefaction) of a renewal process under power-law assumptions, see the 1968 book by Gnedenko and Kovalenko [15], this density had been found as limit density by a combination of thinning followed by rescaling of time and imposing a proper relation between the rescaling factor and the thinning parameter. Likewise one arrives at this law when wanting to construct a certain special class of anomalous random walks, see the 1985 paper by Balakrishnan [1], the anomaly defined by growth of the second moment of the sojourn probability density like a power of time with exponent between 0 and 1. Balakrishnan's paper, having appeared a few years before the fundamental paper of 1989 by Schneider and Wyss [61], is difficult to read as it is written in a style different from the present one, so we will not go into details here. But let it be said that by well-scaled passage to the limit from CTRW (again under suitable power-law assumptions in space and time) he obtained the space-time fractional diffusion equation in the form of an equivalent integro-differential equation. Unfortunately, Balakrishnan's paper did not find the attention it would have deserved. However, due to the sad fact that the Mittag-Leffler function played too long a rather neglected role in treatises on special functions. Balakrishnan as well as Gnedenko and Kovalenko contented themselves with presenting their results only in the Laplace domain; they did not identify their limit density as a Mittag-Leffler type function.

Having worked ourselves for some time on questions of well-scaled passage to the diffusion limit from CTRW to fractional diffusion, see [21–23, 26, 45, 60], we got from the theory of thinning the idea that it should be possible to carry out the passages to the limit separately in space and in time. In time this can be done by a combination of rescaling time and respeeding the underlying process (formally treating it as a CTRW with unit steps in space). In fact, *thinning* in the sense of Gnedenko and Kovalenko transforms the original renewal process into one that is running more slowly and this effect can be balanced by proper choice of the rescaling factor. The result of our combination of rescaling and respeeding for a CTRW governed by a given renewal process with a generic power-law waiting time is a time-fractional CTRW. By another rescaling in space (now under power-law assumption for the jumps) which can be interpreted as a second respeeding we arrive at the already classical space-time fractional diffusion equation. In this way we shed new light on the long time and wide space behavior of continuous time random walks.

In a series of comments at the end of Section 4.6, we have explained how, by what we call *well-scaled* passage to the diffusion limit, the transition from the CTRW to the space-time fractional diffusion process actually can be obtained by merely rescaling time and space without any respeeding at all. However, the separate passages to the limit are more satisfying with respect to mathematical rigour.

Finally, in Section 4.7, we have treated the time-fractional drift process as a properly scaled limit of the counting function of a pure renewal process governed by a waiting-time law of Mittag-Leffler type. Our trick in finding the limiting waiting-time law of this renewal process consists in treating it as a CTRW with positive jumps of size 1 so that its counting number acts as a spatial variable. Then, by suitably rescaling this spatial variable, we obtain the long time behavior of the Mittag-Leffler renewal process as an interesting side result.

Appendix A: The Time-Fractional Derivatives

For a sufficiently well-behaved function $f(t)$ ($t \geq 0$) we define the *Caputo time-fractional derivative* of order β with $0 < \beta < 1$ through

$$\mathcal{L} \left\{ {}_t D_*^\beta f(t); s \right\} = s^\beta \tilde{f}(s) - s^{\beta-1} f(0^+), \quad f(0^+) := \lim_{t \rightarrow 0^+} f(t), \quad (\text{A.1})$$

so that

$${}_t D_*^\beta f(t) := \frac{1}{\Gamma(1-\beta)} \int_0^t \frac{f'(\tau)}{(t-\tau)^\beta} d\tau, \quad 0 < \beta < 1. \quad (\text{A.2})$$

Such operator has been referred to as the *Caputo fractional derivative* since it was introduced by Caputo in the late 1960s for modeling the energy dissipation in the rheology of the Earth, see [4, 5]. Soon later this derivative was adopted by Caputo and Mainardi in the framework of the linear theory of viscoelasticity, see [6].

The reader should observe that the *Caputo fractional derivative* differs from the usual *Riemann–Liouville* (R–L) fractional derivative

$${}_t D^\beta f(t) := \frac{d}{dt} \left[\frac{1}{\Gamma(1-\beta)} \int_0^t \frac{f(\tau) d\tau}{(t-\tau)^\beta} \right], \quad 0 < \beta < 1. \quad (\text{A.3})$$

Both the derivatives are related to the R–L fractional integral, which is defined for any order $\beta > 0$ as

$${}_t J^\beta f(t) := \frac{1}{\Gamma(\beta)} \int_0^t \frac{f(\tau) d\tau}{(t-\tau)^{1-\beta}}, \quad \beta > 0, \quad (\text{A.4})$$

so that $\mathcal{L} \{ {}_t J^\beta f(t); s \} = s^{-\beta} \tilde{f}(s)$. Incidentally ${}_t J^\alpha {}_t J^\beta = {}_t J^{\alpha+\beta}$ for $\alpha, \beta > 0$. Then, by virtue of Eqs. (A.2)–(A.4), the two fractional derivatives read as

$${}_t D^\beta := {}_t D^1 {}_t J^{1-\beta}, \quad 0 < \beta < 1, \quad (\text{A.5})$$

$${}_t D_*^\beta := {}_t J^{1-\beta} {}_t D^1, \quad 0 < \beta < 1. \quad (\text{A.6})$$

In particular, the R–L derivative of order β is the left inverse of the corresponding R–L fractional integral in that ${}_t D^\beta {}_t J^\beta f(t) = f(t)$.

We note the relationships between the two fractional derivatives (when both of them exist), for $0 < \beta < 1$,

$${}_t D_*^\beta f(t) = {}_t D^\beta [f(t) - f(0^+)] = {}_t D^\beta f(t) - \frac{t^{-\beta}}{\Gamma(1-\beta)} f(0^+). \quad (\text{A.7})$$

As a consequence we can interpret the Caputo derivative as a sort of regularization of the R-L derivative as soon as $f(0^+)$ is finite; in this sense such fractional derivative was independently introduced in 1968 by Dzherbashyan and Nersesian [9], as pointed out by Kochubei, see [33, 34]. In this respect the regularized fractional derivative is sometimes referred to as the *Caputo-Dzherbashyan derivative*.

We observe the different behavior of the two fractional derivatives (A.2), (A.3) at the end points of the parameter interval $(0, 1)$, as it can be noted from their definitions in operational terms (A.5), (A.6). In fact, while for $\beta \rightarrow 1^-$ both the derivatives reduce to ${}_t D^1$, due to the fact that the operator ${}_t J^0 = I$ commutes with ${}_t D^1$, for $\beta \rightarrow 0^+$ we have

$$\beta \rightarrow 0^+ \implies \begin{cases} {}_t D^\beta f(t) \rightarrow {}_t D^1 {}_t J^1 f(t) = f(t), \\ {}_t D_*^\beta f(t) \rightarrow {}_t J^1 {}_t D^1 f(t) = f(t) - f(0^+). \end{cases} \quad (\text{A.8})$$

The above behaviors have induced us to keep for the R-L derivative the same symbolic notation as for the standard derivative of integer order, while for the Caputo derivative to decorate the corresponding symbol with subscript $*$.

For the R-L derivative the Laplace transform reads for $0 < \beta < 1$

$$\begin{aligned} \mathcal{L} \left\{ {}_t D^\beta f(t); s \right\} &= s^\beta \tilde{f}(s) - g(0^+), \\ g(0^+) &= \lim_{t \rightarrow 0^+} g(t), \quad g(t) := {}_t J^{(1-\beta)} f(t). \end{aligned} \quad (\text{A.9})$$

Thus the rule (A.9) is more cumbersome to be used than (A.1) since it requires the initial value of an extra function $g(t)$ related to the given $f(t)$ through an R-L fractional integral. However, when $f(0^+)$ is finite we recognize $g(0^+) = 0$.

In the limit $\beta \rightarrow 1^-$ both the derivatives reduce to the derivative of the first order so we recover the corresponding standard formula for the Laplace transform:

$$\mathcal{L} \left\{ {}_t D^1 f(t); s \right\} = s \tilde{f}(s) - f(0^+). \quad (\text{A.10})$$

We conclude this appendix noting that in a proper way both the derivatives can be generalized for any order $\beta > 1$, see e.g., [19, 53].

Appendix B: The Space-Fractional Derivatives

Let us first recall that a generic linear pseudodifferential operator A , acting with respect to the variable $x \in \mathbf{R}$, is defined through its Fourier representation, namely

$$\mathcal{F}\{A f(x); \kappa\} := \int_{-\infty}^{+\infty} e^{i\kappa x} A f(x) dx = \widehat{A}(\kappa) \widehat{f}(\kappa), \quad \kappa \in \mathbf{R} \quad (\text{B.1})$$

where $\widehat{A}(\kappa)$ is referred to as the symbol of A , formally given as

$$\widehat{A}(\kappa) = (A e^{-i\kappa x}) e^{+i\kappa x}. \quad (\text{B.2})$$

The fractional Riesz derivative ${}_x D_0^\alpha$ is defined as the pseudodifferential operator with symbol $-|\kappa|^\alpha$. This means that for a sufficiently well-behaved (generalized) function $f(x)$ ($x \in \mathbf{R}$) we have

$$\mathcal{F}\{{}_x D_0^\alpha f(x); \kappa\} = -|\kappa|^\alpha \widehat{f}(\kappa), \quad \kappa \in \mathbf{R}. \quad (\text{B.3})$$

The symbol of the Riesz fractional derivative is nothing but the logarithm of the characteristic function of the generic symmetric *stable* (in the Lévy sense) probability density, see [11, 12, 57]. Noting $-|\kappa|^\alpha = -(\kappa^2)^{\alpha/2}$, we recognize that

$${}_x D_0^\alpha = - \left(-\frac{d^2}{dx^2} \right)^{\alpha/2}. \quad (\text{B.4})$$

In other words, the Riesz derivative is a symmetric fractional generalization of the second derivative to orders less than 2. In an explicit way the Riesz derivative reads, for $0 < \alpha < 2$,

$$\begin{aligned} {}_x D_0^\alpha f(x) &= \frac{d^\alpha}{d|x|^\alpha} f(x) \\ &= \Gamma(1 + \alpha) \frac{\sin(\alpha\pi/2)}{\pi} \int_0^\infty \frac{f(x + \xi) - 2f(x) + f(x - \xi)}{\xi^{1+\alpha}} d\xi, \end{aligned} \quad (\text{B.5})$$

where in the LHS we have also adopted the alternative and illuminating notation introduced by Zaslavsky, see e.g., [56]. This operator is referred to as the *Riesz fractional derivative* since it is obtained from the inversion of the fractional integral originally introduced by Marcel Riesz in the late 1940s, known as the *Riesz potential*, see e.g., [57]. It is based on a suitable regularization of a hypersingular integral, according to a method formerly introduced by Marchaud in 1927.

Remark Straightforward generalization to the *Riesz–Feller derivative* of order α and skewness θ is possible. Such pseudodifferential operator is denoted by us as

$${}_x D_\theta^\alpha, \quad \text{with} \quad 0 < \alpha \leq 2, \quad \theta \in \mathbf{R}, \quad |\theta| \leq \min\{\alpha, 2 - \alpha\}. \quad (\text{B.6})$$

In this case we have

$$\mathcal{F}\{ {}_x D_\theta^\alpha f(x); \kappa \} = -|\kappa|^\alpha i^\theta \operatorname{sign} \kappa \hat{f}(\kappa) \quad \kappa \in \mathbf{R}. \quad (\text{B.7})$$

In an explicit way the Riesz–Feller derivative reads, for $0 < \alpha < 2$,

$$\begin{aligned} {}_x D_\theta^\alpha f(x) &= \frac{\Gamma(1 + \alpha)}{\pi} \left\{ \sin[(\alpha + \theta)\pi/2] \int_0^\infty \frac{f(x + \xi) - f(x)}{\xi^{1+\alpha}} d\xi \right. \\ &\quad \left. + \sin[(\alpha - \theta)\pi/2] \int_0^\infty \frac{f(x - \xi) - f(x)}{\xi^{1+\alpha}} d\xi \right\}. \end{aligned} \quad (\text{B.8})$$

Note that in (B.7) that $i^\theta \operatorname{sign} \kappa = \exp[i(\operatorname{sign} \kappa)\theta\pi/2]$. Thus the symbol of the Riesz–Feller fractional derivative is the logarithm of the characteristic function of the more general (strictly) *stable* probability density, closely following the Feller parameterization, see [11,12] revisited by the present authors in [20].

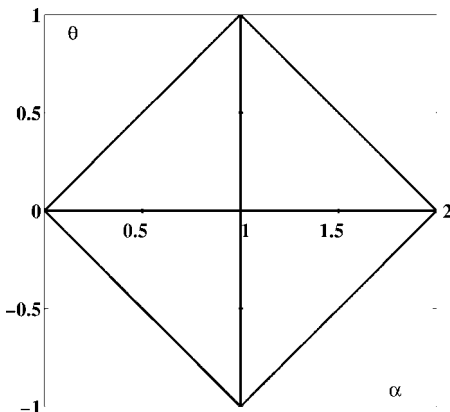


Figure B.1 The Feller–Takayasu diamond.

According to our notation, the strictly stable density of order α and skewness θ is denoted by $L_\alpha^\theta(x)$. We note that the allowed region for the parameters α and θ turns out to be a diamond in the plane $\{\alpha, \theta\}$ with vertices in the points $(0, 0)$, $(1, 1)$, $(2, 0)$, $(1, -1)$, that we call the *Feller–Takayasu diamond*, see Figure B.1. For more details we refer the reader to [42], where series representations and numerical plots of the stable densities $L_\alpha^\theta(x)$ are found. In particular, we recall that the extremal stable densities obtained for $\theta = \pm\alpha$ with $0 < \alpha < 1$ are unilateral, with support in \mathbf{R}^\mp , respectively.

Appendix C: The Mittag-Leffler Function

The Mittag-Leffler function with parameter β is defined as

$$E_\beta(z) := \sum_{n=0}^{\infty} \frac{z^n}{\Gamma(\beta n + 1)}, \quad \beta > 0, \quad z \in \mathbf{C}. \quad (\text{C.1})$$

It is an entire function of order β and reduces for $\beta = 1$ to $\exp(z)$. For detailed information on the functions of Mittag-Leffler type the reader may consult e.g., [10, 19, 32, 39, 53, 57] and references therein.

Hereafter, we find it convenient to summarize the most relevant features of the functions

$$\Psi(t) := E_\beta(-t^\beta), \quad 0 < \beta < 1, \quad (\text{C.2})$$

$$\phi(t) := -\frac{d}{dt}E_\beta(-t^\beta), \quad 0 < \beta < 1, \quad (\text{C.3})$$

that turn out to be the most relevant functions of Mittag-Leffler type for our purposes. Both of them reduce to the exponential function $\exp(-t)$ in the limit as $\beta \rightarrow 1$.

We begin to quote their expansions in power series of t^β (convergent for $t \geq 0$) and their asymptotic representations for $t \rightarrow \infty$,

$$\Psi(t) = \sum_{n=0}^{\infty} (-1)^n \frac{t^{\beta n}}{\Gamma(\beta n + 1)} \sim \frac{\sin(\beta\pi)}{\pi} \frac{\Gamma(\beta)}{t^\beta}, \quad (\text{C.4})$$

$$\phi(t) = \frac{1}{t^{1-\beta}} \sum_{n=0}^{\infty} (-1)^n \frac{t^{\beta n}}{\Gamma(\beta n + \beta)} \sim \frac{\sin(\beta\pi)}{\pi} \frac{\Gamma(\beta + 1)}{t^{\beta+1}}. \quad (\text{C.5})$$

The Laplace transforms of $\Psi(t)$ and $\phi(t)$ can easily be obtained by transforming the series (C.4), (C.5) term by term, respectively, they read

$$\tilde{\Psi}(s) = \frac{s^{\beta-1}}{1+s^\beta}, \quad \tilde{\phi}(s) = \frac{1}{1+s^\beta}, \quad \operatorname{Re} s > 0. \quad (\text{C.6})$$

For $0 < \beta < 1$ both the functions $\Psi(t)$, $\phi(t)$ keep the complete monotonicity of the limiting exponential function of $\exp(-t)$. Complete monotonicity of

a function $f(t)$ means, for $n = 0, 1, 2, \dots$, and $t \geq 0$, $(-1)^n \frac{d^n}{dt^n} f(t) \geq 0$, or equivalently, its representability as (real) Laplace transform of a nonnegative function or measure, see e.g., [12].

Recalling the theory of the Mittag-Leffler functions of order less than 1, we obtain for $0 < \beta < 1$ the following representations, see e.g., [19],

$$\Psi(t) = \frac{\sin(\beta\pi)}{\pi} \int_0^\infty \frac{r^{\beta-1} e^{-rt}}{r^{2\beta} + 2r^\beta \cos(\beta\pi) + 1} dr, \quad t \geq 0, \quad (\text{C.7})$$

$$\phi(t) = \frac{\sin(\beta\pi)}{\pi} \int_0^\infty \frac{r^\beta e^{-rt}}{r^{2\beta} + 2r^\beta \cos(\beta\pi) + 1} dr, \quad t \geq 0. \quad (\text{C.8})$$

In Figures C.1 and C.2 we exhibit plots of the functions $\Psi(t)$ and $\phi(t)$ in logarithmic and linear scales, respectively.

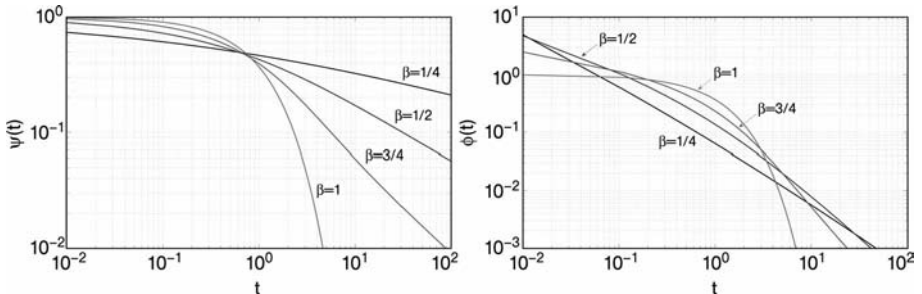


Figure C.1 The functions $\Psi(t)$ (left) and $\phi(t)$ (right) in logarithmic scales.

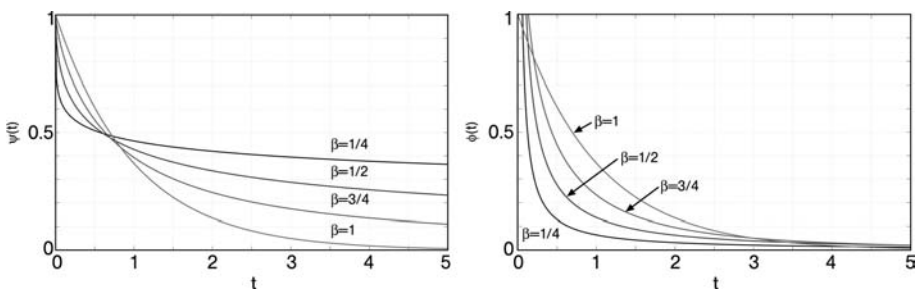


Figure C.2 The functions $\Psi(t)$ (left) and $\phi(t)$ (right) in linear scales.

References

- 1 V. Balakrishnan, Anomalous diffusion in one dimension, *Physica A* **132** (1985), 569–580.
- 2 E. Barkai and R.J. Silbey, Fractional Kramers equation, *J. Phys. Chem. B* **104** (2000), 3866–3874.
- 3 E. Barkai and I.M. Sokolov, On Hilfer's objection to the fractional time diffusion equation, *Physica A* **373** (2007), 231–236.
- 4 M. Caputo, Linear models of dissipation whose Q is almost frequency independent, Part II. *Geophys. J. R. Astr. Soc.* **13** (1967), 529–539.
- 5 M. Caputo, *Elasticità e Dissipazione*. Bologna, Zanichelli (1969).
- 6 M. Caputo and F. Mainardi, Linear models of inelastic solids, *Riv. Nuovo Cimento* (Ser. II) **1** (1971), 161–198.
- 7 D.R. Cox, *Renewal Theory*, 2nd edn., Methuen, London (1967).
- 8 M.M. Dzherbashyan, *Integral Transforms and Representations of Functions in the Complex Plane*, Moscow, Nauka (1966). In Russian. [Note that there is also the transliteration as Djrbashyan]
- 9 M.M. Dzherbashyan and A.D. Nersesian, Fractional derivatives and the Cauchy problem for differential equations of fractional order. *Izv. Acad. Nauk Armjanskvy SSR, Matematika* **3** (1968), 3–29. In Russian.
- 10 A. Erdélyi, W. Magnus, F. Oberhettinger, and F.G. Tricomi, *Higher Transcendental Functions*, Vol. 3, McGraw-Hill, New York (1953–1954).
- 11 W. Feller, On a generalization of Marcel Riesz' potentials and the semi-groups generated by them, *Meddelanden Lunds Universitets Matematiska Seminarium (Comm. Sém. Mathém. Université de Lund)*. Tome suppl. dédié à M. Riesz, Lund, 1952, pp. 73–81.
- 12 W. Feller, *An Introduction to Probability Theory and its Applications*, Vol. 2, 2nd edn., Wiley, New York (1971). [1st edn. 1966]
- 13 I.M. Gel'fand and G.E. Shilov, *Generalized Functions*, Vol. I. Academic Press, New York and London (1964).
- 14 B.V. Gnedenko and A.N. Kolmogorov, *Limit Distributions for Sums of Independent Random Variables*, Addison-Wesley, Cambridge, MA (1954). [Translated from the Russian edition, Moscow 1949, with notes by K.L. Chung, revised 1968]
- 15 B.V. Gnedenko and I.N. Kovalenko, *Introduction to Queueing Theory*, Israel Program for Scientific Translations, Jerusalem (1968).
- 16 R. Gorenflo and E. Abdel-Rehim, From power laws to fractional diffusion: the direct way, *Vietnam J. Math.* **32** SI (2004), 65–75.
- 17 R. Gorenflo, Yu. Luchko, and F. Mainardi, Analytical properties and applications of the Wright function, *Fractional Calculus Appl. Anal.* **2** (1999), 383–414. [E-print arXiv:math-ph/0701069]
- 18 R. Gorenflo, Yu. Luchko, and F. Mainardi, Wright functions as scale-invariant solutions of the diffusion-wave equation, *J. Comput. Appl. Math.* **118** (2000), 175–191.
- 19 R. Gorenflo and F. Mainardi, Fractional calculus: integral and differential equations of fractional order. In A. Carpinteri and F. Mainardi (Editors), *Fractals and Fractional Calculus in Continuum Mechanics*, Springer, Wien and New York (1997), pp. 223–276. [<http://www.fracalmo.org>]
- 20 R. Gorenflo and F. Mainardi, Random walk models for space fractional diffusion processes, *Fractional Calculus Appl. Anal.* **1** (1998), 167–191.
- 21 R. Gorenflo and F. Mainardi, Fractional diffusion processes: probability distributions and continuous time random walk, in: G. Rangarajan and M. Ding (Editors), *Processes with Long Range Correlations*, Springer, Berlin (2003), pp. 148–166. [Lecture Notes in Physics, No. 621]
- 22 R. Gorenflo and F. Mainardi, Simply and multiply scaled diffusion limits for continuous time random walks, in: S. Benkadda, X. Leoncini, and G. Zaslavsky (Editors), *Proceedings of the International Workshop on Chaotic Transport and Complexity in Fluids and Plasmas* Carry Le Rouet (France) 20–25 June 2004, IOP (Institute of Physics) *Journal of Physics: Conference Series* **7** (2005), 1–16.
- 23 R. Gorenflo, F. Mainardi, E. Scalas, and M. Raberto, Fractional calculus and

- continuous-time finance III: the diffusion limit, in: M. Kohlmann and S. Tang (Editors), *Mathematical Finance*, Birkhäuser, Basel (2001), pp. 171–180.
- 24** R. Gorenflo, F. Mainardi, and H.M. Srivastava, Special functions in fractional relaxation-oscillation and fractional diffusion-wave phenomena, in: D. Bainov (Editor), *Proceedings VIII International Colloquium on Differential Equations, Plovdiv 1997* VSP, Utrecht, 1998, pp. 195–202.
- 25** R. Gorenflo, F. Mainardi, and A. Vivoli, Continuous time random walk and parametric subordination in fractional diffusion, *Chaos, Solitons and Fractals* **34** (2007), 87–103. [E-print arXiv:cond-mat/0701126]
- 26** R. Gorenflo, A. Vivoli, and F. Mainardi, Discrete and continuous random walk models for space–time fractional diffusion, *Nonlinear Dynamics* **38** (2004), 101–116.
- 27** R. Hilfer, Exact solutions for a class of fractal time random walks, *Fractals* **3** (1995), 211–216.
- 28** R. Hilfer, On fractional diffusion and continuous time random walks, *Physica A* **329** (2003), 35–39.
- 29** R. Hilfer and L. Anton, Fractional master equations and fractal time random walks, *Phys. Rev. E* **51** (1995), R848–R851.
- 30** T. Huillet, Renewal processes and the Hurst effect, *J. Phys. A* **35** (2002), 4395–4413.
- 31** T. Huillet, On the waiting time paradox and related topics, *Fractals* **10** (2002), 1–20.
- 32** V. Kiryakova, *Generalized Fractional Calculus and Applications*. Harlow, Longman (1994). [Pitman Research Notes in Mathematics, Vol. 301]
- 33** A.N. Kochubei, A Cauchy problem for evolution equations of fractional order, *Diff. Equ.* **25** (1989), 967–974. [English translation from the Russian Journal *Differentsial'nye Uravneniya*]
- 34** A.N. Kochubei, Fractional order diffusion, *Diff. Equ.* **26** (1990), 485–492. [English translation from the Russian Journal *Differentsial'nye Uravneniya*]
- 35** M. Kotulski, Asymptotic distributions of continuous-time random walks: a probabilistic approach, *J. Stat. Phys.* **81** (1995), 777–792.
- 36** T.J. Kozubowski and S.T. Rachev, Univariate geometric stable laws, *J. Comput. Anal. Appl.* **1**, (1999), 177–217.
- 37** F. Mainardi, Fractional relaxation-oscillation and fractional diffusion-wave phenomena. *Chaos, Solitons and Fractals* **7** (1996), 1461–1477.
- 38** F. Mainardi, Fractional calculus: some basic problems in continuum and statistical mechanics, in A. Carpinteri and F. Mainardi (Editors), *Fractals and Fractional Calculus in Continuum Mechanics*, Springer, Wien and New York, 1997, pp. 291–348.
- 39** F. Mainardi and R. Gorenflo, On Mittag-Leffler-type functions in fractional evolution processes, *J. Comput. Appl. Math.* **118** (2000), 283–299.
- 40** F. Mainardi, R. Gorenflo, and E. Scalas, A fractional generalization of the Poisson processes. *Vietnam J. Mathematics* **32** SI (2004), 53–64. [E-print arXiv:math-PR/0701454]
- 41** F. Mainardi, R. Gorenflo, and A. Vivoli, Renewal processes of Mittag-Leffler and Wright type, *Fractional Calculus Appl. Anal.*, **8** (2005), 7–38. [E-print arXiv:math-PR/0701455]
- 42** F. Mainardi, Yu. Luchko, and G. Pagnini, The fundamental solution of the space–time fractional diffusion equation, *Fractional Calculus Appl. Anal.* **4** (2001), 153–192. [E-print arXiv:cond-mat/0702419]
- 43** F. Mainardi and G. Pagnini, The Wright functions as solutions of the time fractional diffusion equations, *Appl. Math. Comput.* **141** (2003), 51–62.
- 44** F. Mainardi, M. Raberto, R. Gorenflo, and E. Scalas, Fractional calculus and continuous-time finance II: the waiting time distribution, *Physica A* **287** (2000), 468–481.
- 45** F. Mainardi, A. Vivoli, and R. Gorenflo, Continuous time random walk and time fractional diffusion: a numerical comparison between the fundamental solutions, *Fluct. Noise Lett.* **5** (2005), L291–L297.
- 46** M.M. Meerschaert, D.A. Benson, H.-P. Scheffler, and B. Baeumer, Stochastic solutions of space fractional diffusion equation, *Phys. Rev. E* **65** (2002), 041103-1/4.
- 47** R. Metzler, E. Barkai, and J. Klafter, Anomalous diffusion and relaxation

- close to thermal equilibrium: a fractional Fokker–Planck equation approach, *Phys. Rev. Lett.* **82** (1999), 3563–3567.
- 48** E.W. Montroll and H. Scher, Random walks on lattices, IV: Continuous-time walks and influence of absorbing boundaries, *J. Stat. Phys.* **9** (1973), 101–135.
- 49** E.W. Montroll and G.H. Weiss, Random walks on lattices, II, *J. Math. Phys.* **6** (1965), 167–181.
- 50** E.W. Montroll and D.J. West, On an enriched collection of stochastic processes, in E.W. Montroll and J. Leibowitz (Editors), *Fluctuation Phenomena*, North-Holland, Amsterdam, 1979, pp. 61–175. [Studies in Statistical Mechanics, Vol. VII]
- 51** R.N. Pillai, On Mittag-Leffler functions and related distributions, *Ann. Inst. Statist. Math.* **42** (1990), 157–161.
- 52** A. Piryatinska, A.I. Saichev, and W.A. Woyczyński, Models of anomalous diffusion: the subdiffusive case, *Physica A* **349** (2005), 375–420.
- 53** I. Podlubny, *Fractional Differential Equations*. Academic Press, San Diego (1999).
- 54** A. Renyi, A characteristic of the Poisson stream, *Proc. Math. Inst. Hungarica Acad. Sci.* **1** (4) (1956), 563–570. [In Hungarian]
- 55** S.M. Ross, *Introduction to Probability Models*, 6th edn., Academic Press, New York, (1997).
- 56** A.I. Saichev and G.M. Zaslavsky, Fractional kinetic equations: solutions and applications, *Chaos* **7** (1997), 753–764.
- 57** S.G. Samko, A.A. Kilbas, and O.I. Marichev, *Fractional Integrals and Derivatives: Theory and Applications*, Gordon and Breach, New York (1993) [Translation from the Russian edition, Nauka i Tekhnika, Minsk (1987)].
- 58** E. Scalas, The application of continuous-time random walks in finance and economics, *Physica A* **362** (2006), 225–239.
- 59** E. Scalas, R. Gorenflo, and F. Mainardi, Fractional calculus and continuous-time finance, *Physica A* **284** (2000), 376–384.
- 60** E. Scalas, R. Gorenflo, and F. Mainardi, Uncoupled continuous-time random walks: Solution and limiting behavior of the master equation, *Phys. Rev. E* **69** (2004), 011107-1/8.
- 61** W.R. Schneider and W. Wyss, Fractional diffusion and wave equations, *J. Math. Phys.* **30** (1989) 134–144.
- 62** I.M. Sokolov, J. Klafter, and A. Blumen, Do strange kinetics imply unusual thermodynamics? *Phys. Rev. E* **64** (2001), 021107-1/4.
- 63** T. Szàntai, Limiting distribution for the sums of random number of random variables concerning the rarefaction of recurrent events, *Studia Scientiarum Mathematicarum Hungarica* **6** (1971), 443–452.
- 64** T. Szàntai, On an invariance problem related to different rarefactions of recurrent events. *Studia Scientiarum Mathematicarum Hungarica* **6** (1971), 453–456.
- 65** V.V. Uchaikin and V.V. Saenko, Stochastic solution of partial differential equations of fractional orders, *Siberian J. Num. Math.* **6** (2003), 197–203.
- 66** G.H. Weiss, *Aspects and Applications of Random Walks*, North-Holland, Amsterdam (1994).
- 67** K. Weron and M. Kotulski, On the Cole–Cole relaxation function and related Mittag-Leffler distribution, *Physica A* **232** (1995), 180–188.
- 68** D.V. Widder, *The Laplace Transform*, Princeton University Press, Princeton (1946).

5

Introduction to the Theory of Lévy Flights

Alexei V. Chechkin, Ralf Metzler, Joseph Klafter, and Vsevolod Yu. Gonchar

Lévy flights are Markovian stochastic processes whose individual jumps have lengths that are distributed with the probability density function (PDF) $\lambda(x)$ decaying at large x as $\lambda(x) \simeq |x|^{-1-\alpha}$ with $0 < \alpha < 2$. Due to the divergence of their variance, $\langle x^2(t) \rangle \rightarrow \infty$, extremely long jumps may occur, and typical trajectories are self-similar, on all scales showing clusters of shorter jumps interspersed by long excursions. In fact, the trajectory of a Lévy flight has fractal dimension $d_f = \alpha$ [1]. Similar to the emergence of the Gaussian as limit distribution of independent identically distributed (iid) random variables with finite variance due to the central limit theorem, Lévy stable distributions represent the limit distributions of iid random variables with diverging variance [1–3]. In that sense, the Gaussian distribution represents the limiting case of the basin of attraction of the so-called generalized central limit theorem for $\alpha = 2$ [1–4].

Measurable quantities that follow Lévy statistics are widely known in nature. Thus, paleoclimatic-time series exhibit a distinct behavior that bears clear signatures of Lévy noise [5]. The foraging behavior of bacteria and higher animals relies on the advantages of Lévy distributed excursion lengths [6–13], which optimize the search compared to Brownian search. The latter tends to significant oversampling in one and two dimensions. In hopping processes along a polymer, where shortcuts across chemically remote segments, that due to looping come in close contact in the embedding space, Lévy flights occur in the annealed limit [14–16]. The spreading of diseases, due to the high degree of connectivity by air traffic of remote geographic locations involves Lévy travel lengths and thus causes a fast worldwide spreading [17]. Similarly, extensive tracking of one dollar bills reveals Lévy statistics [18].

Signatures of Lévy statistics were also documented in the study of the position of a single ion in a one-dimensional optical lattice, in which diverging fluctuations could be observed in the kinetic energy [19]. The occurrence of Lévy flights in energy space for single molecules interacting with two-level systems via long-range interactions was discussed in Refs. [20, 21]. Lévy sta-

tistics has been identified in random single-molecule line shapes in glass formers [22].

Finally, it has been revealed that Lévy statistics governs the distribution of trades in economical contexts [23–25]. Lévy flights are also connected to questions of ergodicity breaking due to the divergence of the variance of the jump length distribution [26].

In what follows we give a detailed introduction to the physical and mathematical foundation of Lévy processes, and explore their dynamic and stationary behavior.

5.1

Lévy Stable Distributions

For sums of independent, iid random variables with proper normalization to the sample size, the generalized central limit theorem guarantees the convergence of the associated PDF to a Lévy stable (LS) PDF even though the variance of these random variables diverges [1–3, 27]. In general, an LS PDF is defined through its characteristic function of the probability density [28, 29], that is, its Fourier transform,

$$\begin{aligned} p_{\alpha,\beta}(k; \mu, \sigma) &= \mathcal{F}\{p_{\alpha,\beta}(x; \mu, \sigma)\} \equiv \int_{-\infty}^{\infty} dx e^{ikx} p_{\alpha,\beta}(x; \mu, \sigma) \\ &= \exp \left[i\mu k - \sigma^{\alpha} |k|^{\alpha} \left(1 - i\beta \frac{k}{|k|} \varpi(k, \alpha) \right) \right], \end{aligned} \quad (5.1)$$

where

$$\varpi(k, \alpha) = \begin{cases} \tan \frac{\pi \alpha}{2} & \text{if } \alpha \neq 1, 0 < \alpha < 2, \\ -\frac{2}{\pi} \ln |k| & \text{if } \alpha = 1. \end{cases} \quad (5.2)$$

Thus, one can see that, in general, the characteristic function and, respectively, the LS PDF are determined by the four real parameters: α , β , μ , and σ . The exponent $\alpha \in [0, 2]$ is the index of stability, or the Lévy index, $\beta \in [-1, 1]$ is the skewness parameter, μ is the shift parameter, and $\sigma > 0$ is a scale parameter. The index α and the skewness parameter β play a major role in our considerations, since the former defines the asymptotic decay of the PDF, whereas the latter defines the asymmetry of the distribution. The shift and scale parameters play a lesser role in the sense that they can be eliminated by proper scale and shift transformations,

$$p_{\alpha,\beta}(x; \mu, \sigma) = \frac{1}{\sigma} p_{\alpha,\beta} \left(\frac{x - \mu}{\sigma}; 0, 1 \right). \quad (5.3)$$

Due to this property, in what follows we set $\mu = 0, \sigma = 1$, and denote the Lévy stable PDF $p_{\alpha,\beta}(x; 0, 1)$ by $p_{\alpha,\beta}(x)$. We note the important symmetry property of the PDF, namely

$$p_{\alpha,-\beta}(x) = p_{\alpha,\beta}(-x). \quad (5.4)$$

For instance, the asymptotics of the PDF $p_{\alpha<1,1}(x), x \rightarrow 0$ ($x > 0$) or $x \rightarrow \infty$ have the same behavior as $p_{\alpha<1,-1}(x), x \rightarrow 0$ ($x < 0$) or $x \rightarrow -\infty$.

One easily recognizes that a stable distribution $p_{\alpha,\beta}(x)$ is *symmetric* if and only if $\beta = 0$. Stable distributions with skewness parameter $\beta = \pm 1$ are called *extremal*. One can prove that all extremal stable distributions with $0 < \alpha < 1$ are one sided, the support being the positive semiaxis if $\beta = +1$, and the negative semiaxis if $\beta = -1$. For instance, $p_{0<\alpha<1,1}(x)$ is only defined for $x \geq 0$.

Only in three particular cases can the PDF $p_{\alpha,\beta}(x)$ be expressed in terms of elementary functions:

(i) Gaussian distribution, $\alpha = 2$,

$$p_2(x) = \frac{1}{\sqrt{4\pi}} \exp\left(-\frac{x^2}{4}\right). \quad (5.5)$$

In the Gaussian case β is irrelevant since $\tan \pi = 0$, and the variance is equal to 2. In this case, the generalized central limit theorem coincides with the traditional central limit theorem.

(ii) Cauchy distribution, $\alpha = 1, \beta = 0$,

$$p_{1,0}(x) = \frac{1}{\pi(1+x^2)} ; \quad (5.6)$$

(iii) Lévy–Smirnov distribution, $\alpha = 1/2, \beta = 1$,

$$p_{1/2,1}(x) = \begin{cases} \frac{1}{\sqrt{2\pi}} x^{-3/2} \exp\left(-\frac{1}{2x}\right), & x \geq 0 \\ 0, & x < 0. \end{cases} \quad (5.7)$$

This probability law appears, e.g., in the first passage problem for a Brownian particle on the semi-infinite domain [27], supporting that even in classical Brownian dynamics Lévy stable laws and therefore diverging moments appear.

Stable distributions for arbitrary α can be expressed via the Fox H -functions [30]. Such a representation for all stable densities was obtained in [31]. The properties of H -functions are presented in detail in [32, 33]. In our tutorial review we do not dwell on representations for general α .

Lévy stable laws are of interest for their asymptotic behavior: The symmetric stable PDF scales asymptotically as [34, 35]

$$p_{\alpha,0}(x) \approx C_1(\alpha) / |x|^{1+\alpha}, \quad x \rightarrow \pm\infty, \quad (5.8)$$

where

$$C_1(\alpha) = \frac{1}{\pi} \sin(\pi\alpha/2) \Gamma(1+\alpha). \quad (5.9)$$

Respectively, for all LS PDFs with $\alpha < 2$ the variance diverges, $\langle x^2 \rangle = \infty$. Conversely, all fractional moments $\langle |x|^q \rangle < \infty$ for all $0 < q < \alpha < 2$. The shapes of symmetric stable PDFs are shown in Figure 5.1 in a linear, log-linear and log-log scales.

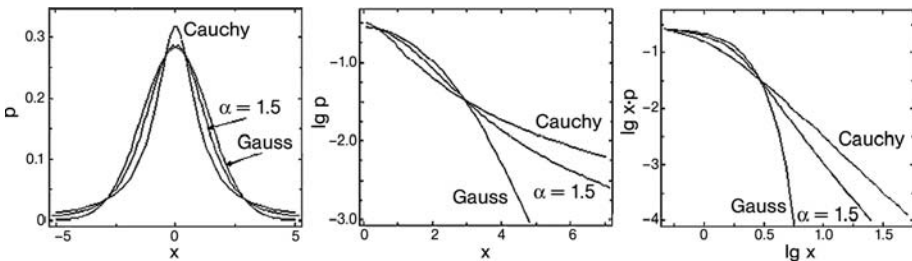


Figure 5.1 The shapes of symmetric stable laws are depicted for Gaussian, $\alpha = 1.5$ and Cauchy PDFs, from the left to the right in linear, log-linear and log-log scales. One can see from the left figure showing the central parts of the PDFs that the Cauchy distribution has a more pronounced peak at the origin but basically all the three PDFs in the central part are similar to each other. The differences are becoming more pronounced in a log-linear scale, which is well suited for showing the intermediate behavior between the central part

of the PDF and the asymptotics. Note that in the log-linear scale the Cauchy distribution (in fact, as all the symmetric stable distributions) is concave far from its maximum at the origin, whereas the Gaussian distribution is convex. And, at last, in a log-log scale on the right figure one can see the large difference between the PDFs in the asymptotics, which are linear for $\alpha < 2$ here, see Eq. (5.8). The slope in the log-log scale is determined by the Lévy index α according to Eq. (5.8). The Gaussian distribution is convex.

Symmetric stable PDFs will be mostly used in our review. We also touch upon the behavior of extremal stable laws with $\beta = 1$, which find applications in different problems, for instance, as waiting time or first-passage-time distributions. At $x \rightarrow \infty$ their asymptotes have the same behavior as that of the symmetric PDFs (Eqs. (5.8) and (5.9)). At $x \rightarrow 0$ the extremal one-sided stable distribution with $0 < \alpha < 1$ behaves as [36, 37]

$$p_{\alpha,1}(x) \approx C_2(\alpha) x^{-1-\eta(\alpha)/2} \exp \left[-C_3(\alpha) x^{-\eta(\alpha)} \right], \quad x \rightarrow 0, \quad 0 < \alpha < 1, \quad (5.10)$$

where $\eta(\alpha) = \alpha/(1-\alpha)$, and coefficients C_2, C_3 depend on α . Thus, at small x the PDF falls off exponentially. The extremal two-sided stable distribution

with $1 < \alpha < 2$ exhibits a similar exponential decay at $x \rightarrow -\infty$,

$$p_{\alpha,1}(x) \approx \bar{C}_2(\alpha) |x|^{-1+\bar{\eta}(\alpha)/2} \exp\left[-\bar{C}_3(\alpha) |x|^{\bar{\eta}(\alpha)}\right], \quad x \rightarrow -\infty, \quad 1 < \alpha < 2, \quad (5.11)$$

with $\bar{\eta}(\alpha) = \alpha/(\alpha - 1)$, and another coefficients \bar{C}_2 , \bar{C}_3 . Both extremal stable PDFs are shown schematically in Figure 5.2.

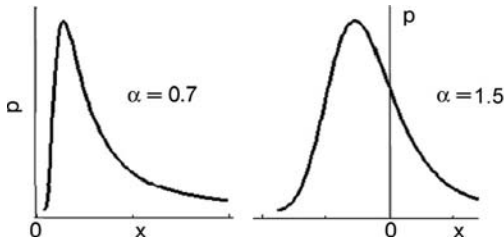


Figure 5.2 Sketch of one-sided (left) and two-sided (right) extremal LS PDFs with $\beta = 1$.

5.2

Underlying Random Walk Processes

Consider a continuous time random walk process defined in terms of decoupled jump length and waiting time distributions $\lambda(\xi)$ and $\psi(\tau)$ [38, 39]. Each jump event of this random walk is characterized by a jump length ξ drawn from the distribution λ , and the time τ between two jump events is distributed according to ψ (note that an individual jump is supposed to occur spontaneously). As we will see, random processes whose jump lengths or waiting times are distributed according to an LS PDF exhibit anomalies, that is, no longer follow the laws of Brownian motion. In absence of an external bias, continuous time random walk theory connects $\lambda(\xi)$ and $\psi(\tau)$ with the probability distribution $f(x, t)$ to find the random walker at a position in the interval $(x, x+dx)$ at time t . In Fourier-Laplace space, $f(k, u) \equiv \mathcal{F}\{\mathcal{L}\{f(x, t); t \rightarrow u; x \rightarrow k\}\}$, this relation reads [40]

$$f(k, u) = \frac{1 - \psi(u)}{u} \frac{1}{1 - \lambda(k)\psi(u)}, \quad (5.12)$$

where $\mathcal{L}\{f(t)\} \equiv \int_0^\infty \exp(-ut)f(t) dt$.

The following cases can be distinguished:

- (i) $\lambda(\xi)$ is Gaussian with variance σ^2 and $\psi(\tau) = \delta(\tau - \tau_0)$. Then, to a leading order in k^2 and u , respectively, one obtains $\lambda(k) \simeq 1 - \sigma^2 k^2$ and

$\psi(u) \simeq 1 - u\tau_0$. From relation (5.12) one recovers the Gaussian probability density $P(x, t) = \sqrt{1/(4\pi Kt)} \exp\{-x^2/(4Kt)\}$ with diffusion constant $K = \sigma^2/\tau_0$. The corresponding mean square displacement grows linearly with time:

$$\langle x^2(t) \rangle = 2Kt. \quad (5.13)$$

This case corresponds to the continuum limit of regular Brownian motion. Note that here and in the following, we restrict the discussion to one dimension.

- (ii) Assume $\lambda(\xi)$ is still a Gaussian, while for the waiting time distribution $\psi(\tau)$, we choose a one-sided LS PDF with stable index $0 < \alpha < 1$. Consequently, $\psi(u) \simeq 1 - (u\tau_0)^\alpha$, and the characteristic waiting time $\int_0^\infty \psi(\tau)\tau d\tau$ diverges. Due to this lack of a time scale separating microscopic (single jump events) and macroscopic (on the level of $f(x, t)$) scales, $f(x, t)$ is no more Gaussian, but given by a more complex H -function [31, 41, 42]. In Fourier space, however, one finds a quite simple analytical form of the characteristic function $f(k, t)$ in terms of the Mittag-Leffler function [41],

$$f(k, t) = E_\alpha \left(-K_\alpha k^2 t^\alpha \right), \quad (5.14)$$

which can be presented in the form of a series as [43]

$$E_\alpha \left(-K_\alpha k^2 t^\alpha \right) = \sum_{n=0}^{\infty} \frac{(K_\alpha k^2 t^\alpha)^n}{\Gamma(1 + \alpha n)}.$$

This function turns from an initial stretched exponential behavior $f(k, t) \approx 1 - K_\alpha k^2 t^\alpha / \Gamma(1 + \alpha) \sim \exp\{-K_\alpha k^2 t^\alpha / \Gamma(1 + \alpha)\}$ to a terminal power-law behavior $f(k, t) \approx (K_\alpha k^2 t^\alpha \Gamma(1 - \alpha))^{-1}$ [41]. In the limit $\alpha \rightarrow 1$, it reduces to the traditional exponential $f(k, t) = \exp(-Kk^2 t)$ with finite characteristic relaxation time. Also the mean squared displacement changes from its linear to the power-law dependence

$$\langle x^2(t) \rangle = \frac{2K_\alpha}{\Gamma(1 + \alpha)} t^\alpha, \quad (5.15)$$

with $K_\alpha = \sigma^2/\tau_0^\alpha$. This is the case of subdiffusion. We note that in x, t space the dynamical equation is the diffusion-like equation with partial fractional derivative in time (time-fractional diffusion equation) [31]. In more detail the time-fractional diffusion equation is discussed in Chapter 4 written by R. Gorenflo and F. Mainardi. In the presence of an external potential, it generalizes to the time-fractional Fokker–Planck equation [41, 42, 44].

- (iii) Finally, take $\psi(\tau) = \delta(\tau - \tau_0)$ sharply peaked, but $\lambda(\xi)$ of Lévy stable form with index $0 < \alpha < 2$. The resulting process is Markovian, but with diverging variance. It can be shown that the fractional moments scale like [45]

$$\langle |x(t)|^q \rangle \propto (K_\alpha t)^{q/\alpha}, \quad (5.16)$$

where $K_\alpha = \sigma^\alpha / \tau_0$. We can therefore rescale this fractional moment according to $\langle |x(t)|^q \rangle^{2/q} \propto (K_\alpha t)^{2/\alpha}$ to see the “superdiffusive” character. Actual superdiffusion within the continuous time random walk framework requires the introduction of finite velocities and using the Lévy walk process [46]. From Eq. (5.12) one can immediately obtain the Fourier image of the associated PDF,

$$f(k, t) = \exp \{ -K_\alpha |k|^\alpha t \}. \quad (5.17)$$

From Eq. (5.1) this is but the characteristic function of a symmetric LS PDF with the index of stability α , and this type of random walk process is most aptly coined a Lévy flight. The characteristic function has regular exponential relaxation in time, and a Lévy flight process is in fact Markovian [47]. The PDF in position space is no more sharply localized like in the Gaussian or subdiffusive case, and it has the diverging variance. We will see below how the presence of steeper than harmonic external potentials cause a finite variance of the Lévy flight, although a power-law form of the probability density remains.

For illustration, we show in Figure 5.3 the trajectory of a Lévy flight compared to a Gaussian walk. The clustered character of the Lévy flight separated by occasional long excursions is distinct. A Lévy flight trajectory has fractal dimension $d_f = \alpha$.

5.3 Space Fractional Fokker–Planck Equation

To derive the dynamic equation of a Lévy flight in the presence of an external force field $F(x) = -dU(x)/dx$, we pursue two different routes.

One starts from the Langevin equation

$$\frac{dx}{dt} = -\frac{1}{m\gamma} \frac{dU(x)}{dx} + \xi_\alpha(t), \quad (5.18)$$

driven by white Lévy stable noise $\xi_\alpha(t)$, defined through $L(\Delta t) = \int_t^{t+\Delta t} \xi_\alpha(t') dt'$ being a symmetric LS PDF of index α with characteristic function $p_{\alpha,0}(k, \Delta t) = \exp(-K_\alpha |k|^\alpha \Delta t)$ for $0 < \alpha \leq 2$. As with standard Langevin

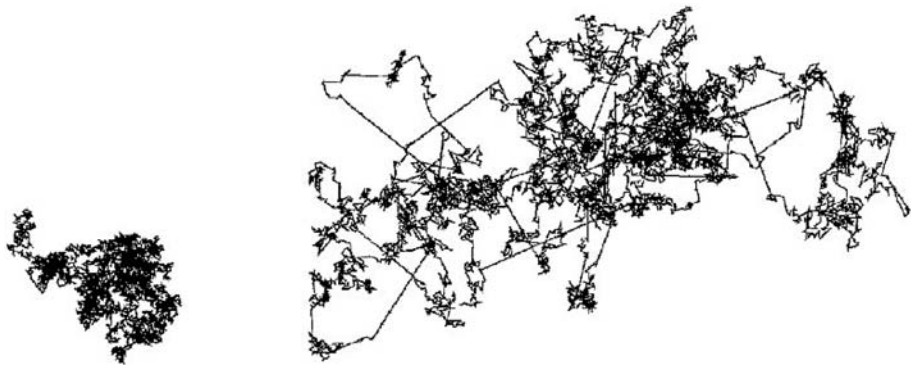


Figure 5.3 Comparison of the trajectories of a Gaussian (left) and a Lévy (right) process, the latter with index $\alpha = 1.5$. Both trajectories are statistically self-similar. The Lévy process trajectory is characterized by the island structure of clusters of smaller steps, connected by a long step. Both walks are drawn for the same number of steps (≈ 7000).

equations, K_α denotes the *noise intensity* of physical dimension $[K_\alpha] = \text{cm}^\alpha/\text{s}$, m is the mass of the diffusing (test) particle, and γ is the friction constant characterizing the dissipative interaction with the bath of surrounding particles. It was shown [48–51] that the kinetic equation corresponding to the Langevin description (5.18) has the form

$$\frac{\partial}{\partial t} f(x, t) = \left(-\frac{\partial}{\partial x} \frac{F(x)}{m\gamma} + K_\alpha \frac{\partial^\alpha}{\partial |x|^\alpha} \right) f(x, t), \quad (5.19)$$

which is called *space-fractional Fokker–Planck equation* (space-FFPE). Remarkably, the presence of the Lévy stable $\lambda(\xi)$ only affects the diffusion term, while the drift term remains unchanged [48, 49]. The symbol $\partial^\alpha / \partial |x|^\alpha$ introduced in Ref. [52] denotes the *symmetric Riesz space fractional derivative*, which represents an integro-differential operator defined through

$$\frac{\partial^\alpha}{\partial |x|^\alpha} f(x, t) = \frac{-1}{2 \cos(\pi\alpha/2) \Gamma(2-\alpha)} \frac{\partial^2}{\partial x^2} \int_{-\infty}^{\infty} \frac{f(x', t)}{|x-x'|^{\alpha-1}} dx' \quad (5.20)$$

for $1 < \alpha < 2$, $-\infty < x, x' < \infty$, and a similar form for $0 < \alpha < 1$ [53, 54]. In Fourier space, for all $0 < \alpha \leq 2$ the simple relation

$$F \left\{ \frac{\partial^\alpha}{\partial |x|^\alpha} f(x, t) \right\} = -|k|^\alpha f(k, t) \quad (5.21)$$

holds. For more details about fractional derivatives see Chapter 2 written by *R. Hilfer*. The space fractional diffusion equation with asymmetric derivatives, its numerical solution, and application to plasma physics are discussed

in Chapter 6 by *D. del-Castillo-Negrete*. In the Gaussian limit $\alpha = 2$, all relations above reduce to the familiar second-order derivatives in x and thus the corresponding $f(x, t)$ is governed by the standard Fokker–Planck equation.

Another approach starts with a generalized version of the continuous time random walk; compare Ref. [49] for details. To include the local asymmetry of the jump-length distribution due to the force field $F(x)$, we introduce [49, 55] the generalized transfer kernel $\Lambda(x, x') = \lambda(x - x')[A(x')\Theta(x - x') + B(x')\Theta(x' - x)]$ (and, therefore $\Lambda(x, x') = \Lambda(x'; x - x')$). As in standard random walk theory (compare [56]), the coefficients $A(x)$ and $B(x)$ define the local asymmetry for jumping left and right, depending on the value of $F(x)$. Here, $\Theta(x)$ is the Heaviside jump function. With the normalization $\int \Lambda(x', \Delta) d\Delta = 1$, the space-FFPE, Eq. (5.19), is obtained.

A subtle point about the FFPE (5.19) is that it does not uniquely define the underlying trajectory [57]; however, *starting from* our definition of the process in terms of the stable jump length distribution $\lambda(\xi) \sim |\xi|^{-1-\alpha}$, or its generalized pendant $\Lambda(x, x')$, the FFPE (5.19) truly represents a Lévy flight in the presence of the force $F(x)$.

We also note that other forms of the space-FFPE exist [58, 59], which describe different physical situations observed in experiment [60]; in particular, they describe the systems relaxing to the Boltzmann distribution, which is not the case for the systems obeying Eqs. (5.18) and (5.19), as we will see below.

5.4

Free Lévy Flights in the Semi-Infinite Domain

5.4.1

First Passage Time and Leapover Properties

We consider two coupled properties of Lévy flights: the first passage time (FPT) and the first passage leapover (FPL). Considering a particle that starts at the origin and performs random jumps with independent increments chosen from a Lévy stable probability law with the PDF $p_{\alpha, \beta}(x)$, the FPT measures how long it takes the particle to arrive at or cross a target. For processes with broad jump length distributions, another quantity is of interest, namely, the statistics of the first passage leapovers, that is the distance the random walker overshoots the threshold value $x = d$ in a single jump. Figure 5.4 illustrates schematically the leapover event.

Information on the leapover behavior is important to the understanding of how far search processes of animals for food [8, 10] or of proteins for their specific binding site along DNA overshoot their target [16], or to define better stock market strategies determining when to buy or sell a certain share instead

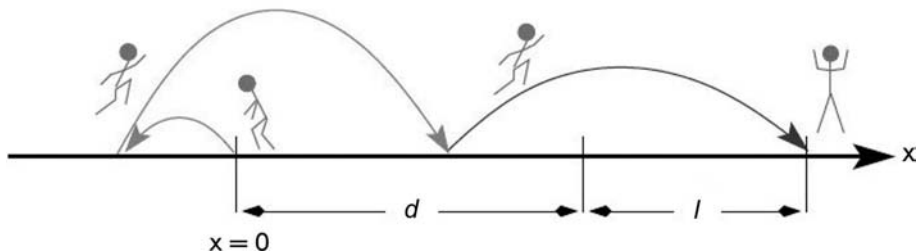


Figure 5.4 Schematic representation of the leapover problem: the random walker starts at $x = 0$ and after a number of jumps crosses the point $x = d$, overshooting it by a distance l . For narrow jump length distributions, each jump is so small that crossing the point d is equal to arriving at this point [61].

of a given threshold price [25]. Examples of the leapovers for the trajectories of symmetric and extremal one-sided Lévy motion are demonstrated in Figure 5.5. It is quite obvious that the smaller α is the larger are the jumps and, as one might expect, the larger is also the size of leapover.

One might naively assume that for Lévy flights the FPT PDF should decay quicker, than for a narrow jump length distribution. However, as we have a symmetric jump length distribution PDF, the long outliers characteristic for these Lévy flights can occur both toward and away from the absorbing barrier. From this point of view it is not totally surprising that for all Markovian processes with a symmetric jump-length distribution the celebrated *Sparre Andersen theorem* [62, 63] proves, without knowledge of any details of $\lambda(\xi)$, that the asymptotic behavior of the first passage time density universally follows $p(t) \propto t^{-3/2}$, and thus the mean FPT is infinite. The details of the specific form of $\lambda(\xi)$ only enter the prefactor, and the preasymptotic behavior. A special case of the Sparre Andersen theorem was proved in Ref. [64] when the particle is released at $x_0 = 0$ at time $t = 0$, and after the first jump an absorbing boundary is installed at $x = 0$. This latter case was simulated extensively in Ref. [65].

Using the general theorem of FPT and FPL properties of homogeneous processes with independent increments [47], the corresponding properties for symmetric and extremal one-sided LFs were derived. The basic results are as follows. For the symmetric LFs with index α and intensity K_α , starting at distance d from the boundary the asymptotics of the FPT PDF reads as [61]

$$p(\tau_d) \approx \frac{d^{\alpha/2}}{\alpha \sqrt{\pi K_\alpha} \Gamma(\alpha/2)} \tau_d^{-3/2} \quad (5.22)$$

Thus, not only the $t^{-3/2}$ is reproduced, but also the prefactor, compared to the

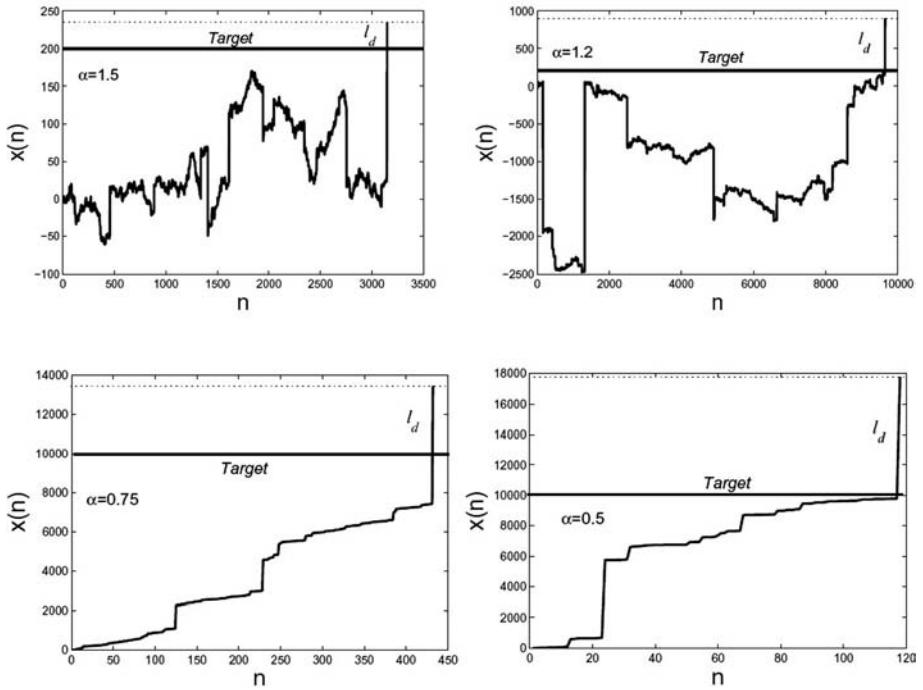


Figure 5.5 Trajectories obtained from numerical simulations with symmetric Lévy motion (top) and extremal one-sided Lévy motion with positive jumps (bottom); n is the number of time steps. As α becomes smaller larger jumps are more probable. The target is lo-

cated at $d = 200$ in case of symmetric motion and at $d = 10^4$ in case of one-sided motion. Note the different scales for the different α values. The target location is shown by the full line and the leapover distance by the broken line.

asymptotic study in Ref [69]. The distribution of FPL l_d reads [61]

$$f(l_d) = \frac{\sin(\pi\alpha/2)}{\pi} \frac{d^{\alpha/2}}{l_d^{\alpha/2} (d + l_d)}. \quad (5.23)$$

Surprisingly, for symmetric LFs with jump-length distribution $p_{\alpha,0}(\xi) \sim |\xi|^{-1-\alpha}$ ($0 < \alpha < 2$) the distribution of leapover lengths across d is distributed like $f(l_d) \sim l_d^{-1-\alpha/2}$ at large l_d , i.e., it is much broader than the original jump-length distribution. For a phenomenological explanation of the leapover asymptotic behavior, we use the “superdiffusive” nature of the motion of the Lévy particle during time interval τ_d , $x \propto \tau_d^{1/\alpha}$, where τ_d has a PDF with the Sparre Andersen “ $-3/2$ ” asymptotics. The leapover is therefore $l_d \sim Q\tau_d^{1/\alpha} - d$, where Q is a (dimensional) constant. Applying $f(l_d) = f(\tau_d) d\tau_d/dl_d$, indeed leads to $f(l_d) \sim l_d^{-1-\alpha/2}$ at $l_d \gg d$. This is a remarkable finding: while $p_{\alpha,0}(x)$ for $1 < \alpha < 2$ has a finite characteristic length $\langle |x| \rangle$, the mean leapover value is infinite for all α s. Another interesting

(however, obvious from dimensional arguments) feature is that the leapover PDF does not depend on the intensity of the Lévy flights K_α . Both features are confirmed by extensive simulations, for more details refer to [61]. Note that $f(l_d)$ is normalized. In the limit $\alpha \rightarrow 2$, $f(l_d)$ tends to zero if $l_d \neq 0$ and to infinity at $l_d = 0$ corresponding to the absence of leapovers in the Gaussian continuum limit.

In contrast, the FPL PDF for extremal LFs with $0 < \alpha < 1$ obtained from the general theorem has the form [61]

$$f(l_d) = \frac{\sin(\pi\alpha)}{\pi} \frac{d^\alpha}{l_d^\alpha (d + l_d)}, \quad (5.24)$$

which corresponds to the results obtained in Ref. [66] from a different method. Thus, for the extremal one-sided LF, the scaling of the leapover is exactly the same as for the jump-length distribution, namely, with exponent α . The FPT PDF is expressed via the so-called M -function [61] (special case of the Wright function [54, 67]), and the mean value of the FPT is finite and reads as

$$\langle \tau_d \rangle = \frac{d^\alpha \cos(\pi\alpha/2)}{K_\alpha \Gamma(1+\alpha)}. \quad (5.25)$$

Again, the results (5.24), (5.25) compare favorably with simulations [61, 68].

5.4.2

Lévy Flights and the Method of Images

As it is well known in the theory of Brownian motion, the method of images allows one to get the solution of the diffusion equation in semi-infinite and finite domains as combination of the solutions on the infinite axis [27, 63]. That is, given the initial condition $\delta(x - x_0)$, $x_0 > 0$, the solution $f_{\text{im}}(x, t)$ for the absorbing boundary problem, $f_{\text{im}}(0, t) = 0$, according to the method of images in the semi-infinite domain corresponds to the difference

$$f_{\text{im}}(x, t) = W(x - x_0, t) - W(x + x_0, t) \quad (5.26)$$

in terms of free propagator W , i.e., a negative image solution originating at $-x_0$ balances the probability flux across the absorbing boundary. However, it was demonstrated in Ref. [69] that being applied to the LFs, the method of images produces a result, which is inconsistent with the universal behavior of the FPT PDF. Indeed, the corresponding (pseudo-) FPT PDF $p_{\text{im}}(t)$ is calculated as a negative time derivative of the survival probability [27],

$$p_{\text{im}}(t) = -\frac{d}{dt} \int_0^\infty f_{\text{im}}(x, t) dx, \quad (5.27)$$

which leads to the long t form [69]

$$p_{\text{im}}(t) \sim 2\Gamma(1/\alpha)x_0 / \left(\pi\alpha K_\alpha^{1/\alpha} t^{1+1/\alpha}\right) \quad (5.28)$$

for the image method. In the Gaussian limit $\alpha = 2$, Eq. (5.28) produces $p_{\text{im}}(t) \sim x_0 / \sqrt{4\pi K t^3}$, in accordance with Eq. (5.22). Conversely, for general $1 < \alpha < 2$, $p_{\text{im}}(t)$ according to Eq. (5.28) would decay faster than $t^{-3/2}$. Therefore, the method of images breaks down for LFs due to their nonlocal nature, displayed by the integrals in Eqs. (5.19) and (5.21), see the detailed discussion in [57, 69].

5.5

Lévy Flights in External Fields

An important point is to understand the behavior of LFs in the presence of external potentials, that is “*confined*” LFs or the barrier crossing of LFs. Although the stage has been set for the study of such properties of LFs, rather limited information is available. In what follows, we briefly review the description of LFs in external fields in terms of the Langevin equation with white Lévy noise and the space-fractional Fokker–Planck equation, and demonstrate interesting and *a priori* unexpected statistical properties of confined LFs.

5.5.1

Reminder: Stationary Solution of the Fokker–Planck Equation, $\alpha = 2$

We remind that the stationary solution of the (standard) Fokker–Planck equation (in dimensionless variables) on the infinite axis,

$$\frac{d}{dx} \left(\frac{dU}{dx} f \right) + \frac{d^2 f}{dx^2} = 0, \quad -\infty < x < \infty, \quad (5.29)$$

is given by the well-known Boltzmann formula,

$$f(x) = C \exp(-U(x)), \quad \int_{-\infty}^{\infty} dx f(x) = 1. \quad (5.30)$$

In particular, for one-well potentials the stationary solution is unimodal, that is, it has one hump whose location coincides with the location of the well, and exhibits fast exponential decay away from the origin.

5.5.2

Lévy Flights in an Harmonic Potential

Let us find the stationary solution of the space-FFPE with harmonic potential, $U(x) = x^2/2$. The direct way to solve Eq. (5.19) is applying the Fourier trans-

form (we remind that in Fourier space the Riesz derivative $d^\alpha f(x)/d|x|^\alpha$ turns into $(-|k|^\alpha) f(k)$), which for the stationary state gives

$$\frac{df}{dk} = -\operatorname{sgn}(k) |k|^{\alpha-1} f(k), \quad f(k=0) = 1. \quad (5.31)$$

The solution is

$$f(k) = \exp(-|k|^\alpha / \alpha), \quad (5.32)$$

that is the characteristic function of symmetric stable law, see Eq. (5.1). The two properties of the stationary PDF in an harmonic potential follow immediately from Eq. (5.32): (i) unimodality (one hump at the origin), and (ii) slowly decaying power-law asymptotics, $f(|x| \rightarrow \infty) \approx C_\alpha |x|^{-1-\alpha}$, where $C_\alpha = \pi^{-1}\Gamma(\alpha) \sin(\pi\alpha/2)$ (compare with Eqs. (5.8) and (5.9)). It implies that the second moment is infinite, and that the harmonic force is not “strong” enough to “confine” LFs. The LFs does not leave their basin of attraction defined by the external Lévy noise of index α .

5.5.3

Lévy Flights in a Quartic Potential, $1 \leq \alpha < 2$

With a quartic potential, $U(x) = x^4/4$, the equation for the characteristic function in the stationary state follows from Eq. (5.19),

$$\frac{d^3 f}{dk^3} = \operatorname{sgn}(k) |k|^{\alpha-1} f(k). \quad (5.33)$$

This equation is solved with the use of the following boundary conditions and properties of the characteristic function: (i) $f(|k| = \pm\infty) = 0$; (ii) $f(k=0) = 1$ (normalization); (iii) $f(k) = f^*(k) = f(-k)$, where $*$ stands for complex conjugation; here the first equality is a consequence of the Khintchin theorem (reality of characteristic function for symmetric PDF), whereas the second equality is the consequence of the Bochner–Khintchin theorem (positive definiteness of characteristic function); and (iv) $df^{(p)}(0)/dk^p = 0$, $p = 1, 3, 5, \dots$, because odd moments (if they exist) are equal zero due to symmetry of the PDF, and we restrict ourselves to the class of characteristic functions which are “smooth enough” in the origin.

Let us first consider the particular Cauchy case, $\alpha = 1$, for which the solution of Eq. (5.33) is straightforward [70],

$$\hat{f}(k) = \frac{2}{\sqrt{3}} \exp\left(-\frac{|k|}{2}\right) \cos\left(\frac{\sqrt{3}|k|}{2} - \frac{\pi}{6}\right). \quad (5.34)$$

Inverse Fourier transform yields the PDF,

$$f(x) = \frac{1}{\pi(1-x^2+x^4)}. \quad (5.35)$$

We observe surprisingly that the variance of the solution (5.35) is finite,

$$\langle x^2 \rangle = 1, \quad (5.36)$$

due to long-tailed asymptotics $f(x) \propto x^{-4}$. In addition, as shown in Figure 5.6, this solution has two global maxima at $x_{\max} = \pm 1/\sqrt{2}$ along with the local minimum at the origin (that is the position of the initial condition).

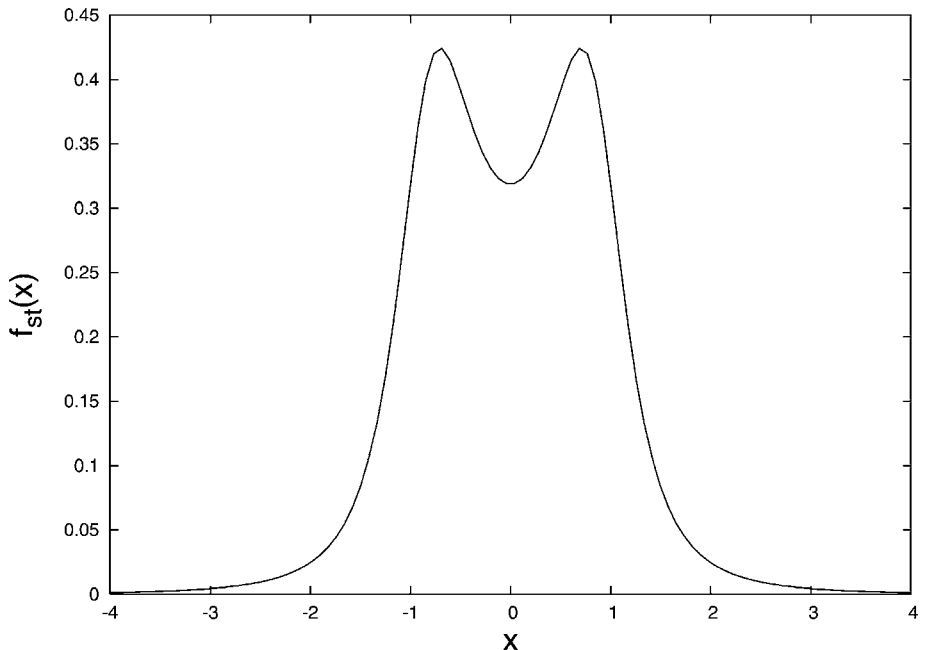


Figure 5.6 Stationary PDF (5.35) of the Cauchy-Lévy flight in a quartic potential.

Equation (5.33) was analyzed in [71] in detail, and the two properties, bimodality and steep asymptotics, $f(x) \approx C_\alpha |x|^{-\alpha-3}$, $|x| \rightarrow \infty$, that is the finite variance, were discovered for the Lévy flights in quartic potential for the whole range of the Lévy indices between 1 and 2. In Figure 5.7 the profiles of stationary PDFs (obtained by an inverse Fourier transformation) are shown for different Lévy indices from $\alpha = 1$ at the top of the figure up to $\alpha = 2$ at the bottom. It is seen that the bimodality is most strongly expressed for $\alpha = 1$. With the Lévy index increasing, the bimodal profile smoothes out and, finally, it turns to a unimodal one at $\alpha = 2$, that is, the Boltzmann distribution.

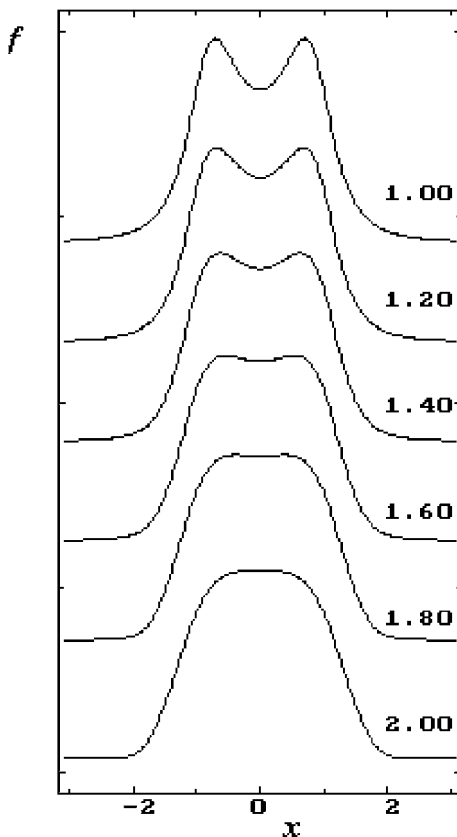


Figure 5.7 Profiles of stationary PDFs of the quartic oscillator for different Lévy indices, from $\alpha = 1$ (at the top) to $\alpha = 2$ (at the bottom).

5.5.4

Lévy Flights in a More General Potential Well

In more general one-well potentials of the type

$$U(x) = \frac{|x|^c}{c}, \quad (5.37)$$

the turnover from unimodal to bimodal form of $f(x)$ in stationary state occurs exactly when c becomes larger than 2. Moreover, the asymptotics of the PDF in the potential (5.37) are given by $f(x) \approx C_\alpha / |x|^{\alpha+c-1}$, $|x| \rightarrow \infty$. It implies that the variance is finite only if $c > 4 - \alpha$, that is the potential wall is “steep enough.” Remarkably, C_α appears to be a “universal” constant, i.e., it does not depend on c , analogously to harmonic and quartic potentials. Both properties of stationary states can be obtained by using different representation of the Riesz derivative in Eq. (5.18) [72]. An interesting effect is observed during relaxation to the bimodal stationary state, starting at $t = 0$ from a narrow

Gaussian-like distribution in the origin. At $2 < c \leq 4$ the bifurcation occurs from a unimodal to a bimodal state, and the corresponding bifurcation time as a function of α , $1 \leq \alpha < 2$, has a minimum at some intermediate value. In the potential well with $c > 4$ two bifurcations occur: first, from unimodal to a transient trimodal state and then from the trimodal to a bimodal one. In the stationary state a bimodal distribution is always observed. The details of the behavior of Lévy flights in a general potential well are given in [72]. From a reverse engineering point of view, Lévy flights in confining potentials are studied in [73].

5.5.5

Kramers Problem for Lévy Flights

Many physical and chemical problems are related to the crossing of an energetic barrier, driven by external noise, such as dissociation of molecules, nucleation processes, or the escape from an external, confining potential of finite height [74]. A particular example of LF barrier crossing in a double-well potential was proposed for a long-time series of paleoclimatic data [5]. Detailed numerical investigations of the LF barrier crossing were performed in [75–77]. In [77] an analytical theory of the escape over a barrier in a symmetric bistable potential was developed based on the space-FFPE for the particular Cauchy case $\alpha = 1$. Another analytical approach which is different from space-FFPE and is purely probabilistic was developed in [78]. The results of analytical and numerical approaches are the following. Similar to Brownian motion, an exponential decay of the survival probability in the initial well was found, $p(t) = T_c^{-1} \exp(-t/T_c)$, as demonstrated in Figure 5.8.

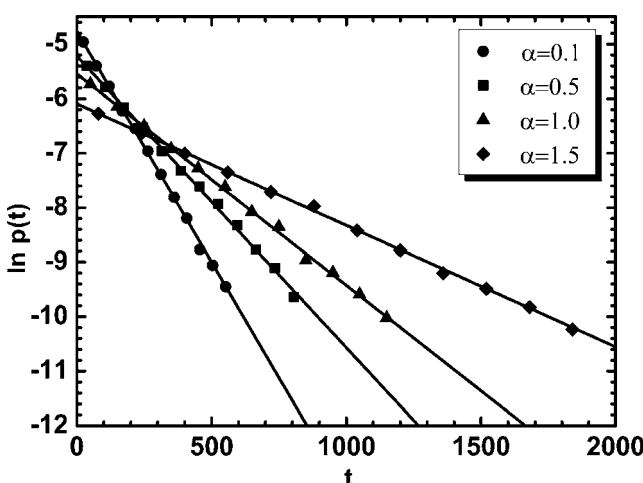


Figure 5.8 Escape time probability density functions in dependence of time for the bistable potentials. In logarithmic versus linear plot, the exponential dependence is obvious.

More interesting is the question how the mean escape time T_c behaves as a function of the noise parameters K_α and α . While in the regular Kramers problem with Gaussian driving noise the Arrhenius-type activation $T_c = A \exp(h/D)$ is followed, where h is the barrier height and the prefactor A includes details of the potential; in the case of Lévy noise-driven escape, a power-law form

$$T_c(\alpha, D) = \frac{C(\alpha)}{D^{\mu(\alpha)}} \quad (5.38)$$

was proposed [75, 79]. This behavior is distinctly visible in Figure 5.9 in the form of the parallel lines in the log-log scale. Indeed, detailed investigations [77] show that the scaling exponent $\mu(\alpha)$ is approximately 1 for all α strictly smaller than 2, see Figure 5.10.

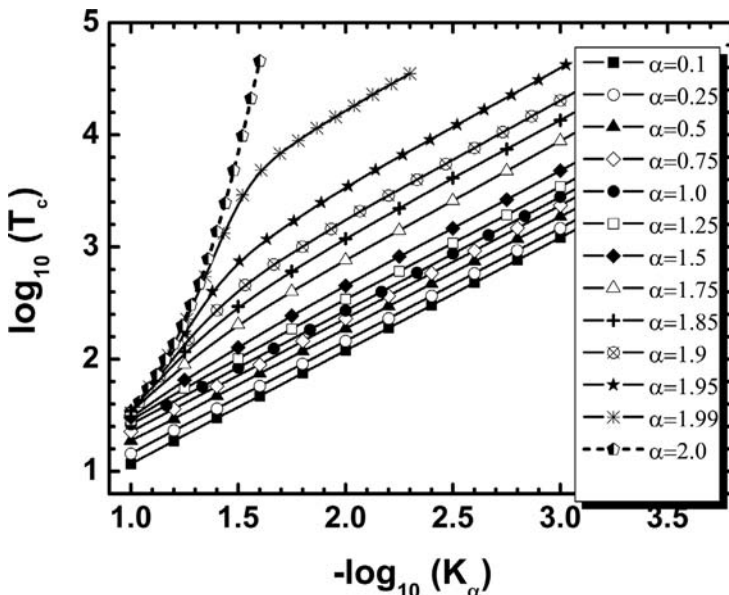


Figure 5.9 Characteristic escape time as a function of the diffusivity D for the symmetric bistable potential.

As already proposed in Ref. [79] and derived in [78] in a different model, this means that, apart from a prefactor, the Lévy flight is insensitive to the external potential for the barrier crossing. For large values of D deviations from the scaling are observed: eventually it will only take a single jump to cross the barrier when $D \rightarrow \infty$. We also note that in Ref. [76] the escape problem was investigated numerically for asymmetric LFs, $\beta \neq 0$.

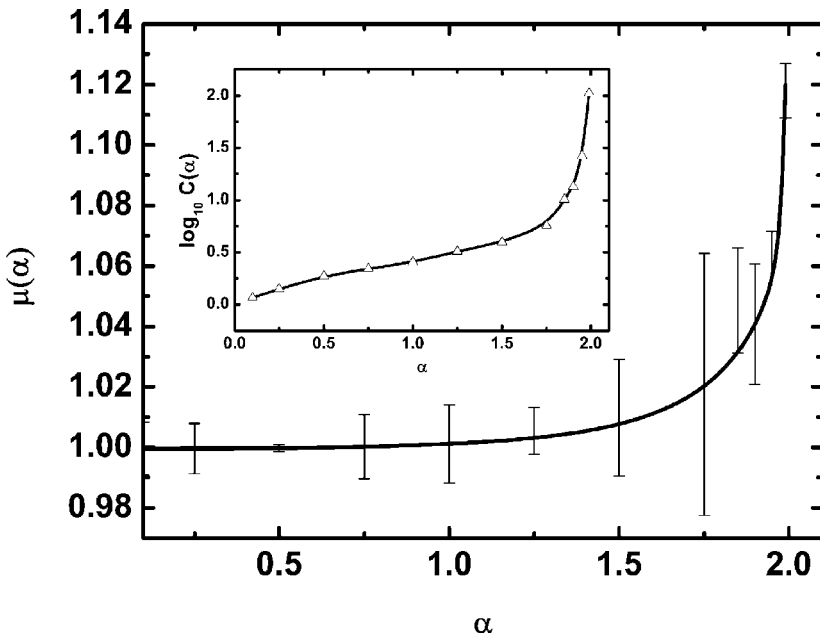


Figure 5.10 Dependences of $\mu(\alpha)$ and $C(\alpha)$ for the symmetric bistable potential.

5.6 Lévy Flights in Phase Space

In the phase space spanned by position and velocity coordinates x and v the basic equation of the Brownian motion is the Klein–Kramers equation for the PDF $f(x, v, t)$ [80,81]. The equivalent Langevin description is based on the two first-order differential equations for space coordinate and velocity, with white Gaussian noise source. The Langevin description can be generalized by including a white Lévy noise source instead of the Gaussian. Correspondingly, we arrive at the generalized velocity-fractional Klein–Kramers equation.

5.6.1 Langevin Description

Our starting point is the coupled Langevin equations in the phase space (x, v) , which are written as

$$\frac{dx}{dt} = v, \quad \frac{dv}{dt} = -\gamma v + \frac{F}{m} + \zeta_\alpha(t), \quad (5.39)$$

where γ is the friction constant, which in general may be v -dependent, $F = -dU/dx$ is a deterministic force, U is a potential energy, and $\zeta_\alpha(t)$ is stationary white Lévy noise with the Lévy index α . The white Lévy noise is de-

fined in a way analogous to Section 5.3, that is $L(\Delta t) = \int_t^{t+\Delta t} \zeta_\alpha(t') dt'$ being a symmetric LS PDF of index α with characteristic function $p_{\alpha,0}(\kappa, \Delta t) = \exp(-D_\alpha |\kappa|^\alpha \Delta t)$ for $0 < \alpha \leq 2$, D_α is the noise intensity, $[D_\alpha] = \text{cm}^\alpha/\text{s}^{1+\alpha}$. If we neglect inertia effects in Eq. (5.39), $dv/dt = 0$, we arrive at the overdamped Langevin equation and the kinetic description presented in Section 5.3, where $\xi_\alpha(t) = \zeta_\alpha(t)/\gamma$.

5.6.2

Velocity-Fractional Klein–Kramers Equation

It can be shown that the kinetic description equivalent to the Langevin description, Eq. (5.39), is given by the *velocity-fractional Klein–Kramers equation* (velocity-FKKE) [82–84],

$$\frac{\partial f}{\partial t} + v \frac{\partial f}{\partial x} + \frac{F}{m} \frac{\partial f}{\partial v} = \frac{\partial}{\partial v} (\gamma v f) + D_\alpha \frac{\partial^\alpha f}{\partial |v|^\alpha}, \quad (5.40)$$

where the last term in the right-hand side is the Riesz fractional velocity derivative, defined, in analogy with definition (5.21), via the velocity Fourier transform of the PDF, whereas the other terms are the usual terms of the Klein–Kramers equation. At $\alpha = 2$ Eq. (5.40) is the (standard) Klein–Kramers equation for the systems driven by white Gaussian noise.

5.6.3

Space-Homogeneous Relaxation in Absence of External Field

We are looking for the solution $f(v, t)$ of the *velocity-fractional Rayleigh equation*

$$\frac{\partial f}{\partial t} = \frac{\partial}{\partial v} (\gamma v f) + D_\alpha \frac{\partial^\alpha f}{\partial |v|^\alpha}, \quad (5.41)$$

with the initial condition $f(v, t = 0) = \delta(v - v_0)$. Passing to the velocity-Fourier transform of the PDF,

$$f(v, t) = \int_{-\infty}^{\infty} \frac{d\kappa}{2\pi} \exp(-i\kappa v) f(\kappa, t), \quad (5.42)$$

we get the solution for the characteristic function [82],

$$f(\kappa, t) = \exp \{ i\kappa v_0 e^{-\gamma t} - |\kappa|^\alpha \chi(t) \}, \quad (5.43)$$

where $\chi(t) = (D_\alpha/\alpha\gamma)(1 - e^{-\alpha\gamma t})$. We see that the PDF tends to a stationary solution which is a Lévy stable distribution in velocity, with relaxation time $\tau_v = 1/\alpha\gamma$. The stationary Maxwell solution appears only in the Gaussian case, $\alpha = 2$, $D_2 \equiv D$,

$$f_{st}(v; \alpha = 2) = \left(\frac{\gamma}{2\pi D} \right)^{1/2} \exp \left(-\frac{\gamma v^2}{2D} \right). \quad (5.44)$$

This is the equilibrium PDF of Brownian motion. It is characterized by the temperature of the surrounding medium T . For Brownian motion, there is a well-known relation between noise intensity D in the Langevin equation, friction coefficient γ , and temperature T : $D = \gamma k_B T / m$, where m is the mass of Brownian particle, k_B is Boltzmann constant. Temperature is a measure of the mean kinetic energy of a Brownian particle, $\langle E_{\text{kin}} \rangle = m \langle v^2 \rangle / 2 = k_B T / 2$. The last two relations are examples of fluctuation–dissipation relations. In this case the random source in the Langevin equation is called the source of internal fluctuations. There exist cases when these relations are not fulfilled, as it happens, for example in autooscillatory systems. In this case it is said that $\zeta_2(t)$ is a source of external (relative to the system considered) fluctuations. However, the stationary Maxwell–Boltzmann distribution still exists [81]. For Lévy motion, there are no fluctuation–dissipation relations, that is why one can talk about $\zeta_\alpha(t)$ as a source of external fluctuations, only. Moreover, the stationary PDF is not Maxwellian but instead has the more general form of a stable distribution. At present no theory of the equilibrium state exists, which would be based on stable distributions.

5.6.4

Space-Inhomogeneous Relaxation in the Absence of an External Field

Similar to Brownian motion, the space-inhomogeneous relaxation in a force-free case can be divided into two stages which are described in the framework of the velocity-FKKE: a “fast” stage, at which a stationary stable PDF over velocity is formed, and a “slow” diffusion stage, at which relaxation in the position coordinate occurs [84]. The latter process can be described asymptotically as the Lévy stable process with independent increments. The characteristic time of the velocity relaxation is τ_v , whereas the relaxation time in position coordinate is $\tau_x \approx (\gamma L)^\alpha / D_\alpha$, where L is an external size of the system considered. For systems large enough one has $\tau_x \gg \tau_v$, and the two-stage representation of relaxation process is valid. The diffusion stage of relaxation can be described in the framework of the space-FFPE, with the fractional moments of the PDF scaling according to Eq. (5.16) with $K_\alpha = D_\alpha / \gamma^\alpha$.

5.6.5

Relaxation of the Linear Oscillator [84]

When studying the relaxation behavior of a linear oscillator, $F(x) = -m\omega^2 x$, it is worthwhile to distinguish between two cases: an overdamped oscillator, $\omega/\gamma \ll 1$; and a weakly damped oscillator, $\omega/\gamma \gg 1$. Both cases are of special importance in the kinetic theory. The relaxation process is very different in the two cases.

The relaxation of an overdamped oscillator, similar to space-inhomogeneous relaxation, has two stages, which are described in the framework of the Kramers equation: a “fast” stage, at which during the time interval $\tau_v = 1/\alpha\gamma$ a stationary stable PDF in velocity is formed; and a “slow” diffusion stage, at which during the time interval $\tau_x = \gamma/\alpha\omega^2$ a stationary stable PDF in position coordinate emerges. At the diffusion stage the relaxation of an overdamped oscillator can be described in the framework of the space-FFPE.

For a weakly damped oscillator in the theory of Brownian motion a method was developed, which allows one to simplify the kinetic description by using slowly varying (within period of oscillations) random variables [81]. The generalization of this approach to the case of a weakly damped Lévy oscillator leads to the fractional kinetic equation in the slow variables \tilde{x} , \tilde{v} ,

$$\frac{\partial}{\partial t} f(\tilde{x}, \tilde{v}, t) = \frac{\gamma}{2} \frac{\partial}{\partial \tilde{x}} (\tilde{x} f) + \frac{\gamma}{2} \frac{\partial}{\partial \tilde{v}} (\tilde{v} f) + D_{\tilde{x}} \frac{\partial^\alpha f}{\partial |\tilde{x}|^\alpha} + D_{\tilde{v}} \frac{\partial^\alpha f}{\partial |\tilde{v}|^\alpha}, \quad (5.45)$$

where $D_{\tilde{x}} = D_\alpha/2\omega^\alpha$, and $D_{\tilde{v}} = D_\alpha/2$ (for derivation see the Appendix in Ref. [84]). It follows from Eq. (5.45) that for a weakly damped oscillator both velocity and coordinate relax with the same relaxation time $\tau_v = \tau_x = \tau = 2/\alpha\gamma$, and thus there is no separation between the kinetic and diffusion stages. In a stationary state the PDF is a Lévy stable in space and velocity, with the characteristic function

$$f_{st}(k, \kappa) = \exp \left(-\frac{2D_{\tilde{x}}}{\alpha\gamma} |k|^\alpha - \frac{2D_{\tilde{v}}}{\alpha\gamma} |\kappa|^\alpha \right) \quad (5.46)$$

Equation (5.46) reduces to Maxwell–Boltzmann distribution for $\alpha = 2$.

5.6.6

Relaxation in a Magnetized Plasma

We here present a model example of magnetized plasma relaxation in the presence of a random electric field obeying Lévy statistics [85]. We consider a charged test particle with mass m and charge e , embedded in a constant external magnetic field $\vec{B} \parallel \vec{e}_z$ and subjected to a stochastic electric field $\vec{\epsilon}(t)$. We also assume, as in the classical problem for a charged Brownian particle [86, 87], that the particle is influenced by the linear friction force $-\gamma m \vec{v}$. The Langevin equations of motion read

$$\frac{d\vec{r}}{dt} = \vec{v}, \quad \frac{d\vec{v}}{dt} = \frac{e}{mc} (\vec{v} \times \vec{B}) - \gamma \vec{v} + \frac{e}{m} \vec{\epsilon}, \quad (5.47)$$

where the field $\vec{\epsilon}(t)$ is assumed to be (i) homogenous and isotropic; (ii) stationary white Lévy noise with intensity D_ϵ . The assumption about non-Gaussian statistics allows us to consider anomalous diffusion and non-Maxwellian

heavy-tailed PDFs, both properties shown to be inherent to a strongly nonequilibrium cosmic and laboratory magnetized plasmas, see, e.g., [88] and references therein. Figure 5.11 shows typical trajectories of the Brownian and Lévy particles in the plane perpendicular to the magnetic field.

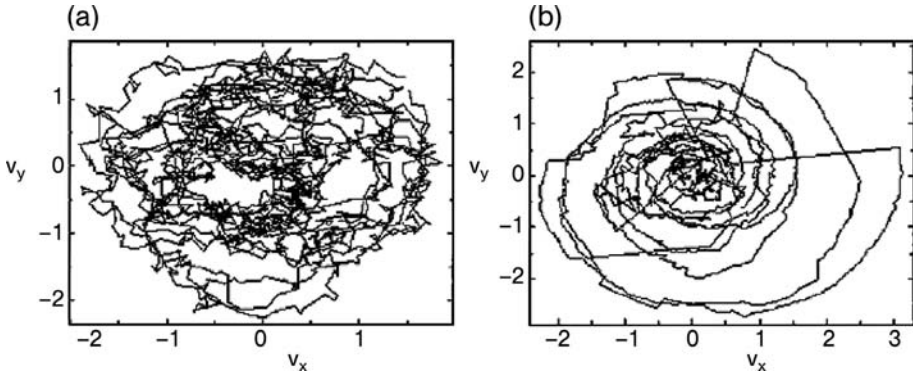


Figure 5.11 Numerical solution to the Langevin equations: trajectory on $(v_x - v_y)$ plane perpendicular to the ambient magnetic field for (a) $\alpha = 2$, and (b) $\alpha = 1.2$. For the latter, Lévy flights for a charged particle are clearly seen [85].

The kinetic equation, equivalent to the Langevin description has the form

$$\frac{\partial f}{\partial t} + \vec{v} \frac{\partial f}{\partial \vec{r}} + \Omega(\vec{v} \times \vec{e}_z) \frac{\partial f}{\partial \vec{v}} = \gamma \frac{\partial}{\partial \vec{v}} (\vec{v} f) - D_\alpha (-\Delta_{\vec{v}})^{\alpha/2} f, \quad (5.48)$$

where $\Omega = eB/mc$, $B \equiv |\vec{B}|$, $D_\alpha = e^\alpha D_e/m^\alpha$, and $(-\Delta_{\vec{v}})^{\alpha/2}$ is the fractional Riesz potential, which is defined via its Fourier transform in velocity as (compare with Eq. (5.21))

$$F_v \left\{ (-\Delta_{\vec{v}})^{\alpha/2} f(\vec{r}, \vec{v}, t) \right\} = |\vec{\kappa}|^\alpha f(\vec{r}, \vec{\kappa}, t). \quad (5.49)$$

At $\alpha = 2$ Eq. (5.48) is reduced to Klein-Kramers equation for a charged Brownian particle in a magnetic field [87].

The general solution of Eq. (5.48) is obtained by the method of characteristics [85]. In the absence of a magnetic field there are two stages of relaxation in this problem: in the first, “fast” stage, the velocity relaxation leads to non-Maxwellian stationary states, for which the velocity PDF is the Lévy stable distribution. The PDF of energy has power-law tails decaying as $f_{st}(E) \propto E^{-(1+\alpha/2)}$. At the second, “diffusion” stage, the charged particle exhibit superdiffusion with the typical displacement behaving as

$$\Delta r \sim \langle r^q \rangle^{1/q} \propto \frac{t^{1/\alpha}}{B}. \quad (5.50)$$

Recalling that the classical diffusion law across a magnetic field gives

$$\langle r^2 \rangle \propto \frac{t}{B^2}, \quad (5.51)$$

we conclude that the diffusion described by the velocity-fractional Klein-Kramers equation demonstrates an anomalous behavior with time and remains classical with respect to the magnetic field dependence.

5.6.7

Damped Lévy Flights [89]

At higher velocities the friction experienced by a moving body starts to depend on the velocity itself [90]. Such nonlinear friction is known from the classical Riccati equation $mdv/dt = mg - Av^2$ for the fall of a particle of mass m in a gravitational field with acceleration g [91] (A is a positive constant), or autonomous oscillatory systems with a friction that is nonlinear in the velocity [90, 92]. The occurrence of a nonconstant friction coefficient $\gamma(v)$ leading to a nonlinear dissipative force was highlighted in Klimontovich's theory of nonlinear Brownian motion [93]. It is therefore natural that higher order, nonlinear friction terms also occur in the case of Lévy processes.

We consider Lévy flights in velocity space as governed by the Langevin equation (compare with Eq. (5.39))

$$\frac{dv}{dt} = -\gamma(v)v + \zeta_\alpha(t), \quad (5.52)$$

where the nonlinear friction coefficient is represented as a series in even powers of v ,

$$\gamma(v) = \gamma(-v) = \gamma_0 + \gamma_2 v^2 + \cdots + \gamma_{2n} v^{2n} + , \quad \gamma_{2n} > 0. \quad (5.53)$$

This Langevin picture is equivalent to the velocity-fractional Rayleigh equation, Eq. (5.41), but with the friction coefficient being a function of v . The analysis of this equation is similar to that of space-FFPE for LFs in steep potentials, see Section 5.4. The presence of the first higher order correction, $\gamma_2 v^2$, rectifies the Lévy motion such that the asymptotic power law becomes steeper and the variance finite. When even higher order corrections are taken into consideration, also higher order moments become finite. We show an example in Figure 5.12 for the second moment: compare the "smooth" behavior of the finite moments with the scattering behavior of the infinite moment. Here, the strong fluctuations observed in numerical simulations are manifestation of the theoretical infinity.

The effect on the stationary velocity distribution $f(v) = \lim_{t \rightarrow \infty} f(v, t)$ for higher order corrections in Eq. (5.53) is demonstrated in Figure 5.13: while for

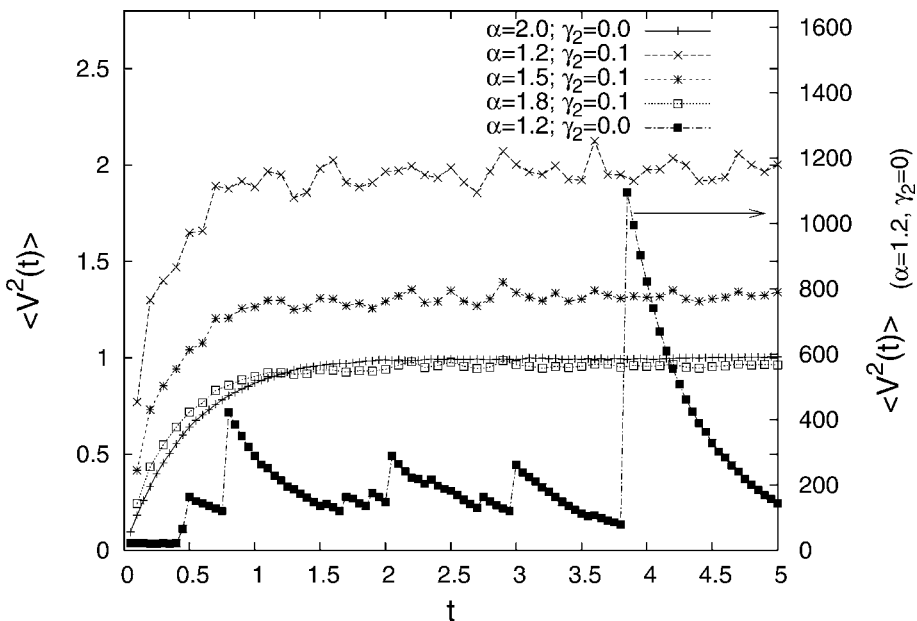


Figure 5.12 Variance $\langle v^2(t) \rangle$ as a function of time t , with the quartic and higher velocity terms set to zero in Eq. (6.16), and $\gamma_0 = 1.0$ for all cases. The variance is finite for the cases $\alpha = 2$, $\gamma_2 = 0.0$; $\alpha = 1.2$, $\gamma_2 = 0.1$; $\alpha = 1.5$, $\gamma_2 = 0.1$; $\alpha = 1.8$, $\gamma_2 = 0.1$. These correspond to the left ordinate. For the case $\alpha = 1.2$, $\gamma_2 = 0.0$, the variance diverges, strong fluctuations are visible; note the large values of this curve corresponding to the right ordinate.

smaller v the character of the original Lévy stable behavior is preserved (the original power-law behavior, that is, persists to intermediately large v), for even larger v the corrections due to the dissipative nonlinearity are visible in the transition(s) to steeper slope(s).

5.7

Power-Law Truncated Lévy Flights

Since Lévy flights have been introduced into statistical physics, it has become clear that special attention must be given to the fact that due to their heavy tails they are characterized by diverging moments. While the hopping along a coiled polymer allows for shortcuts at polymer loops, leading to an LF in the chemical coordinate along the chain but local jumps in the physical embedding space [14–16]; or while diffusion in energy space with diverging variance does not violate physical principles [20], particles of finite mass always must have a finite variance. A few approaches have been suggested to over-

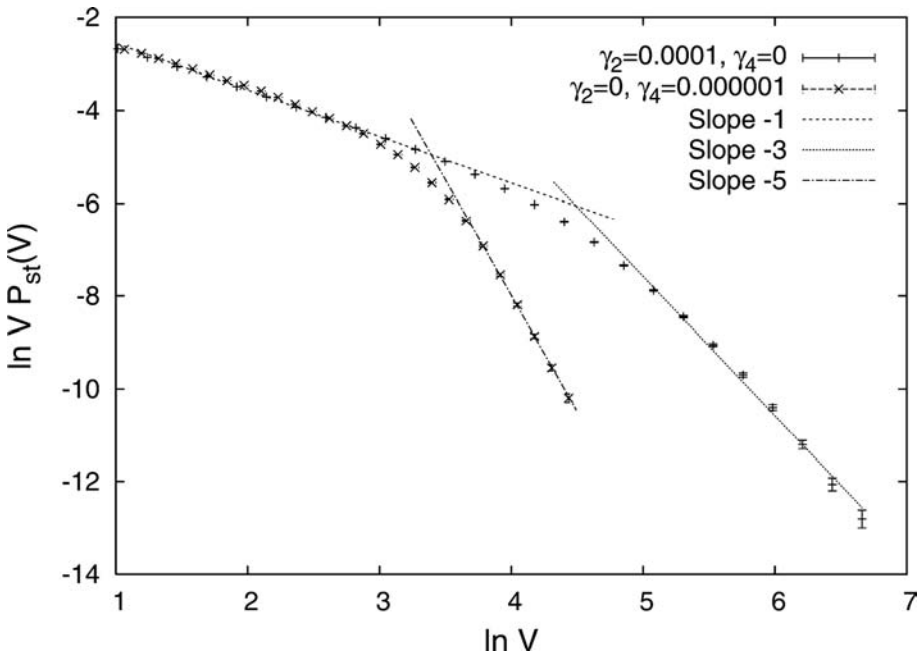


Figure 5.13 Stationary PDF $f(v)$ for $\gamma_0 = 1.0$ and (i) $\gamma_2 = 10^{-4}$ and $\gamma_4 = 0$; and (ii) $\gamma_2 = 0$ and $\gamma_4 = 10^{-6}$; with $\alpha = 1.0$. The lines indicate the slopes -1 , -3 , and -5 .

come this divergence. These include the introduction of the concept of Lévy walks including a spatiotemporal coupling such that at finite times only finite windows in space may be explored [94]; confining Lévy flights by external potentials (Section 5.5); damped Lévy flights (Section 5.6); and introduction of truncation procedures [95, 96]. Each of the approaches represents a different physical situation, but they all made it possible for Lévy processes to be applicable in a variety of areas. In many cases, the Lévy flight behavior corresponds to intermediate asymptotics. At very large values of the variable some cutoffs enter, so that the moments exist. Truncated Lévy flights, a process showing a slow convergence to a Gaussian, were introduced by Mantegna and Stanley [95] and have been used in econophysics ever since, see Refs. [97, 98], in turbulence [99] and in plasma physics [100]. The truncated Lévy flight is a Markovian-jump process, with the length of jumps showing a power-law behavior up to some large scale. At larger scales the power-law behavior crosses over to a faster decay, so that the second moment of the jump lengths exists. In this case the central limit theorem applies, so that at very long times the distribution of displacements converges to a Gaussian; this convergence however may be extremely slow and cannot be observed in many experimental realizations. In such cases, a statistical description in terms of LFs is perfectly

in order. In those cases where cutoffs become relevant, the transition of the dynamics needs to be studied. The original work concentrated on numerical simulations of the process which assumed a Θ -function cutoff. Koponen [96] slightly changed the model by replacing the Θ -function cutoff by an exponential one and obtained a useful analytical representation for the model. However, further investigations have shown that the models with sharp (Θ -function or exponential) cutoffs predicting a Gaussian or an exponential tail of the PDF are not always appropriate [98].

The equation proposed for truncated Lévy flights with power-law cutoff has the following form [101]:

$$\left(1 - K_\alpha \frac{\partial^{2-\alpha}}{\partial|x|^{2-\alpha}}\right) \frac{\partial f(x, t)}{\partial t} = K \frac{\partial^2 f(x, t)}{\partial x^2}. \quad (5.54)$$

Equation (5.54) is in fact a special case of distributed-order diffusion equations [102], which were introduced for the description of anomalous nonscaling behavior. The positivity of the solution is proved in [101].

Equation (5.54) can be easily solved in Fourier space. For the characteristic function we have the solution corresponding to the initial condition $f(x, t=0) = \delta(x)$

$$f(k, t) = \exp\left(-\frac{Kk^2}{1 + K_\alpha |k|^{2-\alpha}}\right). \quad (5.55)$$

The second moment of the solution evolves as in normal diffusion: $\langle x^2(t) \rangle = -(\partial^2 f(k, t) / \partial k^2)_{k=0} = 2Kt$. However, in the intermediate domain of x the distribution shows the behavior typical for Lévy flights; namely for k large enough, i.e., for $K_\alpha |k|^{2-\alpha} \gg 1$, the characteristic function has the form

$$f(k, t) = \exp\left(-\frac{K}{K_\alpha} |k|^\alpha t\right), \quad (5.56)$$

i.e., it corresponds to the characteristic function of the Lévy distribution. Assuming $\alpha < 2$, we get the following expansion for $f(k, t)$ near $k = 0$:

$$f(k, t) \simeq 1 - Kk^2 t + KK_\alpha t |k|^{4-\alpha} + \dots \quad (5.57)$$

From this expression it is evident that $f(k, t)$ always lacks the fourth derivative at $k = 0$ (for $1 < \alpha < 2$ it even lacks the third derivative), which means that the fourth moment of the corresponding distribution diverges. The absence of higher moments of the distribution explains the particular nature of the truncation implied by our model: the Lévy distribution is truncated by a power law with a power between 3 and 5.

Thus, for all $0 < \alpha < 2$ the corresponding distributions have a finite second moment and, according to the central limit theorem (slowly!) converge to

a Gaussian. For the case $0 < \alpha < 1$ (when $\langle |x|^3 \rangle < \infty$) the speed of this convergence is given by the Berry–Esseen theorem, as noted in Ref. [103]. The convergence criteria for $1 < \alpha < 2$ can be obtained using theorems of Chapter XVI of Ref. [27].

This transition from the initial Lévy-like distribution to a Gaussian is illustrated in Figure 5.14, obtained by a numerical inverse Fourier transform of the characteristic function, Eq. (5.55). Here the case $\alpha = 1$, $K = K_\alpha = 1$ is shown. To combine the functions for $t = 0.001$ and $t = 1000$ in the same plot we rescale them in such a way that the characteristic width of the distribution (defined by $\int_0^{W(t)} f(x, t) dx = 1/4$) is the same. The behavior of the PDF to be at the origin $f(0, t)$ as a function of t is shown on the double logarithmic scales in Figure 5.15. Note the crossover from the initially fast decay $f(0, t) \propto t^{-1/\alpha}$ (Lévy superdiffusion) to the final form $f(0, t) \propto t^{-1/2}$ typical for normal diffusion. This crossover was actually observed when analyzing experimental data in tokamak-edge turbulence [100]. Thus, Eq. (5.54) with the exponent α obtained from fluctuations data may be applied to describe the evolution of the PDF of the potential and electric field fluctuations measured in tokamak-edge plasmas.

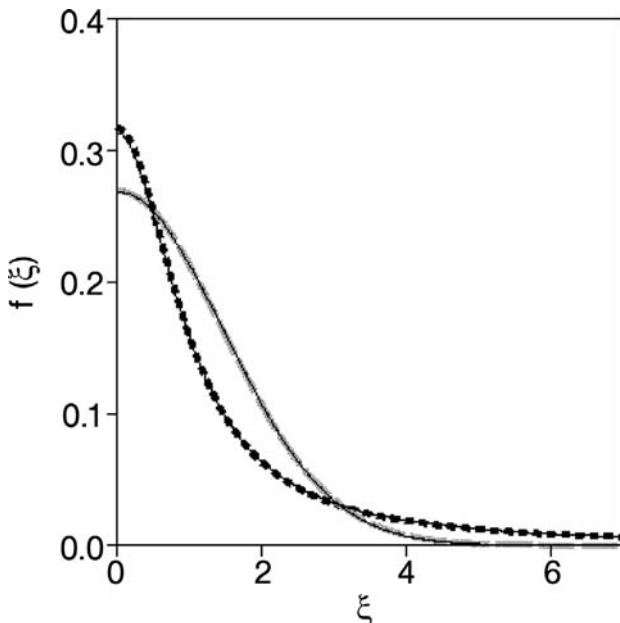


Figure 5.14 The rescaled PDF $f(\xi) = W(t)f(x, t)$ is shown for $t = 0.001$ (dotted line) and for $t = 1000$ (full line) as a function of a rescaled displacement $\xi = x/W(t)$. The corresponding thin lines denote the limiting Cauchy and Gaussian distributions under the same rescaling.

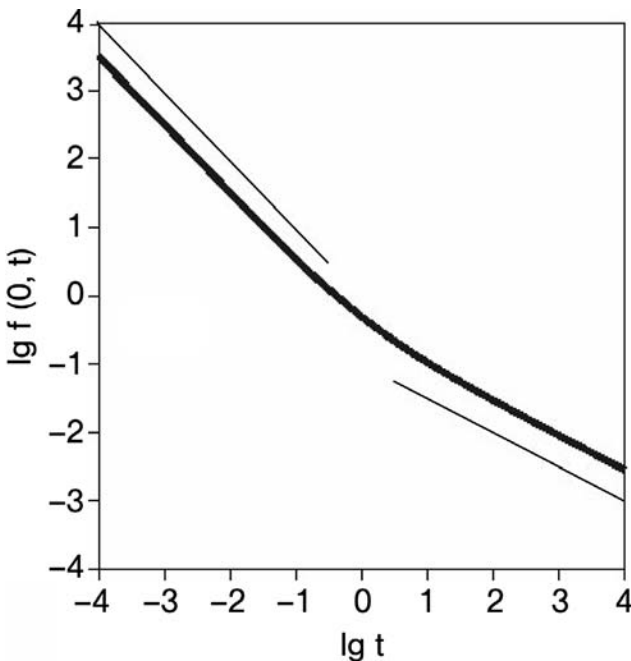


Figure 5.15 The PDF to be at the origin $f(0, t)$ as a function of time. Note the double logarithmic scales. The thick solid line has the slope -1 (with $\alpha = 1$), and corresponds to the superdiffusive decay at small times, and the slope $-1/2$, as in the case of normal diffusion, at large times.

The asymptotics of the PDF at large x is determined by the first nonanalytical term in the expansion, Eq. (5.57), i.e., by $KK_\alpha t |k|^{4-\alpha}$. By making the inverse Fourier transformation of this term and using the Abel method of summation of an improper integral, we get

$$f(x, t) \simeq \frac{\Gamma(5 - \alpha)}{\pi} \frac{\sin(\pi\alpha/2)}{x^{5-\alpha}} \frac{KK_\alpha t}{|k|^{4-\alpha}}, \quad x \rightarrow \infty. \quad (5.58)$$

Thus, in this case the Lévy distribution is truncated not by a Θ - or an exponential function, but by a steeper power law, with a power $\beta = 5 - \alpha$.

This truncation is clearly shown in Figure 5.16 in a log-log scale. At small times the Cauchy asymptote x^{-2} is replaced by the faster decaying asymptote x^{-4} . At large times the Gaussian-like central part of the PDF has a power-law-asymptotic behavior, which again decays as x^{-4} . With increasing time, the central Gaussian part enlarges, and the region of power-law asymptotics shifts toward larger values of x .

Another example for a possible application, a Lévy flight truncated by another, with faster decaying power law, is a much better model for the behavior of commodity prices. Thus, the discussion in Ref. [98] shows that the cumulative distribution function of cotton prices may correspond to a power-law

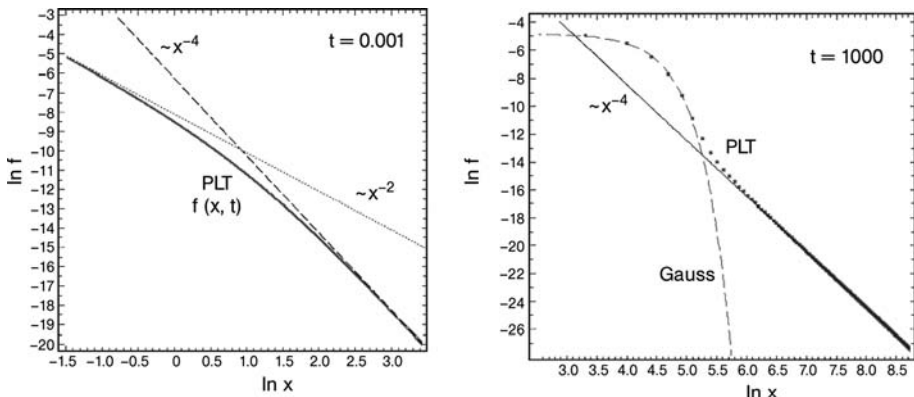


Figure 5.16 Time evolution of power-law truncated (PLT) Lévy flights.

On the left: the solution of Eq. (5.54) at small time is shown by the thick solid line. Thin solid and dashed lines show the asymptotics x^{-2} and x^{-4} , respectively. On the right: the solution of Eq. (5.54) at large time is shown by dots. The Gaussian distribution is depicted by the dashed line. The thin solid line demonstrates the asymptote x^{-4} .

behavior of $1 - F(x) = \int_x^\infty f(y) dy \propto x^{-\alpha}$ with the power $\alpha = 1.7$ in its middle part and the heavy tail decaying as a power law $1 - F(x) \propto x^{-\beta}$ with $\beta \approx 3$. Thus, our equation (which is the simplest form for an equation for truncated Lévy flights) adequately describes this very interesting case giving $\beta = 3.3$. It is likely that fractional equations of the type considered here might be a valuable tool in economic research.

It is worthwhile to note that power-law truncated Lévy flights possess an interesting property: they can be considered as a process subordinated to a Wiener process under the operational time given by the truncated one-sided (extreme) Lévy law of index $\alpha/2$ [101]. The subordination property also sheds light on the possible nature of truncated Lévy distributions in economic processes. The truncated Lévy process can be interpreted as a simple random walk with a finite variance. However, the number of steps of the random walk (the number of transactions) per unit time is not fixed, but fluctuates strongly. The implications of such models to economics were considered in [104]. In our case the distribution function of the number of steps itself has a form of a truncated one-sided Lévy law.

5.8 Summary

Lévy flights represent a widely used tool in the description of anomalous stochastic processes. By their mathematical definition, Lévy flights are Markov-

ian and their statistical limit distribution emerges from independent identically distributed random variables, by virtue of the generalized central limit theorem. Despite their popularity, comparatively long history, and their Markovian nature, Lévy flights are not fully understood. The proper formulation in the presence of nontrivial boundary conditions, their behavior in external potentials both infinitely high and finite, as well as their thermodynamical meaning are under ongoing investigation. This is discussed in the reviews [41, 42, 105], with numerous examples listed. We also recommend the introductory articles [106] and [107] devoted to these and closely related topics.

In this review, we have addressed some of the fundamental properties of random processes, these being the behavior in external force fields, the first passage behavior, as well as the Kramers-like escape over a potential barrier. We have shown that dissipative nonlinear mechanisms cause a natural cutoff in the PDF, so that within a finite experimental range the untruncated Lévy flights provide a reasonable physical description. We also considered power-law truncated Lévy flights showing transition from the Lévy to Gaussian law behavior in the course of time.

While the continuous time random walk model for Lévy flights in the absence of nontrivial boundary conditions or external potentials is a convenient description, in all other cases the fractional Fokker–Planck equation or, equivalently, the Langevin equation with white Lévy stable noise are the description of choice. These equations in most cases cannot be solved exactly, however, it is usually straightforward to obtain the asymptotic behavior, or to solve them numerically.

References

- 1** B.D. Huges. *Random Walks and Random Environments*, vol. 1, Oxford University Press, Oxford, 1995.
- 2** P.P. Lévy, *Théorie de l'Addition des Variables Aléatoires*, 2nd edn., Gauthier-Villars, Paris 1954. (1st edn., 1937).
- 3** B.V. Gnedenko, A.V. Kolmogorov. *Limit Distributions for Sums of Independent Random Variables*, Addison-Wesley, Cambridge, MA, 1954. (Russian edition: 1949).
- 4** J.-P. Bouchaud and A. Georges, Phys. Rev. A **41**, 1156 (1990).
- 5** P.D. Ditlevsen, Geophys. Res. Lett. **26**, 1441 (1999).
- 6** M.F. Shlesinger and J. Klafter, in: *On Growth and Form*, edited by H.E. Stanley and N. Ostrowsky, Martinus Nijhoff Publishers, Amsterdam, pp. 279–283 (1986).
- 7** G.M. Viswanathan et al., Nature **401**, 911 (1999).
- 8** A.M. Reynolds and M.A. Frye, PLoS ONE **2**(4), e354 (2007).
- 9** R.P.D. Atkinson, C.J. Rhodes, D.W. Macdonald, and R.M. Anderson, OIKOS **98**, 134 (2002).
- 10** G. Ramos-Fernandez et al., Behav. Ecol. Sociobiol. **55**, 223 (2003).
- 11** F. Bartumeus, Fractals **15**, 151 (2007).
- 12** F. Bartumeus et al., Phys. Rev. Lett. **88**, 097901 (2002).

- 13** M.A. Lomholt, T. Koren, R. Metzler, and J. Klafter, Proc. Natl. Acad. Sci., at press.
- 14** I.M. Sokolov, J. Mai, and A. Blumen, Phys. Rev. Lett. **79**, 857 (1997).
- 15** D. Brockmann and T. Geisel, Phys. Rev. Lett. **91**, 048303 (2003).
- 16** M.A. Lomholt, T. Ambjörnsson, and R. Metzler, Phys. Rev. Lett. **95**, 260603 (2005).
- 17** L. Hufnagel, D. Brockmann, and T. Geisel, Proc. Natl. Acad. Sci. **101**, 15124 (2004).
- 18** D. Brockmann, L. Hufnagel, and T. Geisel, Nature **439**, 462 (2006).
- 19** H. Katori, S. Schlipf, and H. Walther, Phys. Rev. Lett., **79**, 2221 (1997).
- 20** G. Zumofen and J. Klafter, Chem. Phys. Lett. **219**, 303 (1994).
- 21** E. Barkai and R. Silbey, Chem. Phys. Lett. **310**, 287 (1999).
- 22** E. Barkai, R. Silbey, and G. Zumofen, Phys. Rev. Lett. **84**, 5339 (2000).
- 23** B.B. Mandelbrot, J. Bus, **36**, 394 (1963).
- 24** R.N. Mantegna and H.E. Stanley, Nature **383**, 587 (1996).
- 25** J.-P. Bouchaud and M. Potters, *Theory of Financial Risks*, Cambridge University Press, Cambridge, UK, 2000.
- 26** E. Lutz, Phys. Rev. Lett. **93**, 190602 (2004).
- 27** W. Feller, *An Introduction to Probability Theory and its Applications*, vol. 2., Wiley, New York, 1971.
- 28** V.M. Zolotarev, *One-Dimensional Stable Distributions*, American Mathematical Society, Providence, RI, 1986 (Russian edition: 1983).
- 29** G. Samorodnitsky, M.S. Taqqu, *Stable Non-Gaussian Random Processes*, Chapman & Hall, New York, 1994, p. 619.
- 30** C. Fox, Trans. Am. Math. Soc. **98**, No.3, 395 (1961).
- 31** W.R. Schneider, Stable distributions: Fox function representation and generalization. in: S. Albeverio, G. Casati, D. Merlini (eds.), *Stochastic Processes in Classical and Quantum Systems*, Lecture Notes in Physics, Springer, Berlin, 1986, pp. 497–511.
- 32** A.M. Mathai, R.K. Saxena, *The H-Functions with Applications in Statistics and Other Disciplines*, Wiley Eastern, New Delhi, 1978, p. 235.
- 33** H.M. Srivastava, K.G. Gupta, S.P. Goyal, *The H-Functions of One and Two Variables with Applications*, South Asian Publisher, New Delhi, 1982, p. 186.
- 34** H. Pollard, Bull. Am. Math. Soc. **52**, 908 (1946).
- 35** H. Bergström, Ark. Math. **2**, 375 (1952).
- 36** Y.V. Linnik, Dokl. Akad. Nauk SSSR **94**, 619 (1954).
- 37** A.V. Skorokhod, Dokl. Akad. Nauk SSSR **98**, 731 (1954).
- 38** E.W. Montroll and G.H. Weiss, J. Math. Phys. **10**, 753 (1969).
- 39** E.W. Montroll and H.J. Scher, J. Stat. Phys. **9**, 101 (1973).
- 40** J. Klafter, A. Blumen, and M.F. Shlesinger, Phys. Rev. A **35**, 3081 (1987).
- 41** R. Metzler and J. Klafter, Phys. Rep. **339**, 1 (2000).
- 42** R. Metzler and J. Klafter, J. Phys. A **37**, R161 (2004).
- 43** A. Erdélyi, *Bateman Manuscript Project Higher Transcendental Functions*, Vol. III, McGraw-Hill, New York, 1955.
- 44** R. Metzler, E. Barkai, and J. Klafter, Phys. Rev. Lett. **82**, 3563 (1999).
- 45** R. Metzler and T.F. Nonnenmacher, Chem. Phys. **284**, 67 (2002).
- 46** M.F. Shlesinger, G.M. Zaslavsky, and J. Klafter, Nature **363**, 31 (1993).
- 47** I.I. Gikhman and A.V. Skorohod, *Theory of Stochastic Processes II*, Springer, Berlin, 1975.
- 48** H.C. Fogedby, Phys. Rev. Lett. **73**, 2517 (1994); H.C. Fogedby, Phys. Rev. E **58**, 1690 (1998).
- 49** R. Metzler, E. Barkai, and J. Klafter, Europhys. Lett. **46**, 431 (1999).
- 50** S. Jespersen, R. Metzler, and H.C. Fogedby, Phys. Rev. E **59**, 2736 (1999).
- 51** A. Dubkov and B. Spagnolo, Fluctuat. Noise Lett. **5**, L267–L274 (2005).
- 52** A.I. Saichev and G.M. Zaslavsky, Chaos **7**, 753 (1997).
- 53** S.G. Samko, A.A. Kilbas, and O.I. Marichev, *Fractional Integrals and Derivatives, Theory and Applications*, Gordon and Breach, New York, 1993.

- 54** I. Podlubny, *Fractional Differential Equations*, Academic Press, San Diego, CA, 1998.
- 55** R. Metzler, Euro. Phys. J. B**19**, 249 (2001).
- 56** G.H. Weiss. *Aspects and Applications of the Random Walk*, North-Holland, Amsterdam, 1994.
- 57** I.M. Sokolov and R. Metzler, J. Phys. A **37**, L609 (2004).
- 58** I.M. Sokolov, J. Klafter, and A. Blumen, Phys. Rev. E **64**, 021107 (2001).
- 59** D. Brockmann and I.M. Sokolov, Chem. Phys. **284**, 409 (2002).
- 60** Ya. Gambin, G. Massiera, L. Ramos, Ch. Ligoure, and W. Urbach, Phys. Rev. Lett. **94**, 110602 (2005).
- 61** T. Koren, M.A. Lomholt, A.V. Chechkin, J. Klafter, and R. Metzler, Phys. Rev. Lett. **99**, 160602 (2007).
- 62** E. Sparre Andersen, Math. Scand. **1**, 263 (1953); E. Sparre Andersen, Math. Scand. **2**, 195 (1954).
- 63** S. Redner. *A Guide to First-Passage Processes*, Cambridge University Press, Cambridge, UK, 2001.
- 64** U. Frisch and H. Frisch, in: *Lévy Flights and Related Topics in Physics*, edited by M.F. Shlesinger, G.M. Zaslavsky, and U. Frisch, Lecture notes in physics, vol. 450, Springer, Berlin, 1995.
- 65** G. Zumofen and J. Klafter, Phys. Rev. E **51**, 2805 (1995).
- 66** I. Eliazar and J. Klafter, Physica A **336**, 219 (2004).
- 67** F. Mainardi, in: *Fractals and Fractional Calculus in Continuum Mechanics*, edited by A. Carpinteri and F. Mainardi, CISM Courses and Lectures, vol. 378, Springer, Wien, 1997, p. 291.
- 68** T. Koren, A.V. Chechkin, and J. Klafter, Physica A **379**, 10 (2007).
- 69** A.V. Chechkin, R. Metzler, V.Yu. Gonchar, J. Klafter, and L.V. Tanatarov, J. Phys. A: Math. Gen. **36**, L537 (2003).
- 70** A.V. Chechkin, J. Klafter, V.Yu. Gonchar, R. Metzler, and L.V. Tanatarov, Phys. Rev E **67**, 010102(R) (2003).
- 71** A.V. Chechkin, V.Yu. Gonchar, J. Klafter, R. Metzler, L. Tanatarov, Chem. Phys. **284**, 233 (2002).
- 72** A.V. Chechkin, V.Yu. Gonchar, J. Klafter, R. Metzler, and L.V. Tanatarov, J. Stat. Phys. **115**, 1505 (2004).
- 73** I. Eliazar and J. Klafter, J. Stat. Phys. **111**, 739 (2003).
- 74** P. Hänggi, P. Talkner, and M. Borkovec, Rev. Mod. Phys. **62**, 251 (1990).
- 75** A.V. Chechkin, V.Yu. Gonchar, J. Klafter, and R. Metzler, Europhys. Lett. **75**, 348 (2005).
- 76** B. Dybiec, E. Gudowska-Nowack, and P. Hänggi, Phys. Rev. E **75**, 021109 (2007).
- 77** A.V. Chechkin, O.Yu. Sliusarenko, R. Metzler, and J. Klafter, Phys. Rev. E **75**, 041101 (2007).
- 78** P. Imkeller and I. Pavlyukevich, J. Phys. A **39**, L237 (2006); P. Imkeller and I. Pavlyukevich, Stochastic Proc. Appl. **116**, 611 (2006).
- 79** P.D. Ditlevsen, Phys. Rev. E **60**, 172 (1999).
- 80** H. Risken, *The Fokker–Planck Equation*, Springer, Berlin, 1989.
- 81** Yu.L. Klimontovich, *Statistical Physics*, Nauka, Moscow, 1982; Harwood Academic, New York, 1986.
- 82** B.J. West and V. Seshadri, Physica A **113**, 203 (1982).
- 83** F.E. Peseckis, Phys. Rev. A **36**, 892 (1987).
- 84** A.V. Chechkin, and V. Yu. Gonchar, Journ. Exp. Theor. Phys. **91**, 635 (2000).
- 85** A.V. Chechkin, V. Yu. Gonchar, and M. Szydlowski, Phys. Plasmas **9**, 78 (2002).
- 86** B. Kursunoglu, Ann. Phys. (N.Y.) **17**, 259 (1962).
- 87** B. Kursunoglu, Phys. Rev. **132**, 21 (1963).
- 88** J.A. Krommes, Phys. Rep. **360**, 1 (2002).
- 89** A.V. Chechkin, V.Yu. Gonchar, J. Klafter, and R. Metzler, Phys. Rev. E **72**, 010101(R) (2005).
- 90** N.N. Bogoliubov and Y.A. Mitropolsky, *Asymptotic Methods in the Theory of Non-Linear Oscillations*, Hindustan Publication, Delhi, 1961 (distributed by Gordon&Breach, New York).
- 91** H. Davis, *Introduction to Nonlinear Differential and Integral Equations*, Dover Publications, New York, 1962.

- 92** A.A. Andronov, C.E. Chaikin, and S. Lefschetz, *Theory of Oscillations*, University Press, Princeton, NJ, 1949.
- 93** Yu.L. Klimontovich, *Turbulent Motion and the Structure of Chaos: A New approach to the Statistical Theory of Open Systems*, Kluwer, Dordrecht, 1992.
- 94** M.F. Shlesinger, B.J. West, and J. Klafter, Phys. Rev. Lett. **58**, 1100 (1987).
- 95** R.N. Mantegna and H.E. Stanley, Phys. Rev. Lett. **73**, 2946 (1994).
- 96** I. Koponen, Phys. Rev. E **52** 1197 (1995).
- 97** R.N. Mantegna and H.E. Stanley, J. Stat. Phys. **89**, 469 (1997).
- 98** H.E. Stanley, Physica A **318** (2003) 279.
- 99** B. Dubrulle, J.-Ph. Laval, Eur. Phys. J. B **4**, 143 (1998).
- 100** R. Jha, P.K. Kaw, D.R. Kulkarni, and J.C. Parikh, ADITYA Team, Phys. Plasmas **10**, 699 (2003).
- 101** I.M. Sokolov, A.V. Chechkin, and J. Klafter, Physica A **336**, 245 (2004).
- 102** A.V. Chechkin, R. Gorenflo, and I.M. Sokolov, Phys. Rev. E **66**, 046129 (2002).
- 103** M.F. Shlesinger, Phys. Rev. Lett. **74**, 4959 (1995).
- 104** P.K. Clark, Econometrica **41**, 135 (1973).
- 105** A.V. Chechkin, V.Yu. Gonchar, J. Klafter, and R. Metzler, in: *Fractals, Diffusion, and Relaxation in Disordered Complex Systems*, edited by W.T. Coffee and Yu.P. Kalmykov, A Special Volume of Advances in Chemical Physics **133B**, 439 (2006).
- 106** J. Klafter, M.F. Shlesinger, and G. Zumofen, Phys. Today **49**, No.2, 33 (1996).
- 107** I.M. Sokolov and J. Klafter, A. Blumen, Phys. Today **55**, November, 48 (2002).

6

Fractional Diffusion Models of Anomalous Transport

Diego del-Castillo-Negrete

6.1

Introduction

In the standard diffusion paradigm, the transport of a scalar quantity, f , e.g., temperature or density, is characterized by the Fourier–Fick’s law, $q = -\chi \partial_x f$, that establishes a local relationship between the flux, q , and the gradient of f . This relation, together with the conservation law, $\partial_t f = -\partial_x q$, leads to the well-known diffusion equation, $\partial_t f = \partial_x (\chi \partial_x f)$, where χ is the diffusion coefficient. From the point of view of statistical mechanics, diffusive transport can be conceived as the macroscopic manifestation of an underlying “microscopic” uncorrelated, Gaussian stochastic process, i.e., a Brownian random walk. However, despite its relative success, this diffusion equation fails to describe anomalous transport processes. In the case of particle transport, anomalous transport is often characterized by non-Gaussian probability distributions functions (PDFs) of the particles displacements and by the nondiffusive scaling of the corresponding statistical moments. The goal of this chapter is to discuss the application of fractional diffusion to model this type of transport.

Fractional diffusion models are formulated using fractional derivative operators instead of regular derivatives. Fractional derivatives are integro differential operators that extend the notion of derivative to fractional orders. It is interesting to point out that despite the fact that the origins of fractional calculus go back to the origins of standard calculus, the use of fractional operators in modeling transport and the development of numerical integration methods is a fairly recent and rapidly developing area of applied mathematics.

A clear link between fractional diffusion and anomalous transport is provided by the theory of random walks. The simplest type of random walk is the Brownian motion in which the dynamics is governed by an uncorrelated, Markovian, Gaussian stochastic process. In this case, the dynamics can be described at a macroscopic level using the diffusion equation. This connection, which goes back at least as far as the works of Einstein, Smoluchowsky, and Bachelier in the early 1900s, not only provides an inspiring view of the diffusion model but also points out its limitations. In particular, when the ran-

dom walk involves correlations, non-Gaussian statistics, or non-Markovian “memory” effects, the diffusion equation fails to describe the macroscopic limit. In a seminal work, Montroll and Weiss [1, 2] proposed a generalization of the Brownian random walk called the continuous time random walk (CTRW) model that allows the incorporation of nondiffusive effects. In particular, the CTRW allows the use of algebraically decaying PDFs describing memory effects, and non-Gaussian, algebraically decaying PDFs describing large jumps. As we will describe in detail below, in the continuum limit, the CTRW model leads to the fractional diffusion equation in which the fractional order of the fractional derivatives in space and time depends on the algebraic decay exponents of the jumps and waiting time PDFs, respectively.

The fractional diffusion equation is able to reproduce key aspects of anomalous transport including the non-Gaussian self-similar nature of the PDFs of particle displacement and the anomalous scaling of the moments. Also, the integro-differential nature of the fractional derivative operators allows the description of spatiotemporal nonlocal transport processes. In particular, in fractional diffusion, the local Fourier–Fick’s law is replaced by an integral operator in which the flux at a given point in space depends globally on the spatial distribution of the transported scalar and on the time history of the transport process.

The main objectives of this chapter are (i) use the CTRW to motivate the meaning of fractional diffusion in the context of passive scalar transport in fluids, (ii) review the phenomenology and basic formal properties of fractional diffusion, (iii) discuss the application of fractional diffusion to model transport of passive tracers in turbulence, and (iv) present numerical methods for the study of fractional diffusion in finite-size domains. Although our interest in these problems is mainly motivated by the study of transport in fluids and plasmas, the discussion and results presented in this paper should be of wider applicability and interest.

The organization of the rest of this chapter is as follows. Section 6.2 presents basic concepts of anomalous transport and introduces the fractional diffusion equation. The discussion is based on the study of transport of passive tracers in flows with coherent structures. It is shown that this system can be naturally described using the CTRW model. The fractional diffusion equation is then obtained as a macroscopic transport equation describing the continuum limit of the CTRW. Section 6.3 presents a brief review of basic concepts of fractional calculus in order to make the rest of the chapter as self-contained as possible. This section also discusses the interplay of regular and fractional diffusion, and the role of truncated Lévy processes in anomalous transport which are problems of interest in applications. The last part of this section discusses nonlocality and uphill transport and presents an application of fractional diffusion to turbulent transport. Many applied transport problems in-

volve finite-size domains with physical boundary conditions. However, the use of fractional derivative operators in this case is nontrivial due to the potential singularity of these operators at the boundaries. To address this issue, Section 6.4 formulates fractional diffusion models in finite-size domains and presents finite-differences numerical integration techniques. The numerical methods are illustrated with the solution of fractional diffusion boundary value problems of interest to anomalous heat transport in plasma physics.

6.2 Anomalous Transport

This section introduces basic concepts of anomalous transport [3] and motivates the origin and meaning of fractional diffusion. We focus on transport of passive tracers in flows with coherent structures. In this system, transport is dominated by vortices that trap tracers for long times and zonal flows that advect tracers for long distances. The trajectories of tracers in this problem exhibit random behavior with non-Gaussian statistics that cannot be modeled using the Brownian random walk model. In particular, experimental [4] and numerical [5, 6] results show that the combined effect of vortex trapping and zonal flow advection leads to nondiffusive anomalous transport. This fluid mechanics problem is used to provide a physical motivation for the CTRW model [1, 2] that allows the incorporation of long-range (algebraic decaying) trapping and jump probability distribution functions (PDFs). We discuss how the fractional diffusion equation follows naturally from the continuum limit of the CTRW in a way similar to how the standard diffusion equation follows from the Brownian random walk [7–10].

6.2.1

Anomalous Transport of Tracers in Flows with Coherent Structures

Passive tracers in fully developed, homogeneous, isotropic turbulence exhibit Brownian random motion. In this case, transport is normal and can be modeled using advection–diffusion equations with effective, i.e., renormalized, diffusivities, and advection velocities [11]. However, in the presence of coherent structures like vortices and zonal flows, the situation is quite different. The competition of the trapping effect of vortices and the large displacements induced by zonal flows typically gives rise to nondiffusive anomalous transport. Understanding this type of transport is a problem of significant interest in geophysical fluid dynamics, laboratory experiments, engineering, and plasma physics due to the ubiquitousness of coherent structures in these systems.

The role of vortices and zonal flows in anomalous transport is clearly illustrated in the experiment discussed in Ref. [4] and in the corresponding chaotic advection model proposed in Refs. [5, 6]. The experiment consists of a rapidly rotating annulus in which a forcing mechanism induces a strong azimuthal zonal flow. When the forcing exceeds a threshold, the zonal flow destabilizes and generates a chain of vortices that rotates around the annulus. Tracer transport in the experiment is studied by tracking small, neutrally buoyant particles with negligible drag. In the model, transport of tracers is described using a Hamiltonian chaotic advection dynamical system. Figure 6.1 shows the flow pattern in the co-rotating reference frame of the vortex chain as revealed by individual particle streaks in the experiment and in the model. In this reference frame, the flow is time independent and tracers either remain trapped in vortices or encircle the annulus following the inner or outer zonal flows flanking the vortices. To produce chaotic transport in the experiment, a time-dependent perturbation is added by modulating the forcing of the zonal flow. In the model, chaotic transport is achieved by introducing a time-dependent Hamiltonian perturbation that breaks the integrability (KAM tori) of the unperturbed system. Because of the time-dependent perturbation, the tracers alternate in a seemingly unpredictable way between being trapped in the vortices and moving following the zonal flows as shown in Figure 6.2.

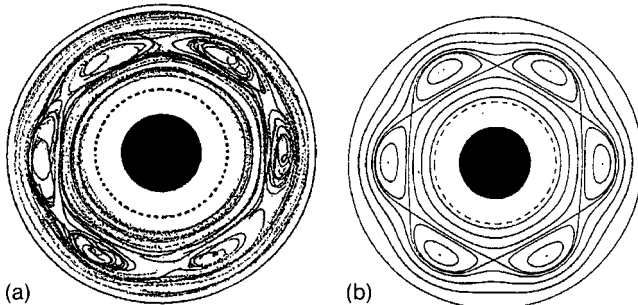


Figure 6.1 Comparison between the velocity field in the rotating annulus experiment, as revealed by particle streaks (a) (after Ref. [4]), and a contour plot of the unperturbed streamfunction (Hamiltonian) of the chaotic advection model in Ref. [5], (b). When the flow velocity is time independent in the reference frame of the vortex chain, tracers are either trapped in the vortices or move around the annulus carried by the zonal flows flanking the vortex chain.

The two most commonly used statistical measures of transport are the mean, $M(t)$, and the variance, $\sigma^2(t)$, defined as

$$M(t) = \langle \delta x \rangle, \quad \sigma^2(t) = \langle [\delta x - \langle \delta x \rangle]^2 \rangle, \quad (6.1)$$

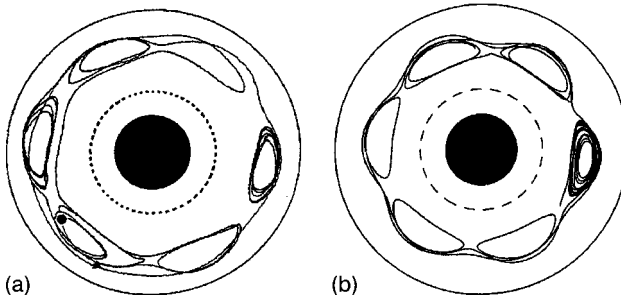


Figure 6.2 Comparison between a typical chaotic particle trajectory in the experiment (a) (after Ref. [4]), and the model in Ref. [5], (b). When the flow velocity is time dependent in the reference frame of the vortex chain, tracers alternate chaotically between being trapped in the vortices and moving following the zonal flows.

where $\langle \rangle$ denotes average over an ensemble of initial conditions, and $\delta x = x(t) - x(0)$ is the particle displacement, which in the case of the annulus experiment corresponds to the azimuthal displacement in the direction of the zonal flows. Because radial particle motion is bounded by the zonal flows and by the annulus boundaries, transport in this direction is not relevant. Also, when computing δx , the net arc length of the particle displacement is considered and not the angular displacement which is trivially bounded by 2π due to the periodicity of the system. Transport is characterized by the long-time behavior of M , σ^2 , and the PDF of particle displacements, $P(\delta x, t)$. A naive approach to this problem would assume that, at long times, the dynamics of P is governed by an advection–diffusion equation of the form

$$\partial_t P + V \partial_x P = \partial_x (\chi \partial_x P), \quad (6.2)$$

with mean transport velocity V , and effective diffusivity χ , defined as

$$V = \lim_{t \rightarrow \infty} \frac{M(t)}{t}, \quad \chi = \lim_{t \rightarrow \infty} \frac{\sigma^2(t)}{2t}. \quad (6.3)$$

As mentioned before, this approach has been successfully applied in the study of transport in fully developed turbulence in the absence of coherent structures. However, the presence of coherent structures alters the statistics of the passive tracers and typically gives rise to anomalous advection and/or anomalous diffusion. This type of transport is characterized by the anomalous scaling

$$M \sim t^\zeta, \quad \sigma^2 \sim t^\gamma, \quad (6.4)$$

with $\zeta \neq 1$ and $\gamma \neq 1$. In the subdiffusion regime, $0 < \gamma < 1$, the variance grows slower than in the diffusive case implying $\chi = 0$ in Eq. (6.3). On the

other hand, when $1 < \gamma < 2$, there is superdiffusion and the variance grows faster than in a diffusive process implying a divergent, $\chi = \infty$, effective diffusivity. A similar terminology is applied to anomalous advection, with $\zeta < 1$ ($\zeta > 1$) corresponding to anomalous subadvection (superadvection). In the rotating annulus experiment, transport is superdiffusive with the experimentally determined exponent, $\gamma_{\text{exp}} = 1.65 \pm 0.15$. As shown in Figure 6.3, the scaling exponent in the model, $\gamma_{\text{mod}} = 1.57$, agrees with the measured exponent within experimental uncertainty. The figure also shows time series of typical trajectories in the model exhibiting trapping and flight events of different duration.

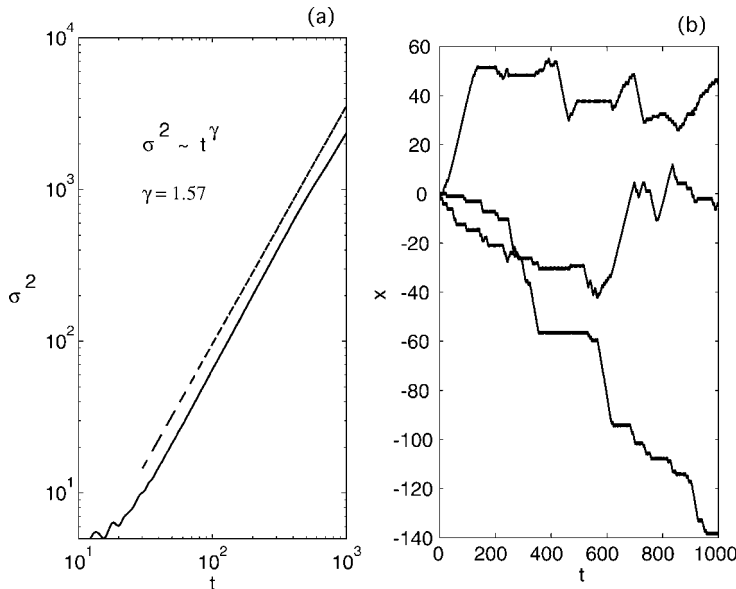


Figure 6.3 Scaling of the variance, σ^2 , (left panel) and typical trajectories of passive tracers (right panel) in the model [5]. The model exhibits superdiffusive scaling with $\gamma = 1.57$ which agrees well with the experimental result $\gamma = 1.65 \pm 0.15$ reported in Ref. [4].

Anomalous transport is closely related to the decay of the Lagrangian velocity autocorrelation function

$$\mathcal{C} = \langle u(0)u(\tau) \rangle, \quad (6.5)$$

where $u(t) = dx/dt$ is the velocity along the trajectory. According to Taylor's relation, $d\sigma^2/dt = 2 \int_0^t \mathcal{C}(\tau) d\tau$. When \mathcal{C} decays rapidly, the integral in this relation converges, and the effective diffusivity can be defined as the limit

$$\chi = \lim_{t \rightarrow \infty} \int_0^t \mathcal{C}(\tau) d\tau, \quad (6.6)$$

which is a particular case of the Green–Kubo formula. However, if the Lagrangian correlation exhibits slow algebraic decay of the form

$$\mathcal{C} \sim \tau^{-v}, \quad (6.7)$$

with $v < 1$, the effective diffusivity in Eq. (6.6) diverges as in the case of superdiffusive transport with $\gamma = 2 - v$.

In addition to the moments and the Lagrangian velocity autocorrelation, two useful diagnostics in the study of anomalous transport in the presence of coherent structures are the PDF of trapping events of duration t , $P_{\text{trap}}(t)$, and the PDF of flight events of duration t , $P_{\text{flight}}(t)$. A trapping event is defined as a portion of a trajectory that encircles a vortex at least once without leaving it, and a flight event is defined as any portion of a trajectory that is not a trapping event. As shown in Figure 6.3, particle trajectories consist of sequences of trapping and flight events of different duration. In the rotating annulus experiment it was observed that both P_{trap} and P_{flight} exhibit algebraic decay of the form $P_{\text{trap}} \sim t^{-v}$ and $P_{\text{flight}} \sim t^{-\mu}$ with the experimentally measured exponents $v_{\text{exp}} = 1.6 \pm 0.3$ and $\mu_{\text{exp}} = 2.3 \pm 0.2$, respectively. In good agreement with the experiment, the scaling exponents in the model are $v_{\text{mod}} = 1.8$ and $\mu_{\text{mod}} = 2.4$ [5].

Since power laws are scale invariant, the algebraic decay of P_{trap} and P_{flight} implies that there is not a characteristic transport scale and that the distribution of trapping and flight events is statistically self-similar. The slow decay of algebraic tails is also directly linked to intermittency, i.e., the significant presence of very large trapping and flight events. Most importantly, the m th moment, of the flights PDF, $\langle t^m \rangle = \int t^m P_{\text{flight}} dt$, diverges for $m \geq \mu - 1$, and the m th moment, of the trapping PDF diverges for $m \geq v - 1$. Assuming that the jump velocity of particles is constant, the case $\mu < 3$ corresponds to Lévy flights for which the second moment diverges in an unbounded domain. Along with the anomalous scaling of the moments, the Lagrangian velocity autocorrelation, and the trapping and flights PDFs, anomalous transport is characterized by non-Gaussian PDFs of particle displacements. In particular, in the presence of strong zonal flows (like in the rotating annulus experiment) $P(\delta x, t)$ exhibits algebraic decaying tails [5].

The relevance of coherent structures on transport goes beyond rotating fluids. Magnetically confined plasmas also exhibit coherent structures that have a nontrivial influence on transport. There is in fact a close analogy between these two problems, and transport models, like the one discussed above for the annulus experiment, are applicable, under suitable approximations, to magnetized plasmas [6]. In Section 6.3, we will study in more detail anomalous transport and fractional diffusion in plasma turbulence.

6.2.2

Continuous Time Random Walk Model and Fractional Diffusion

The motion of tracers in isotropic fully developed turbulence is well described by the Brownian random walk. However, the description of tracers in the presence of coherent structures, like in the rotating annulus experiment, requires a richer model able to incorporate the trapping effect of vortices and the flights induced by zonal flows described above. The CTRW model [1,2,12,13] is a natural description of this type of anomalous transport. The CTRW describes an ensemble of particles that at times, $\tau_1, \tau_2, \dots, \tau_i \dots$, experience a displacement, or jump, of size $x_1, x_2, \dots, x_i \dots$. Both the waiting times, $t_i = \tau_i - \tau_{i-1}$, and the jumps, x_i , are random variable drawn from a waiting-time PDF $\psi(t)$ and a jump PDF $\eta(x)$, respectively. This model generalizes the Brownian walk in two ways. First, contrary to the Brownian random walk where particles are assumed to jump at discrete fixed time intervals, the CTRW model allows the possibility of incorporating waiting times. In addition, the CTRW model allows the possibility of using general, non-Gaussian jump distribution functions with divergent moments to account for Lévy flights. Given ψ and η , the probability of finding a tracer at position x and time t is determined by the Montroll–Weiss equation [1,2]

$$\begin{aligned} P(x, t) &= \delta(x) \int_t^\infty \psi(t') dt' \\ &+ \int_0^t \psi(t-t') \left[\int_{-\infty}^\infty \eta(x-x') P(x', t') dx' \right] dt'. \end{aligned} \quad (6.8)$$

The first term on the right-hand side is the contribution to P of particles that have not moved during the time interval $(0, t)$, and the second term denotes the contribution to P of particles located at x' and jumping to x during this time interval. Equation (6.8) can also be written as the generalized master equation

$$\partial_t P = \int_0^t dt' \phi(t-t') \int_{-\infty}^\infty dx' [\eta(x-x') P(x', t') - \eta(x-x') P(x, t')] , \quad (6.9)$$

where ϕ is the memory function. The spatial integral on the right-hand side represents the gain–loss process for P at x . In particular, since $\eta(x-x')$ determines the transition probability between x and x' , the first term inside the square bracket gives the increase of P due to particles moving to x , while the second term describes the decrease of P due to particles moving away from x . In Fourier–Laplace variables,

$$\mathcal{F}[\eta] = \hat{\eta}(k) = \int_{-\infty}^\infty e^{ikx} \eta(x) dx , \quad \mathcal{L}[\phi] = \tilde{\phi}(s) = \int_0^\infty e^{st} \phi(t) dt , \quad (6.10)$$

the Montroll–Weiss master equation (6.9) takes the form

$$\hat{P}(k, s) = \frac{1 - \tilde{\psi}(s)}{s} \frac{1}{1 - \tilde{\psi}(s)\hat{\eta}(k)}. \quad (6.11)$$

where the relation between the waiting time PDF and the memory function is given by $\tilde{\phi} = s\tilde{\psi}/(1 - \tilde{\psi})$ [13]. In the Markovian approximation, memory effects are neglected and $\phi = \delta(t)$. In this case, $\psi = e^{-t}$ and, as expected, Eq. (6.9) reduces to the standard master equation [14].

The CTRW master equation contains “too much” microscopic kinetic information that is to some degree irrelevant for the description of transport at the macroscopic scale of interest. For example, in a random walk simulation the positions and velocities of a very large number of particles are individually tracked, although what is relevant from the macroscopic transport point view is the long time, coarse grain (with respect to the microscopic scales) evolution of the single-particle distribution function. This motivates working with the continuum, fluid limit of the master equation as opposed to the full kinetic description of the underlying random walk. This limit is obtained by taking the leading order terms in the long wavelength, $k \rightarrow 0$, and time asymptotic, $s \rightarrow 0$, expansion of Eq. (6.11). A key aspect of the fluid limit is that only the asymptotic behavior, i.e., the tails of the η and ψ PDFs matter. This is a significant advantage over the use of the kinetic master equation that requires the detailed knowledge of these functions. Below we present a simplified discussion of the fluid limit of the CTRW. A more formal and general discussion can be found in Refs. [7–10].

As expected, in the Markovian–Gaussian case

$$\psi(t) = \mu e^{-\mu t}, \quad \eta(x) = \frac{1}{\sqrt{2\pi}\sigma} e^{-x^2/(2\sigma^2)}, \quad (6.12)$$

where $\langle t \rangle = 1/\mu$ is the characteristic waiting time and $\sigma^2 = \langle x^2 \rangle$ is the characteristic mean square jump, the fluid limit of the master equation Eq. (6.11) leads to the standard diffusion equation

$$\partial_t P = \chi \partial_x^2 P. \quad (6.13)$$

To see this, note that in the limits $s \rightarrow 0$ and $k \rightarrow 0$, the Fourier–Laplace transforms of Eq. (6.12) implies

$$\begin{aligned} \tilde{\psi}(s) &= \frac{1}{1 + s\langle t \rangle} \approx 1 - \langle t \rangle s + \dots, \\ \hat{\eta}(k) &= e^{-\sigma^2 k^2/2} \approx 1 - \frac{\sigma^2}{2} k^2 + \dots. \end{aligned} \quad (6.14)$$

Using Eqs. (6.14), Eq. (6.11) reduces to leading order in s and k^2 to

$$s \hat{P}(s, k) - 1 = -\chi k^2 \hat{P}, \quad (6.15)$$

where χ is assumed to scale as $\chi \sim \langle x^2 \rangle / (2\langle t \rangle)$. Using the basic properties of the Laplace–Fourier transforms,

$$\mathcal{L} [\partial_t P] = s \tilde{P}(x, s) - P(x, 0), \quad \mathcal{F} [\partial_x^2 P] = -k^2 \hat{P}(k, t), \quad (6.16)$$

the inversion of the Fourier–Laplace transforms in Eq. (6.15), gives the diffusion equation in Eq. (6.13) for $P(x, 0) = \delta(x)$.

However, the situation is quite different in the case of algebraic decaying PDF of the form

$$\psi \sim t^{-(\beta+1)}, \quad \eta \sim |x|^{-(\alpha+1)}, \quad (6.17)$$

where for simplicity we have assumed that η is symmetric. As in the case of transport in the presence of vortices and zonal flows discussed above, the use of this type of algebraic decaying PDFs is motivated by the significant probability of very large trapping events and very large flight events. Note that for $0 < \beta < 1$, $\langle t \rangle$ diverges, and there is not a characteristic waiting time. Similar, for $\alpha < 2$, $\langle x^2 \rangle$ diverges, indicating a lack of characteristic transport scale. The asymptotic behavior in Eq. (6.17) implies the scaling

$$\tilde{\psi}(s) \approx 1 - s^\beta + \dots, \quad \hat{\eta}(k) \approx 1 - |k|^\alpha + \dots \quad (6.18)$$

Substituting Eq. (6.18) into Eq. (6.11) we get to leading order

$$s^\beta \hat{P}(k, s) - s^{\beta-1} = -\chi |k|^\alpha \hat{P}(k, s). \quad (6.19)$$

The final step to obtain the macroscopic transport equation is to invert the Fourier–Laplace transforms in Eq. (6.19) which can be viewed as a fractional generalization of Eq. (6.15). This inversion can be formally written as

$${}_0^c D_t^\beta P = \chi D_{|x|}^\alpha P, \quad (6.20)$$

where

$$\mathcal{L} [{}_0^c D_t^\beta P] = s^\beta \tilde{P}(x, s) - s^{\beta-1} \delta(x), \quad \mathcal{F} [D_{|x|}^\alpha P] = -|k|^\alpha \hat{P}(k, t), \quad (6.21)$$

for $0 < \beta < 1$. Equation (6.21) is a natural generalization of Eq. (6.16) to fractional order, and this motivates the formal identification of the operator ${}_0^c D_t^\beta$ as a “fractional time derivative” and the operator $D_{|x|}^\alpha$ as a “fractional space derivative.” In the next section we will make this notion precise and show that these operators (which are in fact integro-differential operators in real space) share many of the basic properties of regular derivatives.

6.3 Fractional Diffusion

This section presents some fundamental aspects of fractional diffusion. Following a brief summary of basic results from fractional calculus, we review

the solution of the fractional diffusion equation in an unbounded domain with constant diffusivity. We also discuss the interplay of regular and fractional diffusion. This is a problem of practical interest because in applications these two transport mechanisms are usually present. As discussed in the previous section, in the context of the CTRW, fractional diffusion can result from the presence of Lévy flights. However, the divergence of the second-moment characteristic of Lévy flights is problematic from the physics point of view. To circumvent this problem, we discuss in this section the role of truncated Lévy process in the CTRW and in the formulation of fractional transport models [10]. In the last two subsections we study the problem of nonlocality and uphill transport [15] and the application of fractional diffusion to the study of passive scalar transport in turbulence [16, 17].

6.3.1

Fractional Derivatives

In this subsection we briefly review some useful basic results of fractional calculus to make the discussion in the subsequent sections as self-contained as possible. It is not our intention to present a systematic discussion of this vast topic, further information can be found in Refs. [18, 19], and in the contributions by Hilfer, and Gorenflo and Mainardi in this volume [20, 21].

A convenient way of introducing the fractional derivative is by first defining the fractional integral. Let f be a real-valued function, and consider the n th order integration of f ,

$${}_a D_x^{-n} f = \int_a^x dx_1 \int_a^{x_1} dx_2 \dots \int_a^{x_{n-1}} dx_n f(x_n), \quad (6.22)$$

where a is a constant. This expression can equivalently be written as

$${}_a D_x^{-n} f = \frac{1}{(n-1)!} \int_a^x \frac{f(y)}{(x-y)^{1-n}} dy. \quad (6.23)$$

A straightforward formal extension of Eq. (6.23) to noninteger order ν leads to

$${}_a D_x^{-\nu} f = \frac{1}{\Gamma(\nu)} \int_a^x \frac{f(y)}{(x-y)^{1-\nu}} dy, \quad (6.24)$$

where Γ is the gamma function, which as it is well-known generalizes the factorial to noninteger values. Equation (6.24) is the Riemann–Liouville fractional integral of order ν . Based on the fractional integral, the fractional derivative of order α is defined as

$${}_a D_x^\alpha f = \frac{\partial^m}{\partial x^m} \left[{}_a D_x^{-(m-\alpha)} f \right], \quad (6.25)$$

where m is the smallest integer greater than α . As expected, ${}_aD_x^\alpha {}_aD_x^{-\alpha} f = f$, and, for integer $\alpha = n$, ${}_aD_x^n f = \partial^n f / \partial x^n$. Substituting (6.24) into (6.25) leads to the Riemann–Liouville fractional derivative of order α ,

$${}_aD_x^\alpha f = \frac{1}{\Gamma(m-\alpha)} \frac{\partial^m}{\partial x^m} \int_a^x \frac{f(y)}{(x-y)^{\alpha+1-m}} dy, \quad (6.26)$$

where $m-1 \leq \alpha < m$ with m a positive integer. The fractional derivative in Eq. (6.26) at x depends on the behavior of the function f to the “left” of x , i.e., in the interval (a, x) . This is the reason why, in a more precise terminology, Eq. (6.26) is called the left Riemann–Liouville fractional derivative. The right Riemann–Liouville fractional derivative is defined by considering the integral in the interval (x, b) ,

$${}_xD_b^\alpha f = \frac{(-1)^m}{\Gamma(m-\alpha)} \frac{\partial^m}{\partial x^m} \int_x^b \frac{f(y)}{(y-x)^{\alpha+1-m}} dy. \quad (6.27)$$

The most general Riemann–Liouville fractional derivative consists of a superposition of the left and right derivatives

$$D_x^\alpha = l {}_aD_x^\alpha + r {}_xD_b^\alpha, \quad (6.28)$$

where l and r are weighting factors defined as

$$l = -\frac{(1-\theta)}{2\cos(\alpha\pi/2)}, \quad r = -\frac{(1+\theta)}{2\cos(\alpha\pi/2)}, \quad (6.29)$$

where $-1 < \theta < 1$ is the asymmetry parameter. Results from regular calculus extend naturally to fractional integrals and fractional derivatives. For example,

$${}_0D_x^{\mp\nu} x^\mu = \frac{\Gamma(\mu+1)}{\Gamma(\mu\pm\nu+1)} x^{\mu\pm\nu}. \quad (6.30)$$

The composition of derivatives of integer order and fractional derivatives satisfies

$${}_aD_x^\alpha f = \partial_x \left[{}_aD_x^{\alpha-1} f \right], \quad {}_xD_b^\alpha f = -\partial_x \left[{}_xD_b^{\alpha-1} f \right]. \quad (6.31)$$

The values of a and b define the domain of the definition of the fractional operators. When $a = -\infty$ and $b = +\infty$,

$${}_{-\infty}D_x^\alpha e^{ikx} = (ik)^\alpha e^{ikx}, \quad {}_xD_\infty^\alpha e^{ikx} = (-ik)^\alpha e^{ikx}, \quad (6.32)$$

which implies

$$\mathcal{F} [{}_{-\infty}D_x^\alpha f] = (-ik)^\alpha \hat{f}, \quad \mathcal{F} [{}_xD_\infty^\alpha f] = (ik)^\alpha \hat{f}, \quad (6.33)$$

where $\mathcal{F}[f]$ is the Fourier transform defined in Eq. (6.10). In the case $\theta = 0$, the fractional operator in Eq. (6.28) with $a = -\infty$ and $b = \infty$ reduces to the symmetric fractional derivative

$$D_{|x|}^\alpha = -\frac{1}{2 \cos(\pi\alpha/2)} [-_\infty D_x^\alpha + {}_x D_\infty^\alpha], \quad (6.34)$$

formally introduced in Eq. (6.20) when studying the continuum limit of the CTRW. Using Eq. (6.33), it is straightforward to show that Eq. (6.34) satisfies Eq. (6.21).

For finite values of a and b , the left and right Riemann–Liouville fractional derivative operators are in general singular at $x = a$ and $x = b$, respectively. To understand the nature of this singular behavior consider a differentiable function f . Expanding in Taylor series around $x = a$ and taking the fractional derivative of each term using Eq. (6.30) we get

$$\begin{aligned} {}_a D_x^\alpha f &= \frac{1}{\Gamma(1-\alpha)} \frac{f(a)}{(x-a)^\alpha} + \frac{1}{\Gamma(2-\alpha)} \frac{f'(a)}{(x-a)^{\alpha-1}} \\ &\quad + \sum_{k=0}^{\infty} \frac{f^{(k+2)}(a)(x-a)^{k+2-\alpha}}{\Gamma(k+3-\alpha)}. \end{aligned} \quad (6.35)$$

The key issue is that, for $1 < \alpha < 2$ and finite a , the first two terms on the right-hand side are singular unless $f(x=a) = f'(x=a) = 0$. The same problem is encountered with the right Riemann–Liouville derivative which is singular at $x = b$ for $1 < \alpha < 2$ unless $f(x=b) = f'(x=b) = 0$. In general, for $m-1 \leq \alpha < m$, there are m singular terms in the Taylor series and the regularity of the Riemann–Liouville derivatives at the boundaries requires $f^{(k)}(x=a) = f^{(k)}(x=b) = 0$ for $k = 1, \dots, m-1$. Equation (6.35) can be rewritten as

$${}_a D_x^\alpha [f(x) - f(a) - f'(a)(x-a)] = \sum_{k=0}^{\infty} \frac{f^{(k+2)}(a)(x-a)^{k+2-\alpha}}{\Gamma(k+3-\alpha)}, \quad (6.36)$$

where, for $1 < \alpha < 2$, the right-hand side is regular. This motivates the definition of the regularized, left Caputo fractional derivative in space of order α , with $1 < \alpha < 2$ as

$${}_a^c D_x^\alpha f = {}_a D_x^\alpha [f(x) - f(a) - f'(a)(x-a)], \quad (6.37)$$

in which the singularity is absorbed in the operator by subtracting the appropriate boundary terms. In general, for $n-1 < \alpha < n$, n boundary terms need to be subtracted from the argument of the Riemann–Liouville derivative. Integrating by parts, the regularized fractional derivative can be written as

$${}_a^c D_x^\alpha f = \frac{1}{\Gamma(n-\alpha)} \int_a^x \frac{f^{(n)}(y)}{(x-y)^{\alpha-n+1}} dy. \quad (6.38)$$

In an analogous way, for $1 < \alpha < 2$, the right Caputo fractional derivative is defined as

$${}_x^c D_b^\alpha f = {}_x D_b^\alpha [f(x) - f(b) + f'(b)(b - x)] . \quad (6.39)$$

As with the left derivative, for $n - 1 < \alpha < n$, n boundary terms need to be subtracted and the regularized operator becomes

$${}_x^c D_b^\alpha f = \frac{(-1)^n}{\Gamma(n - \alpha)} \int_x^b \frac{f^{(n)}(y)}{(y - x)^{\alpha-n+1}} dy . \quad (6.40)$$

As expected, the operators in Eqs. (6.38) and (6.40) reduce to the Riemann–Liouville fractional derivatives in the limits $a \rightarrow -\infty$ and $b \rightarrow \infty$. An important difference between these two types of operators is that the regularized derivatives of a constant vanish, whereas the Riemann–Liouville derivatives of a constant in general do not vanish. This property allows the existence of well-defined equilibrium solutions like the uniform states in the fractional Fisher–Kolmogorov equation describing front propagation [22].

For the definition of the fractional derivative in time one can in principle use the left Riemann–Liouville definition (6.26)

$${}_0 D_t^\beta f = \frac{1}{\Gamma(1 - \beta)} \frac{\partial}{\partial t} \int_0^t \frac{f(\tau)}{(t - \tau)^\beta} d\tau , \quad (6.41)$$

for $0 < \beta < 1$. Because of causality, the right fractional derivative, which would depend on the “future,” plays no role. However, Eq. (6.41) is problematic because its Laplace transform, Eq. (6.16),

$$\mathcal{L} \left[{}_0 D_t^\beta f \right] = s^\beta \tilde{f}(s) - \left[{}_0 D_t^{-(1-\beta)} f \right](0) . \quad (6.42)$$

depends on the initial value of the fractional integral of f rather than the initial value of f which is typically given in physical applications. In addition, as discussed above, Eq. (6.41) is in general singular at the lower boundary $t = 0$. A solution of this problem is provided by using the Caputo definition of the fractional derivative

$${}_0^c D_t^\beta f = \frac{1}{\Gamma(1 - \beta)} \int_0^t \frac{\partial_\tau f(\tau)}{(t - \tau)^\beta} d\tau . \quad (6.43)$$

The Laplace transform of this operator, which was formally introduced in the study of the continuum limit of the CTRW in Eq. (6.20), depends on the initial value of f ,

$$\mathcal{L} \left[{}_0^c D_t^\beta f \right] = s^\beta \tilde{f}(s) - s^{\beta-1} f(0) . \quad (6.44)$$

6.3.2

Fractional Diffusion Equation: Green's Function and Self-Similar Scaling

In this subsection we review the fundamental solution of the fractional diffusion equation,

$${}_0^c D_t^\beta f = \chi_f [l {}_{-\infty} D_x^\alpha + r {}_x D_\infty^\alpha] f + \chi_d \partial_x^2 f, \quad (6.45)$$

in a one-dimensional unbounded domain, $x \in (-\infty, \infty)$. The operator on the left-hand side is the Caputo fractional time derivative of order β defined in Eq. (6.43) with $0 < \beta < 1$. The operator on the right-hand side is the general fractional space derivative in Eq. (6.28) with $0 < \alpha < 2$, and χ_f is the fractional diffusion coefficient. The weighting factors l and r are defined in Eq. (6.29). In addition to the fractional operator, the right-hand side contains a standard diffusive term with diffusivity χ_d . Including this term is important because in many transport problems, both, fractional and regular diffusion are present. In the pure fractional symmetric case, $\theta = 0$ and $\chi_d = 0$, Eq. (6.45) reduces to the transport equation in Eq. (6.20) describing the fluid limit of the symmetric CTRW.

Using the identities in Eq. (6.31), Eq. (6.45) can be written in the flux-conserving form

$$\partial_t f = -\partial_x [q_l + q_r + q_d], \quad (6.46)$$

where

$$q_d = -\chi_d \partial_x f, \quad (6.47)$$

and q_l and q_r are nonlocal fluxes defined according to

$$q_l = -l \chi_f {}_0 D_t^{1-\beta} {}_{-\infty} D_x^{\alpha-1} f, \quad q_r = r \chi_f {}_0 D_t^{1-\beta} {}_x D_\infty^{\alpha-1} f. \quad (6.48)$$

For the diffusive transport channel, the Fourier–Fick's law in Eq. (6.47) imposes a local relation between the flux and the gradient of f . However, according to Eqs. (6.48), fractional diffusion incorporates spatial, nonlocal couplings between the flux and f through the integro-differential operators ${}_a D_x^{\alpha-1}$ and ${}_x D_b^{\alpha-1}$, and the possibility of non-Markovian (memory) effects through the operator ${}_0 D_t^{1-\beta}$.

The solution of the initial value problem in Eq. (6.45) with $f(x, t = 0) = f_0(x)$ is

$$f(x, t) = \int_{-\infty}^{\infty} f_0(x') G(x - x', t) dx', \quad (6.49)$$

where the Green's function (propagator) G is the solution of the initial value problem $G(x, t = 0) = \delta(x)$ with $\delta(x)$ the Dirac delta function. Using

Eqs. (6.33) and (6.44), the Fourier–Laplace transform of Eq. (6.45) leads to the solution

$$\hat{G} = \frac{s^{\beta-1}}{s^\beta - \Lambda(k)}, \quad (6.50)$$

where

$$\begin{aligned} \Lambda &= \chi_f [l(-ik)^\alpha + r(ik)^\alpha] - \chi_d k^2 \\ &= -\chi_f |k|^\alpha \left[1 + i\theta \frac{k}{|k|} \tan\left(\frac{\alpha\pi}{2}\right) \right] - \chi_d k^2, \end{aligned} \quad (6.51)$$

for $\alpha \neq 1$. Introducing the Mittag-Leffler function [18, 21]

$$E_\beta(z) = \sum_{n=0}^{\infty} \frac{z^n}{\Gamma(\beta n + 1)}, \quad \mathcal{L}[E_\beta(c t^\beta)] = \frac{s^{\beta-1}}{s^\beta - c}, \quad (6.52)$$

the inversion of the Fourier–Laplace transform in Eq. (6.50) gives

$$G(x, t) = \frac{1}{2\pi} \int_{-\infty}^{\infty} e^{-ikx} E_\beta(\Lambda t^\beta) dk. \quad (6.53)$$

In the absence of regular diffusion, $\chi_d = 0$, the scaling relation $\Lambda(\mu k) = \mu^\alpha \Lambda(k)$ implies

$$G(x, \mu t) = \mu^{-\beta/\alpha} G(\mu^{-\beta/\alpha} x, t). \quad (6.54)$$

That is, the solution at time μt can be obtained from a rescaling of the solution at time t . In renormalization group language, G is a fixed point of the renormalization transformation $(G; x, t) \rightarrow (\mu^{-\beta/\alpha} G; \mu^{-\beta/\alpha} x, \mu^{-1}t)$. In this case, introducing the similarity variable $\eta = x t^{-\beta/\alpha}$, the Green's function can be written as

$$G(x, t) = t^{-\beta/\alpha} K(\eta), \quad K(\eta) = \frac{1}{2\pi} \int_{-\infty}^{\infty} e^{-i\eta k} E_\beta[\Lambda(k)] dk. \quad (6.55)$$

This self-similar scaling behavior breaks down when regular diffusion is added, i.e., for $\chi_d \neq 0$. The interplay between regular and fractional diffusion will be studied in more detail in the next section. Further details of the solution of the initial value problem and useful asymptotic and convergent expansions of the Green's function can be found in Refs. [7, 12, 23].

Of particular interest is the asymptotic, $\eta \gg 1$, behavior of K ,

$$K \sim \eta^{-(1+\alpha)}, \quad (6.56)$$

and the convergent, $\eta \ll 1$, expansion

$$K = A\eta^{\alpha-1} + \dots, \quad (6.57)$$

where A is a constant. Using Eq. (6.56), it follows from Eq. (6.55) that for a fixed $t = t_0$,

$$G(x, t_0) \sim x^{-(1+\alpha)}, \quad x \gg (\chi_f^{1/\beta} t_0)^{\beta/\alpha}. \quad (6.58)$$

Introducing the time similarity variable $\xi = t|x|^{-\alpha/\beta}$, the Green's function can be written as

$$G(x, t) = |x|^{-1} \xi^{-\beta/\alpha} K(\xi^{-\beta/\alpha}). \quad (6.59)$$

Using Eqs. (6.56) and (6.57), it follows from Eq. (6.59) that for fixed $x = x_0$,

$$G(x_0, t) \sim \begin{cases} t^\beta & \text{for } t \ll (\chi_f^{-1} x_0^\alpha)^{1/\beta} \\ t^{-\beta} & \text{for } t \gg (\chi_f^{-1} x_0^\alpha)^{1/\beta} \end{cases} \quad (6.60)$$

That is, the order of the fractional derivative in space, α , determines the algebraic asymptotic scaling of the propagator in space for a fixed time, and the order of the fractional derivative in time, β , determines the asymptotic algebraic scaling of the propagator in time for a fixed x . These two properties provide a useful “rule of thumb” to construct fractional models given the spatiotemporal asymptotic scaling properties of the propagator.

In the absence of memory effects, $\beta = 1$, $E_\beta(z) = e^z$, and $K(\eta) = (1/2\pi) \int e^{-i\eta k + \Lambda(k)} dk$. As expected, in the case of regular diffusion, $\alpha = 2$, $\Lambda \sim -k^2$, and G is a Gaussian distribution. For $0 < \alpha < 2$ the solution corresponds to an α -stable Lévy distribution

with skewness θ . This follows directly from the fact that Λ in Eq. (6.51) is the exponent of the characteristic function of the α -stable Lévy distributions, $L_{\alpha,\theta}$, in the Lévy–Khintchine representation [24],

$$\hat{L}_{\alpha,\theta}(k) = e^{\Lambda(k)}. \quad (6.61)$$

The appearance of Lévy distributions is natural and directly related to the close connection between fractional diffusion and the CTRW discussed in the previous section.

6.3.3

Interplay of Regular and Fractional Diffusion

Standard diffusion can have nontrivial effects on fractional transport. For example, when $\chi_d \neq 0$, $\Lambda(\mu k) \neq \mu^\alpha \Lambda(k)$, and the exact self-similarity in Eq. (6.54) breaks down. The effect of regular diffusion on a decaying pulse

is illustrated in Figure 6.4 that shows the results of the numerical integration of Eq. (6.45) with $\alpha = 1.5$, $\beta = 1$, and $\theta = 0$ for the initial condition

$$f_0(x) = \frac{1}{\sqrt{2\pi}\sigma_0} \exp\left[-\frac{1}{2}\left(\frac{x-\mu}{\sigma_0}\right)^2\right], \quad (6.62)$$

with $\mu = 0.5$, and $\sigma_0 = 0.003$. Details of the numerical method will be discussed in the next section. The effects of Gaussian diffusion are mostly present in the core of the distribution, and are negligible in the tails. This is consistent with the probabilistic interpretation since Gaussian diffusion leads to short displacements that dominate the core of the distribution. As time advances, the Gaussian core expands. However, for large enough x , the algebraic tails persist and transport is dominated by fractional diffusion. In particular, the scaling in time of the decay of the pulse transitions from a Gaussian scaling at short times to an asymptotic superdiffusive scaling at long times is given as

$$f(0,t) \sim \begin{cases} (\chi_d t)^{-1/2} & \text{for } t \sim 0 \\ (\chi_f t)^{-1/\alpha} & \text{for } t \gg 1. \end{cases} \quad (6.63)$$

This result is based on the following arguments. According to Eq.(6.55), for $\beta = 1$, $\theta = 0$, and a sharply localized initial condition, $f \sim \delta(x)$,

$$f(0,t) = \frac{1}{\pi} \int_0^\infty dk \cos(\theta\omega\chi_f k^\alpha t) \exp\left[-(\chi_f k^\alpha + \chi_d k^2)t\right], \quad (6.64)$$

where $\omega = \tan(\alpha\pi/2)$. Changing the integration variable to $z = (\chi_d t)^{1/2}k$,

$$f(0,t) = \frac{(\chi_d t)^{-1/2}}{\pi} \int_0^\infty \Omega e^{-z^2} dz, \quad (6.65)$$

where $\Omega = \cos(\theta\omega u) e^{-u}$ and $u = \chi_d^{-\alpha/2} \chi_f t^{(2-\alpha)/2} z^\alpha$. In the limit $t \rightarrow 0$, $\Omega = 1 + O(t^{(2-\alpha)/2})$ which according to Eq. (6.65) implies the small t scaling in Eq. (6.63) to the lowest order. To study the $t \rightarrow \infty$ limit we change the integration variable to $z = (\chi_f t)^{1/\alpha} k$ and write

$$f(0,t) = \frac{(\chi_f t)^{-1/\alpha}}{\pi} \int_0^\infty \Omega \cos(\theta\omega z^\alpha) e^{-z^\alpha} dz, \quad (6.66)$$

where $\Omega = \exp\left[-\chi_d \chi_f^{-2/\alpha} z^2 t^{-\frac{(2-\alpha)}{\alpha}}\right]$. In the $t \rightarrow \infty$ limit, $\Omega = 1 + O(t^{-(2-\alpha)/\alpha})$ which according to Eq. (6.66) implies the asymptotic behavior in Eq. (6.63) to the lowest order. Further details on the role of regular diffusion in fractional transport can be found in Ref. [25].

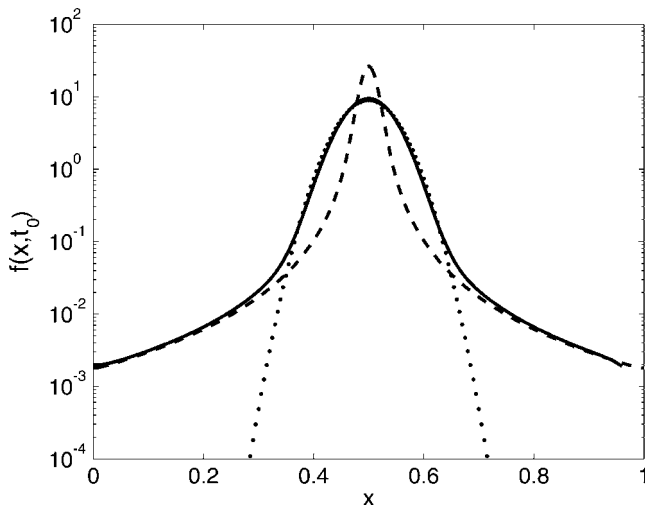


Figure 6.4 Log–normal plot of decaying pulse under the influence of standard and fractional diffusion. The dotted curve corresponds to standard diffusion with $\chi_d = 10$, and the dashed curve corresponds to fractional diffusion with $\alpha = 1.5$, $\theta = 0$, and $\chi_f = 1$. The solid curve is the profile when both the transport mechanisms are present.

6.3.4

Fractional Diffusion Equation for Truncated Lévy Processes

In the discussion of the fluid limit of the CTRW, it was shown that in the Markovian–Gaussian case, Eq. (6.12), which neglects memory effects in the waiting time and assumes a jump PDF with finite moments, the master equation leads to the diffusion equation. On the other hand, when memory and long jumps are included through algebraic decaying PDFs of the form in Eq. (6.17), the fluid limit leads to the fractional diffusion equation. It is tempting to conclude that these two cases encompass all the fundamentally different fluid limits of separable CTRWs. After all, in the absence of memory, the generalized central limit theorem implies that the sum of individual particle displacements converges asymptotically to either a Gaussian (described by the diffusion equation) if $\eta(x)$ has a finite second moment, or to a Lévy α -stable distribution (described by the fractional equation) if $\eta(x)$ has a divergent second moment. However, it is important to keep in mind that although the dynamics asymptotically converges either to a Gaussian or to a Lévy stable distribution, the convergence rate could be very slow. An example is provided by the truncated Lévy processes introduced in Refs. [26, 27] as a way to eliminate the arbitrary large flights produced by Lévy α -stable distributions. Since truncated Lévy distributions have finite second moments, Gaussian convergence is expected. However, as observed in Refs. [26–28] and several subsequent

studies, the convergence rate is so slow that for practical purposes (i.e., for time scales typical considered in applications) the process can be considered non-Gaussian but *not* described by Lévy α -stable distributions.

Truncated Lévy processes have found application in finance [29], fluids [30], astrophysics [31], and plasma physics [32]. However, despite their apparent importance, little is known about the role of truncated Lévy distributions in CTRW models, and most importantly about the role of the truncation effects in the formulation of macroscopic transport equations with memory. In Ref. [33] a special case of a distributed order fractional diffusion equation was proposed to describe a power-law truncated Lévy process in the absence of memory. In this case, a Lévy distribution with a power-law decay of order $1 + \alpha$ is truncated by a steeper power-law distribution with decay $5 - \alpha$. More recently, the study of the fluid limit of the CTRW was extended to include a wider class of jump PDFs with particular interest on exponentially truncated Lévy processes [10]. In the Lévy-Khintchine representation [34] the characteristic function (Fourier transform) $\hat{\eta}$ of the jump PDF η can be written as

$$\Lambda = \ln \hat{\eta} = aik - \frac{1}{2}\sigma^2 k^2 + \int_{-\infty}^{\infty} [e^{ikx} - 1 - iku(x)] w(x) dx, \quad (6.67)$$

where a is a constant, $\sigma \geq 0$, and the function $u(x)$ is included to regularize the integrand at the origin. The specific type of distribution is determined by the Lévy density $w(x)$ which satisfies $\int \min\{1, x^2\} w(x) dx < \infty$. According to this representation, a Lévy process consists of a combination of a drift component parameterized by a , a Brownian (Gaussian) component parameterized by σ^2 , and a jump component represented by the Lévy density w .

As discussed in Ref. [10], the fluid limit of the Montroll–Weiss master equation in Eq. (6.11) for η given in Eq. (6.67) is

$${}_0^c D_t^\beta \hat{f}(k, t) = \Lambda \hat{f}, \quad (6.68)$$

which in real space can be written as

$$\begin{aligned} {}_0^c D_t^\beta f &= -a \partial_x f + \frac{1}{2} \sigma^2 \partial_x^2 f \\ &\quad + \int_{-\infty}^{\infty} [f(x - y, t) - f(x, t) + u(y) \partial_x f] w(y) dy, \end{aligned} \quad (6.69)$$

where the integral operator on right-hand side of Eq. (6.69) is the infinitesimal generator of a general Lévy process, see also Refs. [35, 36]. As expected, for a Lévy density

$$w_{LS}(x) = \begin{cases} \chi_f \frac{(1+\theta)}{2} |x|^{-(1+\alpha)} & \text{for } x < 0, \\ \chi_f \frac{(1-\theta)}{2} x^{-(1+\alpha)} & \text{for } x > 0, \end{cases} \quad (6.70)$$

corresponding to a Lévy α -stable process with algebraic decaying jump distribution, Eq. (6.69) leads to Eq. (6.45) with $\chi_d = \sigma^2/2$ and the extra advection term $-a\partial_x f$ on the right-hand side.

In the case of exponentially truncated Lévy processes [27], the Lévy density is given by

$$w_{ET}(x) = \begin{cases} \chi_f \frac{(1+\theta)}{2} |x|^{-(1+\alpha)} e^{-\lambda|x|} & \text{for } x < 0, \\ \chi_f \frac{(1-\theta)}{2} x^{-(1+\alpha)} e^{-\lambda x} & \text{for } x > 0, \end{cases} \quad (6.71)$$

for $0 < \alpha \leq 2$, $\chi_f > 0$, $-1 \leq \theta \leq 1$, and $\lambda \geq 0$. The damping parameter λ controls the ‘strength’ of the exponential decay of the tails. In this case, the integral in Eq. (6.67) leads to the characteristic exponent [27]

$$\Lambda_{ET} = iak - \frac{\sigma^2}{2}k^2 - \frac{\chi_f}{2 \cos(\alpha\pi/2)} \begin{cases} (1+\theta)(\lambda + ik)^\alpha + (1-\theta)(\lambda - ik)^\alpha - 2\lambda^\alpha, \\ (1+\theta)(\lambda + ik)^\alpha + (1-\theta)(\lambda - ik)^\alpha - 2\lambda^\alpha - 2ik\alpha\theta\lambda^{\alpha-1}, \end{cases} \quad (6.72)$$

for $0 < \alpha < 1$ and $1 < \alpha \leq 2$, respectively. It is straightforward to observe that for $\lambda > 0$ η has finite moments of all orders. Substituting Eq. (6.72) into Eq. (6.68) and using

$$\begin{aligned} \mathcal{F}\left[e^{-\lambda x} {}_{-\infty}D_x^\alpha e^{\lambda x} f\right] &= (\lambda - ik)^\alpha \hat{f}, \\ \mathcal{F}\left[e^{\lambda x} {}_x D_\infty^\alpha e^{-\lambda x} f\right] &= (\lambda + ik)^\alpha \hat{f} \end{aligned} \quad (6.73)$$

we obtain, after inverting the Fourier transform,

$${}^c_0D_t^\beta f = -V\partial_x f + \chi_d \partial_x^2 f + \chi_f {}^c_0D_x^{\alpha,\lambda} f - \nu f, \quad (6.74)$$

where the λ -truncated fractional derivative operator of order α , ${}^c_0D_x^{\alpha,\lambda}$, is defined as

$${}^c_0D_x^{\alpha,\lambda} = le^{-\lambda x} {}_{-\infty}D_x^\alpha e^{\lambda x} + re^{\lambda x} {}_x D_\infty^\alpha e^{-\lambda x}, \quad (6.75)$$

where $V = a$ for $0 < \alpha < 1$, and $V = a - v$ for $1 < \alpha < 2$ with

$$v = \frac{\chi_f \alpha \theta \lambda^{\alpha-1}}{|\cos(\alpha\pi/2)|}, \quad (6.76)$$

and

$$\nu = -\frac{\chi_f \lambda^\alpha}{\cos(\alpha\pi/2)}. \quad (6.77)$$

As expected, for $\lambda = 0$ Eq. (6.74) reduces to Eq. (6.45).

The exponentially truncated fractional equation in Eq. (6.74) describes the interplay between memory, long jumps and truncation effects in the intermediate asymptotic regime. As discussed in Ref. [10], this equation exhibits a scaling transition. In particular, as shown in Figure 6.5, the return PDF exhibits a transition from the Lévy stable scaling, $f(0, t) \sim t^{-\beta/\alpha}$, at short times, to the scaling $f(0, t) \sim t^{\beta/2}$ at long times. For $2\beta/\alpha > 1$ this corresponds to a transition from superdiffusive to subdiffusive dynamics. The crossover time to subdiffusive dynamics scales as

$$\tau \sim \lambda^{-\alpha/\beta}. \quad (6.78)$$

This scaling generalizes the ultraslow Gaussian convergence scaling reported in Refs. [26, 28] to the case of non-Markovian, $\beta \neq 1$, processes. It is also observed that the asymptotic behavior of the propagator (Green's function) of the truncated fractional diffusion equation exhibits a transition from algebraic decay (characteristic of superdiffusive processes) for $\lambda^{\alpha/\beta}t \ll 1$ to stretched Gaussian decay (characteristic of subdiffusive processes) for $\lambda^{\alpha/\beta}t \gg 1$ [10].

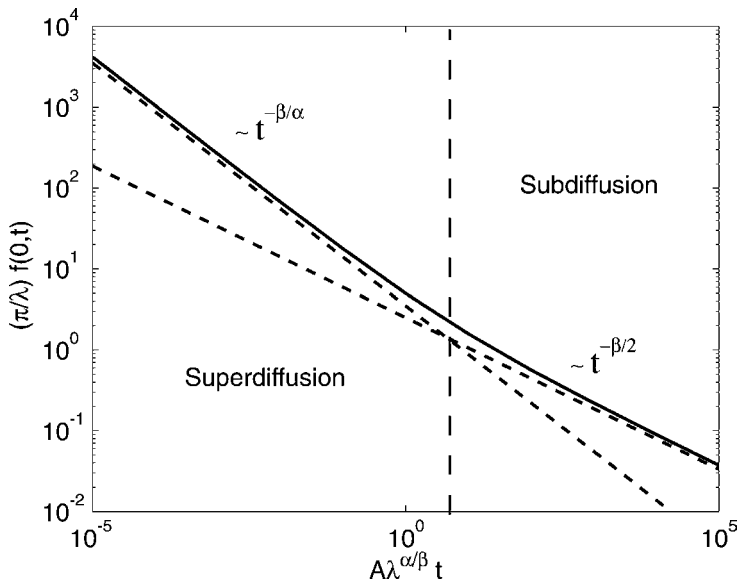


Figure 6.5 Scaling of the probability of first return, $f(0, t)$, according to the truncated fractional diffusion model in Eq. (6.74) with $\alpha = 1.25$, $\beta = 0.75$ and $\theta = 0$. The solid line denotes $f(0, t)$, the steeper dashed line corresponds to the superdiffusive scaling $f(0, t) \sim t^{-\beta/\alpha}$, and the less-steep dashed line corresponds to the subdiffusive scaling $f(0, t) \sim t^{-\beta/2}$. The scaling constant in the horizontal axis is

$$A = [\chi_f / |\cos(\alpha\pi/2)|]^{1/\beta}.$$

6.3.5

Nonlocality and Uphill Transport

The nonlocality of fractional diffusion is evident from the definition of fractional derivatives in terms of integral operators that take into account the global spatial properties of the transported field. As will be discussed in the next section, this leads to the finite-difference representation of the fractional transport operators in terms of dense matrices that introduce long-range couplings, as opposed to the tridiagonal matrices used in diffusive models that only couple nearest neighbors. According to Eq. (6.49) the general solution of the fractional diffusion equation involves a convolution of the Green's function G and the initial condition. As shown in Figure 6.6, in the case of fractional diffusion, the slowly algebraic decaying tails of G give rise to a strong response to the initial condition even at points where the local value of $f(x, t = 0)$ is negligible. To study this effect quantitatively, we integrated the fractional model in Eqs. (6.46)–(6.48) with $\alpha = 1.5$, $\beta = 1$, and $\theta = 0$ for a pulse initial condition of the form in Eq. (6.62) with $\mu = 0.5$, $\sigma_0 = 10^{-3}$. Figure 6.7 shows the results for different values of the Gaussian, χ_d , and the fractional, χ_f , diffusivity. In the absence of fractional diffusion, $(\chi_d, \chi_f) = (1, 0)$, the analytical solution at a point in space $x = x_0$ of the diffusion equation for a sharply localized initial condition gives

$$f(x_0, t) = \frac{A}{\sqrt{t + t_0}} \exp\left(-\frac{B}{t + t_0}\right), \quad (6.79)$$

with $A = 1/(2\sqrt{\pi\chi_d})$, $B = (x_0 - \mu)^2/(4\chi_d)$ and $t_0 = \sigma_0^2/(2\chi_d)$. In this case, as shown in curve (a) of Figure 6.7 the response at short times is exponentially small as a result of the strong locality of Fick's law. The response in the presence of fractional diffusion is drastically different. In the absence of standard diffusion, $(\chi_d, \chi_f) = (0, 1)$, the strong nonlocality of the fractional diffusion operator leads to an approximately linear response as shown in curve (c) of Figure 6.7. This behavior is a direct consequence of the algebraic decay of the Green's function of the fractional diffusion equation. In particular, for a localized initial condition the short time behavior, $t \rightarrow 0$, is dictated by the $x_0/(\chi_f t)^{1/\alpha} \rightarrow \infty$ behavior of the Green's function which implies

$$f(x_0, t) \sim \chi_f \sin\left(\frac{\pi\alpha}{2}\right) \frac{\Gamma(1 + \alpha)}{\pi x_0^{1+\alpha}} t. \quad (6.80)$$

The dashed line in Figure 6.7(a) shows the linear response according to this approximation. As expected, there is good agreement with the numerical result for $t \ll 1$. Curve (d) of this figure shows the response in the presence of standard and fractional diffusion with $\chi_f = 1$ and $\chi_d = 0.25$. Compared to curve (c) it is observed that the nonlocal effects of fractional diffusion are

enhanced by Gaussian diffusion. This result is to be expected since Gaussian diffusion leads to a stronger spreading of the core of the distribution, which when coupled to the long, nonlocal tails induced by fractional diffusion leads to an enhanced response. This effect is more evident in curve (e) for which $\chi_f = \chi_d = 1$. Similarly, comparing curves (a) and (b) for which $(\chi_d, \chi_f) = (1, 0)$ and $(1, 0.25)$, respectively, shows that fractional diffusion enhances the Gaussian response.

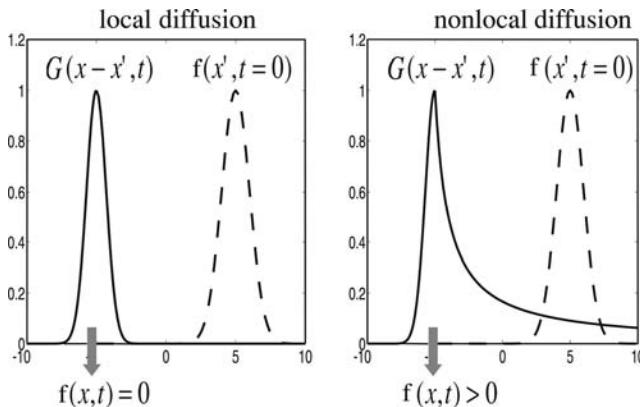


Figure 6.6 Role of the tails of the Green's function G in the solution of the initial value problem for a localized initial condition $f(x', t = 0)$. The plot on the left corresponds to local, standard diffusion for which the Green's function (propagator) is a Gaussian. The plot on the right shows an example of nonlocal, asymmetric fractional diffusion

for which the Green's function is a skewed α -stable Lévy distribution. In the Gaussian case the contributions of the initial conditions far from the peak of the distribution is exponentially small. However, in the fractional case, the slow algebraic decay of the propagator gives rise to a finite response from the nonlocal contribution of the initial condition.

The time evolution of the flux provides further understanding on the non-local response. For the Gaussian case, according to the Fourier–Fick's law, the flux corresponding to f in Eq. (6.79) is given by

$$q_d = -\frac{1}{4\sqrt{\chi_d\pi}} \frac{(\mu - x_0)}{(t + t_0)^{3/2}} \exp\left(-\frac{B}{t + t_0}\right), \quad (6.81)$$

which, as expected, yields a negligible contribution at short times. However, as before, a remarkable contrast is observed in the presence of fractional diffusion. In this case the asymptotic solution in Eq. (6.80) implies the time-independent response

$$q_f \sim -\frac{\Gamma(\alpha)}{\pi} \left(\frac{\chi_f}{x_0^\alpha}\right) \sin\left(\frac{\pi\alpha}{2}\right), \quad (6.82)$$

at short times.

In the standard diffusion model, the Fourier–Fick’s law $q_d = -\chi_d \partial_x f$ implies “downhill” transport, i.e., transport in the direction opposite to the gradient. In the case of a symmetric initial condition, this manifests as a symmetric spreading of the profile with exponential tails. However, fractional diffusion can yield nontrivial, multivalued flux-gradient relations [37]. In particular, regions of “uphill transport” where the flux has the *same* direction as the gradient. As illustrated in Figure 6.8 this can happen in the case of symmetric initial conditions provided there is an asymmetry between the left and the right fractional derivative operators, i.e., if $l \neq r$. Panels (a) and (b) in Figure 6.8 show the evolution of the profile and the flux for the fractional ($\chi_d = 0$, $\chi_f \neq 0$) symmetric case $(\alpha, \theta) = (1.3, 0)$. In this case, although transport is nonlocal and the tails of the profile decay algebraically, the left and right fractional fluxes compensate and there is no uphill transport. On the other hand, in the fractional asymmetric case $(\alpha, \theta) = (1.3, 0.5)$ shown in Figures 6.8(c) and (d), a region of uphill transport is created in the interval $x \approx (0.5, 0.57)$ as a result of the dominance of the right fractional flux.

Figure 6.9 shows plots of the flux–gradient relation and of the standard “effective” diffusivity defined as $\chi_{eff} = -q/\partial_x f$ corresponding to Figure 6.8. In the Fourier–Fick’s law, the flux–gradient relation is linear, $q = -\chi_d \partial_x f$. Fractional diffusion introduces two major differences. First, as shown in Fig-

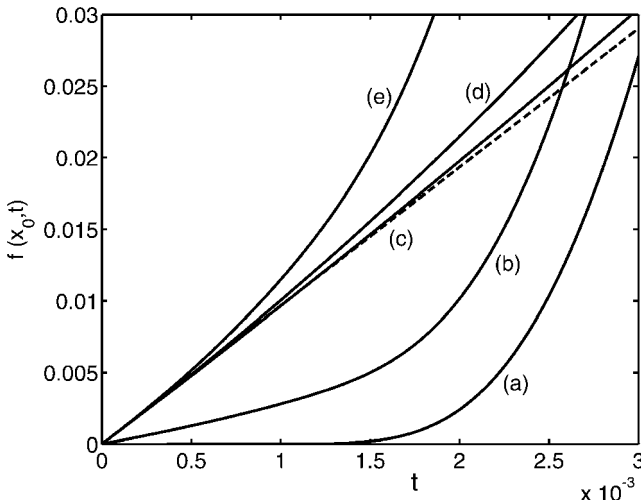


Figure 6.7 Nonlocal response of a decaying pulse with initial condition in Eq. (6.62) according to the fractional model in Eqs. (6.46)–(6.48) with $\alpha = 1.5$, $\beta = 1$, and $\theta = 0$. The plot shows f as a function of time at a fixed point in space $x = x_0$. The labels (a), (b), (c), (d) and (e) correspond to $(\chi_d, \chi_f) = \{(1, 0), (1, 0.25), (0, 1), (0.25, 1), (1, 1)\}$. The straight dashed line shows the asymptotic analytical results according to Eq. (6.80). (Adapted from Ref. [15]).

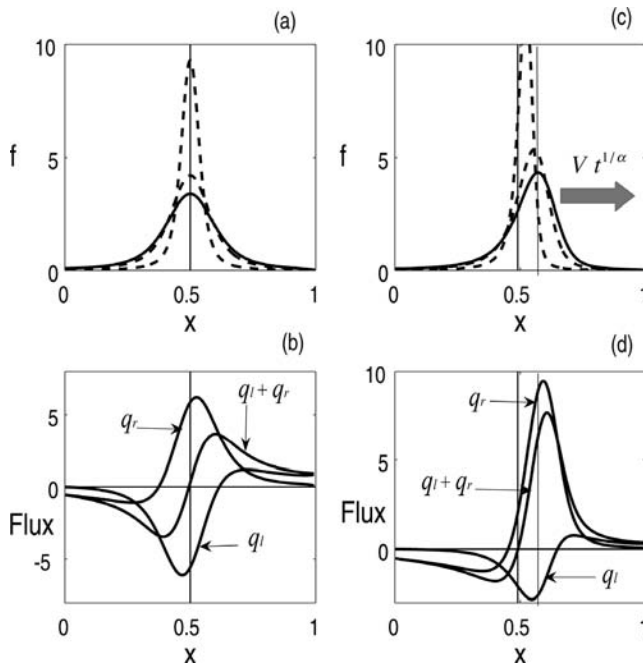


Figure 6.8 Uphill transport in a decaying pulse with initial condition in Eq. (6.62) with $\mu = 0.5$ and $\sigma = 0.0075$ according to the fractional model in Eqs. (6.46)–(6.48) with $\chi_d = 0$, $\chi_f \neq 0$. Panel (a) shows f , and panel (b) the left q_l , right q_r and total $q_l + q_r$ fluxes in the fractional symmetric case $(\alpha, \theta) = (1.3, 0)$. Panels (c) and (d) show f and the fluxes in the fractional asymmetric

case $(\alpha, \theta) = (1.3, 0.5)$. The solid lines in panels (a) and (c) show the profiles at the final time, and the dashed lines the profiles at earlier times. The two vertical lines in (c) and (d) demarcate the region of uphill transport. In the asymmetric case, the drift of the maximum of the profile scales as $Vt^{1/\alpha}$. (Adapted from Ref. [15]).

ures 6.9(a) and (c) the relation is multivalued. That is, in general, a given value of the gradient corresponds to different values of the flux. The second difference is that, as discussed before, nonlocality can create a region of uphill transport in which q and $\partial_x f$ have the same sign. In this case, as shown in Figure 6.9(c), the flux-gradient path crosses the upper left quadrant. In the fractional symmetric case, as shown in Figure 6.9(b), χ_{eff} increases toward the edges. That is, the development of algebraic decaying tails in the fractional model can be “mimicked” by artificially increasing the standard diffusivity in the region of the tails. However, as shown in Figures 6.9(d), the effective diffusivity concept runs into trouble in the case of asymmetric fractional transport. In particular, in the uphill transport region, there is “antidiffusion”, i.e., $\chi_{eff} < 0$. Moreover, because at the peak of the profile the local gradient vanishes but the fractional flux does not necessarily vanishes, χ_{eff} becomes infinity.

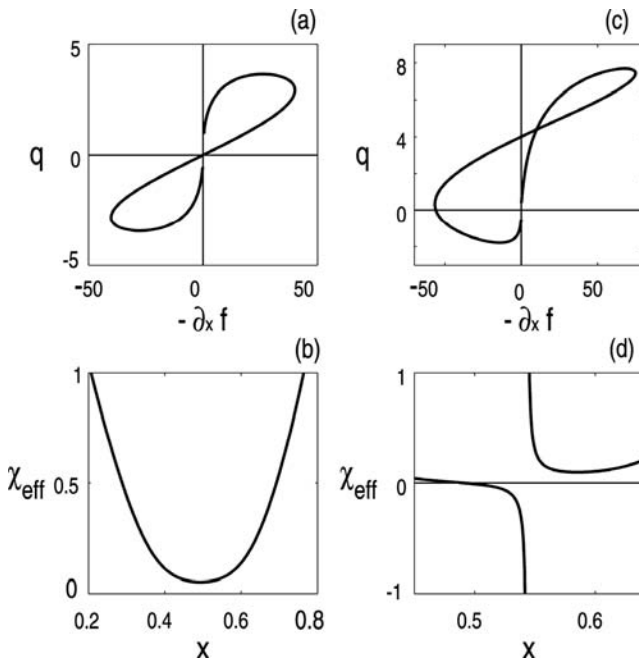


Figure 6.9 Flux-gradient relation and “effective” standard diffusivity, $\chi_{\text{eff}} = -q/\partial_x T$, for a decaying pulse evolving according to the fractional transport model in Eq. (6.45). Panels (a) and (b) correspond to the symmetric fractional case in Figures 6.8(a) and (b). Panels (c) and (d) correspond to the asymmetric fractional case in Figures 6.8(c) and (d).

As shown in Figure 6.8(c), asymmetric fractional diffusion operators can lead to a drift of the peak of the profile. However, despite this drift, in an unbounded domain the first moment of the distribution is conserved, i.e., $\langle x \rangle(t) = \langle x \rangle(0)$. This result provides an intuitive link between the drift of the peak and the development of long-range algebraic tails in the profile. When $l > r$ ($l < r$) the left (right) tail of the profile decays faster than the right (left) tail of the profile and in order to conserve the first moment, the peak of the profile shifts to the left (right). This is consistent with the fact that for $\alpha = 1$ (streaming), the left and right fractional operators become ${}_a D_x^\alpha = \partial_x$ and ${}_x D_b^\alpha = -\partial_x$ which correspond to a negative and positive drifts with velocities $V = -l\chi_f$ and $V = r\chi_f$, respectively.

The position of the peak of the profile, x_m , during the drift scales in time according to

$$x_m(t) = \eta_m \chi_f^{1/\alpha} t^{\beta/\alpha}, \quad (6.83)$$

where η_m is the location of the maximum of the function K in Eq. (6.55). To find an analytic expression for η_m in the case $\beta = 1$, note that $dK/d\eta_m = 0$

implies

$$\int_{-\infty}^{\infty} k e^{-ik\eta_m + \Lambda(k)} dk = 0. \quad (6.84)$$

By symmetry, the real part of the integral vanishes and the imaginary part gives the equation

$$\int_0^{\infty} e^{-\psi} \sin \phi \, dk = 0, \quad (6.85)$$

where $\phi = k \eta_m + \theta \tan(\frac{\alpha\pi}{2}) k^\alpha$ and $\psi = k^\alpha - \ln k$. The function $\sin \phi$ is a rapid oscillating function of k , with first maximum located at k_m , and first nontrivial ($k \neq 0$) zero located at k_z where

$$k_m = \left[\frac{\eta_m}{\alpha \theta |\tan(\frac{\alpha\pi}{2})|} \right]^{\frac{1}{\alpha-1}} \quad k_z = \frac{k_m}{\theta^{1/(\alpha-1)}}, \quad (6.86)$$

for $\theta \neq 0$. The maximum of $e^{-\psi}$ is located at $k_0 = (1/\alpha)^{1/\alpha}$. Let η_a be the value of η_m for which the first nontrivial maximum of $\sin \phi$ coincides with the maximum of $e^{-\psi}$, $k_m = k_0$, and let η_b be the value of η_m for which the first zero of $\sin \phi$ coincides with the maximum of $e^{-\psi}$, $k_z = k_0$. Then, it follows from Eq. (6.86) that

$$\eta_a = \theta \left| \tan\left(\frac{\alpha\pi}{2}\right) \right| \alpha^{1/\alpha}, \quad \eta_b = \eta_a / \alpha. \quad (6.87)$$

The value of the integral is dominated by the contribution around k_0 , $f(\eta_a) > 0$ and $f(\eta_b) < 0$. Therefore $\eta_m \in (\eta_a, \eta_b)$, and, approximating $\eta_m \approx (\eta_a + \eta_b)/2$, it follows that

$$\eta_m = \theta \left(\frac{\alpha+1}{2\alpha} \right) \alpha^{1/\alpha} \left| \tan\left(\frac{\alpha\pi}{2}\right) \right|. \quad (6.88)$$

As expected, in the $\theta = 0$ symmetric case and in the $\alpha = 2$ diffusive limit, the drift vanishes.

6.3.6

Fractional Diffusion Models of Turbulent Transport

Passive scalar transport in a prescribed flow is described by the advection–diffusion equation

$$\partial_t P + \mathbf{V} \cdot \nabla P = \nabla \cdot (\chi \nabla P) + S, \quad (6.89)$$

where P denotes the passive scalar distribution, \mathbf{V} denotes the prescribed velocity flow field, and χ the diffusivity. By passive scalar we mean a field that

does not modify the velocity field \mathbf{V} while being transported. In a first approximation, the temperature and the density can be treated as passive scalars in fluid and plasma transport calculations. The complexity of the passive advection problem depends on the dynamics of \mathbf{V} . The extreme cases of simple spatiotemporal dependence and fully developed turbulence have been studied with relative success. In particular, in the case of fully developed turbulence, strong statistical assumptions including the Gaussian statistics of fluctuations and the lack of correlations allow the construction of renormalized turbulent diffusivity models based on \mathbf{V} [11]. The main challenge is how to deal with flows whose nontrivial spatiotemporal dependence invalidates the restrictive assumptions of fully developed turbulence. We refer to these flows as “structured” since they typically exhibit coherent spatiotemporal structures. We discussed an example of this type of flows in Section 6.2 where we discussed transport in the presence of vortices and zonal flows. There we observed that these coherent structures lead to anomalous, superdiffusive transport. However, the flows discussed in Section 6.2 were not turbulent in the Eulerian sense. In particular, the experimentally measured velocity in the rotating annulus exhibits a deterministic periodic time dependence in the commoving reference frame of the vortices. Consistent with the experiment, the velocity field in the model also exhibits a simple time periodic behavior in the commoving reference frame. Transport in this case is driven by chaotic advection caused by the nonintegrability of the deterministic (nonturbulent) velocity field. In this subsection we consider the problem of passive scalar transport in the presence of coherent structures in the case of turbulent velocity fields. In particular, the goal is to discuss how fractional diffusion operators can provide a phenomenological “renormalization” of turbulent transport in structured flows.

The basic idea of the renormalization approach to turbulent transport is to find an effective operator \mathcal{D} such that $\mathcal{D}\langle P \rangle(x, t)$ and $\langle (\mathbf{V} \cdot \nabla) P \rangle(x, t)$ are phenomenological equivalent from the transport point of view, where x denotes the coordinate direction of interest to transport and $\langle \rangle$ denotes average over the remaining coordinate directions. By phenomenological equivalent we mean that the Green’s function of the operator $(\partial_t + \mathcal{D})$ (which gives the transition probability or propagator) reproduces the average response $\langle P \rangle$ of the advection operator $(\partial_t + \mathbf{V} \cdot \nabla)$ to localized initial conditions of the form $P_0(\mathbf{r}, t = 0) = \delta(x)$. In practical terms this problem is most conveniently formulated in the Lagrangian framework in which the response of the advection equation to $P_0(\mathbf{r}, t = 0) = \delta(x)$ is computed by integrating the characteristics of large ensembles of tracers

$$\frac{d\mathbf{r}_i}{dt} = \mathbf{V}[\mathbf{r}_i(t), t], \quad (6.90)$$

initially localized at $x = 0$ and uniformly distributed in the remaining coordi-

nate directions, where $\mathbf{V}(\mathbf{r}_i, t)$ is the velocity at time t of the i th tracer located at \mathbf{r}_i . In this description the problem corresponds to finding an operator \mathcal{D} whose Green's function reproduces the PDF of the tracer P . In the case of uncorrelated Gaussian turbulence, the Lagrangian tracers exhibit a Brownian random walk, P is a Gaussian probability distribution function, and, consistent with the standard renormalization perturbation theory, [11] \mathcal{D} is a diffusive operator. However, as discussed in Section 6.2, in structured flows, correlations and coherent structures typically give rise to non-Brownian random walks for which P is in general a non-Gaussian PDF. In these cases, fractional derivatives can be used to guide the construction of the effective transport operator \mathcal{D} , provided the underlying stochastic process exhibits self-similar scaling.

An example of the application of this general approach is the study of non-diffusive transport in pressure-gradient driven plasma turbulence in cylindrical geometry presented in Refs. [16, 17]. In this study, radial transport was studied by considering an ensemble of particles sharply localized in radius and uniformly distributed in the azimuthal and axial directions of a cylinder. The Lagrangian particle trajectories were obtained by integrating Eq. (6.90) with \mathbf{V} given by the direct numerical solution of a reduced, resistive 3D fluid model. This is a clear example of a structured turbulent flow in which the combination of large displacements induced by avalanche-like events and long-time trapping events due to coherent eddies gives rise to strongly non-Gaussian tracers distribution functions. In this case, as shown in Figures 6.10 and 6.11 the propagator (Green's function) of the fractional transport model in Eq. (6.45) with $\alpha = 3/4$, $\beta = 1/2$, $\theta = 0$ and $\chi_d = 0$ reproduces the shape and the spatiotemporal scaling of the PDF of the tracers' displacements P for a localized initial condition. Consistent with the analysis presented in Section 6.3 , for fixed $t = t_0$, the PDF decays as $P \sim x^{-(1+\alpha)}$ and for a fixed $x = x_0$, the rise and decay of P with time, scales as $P \sim t^\beta$ and $P \sim t^{-\beta}$, respectively. The parameters α and β are directly related to the Lagrangian statistics of the tracers. In particular, in the fractional model, the anomalous diffusion scaling exponent γ in Eq. (6.4) and the scaling exponent of the Lagrangian autocorrelation function in Eq. (6.7) are given by

$$\gamma = 2\beta/\alpha, \quad v = 2(1 - \beta/\alpha). \quad (6.91)$$

In the case of pressure gradient driven plasma turbulence, $\alpha = 3/4$ and $\beta = 1/2$ imply superdiffusive transport with $\gamma = 4/3$ and $v = 2/3$. These numerical results lead support to the idea that fractional diffusion provides a "phenomenological renormalization" of advective transport of tracers in electrostatic plasma turbulence according to the prescription

$$-\mathbf{V} \cdot \nabla \rightarrow {}_0D_t^{1-\beta} [{}_{-\infty}D_x^\alpha + {}_xD_\infty^\alpha]. \quad (6.92)$$

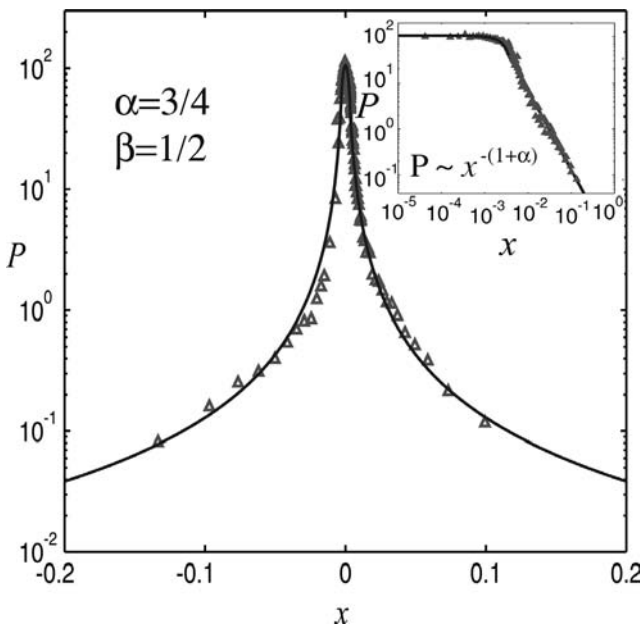


Figure 6.10 Comparison between turbulent transport calculation and fractional diffusion model. The triangles denote the results from the histogram of radial displacements of tracers in a pressure-gradient-driven three-dimensional turbulence model. The solid line is the propagator of the symmetric,

$\theta = 0$, fractional diffusion transport model in Eq. (6.45) with $\alpha = 3/4$, $\beta = 1/2$, $\chi_d = 0$, and $\chi = 0.09$. The log-log plot in the inset shows clear evidence of algebraic decay of the form $P \sim x^{-(1+\alpha)}$. (Adapted from Ref. [17]).

The use of CTRW concepts to construct effective, renormalized macroscopic transport models for stochastic velocity fields (V -Langevin dynamics) with prescribed non-Gaussian statistical properties was pioneered in Ref. [38]. More recently, in Refs. [39–41], the connection between V -Langevin equations, CTRW models and fractional diffusion was discussed in detail. Also, in Ref. [42] it was shown that fractional renormalization concepts can be incorporated in quasilinear calculations of turbulent transport that avoid the restrictive localization hypothesis.

6.4

Fractional Diffusion in Finite-Size Domains

Fractional diffusion has been extensively studied in unbounded, $x \in (-\infty, \infty)$, domains. However, in most applications one has to deal with finite-size domains, e.g., $x \in (a, b)$ with prescribed boundary conditions at $x = a$ and $x = b$. The study of fractional diffusion in this case is delicate because, as discussed

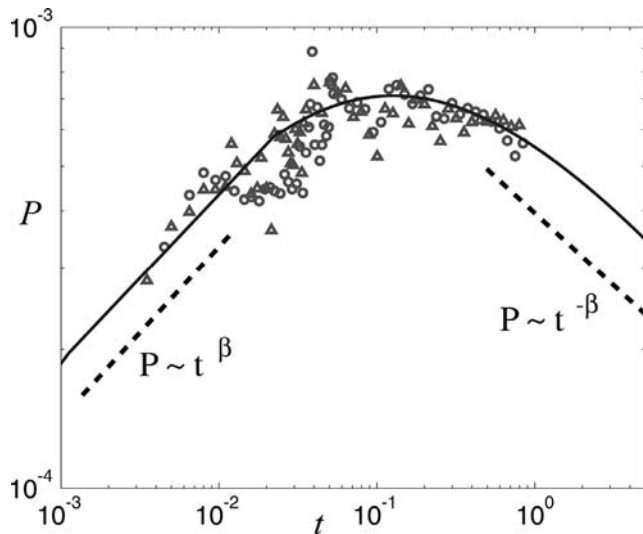


Figure 6.11 Comparison between turbulent transport calculation and fractional diffusion model. The triangles denote the results from the histogram of radial displacements of tracers in a pressure-gradient-driven three-dimensional turbulence model. The solid line is the analytical solution of the symmetric,

$\theta = 0$, fractional diffusion transport model in Eq. (6.45) with $\alpha = 3/4$, $\beta = 1/2$, $\chi_d = 0$, and $\chi = 0.09$. In agreement with the asymptotic result, the dashed lines show that the PDF exhibits algebraic tails with exponent equal to $\beta = 1/2$. (Adapted from Ref. [17]).

in Section 6.3 the left and right Riemann–Liouville fractional derivative operators are in general singular at the lower and upper boundaries. One way to circumvent this problem is to define the fractional spatial derivatives in the Caputo sense. Following Ref. [15], in this section we implement this regularization numerically and discuss solutions of the fractional diffusion equation in a finite-size domain. In particular, we consider steady-state equilibrium solutions and the propagation of pulse perturbations. These problems are mainly motivated by the study of anomalous heat transport in magnetically confined thermonuclear plasmas, but the results should be of interest to other systems.

6.4.1

Finite-Size Domain Model

In the case of constant diffusivity, $\chi_f = \chi_{f0}$, the finite-size domain, $x \in (a, b)$, fractional diffusion model is readily obtained from the unbounded domain model in Eq. (6.45) by substituting the Riemann–Liouville operators by their regularized (in the Caputo sense) counterparts in Eqs. (6.38) and (6.40),

$${}_0^c D_t^\beta f = \chi_{f0} [l_a^c D_x^\alpha + r_x^c D_b^\alpha] f + \chi_d \partial_x^2 f. \quad (6.93)$$

To formulate the model in the case of variable diffusivity, $\chi_f = \chi_f(x)$, we start from Eq. (6.46), and consider the regularization of the spatial fractional derivatives involved in the definition of the fluxes in Eq. (6.48). For $1 < \alpha < 2$, the regularization can be done in two ways. One possibility is to regularize the fractional derivatives of order $0 < \alpha - 1 < 1$ in the fluxes and write

$$q_l = -l\chi_f {}_0D_t^{1-\beta} {}_aD_x^{\alpha-1} [f(x) - f(a)] , \quad (6.94)$$

$$q_r = r\chi_f {}_0D_t^{1-\beta} {}_xD_b^{\alpha-1} [f(x) - f(b)] . \quad (6.95)$$

However, a potential problem with this approach is that, although by construction q_l and q_r are regular at the boundaries, their derivatives might be singular. In particular, at the lower, $x = a$, and upper, $x = b$, boundaries

$$\partial_x q_l \sim \frac{\chi_f(a)f'(a)}{(x-a)^{\alpha-1}}, \quad \partial_x q_r \sim \frac{\chi_f(b)f'(b)}{(b-x)^{\alpha-1}}, \quad (6.96)$$

which, for $1 < \alpha < 2$, in general diverges unless the supplemental boundary condition, $\chi_f(a)f'(a) = \chi_f(b)f'(b) = 0$, is imposed.

An alternative prescription is based on the second-order regularization

$$q_l = -l\chi_f {}_0D_t^{1-\beta} {}_aD_x^{\alpha-1} [f(x) - f(a) - f'(a)(x-a)] , \quad (6.97)$$

$$q_r = r\chi_f {}_0D_t^{1-\beta} {}_xD_b^{\alpha-1} [f(x) - f(b) + f'(b)(b-x)] . \quad (6.98)$$

This regularization is natural in the sense that for constant χ_f , $\partial_x q_l = -l\chi_f {}_0D_t^{1-\beta} {}_aD_x^{\alpha} f$ (and similarly $\partial_x q_r$) involves a fractional operator of order $1 < \alpha < 2$ which as discussed before requires the subtraction of the boundary value of the derivative. In the results reported here we use this regularization.

6.4.2

Finite-Difference Numerical Integration Method

Despite the fact that the analytical study of fractional operators goes back to the origins of regular calculus, the development of numerical integration techniques for partial differential equations with fractional derivatives is a relatively new, rapidly growing area of research. In Ref. [43] the numerical discretization of fractional operators discussed in Ref. [44] was implemented in a finite-difference numerical scheme. The results presented here are based on numerical methods proposed in Ref. [15] which allow spatially dependent diffusivities and the incorporation of physical boundary conditions in finite-size domains. Other recent works devoted to the integration of partial differential equations with fractional derivatives in space and time include Refs. [45, 46].

6.4.2.1 Discretization of Fractional Derivatives

The successful construction of numerical integration methods for fractional diffusion equations depends critically on the use of efficient and accurate techniques for the numerical computation of fractional derivatives. Here, following Ref. [18], we use a finite-difference approach based on the Grunwald–Letnikov representation of the Riemann–Liouville fractional derivative valid for sufficiently smooth functions. According to this representation

$${}_a D_x^\mu f = \lim_{h \rightarrow 0} \frac{-\Delta_h^\mu f}{h^\mu}, \quad {}_x D_b^\mu f = \lim_{h \rightarrow 0} \frac{+\Delta_h^\mu f}{h^\mu}, \quad (6.99)$$

with the left and right finite-difference fractional operators, $\mp \Delta_h^\mu f$ defined as

$$\mp \Delta_h^\mu f(x) = \sum_{j=0}^{m_\mp} w_j^{(\mu)} f(x \mp jh), \quad (6.100)$$

where $m_- = [(x-a)/h]$ and $m_+ = [(b-x)/h]$ and $[]$ denotes the integral part. In the first-order approximation the coefficients $w_j^{(\mu)}$ can be generated recursively using (see Figure 6.12)

$$w_0^{(\mu)} = 1, \quad w_k^{(\mu)} = \left(1 - \frac{\mu+1}{k}\right) w_{k-1}^{(\mu)}, \quad k = 1, 2, \dots, N. \quad (6.101)$$

Without loss of generality we will assume $a = 0$ and $b = 1$, and divide the unit interval $x \in (0, 1)$ into N equally spaced segments with grid points at $\{x_k\}$ for $k = 0, 1, \dots, N$, with $x_0 = 0$, $x_N = 1$, and $x_{k+1} - x_k = 1/N = h$. The field at grid point x_k is denoted as f_k . Based on the Grunwald–Letnikov definition we approximate the left and right fractional derivatives of f at grid point k using

$$[{}_0 D_x^\mu f]_k \approx \frac{1}{h^\mu} \sum_{j=0}^k w_j^{(\mu)} f_{k-j}, \quad [{}_x D_1^\mu f]_k \approx \frac{1}{h^\mu} \sum_{j=0}^{N-k} w_j^{(\mu)} f_{k+j}, \quad (6.102)$$

To discretize the regularized left fractional derivative of order $1 < \alpha < 2$ we write

$${}_0^c D_x^\alpha f = \partial_x \left[{}_0 D_x^{\alpha-1} \right] (f - f_0 - f'_0 x), \quad (6.103)$$

and approximate the first order partial derivative using a *forward difference* approximation

$$[{}_0^c D_x^\alpha f]_k = \frac{{}_0 D_x^{\alpha-1} (f - f_0 - f'_0 x)_{k+1} - {}_0 D_x^{\alpha-1} (f - f_0 - f'_0 x)_k}{h}. \quad (6.104)$$

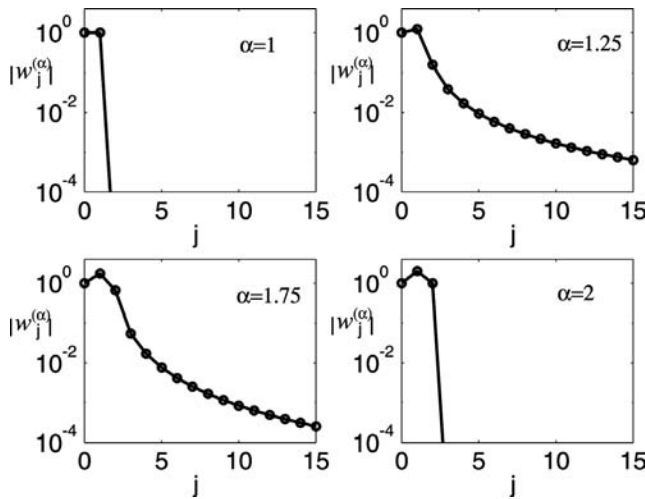


Figure 6.12 Absolute value of the coupling coefficients, $|w_j^{(\alpha)}|$, in the Grunwald–Letnikov finite-difference matrix representation of the fractional derivative. For $\alpha = 1$ the operator reduces to first-order regular derivative and

only $w_1^{(1)}$ and $w_2^{(1)}$ are different from zero. In the case $\alpha = 2$ the operator reduces to the Laplacian operator and the resulting matrix is the standard tridiagonal matrix with nearest neighbor couplings, i.e., $w_i^{(2)} = 0$ for $i > 3$. Intermediate values of α give dense matrices.

Using Eq. (6.102) we then conclude

$$[{}^c D_x^\alpha f]_k = \frac{1}{h^\alpha} \sum_{j=0}^k w_j^{(\alpha)} [f_{k-j+1} - f_0 - f'_0 h(k+1-j)]. \quad (6.105)$$

Recall that, as discussed in Section 6.3, the left fractional derivative gives rise to a drift in the negative direction. In this case, in order to have an upwind discretization scheme (which is the method of choice for advection problems with negative velocity) a forward difference scheme is needed. The proposed discretization can be written in matrix form as

$$[{}^c D_x^\alpha f]_k = h^{-\alpha} \{ \mathcal{D}^\alpha f_k + f_N \delta_{k,N-1} - f_0 V_k - f'_0 h W_k \} \quad (6.106)$$

for $k = 1, 2, \dots, N-1$, where the lower triangular matrix, \mathcal{D}^α is given by

$$\mathcal{D}^\alpha = \begin{pmatrix} w_1^{(\alpha)} & w_0^{(\alpha)} & \dots & \dots & \dots & 0 \\ w_2^{(\alpha)} & w_1^{(\alpha)} & w_0^{(\alpha)} & \dots & \dots & 0 \\ \dots & \dots & \dots & \dots & \dots & \dots \\ w_{N-2}^{(\alpha)} & w_{N-3}^{(\alpha)} & \dots & \dots & w_1^{(\alpha)} & w_0^{(\alpha)} \\ w_{N-1}^{(\alpha)} & w_{N-2}^{(\alpha)} & \dots & \dots & w_2^{(\alpha)} & w_1^{(\alpha)} \end{pmatrix}, \quad f = \begin{pmatrix} f_1 \\ f_2 \\ \dots \\ f_{N-1} \end{pmatrix}, \quad (6.107)$$

$$V_k = \sum_{j=0}^k w_k^{(\alpha)}, \quad W_k = \sum_{j=0}^k (k-j+1)w_k^{(\alpha)}, \quad (6.108)$$

and the values of f_0 and f_N are determined by the boundary conditions. In the limit $\alpha = 2$ the matrix \mathcal{D}^α reduces to the familiar tridiagonal Laplacian matrix with nearest neighbors couplings. However, for $\alpha < 2$ the matrix involves long range coupling which, as Figure 6.12 shows, decays away from the diagonal.

The discretization of the right regularized fractional derivative follows a similar path. However, in this case the right derivative induces a positive drift and in order to have an upwind scheme a backward-difference approximation is needed. The final result can be written in matrix form as

$$[{}_x^c D_1^\alpha f]_k = h^{-\alpha} \left\{ [\mathcal{D}^\alpha]^\dagger f_k + f_0 \delta_{k,1} - f_N V_{N-k} - f'_0 h W_{N-k} \right\} \quad (6.109)$$

for $k = 1, 2, \dots, N-1$, where the upper triangular matrix, $[\mathcal{D}^\alpha]^\dagger$, is the transpose of \mathcal{D}^α . The previous results can be rewritten in a compact matrix as follows:

$$[{}_0^c D_x^\alpha f]_k = h^{-\alpha} [(D^\alpha - C_l) f + U_l]_k, \quad (6.110)$$

$$[{}_x^c D_1^\alpha f]_k = h^{-\alpha} \left[(D^{\alpha\dagger} - C_r) f + U_r \right]_k, \quad (6.111)$$

where the matrices C_ℓ and C_r and the vectors U_ℓ and U_r are determined by the boundary conditions.

6.4.2.2 Finite Difference Scheme

In this subsection we discuss numerical integration techniques for partial differential equations with regular time derivatives and fractional derivatives in space. Since the numerical methods for dealing with standard (Laplacian) diffusion operators are well understood we will not discuss them here.

In the case of constant diffusivity

$$\partial_t f = \chi_f [l {}_0^c D_x^\alpha + r {}_x^c D_1^\alpha] f. \quad (6.112)$$

Defining $f_k^m = f(x = x_k, t = m\Delta t)$ where Δt is the time step, and using a forward difference approximation for the time derivative we write

$$\frac{f^{m+1} - f^m}{\chi_f \Delta t} = \Lambda [l {}_0^c D_x^\alpha + r {}_x^c D_1^\alpha] f^{m+1} + (1 - \Lambda) [l {}_0^c D_x^\alpha + r {}_x^c D_1^\alpha] f^m. \quad (6.113)$$

This weighted average method depends on the parameter $0 \leq \Lambda \leq 1$. For $\Lambda = 0$ ($\Lambda = 1$) it gives a fully explicit (implicit) method. In the case $\Lambda = 1/2$, the method resembles the Crank–Nicholson integration scheme. Substituting Eqs. (6.110)–(6.111) into Eq. (6.113), and defining

$$\mathcal{D}_\theta^\alpha = \ell \mathcal{D}^\alpha + r [\mathcal{D}^\alpha]^\dagger, \quad C_\theta = l C_\ell + r C_r, \quad U_\theta = \ell U_\ell + r U_r, \quad (6.114)$$

we conclude

$$[1 - \nu\Lambda (\mathcal{D}_\theta^\alpha - \mathcal{C}_\theta)] f^{m+1} = [1 + \nu(1 - \Lambda) (\mathcal{D}_\theta - \mathcal{C}_\theta)] f^m + \nu U_\theta, \quad (6.115)$$

where

$$\nu = \chi_f \Delta t / h^\alpha. \quad (6.116)$$

Equation (6.115) reduces the discrete time evolution of f to a matrix inversion problem.

6.4.2.3 Variable Diffusivity

In the case of variable diffusivity we start from the flux conserving formulation

$$\partial f = -\partial_x [q_l + q_r], \quad (6.117)$$

where, as before, we are not including the well-understood diffusive flux q_d and the source S . The scheme can be implemented for arbitrary boundary conditions. However, to simplify the discussion we will assume

$$f'(x = 0, t) = 0, \quad f(x = 1, t) = 0, \quad (6.118)$$

which are the boundary conditions used in the applications discussed below.

The left flux is discretized using the *forward* finite-difference scheme

$$(\partial_x q_l)_k = \frac{(q_l)_{k+1} - (q_l)_k}{h}. \quad (6.119)$$

Applying the Grunwald–Letnikov discretization in Eq. (6.102) to the second-order regularized flux in Eq. (6.97)

$$(q_l)_k = -l \left(\chi_f \right)_k {}_0 D_x^{\alpha-1} (f - f_0 - f'_0 x)_k. \quad (6.120)$$

gives

$$(q_l)_k = -\frac{l \left(\chi_f \right)_k}{h^{\alpha-1}} \left[\sum_{j=0}^{k-1} w_j^{(\alpha-1)} f_{k-j} - f_1 \sum_{j=0}^{k-1} w_j^{(\alpha-1)} \right]. \quad (6.121)$$

Using this expression in Eq. (6.119) and rearranging terms, the derivative of the flux can be written as

$$(\partial_x q_l)_k = -h^{-\alpha} \sum_{j=1}^{N-1} [\mathcal{D}_l - \mathcal{B}_l]_{kj} f_j, \quad (6.122)$$

where the left fractional matrix \mathcal{D}_l and the boundary matrix \mathcal{B}_l depend on α and the diffusivity profile χ_f . The specific form of these matrices can be found in Ref. [15].

The right flux is discretized using the *backward* finite-difference scheme

$$(\partial_x q_r)_k = \frac{(q_r)_k - (q_r)_{k-1}}{h}, \quad (6.123)$$

which in matrix form can be written as

$$(\partial_x q_r)_k = -h^{-\alpha} \sum_{j=1}^{N-1} [\mathcal{D}_r - \mathcal{B}_r]_{kj} f_j, \quad (6.124)$$

where the expressions for the right fractional matrix \mathcal{D}_r and the boundary matrix \mathcal{B}_r can be found in Ref. [15].

Discretizing the time derivative gives

$$\frac{f_k^{m+1} - f_k^m}{\Delta t} = \Lambda [\partial_x (q_l + q_r)]_k^{m+1} + (1 - \Lambda) [\partial_x (q_l + q_r)]_k^m, \quad (6.125)$$

and substituting Eqs. (6.122) and (6.124) we conclude

$$f_k^{m+1} = [1 - \nu \Lambda M]^{-1} [1 + \nu (1 - \Lambda) M] f_k^m, \quad (6.126)$$

where $\nu = \Delta t / h^\alpha$, $0 \leq \Lambda \leq 1$ and

$$M = l (\mathcal{D}_l - \mathcal{B}_l) + r (\mathcal{D}_r - \mathcal{B}_r). \quad (6.127)$$

6.4.3

Examples

In this subsection we present numerical solutions of the fractional diffusion equation

$$\partial_t T = -\partial_x [q_l + q_r + q_d] + S, \quad (6.128)$$

in the finite-size domain $x \in (0, 1)$, where S is an external source,

$$q_d = -\chi_d \partial_x T, \quad (6.129)$$

is the diffusive flux, and q_l and q_r are the second-order regularized fractional fluxes

$$q_l = -l \chi_f {}_a D_x^{\alpha-1} [T(x) - T(0) - T'(0)x], \quad (6.130)$$

$$q_r = r \chi_f {}_x D_1^{\alpha-1} [T(x) - T(1) + T'(1)(1-x)]. \quad (6.131)$$

The two key parameters of the model are α and θ . The parameter α determines the order of the spatial fractional derivative operator. The parameter θ , which according to Eq. (6.29) gives the relative weight of the left and right fluxes in Eqs. (6.97)–(6.98), determines the asymmetry of the fractional diffusion operator.

We assume a fractional diffusivity profile of the form

$$\chi_f = \frac{\chi_{f0}}{2} \left[1 + \tanh\left(\frac{x - A}{B}\right) \right] - \chi_f(0), \quad (6.132)$$

where A and B are constant, and a constant Gaussian diffusivity $\chi_d = \chi_{d0}$. As Figure 6.13 shows, in this case transport near the lower boundary, $x \sim 0$, is dominated by standard diffusive processes and nondiffusive (fractional) processes dominate transport elsewhere. The boundary conditions are $\partial_x T(0, t) = 0$ and $T(1, t) = 0$. For the local diffusive flux, this implies $q_d(0, t) = 0$. However, imposing boundary conditions to nonlocal operators is nontrivial. According to Eq. (6.97), by definition the left-fractional flux vanishes at the lower boundary, i.e., $q_l(0, t) = 0$. For the right-fractional flux, $q_r(0, t) = 0$ is guaranteed by the condition $\chi_f(0) = 0$ in Eq. (6.132). Thus, with the imposed boundary conditions, the total flux vanishes at the lower boundary $(q_d + q_l + q_r)(0, t) = 0$.

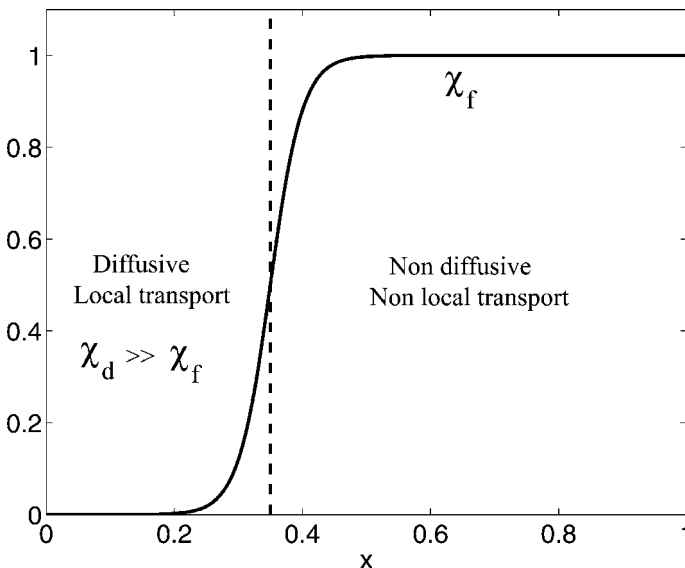


Figure 6.13 Fractional diffusivity profile according to Eq. (6.132). The vertical dashed line separates regions with different transport properties. The $x \sim 0$ region is dominated by standard diffusion, i.e., $\chi_f \ll \chi_d$. On the other hand, at the edge, $x \sim 1$, fractional diffusion plays a dominant role.

The selection of the boundary condition and the diffusivity profile are motivated by the study of anomalous heat transport in magnetically confined fusion plasmas in toroidal geometry. In this context, T represents the plasma temperature, and χ_d, χ_f the heat diffusivities. The variable x represents the coordinate along the minor radius of the torus with $x = 0$ corresponding to the center of the torus (magnetic axis) and $x = 1$ representing the normalized radius of the plasma boundary. In the plasmas of interest, transport near the core, $x \sim 0$, is typically dominated by turbulent diffusion. In this region, nondiffusive transport processes are negligible in comparison with their dominant role near the plasma edge. This basic physics motivates the use of the fractional diffusivity profile in Eq. (6.132). The zero total flux boundary condition at $x = 0$ is motivated by the fact that the radial heat flux at the axis of the torus vanishes. Further plasma physics aspects of the calculations can be found in Ref. [15].

6.4.3.1 Steady State and Anomalous Confinement Time Scaling

Figure 6.14 shows steady state, $\partial_t T = 0$, profiles in the presence of a constant source $S = S_0$, $\chi_{f0} = \chi_{d0}$, $\alpha = 1.5$, $A = 0.2$, $B = 0.1$, and different values of asymmetry parameter θ . For reference, the dashed curve in the figure shows the profile in the case when only regular diffusion is present i.e., for $\chi_{d0} \neq 0$ and $\chi_f = 0$. The asymmetry in the operators has a significant effect on the profiles. In particular, compared to the standard diffusion case (dashed line curve) it is observed that adding a right-fractional diffusion operator actually improves the heat confinement properties of the system as shown by the curve (a). On the other hand, as curve (c) indicates, the left-fractional operator has the opposite effect and leads to a shallower profile. The favorable role of the right-fractional flux is also evident in the symmetric case shown in (b). Figure 6.15 shows the fluxes in the symmetric case corresponding to curve (b) of Figure 6.14. The plot displays four curves denoting the left fractional flux q_l , the right-fractional flux q_r , and the diffusive flux q_d in Eqs. (6.129)–(6.131). The linear profile of the total flux, $q_t = q_d + q_l + q_r$, is consistent with the fact that for a constant source in steady state $q_t = \int S_0 dx = S_0 x$. As expected from Fourier–Fick’s law for a monotonically decreasing profile, the diffusive flux is positive, i.e., “downhill.” However, it is observed that the negative sign of the fractional right q_r gives rise to an “uphill” inward transport contribution that increases the heat confinement properties of the systems.

The scaling of the confinement time τ ,

$$\tau = \frac{1}{P} \int_0^L T(x) dx, \quad P = \int_0^L S(x) dx, \quad (6.133)$$

with the domain size L is of critical importance in the study of heat transport in magnetically confined fusion plasmas [47]. In the case of a toroidal con-

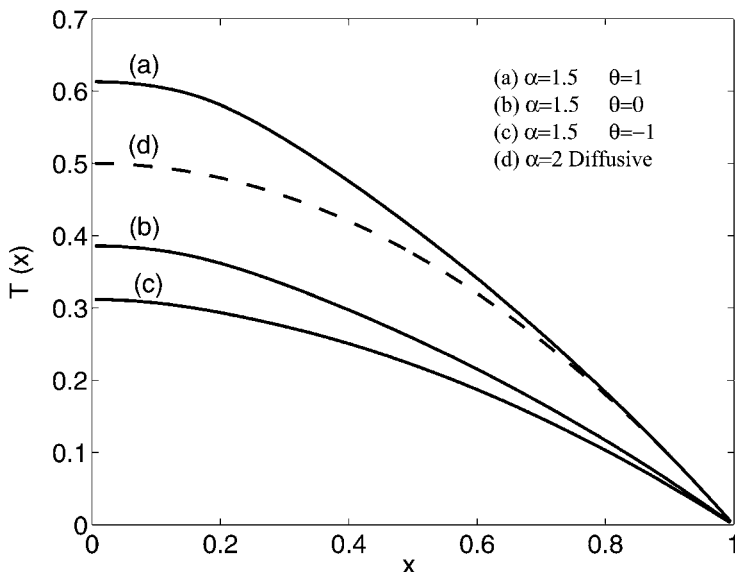


Figure 6.14 Steady-state temperature profiles according to the fractional transport model in Eqs. (6.128)–(6.131) for different values of α and θ , with $S = S_0$ constant source, $\alpha = 1.5$, and $\lambda = 1$. Curve (a) corresponds to an asymmetric, $\theta = 1$, $(l, r) = (\sqrt{2}, \sqrt{2})$ fractional operator; curve (b) corresponds to a symmetric, $\theta = 0$,

$(l, r) = (\sqrt{2}, \sqrt{2})$ fractional operator; and curve (c) corresponds to an asymmetric, $\theta = -1$, $(l, r) = (\sqrt{2}, 0)$ left-fractional operator. Figure 6.14 shows the corresponding fluxes. For reference, the dashed line curve shows the profile in the case of regular diffusion ($\alpha = 2$). (Adapted from Ref. [15]).

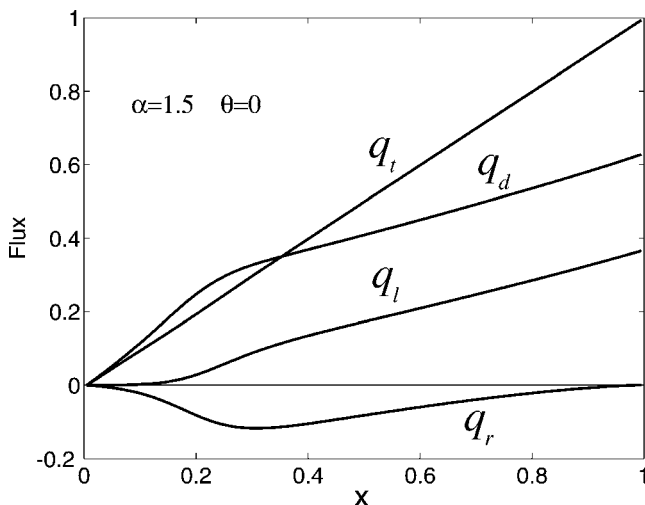


Figure 6.15 Flux as function of x for the steady-state solutions for the fractional symmetric case corresponding to curve (b) in Figure 6.14.

finement device, e.g., a tokamak, L corresponds to the minor radius of the torus. In the diffusive transport model, the Fourier–Fick’s law implies the scaling $\tau \sim L^2$. However, it has been experimentally observed [48] that low-confinement mode plasmas satisfy a less favorable anomalous scaling

$$\tau \sim L^\alpha, \quad 1 < \alpha < 2. \quad (6.134)$$

Figure 6.16 shows that the fractional diffusion transport model is able to reproduce the scaling in Eq. (6.134). Introducing the time and length scales

$$\hat{\tau} = \left(\frac{\chi_{d0}^\alpha}{\chi_{f0}^2} \right)^{1/(1-\alpha)}, \quad \hat{L} = \left(\frac{\chi_{d0}}{\chi_{f0}} \right)^{1/(1-\alpha)}, \quad (6.135)$$

it is observed that for $L/\hat{L} \ll 1$, $\tau/\hat{\tau} \sim (L/\hat{L})^2$, implying diffusive scaling $\tau \sim \chi_d^{-1} L^2$, whereas for $L/\hat{L} \gg 1$, $\tau/\hat{\tau} \sim (L/\hat{L})^\alpha$, implying the anomalous diffusion scaling $\tau \sim \chi_f^{-1} L^\alpha$. The less favorable, anomalous diffusion scaling is due to the left component of the fractional flux which, as observed in Figure 6.15, adds a downhill flux that deteriorates confinement. For fixed χ_d and χ_f , the transition to the anomalous diffusion scaling regime occurs for large L , and for fixed L the transition takes place for $\chi_f \gg \chi_d$.

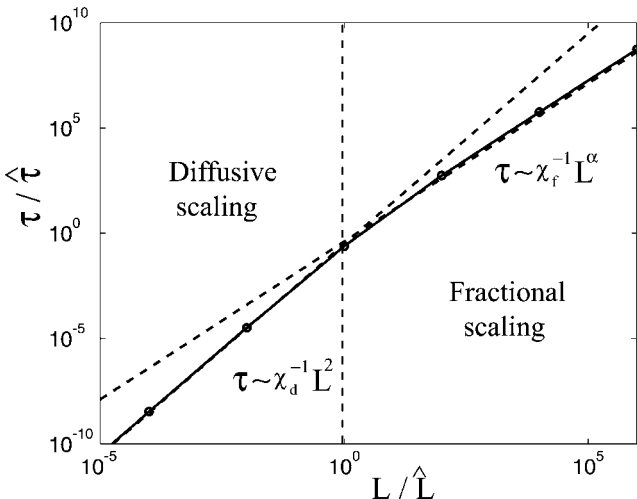


Figure 6.16 Energy confinement time scaling with domain size according to the nonlocal transport model in Eqs. (6.46)–(6.47) and (6.97)–(6.98) with $S = 1$ constant source, $\alpha = 1.5$, $\theta = 0$, and $\lambda = 1$. The plot corresponds to the steady-state profile labeled as (b) in Figure 6.14. The dots joined by the

solid lines denote the numerical results. The dashed lines are power-law fits corresponding to diffusive scaling, $\tau \sim \chi_d^{-1} L^2$, (steeper line), and non-diffusive scaling, $\tau \sim \chi_f^{-1} L^\alpha$ (less steep line) with $1 < \alpha < 2$. (Adapted from Ref. [15]).

6.4.3.2 Profile peaking

One of the puzzles in fusion plasma transport is the explanation of “profile peaking”. In its simplest form, this phenomena manifests as an increase of the temperature (or density) at the core in the absence of a direct source [49]. As shown in Figure 6.17, because of the Fourier–Fick’s law, the boundary condition $\partial_x T(x = 0) = 0$ implies a flat profile, $\partial_x T = 0$, in the absence of a source in the core region. However, in magnetically confined fusion plasmas it is commonly observed that auxiliary off-axis (i.e., outside the core) fueling leads to an increase of the profile in the core. To describe this peaking an ad hoc extra advective “pinch” term is usually added to the transport model. To explore the role of fractional diffusion in this phenomena we integrated the fractional transport model with the localized, off-axis source

$$S(x) = \frac{1}{\sqrt{2\pi}\sigma_s} \exp \left[-\frac{1}{2} \left(\frac{x - \mu_s}{\sigma_s} \right)^2 \right], \quad (6.136)$$

with $\sigma_s = 0.025$ and $\mu_s = 0.75$. For the diffusivities we assume $\chi_d = \chi_{d0} = 1$ and Eq. (6.132) with $A = 0.2$ and $B = 0.1$. It is observed that the asymmetry of the fractional diffusion operators has a critical influence on the central

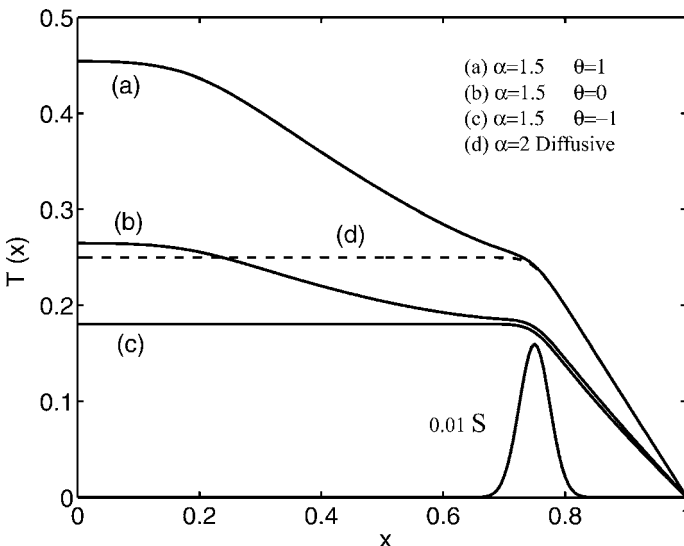


Figure 6.17 Profile peaking with off-axis fueling. Steady-state profiles according to the nonlocal transport model in Eqs. (6.46)–(6.48) for the localized off-axis source in Eq. (6.136), $\alpha = 1.5$, spatial dependent fractional diffusivity in Eq. (6.132), $\chi_d = 1$ and (a) $\theta = 1$, (b) $\theta = 0$ and (c) $\theta = -1$. For reference, the dashed line curve shows the profile

in the diffusive case ($\chi_f = 0$) where peaking does not take place. S shows the source profile (rescaled by 100 for illustration purposes). Figure 6.15 shows the corresponding fluxes. The central peaking in the asymmetric, right-fractional case (a) is a consequence of the strong uphill transport caused by the right-fractional flux q_r .

peaking of the profile. In particular, left-asymmetric operators ($\theta = 1$) lead to flat profiles, whereas right-asymmetric operators ($\theta = -1$) lead to peaked profile. As shown in Figure 6.18, the significant peaking of the profile in the asymmetric $\theta = 1$ case results from the presence of a strong negative left flux. Similar nondiffusive transport phenomenology can also been described in the context of the CTRW in [39, 50, 51].

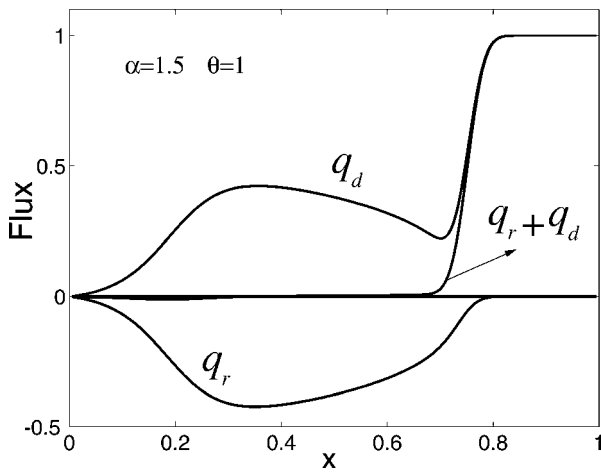


Figure 6.18 Flux as function of x for the off-axis heating steady-state profile (a) in Figure 6.17.

6.4.3.3 Nonlocal Perturbative Transport

Perturbative transport experiments and numerical simulations are a valuable tool to understand plasma transport and to validate and test transport models. These studies follow the transient time response of the plasma to externally applied small perturbations in a relatively controlled setting, see for example Refs. [52, 53] and references therein. The two main types of externally applied perturbations are edge cooling and heating power modulation. In the case of edge cooling, it has been observed in experiments that cold pulses travel from the edge to the core at speeds significantly faster than the typical diffusive time scales hinting to the importance of nonlocal transport processes and raising doubts on the validity of diffusive models [54–56]. Here we briefly discuss the use of the fractional diffusion model as an alternative to diffusive models in the description of these phenomena. The use of fractional diffusion to model nonlocal transport has also been explored in the study of the chemical structure of molecular clouds in astrophysics [57].

The boundary conditions are the same as before – zero total flux at $x = 0$ and constant temperature at the edge $x = 1$. We assume a fractional diffusivity of

the form in Eq. (6.132) with $A = 0.1$ and $B = 0.025$, and a standard diffusivity $\chi_d = 1 - \chi_f$. As shown in Figure 6.19, a steady-state temperature profile $T_0(x)$ was first computed by integrating the transport model with an on-axis source $S(x)$. A pulse perturbation with a localized Gaussian profile centered at $x = 0.75$ was then introduced at $t = 0.01$ and the perturbed temperature $\delta T = T(x, t) - T_0(x)$ and perturbed flux $\delta q = q(x, t) - q_0(x)$ followed in time.

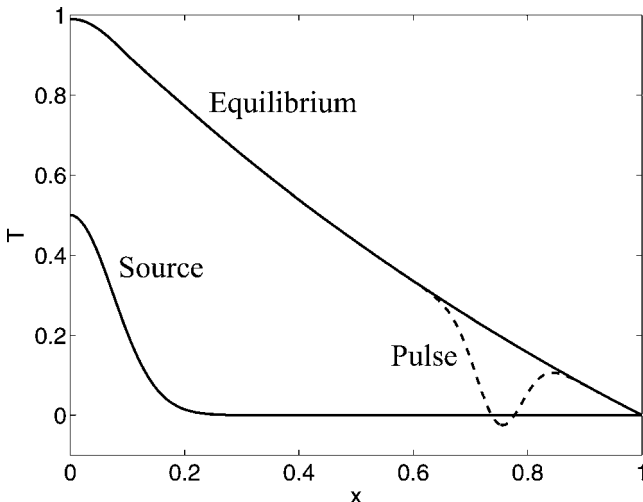


Figure 6.19 Initial condition for the pulse propagation studies. The solid line denotes the initial equilibrium temperature profile for localized on-axis source (shown rescaled for visualization purposes) according to the fractional transport model with $\alpha = 1.5$. The dashed line shows the initial cold pulse perturbation applied at the edge.

Figure 6.20 shows the spatiotemporal evolution of the perturbed temperature, $\delta T(x, t)$, and the perturbed total flux, $\delta q(x, t)$, for $\alpha = 1.75$ and 1.25 , in the symmetric, $\theta = 0$ case. For reference, the diffusive case is also included. In the diffusive case the pulse spreads on a diffusive time scale and the effect of the perturbation at the core is negligible. However, as the second and third columns of Figure 6.20 show, when the value of α is reduced, nonlocal transport yields a fast drop of the temperature at the core. Of particular interest is the case $\alpha = 1.25$ for which the nonlocal response gives rise to a temperature drop at the core larger than the drop experienced at intermediate places as evidenced by the detached “blob” observed in the plot. For small α the perturbed flux exhibits extended areas of large positive values in the region connecting the core. These large positive flux regions are responsible for the temperature transport towards the edge ($x > 0$) leading to the cooling of the core. Figure 6.21 shows the corresponding traces of the normalized temperature perturbation $\hat{\delta}T = \delta T / |\min[\delta T(x, 0)]|$. At the location of the pulse,

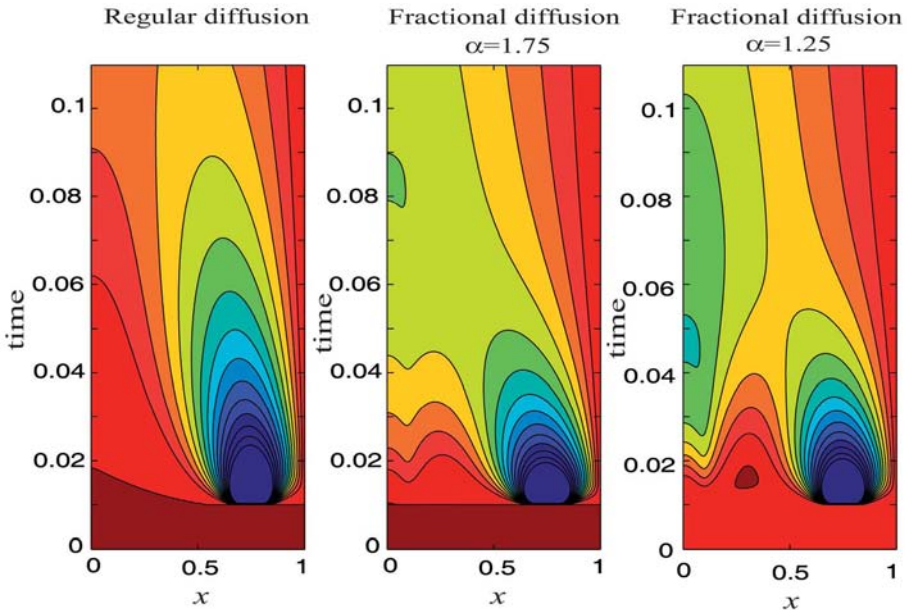


Figure 6.20 Spatiotemporal evolution of a cold pulse temperature perturbation, $\delta T = T(x, t) - T_0(x)$, according to the symmetric, $\theta = 0$, fractional transport model discussed in Chapter 6 with $\alpha = 1.75$ and $\alpha = 1.25$. For reference, the plot in the first column shows the evolution according to the

local, standard diffusion model ($\alpha = 2$). Blue denotes large negative values of δT and red corresponds to $\delta T = 0$. Of particular interest are the detached green “blobs” observed around $x \approx 0$ resulting from the strong non-locality of the fractional model.

$x = 0.75$, the temperature relaxation is dominated by diffusive local transport and very similar behavior is observed independent of the value of α . However, at the core, $x = 0$, a significant delay of the signal is observed in the diffusive case. Further details on perturbative transport including a comparison of the fractional transport model with experimental data can be found in Ref. [56].

6.5 Summary and Conclusions

This chapter discussed the application of fractional diffusion to anomalous transport. This type of transport is characterized by the anomalous scaling of the time evolution of the statistical moments, e.g., the mean and the variance, and by the presence of non-Gaussian PDFs with slowly decaying tails.

As an example of anomalous transport we considered transport of passive tracers in flows with vortices and zonal flows. These coherent structures have a significant influence on transport. In particular, experiments, chaotic advection models, and turbulent transport direct numerical simulations show that the trapping effects of vortices and the advection effects of zonal flows typi-

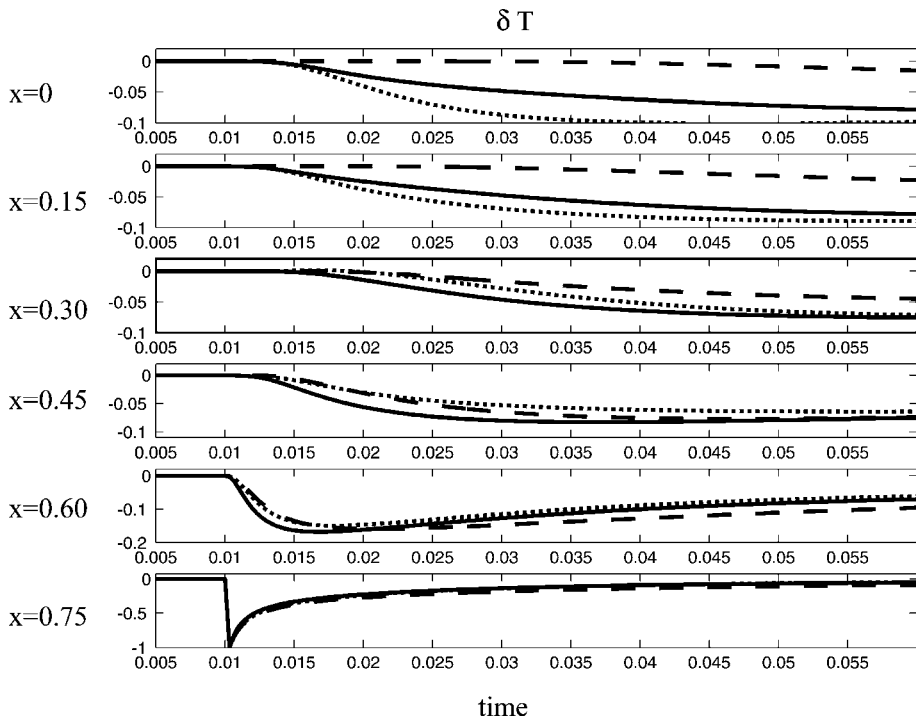


Figure 6.21 Traces of normalized temperature perturbation $\hat{\delta}T = \delta T / |\min[\delta T(x, 0)]|$ at various spatial locations corresponding to the space–time plots shown in Figure 6.20. The dashed line corresponds to the standard diffusion model, the solid line corresponds to $\alpha = 1.75$, and the dotted line corresponds to $\alpha = 1.25$.

cally lead to anomalous transport. One of the most promising approaches to study transport in this case is to use fractional diffusion models. These models involve fractional derivatives that are integro-differential operators that describe, in a unified framework, non-Fickian transport, non-Markovian (“memory”) effects, and nondiffusive scaling. Fick’s law assumes a local relationship between the flux and the gradient of the transported scalar, $q = -\chi \partial_x T$. However, numerical, theoretical, and experimental studies in plasma physics indicate that this locality assumption has limited applicability. This is particularly evident in perturbative transport experiments carried out in magnetically confined fusion plasmas.

For the description of nonlocal and non-Markovian transport one could in principle use other type of integro-differential operators which are not necessarily fractional derivatives. Although this is a direction worth exploring, there are many advantages in using fractional derivatives. From a formal point of view, fractional derivatives are well understood. In particular, fractional calculus provides a sound mathematical framework that allows an in-

depth analytical study of anomalous transport. From the numerical perspective, there are efficient and accurate algorithms to compute fractional derivatives and to numerically integrate fractional diffusion equations. From the physics point of view, fractional operators are appealing because of their close connection with non-Gaussian stochastic processes. In particular, fractional diffusion models naturally arise as macroscopic transport models of non-Brownian random walks in the continuum limit. Also, the self-similarity and scaling properties of fractional diffusion operators allow a natural description of the nondiffusive scaling observed in anomalous transport.

The construction of effective models of passive scalar transport in turbulence is a problem of great interest in geophysical fluid mechanics, engineering, and plasma physics. When the turbulence is fully developed, homogeneous, and isotropic, Gaussian statistics assumptions lead to advection–diffusion models with effective diffusivities and transport velocities. However, when coherent structures, long-range spatiotemporal correlation, and/or non-Gaussian processes are present, this approach breaks down, and there is the need to develop alternative models. A concrete example is the transport of passive tracers in pressure gradient driven plasma turbulence. In this case, fractional diffusion provides an effective model able to describe quantitatively the anomalous space–time scaling of the non-Gaussian PDF of tracers displacements and the superdiffusive scaling of the moments. This result gives support to the idea of using fractional diffusion operators to construct effective, “renormalized” descriptions of anomalous turbulent transport.

The application of fractional diffusion to the description of natural phenomena, in particular laboratory experiments, requires to go beyond the well-understood fractional diffusion equation with constant coefficients in unbounded domains. Two particularly important issues that have to be understood in realistic models of anomalous transport are the role of finite-size domains and truncated Lévy processes. The presence of large particle displacements has been well established in experimental and numerical studies of anomalous transport. However, from a physical point of view, it is evident that particle displacements cannot be arbitrarily large. In particular, it is expected that decorrelations in the trajectories of the tracers, and/or boundary effects, will eventually lead to the truncation of otherwise unbounded transport events. To address this problem, we have discussed the extension of the CTRW model and the corresponding continuum limit to general PDFs of jump displacements and in particular to exponentially truncated Lévy distributions. The description of transport in finite-size domains with physical boundary conditions is another problem of critical importance in applications. Here we have presented numerical solutions of a finite-size domain fractional diffusion model. The numerical method is based on a finite-difference Grunwald–

Letnikov discretization of the regularized fractional derivative operators. The numerical examples presented were motivated by the study of anomalous heat transport in magnetically confined plasmas but the results should be of relevance in other applications. An interesting problem that also requires the numerical integration of regularized fractional derivative operators is the evaluation of barrier options in the fractional Black–Scholes equations modeling the pricing of options in markets with jumps [58].

Acknowledgments

This work was sponsored by the Oak Ridge National Laboratory, managed by UT-Battelle, LLC, for the U.S. Department of Energy under contract DE-AC05-00OR22725.

References

- 1 E. W. Montroll and G. H. Weiss, J. Math. Physics, **6**, 167, (1965).
- 2 E. W. Montroll and M. F. Shlesinger, in *Nonequilibrium Phenomena II. From Stochastics to Hydrodynamics*. Eds. J. L. Lebowitz and E. W. Montroll (Elsevier, The Netherlands, 1984).
- 3 J. P. Bouchaud and A. Georges, Phys. Rep. **195**, 127 (1990).
- 4 T. H. Solomon, E. R. Weeks, and H. L. Swinney, Phys. Rev. Lett. **71**, 3975 (1993).
- 5 D. del-Castillo-Negrete, Phys. Fluids **10**, 576 (1998).
- 6 D. del-Castillo-Negrete, Phys. Plasmas **7**, 1702 (2000).
- 7 A. Saichev and G. M. Zaslavsky, Chaos **7** (4) 753 (1997).
- 8 E. Scalas, R. Gorenflo, and F. Mainardi, Phys. Rev. E, **69**, 011107 (2004).
- 9 R. Metzler and J. Klafter, J. Phys. A – Mathematical and General, **37** (31) R161–R208 (2004).
- 10 A. Cartea and D. del-Castillo-Negrete, Phys. Rev. E **76**, 041105 (2007).
- 11 W. D. McComb, *The Physics of Fluid Turbulence* (Oxford University Press, Great Britain, 1991).
- 12 R. Metzler and J. Klafter, Phys. Rep. **339**, 1, (2000).
- 13 V. M. Kenkre, E. W. Montroll, and M. F. Shlesinger, J. Stat. Phys. **9** (1), 45–50 (1973).
- 14 N. G. Van Kampen, *Stochastic Processes in Physics and Chemistry* (North-Holland, New York, 1981).
- 15 D. del-Castillo-Negrete, Phys. Plasmas **13** 082308 (2006).
- 16 D. del-Castillo-Negrete, B. A. Carreras, and V. E. Lynch, Phys. Plasmas **11**, 3854 (2004).
- 17 D. del-Castillo-Negrete, B. A. Carreras, and V. E. Lynch, Phys. Rev. Lett., **94** 065003 (2005).
- 18 I. Podlubny, *Fractional Differential Equations* (Academic Press, San Diego, 1999).
- 19 S. G. Samko, A. A. Kilbas, and O. I. Marichev, *Fractional Integrals and Derivatives* (Gordon and Breach Science Publishers, Amsterdam, 1993).
- 20 R. Hilfer, “Threefold introduction to fractional derivatives”. This Volumen.
- 21 R. Gorenflo and F. Mainardi, “Continuous time random walks, Mittag-Leffler waiting time and fractional diffusion: mathematical aspects”. This Volume.
- 22 D. del-Castillo-Negrete, B. A. Carreras, and V. E. Lynch, Phys. Rev. Lett. **91**, 018302 (2003).
- 23 F. Mainardi, Y. Luchko, and G. Pagnini, Fractional Calculus and Applied Analysis, **4**, 153–192 (2001).

- 24** G. Samorodnitsky and M. S. Taqqu, *Stable Non-Gaussian Random Processes* (Chapman & Hall, New York, 1994).
- 25** H. Weitzner and G. M. Zaslavsky, Commun. Nonlinear Sci. Numer. Simul. **8**, 273–281 (2003).
- 26** R. N. Mantegna and H.E. Stanley, Phys. Rev. Lett. **73**, 2946 (1994).
- 27** I. Koponen, Phys. Rev. E. **52**, 1197 (1995).
- 28** M. F. Shlesinger, Phys. Rev. Lett. **74**, 4959 (1995).
- 29** R. N. Mantegna and H. E. Stanley, Nature **376**, 46–49 (1995).
- 30** B. Dubrulle and J.-Ph. Laval, Eur. Phys. J. B **4**, 143–146 (1998).
- 31** R. Bruno, L. Sorriso-Valvo, V. Carbone, and B. Bavassano, Europhys. Lett. **66** (1), 146–152 (2004).
- 32** R. Jha, P. K. Kaw, D. R. Kulkami, J. C. Parikh, and the ADITYA Team, Phys. Plasmas **10**, 699 (2003).
- 33** I. M. Sokolov, A. V. Chechkin, and J. Klafter, Physica A, **336**, 245–251 (2004).
- 34** K. Sato, *Lévy Processes and Infinitely Divisible Distributions* (Cambridge University Press, UK, 1999).
- 35** M.M. Meerschaert, D.A. Benson, H.-P. Scheffler, B. Baeumer, Phys. Rev. E **65**, 041103 (2002).
- 36** A. Piryatinska, A.I. Saichev, W.A. Woyczyński, Physica A, **349**, 375–420 (2005).
- 37** P. Paradisi, R. Cessari, F. Mainardi, and F. Tamperi, Physica A, **293**, 130–142 (2001).
- 38** R. Balescu, Phys. Rev. E, **51**, 4807 (1995).
- 39** R. Balescu, *Aspects of Anomalous Transport in Plasmas* (Institute of Physics, Bristol, 2005)
- 40** R. Balescu, “V-Langevin equations, continuous time random walks and fractional diffusion,” <http://arxiv.org/abs/0704.2517>, 19 April, (2007).
- 41** R. Balescu, Chaos Solitons Fractals, **34**, 62–80 (2007).
- 42** R. Sanchez, B. A. Carreras, D. E. Newman, V. E. Lynch, and B. Ph. van Milligen, Phys. Rev. E. **71**, 011111 (2005).
- 43** V. Lynch, B. A. Carreras, D. del-Castillo-Negrete, K. M. Ferreira-Mejias, and H. R. Hicks, J. Comput. Phys. **192**, 406–421 (2003).
- 44** K. B. Oldham and J. Spanier, *The Fractional Calculus* (Academic Press, San Diego, 1974)
- 45** S. B. Yuste and L. Acedo, SIAM J. Num. Anal. **42**, 5, 1862–1874 (2005).
- 46** M. M. Meerschaert and C. Tadjeran, Appl. Num. Math. **56**, 80–90 (2006).
- 47** J. Wesson, *Tokamaks*, second edition (Oxford University Press, New York, 1997)
- 48** S. M. Kaye, C. W. Barnes, M. G. Bell et al. Phys. Fluids B **2**, 2926 (1990).
- 49** T. C. Luce, C. Petty, and J. C. M. de Hass. Phys. Rev. Lett. **68**, 52 (1991).
- 50** B. Ph. van Milligen, R. Sanchez, and B. A. Carreras, Phys. Plasmas **11**, 2272 (2004).
- 51** R. Sanchez, B. Ph. van Milligen, and B. A. Carreras, Phys. Plasmas **12**, 056105 (2005).
- 52** N. Lopez Cardozo, Plasma Phys. Control. Fusion **37**, 799 (1995).
- 53** P. Mantica and F. Ryter, C.R. Phys. **7**, 634 (2007).
- 54** K. W. Gentle, G. Cima, H. Gasquet, and G. A. Hallock et al., Phys. Plasmas **2**, 2292 (1995).
- 55** J. D. Callen and M. W. Kissick, Plasma Phys. Control. Fusion **39**, B173 (1997).
- 56** D. del-Castillo-Negrete, P. Mantica , V. Naulin, J.J. Rasmussen, and JET EFDA contributors, “Non-locality and perturbative transport,” Proceedings of 34nd EPS Plasma Physics Conference, Warsaw, Poland (2007).
- 57** J. J. Martinell, D. del-Castillo-Negrete, A. C. Raga, and D. A. Williams, Mon. Not. R. Astron. Soc. **372**, 213 (2006).
- 58** A. Cartea and D. del-Castillo-Negrete, Physica A **374** (2) 749–763 (2007).

7

Anomalous Kinetics Leads to Weak Ergodicity Breaking

Eli Barkai

7.1

Introduction

Consider a one-dimensional motion of an ensemble of noninteracting Brownian particles in contact with a heat bath with temperature T and in the presence of a binding potential field $V(x)$. In thermal equilibrium the probability to find a member of the ensemble in the domain $x_1 < x < x_2$ is given by Boltzmann's canonical law

$$P_B(x_1 < x < x_2) = \frac{\int_{x_1}^{x_2} \exp\left(-\frac{V(x)}{k_b T}\right)}{Z}, \quad (7.1)$$

where Z is the normalizing partition function. On the other hand consider the dynamics of a single particle. Following the single particle trajectory, the occupation fraction $t_{x_1 < x < x_2}/t$, which is the ratio of the time $t_{x_1 < x < x_2}$ spent by the particle in $x_1 < x < x_2$ and the total measurement time t is investigated. For ergodic motion, in the limit $t \rightarrow \infty$

$$\lim_{t \rightarrow \infty} \frac{t_{x_1 < x < x_2}}{t} = P_B(x_1 < x < x_2). \quad (7.2)$$

What is the physical meaning of a long-measurement time? Brownian dynamics in a finite interval is characterized by a finite relaxation time, which is the time scale on which the particles reach thermal equilibrium. For the simple case of Brownian motion in one dimension between two reflecting walls, with a system of size L , dimension analysis gives the relaxation time of the order of L^2/D , where D is the diffusion constant. A second time scale is more microscopic. According to Einstein, the diffusion constant of a random walker in one dimension is given by

$$D = \frac{\langle (\Delta x)^2 \rangle}{2\langle \tau \rangle}, \quad (7.3)$$

where $\langle (\Delta x)^2 \rangle$ is the variance of the jump lengths, and $\langle \tau \rangle$ is the averaged time between jumps. If $\langle \tau \rangle$ and the relaxation time are finite, for example for

Brownian motion in a binding potential field (e.g., Harmonic potential field), ergodicity is almost trivial in the limit when the measurement time is much longer than these two time scales.

On the other hand anomalous diffusion and transport is characterized in many cases by a diverging relaxation time and a diverging microscopical time scale. For example anomalous subdiffusion in one dimension is characterized by a mean-square displacement [1, 2]

$$\langle x^2 \rangle \sim t^\alpha, \quad (7.4)$$

with $0 < \alpha < 1$. The reader immediately realizes that Einstein's diffusion constant is zero, in the sense that $\lim_{t \rightarrow \infty} \langle x^2 \rangle / t \rightarrow 0$, hence the mentioned relaxation time L^2/D is infinite. Indeed according to the continuous time random walk (CTRW) model, anomalous subdiffusion is found when the waiting time between the jumps $\langle \tau \rangle \rightarrow \infty$, which in turn is related to the Scher-Montroll [3] power-law probability density function (PDF) $\psi(\tau) \sim \tau^{-(1+\alpha)}$ of these waiting times. For such scale-free anomalous diffusion the relaxation and microscopical time scales diverge, and ergodicity is broken weakly.

Strong ergodicity breaking is found when the system is divided into inaccessible regions, and the particle or system once starting in one region of phase space cannot explore others. Bouchaud [4] introduced the profound concept of weak ergodicity breaking. As shown in the manuscript for weak ergodicity breaking, we have no inaccessible regions in phase space, however due to power-law sticking times the dynamics is nonstationary and nonergodic. Since the ergodic hypothesis is the pillar on which statistical mechanics is built, while at the same time power-law waiting times are common, it is natural to investigate the nonergodic properties of anomalous diffusion and relaxation processes which are governed by power-law statistics. In particular what theory replaces Boltzmann–Gibbs theory for dynamics governed by fractional kinetic equations? For example, what is the *distribution* of the occupation fraction for the CTRW model? Is this distribution universal? What is the relation between this distribution and the canonical law (7.1)? What is the distribution of time averages [5], at least for the CTRW model? And what is the exact meaning of weak ergodicity breaking?

In the first part of this chapter, I consider the problem of occupation times in a force field, both for normal and anomalous diffusion, using a fractional Fokker–Planck equation approach [6] (see also the introduction to fractional calculus and the fractional diffusion equation in the chapters of Hilfer and Gorenflo–Mainardi, respectively, though here no prior knowledge of fractional calculus is required). We show that Lamperti's [7] limit theorem describes statistics of occupation times, and quantifies the deviations from ergodicity. Similar conclusion was reached by Bel and myself using a CTRW approach [8]. In the second part of the chapter the problem of occupation

times is considered for deterministic dynamics [9, 10]. Following the approach of Bel and me [9] the dynamics of one-dimensional maps with L unstable fixed points is investigated (see contributions of Altmann–Kantz and Artuso–Cristadoro on anomalous transport in deterministic systems). Statistically similar behaviors are found for the CTRW [8, 11], the Lévy walk [12], random walks in random quenched environments [13], nonergodic blinking quantum dots [12, 14–16], and very recently for a model of gene regulation by DNA-binding proteins [17]. However, I will not survey all these examples, due to lack of space and time.

7.2

Normal Occupation Time Statistics

In this section I consider the problem of occupation times, also called residence times, for Gaussian processes. Consider the trajectory of a single Brownian particle, which starts on x_0 at the beginning of the measurement. The Brownian motion is modeled using

$$\dot{x}(t) = \eta(t), \quad (7.5)$$

where $\eta(t)$ is Gaussian white noise with zero mean. Unlike the example in the previous section the motion now is unbounded. P. Lévy investigated the residence time T^+ of the particle in the domain $x > 0$, and the total observation time is t . Naive expectation is that $T^+/t = 1/2$ with small fluctuations when $t \rightarrow \infty$, namely the particle occupies the domain $x > 0$ for half of the time of observation. However, instead the PDF of T^+/t is given by the arcsine law [18, 19], soon to be derived,

$$f(T^+/t) = \frac{1}{\pi \sqrt{(T^+/t)(1 - T^+/t)}} \quad (7.6)$$

with $0 \leq T^+/t \leq 1$. This PDF has a U shape, which means that for a typical realization of the Brownian trajectory, the particle spends most of the time in one half of space (say $x > 0$) and not in the other ($x < 0$). An intuitive picture is to note that the residence time in $x > 0$ is a sum of sojourn times $T^+ = \sum_{i=1}^N \tau_i^+$ and similarly for the residence time in $x < 0$ $T^- = \sum_{i=1}^N \tau_i^-$, where N is large. The sojourn times τ_i^+ in $x > 0$ and τ_i^- in $x < 0$ are described by the PDF of first passage time of a one-dimensional Brownian particle in half space, since the crossing of $x = 0$ determines the transition from state + to state – and vice versa. It is well known that the PDF of such sojourn times behaves like $\psi(\tau) \sim \tau^{-3/2}$ so the average sojourn time is infinite [18]. This happens since the Brownian particle may wonder very far from the origin and even though it always returns to the origin, it may take it a very long time.

Since T^+ and T^- are sums of random variables with an infinite first moment, they are described by Lévy statistics and they exhibit large fluctuations. In particular, the largest sojourn time is typically of the order of the measurement time t [20]. Simplifying the problem to an extreme, assume that for a typical realization of the process, the largest sojourn time is the only one important, we immediately see that either $T^+ \gg T^-$ or $T^- \ll T^+$ but rarely $T^+ \simeq T^-$. Hence the PDF of the occupation fraction $T^+/(T^+ + T^-)$ has a U shape. We will now make the connection between first passage times and occupation times mathematical.

The basic mathematical theory for the calculation of occupation time statistics for Brownian motion was developed by Kac, and is usually based on the Feynmann–Kac formula (see [19] and references therein). The problem of occupation times of a Brownian particle in the presence of external field was considered recently by Majumdar and Comtet [21]. Using the Kac formalism [19, 21, 22] a backward Fokker–Planck equation was found, whose solution yields statistics of occupation times for normal Gaussian processes. We now consider the problem of occupation times using the backward Fokker–Planck equation approach and show that for an arbitrary potential field the distribution of occupation times is expressed in terms of solutions of the corresponding first passage time problem. This solution gives a general relation between the distribution of occupation times and the corresponding first passage time problem, which in turn can be used to classify general behaviors of normal occupation times.

Consider a one-dimensional overdamped Brownian motion in an external force field $F(x)$. The Smoluchowski Fokker–Planck equation for the concentration of noninteracting particles is

$$\frac{\partial c(x, t)}{\partial t} = D \left[\frac{\partial^2}{\partial x^2} - \frac{\partial}{\partial x} \frac{F(x)}{k_b T} \right] c(x, t). \quad (7.7)$$

As is well known the steady-state solution of this equation is Boltzmann's distribution, provided that the force field $F(x) = -dV(x)/dx$ is binding.

Let $P_{x_0, t}(T^+)$ be the PDF of T^+ . The double-Laplace transform

$$P_{x_0, s}(u) = \int_0^\infty \int_0^\infty e^{-st} e^{-uT^+} P_{x_0, t}(T^+) dt dT^+, \quad (7.8)$$

is defined so that s and t and u and T^+ are Laplace pairs. Majumdar and Comtet [21, 22] found the equation of motion for $P_{x_0, t}(T^+)$ in double-Laplace space

$$D \left[\frac{\partial^2}{\partial x_0^2} + \frac{F(x_0)}{k_b T} \frac{\partial}{\partial x_0} \right] P_{x_0, s}(u) - [s + \Theta(x_0) u] P_{x_0, s}(u) = -1, \quad (7.9)$$

where $\Theta(x_0)$ is the step function: $\Theta(x_0) = 1$ if $x_0 > 0$ otherwise it is zero. This type of equation is called a backward Fokker–Planck equation, the operator on

the left-hand side depends on the initial condition x_0 . Equation (7.9) is solved for the matching boundary conditions

$$\begin{aligned} P_{x_0,s}(u)|_{x_0=0^+} &= P_{x_0,s}(u)|_{x_0=0^-}, \\ \frac{\partial P_{x_0,s}(u)}{\partial x_0}\Big|_{x_0=0^+} &= \frac{\partial P_{x_0,s}(u)}{\partial x_0}\Big|_{x_0=0^-}. \end{aligned} \quad (7.10)$$

We will rederive Eq. (7.9) later as a special limiting case of a more general non-Markovian dynamics.

To prepare for the solution of Eq. (7.9) define the following survival probabilities. For a particle starting on $x_0 < 0$, the survival probability to remain in the domain $x < 0$ during the time interval $(0, t)$ is $W_{x_0}^-(t)$. Let $W_{x_0}^-(s)$ be the Laplace transform of $W_{x_0}^-(t)$ and similarly the Laplace transform of the survival probability in the domain $x > 0$ is $W_{x_0}^+(s)$ for $x_0 > 0$. The key to the solution of the problem of occupation times in half space is to recall the equation for the survival probability of a particle in half space [23]

$$\frac{\partial W_{x_0}^-(t)}{\partial t} = D \left[\frac{\partial^2}{\partial x^2} + \frac{F(x)}{k_B T} \frac{\partial}{\partial x} \right] W_{x_0}^-(t) \quad (7.11)$$

or in Laplace $t \rightarrow s$ space

$$D \left[\frac{\partial^2}{\partial x_0^2} + \frac{F(x_0)}{k_B T} \frac{\partial}{\partial x_0} \right] W_{x_0}^-(s) - s W_{x_0}^-(s) = -1 \quad x_0 < 0, \quad (7.12)$$

and a similar equation holds for $x_0 > 0$. The boundary conditions for Eq. (7.12) are the standard conditions used for the calculation of survival probabilities. Namely, $W_{x_0}^-(s)|_{x_0=0} = 0$ means that the particle reaches the boundary on $x = 0$ instantaneously if the particle starts very close to the absorbing boundary and if $x_0 \rightarrow -\infty$ survival is unity. Initially at time $t = 0$ the survival probability is unity. The solution of Eq. (7.9) for the PDF of the occupation time in Laplace space is

$$P_{x_0,s}(u) = W_{x_0}^-(s) + [1 - s W_{x_0}^-(s)] G_s(u)$$

if $x_0 < 0$,

$$P_{x_0,s}(u) = W_{x_0}^+(s+u) + [1 - (s+u) W_{x_0}^+(s+u)] G_s(u) \quad (7.13)$$

if $x_0 > 0$. From Eq. (7.13) the physical meaning of $G_s(u)$ becomes clear, it is the double-Laplace transform of $G_t(T^+)$ the PDF of the random variable T^+ for a particle starting on $x_0 = 0$. The PDF $G_t(T^+)$ contains the information on the problem of occupation times, while the survival probability was investigated previously by many authors, hence in what follows I investigate $G_t(T^+)$. Using Eq. (7.12) the reader can verify that Eq. (7.13) is indeed the general solution

of the problem of occupation times (Eq. (7.9)). Using the boundary condition $W_{x_0=0}^-(s) = W_{x_0=0}^+(s) = 0$ and the solution (7.13) it is easy to see that the boundary condition $P_{x_0,s}(u)|_{x_0=0^+} = P_{x_0,s}(u)|_{x_0=0^-} = G_s(u)$ in Eq. (7.10) is satisfied.

The second matching boundary condition in Eq. (7.10), on the derivatives of $P_{x_0,s}(u)$ yields $G_s(u)$ using Eq. (7.13)

$$G_s(u) = \frac{J^+(s+u) - J^-(s)}{(s+u)J^+(s+u) - sJ^-(s)}, \quad (7.14)$$

where the currents are

$$J^+(s+u) = \frac{\partial W_{x_0}^+(s+u)}{\partial x_0} \Big|_{x_0=0^+}, \quad J^-(s) = \frac{\partial W_{x_0}^-(s)}{\partial x_0} \Big|_{x_0=0^-}. \quad (7.15)$$

Equations (7.13)–(7.15) are useful since they yield a general relation between statistics of occupation times and survival probability currents. From Eq. (7.15), we learn that the solution of the problem of occupation times is found in terms of two solutions of the corresponding first passage time problems, the first for a particle starting on $x_0 > 0$ and absorbed on $x = 0$ (i.e., J^+) and the second for a particle starting on $x_0 < 0$ and absorbed on $x = 0$ (i.e., J^-). Thus the problem of residence times is solved in three steps:

- (i) Find solutions of two first passage time problems for, $x_0 > 0$ and $x_0 < 0$ in Laplace space.
- (ii) Use Eq. (7.14) to find the solution of the problem of residence times in double-Laplace space.
- (iii) And then use a two-dimensional inverse Laplace transform to get $G_t(T^+)$ from $G_s(u)$.

We now classify behaviors of residence times based on general and widely applicable behaviors of normal first passage times. Survival probabilities in a finite and infinite domain exhibit three typical physical behaviors [18], I consider the right random walk (i.e., $x_0 > 0$) and similar classification holds for the left random walk.

Case 1: The random walk is recurrent, and the average first passage time from x_0 to 0 is finite. Such cases correspond to diffusion in a system of finite size, when the particle cannot escape to infinity, e.g., the driving force field is binding.

Case 2: The random walk is transient, i.e., the survival probability in $x > 0$ is finite in the limit of long times. Such cases happen when the external force drives the particle far from the origin (e.g., an unstable potential $V(x) = -x^2$) and the system is infinite. In that case in the limit of small s

$$W_{x_0}^+(s) \sim \frac{\varepsilon_{x_0}^+}{s}, \quad (7.16)$$

where $\varepsilon_{x_0}^+$ is the survival probability of the particle starting on x_0 , without reaching $x = 0$, when $t \rightarrow \infty$. Similar notation is used for the left random walk, with $\varepsilon_{x_0}^-$.

Case 3: Random walks are recurrent, though the average first passage time is infinite. A particularly common situation is the case when the survival probability decays like $t^{-1/2}$ for long times. This happens if the nondiverging external field $F(x) = 0$ for $x > |x_c|$ and the system is infinite, namely when diffusion controls the long-time dynamics. For such a case [18]

$$W_{x_0}^+(s) \sim \frac{A_{x_0}^+}{s^{1/2}}, \quad s \rightarrow 0, \quad (7.17)$$

where $A_{x_0}^+ > 0$ depends of course on the details of the force field.

We now consider certain general properties of the statistics of occupation times for the three cases.

7.2.1

Ergodicity for Bounded Normal Diffusion

Case 1: The long-time behavior of $G_t(T^+)$ is now investigated. We consider a case when both the left and the right random walks, starting at $x_0 < 0$ or $x_0 > 0$, respectively, are recurrent and the corresponding average first passage times are finite. For this case the small s limit yields

$$W_{x_0}^\pm(s=0) = \langle t_{x_0}^\pm \rangle, \quad (7.18)$$

where $\langle t_{x_0}^\pm \rangle$ is the average time for the particle starting on $x_0 < 0$ (or $x_0 > 0$) to reach the origin for the first time. The small s and u limit, their ratio arbitrary, of Eq. (7.14) gives the long t and T^+ behavior of $G_t(T^+)$

$$G_s(u) \sim \frac{1}{s + u \frac{\frac{\partial \langle t_{x_0}^+ \rangle}{\partial x_0}}{\frac{\partial \langle t_{x_0}^+ \rangle}{\partial x_0} \Big|_{x_0=0} - \frac{\partial \langle t_{x_0}^- \rangle}{\partial x_0} \Big|_{x_0=0}}}. \quad (7.19)$$

The differential equation for $\langle t_{x_0}^+ \rangle$ [23] is obtained from the small s expansion of Eq. (7.12)

$$D \left[\frac{\partial^2}{\partial x_0^2} \langle t_{x_0}^+ \rangle + \frac{F(x_0)}{k_B T} \frac{\partial}{\partial x_0} \langle t_{x_0}^+ \rangle \right] = -1. \quad (7.20)$$

Solving this equation, using a similar equation for $\langle t_{x_0}^- \rangle$, and inverting Eq. (7.19) to the time domain, the expected ergodic behavior is found

$$G_t(T^+) \sim \delta(T^+ - P_B^+ t), \quad (7.21)$$

where P_B^+ is Boltzmann's probability of occupying $x > 0$

$$P_B^+ = \frac{\int_0^\infty e^{-\frac{V(x)}{k_B T}} dx}{Z}, \quad (7.22)$$

where $Z = \int_{-\infty}^\infty \exp -\frac{V(x)}{k_B T} dx$ is the normalizing partition function. One main goal of this manuscript is to show that Boltzmann's ergodic law (7.21) does not hold for fractional diffusion in a binding field.

7.2.2

Occupation Times for Nonrecurrent Diffusion

Case 2: We consider the case where both the left and the right random walks are nonrecurrent. The survival probabilities in the two domains are $\varepsilon_{x_0}^+$ and $\varepsilon_{x_0}^-$, in the long time limit. Then using Eqs. (7.14) and (7.16) for $t \rightarrow \infty$

$$G_t(T^+) \sim \alpha^- \delta(T^+) + \alpha^+ \delta(T^+ - t), \quad (7.23)$$

where

$$\alpha^+ = \frac{\frac{\partial \varepsilon_{x_0}^+}{\partial x_0} \Big|_{x_0=0}}{\frac{\partial \varepsilon_{x_0}^+}{\partial x_0} \Big|_{x_0=0} - \frac{\partial \varepsilon_{x_0}^-}{\partial x_0} \Big|_{x_0=0}} \quad (7.24)$$

and $\alpha^- = 1 - \alpha^+$. Since the particle always manages to escape either to the left or to the right, eventually the particle will either reside in the left domain or the right domain forever, hence the delta functions in Eq. (7.23). The weights of these delta functions are given by the derivatives of the survival probabilities only.

7.2.3

Occupation Times for Unbounded Normal Diffusion

Case 3: We now consider a case where both the left and the right random walks are recurrent, though the average first return time from x_0 to $x = 0$ is infinite, in such a way that Eq. (7.17) is valid. Then in the small s and u limit

$$G_s(u) \sim \frac{s^{-1/2} + \mathcal{R}(s+u)^{-1/2}}{s^{1/2} + \mathcal{R}(s+u)^{1/2}}, \quad (7.25)$$

where the asymmetry parameter is

$$\mathcal{R} = -\frac{\frac{\partial A_{x_0}^+}{\partial x_0} \Big|_{x_0=0}}{\frac{\partial A_{x_0}^-}{\partial x_0} \Big|_{x_0=0}}. \quad (7.26)$$

Transforming to the time domain, using methods in an Appendix of [11], the asymmetric arcsine PDF is found

$$G_t(T^+) \sim \frac{1}{t} f\left(\frac{T^+}{t}\right), \quad (7.27)$$

where

$$f(x) = \frac{1}{\pi} \frac{\mathcal{R}}{x^{1/2} (1-x)^{1/2} [\mathcal{R}^2 (1-x) + x]}. \quad (7.28)$$

When $\mathcal{R} = 1$, we have the arcsine law (7.6). Note that the PDF (7.27) diverges on $T^+/t = 1$ and $T^+/t = 0$, hence events where the particle always occupies (or hardly never occupies) the domain $x > 0$ have a significant contribution.

7.3 Anomalous Diffusion

Anomalous diffusion and relaxation is modeled in this section based on the fractional Fokker–Planck equation (FFPE) [24–26], the concentration of noninteracting particles obeys

$$\frac{\partial^\alpha c(x, t)}{\partial t^\alpha} = D_\alpha \left[\frac{\partial^2}{\partial x^2} - \frac{\partial}{\partial x} \frac{F(x)}{k_b T} \right] c(x, t), \quad (7.29)$$

where D_α is a generalized diffusion coefficient and $0 < \alpha < 1$. A brief mathematical introduction to the FFPE is given in Appendix A. First, recall physical properties of the FFPE. (i) when $F(x) = 0$ and for free boundary conditions we have the fractional diffusion equation [27–30] with anomalous diffusion $\langle x^2 \rangle \propto t^\alpha$. (ii) In the presence of a binding time-independent force field the equilibrium is the Boltzmann distribution [24, 25]. (iii) Generalized Einstein relations are satisfied in consistency with linear response theory [24, 25]. (iv) Relaxation of modes follows the Mittag-Leffler decay, related for example to Cole–Cole relaxation [24, 25]. Applications of fractional diffusion modeling include: Scher–Montroll [3] time-of-flight transport of charge carriers in disordered medium [26], dynamics of ion channels [31], relaxation processes in proteins [32], dielectric relaxation [33], diffusion of DNA through a nanopore [34], and deterministic chaotic diffusion [35, 36]. For reviews and a popular article on fractional kinetics see [35, 37, 38].

Similar to the normal diffusion case, define $P_{x_0, t}(T^+)$ as the PDF of the residence time T^+ in half space $x > 0$, and $P_{x_0, s}(u)$ its double-Laplace transform. As shown in the next subsection the differential equation for $P_{x_0, s}(u)$ for the

dynamics described by the FFPE (7.29) is

$$\begin{aligned} D_\alpha \left[\frac{\partial^2}{\partial x_0^2} + \frac{F(x_0)}{k_B T} \frac{\partial}{\partial x_0} \right] P_{x_0, s}(u) - [s + \Theta(x_0) u]^\alpha P_{x_0, s}(u) \\ = -[s + \Theta(x_0) u]^{\alpha-1}. \quad (7.30) \end{aligned}$$

When $\alpha = 1$, Eq. (7.9) is recovered. The boundary conditions for Eq. (7.30) are identical to the normal diffusion case $\alpha = 1$ given in Eq. (7.4).

Interestingly, the solution of the fractional equation (7.30) is identical to that found for normal diffusion case, namely our main results (7.13)–(7.15) are valid also in the non-Markovian domain $0 < \alpha < 1$. Now $W_{x_0}^\pm(s)$ needed for the calculation of $J^\pm(s)$, is the Laplace transform of the survival probability for the fractional particle. Thus Eqs. (7.13)–(7.15) have some general validity beyond normal Markovian diffusion.

To prove that Eqs. (7.13)–(7.15) are still valid let us first find the differential equation for $W_{x_0}^+(s)$: the survival probability of a fractional particle starting on $x_0 > 0$ in the domain $x > 0$. Using Appendix A

$$D_\alpha \left[\frac{\partial^2}{\partial x_0^2} + \frac{F(x_0)}{k_B T} \frac{\partial}{\partial x_0} \right] W_{x_0}^+(s) - s^\alpha W_{x_0}^+(s) = -s^{\alpha-1}, \quad (7.31)$$

and a similar equation holds for $x_0 < 0$. Equation (7.31) is the fractional generalization of the backward equation for the survival probability equation (7.12). Now using Eq. (7.31) it is easy to verify that Eqs. (7.13)–(7.15) are solutions of the fractional equation (7.30).

7.3.1

Derivation of Fractional Equation for Occupation Times

In this subsection I derive Eq. (7.30) using the assumption that the underlying dynamics is described by the FFPE (7.29). The latter describes long-time behavior of the CTRW [25, 26], which is the underlying random walk process in mind. In the CTRW under investigation a particle performs a one-dimensional random walk on a lattice, with jumps to nearest neighbors only and with random waiting times between jumps. In the CTRW the waiting times between jumps are independent identically distributed random variables, namely the CTRW process is renewed after each jump. The PDF of waiting times is $\psi(t) \propto t^{-(1+\alpha)}$ when $t \rightarrow \infty$ and $0 < \alpha < 1$. The lattice spacing is ϵ , eventually I will consider the continuum limit when ϵ is small. On each lattice point a probability for jumping left and a probability of jumping right is assigned. This dynamics in the continuum limit leads to behavior described by the FFPE, when detailed balance conditions are applied on the

probabilities for jumping left or right [25] (i.e., probabilities to jump left or right are related to external force field and temperature). In what follows I start with some general arguments, assuming only a renewal property of the random walk.

The random position of the particle is $x(t)$. The total time the particle spends on $x \geq 0$ is T^+ , i.e., the occupation time of half space. The particle starts on x_0 and assume that $x_0 \geq 0$. Define the PDF of first passage times, from x_0 to $x = -\epsilon$, as $\psi_{x_0}^+(t)$. The PDF of first passage times from $x = 0$ to $x = -\epsilon$ ($x = -\epsilon$ to $x = 0$) is denoted by $\psi^+(t)$ and $[\psi^-(t)]$, respectively.

Assume that the first passage times PDFs $\psi^+(t)$ and $\psi^-(t)$ do not depend on x_0 and that sojourn times in domain $x > 0$ and $x < 0$ are statistically independent. Such assumption holds for Markovian dynamics but is not obvious otherwise. For the CTRW dynamics the assumption is correct, since the CTRW is a renewal process. The original CTRW process is mapped on a random two-state process

$$\theta_x(t) = \begin{cases} 1 & \text{if } x(t) \geq 0 \\ 0 & \text{if } x(t) < 0 \end{cases} \quad (7.32)$$

and hence $T^+ = \int_0^t \theta_x(t) dt$. Since either the particle is in the domain $x < 0$ or not the dynamics is described by a set of sojourn times

$$\tau_{x_0}, \tau_1^-, \tau_2^+, \tau_3^-, \tau_4^+, \dots$$

Here the PDF of τ_{x_0} is $\psi_{x_0}(t)$, the PDF of τ_1^- is $\psi^-(t)$, the PDF of τ_2^+ is $\psi^+(t)$, etc. All the sojourn times are assumed mutually independent, which means the process is renewed once the particle jumps from $x = 0$ to $x = -\epsilon$ or vice versa.

Let $f_{x_0,t}(T^+)$ be the PDF of T^+ when the total observation time is t . Let $f_{x_0,s}(u)$ be the double-Laplace transform of $f_{x_0,t}(T^+)$. A calculation, using methods of renewal theory, found in the work of Godreche and Luck [39] yields

$$f_{x_0,s}(u) = \frac{1 - \psi_{x_0}^+(s+u)}{s+u} + \psi_{x_0}^+(s+u) \left[\psi^-(s) \frac{1 - \psi^+(s+u)}{s+u} + \frac{1 - \psi^-(s)}{s} \right] \frac{1}{1 - \psi^+(s+u)\psi^-(s)}, \quad (7.33)$$

where $\psi_{x_0}^+(s+u) = \int_0^t \exp[-(s+u)t] \psi_{x_0}^+(t) dt$ is the Laplace transform. If $\psi_{x_0}^+(t) = \psi^+(t) = \psi^-(t)$ a result in [39] is recovered. While I did not provide the derivation of Eq. (7.33), the excellent paper of Godreche and Luck is also tutorial, and the reader should not have difficulty in deriving Eq. (7.33) once Ref. [39] is mastered.

If the particle starts on $x_0 < 0$ then one can show

$$\begin{aligned} f_{x_0,s}(u) = & \frac{1 - \psi_{x_0}^-(s)}{s} + \psi_{x_0}^-(s) \left[\psi^+(s+u) \frac{1 - \psi^-(s)}{s} \right. \\ & \left. + \frac{1 - \psi^+(s+u)}{s+u} \right] \frac{1}{1 - \psi^+(s+u)\psi^-(s)}. \end{aligned} \quad (7.34)$$

Now consider the case when the underlying dynamics is described by the FFPE. By definition the first passage time PDFs are related to survival probabilities according to

$$W_{x_0}^+(t) = 1 - \int_0^t \psi_{x_0}^+(t) dt, \quad (7.35)$$

or using the convolution theorem in Laplace space

$$W_{x_0}^+(s) = \frac{1 - \psi_{x_0}^+(s)}{s}. \quad (7.36)$$

Hence rewrite Eq. (7.33)

$$\begin{aligned} f_{x_0,s}(u) = & W_{x_0}^+(s+u) + [1 - (s+u)W_{x_0}^+(s+u)] \left[\psi^-(s) \frac{1 - \psi^+(s+u)}{s+u} \right. \\ & \left. + \frac{1 - \psi^-(s)}{s} \right] \frac{1}{1 - \psi^+(s+u)\psi^-(s)}. \end{aligned} \quad (7.37)$$

Note that $f_{x_0,s}(u)$ depends on x_0 only through the survival probability $W_{x_0}^+(s+u)$. Apply now the backward Fokker–Planck operator

$$D_\alpha \left[\frac{\partial^2}{\partial x_0^2} + \frac{F(x_0)}{k_B T} \frac{\partial}{\partial x_0} \right]$$

to Eq. (7.37) and use Eq. (7.31), namely assume that the underlying dynamics is described by the FFPE in the continuum limit. Doing so we obtain at once our main result (7.30). Similar method is used for the case $x_0 < 0$ to complete the proof.

Let us derive our main Eq. (7.14) using the continuum approximation. Consider the case when the particle starts on $x_0 = 0$ hence $\psi_{x_0}^+ = \psi^+$ and define

$$\overline{G}_s(u) = f_{x_0=0,s}(u). \quad (7.38)$$

Generally $\overline{G}_s(u)$ is not identical to $G_s(u)$ and now our aim is to find the conditions when these two functions are identical. Using Eq. (7.33)

$$\overline{G}_s(u) = \left[\frac{1 - \psi^+(s+u)}{(s+u)} + \psi^+(s+u) \frac{1 - \psi^-(s)}{s} \right] \frac{1}{1 - \psi^+(s+u)\psi^-(s)}. \quad (7.39)$$

In the continuum limit the following ϵ expansion

$$\psi_\epsilon^-(s) \simeq \psi_{\epsilon=0}^-(s) - \frac{\partial \psi_\epsilon^-}{\partial x}|_{\epsilon=0} \epsilon + \dots \quad (7.40)$$

holds, and a similar expansion for $\psi_\epsilon^+(s)$ is found. The subscript ϵ in Eq. (7.40) is added to emphasize that the PDF of the first passage time from lattice point $-\epsilon$ to the origin 0. Note that $\psi_{\epsilon=0}^-(s) = 1$, since the particle on the origin is immediately absorbed. Inserting the expansion (7.40) in Eq. (7.39) and using a similar expansion for $\psi_\epsilon^+(s+u)$ we see that when $\epsilon \rightarrow 0$

$$\overline{G}_s(u) \sim \frac{\frac{1}{(s+u)} \frac{\partial \psi^+(s+u)}{\partial x_0} \Big|_{x_0=0} - \frac{1}{s} \frac{\partial \psi^-(s)}{\partial x_0} \Big|_{x_0=0}}{\frac{\partial \psi^+(s+u)}{\partial x_0} \Big|_{x_0=0} - \frac{\partial \psi^-(s)}{\partial x_0} \Big|_{x_0=0}}. \quad (7.41)$$

Using Eqs. (7.36) and (7.41) we obtain our main result (7.14) and $\overline{G}_s(u)$ is identical to $G_s(u)$ in the continuum limit of $\epsilon \rightarrow 0$.

7.3.2

Weak Ergodicity Breaking

Consider anomalous dynamics in a binding potential field $V(x)$, e.g., $V(x) = kx^2/2$ with $k > 0$. As I showed already the long-time behavior of $G_t(T^+)$, for normal diffusion, yields an ergodic behavior (7.21). Using the subordination trick (see Appendix), or analyzing Eq. (7.31) I find that for $s \rightarrow 0$

$$W_{x_0}^\pm(s) \sim \frac{(\tau_{x_0}^\pm)^\alpha}{s^{1-\alpha}}, \quad (7.42)$$

and the random walk is recurrent [26]. When $\alpha = 1$, $(\tau_{x_0}^\pm)^\alpha = \langle t_{x_0}^\pm \rangle$ and Eq. (7.18) is valid. For $0 < \alpha < 1$ and in the time domain $W_{x_0}^\pm(t) \propto t^{-\alpha}$, reflecting the long tailed trapping times of the underlying CTRW. The $(\tau_{x_0}^\pm)^\alpha$ are amplitudes which satisfy

$$D_\alpha \left[\frac{\partial^2}{\partial x_0^2} + \frac{F(x_0)}{k_B T} \frac{\partial}{\partial x_0} \right] (\tau_{x_0}^\pm)^\alpha = -1. \quad (7.43)$$

This equation is obtained from the small s expansion of Eq. (7.31). Using Eqs. (7.42) and (7.14) in the limit of small s and u

$$G_s(u) \sim \frac{\mathcal{R}(s+u)^{\alpha-1} + s^{\alpha-1}}{\mathcal{R}(s+u)^\alpha + s^\alpha}, \quad (7.44)$$

where the asymmetry parameter is

$$\mathcal{R} = -\frac{\frac{\partial (\tau^+)^\alpha}{\partial x_0} \Big|_{x_0=0^+}}{\frac{\partial (\tau^-)^\alpha}{\partial x_0} \Big|_{x_0=0^-}}. \quad (7.45)$$

Inverting to the time domain (see Appendix of [11]), the PDF of T^+ in the long-time t limit is described by Lamperti's limit theorem [7]

$$G_t(T^+) \sim \frac{1}{t} \delta_\alpha \left(\mathcal{R}, \frac{T^+}{t} \right), \quad (7.46)$$

where the scaling function is

$$\delta_\alpha(\mathcal{R}, p) \equiv \frac{\sin \pi \alpha}{\pi} \frac{\mathcal{R} p^{\alpha-1} (1-p)^{\alpha-1}}{\mathcal{R}^2 (1-p)^{2\alpha} + p^{2\alpha} + 2\mathcal{R} (1-p)^\alpha p^\alpha \cos \pi \alpha}. \quad (7.47)$$

This function is normalized according to $\int_0^1 \delta_\alpha(\mathcal{R}, p) dp = 1$. When $\alpha = 1$ the ergodic behavior in Eq. (7.21) is reached, while clearly if $\alpha < 1$ we find a nonergodic behavior. The parameter \mathcal{R} is called the asymmetry parameter. It can be calculated by solving Eq. (7.43)

$$\frac{\partial (\tau_{x_0}^+)^{\alpha}}{\partial x_0} \Big|_{x_0=0^+} = \frac{1}{D_\alpha} \int_0^\infty e^{-[V(x')-U(0)]/k_b T} dx', \quad (7.48)$$

$$\frac{\partial (\tau_{x_0}^-)^{\alpha}}{\partial x_0} \Big|_{x_0=0^-} = -\frac{1}{D_\alpha} \int_{-\infty}^0 e^{-[V(x')-U(0)]/k_b T} dx'. \quad (7.49)$$

Using Eqs. (7.45), (7.48), and (7.49)

$$\mathcal{R} = \frac{P_B^+}{1 - P_B^+}, \quad (7.50)$$

where P_B^+ is Boltzmann's probability for finding the particle in the domain $x > 0$ (Eq. (7.22)). Equations (7.46) and (7.50) were found by Bel and myself in [8] using a CTRW approach. One can show that the average occupation time is

$$\langle T^+ \rangle \sim P_B^+ t \quad (7.51)$$

and fluctuations are very large if $\alpha < 1$

$$\langle (T^+)^2 \rangle - \langle T^+ \rangle^2 \sim (1 - \alpha) P_B^+ (1 - P_B^+) t^2. \quad (7.52)$$

For numerical demonstration of the result (7.47), starting from CTRW dynamics, see [8, 11]. Related irreproducibility of time-averaged anomalous currents was numerically demonstrated by Heinsalu et al. [40]. Our results can be generalized for the problem of occupation times in the interval $x_1 < x < x_2$ by replacing P_B^+ with $P_B(x_1 < x < x_2)$ (Eq. (7.1)) in \mathcal{R} (Eq. (7.50)) [11].

7.3.3

Example: Anomalous Diffusion in an Interval

Consider the case where the particle is free to diffuse in an interval of total length $L^+ + L^-$. The particle is initially on the origin $x = 0$ and reflecting boundary conditions are on $x = L^+$ and $x = -L^-$. Statistical properties of T^+ the time spent in $(0, L^+)$ are now investigated.

The survival probability can be calculated using Eq. (7.31)

$$W_{x_0}^+(s) = \frac{1 - \frac{\cosh\left[\sqrt{\frac{s^\alpha}{D_\alpha}}(L^+ - x_0)\right]}{\cosh\left(\sqrt{\frac{s^\alpha}{D_\alpha}}L^+\right)}}{s}, \quad (7.53)$$

and when $\alpha = 1$ we recover a text book result [18]. Using Eq. (7.14)

$$G_s(u) = \frac{(s+u)^{\alpha/2-1} \tanh\left[\frac{(s+u)^{\alpha/2}L^+}{\sqrt{D_\alpha}}\right] + s^{\alpha/2-1} \tanh\left(\frac{s^{\alpha/2}L^-}{\sqrt{D_\alpha}}\right)}{(s+u)^{\alpha/2} \tanh\left[\frac{(s+u)^{\alpha/2}L^+}{\sqrt{D_\alpha}}\right] + s^{\alpha/2} \tanh\left(\frac{s^{\alpha/2}L^-}{\sqrt{D_\alpha}}\right)}. \quad (7.54)$$

For free boundary conditions, namely in the limit where the system size is infinite $L^+ \rightarrow \infty$ and $L^- \rightarrow \infty$

$$G_s(u) = \frac{(s+u)^{\alpha/2-1} + s^{\alpha/2-1}}{(s+u)^{\alpha/2} + s^{\alpha/2}}. \quad (7.55)$$

Inverting to the time domain, the PDF of T^+ is the symmetric Lamperti PDF with index $\alpha/2$

$$G_t(T^+) = \frac{1}{t} \delta_{\alpha/2}\left(1, \frac{T^+}{t}\right). \quad (7.56)$$

When $\alpha = 1$, i.e., the case of normal Gaussian diffusion, the arcsine distribution equation (7.6) is recovered. When $\alpha \rightarrow 0$ the PDF of T^+ is a combination of two delta functions with $T^+ = t$ (particle always on $x > 0$) or $T^+ = 0$ (particle always in $x < 0$).

A different behavior is found for finite L^+ and L^- , then using Eq. (7.54) for short times

$$G_t(T^+) \sim \frac{1}{t} \delta_{\alpha/2}\left(1, \frac{T^+}{t}\right) \quad t \ll \left[\frac{\min(L^+, L^-)^2}{D_\alpha} \right]^{1/\alpha}. \quad (7.57)$$

For these time scales the particle does not interact with the boundaries, and $G_t(T^+)$ is the symmetric Lamperti PDF with index $\alpha/2$. In the long-time limit, corresponding to the small s, u limit, using Eq. (7.54)

$$G_s(u) \sim \frac{(s+u)^{\alpha-1} L^+ + s^{\alpha-1} L^-}{(s+u)^\alpha L^+ + s^\alpha L^-} \quad (7.58)$$

and hence when $t \rightarrow \infty$

$$G_t(T^+) \sim \frac{1}{t} \delta_\alpha \left(\frac{L^+}{L^-}, \frac{T^+}{t} \right). \quad (7.59)$$

This is in agreement with our more general result (Eqs. (7.46) and (7.50)) namely for the case of free diffusion $P_B^+ = L^+/(L^+ + L^-)$ and hence $\mathcal{R} = L^+/L^-$. If $L^+ \neq L^-$ the PDF of T^+ is as expected nonsymmetric, reflecting the tendency of the particle to reside in the larger interval [say $(0, L^+)$ if $L^+ > L^-$] for longer times compared with the smaller domain. We see that the statistics of occupation times exhibits a transition from a symmetric Lamperti PDF with index $\alpha/2$ when diffusion is dominating the dynamics, i.e., for short times, to a generally nonsymmetric Lamperti PDF with index α , for long times when the particle interacts with the boundaries. Other examples are worked out in [6].

7.4

Deterministic Weak Ergodicity Breaking

Let us turn our attention to the problem of occupation times in deterministic systems, showing that statistics of occupations times obtained from stochastic considerations is also found for a class of nonlinear dynamical systems. More importantly, I now explain in further detail what is meant by weak ergodicity breaking, as opposed to strong ergodicity breaking. We do so by considering a one-dimensional map with L unstable fixed points [9], which in the limit of $L \rightarrow \infty$ exhibit anomalous diffusion. Previously, Thaler [10] investigated related maps with two unstable fixed points. In the mathematical literature this problem is related to the so-called infinite ergodic theory, due to the infinite measure of the underlying dynamics [10].

Probably the simplest deterministic maps which lead to normal and anomalous diffusion are one-dimensional maps of the form

$$x_{t+1} = x_t + F(x_t), \quad (7.60)$$

with the following symmetry properties of $F(x)$: (i) $F(x)$ is periodic with a period interval set to 1, i.e., $F(x) = F(x + N)$, where N is an integer. (ii) $F(x)$ is antisymmetric; namely, $F(x) = -F(-x)$, note that t in Eq. (7.60) is a discrete time. Geisel and Thomae [41] considered a family of such maps which behave like

$$F(x) = ax^z \text{ for } x \rightarrow 0_+, \quad (7.61)$$

where $z > 1$. Equation (7.61) defines the property of the map close to its unstable fixed point. In numerical experiments introduced we [9] used the

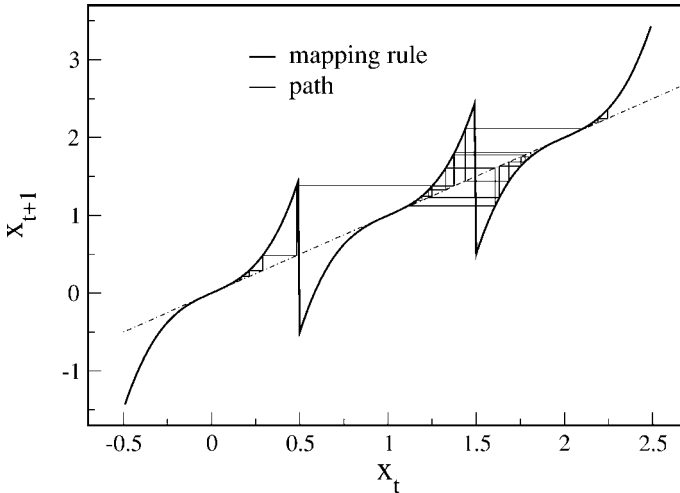


Figure 7.1 The map (Eqs. (7.60) and (7.62)) with $z = 3$ and three unit cells $L = 3$. The dashed line shows the curve $x_{t+1} = x_t$. Fixed points are at $x_t = 0, 1, 2$ and the cells are $(-0.5, 0.5)$, $(0.5, 1.5)$, $(1.5, 2.5)$. A specific realization of the dynamics is also drawn (thin line).

following map:

$$F(x) = (2x)^z, \quad 0 \leq x \leq 1/2, \quad (7.62)$$

which together with the symmetry properties of the map define the mapping for all x . The functional form of the map on a unit interval was introduced by Pomeau and Manneville to describe intermittency [42]. Variations of these maps have been investigated by taking into account time-dependent noise [43], quenched disorder [44], and additional uniform bias which breaks the symmetry of the map [45]. The map with L unit cells and periodic boundary conditions is considered. In Figure 7.1 I show the map, and one realization of a path along three unit cells.

In an ongoing process a walker following the iteration rules may get stuck close to the vicinity of one of the unstable fixed points of the map. It has been shown both analytically and numerically that the PDF of escape times from the vicinity of the fixed points decays as a power law [41]. To see this, one considers the dynamics in a half unit cell, say $0 < x < 1/2$. Assume that at time $t = 0$ the particle is on x^* residing in the vicinity of the fixed point $x = 0$. Close to the fixed point the map (Eq. (7.60)) is approximated with the differential equation $dx/dt = F(x) = ax^z$. The solution is written in terms of the q exponential function, $\exp_q(y) \equiv [1 + (1 - q)y]^{1/(1-q)}$ where $q = z$ and

$$x(t) = x^* \exp_z \left[a x^{*(z-1)} t \right]. \quad (7.63)$$

Invert Eq. (7.63) to obtain the escape time from x^* to a boundary on b ($x^* < b < 1/2$) which is

$$t \simeq \int_{x^*}^b [F(x)]^{-1} dx, \quad (7.64)$$

using Eq. (7.61)

$$t \simeq (1/a) \left[(x^{*1-z})/(z-1) - (b^{1-z})/(z-1) \right]. \quad (7.65)$$

The PDF of escape times $\psi(t)$ is related to the unknown PDF of injection points $\eta(x^*)$, through the chain rule $\psi(t) = \eta(x^*) |dx^*/dt|$. Expanding $\eta(x^*)$ around the unstable fixed point $x^* = 0$ one finds that for large escape times

$$\psi(t) \sim \frac{A}{|\Gamma(-\alpha)|} t^{-1-\alpha}, \quad \alpha = (z-1)^{-1}, \quad (7.66)$$

where A depends on the PDF of injection points, namely on how trajectories are injected from one cell to the other. The parameter A is sensitive to the detailed shape of the map while the parameter z depends only on the behavior of the map close to the unstable fixed points. When $z > 2$ the average escape time diverges [41, 47], which gives rise to aging [36], nonstationarity [46], and anomalous diffusion [41, 47–50].

The map is said to be ergodic if for almost any initial condition (excluding paths starting at fixed points) the path spends equal amounts of time in each cell in the limit of long-measurement time. Namely $t^1/t = 1/L$, where t^1 is the time spent in one of the lattice cells and t is the total measurement time. Another method to quantify the dynamics is to consider the fraction of number of visits per cell n^1/n , where n^1 is the number of visits in one of the lattice cells and n is the total number of visits (or total number of jumps between cells). For maps with finite average escape time $\langle \tau \rangle = \int_0^\infty \tau \psi(\tau) d\tau$, i.e., $z > 2$, the total measurement time $t \sim n \langle \tau \rangle$ and the occupation time of one cell $t^1 \sim n^1 \langle \tau \rangle$ hence $n^1/n = 1/L$, the equalities above should be understood in statistical sense. n^1/n is called the visitation fraction, which plays an important role in the theory of weak ergodicity breaking.

More generally the fraction of occupation times (visitation fraction) in $m \leq L$ cells is $t^m/t (n^m/n)$, where t^m (n^m) is the occupation time (number of visits) in m cells, respectively. For an ergodic system the PDF of the fraction of occupation time is

$$f\left(\frac{t^m}{t}\right) = \delta\left(\frac{t^m}{t} - \frac{m}{L}\right), \quad (7.67)$$

and the visitation fraction is

$$\frac{n^m}{n} = \frac{m}{L} \quad (7.68)$$

in statistical sense, both equalities are valid only in the limit of long-measurement time ($t \rightarrow \infty$). Maps exhibiting strong nonergodicity do not obey Eqs. (7.67) and (7.68). Dynamics obeying Eq. (7.68) but not Eq. (7.67) are said to be weakly nonergodic. When $z > 2$ weak ergodicity breaking is found.

Assuming that the CTRW model is a valid approximation for the dynamics (it is difficult to prove that the CTRW renewal assumption is valid and that the deterministic paths do not hide nontrivial correlations), we can make predictions on the occupation times. First note that for an ensemble of particles the probability that a member of the ensemble occupies cell i , in the limit of long-measurement time is $1/L$. Here an ensemble of particles means an ensemble of initial conditions, for example in simulations [9] choose the initial position of the particles from a uniform distribution in one of the cells. The probability that a member of the ensemble occupies one of m cells is $P_{\text{ens}} = m/L$. Thus the PDF of t^m/t , the occupation fraction in m cells, in the case $z > 2$ is according to Eqs. (7.47) and (7.66)

$$f\left(\frac{t^m}{t}\right) = \delta_{\frac{1}{z-1}}\left(\mathcal{R}, \frac{t_m}{t}\right), \quad (7.69)$$

with

$$\mathcal{R} = \frac{P_{\text{ens}}}{1 - P_{\text{ens}}} = \frac{m}{L - m}, \quad (7.70)$$

which is valid only when t is large.

Following [9] numerical simulations of the map with system of size $L = 9$ are now presented. In Figure 7.2(a) I show two paths generated according to the mapping rule (7.61) and (7.62) with $z = 3$. As one can see each path gets stuck at one of the cells for a time which is of the order of the measurement time. During the measurement the path visits all the L cells many times. In Figure 7.2(b) the case $z = 1.5$, the fraction of occupation time obeys Eq. (7.67) with $m = 1$ namely $t^1/t = 1/L$, with $L = 9$. On the other hand in Figures 7.2(c) and (d) the fraction of occupation time histogram for two initial conditions obtained using $z = 3$. Since each path is localized in one of the cells for a time which is of the order of the total measurement time, the histogram for this case looks very different than that of the ergodic case and clearly Eq. (7.67) is not valid. Histograms of the visitation fraction in each cell are presented in Figure 7.3, for both ergodic ($z = 1.2$) (a) and nonergodic ($z = 3$) (b) maps. The figure demonstrates that for both the cases Eq. (7.68) holds, i.e., the visitation fraction in each cell is given by $1/L$. Hence we are dealing here with

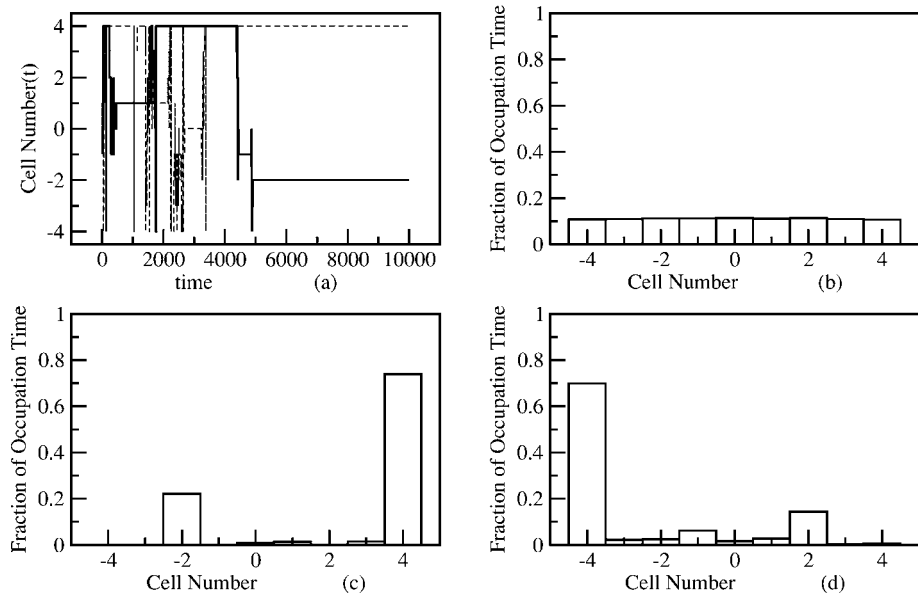


Figure 7.2 (a) Two paths (dashed and solid curves) generated according to the mapping rule with $z = 3$, for each path the particle gets stuck in one of the cells for a time which is of the order of the measurement time.

(b) Histogram of fraction of occupation time for a path with $z = 1.5$. For this ergodic case the fraction of occupation times in the cells are equal. (c)+(d) The same as in (b), but this time for the nonergodic phase with $z = 3$.

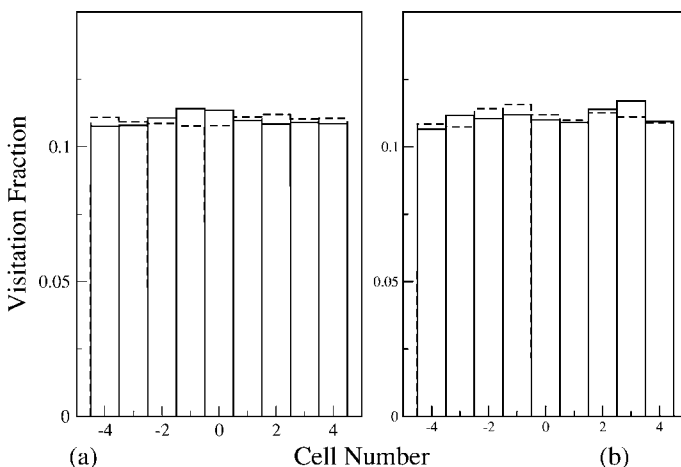


Figure 7.3 Histogram of the visitation fraction in each of the nine lattice cells. (a) $z = 1.2$ (ergodic phase) dashed and solid lines correspond to two initial conditions. (b) The same as (a) but now for the non-

ergodic phase $z = 3$. In both the cases the visitation fractions in each cell are equal, with small fluctuations. Since the visitation fraction is uniform, even in the nonergodic phase, breaking of ergodicity is weak.

weak ergodicity breaking. Clearly Figure 7.2 demonstrates that the fraction of occupation time is random, hence we investigate its distribution.

The assumptions made in the derivation of Eq. (7.69) are tested using numerical simulations of the map. Plots of the PDF of the fraction of occupation time for three different values of z are shown in Figure 7.4. 10^6 trajectories and measured the occupation time of $m = 3$ cells in a system of size $L = 9$ were used. In the ergodic case $z < 2$ the PDF is a delta function centered at m/L (see Figure 7.4(a)). In the nonergodic cases the maximum of $f(t^m/t)$ are at 0 and 1. These events $t^m/t \approx 1$ ($t^m/t \approx 0$) correspond to trajectories where the particle occupies (does not occupy) one of the observed cells for the whole duration of the measurement, respectively. In the nonergodic phase $z > 2$ two types of behaviors are found. For $z = 2.25$ the PDF of fraction of occupation

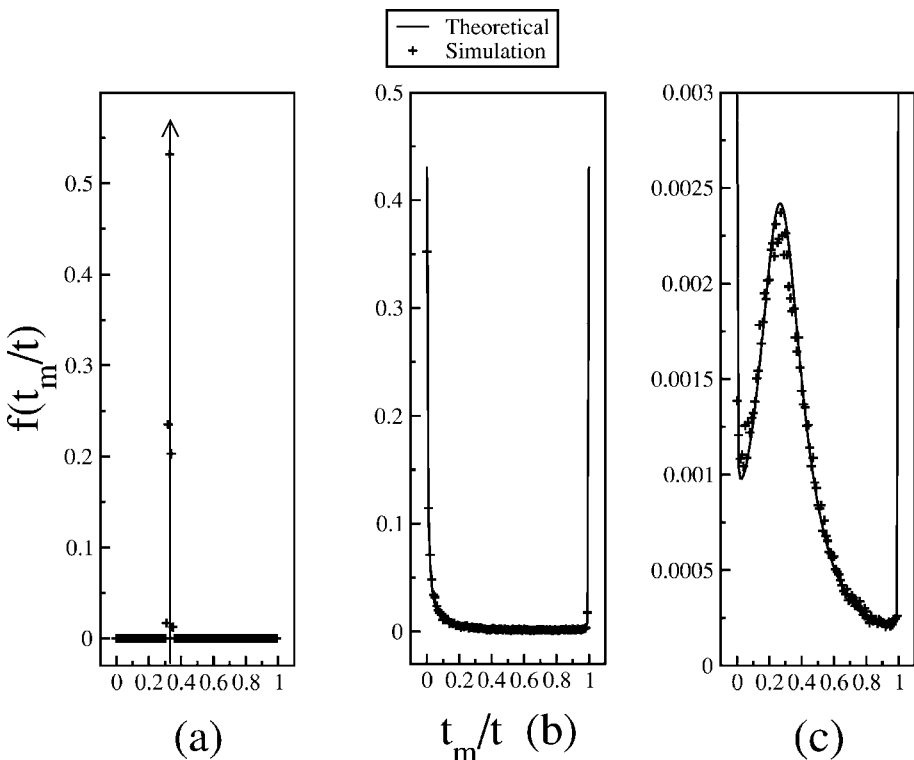


Figure 7.4 (a) The PDF of the fraction of the occupation time t^m/t in $m = 3$ cells, in a system of size $L = 9$ cells for $z = 1.5$. In this ergodic case the PDF is very narrow and centered around m/L . (b) Same as (a), however here $z = 3$. The dynamics is nonergodic, and PDF of the occupation fraction has a U shape, with maximum at 0 and 1.

(c) Same as (a) with $z = 2.25$. In this case a W-shaped PDF is obtained, with a peak at the vicinity of m/L , but yet the maximum are at 0 and 1. The curve is Eq. (7.69) without fitting. Only the parameter z determines the shape of the PDFs, while other details on the shape of the map are unimportant.

time has a W shape, with a peak in the vicinity of m/L . While for $z = 3$, a U shape PDF is found and the probability of obtaining fraction of occupation time equal to m/L is very small. Comparison of theory (Eq. (7.69)) with numerical simulations shows excellent agreement without fitting.

7.5

Discussion

Weak ergodicity breaking has the following meaning:

- (i) The phase space is not divided into mutually inaccessible regions (unlike strong ergodicity breaking), thus the system visits all cells in its phase space for almost all (all but a set of measure zero) initial conditions. Thus for strong ergodicity breaking there is little hope to construct a statistical mechanical theory, since physical properties of each trajectory depend on the initial condition of the system. In contrast for weak ergodicity the phase space is still fully explored, paving the way to statistical analysis of the dynamics, which is not sensitive to the initial condition of the trajectory.
- (ii) For weak ergodicity breaking the visitation fraction for different initial conditions fluctuates very slightly in the limit $t \rightarrow \infty$ (note that for fixed measurement time n and n^m exhibit large fluctuations).
- (iii) The visitation fraction is determined by the probability of finding a member of an ensemble of particles within the given cell [51].
- (iv) The total time the system spends in a cell, or in a domain, fluctuates strongly, and is described by the widely applicable [6, 8, 12, 13, 17] law (Eq. (7.69)).

For the deterministic dynamics investigated, statistics of occupation times is controlled by a single parameter z describing the nonlinearity of the map in the vicinity of the unstable fixed points. Weak ergodicity breaking is clearly related to power-law anomalous diffusion and relaxation, and since these are found in many dynamical systems, it is possible that the nonergodic dynamical behavior found here might be also found in other classes of dynamical systems.

Statistics of occupation times for *binding external fields* exhibits in the limit of long times an ergodic behavior when the diffusion is normal, or weak ergodicity breaking equations (7.46) and (7.50) when diffusion is anomalous. A link between weak ergodicity breaking and fractional calculus was established. The exponent α in the fractional derivative $\partial^\alpha / \partial t^\alpha$ enters in Eq. (7.46) describing the nonergodic properties of the residence times. This is of course the same exponent describing the behavior of the mean-square displacement in the absence of external fields $\langle x^2 \rangle \sim t^\alpha$. Since many processes and systems are modeled today using the fractional calculus approach, it is not out of the

question that weak ergodicity breaking has many applications. Results obtained using fractional kinetic equations must be treated with care, since they describe only ensemble averages, not time averages.

Acknowledgment

This work was supported by the Israel Science Foundation. The second part of the chapter is a brief review of my work with G. Bel. I thank G. Margolin, S. Burov, and G. Bel for fruitful discussions and previous collaborations.

Appendix A

The Fokker–Planck equation for a particle in a force field reads

$$\frac{\partial c(x, t)}{\partial t} = D_1 L_{\text{FP}} c(x, t) \quad (\text{A.1})$$

with the operator

$$L_{\text{FP}} = \frac{\partial^2}{\partial x^2} - \frac{\partial}{\partial x} \frac{F(x)}{k_B T}, \quad (\text{A.2})$$

where D_1 is the diffusion coefficient. To prepare for the FFPE rewrite Eq. (A.1) in an integral form

$$c(x, t) - \delta(x - x_0) = D_1 {}_0 I_t^1 L_{\text{FP}} c(x, t), \quad (\text{A.3})$$

where $\delta(x - x_0)$ are the initial conditions. To obtain the fractional kinetic approach, replace the integral ${}_0 I_t^1$ with a fractional Riemann–Liouville integration, defined as an operation on a function $Z(t)$ according to

$${}_0 I_t^\alpha Z(t) \equiv \frac{1}{\Gamma(\alpha)} \int_0^t \frac{Z(t')}{(t - t')^{1-\alpha}} dt', \quad (\text{A.4})$$

and for our purpose $0 < \alpha < 1$. The FFPE in its integral form is

$$c(x, t) - \delta(x - x_0) = D_\alpha {}_0 I_t^\alpha L_{\text{FP}} c(x, t), \quad (\text{A.5})$$

where D_α is a generalized diffusion coefficient. Several authors present this equation in different ways. Sometimes [24] further differentiation with respect to time is made in Eq. (A.5) to return to a fractional differential equation instead of the fractional integral form. However, following work of Gorenflo and Mainardi, e.g., [29] there is now growing use of Caputo symbols which are more elegant. Such symbols are used in Eq. (7.29), which has the same meaning as Eq. (A.5). Later I use the Laplace $t \rightarrow s$ transform of the FFPE equation (A.5)

$$sc(x, s) - \delta(x - x_0) = D_\alpha s^{1-\alpha} L_{\text{FP}} c(x, s). \quad (\text{A.6})$$

We see that the solution of the FFPE with $\alpha < 1$ is related to the solution of the Fokker–Planck equation when $\alpha = 1$ in Laplace space. To obtain the solution of the FFPE from the solution of the usual Fokker–Planck equation make the replacement $D_1 \rightarrow D_\alpha s^{1-\alpha}$ [24]. This similarity transformation in s space can be inverted to real time [26], and with it one can obtain a solution of the FFPE once the corresponding solution of the usual Fokker–Planck equation is known. This transformation is related to subordination and the inverse Lévy transform [26].

Similarly the survival probability for the normal diffusion case, and the fractional case are related to each other, by a simple transformation in Laplace space [26]. According to Eq. (57) in Ref. [26]

$$W_{\alpha,x_0}^+(s) = \frac{D_1}{D_\alpha} s^{\alpha-1} W_{1,x_0}^+ \left(\frac{D_1}{D_\alpha} s^\alpha \right), \quad (\text{A.7})$$

where $W_{\alpha,x_0}^+(s)$ is the survival probability for the fractional $\alpha < 1$ or the normal case $\alpha = 1$. Using Eqs. (7.12) and (A.7) it is easy to prove the validity of Eq. (7.31).

References

- 1 J. Klafter, M. F. Shlesinger, and G. Zumofen, *Phys. Today* **49**, No. 2, 33 (1996).
- 2 J.P. Bouchaud and A. Georges, *Phys. Rep.* **195** 127 (1990).
- 3 H. Scher, and E. W. Montroll, *Phys. Rev. B* **12** 2455 (1975).
- 4 J. P. Bouchaud, *J. De Physique I* **2** 1705 (1992).
- 5 A. Rebenstok, E. Barkai *Phys. Rev. Lett.* **99**, 210601 (2007).
- 6 E. Barkai, *J. Stat. Phys.* **123** 883 (2006).
- 7 J. Lamperti, *Trans. Am. Math. Soc.* **88** 380 (1958).
- 8 G. Bel and E. Barkai, *Phys. Rev. Lett.* **94** 240602 (2005).
- 9 G. Bel and E. Barkai, *Europhys. Lett.* **74** 15 (2006).
- 10 M. Thaler, *Ergod. Th. & Dynam. Sys.* **22** 1289 (2002).
- 11 G. Bel and E. Barkai, *Phys. Rev. E* **73** 016125 (2006).
- 12 G. Margolin, E. Barkai *Phys. Rev. Lett.* **94** 080601 (2005).
- 13 S. Burov, E. Barkai, cond-mat/0612667 (2006)
- 14 X. Brokmann, J. P. Hermier, G. Messin, P. Desbiolles, J. P. Bouchaud, and M. Dahan, *Phys. Rev. Lett.*, **90** 120601 (2003).
- 15 G. Margolin, V. Protasenko, M. Kuno, E. Barkai, *Advances in Chemical Physics* **133** 327 (2006). G. Margolin et al cond-mat/0506512.
- 16 G. Margolin, V. Protasenko M. Kuno, and E. Barkai, *J. Phys. Chem. B* **110** 19053 (2006).
- 17 M. A. Lomholt, I. M. Zaid, and R. Metzler, *Phys. Rev. Lett.* **98**, 200603 (2007).
- 18 S. Redner, *A Guide to First-Passage Processes* Cambridge University Press, Cambridge, 2001.
- 19 S. N. Majumdar, *Current Science* **89** 2076 (2005).
- 20 see p. 50 in: F. Bardou, J.P. Bouchaud, A. Aspect, and C. Cohen-Tannoudji, *Lévy Statistics and Laser Cooling* Cambridge (2002).
- 21 S. N. Majumdar and A. Comtet, *Phys. Rev. Lett.* **89** 060601 (2002).
- 22 S. Sabhapandit, S. N. Majumdar, and A. Comtet, cond-mat/0601455 (2006).
- 23 C. W. Gardiner, *Handbook of Stochastic Methods* Springer, Berlin, 2003.
- 24 R. Metzler, E. Barkai, and J. Klafter, *Phys. Rev. Lett.* **82** 3563 (1999).
- 25 E. Barkai, R. Metzler, J. Klafter, *Phys. Rev. E* **61** 132 (2000).
- 26 E. Barkai, *Phys. Rev. E* **63** 046118 (2001).
- 27 W. R. Schneider, W. Wyss, *J. Math. Phys.* **30** 134 (1989).
- 28 A. I. Saichev, and G. M. Zaslavsky, *Chaos* **7** 753 (1997).
- 29 R. Gorenflo, A. Vivoli, F. Mainardi, *Nonlinear Dyn.* **38** 101 (2004).
- 30 M. M. Meerschaert, H. P. Scheffler, *J. Appl. Prob.* **41** 623 (2004).
- 31 I. Goychuk and P. Hanggi, *Phys. Rev. E* **70** 051915 (2004).
- 32 G. R. Kneller, *Phys. Chem. Chem. Phys.* **7** 2641 (2005).
- 33 W. T. Coffey, *J. Mol. Liq.* **114** 5 (2004).
- 34 R.C. Lua and A.Y. Grosberg, *Phys. Rev. E* **72** 061918 (2005).
- 35 G. M. Zaslavsky, *Phys. Rep.* **371**, 461 (2002).
- 36 E. Barkai, *Phys. Rev. Lett.* **90** 104101 (2003).
- 37 R. Metzler and J. Klafter, *Phys. Rep.* **339** 1 (2000).
- 38 I. M. Sokolov, J. Klafter, and A. Blumen, *Phys. Today* **55** 48 (2002).
- 39 C. Godreche, and J. M. Luck, *J. Stat. Phys.* **104** 489 (2001).
- 40 E. Heinsalu, M. Patriarca, I. Goychuk, G. Schmid, and P. Hänggi, *Phys. Rev. E* **73** 046133 (2006).
- 41 T. Geisel and S. Thomae, *Phys. Rev. Lett.* **52**, 1936 (1984).
- 42 Y. Pomeau and P. Manneville, *Commun. Math. Phys.* **74**, 189 (1980); P. Manneville, *J. Phys.* **41**, 1235 (1980).
- 43 R. Bettin, R. Mannella, B. J. West, and P. Grigolini, *Phys. Rev. E* **51**, 212 (1995).
- 44 G. Radons, *Phys. Rev. Lett.* **77**, 4748 (1996).
- 45 E. Barkai and J. Klafter, *Phys. Rev. Lett.* **79**, 2245 (1997).
- 46 M. Ignaccolo, P. Grigolini, and A. Rosa, *Phys. Rev. E* **64**, 026210 (2001).

- 47** G. Zumofen and J. Klafter, *Phys. Rev. E* **47**, 851 (1993).
- 48** N. Korabel, A. V. Chechkin, R. Klages, I. M. Sokolov, and V. Yu. Gonchar, *Europhys. Lett.* **70**, 63 (2005).
- 49** S. Tasaki and P. Gaspard, *Physica D* **187**, 51 (2004).
- 50** R. Artuso and G. Cristadoro, *Phys. Rev. Lett.* **90**, 244101 (2003).
- 51** G. Bel and E. Barkai *J. Phys.: Condens. Matter* **17** S4287–S4304 (2005)

Part II Dynamical Systems and Deterministic Transport

Introduction to Part II

While in the first part of the book stochastic descriptions of anomalous transport were highlighted, Part II focuses on deterministic theories. It thus explores the consequences of specific types of nonlinearities in the microscopic equations of motion leading to anomalous transport on macroscopic scales. The currently emerging theory of *Dynamical systems and deterministic transport* as applied to anomalous dynamics can particularly be worked out for low-dimensional models. Part II outlines foundations of this approach in three chapters.

The first contribution by Roberto Artuso and Giampaolo Cristadoro introduces to *Deterministic (anomalous) transport* along the lines of the thermodynamic formalism. For simple models such deterministic techniques yield exact formulas of transport coefficients in terms of periodic orbits, which can be evaluated via cycle expansions. Interesting crosslinks to mathematical dynamical systems theory are provided by means of dynamical zeta functions. These methods are applied to simple (intermittent) one-dimensional maps. Similar models have already been studied by Eli Barkai in the last chapter of the previous Part I from both a stochastic and a deterministic viewpoint. The chapter by Eduardo G. Altmann and Holger Kantz focuses on *Anomalous transport in Hamiltonian systems*. For low-dimensional Hamiltonian dynamics the hypothesis of strong chaos typically leading to normal transport is often violated. In such cases anomalous transport can occur, which in Hamiltonian systems is intimately related to the existence of a mixed phase space with stickiness of trajectories to KAM tori of periodic motion and long-time tails in corresponding observables. Deterministic diffusion in the standard map and tracer diffusion in simple models of incompressible fluids are discussed as examples. Applications of the continuous time random walk model as introduced in Part I of this book yields important insight into the exponents characterizing the anomalous deterministic transport of these systems. The third contribution by Stefano Lepri, Roberto Livi and Antonio Politi introduces to the problem of a microscopic description of heat transport in matter. Attempts to derive Fourier's law of (normal) heat conduction from first prin-

ciples for simple models such as chains of harmonic oscillators first led to rather disappointing results. It turned out that *Anomalous heat conduction* is not the exception but rather the rule even if the oscillator chains are anharmonic. Lepri and colleagues outline the historical development of the problem, leading from Fourier's pioneering work over Boltzmann's and Peierls' groundbreaking contributions to the famous Fermi-Pasta-Ulam model. They classify basic models of harmonic and anharmonic oscillator chains by discussing their properties in terms of Green-Kubo formulas and mode coupling theory. The chapter finishes with anomalous heat conduction in Hamiltonian particle billiards, which establishes an interesting crosslink to models and problems touched upon in the previous two chapters.

8**Deterministic (Anomalous) Transport**

Roberto Artuso and Giampaolo Cristadoro

8.1**Introduction**

A fascinating upshot of dynamical systems theory concerns the possibility that chaos at a microscopic level may induce, once averages are taken, stochastic behavior, for instance by generating normal random-walk like transport properties. As a matter of fact, diffusive properties of deterministic chaotic systems (most remarkable examples being the standard map [1–4], one-dimensional maps [5–7] and Lorentz gas (with finite horizon) [8,9]) have been actively studied since the early stage of chaos theory. An important common feature of the afore-mentioned examples is space periodicity, a property we will extensively use in the next sections.

Systematic investigations of such systems soon revealed the possibility of generating anomalous transport, typically signaled by non-Gaussian scaling of the second moment of the diffusing variable (definitions will be provided in the next section): The origin of such anomalies may be qualitatively tracked down to a weakening of chaotic properties, namely intermittency in one-dimensional maps [10,11], regular islands punctuating the chaotic sea in the standard map [3,12,13], and opening up an infinite horizon for the Lorentz gas [14–16]. Indeed anomalous transport properties represent a relevant phenomenon in statistical mechanics [17]: Our interest here is to provide quantitative techniques that may shed some light on simple examples, and that furthermore may give a clue to universal features of such phenomena.

While it is apparent from many contributions to this volume that such a behavior may be fruitfully scrutinized in terms of random processes (see also [18,19]), our main impetus is to show that crisply deterministic techniques may be applied here, and they are both capable of getting sharp estimates and providing insight on universal behavior (we include a brief discussion of probabilistic approaches in Section 8.6). We point out that the theoretical framework that we here apply to deterministic transport has been employed in a huge number of contexts, both in a classical and in a quantum framework [20–23].

In the next two sections we will give an account of the theoretical approach: further sections will be devoted to the discussion of examples both for normal and anomalous transport.

8.2

Transport and Thermodynamic Formalism

Though the technique we will introduce may be applied to generic dynamical systems, in order to simplify the notation it is convenient to illustrate it within the simplest possible example, so we consider a one-dimensional (discrete-time) mapping f on the real line, enjoying the following symmetry properties:

$$f(-x) = -f(x) \quad (8.1)$$

and

$$f(x+n) = f(x) + n \quad n \in \mathbb{N}. \quad (8.2)$$

The requirement (8.1) is not strictly necessary, it guarantees that no net drift is present in the system (once a uniform initial distribution on a unit cell is taken), so that the discussion of the second moment is easier (we notice that the evaluation of the *first* moment maybe of interest too, as in the discussion of deterministic ratchets [24]: see [25] for an example discussed along the present lines). The condition (8.2) is much more relevant: It encodes space-translation symmetry and it implies that the map on the real line may be viewed as the lift of a circle map \hat{f} on the unit interval:

$$\hat{f}(x) = f(x)|_{\text{mod } 1}. \quad (8.3)$$

This property is also shared by higher dimensional examples to which our technique can be applied: for instance the toral map associated to a Lorentz gas with a square lattice of scatterers is a Sinai billiard with periodic boundary conditions (and this holds in any dimension).¹ Indeed violation of such a property, for instance by introducing a weak quenched disorder, may lead to quite a different physics, see for instance [28] and references therein, where transport properties are considered for such a case, a deterministic analog of random walks in random environments [29, 30].

Given our dynamical system f , we are interested in moments of the diffusing variable:

$$M_q(n) = \langle |x_n - x_0|^q \rangle_0, \quad (8.4)$$

¹) We note, however, that in higher dimensions taking properly into account symmetry properties may require considerable effort [26, 27].

where $\langle \cdots \rangle_0$ denotes an average over initial conditions (typically uniformly distributed on some compact set, for instance an elementary cell). The evaluation of even integer moments may be performed from the generating function

$$\mathcal{G}_n(\beta) = \langle e^{\beta(f^n(x_0) - x_0)} \rangle_0 \quad (8.5)$$

(due to symmetry property (8.1) odd order moments computed from (8.5) vanish). The idea is to deal with the generating function in the same way the partition function is computed in lattice models admitting a transfer matrix, i.e., by expressing (8.5) as the trace of the n th power of a transfer operator. The delicate point is reduction to torus map: as a matter of fact if we just look at the first iterate (and take initial conditions uniformly spread over the unit interval), we get

$$\mathcal{G}_1(\beta) = \int_0^1 dx \int_{-\infty}^{+\infty} dy e^{\beta(f(x) - x)} \delta(y - f(x)) \quad (8.6)$$

so that the “indices” of the kernel are mismatched, coming from two different sets ($[0, 1]$ and $f([0, 1])$). But $\forall y \in \mathbf{R}$ such that $y = f(x)$ there exists one and only one $z \in [0, 1]$ such that $z = \hat{f}(x)$ and $y = z + n_x$, $n_x \in \mathbf{Z}$, so that (8.6) may be rewritten as

$$\mathcal{G}_1(\beta) = \int_0^1 dx \int_0^1 dz e^{\beta(\hat{f}(x) + n_x - x)} \delta(z - \hat{f}(x)). \quad (8.7)$$

Now the starting and arriving domain coincide with the fundamental cell (over which the torus map is defined) and we may introduce a generalized transfer operator [31], acting on smooth functions, \mathcal{L}_β as

$$(\mathcal{L}_\beta h)(x) = \int_0^1 dz h(z) e^{\beta(\hat{f}(z) + n_z - z)} \delta(x - \hat{f}(z)), \quad (8.8)$$

whose (singular) integral kernel is

$$\mathcal{L}_\beta(y, x) = e^{\beta(\hat{f}(y) + n_y - y)} \delta(x - \hat{f}(y)). \quad (8.9)$$

The transfer operator (8.8) is a modification of the usual Perron–Frobenius operator, describing measure evolution for dynamical systems: due to the exponential form of the weight it maintains the semigroup property, and we may write the generating function as

$$\begin{aligned} \mathcal{G}_n(\beta) &= \int_0^1 dx \int_0^1 dy \mathcal{L}_\beta^n(x, y) \\ &= \int_0^1 dx \int_0^1 dz_{n-1} \cdots \int_0^1 dz_1 \int_0^1 dx \mathcal{L}_\beta(x, z_1) \cdots \mathcal{L}_\beta(z_{n-1}, y). \end{aligned} \quad (8.10)$$

This is, as we mentioned at the beginning of the section, the analog of expressing the canonical partition function of a lattice system in terms of a transfer matrix

$$Q_N(T, H) = \sum_{\{\sigma_i\}} e^{-\beta \mathcal{H}(\{\sigma_i\})} = \text{tr } \mathcal{T}^N. \quad (8.11)$$

In equilibrium statistical mechanics the next step is to express the trace as the sum of N th powers of the eigenvalues of \mathcal{T} : the leading eigenvalue determines in such a way the Gibbs free energy per particle in the thermodynamic limit. Here we adopt the same strategy, ignoring the fact that the integral kernel is singular (so that \mathcal{L}_β is not compact, like in ordinary Fredholm theory; the reader interested in a rigorous approach should consult, for instance, [32, 33]) and we label eigenvalues of (8.8) in decreasing order (with respect to their absolute value) $\lambda_0(\beta), \lambda_1(\beta), \dots$. In the large n limit (here the large time limit replaces the thermodynamic limit, $N \rightarrow \infty$ in (8.11)) we may thus write

$$\mathcal{G}_n(\beta) = \int_0^1 dx \int_0^1 dy \mathcal{L}_\beta^n(x, y) \sim \sum_{j=0} \lambda_j(\beta)^n. \quad (8.12)$$

In particular, if the leading eigenvalue is isolated and positive (i.e., some generalized Perron theorem holds) the generating function is asymptotically dominated by powers of $\lambda_0(\beta)$; on the other hand, by power expanding in β we obtain

$$\mathcal{G}_n(\beta) = 1 + \beta \langle (\hat{x}_n - \hat{x}_0) \rangle_0 + \frac{\beta^2}{2!} \langle (\hat{x}_n - \hat{x}_0)^2 \rangle_0 + \mathcal{O}(\beta^3) \sim \lambda_0(\beta)^n \quad (8.13)$$

and we may thus relate the diffusion constant to the leading eigenvalue of the generalized transfer operator in the following way:

$$D = \frac{1}{2} \left. \frac{d^2 \lambda_0(\beta)}{d\beta^2} \right|_{\beta=0}, \quad (8.14)$$

where

$$M_2(n) \sim 2dD \cdot n \quad (8.15)$$

(normal diffusion). As we will see, it may well be the case that D either vanish or diverge (anomalous diffusion).

Such an approach, involving a generalized transfer operator to get the asymptotic behavior of the generating function has been proposed in [26, 34]. Of course, since the asymptotic behavior of the whole generating function is dominated by the leading eigenvalue of the transfer operator, we may generalize (8.14) to yield expressions of higher moments (or cumulants) of the diffusing variable. We will return to this point, but firstly we turn our attention to the way in which the leading eigenvalue $\lambda_0(\beta)$ may be actually computed.

8.3

The Periodic Orbits Approach

The leading eigenvalue $\lambda_0(\beta)$ is the inverse of the smallest $z(\beta)$ solving the secular equation

$$\det(1 - z(\beta)\mathcal{L}_\beta) = 0, \quad (8.16)$$

which, by using the identity $\ln \det(1 - \mathbb{A}) = -\sum m^{-1} \text{tr} \mathbb{A}^m$, may be rewritten as (dependence upon β of z will be implicit in the following)

$$\exp - \sum_{k=1}^{\infty} \frac{z^k}{k} \text{tr} \mathcal{L}_\beta^k = 0. \quad (8.17)$$

Periodic orbits come into play as soon as we evaluate traces and use elementary properties of Dirac's δ : as a matter of fact

$$\begin{aligned} \text{tr} \mathcal{L}_\beta^k &= \int_0^1 dx \mathcal{L}_\beta^k(x, x) \\ &= \sum_{y|\hat{f}^k(y)=y} \frac{e^{\beta n_{(k),y}}}{|1 - \Lambda_{(k),y}|}, \end{aligned} \quad (8.18)$$

which is a sum over periodic points: the weights that are picked up for each of them are the instability

$$\Lambda_{(k),z} = \frac{d\hat{f}^k}{dz}(z) = \prod_{m=0}^{k-1} \hat{f}'(\hat{f}^m(z)) \quad (8.19)$$

and the jumping number of the orbit once unfolded on the real line

$$n_{(k),z} : \hat{f}^k(z) = z + n_{(k),z}. \quad (8.20)$$

Note that both n and Λ will be the same for each point of a given periodic orbit. At each order k (8.18) picks up contributions both from orbits of "prime period" k , and as well from orbits of smaller periods s such that s divides k (in particular fixed points contribute to all orders). Now suppose z is a point of a periodic orbit of prime period s and $k = s \cdot m$, then we have $n_{(k),z} = m \cdot n_{(s),z}$ and $\Lambda_{(k),z} = \Lambda_{(s),z}^m$ thus the only independent quantities entering the former expressions are stabilities and jumping numbers of prime cycles. We now impose the requirement that f is a chaotic map, in the form of a hyperbolicity assumption, that in one dimension simply reads

$$|\hat{f}'(x)| > 1 \quad \forall x \in [0, 1]. \quad (8.21)$$

Typically this property will generate normal transport properties: in Section 8.5 we will see how violation of such an inequality even at a single point will

dramatically modify transport features.² If (8.21) holds than the denominator in (8.18) may always be expanded as a geometric series and we may write

$$\sum_{k=1}^{\infty} \frac{z^k}{k} \sum_{z|f^k(z)=z} \frac{e^{\beta n_{(k),z}}}{|1 - \Lambda_{(k),z}|} = \sum_{\{p\}} \sum_{j=0}^{\infty} \sum_{r=1}^{\infty} \frac{n_p z^{n_p \cdot r}}{n_p \cdot r} \frac{e^{\beta r \sigma_p}}{|\Lambda_p|^r |\Lambda_p^j|^r}, \quad (8.22)$$

where $\sigma_p = n_{(n_p),z_p}$ (z_p being any point of the periodic orbit labeled by p) and, analogously, $\Lambda_p = \Lambda_{(n_p),z_p}$. In Eq. (8.22) $\{p\}$ indicates a sum over all “prime periodic orbits” (of prime period n_p), j is the geometric series index coming from expanding the denominators, while r counts repetitions of prime cycles (as in the original sum each p cycle appears at every $r \cdot n_p$ order). Now we may sum up the r (logarithmic) series, thus getting

$$\det(1 - z\mathcal{L}_\beta) = \exp \sum_{\{p\}} \sum_{j=0}^{\infty} \ln \left(1 - z^{n_p} \frac{e^{\beta \cdot \sigma_p}}{|\Lambda_p| \Lambda_p^j} \right) = \prod_{j=0}^{\infty} \zeta_{\beta,(j)}^{-1}(z), \quad (8.23)$$

where *dynamical zeta functions* are thus defined as

$$\zeta_{\beta,(j)}^{-1}(z) = \prod_{\{p\}} \left(1 - z^{n_p} \frac{e^{\beta \cdot \sigma_p}}{|\Lambda_p| \Lambda_p^j} \right), \quad (8.24)$$

while their infinite product is usually called the spectral determinant

$$F_\beta(z) = \prod_{j=0}^{\infty} \zeta_{\beta,(j)}^{-1}(z) = \det(1 - z\mathcal{L}_\beta). \quad (8.25)$$

When j increases, the coefficients of z^{n_p} in (8.23) become smaller and smaller: this suggests that $z(\beta)$ is a zero of the lowest order zeta function (8.24)

$$\zeta_{\beta,(0)}^{-1}(z) = \prod_{\{p\}} \left(1 - z^{n_p} \frac{e^{\beta \cdot \sigma_p}}{|\Lambda_p|} \right). \quad (8.26)$$

This is checked in exactly solvable models [23], and, under suitable hypotheses, may be proved for particular classes of dynamical systems.

Cycle expansions [21–23] consist in expanding (8.26) into a power series

$$\zeta_{\beta,(0)}^{-1}(z) = 1 - \sum_{m=1}^{\infty} \gamma_m(\beta) z^m. \quad (8.27)$$

2) We remark that while chaos is an efficient randomizing mechanism to induce stochasticity, highly nontrivial transport properties may also appear in systems that lack exponential sensitivity upon initial conditions [35–39].

Finite l -order estimates (that require information coming from periodic orbits whose prime period does not exceed l) come from polynomial truncation of (8.27): this leads to a genuine perturbation scheme if we are able to control how finite order estimates converge to the asymptotic limit. From a mathematical point of view this amounts to investigate analytic properties of dynamical zeta functions, typically by finding a domain in which they are meromorphic: specific examples and heuristic arguments are provided in [23], while a guide to the relevant mathematical literature may be found in [40, 41]. In practice, detailed knowledge on the topology of the system allows one to write the dynamical zeta function (8.26) in such a way that the role of *fundamental cycles* is highlighted :

$$\zeta_{\beta,(0)}^{-1}(z) = 1 - \sum_f \hat{t}_f + \sum_n \hat{c}_n, \quad (8.28)$$

where we have incorporated z in the definition of cycle weights \hat{t} , and we factored away the contribution of cycles which are not shadowed by combination of lower order orbits: in the case of a unrestricted grammar the fundamental cycles are just the contributions from the alphabet's letters [21, 23]. The simplest example comes a complete binary grammar, with alphabet $\{0, 1\}$:³ the expansion of the dynamical zeta function is

$$\begin{aligned} \zeta_{\beta,(0)}^{-1}(z) &= (1 - \hat{t}_0) \cdot (1 - \hat{t}_1) \cdot (1 - \hat{t}_{01}) \cdots \\ &= 1 - \hat{t}_0 - \hat{t}_1 - (\hat{t}_{01} - \hat{t}_0 \cdot \hat{t}_1) \cdots \end{aligned} \quad (8.29)$$

and the fundamental cycles are just the two fixed points, labeled by the alphabet's letter 0 and 1. The fundamental cycles thus provide the lowest order approximation in the perturbative scheme: a general chaotic systems is approximated at the lowest level with its simplest polygonalization, nonuniformity is incorporated perturbatively by considering curvature corrections (\hat{c}^n) of higher and higher order. The whole scheme relies on a symbolic encoding of the dynamics, and while we remark that finding a proper code for a given system is a highly nontrivial task in general, we have to emphasize that this cannot be considered as a shortcut on the theory proposed here, as the topological complexity cannot be eluded in any sensible treatment of general properties of chaotic systems.

To investigate the behavior of higher moments or to scrutinize thoroughly deviations from full hyperbolicity, we need to extend the former considerations in the following way: first we reorder the eigenvalues of the transfer

3) Such is the case for instance for the Bernoulli shift or the quadratic family at Ulam point.

operator so that the dominant ones come first and write in general

$$F_\beta(e^{-s}) = \prod_i (1 - \lambda_i e^{-s}) \quad (8.30)$$

so that

$$\frac{d}{ds} \ln F_\beta(e^{-s}) = \sum_i \frac{\lambda_i e^{-s}}{(1 - \lambda_i e^{-s})} \quad (8.31)$$

and if we now take the inverse Laplace transform, we get

$$\frac{1}{2\pi i} \int_{a-i\infty}^{a+i\infty} ds e^{sn} \frac{d}{ds} \ln [F_\beta(e^{-s})] = \sum_i \lambda_i^n \sim \mathcal{G}_n(\beta). \quad (8.32)$$

As the asymptotic behavior is dominated by the leading eigenvalue we may use the dynamical zeta function instead of the spectral determinant, thus

$$\lambda_0^n(\beta) \sim \frac{1}{2\pi i} \int_{a-i\infty}^{a+i\infty} ds e^{sn} \frac{d}{ds} \ln [\zeta_{\beta,(0)}^{-1}(e^{-s})]. \quad (8.33)$$

When $\beta = 0$, the transfer operator (8.8) coincides with the Perron–Frobenius operator [42] and so $\lambda_0(0) = 1$ (the corresponding eigenfunction being the density of the invariant measure). Even moments are given by Taylor expansion of $\mathcal{G}_n(\beta)$ around $\beta = 0$ (when (8.1) is satisfied odd moments vanish):

$$\begin{aligned} M_k(n) &= \langle (x_n - x_0)^k \rangle_0 = \left. \frac{\partial^k}{\partial \beta^k} G_n(\beta) \right|_{\beta=0} \\ &\sim \left. \frac{\partial^k}{\partial \beta^k} \frac{1}{2\pi i} \int_{a-i\infty}^{a+i\infty} ds e^{sn} \frac{d}{ds} \ln [\zeta_{\beta,(0)}^{-1}(e^{-s})] \right|_{\beta=0} \end{aligned} \quad (8.34)$$

and in particular we may rewrite (8.14) as

$$D = \lim_{n \rightarrow \infty} \frac{d^2}{d\beta^2} \left(\frac{1}{2\pi i} \int_{a-i\infty}^{a+i\infty} ds e^{st} \frac{\partial_s \zeta_{\beta,(0)}^{-1}(e^{-s})}{\zeta_{\beta,(0)}^{-1}(e^{-s})} \right)_{\beta=0}. \quad (8.35)$$

High-order derivatives in the argument of the inverse Laplace transform are then evaluated by making use of Faà di Bruno formula:

$$\frac{d^n}{dt^n} H(L(t)) = \sum_{k=1}^n \sum_{k_1, \dots, k_n} \frac{n!}{k_1! \dots k_n!} \frac{d^k H}{dL^k}(L(t)) \cdot B_{\vec{k}}(L(t)) \quad (8.36)$$

$$B_{\vec{k}}(L(t)) = \left(\frac{1}{1!} \frac{dL}{dt} \right)^{k_1} \cdots \left(\frac{1}{n!} \frac{d^n L}{dt^n} \right)^{k_n} \quad (8.37)$$

$$\vec{k} = \{k_1, \dots, k_n\} \text{ with } \sum k_i = k, \quad \sum i \cdot k_i = n \quad (8.38)$$

In view of formulas like (8.35) or (8.34) transport properties are deduced from dynamical zeta functions, which organize knowledge about the system as encoded in the set of periodic orbits. These relationships provide information both on prefactors (8.35) and on asymptotic growth (8.34): the latter feature is particularly relevant if we are facing the problem of anomalous diffusion, as in this case the important piece of information concerns the *spectrum* $\nu(q)$, determining the asymptotic behavior of q -order moments

$$M_q(n) \sim n^{\nu(q)}. \quad (8.39)$$

Gaussian (normal) transport is described by a single-scale spectrum $\nu(q) = q/2$, while anomalous transport typically shows a nontrivial behavior, which cannot be encoded by a single exponent, but rather typically exhibits a phase transition [43–47].

We notice a remarkable feature of the formula (8.35): it leads to a normal diffusing behavior from a balance between *localized* orbits (those with $\sigma_p = 0$), and *ballistic* orbits (with $\sigma_p \neq 0$): such a balance was also considered in early efforts to explain diffusive properties of sawtooth and cat maps via periodic orbits [48] (see [49] for treatment of the problem according to the present technique).

8.4

One-Dimensional Transport: Kneading Determinant

While in the case of anomalous transport the interest is typically concentrated in understanding the time asymptotic behavior, in normal transport the attention is focused on the prefactor of the second moment (the diffusion coefficient), that carries the crucial information of the process.

If we are interested in using periodic orbit theory for a *precision* calculation of the diffusion coefficient, we will eventually have to face the problem of the full understanding of cycle organization. A good control of the periodic orbit organization is thus necessary if we want to proceed via cycle expansion techniques. In fact, the success of the zeta function approach strongly relies on the ability of the *user* to control the (typically exponential) proliferation of periodic orbits. In particular, the cycle expansion technique guarantees nice convergence properties of the zeta functions once we have identified the set of periodic orbits that build the *fundamental* and *curvature terms* (8.28) [21, 23]. This, in turn, implies a complete understanding of the underlying symbolic dynamic. Unfortunately such a control is rather exceptional and many interesting examples present extreme complexity in orbit coding and control over finite order estimates becomes problematic. As a paradigmatic example, we will consider a simple one-dimensional map of the real line that deterministically generates normal diffusion with a diffusion coefficient that sensitively

depends on the control parameter that define the map [50, 51]. In particular, the cycles organization change discontinuously under parameters variation, thus invalidating any meaningful attempt to directly use periodic orbit theory. This example is used to show how it is possible to build (at least in the one-dimensional case) the *dynamical zeta function* without any need of periodic orbits, using the kneading trajectories of the systems. The kneading trajectories naturally order the admissible symbolic sequences of the systems and thus incorporate all the information needed to generate grammar rules. It seems thus natural to try to directly use these trajectories into an expression closely related to dynamical zeta functions. In fact Milnor and Thurston [52] were able to relate the topological entropy to the determinant of a finite matrix (the kneading determinant) where the entries are formal power series (with coefficients determined by the kneading trajectories). Later Baladi and Ruelle [53] have generalized the result, incorporating a constant weight (see also [54, 55] and references therein for more general results). We will use this extension to derive an explicit expression of the diffusion coefficient in the full parameter range [56].

Let us start by introducing the reference dynamical system [50]: for $\Lambda \geq 2$ let us define the map $g_\Lambda : \mathbb{R} \rightarrow \mathbb{R}$:

$$g_\Lambda(x) = \frac{1}{2} + \Lambda \left(x - \frac{1}{2} \right) \quad x \in [0, 1] \quad (8.40)$$

and extending it on the real line by the symmetry property (8.2). Let $\hat{g}_\Lambda(x) : [0, 1] \rightarrow [0, 1]$ be the circle map corresponding to g_Λ :

$$\hat{g}_\Lambda(x) = g_\Lambda(x)|_{\text{mod } 1}. \quad (8.41)$$

For integer values of the slope Λ dynamical zeta functions may be written down explicitly and the diffusion coefficient D is easily computed from the smallest zero [23, 34, 57–59]:

$$D = \frac{(\Lambda - 1)(2\Lambda - 1 - 3(-1)^\Lambda)}{48}. \quad (8.42)$$

For a generic value of the control parameter the situation is more involved: typically there is an infinite set of pruning rules that do not allow to write down the exact dynamical zeta function. Following the notation of Baladi and Ruelle, we define $\epsilon(x) = \pm 1$, whether $f(x)$ is increasing or decreasing and $t(x)$ as a constant weight for $x \in [a_{i-1}, a_i]$, where $a_0 < a_1 < \dots < a_N$ are the ordered sequence of end points of each branch (see Figure 8.1). The restriction of these functions on the i -interval will take the constant values:

$$\epsilon_i = 1 \quad (8.43)$$

$$t_i = \frac{z e^{\beta \sigma_i}}{\Lambda}, \quad (8.44)$$

where σ_i is the jumping number associated to the i th branch.

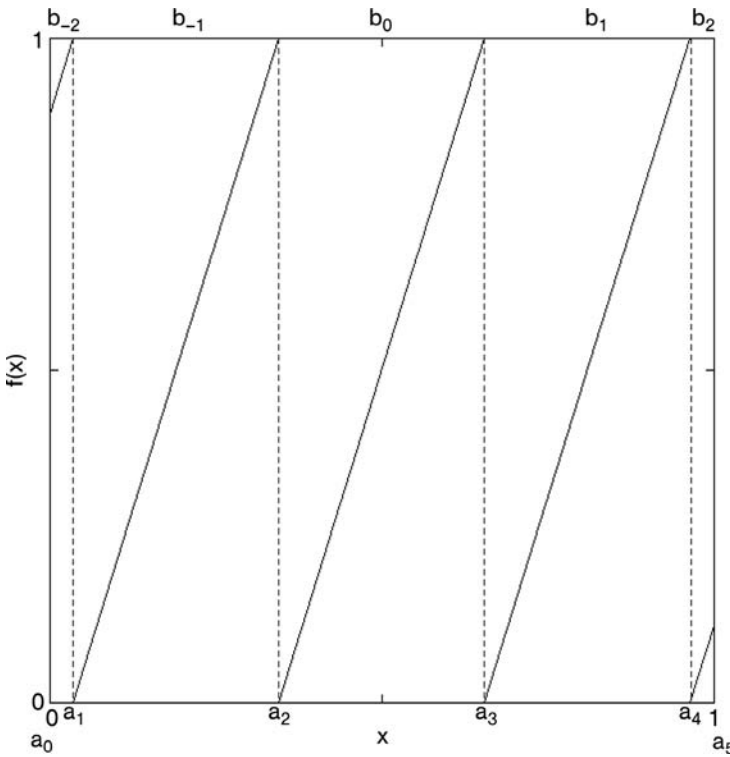


Figure 8.1 The map $\hat{g}_\Lambda(x)$ with $\Lambda = 3.23$.

We associate to each point x the address vector in \mathbb{Z}^{N-1}

$$\vec{\alpha}(x) = [\operatorname{sgn}(x - a_1), \dots, \operatorname{sgn}(x - a_{N-1})] \quad (8.45)$$

and we define the invariant coordinate of x by the formal series

$$\vec{\theta}(x) = \sum_{n=0}^{\infty} \left[\prod_{k=0}^{n-1} (\epsilon t)(\hat{g}_\Lambda^k(x)) \right] \vec{\alpha}(\hat{g}_\Lambda^n(x)) \quad (8.46)$$

with the convention that the product is equal to 1 if $n = 0$ (the invariant coordinate θ is single valued once we put $\epsilon(a_i) = 0$).

Defining $\phi(a^\pm) = \lim_{x \rightarrow a^\pm} \phi(x)$, we compute the discontinuity vector at the critical points a_i for $i = 1, \dots, N-1$:

$$\vec{K}_i(z, \beta) = \frac{1}{2} \left[\vec{\theta}(a_i^+) - \vec{\theta}(a_i^-) \right]. \quad (8.47)$$

The kneading matrix $K(z, \beta)$ is defined as the $(N-1) \times (N-1)$ matrix with \vec{K}_i ; $i = 1, \dots, N-1$ as rows. Let us call $\Delta(z, \beta) = \det K(z, \beta)$ the kneading determinant. It is possible to show that in our case the dynamical zeta function

is equal to the kneading determinant up to a rational function (see [53] for more general results and a proof of relation (8.48)). In particular, if we denote $\{\tilde{p}\}$ the set of prime periodic orbits that include a critical point (i.e., $\hat{g}_\Lambda^{\eta_{\tilde{p}}}(a_i) = a_i$), we have

$$\Delta(z, \beta) = R(z, \beta) \zeta_{\beta, (0)}^{-1}(z) \quad (8.48)$$

$$R(z, \beta) = \left[1 - \frac{1}{2}(\epsilon_1 t_1 + \epsilon_N t_N) \right] \prod_{\{\tilde{p}\}} [1 - t_{\tilde{p}}(z, \beta)]^{-1}. \quad (8.49)$$

Equation (8.48) explicitly relates a quantity build upon periodic orbit of system (the dynamical zeta function) with a quantity build from the iterate of kneading trajectories (the kneading determinant). It is simple to show that in our case the kneading determinant can be explicitly written in terms of the trajectory of the pair of critical points a_0 and a_N :

$$\Delta(z, \beta) = 1 + \frac{z}{2\Lambda} \sum_{i=1}^{N-1} e^{\beta(\sigma_i + 1/2)} \left[e^{\frac{\beta}{2}} \vec{\theta}(a_0^+) - e^{-\frac{\beta}{2}} \vec{\theta}(a_N^-) \right]_i. \quad (8.50)$$

Moreover, we can see from formula (8.48) that the smallest zero of the kneading determinant coincides with the smallest zero of the dynamical zeta function for $\beta \rightarrow 0$ and then we can derive, via the implicit function theorem, the diffusion coefficient as

$$D = -\frac{1}{2} \left(\frac{\partial^2 \Delta(z, \beta)}{\partial \beta^2} / \frac{\partial \Delta(z, \beta)}{\partial z} \right) \Big|_{z=1, \beta=0}. \quad (8.51)$$

By using (8.50) it is in principle possible to explicitly write a (lengthy) expression for the diffusion coefficient in terms of the kneading trajectory (see [56] for details). The evaluation of (8.51) for a parameter choice $\Lambda \in [2, 3]$ is shown in Figure 8.2 and can be compared, for example, with Figure 10 in [50].

Though elegant, such a technique is essentially confined to the $1d$ setting: the difficulties of computing D via (8.35) in higher dimensions is made clear by attempts to get accurate estimates for the case of the Lorentz gas with finite horizon [60–62].

8.5

An Anomalous Example

In many situations the dynamics of a system is far from being completely hyperbolic. Quite often accessible regions of phase space behave quasiregularly and strongly influence the overall properties of the system: trajectories tend to

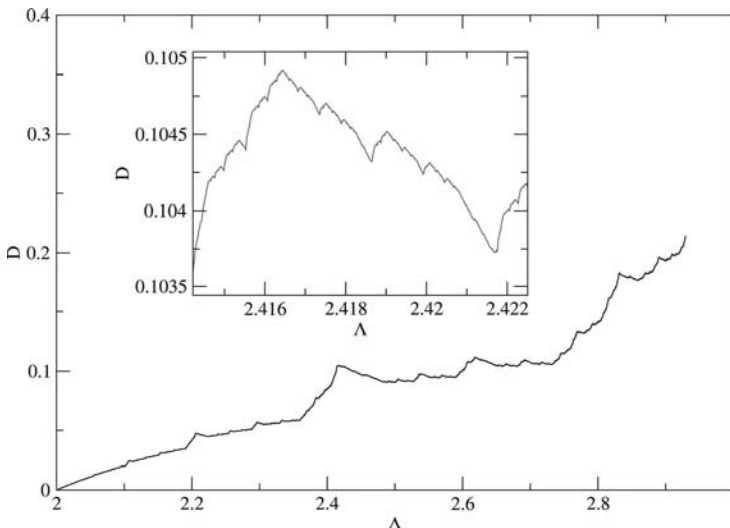


Figure 8.2 Fractal diffusion coefficient as a function of the slope of the map $\hat{g}_\Lambda(x)$ computed from the smallest zero of the dynamical zeta function. The insert is a blow up of a part of the main figure.

stick close to regular regions, slowly moving away from it. Chaotic wandering is then interrupted by long segments of quasiregular motion (see Figure 8.3 for an example in one dimension). This peculiar aspect of the dynamic can modify important quantities like decay of correlation or return time statistics, that typically show a power-law decay. In particular, stickiness of trajectories can induce anomalous diffusion in open systems. In the last few years it has been realized [16, 63–69] that power-law separation of nearby trajectories in weakly chaotic systems (in particular one-dimensional intermittent maps, or infinite horizon Lorentz gas models) deeply modify the analytic properties of zeta functions, which typically exhibit branch points. The modified analytic structure of the zeta function may induce anomalous behavior (nonlinear diffusion [23, 70]): in the thermodynamic language this would correspond to critical behavior, with a gapless transfer operator slowing down correlations decay. While the detailed understanding of the mechanism for stickiness in generic Hamiltonian systems is still an open problem [71–74], it is fruitful to investigate a simpler case, where the analysis can be performed in a detailed way: a one-dimensional map with a marginal fixed point.

The map on the fundamental cell is implicitly defined on $[-1, 1]$ in the following way [45]:

$$x = \begin{cases} \frac{1}{2\gamma} \left(1 + \hat{f}(x)\right)^\gamma & 0 < x < 1/(2\gamma) \\ \hat{f}(x) + \frac{1}{2\gamma} \left(1 - \hat{f}(x)\right)^\gamma & 1/(2\gamma) < x < 1 \end{cases} \quad (8.52)$$

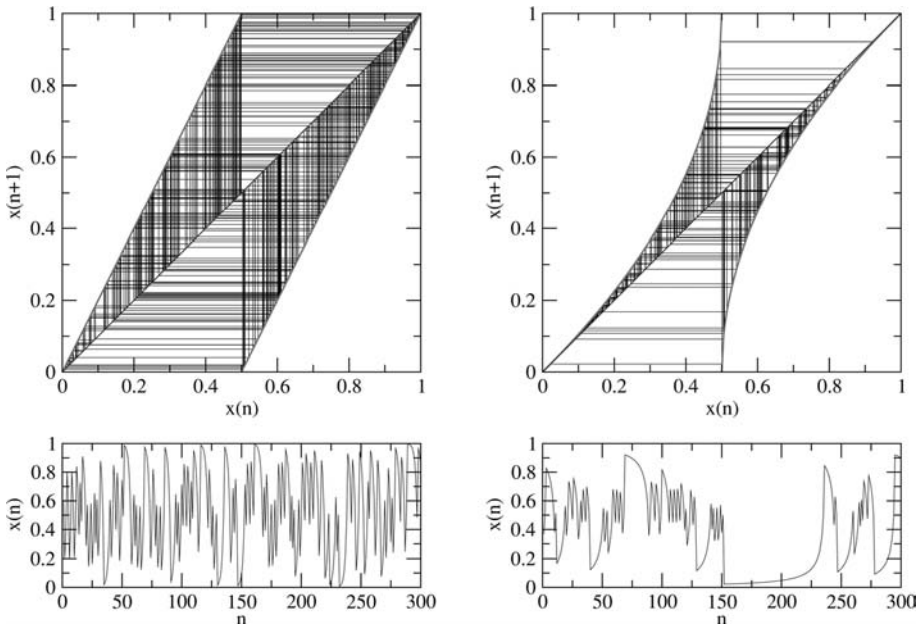


Figure 8.3 A segment of trajectory (300 iterations) with the same initial condition is showed for two torus maps: a completely hyperbolic map (left) and one with intermittent fixed points (right).

for negative values of x the map is defined as $\hat{f}(-x) = -\hat{f}(x)$ (thus satisfying the symmetry requirement (8.1)): the map is plotted in Figure 8.4. The map lacks full hyperbolicity due to the presence of two marginal fixed points (at $x = \pm 1$), where the slope is exactly one. The lift of the map on the real line is defined once we assign jumping numbers $\sigma_L = -1$ to the left branch and $\sigma_R = +1$ to the right branch: whenever a particle remains trapped near a marginal point the corresponding unfolded trajectory on the real line consists of successive jumps to the neighboring cell. Symmetry requirement (8.2) is assumed, so the map is thus extended on the full real line.

The presence of complete branches leads to an unrestricted grammar in the symbolic code $\{L, R\}$, where the corresponding partition obviously consist of $L = [-1, 0]$ and $R = [0, 1]$. However, the presence of the marginal fixed points (\bar{L}, \bar{R}) causes problems in using zeta function techniques: these fixed points have $|\Lambda| = 1$, and cannot be included in any trace formula like (8.18), as they would lead to divergences. In this case we are forced to prune away the (\bar{L}, \bar{R}) fixed points thus moving to a new *countable* infinite alphabet with unrestricted grammar:

$$\{L^j R, R^k L\} \quad j, k \in \mathbb{N}_+ . \quad (8.53)$$

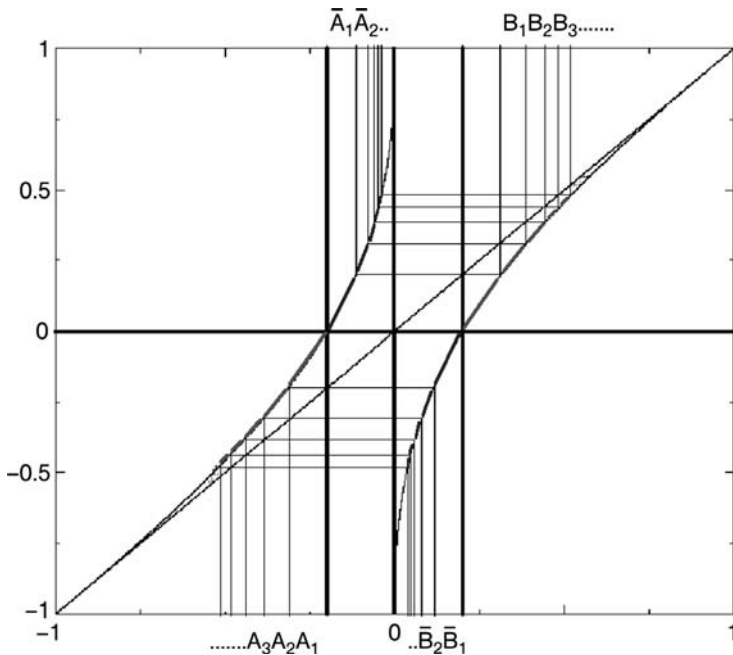


Figure 8.4 Linearization of the map (8.52). Near marginal points, laminar regions, a Gaspard–Wang type partition is used while a finer one is used in the injection zone.

In this new alphabet all $L^n R$ ($R^n L$) cycles lack curvature counterterms (they are not shadowed by any combination of shorter cycles (8.28) and (8.29), due to the lack of the symbols L and R alone) and the fundamental cycle part of the zeta function thus becomes

$$\zeta_{\text{fund}}^{-1}(z) = 1 - t_R - t_{LR} - t_{L^2R} - \cdots - t_{L^nR} - \cdots + (R \rightarrow L), \quad (8.54)$$

where again t indicates the appropriate weight. It is clear that, in contrast with the *normal* example, we do not have a finite order polynomial and the analytic structure of (8.54) will be strongly dependent on the intermittency exponent γ . In order to proceed we need to compute the instabilities and jumping number of the cycles $L^n R$ ($R^n L$) that come closer and closer to the marginal points. Firstly, we note that the slope of the map in the chaotic region is not bounded from above. This feature is intimately connected to the peculiar ergodic properties of the map: it has a *constant* invariant measure [45] for *any* values of γ as is easily seen from the summation property

$$\sum_{y=\hat{f}^{-1}(x)} \frac{1}{\hat{f}'(y)} = 1 \quad (8.55)$$

that follows directly from the expressions (8.52). In this sense the behavior of (8.52) is similar to what happens in an area preserving map example [73], where a parabolic fixed point coexists with a Lebesgue invariant measure, and is quite different from the usual Pomeau–Manneville [75, 76] case, where the torus map has nontrivial ergodic properties: an absolutely continuous invariant measure only exists for $\alpha = 1/(\gamma - 1) > 1$ (see for instance [77] and references therein) while the ergodic behavior is much more complex when $\alpha < 1$; in any case sticking induces peaking of the measure around marginal fixed points (see [78, 79]).

In order to use the peculiarities of the map into the derivation of the instabilities, we can start by identifying for each branch a laminar and an injection regions (for example we call $\bar{B} = [0, 1/(2\gamma)]$ and $B = [1/(2\gamma), 1]$, respectively, the injection and laminar regions of the right branch (see Figure 8.4): \bar{A} and A will denote the symmetric regions in the left subinterval.

Now we refine partitions in the following way: if f_R and f_L denote the right and left branches of the map we set $B_i = f_R^{-i}(\bar{B})$ and $A_i = f_L^{-i}(\bar{A})$: we then refine the turbulent sets by $\bar{A}_i = f_L^{-1}(B_i)$ and $\bar{B}_j = f_R^{-1}(A_j)$. Now in each laminar set the map is linearized according to Gaspard–Wang approximation [78, 79]: linearization in the turbulent sets $\{\bar{A}_i, \bar{B}_j\}$ is then constructed in such a way to preserve the summation property (8.55)

$$\Lambda_{\bar{B}_i}^{-1} = 1 - \Lambda_{A_i}^{-1}. \quad (8.56)$$

The width of the sets A_j is easily seen to shrink with a power law in j :

$$A_k \sim \frac{C}{k^{\alpha+1}}, \quad (8.57)$$

where again $\alpha = 1/(\gamma - 1)$. By using (8.57) and (8.56) we get an estimate of periodic orbits instabilities:

$$\begin{aligned} \Lambda_{A^k B} &= \left[\frac{A_0}{A_1} \frac{A_1}{A_2} \cdots \frac{A_{k-1}}{A_k} \right] \left[1 - \frac{A_k}{A_{k-1}} \right]^{-1} \left[1 - \frac{A_1}{A_0} \right]^{-1} \\ &\sim k^{\alpha+2} \end{aligned} \quad (8.58)$$

This agrees with numerical simulations for the nonlinearized map (see Figure 8.5).

Note that with this partition it is possible to estimate the behavior of the instabilities of all orbits, not only the one accumulating to the marginal point [80]. Once we notice that, for the cycles dominating the zeta function expression, the jumping number is given by the length of the periodic orbit (with the appropriate sign), the dynamical zeta function is (for the linearized map, where curvature corrections vanish):

$$\zeta_{\beta,(0)}^{-1}(z) = 1 - \zeta(\alpha + 2)z \sum_{k=1}^{\infty} \frac{z^k}{k^{\alpha+2}} \cosh(\beta k). \quad (8.59)$$

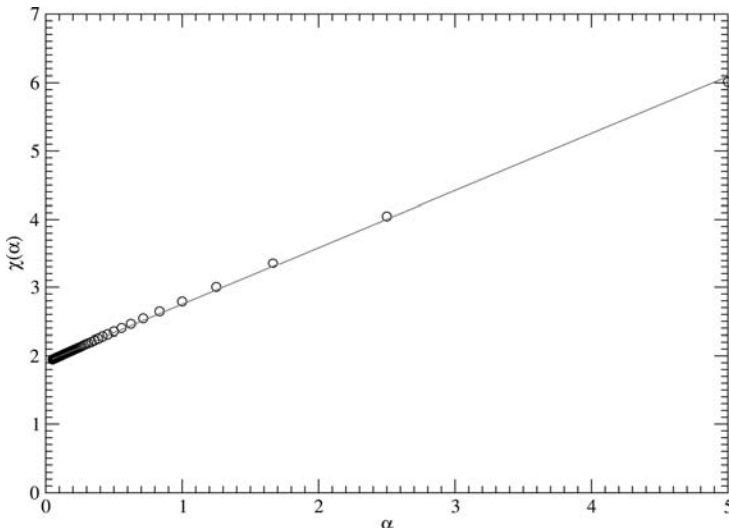


Figure 8.5 The exponent $\chi(\alpha)$ of power-law decay of instabilities $\Lambda_{A^k B} \sim k^{\chi(\alpha)}$ as a function of the parameter α (open circles) and the best fit $\chi(\alpha) = (0.88\alpha + 1.9)$ (full line).

To estimate the asymptotic behavior of the generating function (8.34), we need to single out the leading singularity in the logarithmic derivative of the zeta function. The divergences for $z \rightarrow 1$ in derivatives expansions (8.36) depend on the appearance of the Bose function

$$g_\mu(z) = \sum_{l=1}^{\infty} \frac{z^l}{l^\mu} \quad (8.60)$$

that indeed may alter the analytic features. This function appears as a consequence of the particular sequences of orbits whose stability increases only polynomially with the period (8.58), a signature of nonhyperbolic behavior [23, 78, 79]. We recall how Bose functions behave as $z \rightarrow 1^-$: the result depends upon μ (related to the intermittency exponent)

$$g_\mu(z) \sim \begin{cases} (1-z)^{\mu-1} & \mu < 1 \\ \ln(1-z) & \mu = 1 \\ \zeta(\mu) + C_\mu(1-z)^{\mu-1} + D_\mu(1-z) & \mu \in (1, 2) \\ \zeta(2) + C_2(1-z)\ln(1-z) & \mu = 2 \\ \zeta(\mu) + C_\mu(1-z) & \mu > 2 \end{cases} \quad (8.61)$$

Now look at a generic term in Faà di Bruno expansion of the factor

$$\left. \frac{\partial^n}{\partial \beta^n} \ln \zeta_{\beta, (0)}^{-1}(z) \right|_{\beta=0} \quad (8.62)$$

in (8.34) and denote it by $\mathcal{D}_{k_1 \dots k_n}$. Taking into account that

$$\frac{\partial^i}{\partial \beta^i} \zeta_{\beta, (0)}^{-1}(z) \Big|_{\beta=0} \sim \begin{cases} 0 & i \text{ odd} \\ z g_{\alpha+2-i}(z) & i \text{ even} \end{cases} \quad (8.63)$$

we have that

$$\mathcal{D}_{k_1 \dots k_n} \sim \frac{1}{(\zeta_{0, (0)}^{-1}(z))^k} \prod_j (g_{\alpha+2-j}(z))^{k_j} = \frac{\mathcal{D}_{k_1 \dots k_n}^+}{\mathcal{D}_{k_1 \dots k_n}^-}, \quad (8.64)$$

where the \mathcal{D}^+ pick up the contributions from the product of Bose functions, and all j must be even, due to (8.63).

Since the dynamical zeta function has a simple zero we get

$$\mathcal{D}_{k_1 \dots k_n}^- \sim (1-z)^k, \quad (8.65)$$

while the terms appearing in \mathcal{D}^+ modify the singular behavior near $z = 1$ only for sufficiently high j

$$g_{\alpha-j}(z) \sim \begin{cases} (1-z)^{\alpha+1-j} & j > \alpha \\ \zeta(\alpha+2-j) & j < \alpha \end{cases} \quad (8.66)$$

If all $\{j\}$ are less than α then the singularity is determined by \mathcal{D}^- : keeping in mind that the highest k value is achieved by choosing $j = 2$ and $k_2 = n/2$, we get

$$\nu(q) = \frac{q}{2} \quad q < \alpha. \quad (8.67)$$

When q exceeds α we have to take into account possible additional singularities in \mathcal{D}^+ , and thus we get

$$\rho = \sup_{\{k_1 \dots k_n\}} (k + \sum_{j>\alpha} (j - \alpha) k_j) = \begin{cases} n/2 & n < 2\alpha \\ n + 1 - \alpha & n > 2\alpha \end{cases} \quad (8.68)$$

which, once we take (8.67) into account, yields the full spectrum of transport moments

$$\nu(q) = \begin{cases} q/2 & q < 2\alpha \\ q + 1 - \alpha & q > 2\alpha \end{cases} \quad (8.69)$$

which may also be checked numerically for the full map (see Figure 8.6).

The non trivial structure of the spectrum, which presents a sort of phase transition for $q = 2\alpha$, is a common feature of many systems with anomalous transport properties [43, 46, 47]. In this example we showed how [44] the essential ingredient in the analysis of weakly chaotic systems seems to

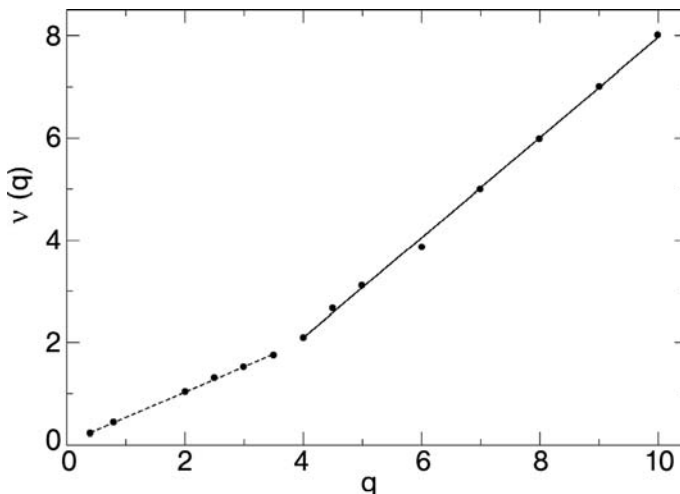


Figure 8.6 Spectrum of the transport moments for the map (8.52) with $\gamma = 1.5$: the best fit on numerical data is $\nu(q) = 0.50q + 0.04$ for the dotted line, and $\nu(q) = 0.98q - 1.82$ for the full line.

be a proper characterization of a particular sequence of periodic orbits: those probing closer and closer dynamical features of the marginal structures: the parameter ruling the presence of a phase transition (and the explicit form of the spectrum) is α , that is the exponent describing the polynomial instability growth of the family of periodic orbits coming closer and closer to the marginal fixed point, and thus describing the sticking to the regular part of the phase space. In this way, differently from prefactors, which depend critically on the fine structure of the map, the spectrum $\nu(q)$ is fully determined by a local analysis near the marginal fixed points, and this corroborates the idea that a single exponent determines the universality class of the system as regards the transport moments. Again if we try to evaluate prefactors in this context, fine details of the full dynamics are needed as shown in [81].

8.6 Probabilistic Approximations

While the approach we described is purely deterministic (and in particular cases can be rigorously justified, even for intermittent systems [68, 69]), we briefly describe now how probabilistic methods may also be employed.

The main point in this class of probabilistic approaches is to suppose that any orbit might be partitioned according to a sequence of times $t_1 < t_2 < \dots < t_n < \dots$ such that the time laps $\Delta_j = t_j - t_{j-1}$ form a sequence of random variables with common distribution $\psi(\Delta) d\Delta$ and the orbit properties

before and after t_n are independent of n . A typical choice for $\{t_j\}$ in the case of intermittent maps consists in collecting the reinjection times in the laminar region: the second property mentioned above is thus related to the “randomization” operated by the chaotic phase. From the stochastic processes point of view this amounts to employ renewal theory [82] to describe the dynamics of the system.

We now illustrate how an approximate form of the distribution $\psi(T)$ may be obtained in the case of Pomeau–Manneville map [11]

$$x_{n+1} = x_n + x_n^z \bmod 1. \quad (8.70)$$

The map consists of two full branches, with support on $[0, p)$ (I_0 the laminar region) and $[p, 1]$ (I_1 the chaotic region), where $p + p^z = 1$. In a continuous time approximation [83, 84], (8.70) is turned into the differential equation

$$\dot{x}_t = x_t^z \quad (8.71)$$

whose solution we write as

$$x_t = \left[\frac{1}{x_0^{z-1}} - (z-1)t \right]^{-\frac{1}{z-1}}. \quad (8.72)$$

From (8.72), we can obtain the exit time $T(x_0)$ for each $x_0 \in I_0$, as x_t will exit I_0 as soon as $x_t \geq p$:

$$T(x_0) = \frac{1}{z-1} \left[\frac{1}{x_0^{z-1}} - \frac{1}{p^{z-1}} \right].$$

Now

$$\psi(T) = \int_0^p dx P(x, T - T(x)), \quad (8.73)$$

where $P(x, t)$ is the probability of being injected at time t from I_1 to $x_0 \in I_0$ (we partition the time sequence so that t_j is the entrance time in the chaotic region). In the limit of large T , the dominant contribution to (8.73) comes from

$$\psi(T) \propto \left| \frac{dx_0(T)}{dT} \right|$$

if we suppose that the reinjection probability is smooth and chaotic residence times vanish sufficiently fast. Within this approximation, we thus get

$$\psi(T) \propto \left((z-1)T + \frac{1}{p^{z-1}} \right)^{-\frac{z}{z-1}} \quad T \gg 0$$

so that

$$\psi(T) \sim \frac{1}{T^{\frac{z}{z-1}}}$$

for large values of T .

From the distribution $\psi(T)$, we can get information about correlation functions: suppose we consider an observable A that may change only during transitions between neighboring time lapses: its autocorrelation function may be written as the time average

$$C_{AA}(t) = \langle A(t_0 + t)A(t_0) \rangle_{t_0} - \langle A \rangle^2. \quad (8.74)$$

Our probabilistic assumption amounts to disregard correlations if t_0 and $t + t_0$ belong to different intervals (yielding a contribution $\langle A \rangle^2$ to $C_{AA}(t)$, while if t_0 and $t + t_0$ belong to the same interval correlation in complete (and the corresponding contribution is $\langle A^2 \rangle$). So, if we denote by $\Phi(t)$ the probability that no lapse transition has occurred between t_0 and $t + t_0$, we easily rewrite the correlation function as

$$C_{AA}(t) = (\langle A^2 \rangle - \langle A \rangle^2) \Phi(t). \quad (8.75)$$

But now Φ may be written in terms of the distribution function as

$$\Phi(t) = \frac{1}{\langle \Delta \rangle} \int_t^\infty du \int_u^\infty d\Delta \psi(\Delta). \quad (8.76)$$

Once we control correlations, the behavior of the second moment, via Green–Kubo formulas [11], is easily found, and the results agree with our deterministic approach (see also [43]).⁴ This approach has been reformulated in a clean way in [85, 86], and its virtues and shortcuts have been scrutinized, in the case of the Lorentz gas with infinite horizon, in [16].

8.7 Conclusions

We have presented the essential features of a theory of deterministic transport (for systems enjoying space periodicity) based upon periodic orbit theory. This technique, besides being crisply deterministic, presents a number of appealing features: It is invariant under smooth conjugacies of the dynamical

4) Of course the original Pomeau–Manneville map is defined on the unit torus, so no transport properties can be established for it: the actual model one considers is a lift on the real line, where the marginal fixed point actually unfolds to a ballistic point (i.e., the laminar branch has a nonzero jumping number).

system and it offers a way to present in a hierarchical way the problem, in cases where typically a perturbative parameter does not exist. It also presents subtle points: for instance the evaluation of the diffusion constant generically requires a considerable amount of control over fine details of the dynamics. The theory also allows to deal with anomalous transport: in particular moments of the diffusing variable may be investigated, and the corresponding spectrum $\nu(q)$ computed. The shape of such a spectrum is found to be determined by cycles probing closer and closer sticking regions: thus only *local* quantities enter the final results and this suggests interesting universal features of deterministic anomalous transport.

References

- 1** Chirikov, B. V., *Phys. Rep.* **52** (1979), p. 263
- 2** Cary, J. R., Meiss, J. D., *Phys. Rev. A* **24** (1981), p. 2664
- 3** Karney, C. F. F., *Physica D* **8** (1983), p. 360
- 4** Rechester, A. B., White, R. B., *Phys. Rev. Lett.* **44** (1980), p. 1586
- 5** Schell, M., Fraser, S., Kapral, R., *Phys. Rev. A* **26** (1982), p. 504
- 6** Geisel, T., Nierwetberg, J., *Phys. Lett.* **48** (1982), p. 7
- 7** Grossman, S., Fujisaka, H., *Phys. Rev. A* **26** (1982), p. 1779
- 8** Bunimovich, L. A., Sinai, Ya. G., *Commun. Math. Phys.* **78** (1981), p. 479
- 9** Bunimovich, L. A., Sinai, Ya. G., Chernov, N. I., *Russ. Math. Surv.* **46** (1991), p. 47
- 10** Geisel, T., Thomae, S., *Phys. Rev. Lett.* **52** (1984), p. 1936
- 11** Geisel, T., Nierwetberg, J., Zacherl, A., *Phys. Rev. Lett.* **54** (1985), p. 616
- 12** Ishizaki, R., Horita, T., Kobayashi, T., Mori, H., *Progr. Theor. Phys.* **85** (1991), p. 1013
- 13** Zaslavsky, G. M., Edelman, M., Niyazov, B. A., *Chaos* **7** (1997), p. 159
- 14** Bleher, P. M., *J. Stat. Phys.* **66** (1992), p. 315
- 15** Dahlqvist, P., *J. Stat. Phys.* **84** (1996), p. 773
- 16** Dahlqvist, P., Artuso, R., *Phys. Lett. A* **219** (1996), p. 212
- 17** Bouchaud, J.-P., Georges, A., *Phys. Rep.* **195** (1990), p. 127
- 18** Metzler, R., Klafter, J., *Phys. Rep.* **339** (2000), p. 1
- 19** Metzler, R., Klafter, J., *J. Phys. A* **37** (2004), p. R161
- 20** Cvitanović, P., *Phys. Rev. Lett.* **61** (1988), p. 2729
- 21** Artuso, R., Aurell, E., Cvitanović, P., *Nonlinearity* **3** (1990), p. 325
- 22** Artuso, R., Aurell, E., Cvitanović, P., *Nonlinearity* **3** (1990), p. 361
- 23** Cvitanović, P., Artuso, R., Mainieri, R., Tanner, G., Vattay, G., *Classical and Quantum Chaos*, www.chaosbook.org, Copenhagen 2006
- 24** Reimann, P., *Phys. Rep.* **361** (2002), p. 57
- 25** Artuso, R., Cavallasca, L., Cristadoro, G., *J. Phys. A* **39** (2006), p. 1285
- 26** Cvitanović, P., Eckmann, J.-P., Gaspard, P., *Chaos, Solitons Fractals* **6** (1995), p. 113
- 27** Cvitanović, P., Eckhardt, B., *Nonlinearity* **6** (1993), p. 277
- 28** Fichtner, A., Radons, G., *New J. Phys.* **7** (2005), p. 30
- 29** Sinai, Ya. G., *Theory Probab. Appl.* **27** (1982), p. 256
- 30** Golosov, A. O., *Commun. Math. Phys.* **92** (1984), p. 491
- 31** Ruelle, D., *Thermodynamics Formalism*, Addison-Wesley, New York, **1978**
- 32** Ruelle, D., *Invent. Math.* **34** (1976), p. 231
- 33** Baladi, V., *Positive Transfer Operators and Decay of Correlations*, World Scientific, Singapore, **2000**
- 34** Artuso, R., *Phys. Lett. A* **160** (1991), p. 528
- 35** Artuso, R., Guarneri, I., Rebuzzini, L., *Chaos* **10** (2000), p. 189

- 36** Alonso, D., Ruiz, A., de Vega, I., *Physica D* 187 (2004), p. 184
- 37** Jepps, O. G., Rondoni, L., *J. Phys. A* 39 (2006), p. 1311
- 38** Sanders, D. P., Larralde, H., *Phys. Rev. E* 73 (2006), p. 026205
- 39** Cecconi, F., del-Castillo-Negrete, D., Falconi, M., Vulpiani, A., *Physica D* 180 (2003), p. 129
- 40** Baladi, V., in *Proceedings of the NATO ASI Real and Complex Dynamical Systems*, Kluwer, Dordrecht, 1995
- 41** Pollicott, M., *Proc. Symp. Pure Math.* 69 (2001), p. 409
- 42** Sinai, Ya. G., *Introduction to Ergodic Theory*, Princeton University Press, Princeton, 1976
- 43** Castiglione, P., Mazzino, A., Muratore-Ginanneschi, P., Vulpiani, A., *Physica D* 134 (1999), p. 75
- 44** Artuso, R., Cristadoro, G., *Phys. Rev. Lett.* 90 (2003), p. 244101
- 45** Pikovsky, A. S., *Phys. Rev. A* 43 (1991), p. 3146
- 46** Armstead, D., Hunt, B. Ott, E., *Phys. Rev. E* 67 (2003), p. 021110
- 47** Armstead, D., Hunt, B. Ott, E., *Phys. Rev. Lett.* 89 (2002), p. 284101
- 48** Dana, I., *Physica D* 39 (1989), p. 205
- 49** Artuso, R., Strepparava, R., *Phys. Lett. A* 236 (1997), p. 469
- 50** Klages, R., Dorfman, J. R., *Phys. Rev. E* 59 (1999), p. 5361
- 51** Groeneveld, J., Klages, R., *J. Stat. Phys.* 109 (2002), p. 821
- 52** Milnor, J., Thurston, W., *Lect. Notes Math.* 1342 (1988), p. 465
- 53** Baladi, V., Ruelle, D., *Ergod. Theor. Dyn. Sys.* 14 (1994), p. 621
- 54** Baladi, V., Ruelle, D., *Invent. Math.* 123 (1996), p. 553
- 55** Baillif, M., Baladi, V., *Ergod. Theor. Dyn. Syst.* 25 (2005), p. 1437
- 56** Cristadoro, G., *J. Phys. A* 39 (2006), p. L151
- 57** Tseng, H.-C., Chen, H.-J., Li, P.-C., Lai, W.-Y., Chou, C.-H., Chen, H.-W., *Phys. Lett. A* 195 (1994), p. 74
- 58** Chen, C.-C., *Phys. Rev E* 51 (1995), p. 2815
- 59** Tseng, H.-C., Chen, H.-J., Chen, H.-W., *Int. J. Mod. Phys. B* 10 (1996), pp. 1913–1934
- 60** Vance, W. N., *Phys. Rev. Lett.* 96 (2002), p. 1356
- 61** Cvitanović, P., Gaspard, P., Schreiber, T., *Chaos* 2 (1995), p. 85
- 62** Lloyd, J., Niemeyer, M., Rondoni, L., Morriss, G. P., *Chaos* 5 (1995), p. 536
- 63** Gallavotti, G., *Rend. Accad. Naz. Lincei* 51 (1977), p. 509
- 64** Prellberg, T., Slawny, J., *J. Stat. Phys.* 66 (1992), p. 503
- 65** Artuso, R., Cvitanović, P., Tanner, G., *Prog. Theor. Phys. Suppl.* 150 (2003), p. 1
- 66** Dahlqvist, P., *Phys. Rev. E* 60 (1999), p. 6639;
- 67** Dahlqvist, P., *Nonlinearity* 10 (1997), p. 159
- 68** Prellberg, T. J., *J. Phys. A* 36 (2003), p. 2455
- 69** Isola, S., *Nonlinearity* 15 (2002), p. 1521
- 70** Artuso, R., Casati, G., Lombardi, R., *Phys. Rev. Lett.* 71 (1993), p. 62
- 71** Karney, C. F. F., *Physica D* 8 (1983), p. 360
- 72** Zaslavsky, G. M., Edelman, M., *Chaos* 10 (2000), p. 135
- 73** Artuso, R., Prampolini, A., *Phys. Lett. A* 246 (1998), p. 407
- 74** Chirikov, B. V., Sheleplyansky, D. L., *Phys. Rev. Lett.* 82 (1999), p. 528
- 75** Manneville, P., Pomeau, Y., *Phys. Lett. A* 75 (1979), p. 1
- 76** Pomeau, Y., Manneville, P., *Commun. Math. Phys.* 74 (1980), p. 189
- 77** Campanino, M., Isola, S., *Forum Math.* 8 (1996), p. 71
- 78** Gaspard, P., Wang, X.-J., *Proc. Natl. Acad. Sci. USA* 85 (1988), p. 4591
- 79** Wang, X.-J., *Phys. Rev. A* 40 (1989), p. 6647
- 80** Artuso, R., Cristadoro, G., *J. Phys. A* 37 (2004), p. 85
- 81** Korabel, N., Klages, R., Chechkin, A. V., Sokolov, I. M., Gonchar, V. Yu., *Phys. Rev. E* 75 (2007), p. 036213
- 82** Feller, W., *An Introduction to Probability Theory and Applications*, Vol. II, Wiley, New York, 1966
- 83** Procaccia, I., Schuster, H., *Phys. Rev. A* 28 (1983), p. 1210
- 84** Hirsch, J. E., Huberman, B. A., Scalapino, D. J., *Phys. Rev. A* 25 (1982), p. 519
- 85** Baladi, V., Eckmann, J.-P., Ruelle, D., *Nonlinearity* 2 (1989), p. 119
- 86** Dahlqvist, P., *Nonlinearity* 8 (1995), p. 11

9**Anomalous Transport in Hamiltonian Systems**

Eduardo G. Altmann and Holger Kantz

9.1**Introduction**

The importance of Hamiltonian dynamical systems is at the same time practical (e.g., simulations in astronomy and fluid dynamics) and fundamental (e.g., microscopic basis of thermodynamics). The reason for this last point is that systems of many interacting particles considered in statistical physics are in a fundamental sense *high-dimensional Hamiltonian* systems. An effective description of such systems is performed under the (implicit) assumption of a suited hypothesis of strong chaos [1]. One example is when transport properties are described using kinetic equations like the Fokker–Planck equation. In contrast, *low-dimensional Hamiltonian* systems are usually not ergodic and correlations do not decay fast, what violates the hypotheses for the derivation of the Fokker–Planck equation and may lead to anomalous transport.

The mechanism leading to anomalous transport in low-dimensional Hamiltonian systems is the topic of this contribution. Normal diffusive transport in deterministic systems has its origin in the chaotic nature of generic systems. However, corrections to this are caused by nonhyperbolicities (or weak chaos, see the contribution by Artuso and Cristadoro in Chapter 8 of this book) and by the generic property of *stickiness* [2, 3]. By this, one denotes a kind of sticking of trajectories to structures in the phase space which causes episodes of regular motion being intertwined into chaotic motion. The characteristics of such intermittent motion depend on the details of the Hamiltonian dynamics. Generic features, however, allow one to establish the analogy between chaotic motion in such systems and a simplified stochastic model, the continuous time random walk (CTRW, outlined in Section 9.2). In this model class, anomalous transport results from long (power-law) tails in the probability density functions (PDFs) of flights and traps. From this perspective, the mechanism responsible for the long-time tails in Hamiltonian systems is the stickiness of chaotic trajectories close to the regions of regular motion (discussed in Section 9.3). We spend considerable effort to illustrate the general aspects of anomalous transport in Hamiltonian systems by an intuitive exam-

ple, namely the model of transport of tracer particles in some incompressible two-dimensional fluid (which is the topic of Section 9.4). A new aspect considered here is the effect of noise perturbations on the anomalous transport in Hamiltonian systems. In our example this corresponds to the action of molecular diffusion.¹

Transport in Hamiltonian systems is a widely studied problem with applications in many different contexts [5–9] (see also the contribution by Lepri, Livi, and Politi in Chapter 10 of this book). We consider here the case of transport of an *ensemble* of trajectories over *large* times and distances in the phase space. This can be quantified by the temporal evolution of the mean squared displacement:

$$\langle \Delta r^2 \rangle = D t^\nu, \quad (9.1)$$

where r is a function of the phase space variables $r = r(\mathbf{p}, \mathbf{q})$ and $\langle \cdot \rangle$ means ensemble average (i.e., average over many trajectories belonging to the same chaotic ergodic component). *Anomalous* transport means in this context that $\langle \Delta r^2 \rangle$ grows nonlinearly in time ($\nu \neq 1$). This is also called anomalous diffusion since it corresponds to a vanishing ($\nu < 1$, subdiffusion) or diverging ($\nu > 1$, superdiffusion) diffusion coefficient. Furthermore, this contribution is restricted to low-dimensional Hamiltonian systems. These systems usually present mixed phase space and the anomalous transport is related to the stickiness close to ballistic ($\nu = 2$) regions. Such kind of anomalous transport was first observed in the standard map [2] which became a paradigmatic example [10–17]. It was later reported in different area-preserving maps [15, 16, 18, 19] and time-continuous systems [20, 21], as well as in a fluid-flow experiment [22, 23].

This chapter is divided as follows. In Section 9.2, anomalous transport is described in the framework of a stochastic model. The basic properties of Hamiltonian chaos that allow the connection to the general stochastic model appear in Section 9.3. These theoretical results are didactically illustrated in Section 9.4, where an intuitively understandable system of fluid dynamics is introduced and investigated numerically. Finally, in Section 9.5 the main results are summarized and discussed.

9.2

Continuous Time Random Walk Model

As in many examples studied in this book, it is useful to interpret the anomalous transport obtained in Hamiltonian systems in terms of a stochastic CTRW

¹⁾ The results contained in this chapter are part of the PhD Thesis [4].

model. In this section we summarize the main results of this model (we follow Refs. [24, 25], for more details and original references see the contribution by Gorenflo and Mainardi in Chapter 4 of this book). Consider trajectories (particles) that move with a constant speed in the direction of negative or positive r . After a given flight time t_f the trajectory remains trapped (constant r) for a time t_t before choosing at random a new direction (with equal probability) and a new flight time. An important assumption is that consecutive flights and traps are completely uncorrelated and thus drawn from invariant PDFs $\psi_f(\tau)$ and $\psi_t(\tau)$, respectively. Anomalous transport may arise in such a model if these PDFs have long tails. Consider that the probability of flying consecutively to one same direction for a time t or greater is given for long times by

$$\psi_f(\tau) \sim \tau^{-\gamma_f}, \gamma_f > 0, \quad (9.2)$$

and, analogously, that the probability of being trapped for a time t or greater is given by

$$\psi_t(\tau) \sim \tau^{-\gamma_t}, \gamma_t > 0. \quad (9.3)$$

The symbol “ \sim ” means that asymptotically the ratio of both sides of the equation tends to a constant. Additional motivation for such power-law distributions come from the stable Lévy distributions that have asymptotically power-law tails.

From the trapping and flying time distributions one can calculate the propagator $P(r, \tau)$ of reaching the point r at a time τ . Going to the Fourier–Laplace space ($r \rightarrow k, \tau \rightarrow u$) the calculation of the mean squared displacement is then given simply by [24]

$$\langle r^2 \rangle = -\frac{\partial}{\partial k} P(k, u)|_{k=0}. \quad (9.4)$$

Depending on the values of the exponents γ_f and γ_t of the PDFs (9.2) and (9.3), different values of the transport exponent ν in Eq. (9.1) are obtained asymptotically in time. The general relation can be written concisely as [25]

$$[\nu]_2 = 2 + [\gamma_t]_1 - [\gamma_f]_2, \quad (9.5)$$

where the following notation was used:

$$[x]_m = \begin{cases} x & \text{if } 0 \leq x \leq m \\ m & \text{if } x > m \end{cases} \quad (9.6)$$

The different explicit relations between ν and $\gamma_{f,t}$ contained in relation (9.5) are illustrated in Figure 9.1. When the flight- and trapping-time PDFs decay

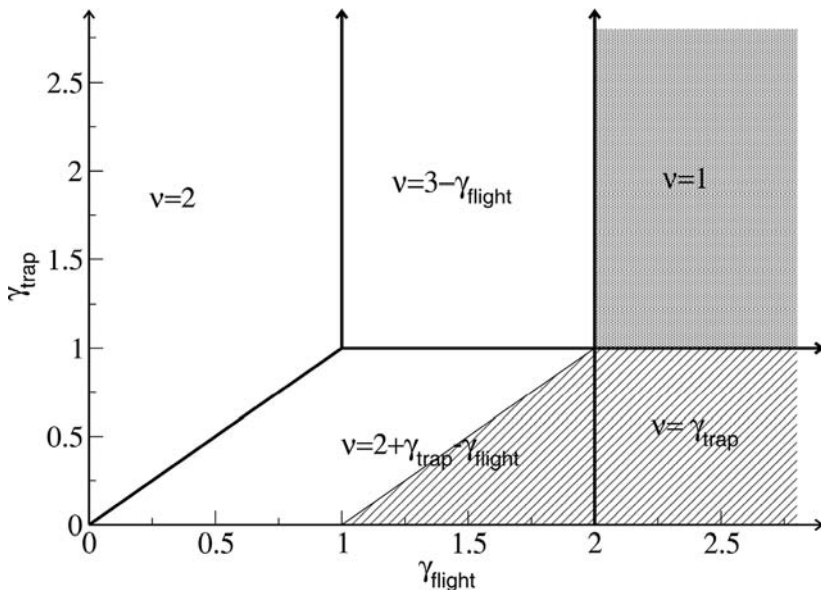


Figure 9.1 Relation between the anomalous transport exponent ν and the exponents of the statistics of flights γ_f and traps γ_t according to Eq. (9.5). Regions of subdiffusion (diagonal lines), normal diffusion (gray), and superdiffusion (white) are indicated [25].

faster than power law (no stickiness) one considers $\gamma \rightarrow \infty$ in (9.5). When both $\gamma_t \rightarrow \infty$ and $\gamma_f \rightarrow \infty$ one hence finds normal diffusion $\nu = 1$. In the more general case of nonsymmetric flights in positive/negative directions a richer behavior is obtained (see Ref. [25]).

9.3

Origin of Long-Time Tails in Hamiltonian System

In this section we present the analogy between the chaotic dynamics in low-dimensional Hamiltonian systems and the CTRW description. The origin of the power-law PDFs presented in the previous section relies on the stickiness of the regular components of the phase space, what has a strong influence on the chaotic trajectories. The main properties of this stickiness mechanism and the restrictions imposed to the CTRW model are discussed.

9.3.1

Phase Space of Hamiltonian Systems

Hamiltonian systems are defined by a single scalar function. $H(\mathbf{p}, \mathbf{q}, t)$ – the *Hamiltonian* – of $2N$ pairs of conjugate variables (q_i, p_i) , which define the

phase space Γ . The dynamics is defined through

$$\begin{aligned}\dot{p} &= -\partial H / \partial q, \\ \dot{q} &= \partial H / \partial p,\end{aligned}\tag{9.7}$$

where the dot indicates derivative with respect to time d/dt . Time discrete systems (maps) $(p, q) \mapsto (p', q')$ can be defined in a similar way [27]. From a broader perspective, Hamiltonian systems are *symplectic* dynamical systems meaning that not only the macroscopic volume of the phase space is preserved (the Liouville theorem) but also microscopic areas (Poincaré integral invariant [26]).

Simple Hamiltonian systems are integrable, in which case a canonical transformation of variables $(p, q) \mapsto (I, \theta)$ leads to $H(I, \theta) = H(I)$. The dynamics (9.7) is then trivial: the full phase space is foliated by tori. Perturbations of integrable Hamiltonian systems $H(I, \theta) = H_0(I) + KH_1(I, \theta)$ are well described by the KAM theory [27–30] that states that almost all tori survive small perturbations. This is easily illustrated using the standard map [29]

$$\begin{aligned}y_{n+1} &= y_n + K \sin(2\pi x_n) \bmod 1, \\ x_{n+1} &= x_n + y_{n+1} \bmod 1,\end{aligned}\tag{9.8}$$

which is a paradigmatic symplectic map and can be thought of being a typical Poincaré section of a continuous Hamiltonian system [27, 29]. In Figure 9.2(a1) the phase space for $K = 0.1$ is shown, where many tori are visible together with a large resonance around an elliptic fixed point at the origin. Increasing the control parameter K one observes that more and more tori are broken and that the phase space becomes increasingly more chaotic. For $K > K_c = 0.15464\dots$ no torus dividing the phase space (running from $x \in [-0.5, 0.5]$) exists. Nevertheless there are regular regions of the phase space around stable (elliptic) periodic orbits that build the so-called KAM islands. This is illustrated in Figure 9.2(a2). Such coexistence of regular and chaotic components in the phase space is a generic feature of Hamiltonian systems [29, 30]. We say that such systems have *mixed phase space*. Increasing even more K , the phase space appear to be filled by a single chaotic trajectory, as shown in Figure 9.2(a3).

9.3.2

Main Properties of Hamiltonian Chaos

There is a fundamental difference between the chaotic dynamics in fully chaotic (hyperbolic) systems and in systems possessing mixed phase space. This is illustrated in Figure 9.2(b) where the distribution of recurrence times $T > \tau$ to a specified region ($|x| > 0.25$) is shown. It follows roughly a *power-*

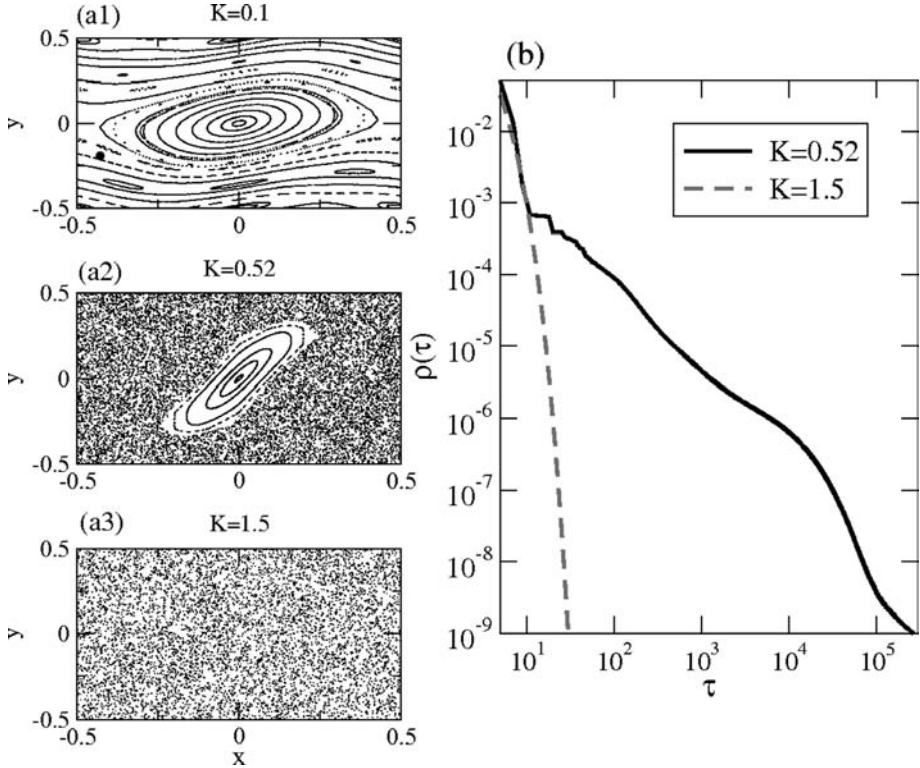


Figure 9.2 (a) Phase space of the standard map (9.8). Invariant tori and a large resonance are seen for (a1) $K = 0.1$; one KAM island is seen for (a2) $K = 0.52$; and a completely chaotic phase space is seen for (a3) $K = 1.5$. (b) Recurrence time distribution of

a single chaotic trajectory to a region away of islands (see Ref. [17] for details). While for $K = 0.52$ the trajectories stick to the border of the KAM island and a power-law like distribution (9.9) is observed, for $K = 1.5$ the distribution decays exponentially.

law

$$\rho(\tau) \sim \tau^{-\gamma}, \quad (9.9)$$

for control parameter $K = 0.52$ (mixed phase space), while it follows an exponential $\rho(\tau) \sim \exp(-a\tau)$ for $K = 1.5$ (fully chaotic). The same distinction is observed also in the decay of survival probabilities, escape rates, and correlations ($C(t) \sim t^{-(\gamma-1)}$ [31]). The reason for these equivalences is that the long-term behavior of all these quantities are determined by the trajectories stuck to the border of the regular regions. Therefore, we call the distribution (9.9) hereafter simply *stickiness distribution* and γ the *stickiness exponent*. Notice that the stickiness distribution (9.9), as well as the PDFs (9.2) and (9.3), are defined as cumulative functions. This means that the values of the corresponding power-law exponents γ , γ_f , and γ_t can be directly compared to each other.

As argued above the origin of long-term correlations and power-law distributions is the stickiness of the chaotic trajectories on the border of the regions of regular motion [2, 3], such as the KAM island in Figure 9.2(a2). The dynamics shows an intermittent behavior alternating between chaotic bursts and intervals of almost regular motion (while the trajectories are stuck to the islands). Even zero measure nonhyperbolic sets may lead to stickiness. Examples are the families of marginally unstable periodic orbits that lead to $\gamma = 2$ [39] and the marginal fixed point discussed in Ref. [32]. Generic mixed phase space in two-dimensional maps² show hierarchical chains of secondary islands and cantori found on all scales. Cantori are invariant Cantor sets that work as partial barriers to the transport close to KAM islands [8, 9]. Using such partial barriers to define states, the transport close to a KAM island was modeled by a random-walk in a Markov-tree [6, 7, 33]. The asymptotic stickiness exponent γ is obtained through the scaling properties of the Cantori and chains of islands on finer and finer scales.

The questions whether a well-defined stickiness exponent γ exists asymptotically and which is its value are fundamental questions of Hamiltonian dynamics. Nonequivalent claims of universality of this exponent exist already for two-dimensional maps [6, 15, 31, 34]. A clear answer to this problem can not be settled numerically due to the extremely slow convergence of the numerical simulations. A representative example of such convergence is presented in Figure 9.2(b) where no well defined power-law exponent is seen. Instead, an oscillating curve around a power-law like decay is effectively observed for all practical observation times [35]. The power-law assumption for the stickiness distribution expressed in relation (9.9) (and, correspondingly the PDFs. (9.2) and (9.3) of the CTRW model introduced in Section 9.2) should be considered as an idealization of the distributions found in typical Hamiltonian systems. The oscillations are system and parameter dependent since they depend on the details of the phase space structures [36]. A good estimation of the average exponent verified in different system is $\gamma = 1.6$ [4, 34], which according to Ref. [34] should be universal asymptotically in time. The exponent also γ depends strongly on the dimension of the investigated system [17].

If on the one hand an universal value of γ is not observed, on the other hand a general lower bound $\gamma > 1$ can be easily established for all systems in any dimension. This is based on Kac's lemma that states that for closed systems the mean recurrence time is equal to the inverse of the invariant measure of the recurrence region in the phase space [15]. This can be seen as a direct consequence of ergodicity. It immediately leads to the above-mentioned lower bound since for $\gamma < 1$ the mean recurrence time $\langle T \rangle = \int_0^\infty T' \frac{d}{dT} \rho(T') dT'$

2) What correspond to continuous time systems with two or one and a half degrees of freedom?

diverges. As we will see in the next section, this lower bound has important consequences to the anomalous transport in Hamiltonian systems.

9.3.3

Connection to CTRW

The analogy between the CTRW description of Section 9.2 and the intermittent chaotic dynamics described in Section 9.3.2 can be explicitly stated now [12, 18, 24]. While stuck to the border of the regular region the trajectory follows essentially the motion of the trajectories inside the regular region. Between two stickiness events the trajectory spends some (exponentially distributed) time in the chaotic sea, which is enough to destroy the correlations. This justifies the CTRW assumption that consecutive flights and traps are uncorrelated. In order to relate the stickiness distribution (9.9) to the PDFs of flights (9.2) and traps (9.3) one has to determine how the trajectories inside the regular regions move with respect to the observable r one is calculating the transport. There are essentially two cases:

- (a) When the regular region is fixed with respect to r the stickiness distribution corresponds to the PDF of traps (9.3). This is the case of all islands of the standard map shown in Figure 9.2 when the transport is calculated in the $r = y$ direction (i.e., when the map (9.8) is defined on a cylinder by taking the mod(1) function only in the angular component x).
- (b) When the regular region performs a ballistic (uniform) motion in respect to r the stickiness distribution corresponds to the PDF of flights (9.2). This is the case of the original tori (running between $x \in [-0.5, 0.5]$) and of most of the islands (those mapped in one period as $x_0 \mapsto x_0 + q$, where q is an integer) of the standard map when the transport is calculated in the $r = x$ direction [i.e., when the map (9.8) is defined on the entire plane and no mod(1) function is used]. Due to a special symmetry of the standard map (which makes it possible to associate $y + 1 \mapsto y$), for special control parameters K the so-called accelerator modes exists (for other maps see Ref. [19]). They correspond to ballistic islands in the y direction. Usually the anomalous transport is studied in the standard map in the $r = y$ direction for these special values of K [11–13, 15–17, 46].

In the most general case regular regions of both the types (a) and (b) coexist in the phase space in full analogy to the CTRW model of Section 9.2. The velocity of flight is given by the length in r of the ballistic island divided by its period. When more than one region of a given type exists, the ones showing a greater stickiness (smaller γ) should be considered.

In the last paragraph of Section 9.3.2 it was argued that for Hamiltonian systems $\gamma > 1$. Imposing this constraint to both γ_t and γ_f in Eq. (9.5) it be-

comes clear that the PDF of trapping times is irrelevant and Eq. (9.5) reduces to [20, 24]

$$\nu = \begin{cases} 3 - \gamma_f & \text{if } 1 \leq \gamma_f \leq 2, \\ 1 & \text{if } \gamma_f > 2. \end{cases} \quad (9.10)$$

As it was demonstrated in Ref. [17] and will be shown in Section 9.4.4, noise introduces an intermediate but arbitrarily long regime with $\gamma < 1$. In this case Eq. (9.5) may apply for intermediate times depending on the choice of initial conditions.

The relation between the stickiness exponent γ and the anomalous transport exponent ν expressed in Eq. (9.10) was obtained using the CTRW assumptions [24] (see also Refs. [20, 21]). Nonequivalent relations were proposed in Refs. [13, 15]. In order to clarify this conflicting point the following Refs. [12, 13, 37, 38] are suggested. Quantitative comparisons of the numerically obtained values of γ and ν have to be done extremely carefully since usually no well defined γ is observed. As discussed in Section 9.3.2 this is an intrinsic property of the stickiness phenomenon of Hamiltonian systems.

One consequence of Eq. (9.10) is that anomalous transport appears only as superdiffusion $1 < \nu < 2$, whenever sticky ballistic regions exist. In other words, no asymptotic subdiffusion $0 < \nu < 1$ is possible in Hamiltonian system, differently from the case of one-dimensional maps (see the contribution of Artuso and Cristadoro in Chapter 8 of this book). As presented here, this is a direct consequence of (i) the lower bound $\gamma > 1$ (finite mean recurrence time) discussed in Section 9.3.2; and (ii) the asymmetry between flights and traps present in Eq. (9.5) (the values of m in Eq. (9.6) are $m = 1$ for γ_t and $m = 2$ for γ_f). This asymmetry between sub- and super-diffusion is evident if one writes the diffusion coefficient of a simple diffusive process (e.g., normal random walkers) as

$$D = \frac{\langle l^2 \rangle - \langle l \rangle}{2\langle t \rangle}, \quad (9.11)$$

where l is the jump (flight) size and $\langle t \rangle$ the typical waiting (trapping) time between successive jumps. anomalous transport, which corresponds to a vanishing (subdiffusion) or diverging (superdiffusion) diffusion coefficient, arises if one of the terms in Eq. (9.11) diverges. This happens if the flight- and trapping-time PDFs have broad tails, as assumed in the CTRW description of Section 9.2. Notice that the numerator of expression (9.11) involves the second moment of the flight PDF (requiring thus $0 < \gamma_f < 2$ for superdiffusion) while the denominator involves only the first moment (requiring thus $0 < \gamma_t < 1$ for subdiffusion).

One additional remark is that the results of Eqs. (9.5) and (9.10) are valid up to log-periodicities, which are specially important in the limiting cases be-

tween normal and anomalous transport. The well-known result of anomalous transport $\langle \Delta r^2 \rangle \sim t \ln(t)$ in the Lorentz gas with infinite horizons can be in this sense also interpreted from Eq. (9.10) and the exponent $\gamma = 2$ obtained for the stickiness to marginally unstable periodic orbits (e.g., the orbits bouncing between parallel walls of the Sinai billiard) [39].

9.4 Paradigmatic Fluid Model

The theory of Sections 9.2 and 9.3 is illustrated in this section on an intuitively understandable system of fluid dynamics. A new issue investigated here is the effect of noise perturbations on the anomalous transport of Hamiltonian systems, which is introduced in our model by considering molecular diffusion.

9.4.1

Incompressible Fluid Flows as Hamiltonian Systems

The transport of a passive scalar field $\theta(\vec{x}, t)$ (contaminant), advected by a flow with velocity field $\vec{v}(\vec{x}, t)$, is given by [40, 41]

$$\frac{\partial \theta}{\partial t} + \nabla \cdot (\vec{v}\theta) = D_m \nabla^2 \theta, \quad (9.12)$$

where D_m is the molecular diffusion coefficient. The motion of fluid elements (Lagrangian description) is given by

$$\frac{d\vec{x}}{dt} = \vec{v}(\vec{x}, t) + \eta(t), \quad (9.13)$$

where $\eta(t)$ is a Gaussian stochastic process with zero mean and variance

$$\langle \eta_i(t)\eta_j(t') \rangle = 2D_m \delta_{ij} \delta(t - t').$$

Assume now that the fluid is two-dimensional (negligible vertical velocities) $\vec{x} = (x, y)$ and incompressible

$$\nabla \cdot \vec{v} = 0.$$

These conditions guarantee the preservation of area of the flow (we consider initially $D_m = 0$), what is equivalent to say that there exists a stream function $\psi(x, y, t)$ such that

$$\frac{dx}{dt} = v_x = -\frac{\partial \psi}{\partial y} \quad \text{and} \quad \frac{dy}{dt} = v_y = \frac{\partial \psi}{\partial x}. \quad (9.14)$$

Comparing Eqs. (9.14) and (9.7) it is easy to see the analogy to Hamiltonian dynamics, where the stream function $\psi(x, y, t)$ plays the role of the Hamiltonian $H(p, q, t)$. The conjugate position–momentum variables are in this case both spatial coordinates (x, y) . This makes the experimental realization and visualization of such systems specially easy since *the configuration space is equal to the phase space*. One paradigmatic experiment in this field is the rotating annulus experiment, where quasigeostrophic flows were mimic by a rotating cylindrical container [22]. For certain parameters KAM islands, regions of steady flow, and chaotic regions were observed. In particular, the anomalous transport of the angular position of tracing particles was explored [22, 23]. Hamiltonian models motivated by this experiment were proposed, where anomalous transport was generated either by the stickiness into the border of the KAM islands and tori corresponding to steady flow [42] (as discussed here) or due to the composition of this effect with some irregular (random) temporal behavior [43]. Inspired by these results we introduce below an additional model which is at the same time numerically convenient and of easy visualization.

9.4.2

Specific Model

Consider a long-fluid channel along the x direction with borders at $y = \pm 1$, having basically two flow regimes (as in Ref. [43]): (i) a regime of shear flow where the fluid is steadily flowing along x with sinusoidal velocity profile

$$\psi_1(x, y) = -v_1 \sin(\pi y), \quad (9.15)$$

illustrated in Figure (9.3)(a); (ii) a regime of vortex flow where the fluid remains localized in the channel, given by

$$\psi_2(x, y) = v_2 \cos(2\pi x)(1 - y^2)^2, \quad (9.16)$$

illustrated in Figure (9.3)(b). Note that both the regimes are periodic in x with period 1 and satisfy the boundary condition $v_x(y = \pm 1) = 0$.

The qualitative features of a large class of time-periodic two-dimensional incompressible flows can be approximated by a superposition of these two regimes. The arguments for this claim are the same used in Section 9.3.2 to argue about the generality of the phase space of near-integrable Hamiltonian systems. Additionally, a time discrete system is desired in order to facilitate our numerical simulations. This can be achieved by considering that the stream functions given by Eqs. (9.15) and (9.16) are alternated periodically in time (each one is kept constant for a fixed time t_0). A discrete system mapping the points (x', y') after one period t_n as a function of the points (x, y) before this period is obtained defining generating functions $F_n(x', y)$ as

$$F_n = x'y + \psi(x', y, nt_0)t_0.$$

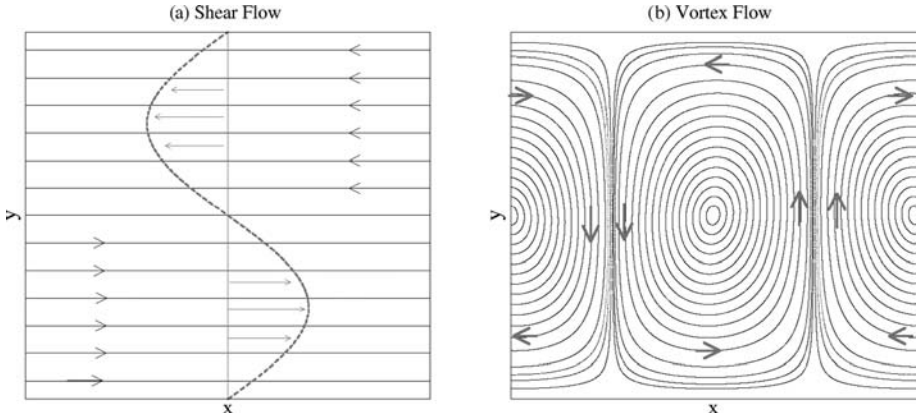


Figure 9.3 Representation of the streamlines of the two fluid regimes discussed in the text and used in order to compose the channel model given by the map (9.18). (a) Shear-flow regime given by Eq. (9.15). (b) Vortex-flow regime given by Eq. (9.16)

The map $T_n(x, y) \rightarrow (x, y)$ is defined implicitly as

$$x = \frac{\partial F_n}{\partial y} \text{ and } y' = \frac{\partial F_n}{\partial x'}. \quad (9.17)$$

In this way the maps $F^{(1)}$ and $F^{(2)}$ are obtained from ψ_1 and ψ_2 , and the composition of this two maps is taken [43]. Considering additionally the noise perturbation discussed above, we arrive at the following implicit map :

$$\begin{aligned} x_n &= x_{n+1} + \lambda \sin(\pi y_n) - \frac{2\rho}{\pi} y_n (1 - y_n^2) \cos[2\pi(x_{n+1})] + \xi \delta_n, \\ y_{n+1} &= y_n - \rho (1 - y_n^2)^2 \sin[2\pi x_{n+1}] + \xi \delta'_n. \end{aligned} \quad (9.18)$$

This model is called hereafter *channel*. The control parameters are $\rho = \pi v_2 t_0 / 2$ – intensity of the vortex regime –, $\lambda = v_1 t_0 / 2$ – intensity of the laminar flow –, and ξ – intensity of the white noise variable δ ($\xi \sim \sqrt{D_m}$). Fixed $\rho = 0.6$ and the value $\lambda = 0.25$ and $\lambda = 1$ were used, exploring later the dependence on ξ . The phase spaces for these two parameters are depicted in Figure 9.4.³ Notice that the periodicity of the channel in x is preserved, what was used in the plot of this figure but is not considered in the transport problems in the next sections. For both parameters one can identify regimes of steady flow near the walls $y \approx \pm 1$ (invariant tori of ballistic motion in x , as in item (b)) of Section 9.3.3), which are remnants of the regime illustrated in Figure 9.3(a). In

3) The implicit map (9.18) is iterated numerically using the Newton–Raphson method. Reflecting boundaries conditions at $|y| = \pm 1$ were used for the noise.

the case $\lambda = 0.25$ there exists additionally a localized KAM island around the elliptic fixed point ($x = 0.5, y = 0$). It can be seen as a remnants of the vortex regime illustrated in Figure 9.3(b) and does not move in x (as in item (a)) of Section 9.3.3).

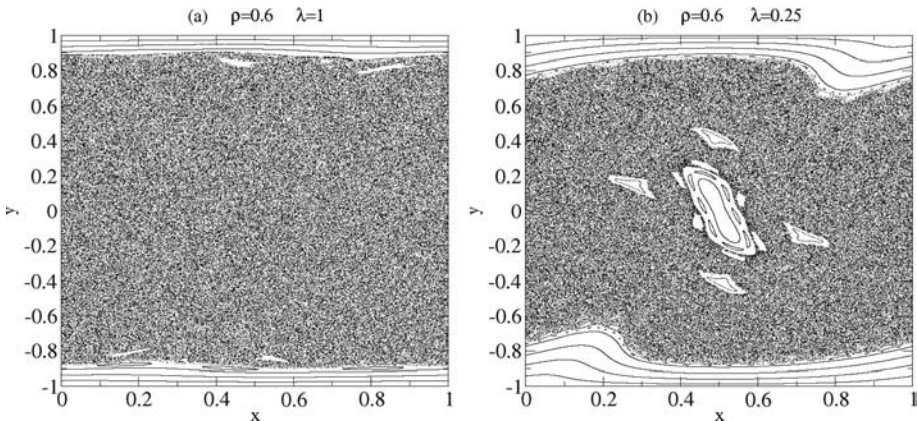


Figure 9.4 Iteration of different initial conditions of the map (9.18). Fixed $\xi = 0, \rho = 0.6$ and (a) $\lambda = 1$ and (b) $\lambda = 0.25$ were used. Laminar flow (tori) are visible close to $y \approx \pm 1$, while an additional localized KAM island is visible around the elliptic fixed point

($x = 0.5, y = 0$) in (b). For these “phase space” plots $0 \leq x < 1$ (map taken on the cylinder) was considered. In the transport simulations $-\infty < x < \infty$ was used, in which case one can think that the above configuration periodically repeats in x .

9.4.3

Transport Properties of Passive Tracers

In this section we consider the transport of a passive scalar contaminant in the $r = x$ direction ($-\infty < x < \infty$) of the channel model (9.18). The transport results from the combination of the molecular diffusion and of the chaotic advection of particles as stated in Eq. (9.12). The advection part of the model corresponds to an Hamiltonian system, as argued in Section 9.4.1. Therefore, the transport in the deterministic channel model ($\xi = 0$) should be described by the models discussed in Sections 9.2 and 9.3. The influence of molecular diffusion is analogous to a noise perturbation to Hamiltonian systems and will be considered only in Section 9.4.4.

Consider initially the motion of individual trajectories in the channel, as illustrated in Figure 9.5 for the two representative control parameters illustrated in Figure 9.4. Motion occurs through a sequence of long flights. In the case $\lambda = 0.25$ one additionally sees the existence of long trappings where the position in x hardly changes. Comparing these regimes with the position in y , shown in the two other panels of this figure, one can identify these events to the stickiness to the upper/bottom steady flow regions (left/right

flights) and to the central localized islands (traps). This is in agreement with the overall picture discussed in Sections 9.3.2 and 9.3.3, where the central island corresponds to a localized regular region of type a) and the border tori to ballistic regular regions of type b). Taking into account this relation, the following computational efficient definitions of flights and traps were used: if the trajectory crossed the axis $y = 0$ during the last 4 iterations it was considered a trap, otherwise it was considered a flight to the positive/negative direction (for y smaller/greater than 0, respectively).⁴ Due to the symmetry $(x, y) \mapsto (1 - x, -y)$ of map (9.18), there is equal probability of flying to the left and to the right and thus no further distinction will be considered (in agreement with the assumptions of the CTRW model of Section 9.2). For long times, the distributions of flights and traps are evidently related to the stickiness to the ballistic and localized regular regions of the phase space shown in Figure 9.4. It is thus not a surprise that the numerical results shown in Figure 9.6(a) resemble the stickiness distribution presented in Figure 9.2(b).

So far statistics of single trajectories were considered. In order to calculate the transport properties of the system, given by the growth of the mean squared displacement as in Eq. (9.1), an ensemble of trajectories is considered next. All initial conditions were chosen inside the large chaotic component of the phase space. The precise initial conditions are irrelevant for long times (in the simulations $x_0 = 0$ and $-0.5 < y_0 < 0.5$). The numerical results for the transport in the x direction of the model (9.18) are shown in Figure 9.6(b) for the two standard control parameters. Again a power-law-like curve with strong oscillations is observed and no power-law exponent can be defined (a curve with $\nu = 1.25$ is plotted for comparison). Nevertheless, the superdiffusive character of the transport is apparent in both cases (see also Figure 9.8).

9.4.4

Effect of Noise Perturbation

The effect of noise on the anomalous transport of Hamiltonian systems is discussed in this section. As a motivation we first estimate the order of magnitude of molecular diffusion in a concrete physical setup. From Eq. (9.13) one sees that the effect of molecular diffusion is simulated as a noise perturbation in the system and D_m is proportional to the variance of the noise: $D_m = 4\xi^2$, where ξ is the amplitude of the noise perturbation considered in model (9.18). The value of the molecular diffusion coefficient is given by the famous Ein-

4) Notice that the value $y = 0$ separates the regions of flows to the left and right and that the bigger chain of secondary islands has period 4 meaning that a typical trajectory stuck to it crosses the axis $y = 0$ twice in this period.

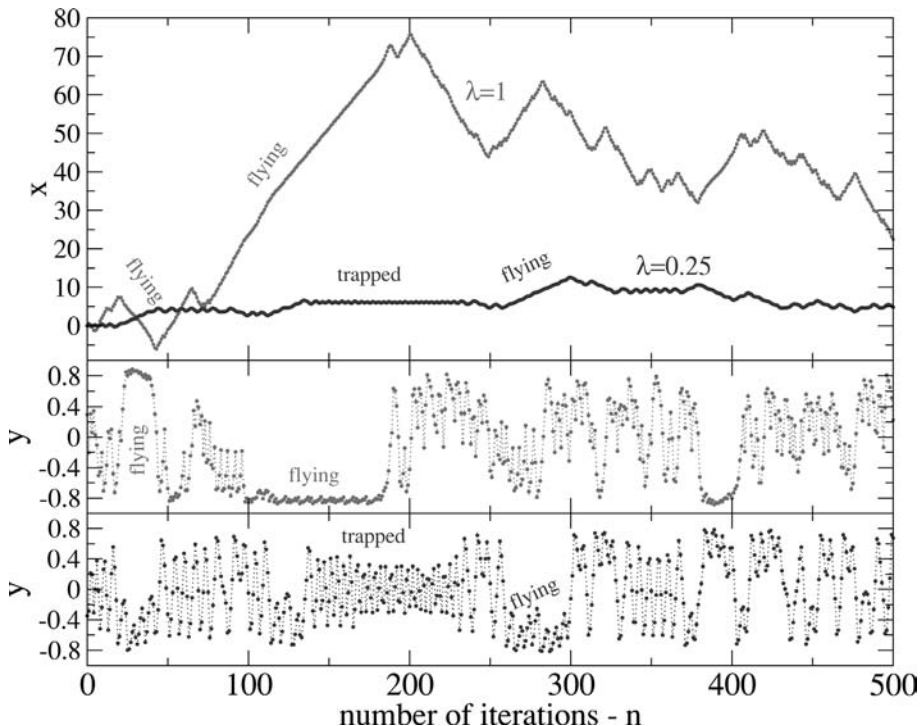


Figure 9.5 Analysis of the temporal evolution of the coordinates x, y of trajectories in the channel (9.18). A single trajectory is shown for each control parameters $\lambda = 0.25$ and $\lambda = 1$ ($\rho = 0.6$ and $\xi = 0$). Long flights are associated to the stickiness to the running tori at $|y| \approx \pm 1$ and long traps are associated to the stickiness to the central islands $|y| < 0.5$ (see Figure 9.4).

stein's relation

$$D_m = \frac{RT}{6\pi N_A \eta_k a}, \quad (9.19)$$

where R is the universal gas constant, N_A the Avogadro number, T the temperature, η_k the kinematic viscosity of the fluid, and a the radius of the corresponding Brownian particle. Consider the following estimations of the above parameters: room temperature $T = 300$ K, viscosity of water/glycerol mixtures $\eta_k \approx 10^{-4}$ m²/s as used in [23], and radius of the particles $a \approx 1$ mm. This leads to $\xi = \sqrt{2D_m} \approx 4 \cdot 10^{-6} \sqrt{\text{cm}^2/\text{s}}$. This value is fairly small (compare to the results below) and it is a reasonable approximation to neglect it for the time scales of the performed experiments, as was done in Refs. [22, 23]. However, if one considers instead particles of a contaminant or dye, that is, passive tracers where the value of a are in the scale of the radius of molecules $a \approx 1A = 10^{-8}$ cm, the estimation leads to $\xi = \sqrt{2D_m} \approx 10^{-2} \sqrt{\text{cm}^2/\text{s}}$. As will

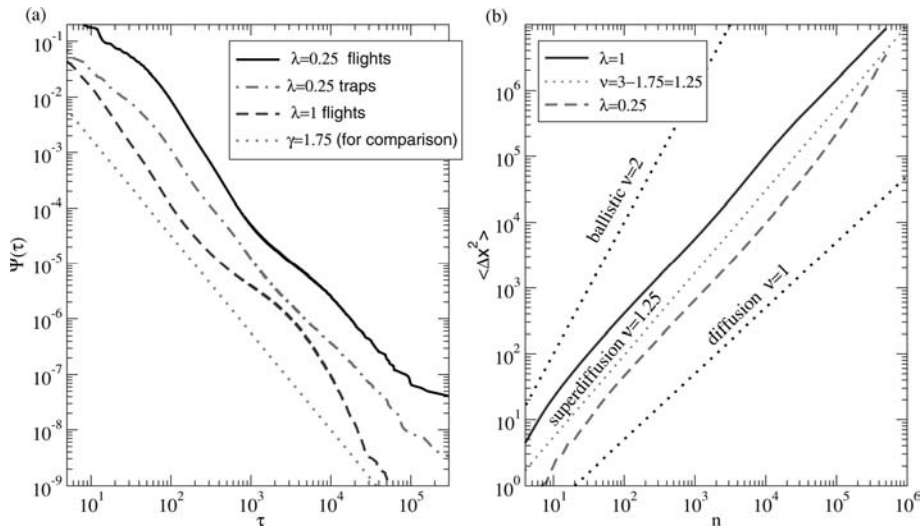


Figure 9.6 (a) PDFs of flights (9.3) and traps (9.2) for $\rho = 0.6$, $\lambda = 0.25$, and PDF of flights (9.2) for $\rho = 0.6$, $\lambda = 1$. The two lower curves were shifted vertically downwards by a factor 5 and 10, respectively, for visualizations purposes. (b) Mean squared displacement of 10^5 initial conditions in the chaotic component as a function of the number of iterations of the map (9.18). Results for

parameters $\lambda = 1$ (upper curve) $\lambda = 0.25$ (lower curve) are shown ($\rho = 0.6$, $\xi = 0$ are fixed). Both curves are between the diffusive ($\nu = 1$) and the ballistic ($\nu = 2$) regimes, what characterizes the anomalous transport. For comparison, in graph (a) a power-laws with $\gamma = 1.75$ is plotted, and in graph (b) the corresponding transport curve with $\nu = 1.25$, obtained through Eq. (9.10).

be evident from the results below, this is in our range of interest if setups in the scale of centimeter and observation times in the scale of hours are considered. Different molecular diffusion coefficients can be easily achieved by changing the type of the contaminant. Apart from molecular diffusion, different fluctuations in the experimental configuration as well as activity of the tracer (spontaneous motion) may exist. The combination of such effects can be modeled by an effective increment of the value of D_m what provides additional motivation to the study of the effect of noise in fluid dynamics.

The effect of additive white noise to the anomalous transport in Hamiltonian systems was previously studied [in the standard map (9.8)]: for the first time in Ref. [45] and recently by us in Ref. [17] where the same approach of this chapter was assumed (see also Refs. [46–49]). We have shown in that reference that the effect of noise on the stickiness phenomenon described in Section 9.3.2 is twofold:

- (i) For intermediate times⁵ it enhances the stickiness distribution by trapping trajectories *inside* the regions corresponding to KAM islands of the
- 5) For short times the perturbed stickiness distribution follows the unperturbed one.

unperturbed system. Inside the island the trajectories perform a normal random walk with step size ξ before leaving it. This introduces an intermediate power-law decay of the stickiness distribution with an intermediate stickiness exponent $\gamma = 0.5$.

- (ii) For long times, stickiness is suppressed and the stickiness distribution decays exponentially. This is due to the finite domain of regular island where effect (i) takes place. Alternatively, one can think that the small structures of the phase space are washed out by the noise.

Effect (ii) corresponds to the typical cutoff of power-law decays in the presence of noise and has as a consequence that asymptotic diffusive transport is obtained for arbitrarily small noise intensities. From the model of simple random walk inside the KAM island mentioned in point (i) we can estimate the time τ^* the trajectories take to leave the regular region to scale as

$$\tau^* \sim 1/\xi^2. \quad (9.20)$$

Indeed, in Ref. [17] we have observed this scaling for the initial time of the exponential decay mention in item (ii) above and also for the onset of normal transport. As will be shown below, effect (i) leads to interesting intermediate regimes of anomalous transport that leave their fingerprints on the value of the asymptotic diffusion coefficient.

Turning back to our fluid model (9.18), we investigate initially the effect of noise perturbation ($\xi \neq 0$) on the distribution of traps and flights. Figure 9.7 compares the unperturbed distribution to the perturbed ones for two noise intensities. The same behavior described in points (i) and (ii) above for the

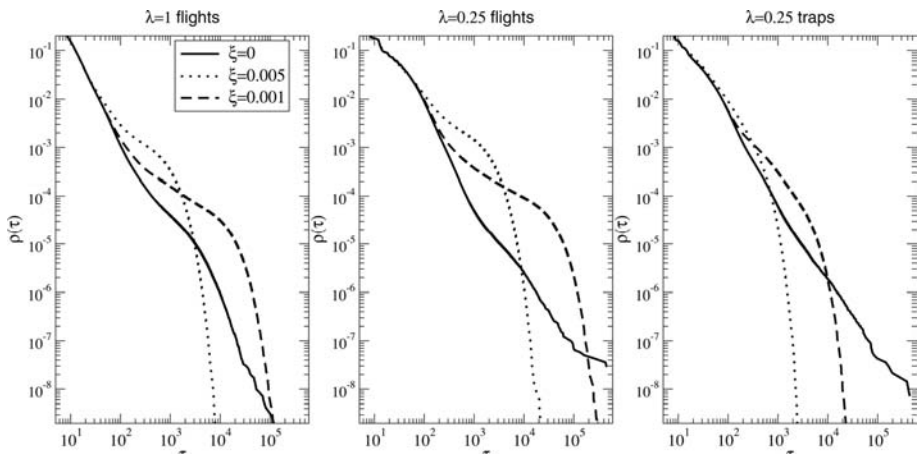


Figure 9.7 Statistical analysis of the flights and traps times as illustrated in Figure 9.5 for three different noise intensities $\sqrt{D_m} \sim \xi = 0, 0.005$, and 0.001 . The control parameters used were: $\rho = 0.6$, $\lambda = 1$ (left graph) and $\rho = 0.6$, $\lambda = 0.25$ (central and right graph).

stickiness distributions are also seen in this case: an intermediate regime of enhanced probability (tending to $\gamma_{f,t} = 0.5$) followed by an asymptotic exponential decay.

As argued above, the transport is normal (diffusive) for any $\xi \neq 0$ at sufficiently large times ($\sim 1/\xi^2 \sim 1/D_m$). This is shown for both control parameters in Figure 9.8, where one sees that for long enough times all curves approach a constant. However, interesting intermediate behaviors in agreement with the two effects mentioned in the beginning of this section can be seen for weak noise. For short times all curves follow the unperturbed anomalous transport; for intermediate times an enhanced transport is observed. Notice that introducing the intermediate stickiness exponent $\gamma = 0.5$ in Eq. (9.10) ballistic motion $v = 2$ is predicted. In the case $\lambda = 0.25$ regions of regular ballistic flow and of trapped flow exist. Nevertheless, in agreement with the CTRW theory behind Eq. (9.5), and since both regions have similar sizes, superdiffusion dominates the intermediate regimes. In the limit of small noise $\xi \rightarrow 0$, the intermediate regime of ballistic motion is increasingly large (trajectories inside the ballistic region). The interval of time that this regime lasts, and consequently the asymptotic diffusion coefficient D_A , scales with the noise intensity ξ as $D_A \sim 1/\xi^2$ as obtained in Eq. (9.20). The asymptotic diffusion coefficient can be thus seen as a consequence of the intermediate regimes [17]. However one should notice that while the intermediate regimes strongly depend on the choice of initial conditions the value of the asymptotic diffusion coefficient D_A is independent of this choice.⁶ In our simulations all initial conditions were chosen inside the region corresponding to the chaotic sea of the deterministic system.

The asymptotic diffusion coefficient measured as a function of the molecular diffusion for both parameters $\lambda = 0.25$ and $\lambda = 1$ is shown in Figure 9.9. This is a physically and experimentally relevant diagram [50]. In the academical case of very large molecular diffusion (left of the figure) the trivial relation $D_A = D_m$ is observed. The opposite limit, of very small molecular diffusion (right of the figure), is the physically relevant one and shows the asymptotic $D_A \sim 1/D_m \sim 1/\xi^2$ regime. This regime was already known by Taylor [44] and was obtained also in Ref. [45]. In the perspective discussed above, this scaling is a result of the enhanced trapping of trajectories inside the ballistic region [17]. For intermediate values of the molecular diffusion strength a minimum and a nontrivial dependence of D_A on D_m is observed. While the transport in the case $\lambda = 1$ is completely analogous to the standard map with ballistic islands, discussed in Ref. [17], the case $\lambda = 0.25$ is more complicated. This is due to the existence, together with the steady

6) When noise is present the system becomes ergodic in the full phase space.

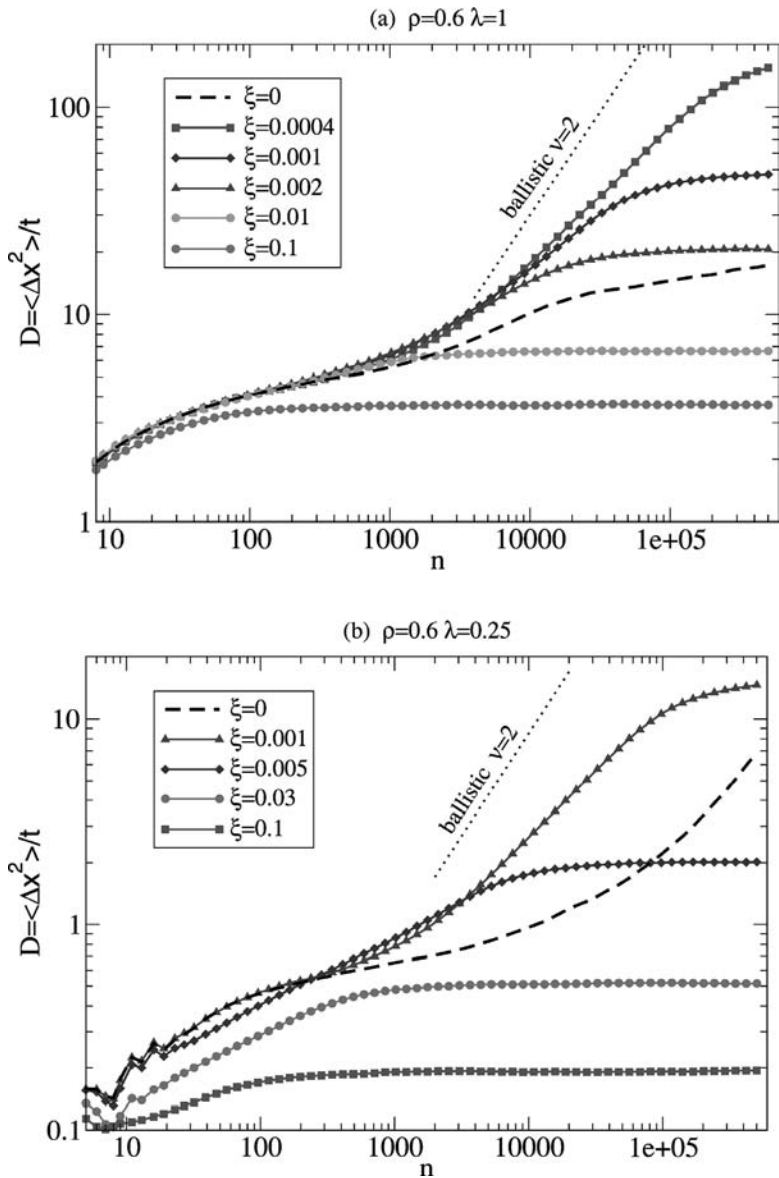


Figure 9.8 Transport along the x component of the channel model (9.18) with different noise intensities (molecular diffusivities) $\xi \propto \sqrt{D_m}$, which is reduced from bottom to top (see legends). 10^5 initial conditions were chosen inside the chaotic sea. The dashed black curve corresponds to

the unperturbed case $\xi = 0$, and show anomalous transport (the same as in Figure 9.6(b)). When the curves become constant (for $t \rightarrow \infty$) transport is normal. Control parameters: $\rho = 0.6$ and (a) $\lambda = 1$; (b) $\lambda = 0.25$.

flow near the borders (ballistic tori), of localized KAM islands where the trajectories may stick or, through molecular diffusivity, even penetrate. In this case the CTRW models with both algebraic trapping and flight distributions has to be considered, as presented in Section 9.2. As argued after Eq. (9.10) the trapping distribution is asymptotically irrelevant in Hamiltonian systems (since $\gamma > 1$). However, molecular diffusion leads to a large intermediate regime of enhanced stickiness with $\gamma \approx 0.5$ and the full expression (9.5) might be relevant for intermediate times.

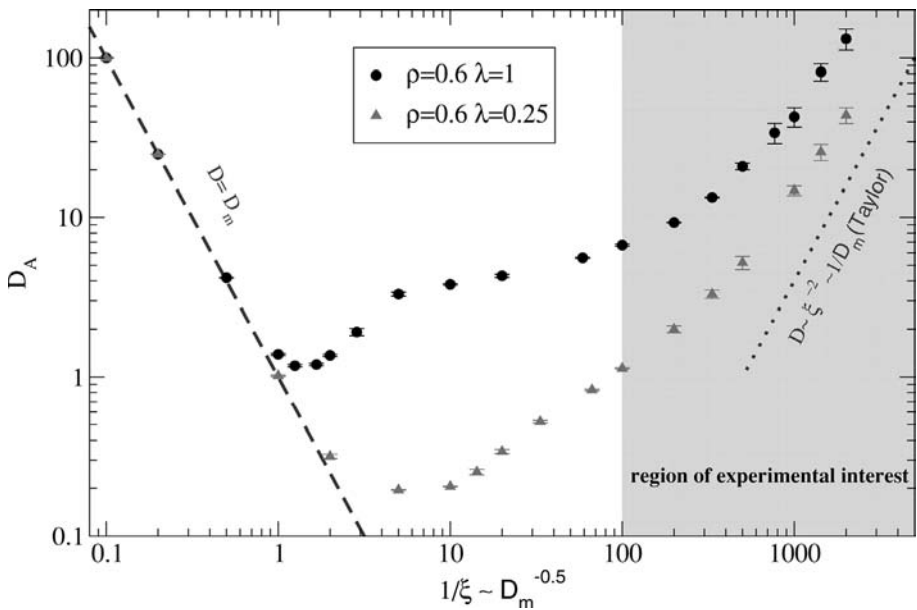


Figure 9.9 Asymptotic diffusion coefficient D_A as a function of the noise intensity (molecular diffusion) $\xi \sim \sqrt{D_m}$ for the two parameters of Figure 9.8, indicated in the legend.

9.5 Discussion

In this chapter we have studied anomalous transport in low-dimensional Hamiltonian systems. Generally, the specific transport properties depend on the system, on the control parameters, and on the initial conditions. However, an effective description of typical solutions can be achieved using CTRW models. The reason is that chaotic dynamics of generic systems can be described as an intermittent process where the origin of the long tails in the distribution of traps and flights relies on an universal mechanism: the stickiness of the chaotic trajectories close to the regions of regular motion. This is a fundamen-

tal and generic property of Hamiltonian dynamics. It introduces long-term correlations in the chaotic dynamics and may lead to anomalous transport (superdiffusion) when stable ballistic trajectories exist.

We have discussed the main properties of the stickiness distribution of Hamiltonian systems with two degrees of freedom. The fundamental difference is between the exponential decay for fully chaotic systems and power-law like decay for systems with mixed phase space. Despite different claims of universality, usually no well defined stickiness exponent γ is observed for finite times due to great oscillations in the distribution. This exponent is related to the transport exponent ν through equation (9.10). Precise quantitative comparisons are difficult to perform due to the oscillations and due to finite time simulations. Nevertheless, remarkable qualitative agreement of the different regimes of stickiness were obtained (e.g., comparing Figure 9.6(a) to Figure 9.6(b) and Figure 9.7 to Figure 9.8). Fundamental properties of Hamiltonian systems guarantee that only superdiffusion may occur asymptotically in time (no subdiffusion).

These results were illustrated through numerical simulations on a fluid model. Additionally, we consider the effect of molecular diffusion (white noise). Different intermediate regimes of anomalous transport are seen in this case, before asymptotic normal diffusion arises. We have shown a nontrivial dependence of the asymptotic diffusion coefficient D_A on the molecular diffusion coefficient D_m : a minimum is obtained between the two asymptotic scaling $D_A \sim D_m$ for large D_m , and $D_A \sim 1/D_m$ for small D_m . In Ref. [17] we have obtained similar results for a high-dimensional Hamiltonian system obtained through the weak coupling of two-dimensional maps. For some parameters, additionally an asymptotic regime of anomalous transport was obtained due to the stickiness to higher dimensional tori.

References

- 1** J.R. Dorfman, *An Introduction to Chaos in Nonequilibrium Statistical Mechanics*, Cambridge University Press, Cambridge, 1999.
- 2** C. F. F. Karney, *Long-time correlations in the stochastic regime*, Physica D **8** (1983), 360.
- 3** B. V. Chirikov and D. L. Shepelyansky, *Correlation-properties of dynamical chaos in Hamiltonian-systems*, Physica D **13** (1984), 395.
- 4** E. G. Altmann *Intermittent chaos in Hamiltonian dynamical systems*, Ph.D. Thesis obtained at the Bergische University Wuppertal, Germany (2007). Supervisor: Prof. Dr. Holger Kantz.
- 5** S. Wiggins, *Chaotic Transport in Dynamical Systems*, Springer, Berlin, 1991.
- 6** J. D. Meiss and E. Ott, *Markov-tree model of intrinsic transport in Hamiltonian systems*, Phys. Rev. Lett. **55** (1985), 2741.
- 7** J. D. Meiss and E. Ott, *Markov-tree model of transport in area-preserving maps*, Physica D **20** (1986), 387.
- 8** R. S. Mackay, J. D. Meiss, and I. C. Percival, *Transport in Hamiltonian systems*, Physica D **13** (1984), 55.
- 9** J. D. Meiss, *Symplectic maps, variational principles, and transport*, Rev. Mod. Phys. **64** (1992), 795.

- 10** R. Ishizaki, T. Horita, T. Kobayashi and H. Mori, *Anomalous diffusion due to accelerator modes in the standard map*, Prog. of Theor. Phys. **85** (1991) 1013.
- 11** Y. H. Ichikawa, T. Kamimura, and T. Hatori, *Stochastic diffusion in the standard map*, Physica D **29** (1987) 248.
- 12** G. Zumofen and J. Klafter, *Random walks in the standard map*, Europhys. Lett. **25** (1994), 565.
- 13** R. B. White, S. Benkadda, S. Kassibrakis, and G. M. Zaslavsky, *Near threshold anomalous transport in the standard map*, Chaos **4** (1998) 757.
- 14** G. M. Zaslavsky and Michael K. Tippett, *Connection between recurrence-time statistics and anomalous transport*, Phys. Rev. Lett. **67** (1991), 3251.
- 15** G. M. Zaslavsky, *Chaos, fractal kinetics, and anomalous transport*, Phys. Rep. **371** (2002), 461.
- 16** G. M. Zaslavsky, *Hamiltonian chaos and fractional dynamics*, Oxford University Press, Oxford, 2005.
- 17** E. G. Altmann and H. Kantz, *Hypothesis of strong chaos and anomalous diffusion in coupled symplectic maps*, Europhys. Lett. **78** (2007), 10008.
- 18** S. Denisov, J. Klafter, and M. Urbakh, *Ballistic flights and random diffusion as building blocks for hamiltonian kinetics*, Phys. Rev. E, **66** 046217 (2002).
- 19** P. Leboeuf, *Normal and anomalous diffusion in a deterministic area-preserving map*, Physica D **116** (1998), 8-20.
- 20** T. Geisel, A. Zacherl, and G. Radons, *Generic $\frac{1}{f}$ noise in chaotic Hamiltonian dynamics*, Phys. Rev. Lett. **59** (1987), 2503.
- 21** T. Geisel, A. Zacherl, and G. Radons, *Chaotic diffusion and $1/f$ -noise of particles in two-dimensional solids*, Z. Phys. B **71** (1988), 117.
- 22** T. H. Solomon, E. R. Weeks, and H. L. Swinney, *Observation of anomalous diffusion and Lévy flights in a two-dimensional rotating flow*, Phys. Rev. Lett. **71** (1993), 3975.
- 23** T. H. Solomon, E. R. Weeks, and H. L. Swinney, *Chaotic advection in a two-dimensional flow: Lévy flights and anomalous diffusion*, Physica D **76** (1994), 70.
- 24** J. Klafter and G. Zumofen, *Lévy statistics in a Hamiltonian system*, Phys. Rev. E **49** (1994), 4873.
- 25** E. R. Weeks, J.S. Urbach, and H. L. Swinney, *Anomalous diffusion in asymmetric random walks with a quasi-geostrophic flow example*, Physica D **91** (1996), 291.
- 26** M. Hazewinkel (Ed.) *Encyclopedia of Mathematics*, Springer, Berlin, 2002.
- 27** E. Ott, *Chaos in dynamical systems*, Cambridge University Press, Cambridge, 2002.
- 28** V. I. Arnold and A. Avez, *Ergodic problems of classical mechanics*, Addison-Wesley, New York, 1989.
- 29** A. L. Lichtenberg and M. A. Lieberman, *Regular and chaotic motion*, Springer, New York, 1983.
- 30** George M. Zaslavsky, *Weak Chaos*, Cambridge University Press, New York, 1991.
- 31** B. V. Chirikov and D. L. Shepelyansky, *Asymptotic statistics of Poincaré recurrences in Hamiltonian systems*, Phys. Rev. Lett. **82** (1999), 528.
- 32** R. Artuso and A. Prampolini, *Correlation decay for an intermittent area-preserving map*, Phys. Lett. A **246** (1998), 407.
- 33** M. Weiss, L. Hufnagel, and R. Ketzmerick, *"Can simple renormalization theories describe the trapping of chaotic trajectories in mixed systems?"*, Phys. Rev. E **67** (2002), 046209.
- 34** G. Cristadoro and R. Ketzmerick, *Universality of Algebraic Decays in Hamiltonian Systems*, Phys. Rev. Lett. **100**, 184101 (2008).
- 35** A. E. Motter, A. P. S. de Moura, C. Grebogi, and H. Kantz, *Effective dynamics in Hamiltonian systems with mixed phase space*, Phys. Rev. E **71** (2005), 036215.
- 36** G. M. Zaslavsky, *Dynamical traps*, Physica D **168-169** (2002), 292.
- 37** G. Zumofen and J. Klafter, *Comment on "Self-similarity and transport in the standard map"*, Phys. Rev. E **59** (1999), 3756.
- 38** S. Benkadda, S. Kassibrakis, R. B. White and G. M. Zaslavsky, *Reply to:"Comment on 'Self-similarity and transport in the standard map'"*, Phys. Rev. E **59** (1999), 3761.
- 39** E. G. Altmann, A. E. Motter, and H. Kantz, *Stickiness in Hamiltonian systems: from sharply divided to hierarchical phase space*, Phys. Rev. E **73** (2006), 026207.
- 40** H. Aref, *Stirring by chaotic advection*, J. Fluid Mech. **143** (1984), 1.

- 41** E. M. Ziemniak, C. Jung and T. Tél, *Tracer dynamics in open hydrodynamical flows as chaotic scattering*, Physica D **76** (1993), 123.
- 42** S. Kovalyov, *Phase space structure and anomalous diffusion in a rotational fluid experiment*, Chaos **10** (2000), 153.
- 43** S. C. Venkataramani, T. M. Antonsen Jr, and E. Ott, *Anomalous diffusion in bounded temporally irregular flows*, Physica D **112** (1998), 412–440.
- 44** G. Taylor, *Dispersion of soluble matter in solvent flowing slowly through a tube*, Proc. R. Soc. London, Ser. A **219** (1953), 186.
- 45** C. F. F. Karney, A. B. Rechester, and R.B. White, *Effect of noise on the standard mapping*, Physica D **4** (1982), 425.
- 46** R. Ishizaki, H. Shibata, and H. Mori, *Effects of external noise on anomalous diffusion in Hamiltonian dynamical systems*, Prog. Theor. Phys. **103** (2000), 245.
- 47** G. Boffetta, D. del Castillo-Negrete, C. López, G. Puccio, and A. Vulpiani, *Diffusive transport and self-consistent dynamics in coupled maps*, Phys. Rev. E **67** (2003), 026224.
- 48** R. Bettin, R. Mannella, and B. J. West, *Influence of the environment on anomalous diffusion*, Phys. Rev. E **51** (1995), 212.
- 49** E. Floriani, R. Mannella, and P. Grigolini, *Noise-induced transition from anomalous to ordinary diffusion : the crossover time as a function of noise intensity*, Phys. Rev. E **52** (1995), 5910.
- 50** L. Biferale, A. Crisanti, M. Vergassola, and A. Vulpiani, *Eddy diffusivities in scalar transport*, Phys. Fluids **7** (1995), 2725.

10

Anomalous Heat Conduction

Stefano Lepri, Roberto Livi, and Antonio Politi

10.1

Introduction

There are challenging problems in physical science, whose understanding needs a long series of efforts and contributions. The problem of obtaining a microscopic description of heat transport in matter is a typical example. This chapter aims at providing the reader an overview on this problem, up to the most recent achievements. Section 10.2 is devoted to a historical summary of the main contributions. We start from Fourier, at the beginning of the 19th century, and we arrive at Fermi and coworkers, at the half of the 20th century, going through Krönig, Clausius, Maxwell, Boltzmann, Debye, and Peierls.

More recent contributions are described in Section 10.3, which deals with the study of heat transport in harmonic systems. Thanks to the linear nature of the interactions, harmonic chains of massive oscillators were the first models which allowed to tackle the problem by a rigorous mathematical treatment. On the other hand, harmonic chains (even in the presence of isotopic disorder) exhibit an ill-defined transport coefficient: the thermal conductivity κ is found to diverge in the limit of infinite system size (*thermodynamic limit*), thus yielding a completely unexpected behavior with respect to the predictions of Fourier law. In fact, this phenomenological law is based on the assumption that heat should flow by diffusing through matter. Conversely, in a homogeneous harmonic chain heat is transferred with the speed of sound (i.e., ballistically) from the hot to the cold chain end. Accordingly, the heat current is independent of the system size and κ diverges proportionally to the system size. In the disordered harmonic chain localization effects prevent the ballistic heat transport observed in the homogeneous chain. Nonetheless, this is not enough to obtain a finite κ : for free boundary conditions κ is found to diverge with the square root of the system size, while for fixed boundary conditions κ is found to vanish like the inverse of the square root of the system size. Accordingly, different boundary conditions change the disordered chain from a heat superconductor to a heat insulator.

As mentioned in Section 10.2, in 1914 P. Debye had already suggested that an effective microscopic theory of heat transport should include nonlinear forces as a basic ingredient to prevent the pathologies inherent the linear nature of harmonic interactions. In Section 10.4, we present a short summary of the main highlights concerning the heat transport problem in chains of anharmonic oscillators, including also a short section dealing with the case of integrable nonlinear models (e.g., the Toda lattice) which exhibit ballistic transport, as in the homogeneous harmonic chain. For nonintegrable systems we show that, despite the nonlinear nature of the interaction, κ is still found to diverge with some power α ($0 < \alpha < 1$) of the system size. This is essentially due to the correlations induced by the one-dimensional nature of these models, which yield *anomalous* transport properties. More precisely, we argue that in anharmonic chains the origin of the exponent α can be traced back to the superdiffusive mechanism, characterizing the transport of energy perturbations through such chains. This also explains why we have borrowed in this context the attribute “anomalous” (also used in the title of this chapter) from the general theory of diffusion processes, where it epitomizes super- and sub-diffusive mechanisms. This choice has also the advantage of keeping a distinction with the harmonic cases, where different physical mechanisms are responsible for the divergent thermal conductivity. It is worth mentioning that related topics contained in this book are the contributions by Altmann and Kantz and by Artuso and Cristadoro. We conclude Section 10.4 by discussing the possibility of classifying such anomalous behavior by collecting different anharmonic models into a few universality classes, corresponding to specific values of α , and by providing some details about the relation between divergent thermal conductivity and anomalous diffusion in anharmonic chains.

10.2

An Historical Perspective

10.2.1

Fourier and the Problem of Heat Transport in the Earth

Since more than two centuries the phenomenon of heat transport in matter is a classical research topic in physics and applied mathematics. Such a long-time lapse testifies to the difficulties encountered in developing a convincing and general theory. Already at the end of the 18th century the design of the first steam engines attracted the interest of the scientists on such a phenomenon. At the same time, thermodynamics was going to gain a prominent position in science by occupying a seat of equal importance as mechanics. Besides the attention induced by technological applications that led to the industrial revolution, the problem of heat transport played a central role in the scientific

debate concerning the geological discoveries, which were unveiling the secrets about the formation of the solar system. In fact, the observation that a thermal gradient is present inside the Earth led many scientists to conjecture that our planet was originally a fire ball, that had progressively cooled down, while keeping in its interior track of its original nature. The Moon was also assumed having undergone the same fate, although its reduced size with respect to the Earth had fastened its cooling. Great efforts and many debates were devoted to this challenging problem, which concerned aspects inherent the very creation of the Universe. The first basic contributions to the problem were provided by the French scientist J.B.J. Fourier already in 1808. His scientific masterpiece entitled "Theorie Analytique de la Chaleur" was finally published in 1822. It contains the first mathematical theory of heat transport in matter. In particular, Fourier provided a convincing explanation for the existence of a thermal gradient inside the Earth. The basic ingredient of Fourier approach was that the phenomenon of heat flow through matter can be described by a diffusion equation, which contains a first-order derivative in time and a second-order derivative in space of the temperature field. As a consequence, such an equation describes an irreversible evolution¹ the thermal energy being substantially lost in a uniform background. Such a consequence deeply challenged the widespread opinion among many of his contemporary scientists that energy must be conserved in physical processes based on the atomistic hypothesis. The reader should consider that at the beginning of the 19th century physical sciences still stood on the firm footing of Newtonian mechanics, which was considered a fundamentally time-reversible theory. No surprise that even later Fourier theory was criticized by scientists like Helmholtz, Maxwell and Clausius.² Nonetheless, his contribution remained for a long time the fundamental mathematical theory which provided a solid basis for any phenomenological interpretation.

10.2.2

From the Old Kinetic Theory to Boltzmann

At the half of the 19th century many scientists were convinced that mechanical and thermodynamic phenomena could be traced back to a common interpretation based on the atomistic nature of matter. The reader should consider that the very structure of an atom, as known today, was going to be unveiled only half a century later, thanks to quantum mechanics. Accordingly, the atomistic assumption of the old kinetic theory had to be viewed as a fruitful hypothesis

1) This is at variance with wave-like equations, where both space and time derivative are second order.

2) For the lack of space we cannot enter here the details of this debate and we address the reader to the book by Brush [1].

for obtaining a proper description of thermodynamics from mechanics. Actually, the atoms of Krönig, Clausius, Maxwell were essentially microscopic massive particles behaving according to the Newtonian laws of mechanics. Collisions among atoms and with the walls of a container were assumed to determine the hydrodynamic properties of a macroscopic fluid, made of an extremely large number of atoms. In practice, the main goal of kinetic theory was the definition of transport coefficients through phenomenological equations describing the stationary evolution of fluxes proportional to the thermodynamic forces. For instance, when dealing with heat transport in matter one defines the thermal conductivity κ through the equation

$$\mathbf{J} = -\kappa \vec{\nabla} T , \quad (10.1)$$

where the heat flux vector \mathbf{J} is the amount of heat transported through the unit surface in unit time and $T(\vec{x}, t)$ is the local temperature.³ This equation represents the formulation of Fourier law according to the kinetic theory. Similar equations define other transport coefficients like the kinematic viscosity (a flux of momentum associated with a velocity gradient applied to the fluid) and the diffusivity (a mass flux associated with a density gradient applied to the fluid). Transport phenomena are manifestly related to out-of-equilibrium conditions determined by an applied gradient. Nonetheless, for consistency reasons one has to assume that equilibrium conditions must hold “locally” in the fluid. One can easily understand the need for such an assumption by considering that in the right-hand side of Eq. (10.1) it appears the temperature field $T(\vec{x}, t)$. This is a well-defined physical quantity provided one assumes that local equilibrium conditions hold, i.e., a local temperature can be defined for a macroscopically small, but microscopically large volume in any space position \vec{x} at any time t .

Thanks to the contribution of the great Austrian physicist L. Boltzmann, equilibrium properties as well as transport phenomena were casted into a unified fundamental description, i.e., the Boltzmann transport equation, which epitomizes his kinetic theory of gases. It is quite peculiar that this crucial progress was formulated in a hostile scientific environment, dominated by a strong reaction against the atomistic hypothesis supported by the German school of energetists led by W. Ostwald and E. Mach. In fact, Boltzmann theory appeared quite contradictory to his contemporaries. It relied upon the assumption that microscopic interactions among atoms in a gas are ruled by elastic collisions which yield the conservation of total momentum and energy

3) The heat current vector is directed from the highest to the lowest temperature, i.e., contrary to the direction of the applied temperature gradient: this is the reason for the minus sign on the right-hand side of Eq. (10.1).

together with time reversibility. On the other hand, Boltzmann proved a theorem according to which his transport equation implies an irreversible evolution towards equilibrium, in agreement with the second law of thermodynamics. This apparently paradoxical scenario was criticized by Zermelo and H. Poincaré.⁴ Boltzmann answered many of their criticisms by pointing out that the necessity of a statistical description of the astronomic number of collision processes inside the gas (fluid) originates the irreversible nature of his equation. Despite his argument was far from mathematical rigour, we know today that Boltzmann physical intuition was essentially correct. Nonetheless, it was not enough to defeat his scientific opponents before his life came to a tragic end in 1906.

10.2.3

The Harmonic Pathology and the Phonons

Boltzmann's ideas provided inspiration to the new generation of physicists, who contributed to the scientific revolution at the turn of the century. Certainly, Max Planck profited significantly from Boltzmann's approach, when he tried to solve the problem of the equilibrium spectrum of the black-body radiation. He treated the problem as a gas of radiation quanta called photons, thus preparing the ground for quantum mechanics. For what concerns transport phenomena, which are the main concern of this paper, it should be noted that another young physicist, the Dutch P. Debye, in 1914 tackled the problem of providing a microscopic foundation to Fourier law of heat transport. In practice, Debye adapted Boltzmann kinetic theory of an ideal gas of particles to a diluted gas of lattice vibrations (phonons) in an ideal solid. He found that the thermal conductivity, κ , should be proportional to $Cv\ell$, where C is the heat capacity and v , ℓ are the phonon mean velocity and free path, respectively. This is a remarkable relation, which gives us the opportunity of realizing the deep conceptual content of Boltzmann approach. Actually, Debye's relation combines typical equilibrium (C) and nonequilibrium observables (κ) through kinetic quantities (v and ℓ). When local equilibrium conditions hold, transport coefficients can be traced back to a standard thermodynamic description. Moreover, Debye realized that a physical model of a solid as a purely harmonic crystal, with elastic forces acting among its constituent atoms, could not provide a correct description of heat transport. Actually, in such a set-up all lattice vibrations propagate freely with the same velocity, so that any energy fluctuation is transported ballistically rather than being diffused through the lattice. This yields pathological effects, like an ill-defined thermal conductivity in the thermodynamic limit. For this reason, Debye conjectured that

⁴⁾ For instance, see the article "Mechanical View and Experience" by H. Poincaré, published in 1893.

in real solids the finiteness of transport coefficients should be attributed to the intrinsic nonlinear nature of the forces acting among the atoms forming its crystal structure. Actually, nonlinear forces can establish an interaction among phonons, which is expected to perturb significantly their tendency of propagating without attenuation in the purely harmonic limit. We want to stress that Debye's conjecture could not be a sufficient condition for recovering the correct diffusive behavior characterizing normal transport features. Nonetheless, it seems the simplest hypothesis for overcoming the conceptual difficulties generated by the linear nature of harmonic forces.

At the beginning of the 1930s quantum theory had already scored much success. In this historical context another young physicist, R. Peierls, during a period spent in Munich, devoted his efforts to reconsider Debye's conjecture in the light of Quantum Theory. More precisely, Peierls formulated a Boltzmann-like equation for describing heat transport in a solid in the low-temperature limit. Peierls' approach is essentially perturbative and phenomenological. Actually, in his model equation for quantized lattice vibrations the anharmonicity necessary for obtaining a genuine diffusion of the energy is introduced by invoking the so-called *Umklapp* processes [2]. In practice, Peierls assumed that in the low-temperature limit any nonlinear effect can be reduced at leading order to a basic scattering process among the quantized lattice vibrations (phonons), irrespectiv of the specific nonlinear nature of the microscopic interactions present in a real solid. It must be stressed that the so-called Boltzmann–Peierls approach marked a crucial improvement in the theory of lattice thermal conductivity. Actually, it predicts the dependence of κ on the temperature, which agrees reasonably well with experimental data in the very low-temperature regime.

10.2.4

The Fermi–Pasta–Ulam (FPU) Numerical Experiment

Despite so many improvements on the knowledge about heat transport in matter, still some basic questions were waiting for a convincing answer at the beginning of the 1950s. For instance, one could wonder under which conditions may local equilibrium be approached in a physically accessible time.

This kind of problems inspired the celebrated numerical experiment designed and performed in 1954 at Los Alamos by E. Fermi, J. Pasta, and S. Ulam. Actually, Fermi was aware of the conceptual difficulties concerning the possibility of constructing a satisfactory microscopic approach to transport theory. Presumably, since a long time he was considering the possibility of verifying the conjecture of Debye about the need of nonlinear forces for guaranteeing finite transport coefficients. Certainly, Peierl's approach provided a suitable theoretical explanation in the frame of a perturbative quantum description.

This notwithstanding, the problem remained still unsolved on the ground of classical physics. The main technical difficulty for working out an effective mathematical approach was the lack of suitable tools for treating nonlinear problems. It should be pointed out that Fermi had an extremely solid mathematical background that allowed him having a clear perception of such difficulties. Fortunately, at the Los Alamos Laboratories he and his coworkers had access to the first digital computer, MANIAC 1. It had been designed by the mathematician J. von Neumann for supporting investigations in several research fields where difficult mathematical problems could not be tackled by rigorous proofs⁵.

Fermi, Pasta, and Ulam realized the possibility of tackling the problem by numerically integrating on MANIAC 1 the classical equations of motion of a suitable model. They considered the simplest representation of a real solid as a one-dimensional chain of equal-mass classical oscillators, interacting through nearest-neighbor nonlinear forces (see Figure 10.1).

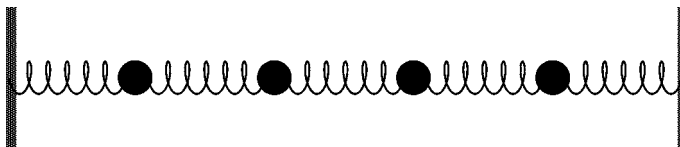


Figure 10.1 Scheme of the chain of nonlinearly coupled oscillators studied in the numerical experiment by Fermi, Pasta, and Ulam.

More precisely, they considered the classical Hamiltonian

$$H = \sum_{n=1}^N \left[\frac{p_n^2}{2m} + \frac{\omega^2}{2}(q_{n+1} - q_n)^2 + \frac{g_s}{s}(q_{n+1} - q_n)^s \right], \quad (10.2)$$

where the integer index n labels the oscillators (N being the total number of them), while q_n and p_n represent the displacement from the equilibrium position and the relative momentum, respectively. Finally, $s > 2$ identifies the power of the nonlinearity and the coupling parameter g_s determines its relative strength. For the sake of simplicity, Fermi, Pasta, and Ulam considered the cases $s = 3, 4$, with g_3, g_4 denoted as α and β , respectively (from which the names “ α ” and “ β ” models).

The reduced dimensionality and the choice of algebraic nonlinearities⁶ were dictated by simplicity arguments and by the limited amount of computational

- 5) It should be mentioned that MANIAC 1 was mainly designed for supporting researches in nuclear physics that yielded the production of the first atomic bomb.
- 6) These simplifications can be easily justified by considering that any interaction between atoms in a crystal is well approximated by introducing a power expansion considering that the amplitude of the atomic oscillations is much smaller than the interatomic distance in real solids at room temperature and pressure.

resources available on such a “primitive” digital computer. Actually, Fermi, Pasta, and Ulam were able to integrate numerically the dynamics of relatively short chains, made of 32 oscillators. Nonetheless, all the basic ingredients for testing Debye’s conjecture were contained in the model.

One should also remind that further basic conceptual implications of this numerical experiment were known from the very beginning to Fermi and his collaborators. In fact, they also expected to verify a common belief that had never been supported by a rigorous mathematical proof: In an isolated mechanical system with many degrees of freedom (i.e., made of a large number of atoms or molecules), a generic nonlinear interaction should eventually lead to equilibrium through energy “thermalization.” On the basis of physical intuition, nobody would object to this expectation if the mechanical system started its evolution from an initial state very close to thermodynamic equilibrium. Nonetheless, the same should be observed also when the energy is initially distributed within a small subset of oscillatory modes. Nonlinearities are expected to make the energy flow toward all modes, until it is equidistributed among all of them and thermal equilibrium is eventually reached.

In this sense the FPU⁷ numerical experiment was intended to test also if and how equilibrium is approached by a relatively large number of nonlinearly coupled oscillators, which obey the classical laws of Newtonian mechanics. Furthermore, the knowledge of the time elapsed before reaching the equilibrium state, i.e., the “relaxation time” τ_r of the chain of oscillators, could have contributed to determining the thermal conductivity.⁸

In their numerical experiment, FPU considered relatively short chains, up to 64 oscillators,⁹ with fixed boundary conditions. Energy was initially stored in just one of the long-wavelength oscillatory modes.

Surprisingly, the scenario conjectured by Fermi did not show up. Contrary to any intuition, the energy did not flow to the higher modes, but was exchanged only among a small number of low modes, before flowing back almost exactly to the initial state, yielding a characteristic recurrent behavior.

In spite of the nonlinearities, neither a tendency toward thermalization, nor a mixing rate of the energy could be identified. The dynamics exhibited regular features very close to those of an integrable system, like in a purely harmonic chain.

7) In the following we shall use the usual acronym for Fermi–Pasta–Ulam.

8) According to Boltzmann’s kinetic theory, τ_r represents an estimate of the time scale of energy exchanges inside the crystal: Debye’s argument predicts that thermal conductivity κ is proportional to the specific heat at constant volume of the crystal, C_v , and inversely proportional to τ_r .

9) Such sizes were already at the limit of computational performances of MANIAC 1, whose execution velocity was much smaller than that of a modern home PC.

Fermi was quite disappointed by the difficulties in finding a convincing explanation. This lacking, he decided not to publicize the results which were finally published in 1965, one decade after his death, in a volume containing his Collected Papers [3]. The FPU report is probably the most striking example of a crucial achievement which never appeared as a regular paper in a scientific journal, but which, nonetheless, has been a major source of inspiration for future developments in science. Actually, while the understanding of the mechanisms of relaxation to equilibrium and ergodicity mainly concerned later efforts of European scientists, some American researchers concentrated their attention in trying to interpret the regular motion of the FPU chain in a different way. The first contribution came from a seminal paper by M.D. Kruskal, a physicist at Princeton, and N.J. Zabusky, a mathematician at the Bell's Laboratories, in 1965 [4]. This was the starting point of the large physical literature on nonlinear lattice vibrations that are nowadays called "solitons" [5].

Apparently, the challenging questions raised by the interpretation of the FPU numerical experiment contributed to relegate the problem of the intrinsic nonlinear nature of thermal conductivity to the backstage of scientific interest. As we shall report in the following section, this is no longer the case.

10.3 Harmonic Systems

10.3.1 Homogeneous Chain

In the harmonic crystal, the heat flux decomposes into the sum of independent contributions associated with the various eigenmodes and the behavior is that of an ideal conductor. This notwithstanding, there are important theoretical questions that may be addressed about the nature of the nonequilibrium states of the system, even beyond a perturbative picture. In the present context, the natural way to proceed consists in putting the system in contact with two heat reservoirs operating at different temperatures T_+ and T_- . Several methods have been proposed based on both deterministic and stochastic algorithms [6]. Regardless the actual thermostating scheme, after a transient, an off-equilibrium stationary state sets in with a net heat current flowing through the lattice. The thermal conductivity of the chain κ is then estimated as the ratio between the time-averaged flux \bar{j} and the overall temperature gradient $(T_+ - T_-)/L$, where $L = aN$ is the chain length (a denoting the lattice spacing). Note that by this latter choice, κ amounts to an effective transport coefficient including both boundary and bulk scattering mechanisms. The average \bar{j} can be estimated in several equivalent ways, depending on the employed thermostating scheme. One possibility is to directly measure the en-

ergy exchanges with the two baths. A more general definition (thermostat-independent) consists in averaging

$$j_n = \frac{a}{2} \sum_n (\dot{q}_{n+1} + \dot{q}_n) F_n , \quad (10.3)$$

which is a microscopic expression appropriate in the context of lattices with nearest-neighbor couplings. Here, $F_n = -V'(q_{n+1} - q_n)$ is a shorthand notation for the force exerted by the n th on the $n + 1$ st oscillator.

10.3.1.1 The Rieder–Lebowitz–Lieb Model

In the above spirit, Rieder, Lebowitz, and Lieb [7] formulated a model that allows a complete analytical characterization of the nonequilibrium states. The model consists of a homogeneous (i.e., equal masses) harmonic chain with fixed boundary conditions in contact with two heat baths at temperatures T_{\pm} , modeled by stochastic forces acting on the first and last particle, respectively

$$\ddot{q}_n = \omega^2(q_{n+1} - 2q_n + q_{n-1}) + \delta_{n1}(\xi_+ - \lambda\dot{q}_1) + \delta_{nN}(\xi_- - \lambda\dot{q}_N), \quad (10.4)$$

where we have assumed unitary masses and the ξ_{\pm} 's are two independent Wiener processes with zero mean and variance $2\lambda_{\pm}k_B T_{\pm}$, where k_B is the Boltzmann constant.

This set of Langevin equations can be solved (see [7] and Appendix B in [6]) by writing down the corresponding Fokker–Planck equation for the probability $P(x)$, where x is a phase-space vector whose components are $x_n = q_n$ for $1 \leq n \leq N$, $x_n = \dot{q}_n$ for $N < n \leq 2N$. All relevant correlations in the stationary nonequilibrium state can be expressed in terms of the auxiliary function $\phi(j)$,

$$\phi(j) = \frac{\sinh(N-j)\theta}{\sinh N\theta}, \quad (10.5)$$

where the parameter θ is determined by solving the equation

$$e^{-\theta} = 1 + \frac{\zeta}{2} - \sqrt{\zeta + \frac{\zeta^2}{4}} \quad (10.6)$$

and $\zeta = \omega^2/\lambda^2$ is the only dimensionless parameter of the model. As it can be seen by direct inspection of correlations, θ defined in Eq. (10.6) measures the inverse length of the boundary layers over which the reservoirs significantly affect the chain dynamics. As expected, θ diverges in the weak coupling limit ($\zeta = \omega^2/\lambda^2 \rightarrow \infty$). For example, the temperature profile $T_n = \langle \dot{q}_n^2 \rangle$ writes

$$T_n = \begin{cases} T_+ - \zeta\eta T\phi(1) & n = 1 \\ T[1 - \eta\zeta\phi(2n-1)] & 1 < n \leq N/2 \\ T[1 + \eta\zeta\phi(2(N-n)-1)] & N/2 < n < N \\ T_- + \nu\eta T\phi(1) & n = N \end{cases} \quad (10.7)$$

where $T = (T_+ + T_-)/2$ is the average temperature and $\eta = (T_+ - T_-)/T$ the rescaled temperature difference. The temperature profile exhibits an unexpected property: the temperature is higher (lower) in the vicinity of the colder (hotter) reservoir (see Figure 10.2), the only exceptions being represented by the first and last particles, respectively. Moreover, because of the exponential decay of $\phi(n)$, in the bulk, the temperature profile is constant as if the system were at equilibrium at temperature T . However, this is only superficially true, as position–velocity correlations significantly differ from the equilibrium ones.

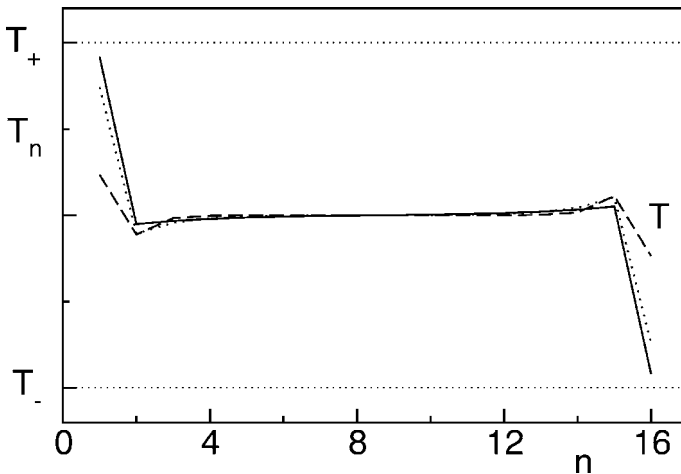


Figure 10.2 The temperature profile for the harmonic chain, formula (10.7), for coupling parameter $\zeta = 0.05, 0.2, 1.0$ (solid, dotted, and dashed lines, respectively).

Also the average local flux j_n can be computed explicitly. In the stationary state, $j_n = j$ independently of the lattice position n . For large N , Eqs. (10.5) and (10.6) imply

$$j = \frac{\omega^2 k_B}{2\lambda} \left[1 + \frac{\omega^2}{2\lambda^2} - \frac{\omega}{\lambda} \sqrt{\frac{\omega^2}{4\lambda^2} + 1} \right] (T_+ - T_-). \quad (10.8)$$

Accordingly, the heat flux is proportional to the temperature *difference* rather than to the local gradient $T_{n+1} - T_n$, as it should be, were the Fourier law to be satisfied. This proves that, as expected, homogeneous harmonic chains do not exhibit normal transport properties, since the effective conductivity $\kappa = jN/(T_+ - T_-) \propto L$, while the bulk conductivity diverges exponentially, as the temperature gradient away from the baths is exponentially small.

The asymptotic expressions

$$j = \begin{cases} \frac{\omega^2}{2\lambda} k_B(T_+ - T_-) & \lambda \gg \omega \\ \frac{\lambda}{2} k_B(T_+ - T_-) & \lambda \ll \omega, \end{cases} \quad (10.9)$$

show that the maximum flux is attained for the optimal value $\lambda/\omega = \sqrt{3}/2$, while j vanishes both in the limit of large and small coupling. While the behavior in the small coupling limit is pretty obvious, the opposite limit can be understood by noticing that the flux is proportional to the difference between the temperature of the thermal bath and the effective temperature of the thermostatted particle: in the strong coupling limit, such a difference vanishes.

The same approach can be adopted to solve the problem for heat baths characterized by stochastic elastic collisions. In fact, very similar expressions are found to hold in that case [7]. Moreover, analogous conclusions can be drawn with reference to free boundary conditions [8].

The solution we have outlined is based on the Fokker–Planck equation and stochastic calculus. An important alternative approach based on transmission coefficients has been presented by Rubin and Greer [9].

10.3.2

Disordered Chain

As it is known, the presence of disorder generally induces localization of the normal modes of the chain and one may thus expect the latter to behave as a perfect thermal insulator. Nonetheless, the actual scenario is much more complicated, depending on boundary conditions and on the properties of the thermostats. For concreteness, we discuss a generalization of model (10.4) in which masses are randomly distributed (isotopic disorder),

$$m_n \ddot{q}_n = q_{n+1} - 2q_n + q_{n-1} + \delta_{n1}(\xi_+ - \lambda \dot{q}_n) + \delta_{nN}(\xi_- - \lambda \dot{q}_N), \quad (10.10)$$

where, for the sake of simplicity ω is set equal to 1 (this implies that now the mass has the dimension of a square time). As for the boundary conditions, for the moment, we leave them unspecified. Before entering a more detailed discussion, it is worth recalling that Lebowitz and collaborators [10, 11] rigorously showed that the system approaches a unique stationary non-equilibrium state for a large class of heat baths.

10.3.2.1 Localization of the Eigenmodes

In the absence of thermal baths, one can look for solutions of the form $q_n = v_n e^{ivt}$ and solve the resulting eigenvalue problem numerically. Upon ordering the eigenvectors with increasing eigenfrequencies v , a distinct difference in their localization properties can be recognized (see Figure 10.3). For small v

(upper panel of Figure 10.3), randomness induces only a relatively weak modulation of the amplitude; a partial localization can be recognized in the intermediate panel, while a clear evidence of localization is visible only for the high-frequency eigenvector reported in the bottom panel.

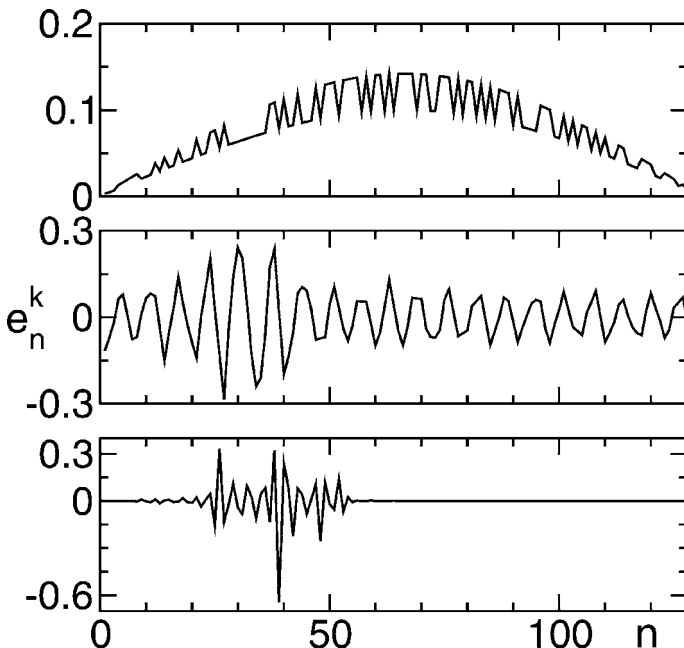


Figure 10.3 The first, 41st, and 100th eigenvector (from top to bottom) in a chain of 130 particles with random masses with an even distribution of 1 and 1/2 values. The increasing localization with increasing eigenvalue is transparent.

A more rigorous analysis can be performed by solving the eigenvalue problem for the discrete Laplacian by a transfer matrix approach. This approach has been successfully employed to solve the Anderson quantum localization problem in the tight-binding approximation [12]. The spectrum can be determined from a recursive equation for the new variable $R_n = v_n/v_{n-1}$. As a result one can compute both the integrated density of states $I(\nu)$ and the inverse localization length γ . In the small-frequency limit, a perturbative calculation yields [6,13]

$$I(\nu) = \frac{\sqrt{\langle m \rangle}}{\pi} \nu \quad , \quad \gamma = \frac{\nu^2 \sigma_m^2}{8a\langle m \rangle}, \quad \text{for } \nu \rightarrow 0 \quad (10.11)$$

where $\langle m \rangle$ and $\sigma_m^2 = \langle m^2 \rangle - \langle m \rangle^2$ stands for the mean and variance of the mass distribution. The fact that γ tends to zero for $\nu \rightarrow 0$ means that low-

frequency modes are almost extended (see again Figure 10.3) and thus significantly contribute to heat transport.

10.3.2.2 The Temperature Profile

Despite the linearity of Eqs. (10.10), an analytic solution can be obtained only in the perturbative regime, $\lambda \ll 1$. It is convenient to introduce the variable $u_n = \sqrt{m_n}q_n$, which allows rewriting the evolution equations (10.10) in the bulk in a symmetric way and, accordingly, to diagonalize them through an orthogonal transformation. By denoting with e_n^k , the n th component of the k th (normalized) eigenvector and introducing the variable $U_k = \sum_n u_n e_n^k$, the equations of motion write as

$$\ddot{U}_k = -v_k^2 U_k - \lambda \sum_j C_{kj} \dot{U}_j + \frac{e_1^k}{\sqrt{m_1}} \xi_+ + \frac{e_N^k}{\sqrt{m_N}} \xi_- , \quad (10.12)$$

where $-v_k^2$ is the real, negative k th eigenvalue of the unperturbed evolution operator and

$$C_{kj} = \frac{e_1^k e_1^j}{m_1} + \frac{e_N^k e_N^j}{m_N} . \quad (10.13)$$

Equation (10.12) shows that the normal modes are coupled among themselves through the interaction with the reservoirs. It follows that by neglecting first-order corrections, the local temperature T_n in the stationary state reads as

$$T_n = \sum_{k=1}^N \frac{(e_n^k)^2}{C_{kk}} \left(T_+ \frac{(e_1^k)^2}{m_1} + T_- \frac{(e_N^k)^2}{m_N} \right) . \quad (10.14)$$

This is basically the expression derived by Matsuda and Ishii [13] (see also [14] for a critical discussion of this result). As a consistency check, one can easily verify that if $T_+ = T_- = T$, then $T_n = T$ for all values of n (this follows from the normalization condition on the eigenvectors). Another limit case is the homogeneous chain for $T_+ \neq T_-$ where the amplitude of all eigenvectors is the same at the two chain ends, implying a flat profile, $T_n = (T_+ + T_-)/2$. In the generic case, the temperature profile is highly irregular (see Figure 10.4) and depends on the specific realization of the disorder, reflecting the complicated spatial structure of the eigenmodes.¹⁰

- 10)** As the temperature profile depends on the actual realization of the disorder, one may wish to look at its ensemble average over independent realizations of the disorder itself. However, numerics indicate that fluctuations of T_n do not vanish in the thermodynamic limit, implying that they do not self-average [6].

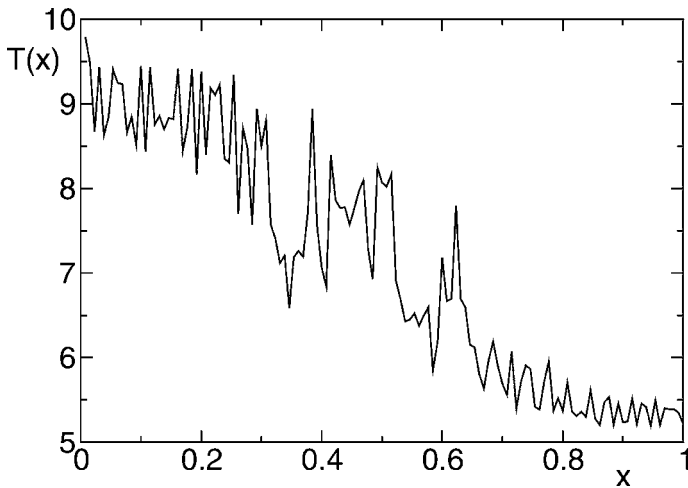


Figure 10.4 Temperature profile versus the rescaled lattice position $x = n/N$ for a given realization of disorder in a chain of length $N = 128$, with $T_+ = 10$ and $T_- = 5$. The T_n are computed from Eq. (10.14), using the eigenvectors obtained from numerical diagonalization.

10.3.2.3 The Heat Flux

For Langevin heat baths, like those in Eqs. (10.4), one can compute the heat flux as the average amount of energy exchanged between the first particle and the hot reservoir, namely

$$j(\lambda, N) = \frac{\lambda}{m_1} (T_+ - T_1) \quad (10.15)$$

(an equivalent expression holds on the opposite boundary). By making use of Eq. (10.14), one obtains [13, 14]

$$j(\lambda, N) = \lambda (T_+ - T_-) \sum_k \frac{(e_1^k)^2 (e_N^k)^2}{m_N (e_1^k)^2 + m_1 (e_N^k)^2} \equiv \sum_k J_k, \quad (10.16)$$

where the k th addendum J_k can be naturally interpreted as the contribution of the k th mode. As intuitively expected, J_k is larger for modes that have larger amplitudes at the boundaries and are thus more strongly coupled with the reservoirs. This interpretation is confirmed by looking at Eq. (10.12). Indeed, in so far as cross-coupling can be neglected, the dynamics of the k th eigenmode is approximately described by the equation

$$\ddot{U}_k = -\omega_k^2 U_k - \lambda C_{kk} \dot{U}_k + \frac{e_1^k}{\sqrt{m_1}} \xi_+ + \frac{e_N^k}{\sqrt{m_N}} \xi_-. \quad (10.17)$$

Standard stochastic calculus shows that, in the stationary regime, the energy exchanged per unit time with the two thermal baths is equal to J_k as defined

by Eq. (10.16). However, heat transport is characterized by more subtle mechanisms than one could infer from this simple picture of independent modes. A perturbative calculation [6] does show that a nonvanishing heat flux is necessarily associated with the existence of *correlations among different modes*. From the dynamical viewpoint, such correlations may be explained from the fact that all eigenmodes are subject (up to a multiplicative factor) to the same noise sources. This may well induce a sort of synchronization among them. In homogeneous chains, this type of coherence has been numerically investigated in Ref. [15].

10.3.2.4 The Thermal Conductivity

Since the high-frequency eigenmodes are strongly localized, only the N_e modes whose localization length is comparable to or larger than the sample size L can contribute significantly to the heat flux (10.16). From Eqs. (10.11), it follows that $\gamma \simeq \sigma_m^2 I^2(\nu)/(a\langle m \rangle^2)$. Upon writing $I = N_e/N$ and imposing $\gamma = 1/L$, one finds that

$$N_e = \frac{\langle m \rangle}{\sigma_m} \sqrt{N}. \quad (10.18)$$

At this point, it becomes crucial to specify the boundary conditions. Let us first consider the case of free ones: the square amplitude of an extended eigenmode in a lattice of size N is on the order of $1/N$. This implies that the contribution to the heat flux of one of such modes is $\lambda(T_+ - T_-)/N$ and, from Eq. (10.16), the heat flux turns out to be

$$j_{free}(\lambda, N) \propto \lambda(T_+ - T_-) \frac{\langle m \rangle}{\sigma_m} \frac{1}{\sqrt{N}}. \quad (10.19)$$

As a result, the conductivity diverges as

$$\kappa_{free} \propto \lambda \frac{\langle m \rangle}{\sigma_m} \sqrt{N}. \quad (10.20)$$

This scaling was first derived in Ref. [13] and later confirmed in Ref. [16] by means of a different approach. On the other hand, for fixed boundary conditions the result is completely different. In this case all eigenmodes must vanish for $n = 0$ and $n = N + 1$. By approximating the site-to-site variation of e_n^k with the wavenumber k/N , we find that the square amplitude of e_1^k and e_N^k is on the order k^2/N^3 . As a consequence, summing all such addenda up to $k = N_e$ in Eq. (10.16) yields

$$j_{fix}(\lambda, N) \propto \lambda(T_+ - T_-) \left(\frac{\langle m \rangle}{\sigma_m} \right)^3 \frac{1}{N^{3/2}}, \quad (10.21)$$

and, accordingly, the thermal conductivity vanishes as

$$\kappa_{fix} \propto \lambda \left(\frac{\langle m \rangle}{\sigma_m} \right)^3 \frac{1}{\sqrt{N}}. \quad (10.22)$$

Altogether, not only boundary conditions affect the scaling behavior of κ , but they give rise to qualitatively different scenarios. On the one hand, the conductivity of disordered harmonic chains with free boundaries diverges in the thermodynamic limit. On the other hand, chains with fixed boundaries behave as good insulators!¹¹

Dhar [17] went even further and showed how the scaling behavior of the conductivity with the system size depends also *on the spectral properties of the heat baths*. More precisely, if $\kappa \propto N^\alpha$, then the exponent α is determined by the low-frequency behavior of the noise spectrum. This implies that a suitable spectral choice can even lead to a finite conductivity! Such a scenario is less unphysical than it may appear at a first glance. Integrability of the motion implies that the only scattering mechanism that determines the heat resistance is the interaction with the baths. It is therefore reasonable that the actual way the energy is transferred to the various modes plays a crucial role.

Before closing this section, let us comment on the difficulties that are encountered when simulating directly disordered chains. The major problem is represented by the extremely slow convergence toward the asymptotic regime that can be explained as follows. Equation (10.12) shows that the effective coupling of each eigenmode with the reservoirs is proportional to its square amplitude at the extrema. For an eigenmode with inverse localization length γ , the coupling is of order $\exp(-\gamma\Delta)$, where Δ is the distance from the localization site which is typically of order N . Therefore, the stationary state is attained over times scales that grow exponentially with N .¹² Serious convergence problems are also found when the leading behavior predicted by Eqs. (10.20) and (10.22) is checked. The asymptotic regimes are usually approached very slowly (say for N greater than 10^3). It is thus clear that sound conclusions about the dependence of the thermal conductivity on the system size may be hard to obtain. These issues are of great importance when dealing

11) This latter scenario is brought to an extremum if a linear on-site force $-Kq_n$ is added to the right-hand side of Eqs. (10.10). The model becomes almost equivalent to the one-dimensional tight-binding model of Anderson localization: the lower band-edge is bounded away from zero and γ does not vanish, meaning that all eigenmodes are exponentially localized. As a result, the conductivity is exponentially small in N .

12) In principle, the same problem applies also to the convergence of the flux $j(\lambda, N)$. From a practical point of view this is however not very relevant, as the contribution of such strongly localized modes is anyhow exponentially negligible.

with nonlinear models where analytical results are not available and make the validity of recent results questionable [18].

10.4

Anomalous Transport in Anharmonic Chains with Momentum-Conserving Potentials

10.4.1

Early Studies

The analysis of linear systems coupled with external thermostats allows characterizing nonequilibrium steady states. However, such models miss the most crucial physical ingredient: nonlinearity, which, according to Debye's arguments, can account for thermal resistance. Following the track opened by the FPU experiment, numerical simulations soon appeared as the most direct way to attack the problem in a fully nonperturbative manner. Indeed, already at the end of the 1960s, some pioneering computer studies were performed by Payton, Rich, and Visscher [19] and Jackson, Pasta, and Waters [20] in steady nonequilibrium conditions. It should be recognized a posteriori that those early studies attacked the problem from the most difficult side, as both anharmonicity and disorder were simultaneously present (random masses [19] or coupling constants [20]). Nevertheless, they have the merit to show how the interplay of the two ingredients can lead to unexpected (and still poorly understood) effects. For instance, the perturbative picture in which anharmonicity and impurities provide two independent (and thus additive) scattering mechanisms does not hold and, in some cases, a larger nonlinearity *enhances* thermal conductivity [19]. A qualitative explanation was put forward by claiming that anharmonic coupling induces an energy exchange between the localized modes, thus leading to an increase of the heat flux. Additional questions that have been investigated were the effect of disorder on the temperature field and the concentration of impurities. Besides the obvious finding that disorder reduces the value of thermal conductivity (for fixed finite-chain length), it was noticed an asymmetric behavior between the case of a few heavy atoms randomly added to an otherwise homogeneous light-atom chain and its converse. The smaller values of the thermal conductivity observed in the former case were traced back to the larger number of localized modes [19].

10.4.2

Green–Kubo Formalism

So far we have mostly dealt with nonequilibrium methods. As it is known, linear response theory provides an alternative approach for investigating transport properties. In fact, whenever the chain length is sufficiently large, local gradients are small and, accordingly, small deviations from an equilibrium state are expected. In these conditions, transport coefficients can be determined from equilibrium fluctuations. More precisely, by introducing the total heat flux

$$J = \sum_n j_n, \quad (10.23)$$

the Green–Kubo formalism tells us that thermal conductivity is determined from the expression [21]

$$\kappa = \frac{1}{k_B T^2} \lim_{t \rightarrow \infty} \lim_{N \rightarrow \infty} \frac{1}{N} \int_0^t dt' \langle J(t') J(0) \rangle, \quad (10.24)$$

where the autocorrelations refer to equilibrium conditions. From the above expression, it follows that κ is a well-defined transport coefficient when it stays finite in the thermodynamic limit $N \rightarrow \infty$. Whenever this is not the case, one can at least define an effective conductivity $\kappa(L)$ by truncating the time integral in the above equation to $t \approx L/c$, where c is the sound velocity (see [6] for a more detailed discussion). In particular, if $\langle J(t) J(0) \rangle \approx t^{-\chi}$ (with $\chi < 1$), it turns out that $\kappa(L) \approx L^{1-\chi} = L^\alpha$, where the exponent α is introduced to denote the divergence rate of thermal conductivity. This allows summarizing the behavior of harmonic chains discussed in the previous section, by stating that $\alpha = 1$ in homogeneous systems, while $\alpha = 1/2$ in disordered ones with free boundary conditions.

In view of the well known correspondence between autocorrelations and power spectra, one can equivalently extract α from the low-frequency behavior of

$$S(\omega) \equiv \int_0^\infty dt \langle J(t) J(0) \rangle e^{i\omega t}. \quad (10.25)$$

In fact, a $t^{-\chi}$ decay of $\langle J(t) J(0) \rangle$ corresponds to an $\omega^{-\delta}$ divergence of $S(\omega)$ with $\delta = 1 - \chi$, so that $\alpha = \delta$. In fact, the best numerical strategy consists in computing the power spectrum $S(\omega)$ as power-law divergences can be better resolved than convergences to zero. In the next sections, we illustrate why and how Fourier's law breaks down in nonlinear systems.

10.4.3

The Quasi-Integrable Limit

A remarkable and general property of FPU-like models is the existence of an energy-density threshold e_c below which almost-regular behavior significantly slows down the relaxation. This originates from the fact that although primary resonances do not overlap, higher order resonances can do, yielding a slower evolution in phase space on a time scale that is inversely proportional to a power of the energy density (see Ref. [22] for a recent review of the topic). The *weak stochasticity* of this regime is confirmed by the smallness of the maximum Lyapunov exponent that is of order e^2 . Conversely, above e_c , equipartition is rapidly approached without any numerical difficulty. For these reasons, e_c is termed as *strong stochasticity threshold*. Its value depends on the leading nonlinearity; for instance, in the FPU- β model, once the physical quantities are expressed in adimensional units such that $m = 1$, $\omega = 1$ and $\beta = 1$, the threshold is $e_c \simeq 0.1$.

This scenario suggests that stationary transport properties below e_c may be strongly affected by the quasi-integrability of the dynamics. Indeed, simulations of the FPU- β model subject to a thermal gradient [23], exhibit a systematic increase of the effective conductivity $\kappa(L)$ with the system size, which is well fitted by a law of the type

$$\frac{1}{\kappa(L)} = \frac{A}{L} + \frac{B}{L^\alpha}. \quad (10.26)$$

The fitted values of the exponent $\alpha \simeq 0.4$ are almost independent of the temperature and indicate a nontrivial behavior at large scales (see below).

By performing microcanonical simulations (with periodic boundary conditions and zero total momentum), it turns out that $S(\omega)$ displays a power-law singularity for ω below some crossover frequency ω_c that decreases upon decreasing the energy density. A quantitative analysis shows that ω_c is roughly proportional to $e^{1.6}$, which is not too far from the e^2 scaling of the Lyapunov exponent in the weakly chaotic regime. It is thus reasonable to infer that the dynamical mechanisms underlying the slow relaxation and the anomalous conduction are basically the same at such low temperatures.

10.4.4

The Strong-Chaos Regime

In the previous section we saw how the almost-regular features of the dynamics may give rise to a breakdown of a macroscopic transport law (the Fourier law in this case). On the basis of the previous discussion, it might be surmised that above the strong stochasticity threshold such anomalies should somehow disappear as the dynamics becomes more “mixing” and the relaxation times shorter. It thus came as a surprise when the anomalous transport features of

the FPU chain were actually discovered to persist also in this regime [24, 25]. The origin of this anomalous behavior is twofold. The first cause is the *reduced dimensionality*. Indeed, strong spatial constraints can significantly alter transport properties: the response to external forces depends on statistical fluctuations which, in turn, crucially depend on the system dimensionality d . This is very much reminiscent of the problem of long-time tails in fluids [26] where, for $d \leq 2$, transport coefficients may *not exist at all*. The second necessary condition is *momentum conservation* [27], i.e., the existence of long-wavelength (Goldstone) modes that are propagating and very weakly damped. This latter condition is necessary for these anomalies to occur and means that no external (i.e., substrate) forces must be present. This is precisely the case of the ding-a-ling model [28] and of other models in the same class (for example the Frenkel–Kontorova model [29, 30] or the nonlinear Klein–Gordon chain [31]). The only remarkable exception to this is the coupled rotor chain [32, 33] where, however, different mechanisms are at work.

A concrete example is given in Figure 10.5 for the FPU model with cubic and quartic nonlinearities. A power-law divergence $\omega^{-\delta}$ of the power spectra $S(\omega)$ is observed in the low- ω region. In addition, the finite-size conductivity increases as a power N^α of the number of oscillators. For the data in Figure 10.5 one finds the values $\delta = 0.30$ and $\alpha = 0.34$, which are consistent with the above reasoning.¹³

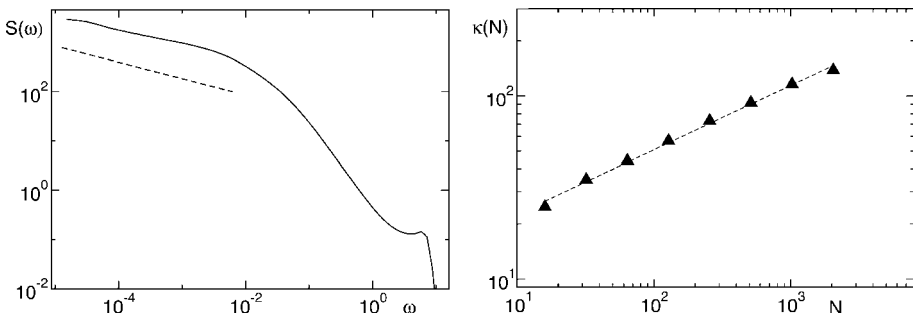


Figure 10.5 Left: Power spectra of the flux J as defined in Eq. (10.3) for the FPU model with cubic and quartic nonlinearities, $g_3 = 0.25$, $g_4 = 1$, $N = 1024$, and $e = 0.5$. Data are averaged over 7000 random initial conditions. To minimize statistical fluctuations, a binning of the data over contiguous

frequency intervals has been performed. The dashed line corresponds to $\omega^{-1/3}$ behavior. Right: finite-size conductivity as measured by nonequilibrium simulations (Nosé–Hoover thermostats) with $T_+ = 0.21$ and $T_- = 0.19$. Dashed line is a power-law fit.

13) To obtain reliable estimates of δ , one must compare the results obtained for different numbers of particles to ensure that finite-size corrections are negligible at least above a size-dependent frequency $\omega_c(N)$. Data fitting is then performed in a scaling range $[\omega_c(N), \omega_s]$, where ω_s is chosen to be well below the knee in Figure 10.5.

10.4.5

Integrable Nonlinear Systems

The harmonic crystal behaves as an ideal conductor because its dynamics can be decomposed into the superposition of independent “channels.” This peculiarity can be generalized to the broader context of integrable nonlinear systems. They are mostly one-dimensional models characterized by the presence of “mathematical solitons,” whose stability is determined by the interplay of dispersion and nonlinearity. This interplay is expressed by the existence of a macroscopic number of *conservation laws* constraining the dynamical evolution. As pointed out by Toda [34], the existence of freely traveling solitons is expected to lead to ballistic transport, i.e., to an infinite conductivity. From the point of view of the Green–Kubo formula, this ideal conducting behavior is reflected by the existence of a nonzero flux autocorrelation at arbitrarily large times. This, in turn, implies that the finite-size conductivity *diverges linearly with the system size*.

Although integrable models are, in principle, exactly solvable, the actual computation of dynamic correlations is technically involved. A more straightforward approach is, nevertheless, available to evaluate the asymptotic value of the current autocorrelation. This is accomplished by means of an inequality due to Mazur [35] that, for a generic observable \mathcal{A} , (with $\langle \mathcal{A} \rangle = 0$) reads as

$$\lim_{\tau \rightarrow \infty} \frac{1}{\tau} \int_0^\tau \langle \mathcal{A}(t) \mathcal{A}(0) \rangle dt \geq \sum_n \frac{\langle \mathcal{A} \mathcal{Q}_n \rangle^2}{\langle \mathcal{Q}_n^2 \rangle} , \quad (10.27)$$

where $\langle \dots \rangle$ denotes the (equilibrium) thermodynamic average, the sum is performed over a set of conserved and mutually orthogonal quantities \mathcal{Q}_n ($\langle \mathcal{Q}_n \mathcal{Q}_m \rangle = \langle \mathcal{Q}_n^2 \rangle \delta_{n,m}$).

Zotos [36] applied the above result to the equal-masses Toda chain with periodic boundary conditions, defined, in reduced units, by the Hamiltonian

$$H = \sum_{l=1}^N \left[\frac{p_l^2}{2} + \exp(-r_l) \right] , \quad (10.28)$$

where $r_l = x_{l+1} - x_l$ is the relative position of neighboring particles. As the model is completely integrable, since it admits N independent constants of the motion, lower bounds on the long time value of $\langle J(t)J(0) \rangle$ can be calculated by the inequality (10.27) [36]. As a result, the lower bound to the conductivity is found to increase monotonously with the temperature. At low T , the growth is linear with a slope comparable to the density of solitons $N_s/N \propto T \ln(2/\pi^2)$. This trend is interpreted as an evidence for the increasing contribution of thermally excited nonlinear modes to ballistic transport.

10.4.6

Universality

It is natural to argue about the universality of the exponent α in Eq. (10.26). Simulation studies of specific models [6] as well as analytic arguments [27], lead to the surmise that anomalous conductivity should occur generically whenever momentum is conserved. Moreover, the exponent α should be largely independent of the microscopic details, as suggested by a the Renormalization-Group (RG) calculation by Narayan and Ramaswamy [27] that predicts $\alpha = (2 - d)/(2 + d)$. For $d = 1$ the resulting value $\alpha = 1/3$ is consistent with the results shown in Figure 10.5 (although some substantial deviations have been observed in specific cases – see the discussion at the end of this section).

Another approach to the problem of anomalous conductivity is mode-coupling theory (MCT), which has been invoked to estimate long-time tails of fluids [26] and to describe the glass transition [37].

In the present context, hydrodynamic considerations would suggest that three fields play a major role, namely, particle, momentum, and energy density. However, as already shown by the RG analysis carried out in Ref. [27], the correct scaling behavior can be inferred by reducing the coarse-grained dynamics to an equation for a single field. The main observable taken into account by MCT is the normalized correlator¹⁴ $G(k, t) = \langle Q^*(k, t)Q(k, 0) \rangle / \langle |Q(k)|^2 \rangle$, where $Q(k, t)$ is the Fourier transform of the displacement field q_n

$$Q(k) = \frac{1}{\sqrt{N}} \sum_{n=1}^N q_n e^{-ikn} \quad (10.29)$$

and which basically amounts to the density–density correlator. Under the only approximation that the coupling with the other correlators can be neglected, the Mori–Zwanzig projection approach leads to [38, 39],

$$\ddot{G}(k, t) + \varepsilon \int_0^t \Gamma(k, t-s) \dot{G}(k, s) ds + \omega^2(k) G(k, t) = 0 \quad (10.30)$$

where particle mass, lattice spacing, and sound velocity are all set to unity. Moreover, the memory kernel $\Gamma(k, t)$ is proportional to $\langle \mathcal{F}(k, t)\mathcal{F}(k, 0) \rangle$ with $\mathcal{F}(k)$ being The Fourier transform of the nonlinear force between particles. Equation (10.30) must be solved with the initial conditions $G(k, 0) = 1$ and $\dot{G}(k, 0) = 0$. Both the coupling constant ε and the frequency $\omega(k)$ are temperature-dependent input parameters, which should be computed

14) The normalization is not necessary, but it has the advantage of simplifying the scaling analysis of the correlator.

independently by numerical simulations or approximate analytical estimates [38,39]. For simplicity, one may restrict to considering their bare values, obtained in the harmonic approximation. In the adopted dimensionless units they read $\varepsilon = 3g_3^2 k_B T / 2\pi$ and $\omega(k) = 2|\sin \frac{k}{2}|$.

The physical interpretation of the above equation is best understood within a Markovian approximation, i.e., replacing the memory function with a Dirac delta. In the small wavenumber limit $k \rightarrow 0$, Eq. (10.30) reduces to

$$\ddot{G}(k, t) + \eta k^2 \dot{G}(k, t) + c^2 k^2 G(k, t) = 0, \quad (10.31)$$

where, for the sake of clarity, we have reintroduced the sound velocity c . Notice that the validity of (10.31) rests on the fact that Γ exhibits a fast decay and that its time integral is finite. This equation describes the response of an elastic string at finite temperature, as predicted by linear elasticity theory. The kinetic coefficient η is a suitable viscosity, describing the internal irreversible processes of the elastic string, i.e., the absorption of “sound” waves.

More in general, Eq. (10.30) can be solved only after introducing a closed expression for the memory kernel Γ . The self-consistent mode-coupling approach amounts to introducing the lowest-order approximation [38,39]

$$\Gamma(k, t) = \omega^2(k) \frac{2\pi}{N} \sum_{p+p'-k=0, \pm\pi} G(p, t) G(p', t), \quad (10.32)$$

where p and p' are multiples of $2\pi/N$ ranging over the whole Brillouin zone (from $-\pi$ to π in our units).

The long-time behavior of G can be obtained by decomposing the variable as the product of a slowly varying term and a “rapid” rotation,

$$G(k, t) = C(k, t) e^{i\omega(k)t} + c.c. \quad . \quad (10.33)$$

This allows reducing Eq. (10.30) to a first order equation for $C(k, t)$ and thereby proving that for small k -values and long times [40,41] $C(k, t) = g(\sqrt{\varepsilon} t k^{3/2})$. Upon inserting this scaling result into the definition of the heat flux, one eventually concludes that the conductivity κ diverges with a rate $\alpha = 1/3$, that is in agreement with the RG theory.

Validation of these theoretical results by simulation is, to some extent, still under debate. Generally speaking, the available numerical estimates range between 0.25 and 0.44 [6,42]. The existence of crossovers among different scaling regimes has been observed [43]. As a word of caution, it must be stressed that obtaining reliable numerical estimates is a challenging task. Even in the most favorable cases of computationally efficient models, such as the one-dimensional gas of hard-point particles with alternating masses [44], finite-size corrections to scaling are sizeable. As a matter of fact, α -values as diverse as 0.33 [45] and 0.25 [46] for comparable parameter choices have been reported.

In spite of the scattered numerical results, the combined pattern emerging from theory and simulations suggests the following scenario. There exists a broad universality class characterized by the exponent $\alpha = 1/3$. The underlying major condition for the observation of this scenario is a nonvanishing pressure. In fact, on the one hand, at zero pressure, one can imagine that the leading nonlinearity invoked in the memory kernel (see Eq. (10.32)), is no longer quadratic, but cubic. An analytical solution of the corresponding mode-coupling equations indeed reveals a different scaling behavior with $\alpha = 1/2$ (see also Ref. [47] and also [48] where the value $\alpha = 2/5$ is predicted). On the other hand, the most sizeable deviations from $\alpha = 1/3$ have indeed been observed in the FPU- β [42] that, by symmetry reasons, is characterized by a zero pressure.

However, it is fair to admit that although zero-pressure models systematically exhibit larger α -values, the agreement between theory and numerics is even more elusive than in the broader universality class of nonzero pressure systems. All in all, one is bounded to conclude that all such models are affected by strong and possibly universal finite-size deviations that are not taken into account by the theories developed so far. In particular, in the MCT framework, it seems necessary to write and solve full equations that take into account the correlators of the three relevant hydrodynamic fields at the same time.

10.4.7

Anomalous Diffusion

It is tempting to tackle the problem of anomalous thermal conductivity by trying to establish a connection with that of anomalous diffusion. In all models that have been mentioned in the previous sections, the particle order is rigorously preserved during the evolution. This is a peculiar feature of one-dimensional systems that is lost in two and higher dimensions. As a consequence, one might expect no diffusion at all. However, one-dimensional systems are characterized by yet another peculiarity, namely long-wavelength fluctuations. In fact, it is well known that one cannot rigorously speak of one-dimensional solids, precisely because of the strong deviations induced by the density fluctuations. We illustrate this with reference to an isolated chain of N particles with periodic boundary conditions. The equilibrium average $\langle |Q(k)|^2 \rangle$ of the k th Fourier mode (10.29) diverges as k^{-2} at small k -values [2], thus implying that $q_n(t)$ is, at any time, basically a diffusive process in space, which returns exactly to the origin after N steps. Accordingly, we expect deviations on the order of \sqrt{N} , which are made possible by the absence of an onsite force, because the internal forces bind any particle to its neighbors but not to fixed external positions. It is therefore very tempting to establish a connection with rough interfaces [49] such as those described by either the Kardar-

Parisi–Zhang (KPZ) equation or the simpler linear Edwards–Wilkinson (EW) equation, both of which exhibit the same type of stationary profiles (notice, however, that the KPZ equation describes nonequilibrium processes).

In the context of roughening processes, the temporal scaling behavior is analysed by letting the interface evolve from an initially flat profile $q_n(0) = 0$ and thereby monitoring the growth of the interface variance $\sigma^2 = \overline{(q - \bar{q})^2}$, where the overline denotes a spatial average. In the case of KPZ and EW interfaces, σ^2 grows as $t^{2/3}$ and $t^{1/2}$, respectively: both indices are suggestive of an anomalous sub-diffusive behavior. If one performs a similar analysis in the context of lattice dynamics, by preparing an initial condition with all particles in the equilibrium position but randomly distributed kinetic energies, it turns out that σ^2 grows linearly in time. Thus, one is led to conclude that this type of diffusion is normal and has no connections with the anomalous transport properties exhibited by such systems.

A completely different approach has been taken by other scientists, who have studied heat transport in ensembles of noninteracting particles. One typical example is that of a point-like particle moving in a long billiard that is connected with two thermal baths at its extrema [50] (see Figure 10.6 for an example). In this framework, the energy is separately transferred by the single particles with their motion from one to the other end of the system. Not unexpectedly, anomalous (superdiffusive) behavior is accompanied by anomalous heat transport [51].

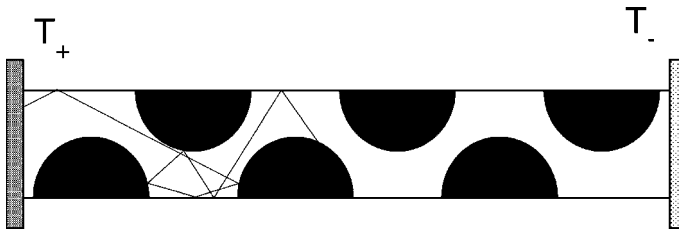


Figure 10.6 The Lorentz channel model [50] consists of a series of semicircles of radius R placed in a triangular lattice along the channel. By construction no particle can move along the horizontal direction without colliding with the disks. The channel is in contact with two baths at different temperatures T_{\pm} .

In order to shed some light about a possible relationship between the two phenomena, it is convenient to make reference to suitable stochastic processes. In this respect, Lévy walks are the best candidates for their generality and robustness. A simple model is that of a particle moving ballistically in between successive “collisions” that are separated in time according to a power law, $\psi(t) \propto t^{-\mu-1}$, $\mu > 0$, while its velocity is $\pm v$ with equal probability. In Ref. [52] it was shown that the probability density

$P(x, t)$ to find in x at time t a particle initially localized at $x = 0$ writes $P(x, t) = P_L(x, t) + t^{1-\mu}[\delta(x - \tilde{v}t) + \delta(x + \tilde{v}t)]$ with

$$P_L(x, t) \propto \begin{cases} t^{-1/\mu} \exp\left[-(\eta x/t^{1/\mu})^2\right] & |x| \lesssim t^{1/\mu} \\ t x^{-\mu-1} & t^{1/\mu} \lesssim |x| < \tilde{v}t \\ 0 & |x| > \tilde{v}t. \end{cases} \quad (10.34)$$

The density $P_L(x, t)$ is independent of details such as the distribution of the particle velocities, but more important is to notice that the growth rate β of the variance depends only on the relevant parameter μ , through the relation $\beta = 3 - \mu$. In this context, the exponent α characterizing the divergence of κ is linked to β by the simple relation $\alpha = \beta - 1$.

The general relevance of this result in the context of billiard-like systems is questionable, since the underlying value μ is likely to be model-dependent if not even specific of some parameter values. Nevertheless, the study of energy diffusion in a gas of hard-point particles (with alternating masses) has revealed that this formalism applies perfectly to energy diffusion (at least in the limit of infinitesimal perturbations). In fact, in Ref. [53] it has been shown that the average energy profile of an initially δ -like distribution follows Eq. (10.34) for $\mu = 5/3$. The relevance of this observation is that the long-time correlations arise as a genuine many-body effect (the nonlinear interaction of long-wavelength modes) and is not postulated *a priori*. This provides a sound basis for the connection between anomalous transport and kinetics (superdiffusion in this case) [51].

The connection between anomalous diffusion and thermal conductivity is further strengthened by noticing that the function $C(k, t)$ introduced in the context of MCT (see Eq. (10.33)) satisfies the fractional differential equation (at least in the limit of $\sqrt{\epsilon}tk^{3/2} \rightarrow 0$),

$$\frac{\partial^\rho}{\partial t^\rho} C(k, t) + \lambda^\rho C(k, t) = 0, \quad (10.35)$$

where $\rho = 4/3$ and $\lambda^\rho = ak^2$ (a is a suitable numerical constant). The solution of Eq. (10.35) is the Mittag-Leffler function $E_\rho(-(\lambda t)^\rho)$ [54] that interpolates between stretched-exponential and power-law decays. The case of interest here ($1 < \rho \leq 2$) corresponds to the so-called fractional oscillations [54]. More details about fractional derivatives can be found in the contribution by del-Castillo-Negrete in Chapter 6 of this book.

Finally, a few words of caution come from the discussion of the underlying dynamical exponent. In space-time critical phenomena, the dependence on the space x - the time t -variable combines in a dependence on the single variable t/x^z for some suitable z that is called the dynamical exponent. From the MCT discussed in the previous section, it turns out that in Fourier space the

relevant variable is $tk^{3/2}$ which implies $z = 3/2$. On the other hand, from the Lévy walk analogy, it turns out that $z = \mu = 5/3$. As both results have been shown to be compatible with $\alpha = 1/3$ this contradiction seems to indicate that there is still something to be further clarified.

References

- 1 S.G. Brush, *The kind of motion we call heat*, North-Holland, Amsterdam 1976.
- 2 R.E. Peierls, *Surprises in Theoretical Physics*, Princeton University Press, Princeton, NJ, 1979.
- 3 E. Fermi, J. Pasta and S. Ulam, in *Collected papers of E. Fermi*, University of Chicago Press, Chicago, 1965, Vol.2, p.78 .
- 4 M.D. Kruskal and N.J. Zabusky, J. Math. Phys. 5, 231 (1964).
- 5 P.G. Drazin and R.S. Johnson, *Solitons: an introduction*, Cambridge University Press, Cambridge 1989.
- 6 S. Lepri, R. Livi, A. Politi, Phys. Rep. 377, 1 (2003).
- 7 Z. Rieder, J.L. Lebowitz, E. Lieb, J. Math. Phys. 8 (1967) 1073.
- 8 N. Nakazawa, Progr. Theor. Phys. Suppl. 45 (1970) 231.
- 9 R.J. Rubin, W.L. Greer, J. Math. Phys. 12 (1971) 1686 .
- 10 A. Casher, J.L. Lebowitz, J. Math. Phys. 12, (1971) 1701 .
- 11 A.J. O'Connor, J.L. Lebowitz, J. Math. Phys. 15, (1974) 692 .
- 12 B. Derrida, E. Garner J. Phys. (Paris) 45 (1984) 1283 .
- 13 H. Matsuda, K. Ishii, Suppl. Prog. Theor. Phys. 45 (1970) 56.
- 14 W.M. Visscher, Prog. Theor. Phys. 46 (1971) 729.
- 15 W. Frizzera, A. Monteil, A. Capobianco, Il Nuovo Cimento D 20 (1998) 1715.
- 16 J.B. Keller, G.C. Papanicolaou, J. Weilenmann, Comm. Pure App. Math. Vol. XXXII (1978) 583.
- 17 A. Dhar, Phys. Rev. Lett. 86 (2001) 5882.
- 18 B. Li, H. Zhao, B. Hu, Phys. Rev. Lett. 86 (2001) 63.
- 19 D.N. Payton, M. Rich, W.M. Visscher, Phys. Rev. 160 (1967) 706.
- 20 E.A. Jackson, J.R. Pasta, J.F. Waters, J. Comput. Phys. 2 (1968) 207.
- 21 R. Kubo, M. Toda and N. Hashitsume, *Statistical Physics II*, Springer Series in Solid State Sciences vol. 31, Springer, Berlin 1991.
- 22 M. Pettini, L. Casetti, M. Cerruti-Sola, R. Franzosi and E.G.D. Cohen, Chaos 15 015106 (2005).
- 23 S. Lepri, R. Livi, A. Politi, Chaos 15 (2005) 015118.
- 24 S. Lepri, R. Livi, A. Politi, Phys. Rev. Lett. 78 (1997) 1896.
- 25 S. Lepri, R. Livi, A. Politi, Physica D 119 (1998) 140.
- 26 Y. Pomeau, R. Résibois, Phys. Rep. 19 (1975) 63.
- 27 O. Narayan, S. Ramaswamy, Phys. Rev. Lett. 89, (2002) 200601 .
- 28 G. Casati, J. Ford, F. Vivaldi, W.M. Visscher, Phys. Rev. Lett. 52 (1984) 1861.
- 29 M.J. Gillan, R.W. Holloway, J. Phys. C 18 (1985) 5705.
- 30 B. Hu, B. Li, H. Zhao, Phys. Rev. E 57 (1998) 2992.
- 31 K. Aoki, D. Kusnezov, Phys. Lett. A 265 (2000) 250.
- 32 C. Giardiná, R. Livi, A. Politi, M. Vassalli, Phys. Rev. Lett. 84 (2000) 2144.
- 33 O. V. Gendelman, A. V. Savin, Phys. Rev. Lett. 84 (2000) 2381.
- 34 M. Toda, Phys. Scr. 20 (1979) 424.
- 35 P. Mazur, Physica 43 (1969) 533.
- 36 X. Zotos, J. Low Temp. Phys. 126 (3-4) (2002) 1185.
- 37 W. Götze in *Liquids, freezing and the glass transition*, edited by J. P. Hansen, D.

- Levesque and J. Zinn-Justin, North-Holland, Amsterdam 1991; R. Schilling in *Collective dynamics of nonlinear and disordered systems*, edited by G. Radons, W. Just and P. Häussler, Springer, Berlin, 2003.
- 38** J. Scheipers, W. Schirmacher, *Z. Phys. B* **103**, (1997) 547.
- 39** S. Lepri, *Phys. Rev. E* **58** (1998) 7165.
- 40** L. Delfini, S. Lepri, R. Livi, A. Politi, *Phys. Rev. E* **73**, (2006) 060201(R).
- 41** L. Delfini, S. Lepri, R. Livi, A. Politi, *J. Stat. Mech.* (2007) P02007.
- 42** S. Lepri, R. Livi, A. Politi, *Phys. Rev. E* **68** (2003) 067102 .
- 43** J. S. Wang and B. Li, *Phys. Rev. Lett.* **92**, (2004) 074302
- 44** T. Hatano, *Phys. Rev. E* **59** (1999) R1.
- 45** P. Grassberger, W. Nadler, L. Yang, *Phys. Rev. Lett.* **89**, 180601 (2002).
- 46** A. Dhar, *Phys. Rev. Lett.* **86** 3554 (2001); G. Casati, T. Prosen, *Phys. Rev. E* **67**, 015203 (2003)
- 47** G.R. Lee-Dadswell, B.G. Nickel and C.G. Gray, *Phys. Rev. E* **72** (2005) 031202 .
- 48** A. Peverzhev, *Phys. Rev. E* **68**, (2003) 056124 .
- 49** A.-L. Barabasi, H.E. Stanley, *Fractal Concepts in Surface Growth*, Cambridge University Press, Cambridge, 1995.
- 50** D. Alonso, R. Artuso, G. Casati and I. Guarneri, *Phys. Rev. Lett.* **82**, 1859 (1999); D. Alonso, A. Ruiz, and I. de Vega *Phys. Rev. E* **66**, 066131 (2002).
- 51** S. Denisov, L. Klafter J and M. Urbakh, *Phys. Rev. Lett.* **91** 194301 (2003).
- 52** A. Blumen, G. Zumofen and J. Klafter, *Phys. Rev. A* **40** 3964 (1989).
- 53** P. Cipriani, S. Denisov, A. Politi *Phys. Rev. Lett.* **94**, 244301 (2005)
- 54** F. Mainardi, *Chaos, Solitons and Fractals* **7** 1461 (1996).

Part III Anomalous Transport in Disordered Systems

Introduction to Part III

Many systems in nature can to a good approximation be considered as being disordered. Prominent examples reach from structural glasses or porous materials to biological systems such as living cells or actin networks. Transport in such systems is often anomalous, in many cases subdiffusive, but superdiffusive motion is also observed. Because of its importance for natural systems the following Part III, consisting of four chapters, is devoted to *Anomalous transport in disordered systems*.

Disordered systems and their transport properties are notoriously difficult to deal with, even numerically. Therefore analytically solvable models play an import role in this field. The introductory contribution to this part by Jean-Phillipe Bouchaud is devoted to such models with emphasis on glassy behavior. Its title *Anomalous relaxation in complex systems: from stretched to compressed exponentials* indicates another fundamental aspect considered, namely the non-trivial interplay between anomalous relaxation and anomalous transport. In this context recent results for soft glassy materials and granular systems are highlighted. The second contribution by Walter Kob and his coworkers, *Anomalous transport in glassforming liquids*, basically reviews recent progress with a prototype model for structural glass formers, the binary Lennard-Jones fluid. For this model, which is generally accepted as capturing essentials of real glassforming liquids, molecular dynamics simulations give detailed insights into the microscopic processes involved in the self-organized emergence of disorder in these systems. In addition, it allows the testing of concepts such as mobile regions and basins in configuration space of these many particle systems and its signatures in measurable quantities. The third chapter in this part, *Subdiffusion limited reactions* by Santos Bravo Yuste, Katja Lindenberg, and Juan Jesus Ruiz-Lorenzo, introduces another important aspect into the field of anomalous transport, the possibility of reactions or transformations between e.g. chemical species. While reaction-diffusion processes for the case of normal diffusion and the governing partial differential equations are nowadays well understood, research on their analogue in case of subdiffusive processes, most relevant for disordered systems, is still in its in-

fancy. This article reviews the state of the art and the unsolved problems in this field. The last contribution of this part by Karl Heinz Hoffmann and Janett Prehl considers in depth one of the important system classes leading to subdiffusive behavior, systems with an approximately fractal structure. In the chapter *Anomalous transport on disordered fractals* first the fundamentals of anomalous transport on regular fractals, including the possible numerical treatments are reviewed. Based on that, a detailed study of the subtle influence of disorder within the fractal structure is presented. Among others it is explained how disorder, counter intuitively, may even enhance transport in comparison to the regular case. The short-comings of fractional partial differential equations, as treated in Part I of this book, for the description of transport on fractals are pointed out and alternative approaches based on similarity groups are presented.

11

Anomalous Relaxation in Complex Systems: From Stretched to Compressed Exponentials

Jean-Philippe Bouchaud

11.1

Introduction

Normal diffusion usually refers to plain Brownian motion and describes situations where the mean-square displacement of a particle (or the variance of the (log)-price of a financial asset) grows linearly with time. This property is in general only valid when time is sufficiently large compared to a microscopic correlation time. The diffusion law $R^2 \propto Dt$ is indeed tantamount to a complete decorrelation between successive displacements. *Anomalous diffusion*, on the other hand, describes all other cases, where the normal diffusion law fails to describe the data, at least over some time interval $[t_<, t_>]$ where the logarithmic slope $2\nu(t) \equiv \partial \ln R^2 / \partial \ln t$ is observed to be either smaller than one (subdiffusion) or larger than one (superdiffusion) [1]. Of course, the effect is only interesting if the time interval $[t_<, t_>]$ is wide enough to delimit a genuinely anomalous regime, and not a trivial crossover. One mechanism leading to anomalous diffusion is the existence of persistent (or antipersistent) correlations up to time interval $t_>$. Positive correlations of displacements lead to superdiffusion, whereas negative correlations lead to subdiffusion. For example, diffusion of particles in hydrodynamical flows often lead to superdiffusion since particles are coherently convected along streamlines over some length scale [1]. Conversely, particles in a potential field tend to be trapped in minima, where they execute numerous back-and-forth oscillations, and therefore anticorrelated motion, before being able to escape [1]. Another important mechanism generating superdiffusion is the existence of *jumps* with a broad distribution of possible sizes, leading to “Lévy flights” [2].

Normal diffusion is also characterized by a Gaussian diffusion profile, i.e., the distribution of the displacement \vec{R} between t_0 and $t_0 + t$ is given by

$$P(\vec{R}, t) = \frac{1}{(\sqrt{4\pi D t})^d} \exp \left[-\frac{R^2}{4Dt} \right]. \quad (11.1)$$

The relaxation of a density fluctuation of wavevector \vec{q} , created at time t_0 , is easily computed to be *exponential*:¹

$$C(\vec{q}, t) = \frac{1}{N} \left\langle \sum_j \exp [i\vec{q} \cdot (\vec{r}_j(t_0 + t) - \vec{r}_j(t_0))] \right\rangle = \exp(-Dq^2 t), \quad (11.2)$$

with relaxation time $1/Dq^2$ equal to the diffusion time over the scale $1/q$. Therefore, normal diffusion is associated to what is usually considered to be “normal” – i.e., exponential – relaxation. The aim of this short review is to discuss possible forms of anomalous relaxation in complex systems, in particular the relation between anomalous diffusion and nonexponential relaxation.

11.2

Stretched Exponential Relaxations

Stretched exponential relaxation refers to cases where the correlation function decays as $\ln C(t) \propto -t^\beta$ with $\beta < 1$. A simple model where this behavior is exactly observed is the case where subdiffusion is induced by an antipersistent Gaussian process (also called *fractional Brownian motion* [3]), in which case the diffusion profile is given by

$$P(\vec{R}, t) = \frac{1}{(\sqrt{4\pi D_\beta t^\beta})^d} \exp \left[-\frac{R^2}{4D_\beta t^\beta} \right], \quad \beta < 1. \quad (11.3)$$

The density relaxation is then trivially given by $C(\vec{q}, t) = \exp(-D_\beta q^2 t^\beta)$. However, it is hard to think of a physical system for which this model applies directly. A more generic model for subdiffusion is anomalous trapping, for which, as we discuss now, the correlation indeed decays as a stretched exponential but only at small times.

11.2.1

Trapping-Induced Subdiffusion

We therefore consider the trap model where a particle hops on a regular lattice in d dimensions; each node of the lattice is an energy valley of random depth E , which traps the particle for a certain random time, before an activated event occurs and allows the particle to jump to a neighboring site. One

1) Here we imagine that particles do not interact and that there is no difference between the individual and collective diffusion constant D . More generally, there is a difference between the relaxation of tracer particles (of small concentration) and of the density of interacting host particles.

should distinguish the *annealed* case where the depth E is drawn anew at every jump of the particle from the *quenched* case where the depth E of each site is drawn once and for all and does not evolve with time. However, in $d > 2$, the particle typically visits each trap a finite number of times and the difference between the two models is immaterial at long times. We will therefore focus on the first case, which is much easier to solve analytically, and return to the quenched case in $d = 1$ at the end of this section.

Conditioned to being in a trap of depth E and at temperature T , the exit time τ is distributed according to

$$\Psi_E(\tau) = \Gamma_0 e^{-\beta E} e^{-(\Gamma_0 e^{-\beta E})\tau}, \quad (11.4)$$

where Γ_0 is a microscopic frequency and $\beta \equiv 1/T$ (we set $k_B = 1$ throughout the paper). If $\rho(E)$ denotes the *a priori* probability distribution of the depth E of the traps, the particle performs a random walk among traps with a distribution of trapping times

$$\Psi(\tau) = \int_0^\infty dE \rho(E) \Psi_E(\tau). \quad (11.5)$$

We will consider below the case where $\rho(E) = 1/T_g \exp(-E/T_g)$ (exponential model), for which a true dynamical phase transition appears: diffusion is asymptotically normal for $T > T_g$, but subdiffusion set in for $T < T_g$, with an anomalous diffusion exponent ν (defined in Section 11.1) given by $\nu = T/2T_g < 1/2$. The exponential model is such that the upper limit $t_>$ of the time domain where subdiffusion is observed is infinite. Other cases could be considered as well, such as a Gaussian distribution of depths, but in that case $t_>$ would be finite and a crossover to normal diffusion would eventually set in. However, the following conclusions will still hold in an intermediate time domain, which can become very large when $T \rightarrow 0$ (see the detailed discussion in [4]).

Interestingly, the subdiffusive phase $T < T_g$ of the exponential model is also *nonstationary*, in the sense that all dynamical properties depend on the age of the system [4–6]. More precisely, if the initial ($t_0 = 0$) position of the particle is chosen randomly, the two-time correlation function

$$C(\vec{q}, t + t_w, t_w) = \left\langle e^{i\vec{q} \cdot (\vec{r}(t+t_w) - \vec{r}(t_w))} \right\rangle \quad (11.6)$$

strongly depends on t_w for $T < T_g$, but becomes time translation invariant and given by Eq. (11.2) for $T > T_g$, at least when $\Gamma_0 t_w \gg 1$. The *aging* properties of the low-temperature phase are strongly reminiscent of the phenomenology of glasses and spin glasses below their glass transition [7], hence justifying the notation T_g for the critical temperature of the model.

The exact computation of $C(\vec{q}, t + t_w, t_w)$ was presented in [4]. After a series of manipulations, one obtains the following result for the Laplace transform $\tilde{C}(\vec{q}, \lambda, t_w) = \int_0^\infty dt e^{-\lambda t} C(\vec{q}, t + t_w, t_w)$:

$$\tilde{C}(\vec{q}, \lambda, t_w) = \tilde{\Pi}(\lambda, t_w) \left[\frac{1 - \zeta_d(\vec{q})}{1 - \tilde{\Psi}(\lambda) \zeta_d(\vec{q})} \right] + \frac{1}{\lambda} \frac{1 - \tilde{\Psi}(\lambda)}{(\zeta_d(\vec{q}))^{-1} - \tilde{\Psi}(\lambda)}, \quad (11.7)$$

where we have introduced

$$\zeta_d(\vec{q}) = \frac{1}{d} \sum_{\kappa=1}^d \cos(q_\kappa a) \quad (11.8)$$

and the following Laplace transforms:

$$\tilde{\Psi}(\lambda) = \int_0^\infty d\tau e^{-\lambda\tau} \Psi(\tau); \quad \tilde{\Pi}(\lambda, t_w) = \int_0^\infty dt e^{-\lambda t} \Pi(t + t_w, t_w), \quad (11.9)$$

where $\Pi(t + t_w, t_w)$ is the probability not to have jumped between t_w and $t_w + t$. The above formulas are general and do not depend on the specific choice of $\rho(E)$. In the case of an exponential density of trap depths, and when $\mu = T/T_g < 1$, the correlation function Π is known and its Laplace transform reads [4, 6]

$$\tilde{\Pi}(\lambda, t_w) \simeq \frac{1}{t_w} \int_0^\infty du e^{-(\lambda t_w)u} \frac{\sin \pi \mu}{\pi} \int_{\frac{u}{1+u}}^1 dv (1-v)^{\mu-1} v^{-\mu} \quad (11.10)$$

with the asymptotic behaviors

$$\tilde{\Pi}(\lambda, t_w) \underset{\lambda t_w \ll 1}{\simeq} \frac{1}{\Gamma(1+\mu)} \frac{(\lambda t_w)^\mu}{\lambda} \quad (11.11)$$

$$\tilde{\Pi}(\lambda, t_w) \underset{\lambda t_w \gg 1}{\simeq} \frac{1}{\lambda} \left[1 - \frac{1}{\Gamma(\mu)} \frac{1}{(\lambda t_w)^{1-\mu}} \right]. \quad (11.12)$$

Interestingly, the correlation function Π depends on the ratio t/t_w when $\mu < 1$: the characteristic time needed to leave a trap is therefore proportional to the age of the system. For $\mu > 1$, on the other hand, one would find that Π only depends on $\Gamma_0 t$ and not on t_w – the problem is *time translation invariant* in that case, as usual for equilibrium dynamics.

Coming back to Eq. (11.7), it is convenient to introduce the subdiffusion time t_q defined as

$$(\Gamma_0 t_q)^\mu = \frac{2d}{(qa)^2} \quad (11.13)$$

corresponding to the typical time needed by the particle to spread over a region of size $1/q$. There are therefore three time scales in (11.7): λ^{-1} , t_q , t_w . We

are interested in the region where all three are much larger than the microscopic time scale Γ_0^{-1} , where the results become universal in the sense that they only depend on the exponential form of $\rho(E)$ at large E , and not on the details of $\rho(E)$ for finite E . Still we have to distinguish various time regimes in (11.7). Let us first consider *young* systems, for which $t_w \ll t_q, t$. In this case, we find that at small times $t \ll t_q$, the correlation decays as a stretched exponential with exponent $\mu < 1$:²

$$\ln C(\vec{q}, t + t_w, t_w) \simeq -\frac{\text{sinc}[\pi\mu]}{\Gamma(1+\mu)} \left(\frac{t}{t_q}\right)^\mu \quad \text{for } t_w \ll t \ll t_q, \quad (11.14)$$

whereas at large times $t \gg t_w$, the correlation decays as a power law (much slower than a stretched exponential):

$$C(\vec{q}, t + t_w, t_w) \simeq \Gamma(1+\mu) \left(\frac{t}{t_q}\right)^{-\mu} \quad \text{for } t_w \ll t_q \ll t. \quad (11.15)$$

In the aging regime, on the other hand, we find at small times

$$\ln C(\vec{q}, t + t_w, t_w) \simeq -\text{sinc}[\pi(1-\mu)] \left(\frac{t}{t_w}\right)^{1-\mu} \quad \text{for } t_q \ll t \ll t_w, \quad (11.16)$$

$$\ln C(\vec{q}, t + t_w, t_w) \simeq -\frac{\text{sinc}[\pi\mu]}{\Gamma(\mu)} \frac{t}{t_q^\mu t_w^{1-\mu}} \quad \text{for } t \ll t_w \text{ and } t \ll t_q \quad (11.17)$$

and finally, at long times:

$$C(\vec{q}, t + t_w, t_w) \simeq \text{sinc}[\pi\mu] \left(\frac{t}{t_w}\right)^{-\mu} \quad \text{for } t_q \ll t_w \ll t \quad (11.18)$$

There are four interesting points to notice:

- For qa very large, such that $t_q \ll t, t_w$, we find the same asymptotic behaviors as for $\Pi(t + t_w, t_w)$. Physically, this means that as soon as the particle has jumped once, the rapidly oscillating correlation function averages to zero. Hence, only the particles *which have not yet moved* contribute to the correlation.
- There are two regimes where the correlation function behaves similarly to a stretched exponential, but *only at small times*, when $t_q \ll t \ll t_w$ or $t_w \ll t \ll t_q$. The exponent β of this stretched exponential is however different in both cases: it is equal to $\beta = \mu$ when $t_w \ll t \ll t_q$, and equal to $\beta = 1 - \mu$ in the other case.
- In the regime $t \ll t_w, t_q$, we find an interesting subaging behavior, where $C(\vec{q}, t + t_w, t_w)$ is a function of $t/t_w^{1-\mu}$, see the discussions in [7–9].

2) We define in the following $\text{sinc}x = \sin x/x$.

- The frequency-dependent susceptibility defined by

$$\begin{aligned}\chi(\vec{q}, \omega, t_w) &= 1 + i\omega \int_0^\infty dt e^{i\omega t} C(\vec{q}, t_w + t, t_w) \\ &\equiv 1 + i\omega \tilde{C}(\vec{q}, -i\omega, t_w),\end{aligned}\quad (11.19)$$

behaves in a Cole–Cole fashion for young systems:

$$\chi(\vec{q}, \omega, t_w = 0) \simeq \frac{1}{1 + (-i\omega t_q)^\mu} \quad (11.20)$$

for $\omega \ll \Gamma_0$, $qa \ll 1$. In the aging regime $\omega t_w \gg 1$, the behavior of χ is given by

$$\chi(\vec{q}, \omega, t_w) \simeq \frac{1}{\Gamma(\mu)(-i\omega t_w)^{1-\mu}}. \quad (11.21)$$

A similar expression was obtained in the context of spin glasses in [6], and discussed further in the context of experimental data in [7]. Note that the noise spectrum $S(\omega)$ of the system is related to the susceptibility through a fluctuation–dissipation relation $S(\omega) \propto \chi''(\omega)/\omega$.

Two further remarks on this spatial-trap model: (a) the marginal case $T = T_g$, $\mu = 1$ is quite interesting, since it exhibits exact dynamical ultrametricity [10] and weakly aging $1/f$ noise, see Eq. (11.21) above and [6, 7]; (b) the quenched case in $d = 1$ reveals a number of subtle peculiarities, discussed in [8]. In particular, the diffusion exponent ν is now given by $\nu = \mu/(1 + \mu)$. Using the results of [8], one finds that in the case of *young* systems, the result for the correlation function reads

$$\ln C(\vec{q}, t + t_w, t_w) \sim - \left(\frac{t}{t_q} \right)^{\frac{2\mu}{1+\mu}}; \quad C(\vec{q}, t + t_w, t_w) \sim \left(\frac{t_q}{t} \right)^\mu, \quad (11.22)$$

for $t \ll t_q$ and $t \gg t_q$, respectively, with now t_q given by $qa(\Gamma_0 t_q)^\nu = 1$. The above shape is different from the annealed case, but the initial decay is still of the stretched exponential type. The asymptotic behavior of $C(\vec{q}, t + t_w, t_w)$ in the aging regime can also be inferred from the results of [11]. We also refer to Refs. [12] for more work on the trap model and some application to glassy dynamics.

11.2.2

Two-Step Relaxation

In the above model, there is no intranode dynamics: traps are assumed to have no spatial extension. This is clearly unrealistic and the short-time, high- q behavior of the correlation function should be sensitive to the intratrapping dynamics. As a simple model for this, we consider harmonic potential wells

again organized at the node of a regular lattice. Each particle oscillates at the bottom of the well, and with a small probability per unit time proportional to $\Lambda = \Gamma_0 \exp(-E/T)$ the particle hops to its nearest neighbor site, where it lands at random with the equilibrium probability inside the harmonic well. We neglect for the moment the fluctuations of E , which is justified when $T \gg T_g$. The position of a particle at time t will be written as

$$\vec{r}(t) = \vec{R}(t) + \vec{\delta}(t), \quad (11.23)$$

where $\vec{R}(t)$ labels the lattice site to which the particle “belongs” at time t , and $\vec{\delta}(t)$ is the position of the particle within the well, the center of the well being defined by $\vec{\delta}(t) = 0$. The probability for the particle not jumping site between t_0 and $t_0 + t$ is

$$\Pi(t) = \exp(-\Lambda t). \quad (11.24)$$

If the particle has not jumped, then $\delta(t_0 + t) - \delta(t_0)$ is a Gaussian variable of variance given by

$$\langle (\delta(t_0) - \delta(t_0 + t))^2 \rangle = 2\Delta_0^2[1 - \exp(-\gamma t)], \quad (11.25)$$

where Δ_0 is the width of the explored region of the well, and γ the inverse relaxation time in the well. If on the other hand at least one jump has occurred between t_0 and $t_0 + t$, one has

$$\langle (\delta(t_0) - \delta(t_0 + t))^2 \rangle = 2\Delta_0^2. \quad (11.26)$$

Our aim is again to compute the correlation function

$$C(\vec{q}, t) = \langle e^{i\vec{q} \cdot (\vec{r}(t_0) - \vec{r}(t_0 + t))} \rangle. \quad (11.27)$$

This quantity can be easily computed by separating the no jump situations from the situations where at least one jump has taken place. One finds

$$\begin{aligned} C(\vec{q}, t) &= \Pi(t) e^{-q^2 \Delta_0^2 [1 - \exp(-\gamma t)]} \\ &\quad + (1 - \Pi(t)) e^{-q^2 \Delta_0^2} \langle e^{i\vec{q} \cdot (\vec{R}(t_0) - \vec{R}(t_0 + t))} \rangle_J, \end{aligned} \quad (11.28)$$

where the subscript J indicates that at least one jump has taken place. Clearly, this last average is related to the unconditional average by

$$\langle e^{i\vec{q} \cdot (\vec{R}(t_0) - \vec{R}(t_0 + t))} \rangle = \Pi(t) + (1 - \Pi(t)) \langle e^{i\vec{q} \cdot (\vec{R}(t_0) - \vec{R}(t_0 + t))} \rangle_J. \quad (11.29)$$

Finally, the unconditional average is a classic result of random walk theory on lattices:

$$\langle e^{i\vec{q} \cdot (\vec{R}(t_0) - \vec{R}(t_0 + t))} \rangle = \exp[\Lambda t(\zeta_d(\vec{q}) - 1)]. \quad (11.30)$$

In the limit $qa \ll 1$, the final result reads (see [13] for similar calculations):

$$C(\vec{q}, t) = \Pi(t) \left[e^{-q^2 \Delta_0^2 [1 - \exp(-\gamma t)]} - e^{-q^2 \Delta_0^2} \right] + e^{-q^2 \Delta_0^2} e^{-\Lambda(qa)^2 t}. \quad (11.31)$$

Note that $C(\vec{q}, t=0) = C(\vec{q}=0, t) = 1$, as it should. Suppose $\Lambda t \ll 1$ (i.e., the probability of a jump is very small, $\Pi(t) \approx 1$) and $\gamma t \gg 1$, corresponding to full equilibration within the initial well. In this limit, one then finds

$$C(\vec{q}, t) \approx f [1 + q^2 \Delta_0^2 \exp(-\gamma t)], \quad (11.32)$$

i.e., an exponential convergence toward a plateau value $f = e^{-q^2 \Delta_0^2}$. If on the other hand $\Lambda t \ll 1$, many jumps have occurred ($\Pi(t) \approx 0$) and

$$C(\vec{q}, t) \approx f e^{-\Lambda(qa)^2 t}. \quad (11.33)$$

The parameter f measures the relative weight of the two relaxation processes (intratrap and intertrap); and has the following interpretation: if one plots the above relaxation function in a log–lin representation, one observes two-step relaxation, with a *quasplateau* of the correlation function, of height f . The fast, intratrap process does lead to a complete decorrelation – on the contrary, for time scales much smaller than γ^{-1} , the system appears to be nonergodic (it keeps a nonzero correlation with its initial state); the strength of this non-ergodicity is measured by f . The quantity f is called the nonergodicity, or Edwards–Anderson parameter, in the context of glassy dynamics. The above simple model also allows to discuss in very simple terms the non-Gaussian parameter α often discussed in this context. A purely Gaussian probability density is such that $\ln C(\vec{q}, t) \propto q^2$. The kurtosis α is in fact related to the coefficient of the q^4 term of the expansion of $\ln C(\vec{q}, t)$ in the vicinity of $\vec{q} = 0$. One finds that $\alpha(t) \sim [1 - \Pi(t)]/t^2$ for small t and $\alpha(t) \sim \Pi(t)/t^2$ at large t . In the naive model above, $1 - \Pi(t) = \Lambda t$ at small t , leading to a diverging kurtosis at small times. This is however an artefact of the instant “jump” description of the way a particle exits from a trap. A more realistic model should account for the fact that the time needed to exit a trap cannot be infinitely small, leading to a much smaller value of $1 - \Pi(t)$ at small t and therefore a vanishing $\alpha(t)$ in that limit. Therefore, we expect $\alpha(t)$ to peak around the typical time needed to exit a trap, before decaying back to zero at larger times, as often seen in experimental or numerical data (see, e.g., [14]).

When the fluctuations of the depths E are reinstalled, in particular in the glassy phase $T < T_g$, one finds that the above short-time behavior of $C(\vec{q}, t)$ is unaffected, while the long-time behavior is still given by the expression of the previous section, up to a factor f which describes the initial fast fall-off of the correlation function.

11.2.3

Superposition of Relaxation Times and Stretched Exponentials

In the models considered above, the stretching of the relaxation is associated to (sub-)diffusive entities. This needs not be the case; in some cases there is relaxation but no transport. Suppose, for example, that the physics is governed by two-level systems, rotors, or dipoles which do not wander in space at all, but feel a random field which makes the local relaxation time τ random as well. More precisely, suppose that there is a whole spectrum of independent, exponential relaxation processes, with a density of relaxation times $\rho(\tau)$, and that each elementary relaxation process contributes equally to the correlation function, so that

$$C(t) = \int_0^\infty \rho(\tau) e^{-t/\tau} d\tau. \quad (11.34)$$

Suppose further that the resulting correlation function $C(t)$ can be well fitted by a stretched exponential:

$$C(t) \approx \exp - (\gamma t)^\beta, \quad (11.35)$$

what can we infer about the shape of the density of relaxation times $\rho(\tau)$? After a very small time, the correlation function has dropped from its initial value of 1 by an amount $\Delta C \sim \int_0^t \rho(\tau) d\tau$: all relaxation times larger than t have not had time to relax yet, whereas all relaxation times smaller than t have already relaxed. Equating this result with the initial decay of the stretched exponential, one finds

$$\int_0^t \rho(\tau) d\tau \approx (\gamma t)^\beta \longrightarrow \rho(\tau) \propto_{\tau \rightarrow 0} \gamma^\beta \tau^{\beta-1}, \quad (11.36)$$

showing an (integrable) divergence of the density of small relaxation times.

Therefore, although stretched exponential relaxation is usually associated with *slow* relaxation, the above result implies a *profusion of short-time scales* in the system. However, since the long-time behavior of the relaxation is much slower than an exponential, there must also be abundant long-time scales. How abundant can be guessed by a saddle point calculation? Suppose that $\rho(\tau)$ decays itself, for large τ as $\exp(-B\tau^{\beta'})$. This implies, for large t , a decay of $C(t)$ given by

$$\ln C(t) \simeq - \frac{B^{1-\beta}}{\beta^\beta (1-\beta)^{1-\beta}} t^\beta \quad \beta \equiv \frac{\beta'}{1+\beta'}, \quad (11.37)$$

up to subleading power-law corrections. For example, a significantly stretched relaxation $\beta = 0.5$ corresponds to $\beta' = 1$, i.e., an exponential decay of long-relaxation times [15]. Therefore, only a very limited density of

very large relaxation times is enough to transform a pure exponential relaxation into a stretched one. The pure exponential case corresponds formally to $\beta' = \infty$, i.e., no long times at all.

More generally, any nontrivial distribution of relaxation times leads to a relaxation function that is faster than exponential on short times and slower than exponential on large times, in the following sense: define the average relaxation time as $\langle \tau \rangle = \int_0^\infty C(t) dt = \int_0^\infty \tau \rho(\tau) d\tau$; the reference exponential relaxation is taken to decay over this average time. Then, the initial slope of the relaxation is given by

$$-\frac{dC}{dt} = \int_0^\infty \frac{1}{\tau} \rho(\tau) d\tau = \left\langle \frac{1}{\tau} \right\rangle \geq \frac{1}{\langle \tau \rangle}, \quad (\text{provided } \left\langle \frac{1}{\tau} \right\rangle < +\infty), \quad (11.38)$$

where the equality is reached only if there is a single relaxation time scale, $\rho(\tau) = \delta(\tau - \gamma^{-1})$. Conversely, for large time scales, one can easily show that the relaxation can only be slower than $\exp(-t/\langle \tau \rangle)$.

An important case, which superficially corresponds to the trap model discussed above, is

$$\rho(\tau) = \frac{\mu \tau_0^\mu}{\tau^{1+\mu}} \Theta(\tau - \tau_0), \quad (11.39)$$

i.e., a power-law density of relaxation times. The cutoff for small τ (that could be chosen to be less abrupt) and the condition $\mu > 0$ are needed for the distribution to be normalizable. Because of the cutoff, $\left\langle \frac{1}{\tau} \right\rangle < +\infty$; the initial slope of the $C(t)$ is then finite and the short-time decay is regular, at variance with the stretched exponential case described above. However, the long-time decay is in that case much slower than stretched exponential:

$$C(t) = \int_{\tau_0}^\infty \frac{\mu \tau_0^\mu}{\tau^{1+\mu}} e^{-t/\tau} d\tau \simeq_{t \rightarrow \infty} \Gamma(\mu) \left(\frac{\tau_0}{t} \right)^\mu. \quad (11.40)$$

The above result is valid for all values of μ , in particular when $\mu < 1$, which corresponds to an infinite average relaxation time. At this stage, the reader might feel completely nonplussed: why all the *aging properties* that we found within the trap model when $\mu < 1$ seem to have disappeared? The answer is that the two models are in fact fundamentally different. In the trap model, particles progressively discover their environment and, as they explore space further, they fall in deeper and deeper traps which they never encountered before. When $T < T_g$, the deepest trap encountered at time t_w is so much deeper than all the others that it dominates the dynamics. In the second model, on the other hand, there is a relaxing entity for each and every trap, and therefore the whole distribution of relaxation time is probed right away. There is no aging whatsoever in that case.

It should be noted that a stretched exponential fit to nonexponential relaxation is often an acceptable fit of empirical (or numerical) data. For example, when $\tau \propto \exp(E/T)$ with a Gaussian distribution of barrier heights, the relaxation obtained from Eq. (11.34) can still be approximatively fitted by a stretched exponential, with, as a rough rule of thumb [4]:

$$\beta \approx \frac{T}{\sqrt{T^2 + E_0^2}}, \quad (11.41)$$

where E_0 is the width of barrier distribution. When a stretched exponential fit is attempted, it is important to specify whether it is supposed to be faithful to the initial decay of the relaxation $t \leq \gamma^{-1}$, and hence to probe the profusion of high frequencies in the system, or if it is rather the long time ($t \gg \gamma^{-1}$) aspect of the phenomenon which is targeted, which is often the regime where exact analytical results are available but where the correlation is so small $-\ln C(t) \gg 1$ that it nearly impossible to measure. To illustrate this point, it is interesting to discuss the problem of survival of a Brownian particle in a random environment, where infinitely deep traps are randomly scattered in a d -dimensional space. For this problem, a rigorous result, due to Donsker and Varadhan [16], asserts that the total survival probability, averaged over the starting point of the Brownian particle, decays asymptotically as a stretched exponential, with $\beta = d/(d+2)$. This result can be simply understood using the above relation, Eq. (11.37), between β' and β : in the model at hand, long times are associated with exceptionally large regions free of traps where the particle can survive much longer than on average. These occur with probability $\ln p \propto -L^d$, and the associated survival time is $\tau(L) \sim L^2/D$, from which one immediately concludes that $\beta' = d/2$. Although this result is rigorous, its domain of validity is, in $d \geq 2$, so far into the asymptotic regime that it is of little interest, at least for numerical or experimental purposes, because the number of surviving particles in this regime is exponentially small. For intermediate times, one finds that the survival probability can be fitted by a stretched exponential, but with an effective value of $\beta \neq d/(d+2)$. We should also mention that this survival model is in fact very subtle: although the average survival probability is given by the above Donsker–Varadhan result, the survival of a given particle with fixed initial position decays as $-\ln C(t) \sim t/\ln t!$ We refer to the insightful papers of Ben Arous et al. [17, 18] for a comprehensive account of this result.

11.3

Models of Compressed Exponentials

Again, a trivial model leading to both superdiffusion and compressed exponential relaxation (i.e., $\beta > 1$) is when the noise driving the particle is a long-ranged persistent Gaussian process, in which case the diffusion profile is given by

$$P(\vec{R}, t) = \frac{1}{(\sqrt{4\pi D_\beta t^\beta})^d} \exp\left[-\frac{R^2}{4D_\beta t^\beta}\right], \quad \beta > 1 \quad (11.42)$$

and therefore $C(\vec{q}, t) = \exp(-D_\beta q^2 t^\beta)$, which is faster than exponential when $\beta > 1$. As we noticed for antipersistent Brownian motion, physical situations where this model applies directly are scarce. In fact, natural models for superdiffusion do *not* lead to compressed exponentials, as we now discuss. We then turn to the necessary ingredients needed to explain why compressed exponential relaxations have recently been observed in a variety of soft glassy materials – where one would have rather expected, because of their glassiness, stretched exponentials! On the other hand, exactly as stretched exponential relaxation means superabundance of short relaxation times, compressed exponential relaxation requires that no fast relaxation channels exist.

11.3.1

Superdiffusion and Lévy Flights

The best known model of superdiffusion is a random walk with a distribution of jump size ℓ , which decays for large ℓ as

$$P(\ell) \sim \frac{\mu \ell_0^\mu}{\ell^{1+\mu}}, \quad (11.43)$$

with $\mu < 2$ such that the variance of the distribution diverges. In this case, one knows that for large times, the distribution of the total displacement of the particle is given by a Lévy stable law of index μ :³

$$P(R, t) \propto \frac{1}{t^\nu} L_\mu\left(\frac{R}{t^\nu}\right); \quad \nu = \frac{1}{\mu}, \quad (11.44)$$

where we have been sloppy with prefactors and constants. The crucial point is that although L_μ has no simple expression in general (except for $\mu = 2$ where it reduces to the Gaussian and $\mu = 1$ where it is the Cauchy distribution), its Fourier transform is extremely simple. In fact, the relaxation of a density perturbation is an unspectacular exponential:

$$C(q, t) = \exp(-D q^\mu t). \quad (11.45)$$

³) For simplicity, we restrict here to one-dimensional Lévy flights.

Although diffusion is anomalous, relaxation is normal! The only anomalous feature is the scaling of the wavevector q , raised to the power μ rather than q^2 for normal diffusion. Exactly this behavior was observed for tracer particles in a system of polydisperse, elongated micelles [19]. The very strong contrast between the diffusion constant of small micelles and long micelles was argued to be responsible for the broad distribution of jump sizes, and in turn for the Lévy flight motion clearly observed experimentally [19].

Another well-studied case of superdiffusion is random advection in long range correlated hydrodynamical flows. Consider the following Langevin equation for a particle in a $d = 3$ random flow:

$$\frac{d\vec{x}}{dt} = -\vec{V}(\vec{x}) + \vec{\eta}(\vec{x}, t), \quad (11.46)$$

where $\vec{\eta}$ is the usual Langevin noise and \vec{V} is a divergence free random convection field, with long-ranged correlations:

$$\langle V_i(\vec{x}) V_j(\vec{y}) \rangle \underset{|\vec{x}-\vec{y}| \rightarrow \infty}{\simeq} T_{ij} |\vec{x} - \vec{y}|^{-a}, \quad a < 2, \quad (11.47)$$

where T is a tensor ensuring that \vec{V} is indeed an incompressible flow. This model, with $a = -2/3$ can be seen as a very rough model of tracer dispersion in a turbulent flow with Kolmogorov scaling – in order to be more realistic one should allow the flow field to become time dependent, with a correlation that includes a function of $(t - t') / |\vec{x} - \vec{y}|^{2/3}$. For the above static turbulence model, one can show that diffusion is anomalous with a diffusion exponent exactly given by $\nu = 2/(2 + a) > 1/2$ (see [1]), leading to the Richardson scaling $\nu = 3/2$ for $a = -2/3$. The shape of diffusion profile at large times is not exactly known. However, since the simplest self-consistent resummation scheme of the perturbation theory for this problem (called mode coupling or direct interaction approximation (DIA) in different contexts [20]) gives the exact diffusion exponent ν , one can hope that it also leads to an accurate shape of the diffusion profile. More precisely, the DIA suggests that the Fourier–Laplace transform of $P(\vec{R}, t)$ reads, in the long wavelength, low-frequency limit [1]:

$$C(\vec{q}, \lambda) \approx \frac{1}{\lambda + Dq^{1/\nu}}, \quad (11.48)$$

which is exactly the Fourier–Laplace transform of a Lévy distribution! The interesting consequence is that diffusion in a long-range correlated hydrodynamical flow is equivalent, at long times and in the scaling regime $R \sim t^\nu$, to a Lévy flight (provided of course the DIA is trustworthy). But it also means that this model cannot generate compressed exponentials!

11.3.2

Rearrangement-Induced Stress Fields in Elastic Media

Still, one of the major experimental surprise of the last decade is the discovery of compressed exponential relaxation in a bevy of different soft matter materials, ranging from polystyrene microsphere gels, diblock copolymers, laponite, etc. [21]. These systems have very slow dynamics and rheological properties typical of glasses or jammed granular media, which would have suggested that relaxation functions would be found, as in glasses, to be stretched exponentials. More precisely, one finds experimentally that the correlation function decays as

$$C(\vec{q}, t) = \exp[-A(qt)^\beta], \quad (11.49)$$

with $\beta \approx 3/2 > 1$. A notable feature of the above result is the scaling between space and time $q^{-1} \sim t$, characteristic of ballistic effects. It was suggested early on [22] that such a result might be related to the elasticity of these materials which mediate the long-ranged stress fields generated when a local rearrangement occurs. In this section, we show how a more detailed model of the deformation induced by these local events can give rise to anomalous q and t behavior of the structure function [23].

11.3.2.1 The Model

Following [22], we assume that the dominant mechanism is the random appearance of localized rearrangements. For example, in the system studied in [22], the microparticles forming the gel attract each other rather strongly, the gel tends to restructure locally so as to create dense packings of particles. Since the collapsing particles belong to a gel network, their motion will induce a certain strain field around them; other particles therefore move and dynamical light scattering probes this motion. Similarly, in other soft elastic media, any local rearrangement will induce a strain that propagates into the system. A rearrangement of particles will result in a force dipole of intensity P_0 in a certain direction \vec{n} . When the dipole is formed at point \vec{r}_0 , the elastic strain field \vec{u} at point \vec{r} can be computed assuming a simple central force elasticity:

$$K\Delta\vec{u} = -\vec{f}(\vec{r}), \quad (11.50)$$

where K is a compression modulus and $\vec{f}(\vec{r})$ is a local force dipole of the form:

$$\vec{f}(\vec{r}) = f_0 \left[\vec{\epsilon} \cdot \vec{\nabla} \delta(\vec{r} - \vec{r}_0) \right] \vec{n}, \quad (11.51)$$

where we will assume that $\vec{\epsilon} = \epsilon\vec{n}$, i.e, the mean displacement of the particles creates a force in the same direction. This dipolar force can be simply expressed by its Fourier transform:

$$\vec{f}(\vec{k}) = iP_0 (\vec{k} \cdot \vec{n}) \vec{n} \exp(-i\vec{k} \cdot \vec{r}_0) \quad (11.52)$$

with $P_0 = f_0 \epsilon$.⁴ The solution of Eq. (11.50) is of course

$$\vec{u}(\vec{r}) = -\frac{P_0}{4\pi K} \frac{(\vec{r} - \vec{r}_0) \cdot \vec{n}}{|\vec{r} - \vec{r}_0|^3} \vec{n}. \quad (11.53)$$

The r^{-2} dependence of the strain field has an immediate consequence which will be of importance in the following: if there is a finite density of force dipoles randomly scattered in space, the probability that the stress at a given point has an amplitude u decays for large u as $u^{-5/2}$, which has a diverging variance. (This divergence is however cutoff if the finite size of the dipoles is taken into account). This property of the distribution of displacements and stresses will be responsible for the unusual q -dependence of the correlation function.

Now, let us assume that the rearrangement events are not instantaneous but take place slowly, over a certain time scale θ . This will turn out to be crucial in the following. A given event j starts at time t_j and is completed at time $t_j + \theta$; the dipole intensity $P(t)$ at time t is a certain function of $(t - t_j)/\theta$, which can be taken to be approximately linear: $P_j(t) = P_0(t - t_j)/\theta$ before saturating at P_0 when the collapse is completed. The dynamics of the individual particles is presumably dominated by viscous friction, therefore we write the following equation of motion for the strain field \vec{u} :

$$\gamma \frac{\partial \vec{u}(\vec{r}, t)}{\partial t} = K \Delta \vec{u} + \sum_j \vec{f}_j(\vec{r}, t) + \vec{\eta}(\vec{r}, t), \quad (11.54)$$

where the Fourier transform of the dipolar force is

$$\vec{f}_j(\vec{k}, t) = iP_j(t) (\vec{k} \cdot \vec{n}_j) \vec{n}_j \exp(-i\vec{k} \cdot \vec{r}_j) \quad (11.55)$$

and γ is a friction coefficient, and $\vec{\eta}$ is the thermal random force due to the viscous bath, uncorrelated in time and in direction. We will finally assume in the following that these events occur randomly in space and time, with a certain rate ρ per unit volume and unit time, and with a random orientation of the force dipole \vec{n} . The quantity K/γ is a diffusion constant that we will call D . Equation (11.54) defines the model that we want to study and from which we will compute the correlation function (or dynamical structure factor) $C(q, t)$, defined as

$$C(q, t) = \langle \exp [i\vec{q} \cdot (\vec{u}(\vec{r}, t_0 + t) - \vec{u}(\vec{r}, t_0))] \rangle, \quad (11.56)$$

where the brackets refer to a spatial average over \vec{r} or, equivalently, over the random location and time of the rearrangement events. In the following, we

4) Note that a more refined model with shear modulus could also be considered, but would only change some numerical factors in the following calculations.

will neglect the thermal random force, which would add a Debye–Waller short time diffusive contribution to the dynamical structure factor, and set $\vec{\eta} = 0$. However, the presence of $\vec{\eta}$ has an indirect crucial effect since the local rearrangements are probably thermally activated.

11.3.2.2 The Slow Rearrangement Regime

A first step is to calculate the Fourier transform of the *time derivative* of the displacement field $\vec{u}(\vec{r}, t)$ created by a single dipole located at \vec{r}_j , in direction \vec{n}_j , that we denote $\vec{v}(\vec{k}, t|\vec{r}_j, \vec{n}_j, t_j)$. One finds

$$\begin{aligned}\vec{v}(\vec{k}, t|\vec{r}_j, \vec{n}_j, t_j) &= -i\exp(-i\vec{k} \cdot \vec{r}_j) \frac{P_0 \vec{n}_j}{\theta} \frac{\vec{n}_j \cdot \vec{k}}{Kk^2} \exp(-Dk^2 t) \\ &\quad \left[\exp(Dk^2 t_j) - \exp(Dk^2 \min(t_j + \theta, t)) \right].\end{aligned}\quad (11.57)$$

The displacement difference between t and $t + \tau$ can therefore be expressed as

$$\vec{u}(\vec{r}, t_0 + t) - \vec{u}(\vec{r}, t_0) = \int_{t_0}^{t_0+t} dt' \sum_{j/t_j < t'} \int \frac{d^3 \vec{k}}{(2\pi)^3} \exp(i\vec{k} \cdot \vec{r}) \vec{v}(\vec{k}, t_0|\vec{r}_j, t_j). \quad (11.58)$$

The analysis of this expression reveals that there are several cases to consider for the relative position of the time t_j when the j th event takes place and the other relevant times. We refer to [23] for further details. In the course of the analysis, one finds that a new, q -dependent time scale τ_q appears, defined as

$$\tau_q \equiv \frac{D\theta}{qv_0} \theta, \quad (11.59)$$

such that, depending on the ratio t/τ_q , the dominant contribution to the decay of $C(q, t)$ comes from different regions of the t', t_j plane. In the slow regime where the rearrangement time θ is larger than the lag t , the final result reads

$$C(q, t) = \exp \left[-A' \rho \theta (D\theta)^{3/2} \left(\frac{t}{\tau_q} \right)^{3/2} \right] \quad (t \ll \tau_q), \quad (11.60)$$

which has the compressed exponential form found in [22], in particular, it indeed only depends on $(qt)^{3/2}$. (The numerical value of the prefactor A' can be computed exactly to be 1.67996...) This result is however only valid in the short-time regime $t \ll \theta$ and $t \ll \tau_q$. Note that the combination $\hat{\rho} \equiv \rho \theta (D\theta)^{3/2}$ is adimensional and represents the average number of events taking place within a time interval θ and within a diffusion volume $(D\theta)^{3/2}$.

11.3.2.3 Other Regimes

Other regimes can be analyzed similarly (see [23]), and lead to different scaling behaviors for $C(q, t)$. A summary of the results in terms of $\Xi(q, t) \equiv$

$-\log C(q, t)$ is as follows. The two physical cases depend on the relative position of τ_q and $\tilde{\tau}_q = qv_0/D = \theta^2/\tau_q$. For $D\theta \ll qv_0$ one finds $\tau_q \ll \theta \ll \tilde{\tau}_q$ and:

$$\Xi \sim \begin{cases} (qt)^{3/2} & (t \ll \tau_q); \\ (qt)^{5/4} & (\tau_q \ll t \ll \tilde{\tau}_q); \\ q^{3/2}t & (t \gg \tilde{\tau}_q). \end{cases} \quad (11.61)$$

Note the appearance of a second compressed exponential regime with $\beta = 5/4$. For $D\theta \gg qv_0$, this $(qt)^{5/4}$ regime is squeezed out and the results are simply:

$$\Xi \sim \begin{cases} (qt)^{3/2} & (t \ll \theta); \\ q^{3/2}t & (t \gg \theta), \end{cases} \quad (11.62)$$

where we have skipped all prefactors. The late time, purely exponential regime in $q^{3/2}t$ in fact reads: $\rho v_0^{3/2} q^{3/2} t$, which can be simply understood. The factor ρt simply counts the average number of events per unit volume between t_0 and $t_0 + t$, and $q^{3/2}$ reflects the fact that the distribution of local displacements u decays as $u^{-5/2}$ and has a diverging variance. For a distribution with a finite variance, one would obtain the usual q^2 dependence.

The mechanism leading to a compressed exponential at short times is the fact that the motion of particles is not diffusive in this regime, but rather ballistic, due to a local drift of the structure imposed by slow events taking place elsewhere. Clearly, if θ was very small (corresponding to instantaneous rearrangements), one would lose the compressed exponential behavior altogether and observe simple exponential decay with an anomalous $q^{3/2}$ scaling, exactly as for Lévy flights (see Eq. (11.45)). The fact that the motion of particles is *coherent* over a rather long time scale θ is crucial to observe the small time slow decorrelation $1 - C(t) \sim t^{3/2}$. As recently noted [24], this ballistic-like motion might be a generic property of glassy system, where “crossing a barrier” means a slow, collective rearrangement of many particles in an orderly manner. There might therefore be deep interrelations between compressed exponential relaxation, cooperative effects, and dynamical heterogeneities (for recent reviews, see [14, 25, 26] and references therein).

11.4 Conclusion

We have tried to give an overview of the physical mechanisms leading to *anomalous relaxation*, and the relation of this phenomenon with anomalous diffusion and transport. Whereas in some cases these two notions are indeed deeply related, this needs not to be the case. We have shown in particular that

stretched exponential relaxation can be found in trap models where subdiffusion occurs, but only as a short time approximation, and in a nonstationary (aging) situation. At long times, the relaxation becomes a power law in time. We have pointed out that stretched exponential relaxation, while being slow at long times, in fact reveals the existence of *fast* relaxation processes at short times. We have emphasized the fact that any distribution of relaxation times will lead to a relaxation function resembling, at least within some time interval, a stretched exponential; therefore one should be very careful about the physical consequences one infers from a stretched exponential fit of experimental (or numerical) data points, in particular the physical meaning of the stretching exponent β .

Models leading to compressed exponentials are much more scarce. In particular, the dynamical structure factor of particles undergoing Lévy flight motion is a simple exponential in time. Similarly, superdiffusion in random advection flows lead, at least within some approximations, to a simple exponential in time; it would be interesting to know under what conditions this is an exact result. Still, compressed exponentials have now been observed in a variety of systems, from soft glassy materials to granular packs. We have discussed a generic model for compressed exponentials where slow rearrangement events occur randomly in space and create long-ranged elastic strains, leading to $\beta = 3/2$.

Acknowledgments

This review is heavily based on work I have been involved in during the last 15 years or so. I thank in particular G. Ben Arous, E. Bertin, L. Berthier, G. Biroli, M. Cates, L. Cipelletti, L. Cugliandolo, D. Dean, O. Dauchot, A. Georges, J. Kurchan, F. Lechenault, Ph. Maass, M. Mézard, C. Monthus, E. Pitard, D. Reichman, P. Sollich, H. Yoshino, and M. Wyart for many useful discussions on these and related matters. I also thank Eric Bertin and Giulio Biroli for carefully reading the manuscript. Finally, I want to thank Rainer Klages and Gunter Radons for giving me the opportunity to write this piece.

References

- 1** see e.g., J.-P. Bouchaud, A. Georges, *Anomalous diffusion in random media: statistical mechanisms, models and physical applications*, Phys. Rep. **195**, 127 (1990).
- 2** *Lévy Flights and Related Topics in Physics*, Eds: M. F. Shlesinger, G. M. Zaslavsky, U. Frisch, Lecture Notes in Physics, vol. 450.
- 3** B. B. Mandelbrot, J. W. Van Ness, *Fractional Brownian motions, fractional noises and applications*, SIAM Rev., **10**, 422 (1968).
- 4** C. Monthus, J.-P. Bouchaud, *Trap models and phenomenology of glasses*, J. Phys. A: Math. Gen. **29**, 3847 (1996).
- 5** G. Ben Arous, J. Černý, *Dynamics of trap models*, math.PR/0603344.

- 6** J. P. Bouchaud, D. S. Dean, *Aging on Parisi's tree*, J. Physique I (France) **5**, 265 (1995).
- 7** J.-P. Bouchaud, L. Cugliandolo, J. Kurchan, M. Mézard, *Out of equilibrium dynamics in spin-glasses and other glassy systems; in Spin-Glasses and Random Fields*, edited by A. P. Young (World Scientific, Singapore, 1998).
- 8** E. Bertin, J. P. Bouchaud, *Subdiffusion and localization in the one-dimensional trap model*, Phys. Rev. E **67**, 026128 (2003).
- 9** B. Rinn, Ph. Maass, J. P. Bouchaud, *Hopping in the glass configuration space: subaging and generalized scaling laws*, Phys. Rev. B **64**, 104417 (2001).
- 10** E. Bertin, J. P. Bouchaud, *Dynamical ultrametricity in the critical trap model*, J. Phys. A: Math. Gen. **35**, 3039 (2002).
- 11** E. Bertin, J. P. Bouchaud, *Linear and non-linear response in the aging regime of the one-dimensional trap model*, Phys. Rev. E **67**, 065105 (2003).
- 12** J. C. Dyre, *Master-equation approach to the glass transition*, Phys. Rev. Lett. **58**, 792 (1987), Phys. Rev. **B51** (12), 276 (1995); T. Odagaki, *Glass transition singularities*, Phys. Rev. Lett. **75**, 3701 (1995); P. Sollich, F. Lequeux, P. Hebraud, M. E. Cates, *Rheology of soft glassy materials*, Phys. Rev. Lett. **78**, 2020 (1997); R. A. Derry, D. R. Reichman, J. P. Bouchaud, *Trap models and slow dynamics in supercooled liquids*, Phys. Rev. Lett. **90**, 025503 (2003); A. Heuer, B. Doliwa, A. Saksengwijit, *Does the potential energy landscape of a supercooled liquid resemble a collection of traps?*, Phys. Rev. E **72**, 021503 (2005).
- 13** L. Berthier, D. Chandler, J.P. Garrahan, *Length scale for the onset of Fickian diffusion in supercooled liquids*, Euro. Phys. Lett. **69**, 320 (2005).
- 14** see e.g., W. Kob, C. Donati, S. J. Plimpton, P. H. Poole, S. C. Glotzer, *Dynamical heterogeneities in a supercooled Lennard-Jones liquid*, Phys. Rev. Lett. **79**, 2827 (1997).
- 15** see e.g., J. S. Langer, S. Mukhopadhyay, *Anomalous diffusion and stretched exponentials in heterogeneous glass-forming materials*, arXiv:0704.1508 for a very recent contribution on this subject. Older papers include: I. A. Campbell, J.-M. Flesselles, R. Jullien, R. Botet, *Nonexponential relaxation in spin glasses and glassy systems*, Phys. Rev. B **37**, 3825 (1988); J. T. Bendler, M. F. Shlesinger, *Defect diffusion and a two-fluid model for structural relaxation near the glass–liquid transition*, J. Phys. Chem. **96**, 3970 (1992).
- 16** M. Donsker, S. R. Varadhan, *On the number of distinct sites visited by a random walk*, Comm. Pure Appl. Math. **32**, 721 (1979).
- 17** G. Ben Arous, S. A. Molchanov, A.F. Ramirez, *Transition from the annealed to the quenched asymptotics for a random walk on random obstacles*, Ann. Probab. **33**, 2149 (2005).
- 18** G. Ben Arous, L. V. Bogachev, S. A. Molchanov, *Limit theorems for sums of random exponential*, Probability Theory and Related Fields, **132**, 579 (2005).
- 19** A. Ott, J. P. Bouchaud, D. Langevin, W. Urbach, *Anomalous diffusion in "living polymers": A genuine Lévy flight?*, Phys. Rev. Lett. **65**, 2201 (1990); J. Phys. II France **1**, 1465 (1991).
- 20** W. D. McComb, *Renormalisation Methods*, Oxford University Press, Oxford, 2004.
- 21** L. Cipelletti, L. Ramos, *Slow dynamics in glassy soft matter*, J. Phys.: Condens. Matter **17**, R253 (2005), see also: R. Bandyopadhyay, D. Liang, J. L. Harden, R. L. Leheny, *Slow dynamics, aging, and glassy rheology in soft and living matter*, e-print cond-mat/0606466.
- 22** L. Cipelletti, S. Manley, R. C. Ball, D. A. Weitz, *Universal aging features in the restructuring of fractal colloidal gels*, Phys. Rev. Lett. **84**, 2275–2278 (2000).
- 23** J.-P. Bouchaud, E. Pitard, *Anomalous dynamic light scattering in soft glassy gels*, Eur. Phys. J. E **6**, 231 (2001).
- 24** F. Lechenault, O. Dauchot, G. Biroli, J.-P. Bouchaud, *Experimental evidence of critical scaling and heterogeneous superdiffusion across the Jamming transition*, Euro. Phys. Lett., to appear (2008).
- 25** M. D. Ediger, *Spatially heterogeneous dynamics in supercooled liquids*, Annu. Rev. Phys. Chem. **51**, 99 (2000); R. Richert, *Heterogeneous dynamics in liquids: fluctuations in space and time*, J. Phys.: Condens. Matter **14**, R703 (2002).
- 26** L. Berthier, G. Biroli, J.-P. Bouchaud, W. Kob, K. Miyazaki, D. R. Reichman, *Spontaneous and induced dynamic fluctuations in glass-formers*, cond-mat/0609656 and 0609658, J. Chem. Phys. **126**, 184503 (2007) and J. Chem. Phys. **126**, 184504 (2007).

12

Anomalous Transport in Glass-Forming Liquids

Walter Kob, Gustavo A. Appignanesi, J. Ariel Rodríguez Fris, and Ruben A. Montani

12.1

Introduction

If one measures the viscosity η of a liquid as a function of temperature T one finds that $\eta(T)$ increases quite rapidly with decreasing T . For many liquids it is not possible to investigate the T -dependence of η in a large range of the viscosity since they crystallize at their melting temperature T_m . However, there is a large class of liquids, the so-called glass formers, for which the crystallization dynamics is so slow that it becomes possible to investigate their properties also in the supercooled state, i.e., for $T < T_m$. For these systems it is found that the T -dependence of η is smooth and shows no particular features at T_m . This can, e.g., be seen in Figure 12.1, where we plot the logarithm of the viscosity of various glass-forming liquids as a function of inverse temperature. Note that these systems have characteristic temperatures (T_m , boiling temperature, etc.) that are very different since their atomic interactions are very different. In order to represent the data for the various systems on the same scale, we therefore plot η as a function of the reduced temperature T_g/T , where T_g is the temperature at which the viscosity is 10^{13} Poise.¹ From this figure we recognize that in the accessible range of η the viscosity is indeed a smooth function of temperature and shows no sign of a singular behavior. (Although in this graph we do not show the location of the melting temperature T_m , it is found empirically that $T_g/T_m \approx 0.6$, i.e., is in the reduced temperature range shown in the plot.) Even more important is the fact that a relatively small change in T , let us say a factor 2–3, leads to a dramatic change of the viscosity (13–15

¹) The choice of this value for the definition of T_g is quite arbitrary. It corresponds to a viscosity at which the relaxation times of the system are typically 10^1 – 10^3 s, i.e., are on “human” time scales. However, if T_g is defined in a manner that is not too different, the resulting graph, and all the conclusions that can be drawn from it, remains basically unchanged.

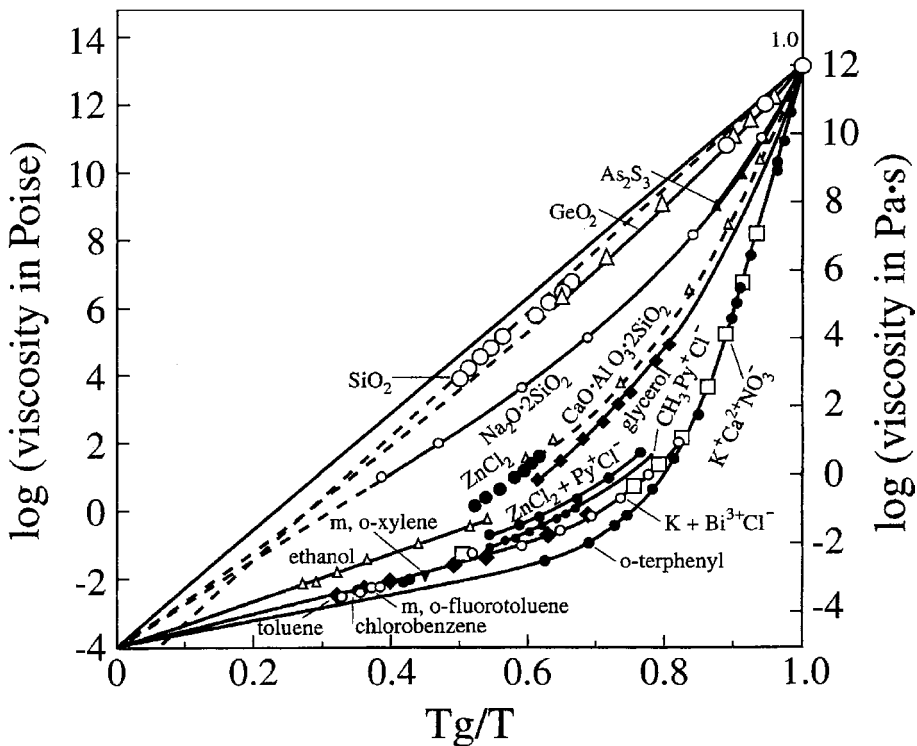


Figure 12.1 Logarithm of the viscosity as a function of (reduced) temperature T_g/T , where T_g is defined as $\eta(T_g) = 10^{13}$ Poise. Adapted from Ref. [2].

decades!). This strong T -dependence of the transport coefficient, which is also found in other quantities, such as the diffusion constant D or the relaxation time τ of the system, is one of the surprising properties of glass-forming systems for which there is presently still no complete theoretical explanation [1].

The observation that η shows such a strong T -dependence is even more astonishing if one compares it with the one of structural properties (e.g., the static structure factor) or thermodynamic quantities (density, specific heat, etc.) of the system. These observables show all a very smooth and *weak* T -dependence in that, e.g., the structure factor shows a main peak that becomes a bit sharper and increases somewhat its height, the density changes by 10–20%, and the specific heat changes by a factor of 2–3. Thus all these changes are significantly smaller than the ones observed in the quantities related to the *dynamics* of the system. This strong difference between the T -dependence of the dynamic quantities from the one of static quantities makes it a great challenge to come up with a theory that is able to give a satisfying explanation for these observations, although there is presently one theory, the so-called

mode-coupling theory of the glass transition [3–5], that is able to rationalize the dynamic features of glass-forming liquids at least at high and intermediate (reduced) temperatures. Coming up with a complete theoretical description for the slowing down of the dynamics is *the* fundamental problem in the field of glass-forming liquids [1].

Note that so far we have only discussed the properties of the system *at equilibrium* (and have neglected the fact that in principle the system should crystallize for $T < T_m$). Since the time to equilibrate the system is proportional to its relaxation time, which in turn is roughly proportional to the viscosity, it is evident that at low T it becomes increasingly difficult to reach equilibrium, since the necessary time scales increase very quickly with decreasing T . Thus a given fixed experimental time for equilibration, t_{equil} , corresponds to a temperature T_{glass} with $\tau(T_{\text{glass}}) = t_{\text{equil}}$, i.e., for $T < T_{\text{glass}}$ the system is not in equilibrium, i.e., it is a *glass*. Since a glass is an out-of-equilibrium system, and thus will age, the usual machinery of standard statistical mechanics is no longer applicable and therefore it is not surprising that from a theoretical point of view such systems are understood even less than (equilibrium) glass-forming liquids [6].

It can be expected that a system that shows such a strong T -dependence of its dynamics has also nontrivial features in its *microscopic* dynamics. That this expectation is indeed born out can be demonstrated by investigating the time dependence of quantities like $\langle r^2(t) \rangle$, the mean-squared displacement (MSD) of a tagged particle, or $F_s(q, t)$, the intermediate scattering function. The MSD is defined as

$$\langle r^2(t) \rangle = N^{-1} \sum_{j=1}^N \langle |\mathbf{r}_j(t) - \mathbf{r}_j(0)|^2 \rangle, \quad (12.1)$$

where N is the number of particles in the system and $\mathbf{r}_j(t)$ is the position of particle j at time t . In Figure 12.2 we show the time dependence of the MSD for the case of a simple glass former, a binary Lennard-Jones system whose properties will be discussed below. From this figure we recognize that at high temperatures the MSD shows two regimes: At short times a so-called ballistic regime in which we have $\langle r^2(t) \rangle \propto t^2$ since the displacement of the particles is just linear in time and at long times a “diffusive regime” in which $\langle r^2(t) \rangle \propto t$. In this latter regime the tagged particle collides with the other particles and thus makes for sufficiently long times a motion that is random and which can be characterized by a random (Gaussian) process.

For low temperatures the time dependence of the MSD is more complex (bottom curves in Figure 12.2): Although one finds again the ballistic and diffusive regimes at short and long times, respectively, these two regimes are separated by a time window in which the MSD shows only a very weak t -dependence. This intermediate regime is due to the so-called cage effect, i.e.,

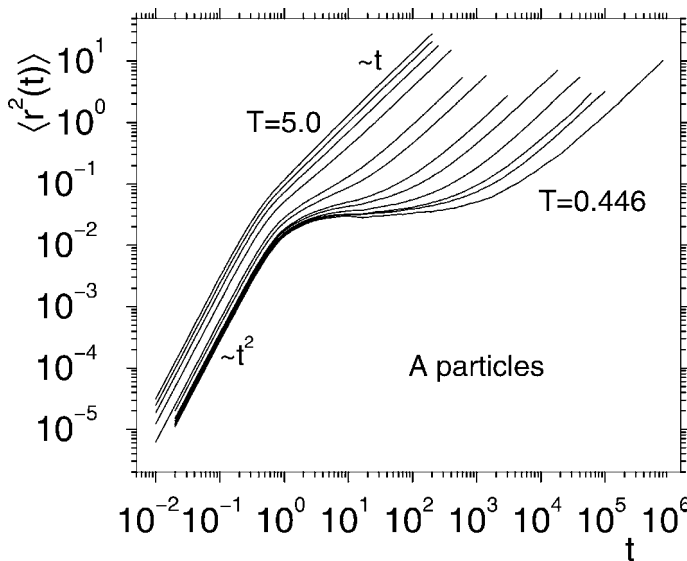


Figure 12.2 Time dependence of the MSD of a tagged particle in a binary Lennard-Jones system. The curves correspond to the (reduced) temperatures $T = 5.0, 4.0, 3.0, 2.0, 1.0, 0.8, 0.6, 0.55, 0.50, 0.475, 0.466$, and 0.446 (from left to right). From Ref. [7].

the fact that for intermediate times the tagged particle is trapped by its surrounding neighboring particles and thus undergoes a rattling motion. Note that the duration of this temporary trapping increases quickly with decreasing temperature, see Figure 12.2, and thus it is evident that in order to understand the slowing down of the dynamics of the system it is necessary to study the behavior of the system on this time regime and to find the answers to the following questions: What is the motion of the particles in this time window? What is the mechanism that allows the particles to leave their cage? Is there a typical time scale for this process or does one have a nontrivial distribution? Can the exit from the cage be understood in a single particle picture or is this a cooperative effect that involves also the neighboring particles? Below we will discuss some results from computer simulations that should help to find some answers to these questions.

A further quantity that allows to obtain interesting information on the relaxation dynamics of the system is the self-intermediate scattering function which is defined as [8]

$$F_s(q, t) = N^{-1} \sum_{j=1}^N \langle \exp[i\mathbf{q} \cdot (\mathbf{r}_j(t) - \mathbf{r}_j(0))] \rangle, \quad (12.2)$$

where \mathbf{q} is the wave vector and $q = |\mathbf{q}|$. Thus $F_s(q, t)$ describes how a density fluctuation of the particles on a length scale $2\pi/q$ decays as a function of time.

The typical behavior of $F_s(q, t)$ is shown in Figure 12.3. At high temperatures, $F_s(q, t)$ decays quickly to zero and at long times its shape can be approximated well by an exponential function. Such a behavior is the one expected for a particle that makes a simple random walk and thus obeys Gaussian statistics, i.e., the van Hove time-correlation function is a Gaussian [8].

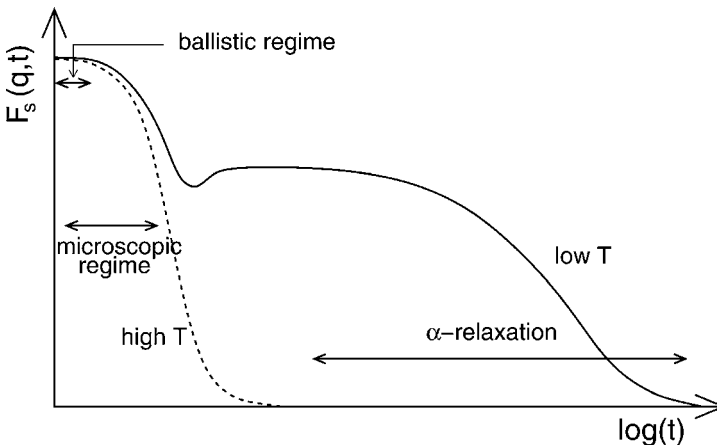


Figure 12.3 Schematic plot of the time dependence of a time-correlation function at high (left) and low (right) temperatures.

For low temperatures the situation is very different. At short times the shape of $F_s(q, t)$ is similar to the one at high T (see Figure 12.3). However, for intermediate times the time-correlation function shows a plateau. The reason for this feature is again the cage effect mentioned above, i.e., the temporary trapping of the particle by its surrounding neighbors. Only at much longer times the particles are able to escape this cage and hence $F_s(q, t)$ goes to zero. In contrast to the case of high T , this ultimate decay (which is also often called “ α -relaxation”) can, however, not be described by an exponential. Instead the so-called Kohlrausch–Williams–Watts function (KWW) [9, 10], given by

$$A \exp(-(t/\tau)^\beta), \quad (12.3)$$

gives a good description of the correlator. Here A is a prefactor that gives, basically, the height of the plateau in $F_s(q, t)$ and $\beta \leq 1$ is the so-called stretching parameter. The fact that $\beta < 1$ implies that the relaxation dynamics of the system is “anomalous,” i.e., non-Debye. Note that $F_s(q, t)$ is a system averaged quantity, i.e., *a priori* this correlator does not allow to draw any conclusion on the dynamics of an individual particle. In particular the fact that $\beta < 1$ can be the result of two extreme scenarios [11]: the completely homogeneous one and the completely heterogeneous one. In the former case the trajectory of *each* particle observed on the time scale τ from Eq. (12.3) gives rise to a decor-

relation that is described well by the KWW law. Thus in this case the nature of the trajectory must be different from a Gaussian one and one has to explain why this is so, i.e., give a description of a microscopic process that gives rise to a time-correlation function that has the form of the KWW law. One possibility is, e.g., a continuous time random walk [12–14]. In the heterogeneous case the individual trajectories of the particles are Gaussian processes (on the time scale τ !) but different particles have a different value for τ . Since $F_s(q, t)$ is the average over all the particles, the stretching can be rationalized as a result of a superposition of different Debye laws, i.e., exponentials. In such a scenario one has of course to explain why (identical!) particles show, on the time scale τ , a different relaxation dynamics. (For *very* long times all the particles have of course the same statistical properties since we assume that the system is ergodic.) One possibility is that each particle has at time zero a local environment that is somewhat different and therefore makes that the dynamics of the particle also depends on the particle considered. Evidence for the presence of such an influence has indeed been given, e.g., in Refs. [15,16], but the details of this influence, which is also called dynamical heterogeneity, are presently still not understood [17–19]. In the following, we will therefore discuss the results of computer simulations that have been done to investigate the relaxation dynamics of glass-forming liquids with respect to the dynamical heterogeneities.

12.2 Model

The system we are investigating is a binary Lennard–Jones mixture with particles which we will denote by A (80%) and B (20%). All particles have the same mass m and interact via the potential $V_{\alpha\beta}(r) = 4\epsilon_{\alpha\beta}[(\sigma_{\alpha\beta}/r)^{12} - (\sigma_{\alpha\beta}/r)^6]$, with $\alpha, \beta \in \{A, B\}$. In the following we will use reduced units with σ_{AA} and ϵ_{AA} the unit of length and energy, respectively, and $\sqrt{m\sigma_{AA}^2/48\epsilon_{AA}}$ as unit of time. The parameters of the interactions are thus given by $\sigma_{AA} = 1.0$, $\sigma_{AB} = 0.8$, $\sigma_{BB} = 0.88$, $\epsilon_{AA} = 1.0$, $\epsilon_{AB} = 1.5$, and $\epsilon_{BB} = 0.5$. The resulting Newton's equation of motion have been integrated using the velocity Verlet algorithm with a step size of 0.02 [20]. The simulations have been done at a reduced particle density of 1.2 and all the results represent the behavior of the system *in equilibrium*. More details on the static and thermodynamic properties of this model can be found in Refs. [7,21,22].

12.3 Results

One simple quantity that allows to determine whether or not the trajectories of the particles obey Gaussian statistics is the so-called non-Gaussian parameter [23] which is given by

$$\alpha_2(t) = \frac{3\langle r^4(t) \rangle}{5\langle r^2(t) \rangle^2} - 1. \quad (12.4)$$

For a Gaussian process this quantity is strictly zero and thus any nonzero value indicates a nontrivial dynamics. The time dependence of α_2 for the A particles at intermediate and low T is shown in Figure 12.4.

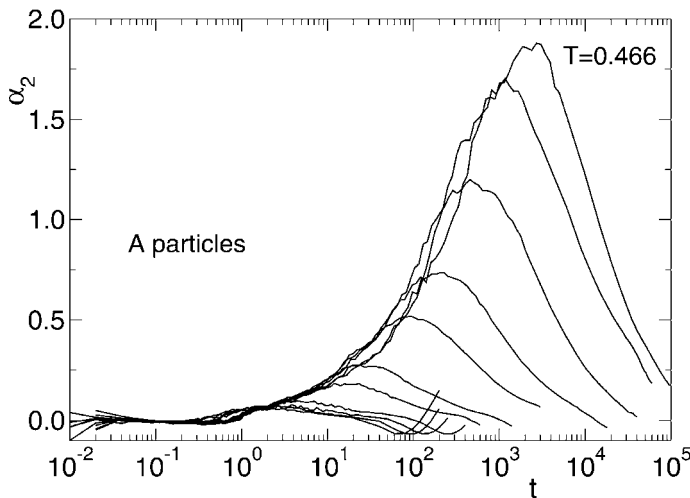


Figure 12.4 Non-Gaussian parameter α_2 versus t for the A particles of a binary Lennard–Jones system. Temperatures from right to left: 0.466, 0.475, 0.5, 0.55, 0.6, 0.8, 1.0. Adapted from Ref. [7].

We see that at short times $\alpha_2(t)$ is zero since in this time regime the particles undergo a ballistic motion, i.e., they behave like a free gas which, due to the Maxwell distribution of the velocities of the particles, is a Gaussian system. For intermediate times the non-Gaussian parameter increases rapidly, attains a maximum at a time that we denote by t^* , and then it decreases again to zero since at very long times the behavior of the particles is diffusive, i.e., Gaussian. Note that with decreasing T the location of the maximum shifts to longer times and that also its height increases. This means that the non-Gaussianity of the motion increases with decreasing T and that the time scale at which it is most pronounced becomes larger and larger.

The time dependence of α_2 does, of course, not allow to identify the nature of the microscopic process that gives rise to the non-Gaussian behavior of the

relaxation dynamics since it is just a system averaged quantity. One possibility to gain insight into the nature of this process is to look directly at the trajectories of individual particles. Since the non-Gaussian behavior seems to be most pronounced on the time scale t^* , it is natural to study these trajectories on this time scale. One possibility to characterize the dynamics of the individual particles is to look at their displacement within a given time: $\delta_i(t', t' + t) = |\mathbf{r}_i(t' + t) - \mathbf{r}_i(t')|$. The distribution of this quantity, averaged over the particles i and time t' , is thus just the well-known self part of the van Hove function $G_s(r, t)$ given by [8]

$$G_s(r, t) = N^{-1} \sum_{i=1}^N \langle \delta(r - |\mathbf{r}_i(t) - \mathbf{r}_i(0)|) \rangle. \quad (12.5)$$

In Figure 12.5 we show this distribution function for the A particles at time $t = t^*$. Also included in the graph is $G^0(r, t)$, the van Hove function of a *Gaussian* process, which at $t = t^*$ has the same second moment, i.e., the same mean-squared displacement. The comparison of the two curves shows that $G_s(r, t^*)$ has a tail that extends to relatively large distances, i.e., that there are parti-

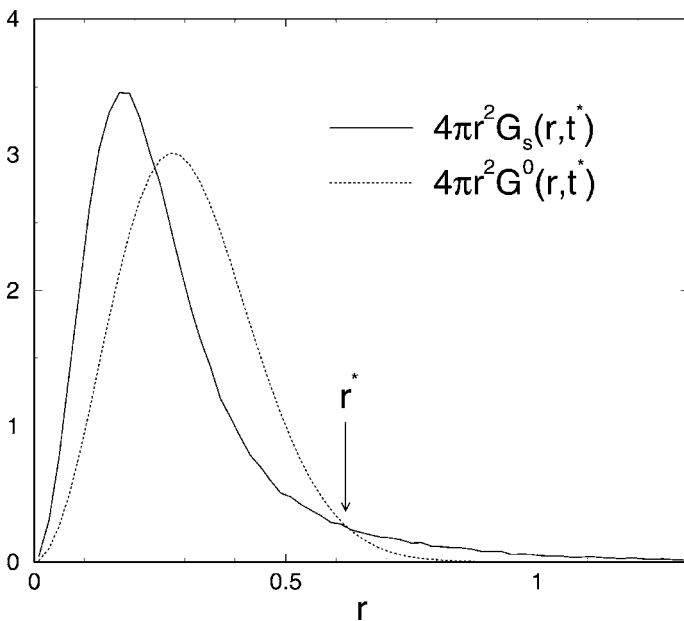


Figure 12.5 Self part of the van Hove distribution function $G_s(r, t^*)$ for a supercooled Lennard-Jones system, where t^* is the time at which the non-Gaussian parameter $\alpha_2(t)$ shows a maximum (see Figure 12.4). The dotted curve is the same distribution for a Gaussian process which has the same MSD as the particles in the Lennard-Jones system. The two distribution intersect at a distance r^* , which we use to define “mobile” particles $T = 0.45$. From Ref. [24].

cles that have moved farther than can be expected from a Gaussian process. (and since the second moment of $G_s(r, t^*)$ is the same as the one of $G^0(r, t^*)$ it follows that there must be more particles that are moving slower than can be expected from a Gaussian process.). In the following, we will define as “mobile” all the particles that have moved within the time t^* a distance larger than r^* , the intersection of $G_s(r, t^*)$ and $G^0(r, t^*)$. One finds that at low temperatures around 5% of the particles are mobile. Naively one would expect that the location of the mobile particles in the simulation box is random, i.e., there is no correlation between the position of the mobile particles. This is indeed

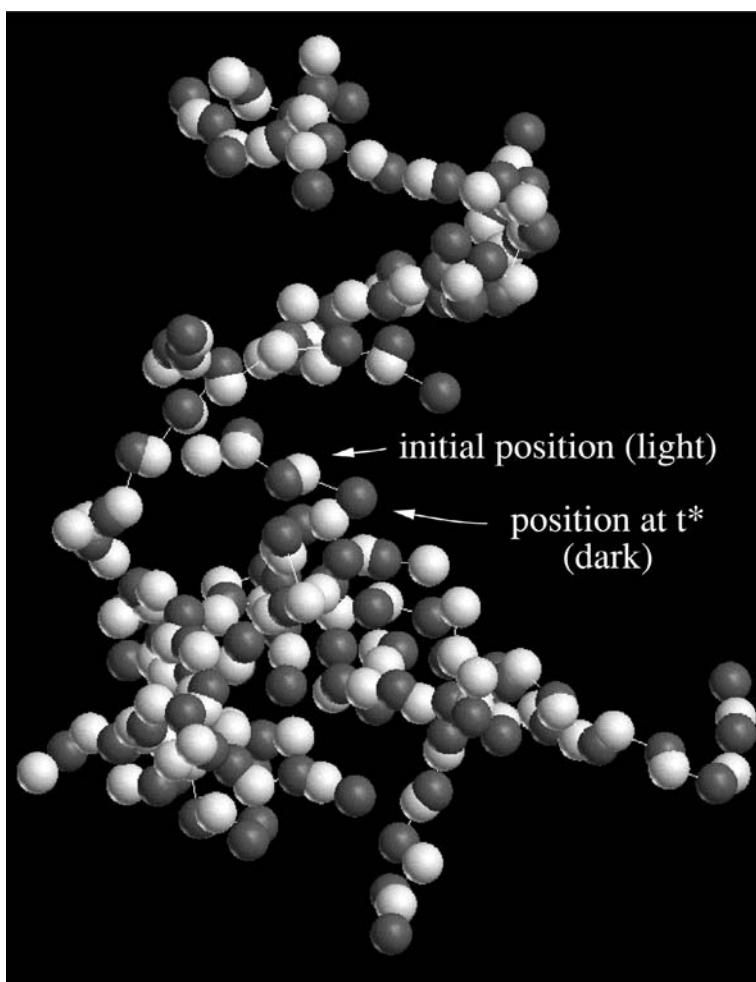


Figure 12.6 Cluster of mobile particles. At $t = 0$ the particles occupy the positions given by the white spheres and at $t = t^*$ they are at the positions given by the gray spheres. Adapted from Ref. [16].

true at high temperatures. However, for intermediate and low temperatures one finds that these mobile particles form clusters, i.e., are strongly correlated. One example of such a cluster is shown in Figure 12.6 where the light spheres represent a snapshot of the mobile particles at $t = 0$. Thus we recognize that at low temperatures the mobile particles form structures that are rather low dimensional/string-like, i.e., not compact. What is the motion of the mobile particles on the time scale t^* ? To answer this question we have also included in Figure 12.6 the position of the mobile particles at $t = t^*$ (gray spheres). We see that these final positions form again a connected cluster and, more important, that this final cluster has a strong overlap with the initial one. A detailed analysis of the motion of the mobile particles shows that most of them leave the position at $t = 0$ in order to occupy at $t = t^*$ a position which was occupied by another mobile particle at $t = 0$, thus reminiscent to a congo-line [16, 24]. We therefore can conclude that the motion of the particles is extremely cooperative and this is one of the reasons for the non-Gaussian dynamics of the system although, as we will see below, not the only one.

Furthermore, we note that the cluster of mobile particles spans the whole system. A detailed analysis shows, however, that the cluster is not the outcome of a single event but instead is the result of string motions of particles as described above but that occur asynchronously [25, 26]. That is, fast string motions in different regions of the system occur at different times within the t^* timespan, thus building up the global cluster of mobility.

The existence of the cooperatively relaxing clusters such as the one shown in Figure 12.6 rises the question to what extent this type of motion is a particularity for Lennard-Jones systems or whether such a behavior can also be found in real life. Weeks et al. and van Kegel et al. have used confocal microscopy to track the motion of individual particles in a dense colloidal suspension [27, 28], i.e., a system which is known to be a good glass former [29–32]. This technique thus allowed to identify mobile particles in the same way as in the computer simulation and thus to see whether these particles form string-like clusters. Surprisingly enough, this is indeed the case, thus giving evidence that the relaxation dynamics in hard sphere like systems is indeed related to the presence of cooperatively rearranging clusters that are similar to the ones found in the computer simulation. We remind at this place that more than 40 years ago Adam and Gibbs proposed a relatively simple model for the relaxation dynamics in glass-forming liquids in which particles are members of a “cooperatively rearranging region” (CRR) which undergoes a spontaneous relaxation [1, 33]. Thus the clusters found in the simulations and in the colloidal systems, where the first strong indication that the CRRs proposed by Adam and Gibbs, actually existed in real systems. Further support for such clusters come from other experimental approaches and other computer simulations (see Refs. [17–19, 34] and references therein).

Although the simulations and experiments discussed so far clearly show that glass-forming systems show dynamical heterogeneities one still has to wonder to what extent the occurring clusters are relevant for the α -relaxation of the system, i.e., the second step in the correlation function shown in Figure 12.2. We remind that at any instance only around 5% of the particles are mobile, i.e., only a small fraction. In order to answer this question it is useful to investigate to what extent the (temporal) presence of such a string-like cluster is (temporarily) correlated with the relaxation of the system, i.e., the α -relaxation. The latter can, e.g., be monitored by investigating the instantaneous (system-averaged) displacement of the particles, i.e., $\langle \delta_i(t, t + t') \rangle_i$, where $\langle \dots \rangle_i$ stands for the average over the particles. It is evident that in a macroscopically large system there will be always some string-like clusters and since, in a large system, also the quantity $\langle \delta_i(t, t + t') \rangle_i$ will not depend on t it is difficult to demonstrate for a *large* system that there is indeed a correlation between the occurrence of a string-like cluster and the α -relaxation. Fortunately this problem can be avoided by considering relatively small systems since then it can be expected that at any given time there is only *one* string-like cluster present in the system and thus it is easy to see whether or not its presence is related to a fast relaxation. In the following, we will therefore present the results of simulations of systems that have only 150 particles. We emphasize at this point that it is found that the *average* relaxation dynamics of such a small system is not very different from the one of a large system, i.e., the average dynamics (as well as the structural properties of the system) show only very mild finite size effects.

It turns out that in order to investigate the relaxation dynamics of such a many-particle system it is useful to make a two-time plot [35]. Thus one considers the so-called distance matrix

$$\Delta^2(t', t'') = \frac{1}{N} \sum_{i=1}^N |\mathbf{r}_i(t') - \mathbf{r}_i(t'')|^2 \quad , \quad (12.6)$$

a quantity that contains information to what extent a configuration at time t'' is correlated to a configuration at time t' . Note that although *on average* such a correlation will depend only on the time difference $|t'' - t'|$, in general Δ^2 will indeed depend on both time arguments, *if the system size is finite*.

For high temperatures Δ^2 increases quickly if $|t'' - t'|$ is large since the relaxation dynamics is fast, i.e., the system moves quickly through configuration space. Thus a contour plot of Δ^2 as a function of t' and t'' shows a narrow valley along the diagonal $t' = t''$ and large values for $t' \neq t''$.

The situation is very different for low temperatures as can be seen in Figure 12.7 where we show the t' and t'' dependence of Δ^2 for a system at $T = 0.5$. Apart from the valley along the diagonal we see that Δ^2 has also low values for Δ^2 for $t' \neq t''$ and that the regions with low Δ^2 have quite sharp limits. The

presence of these sharply delimited regions of low Δ^2 thus shows that the system is often stuck in configuration space and then moves *quickly* to a different part of configuration space.

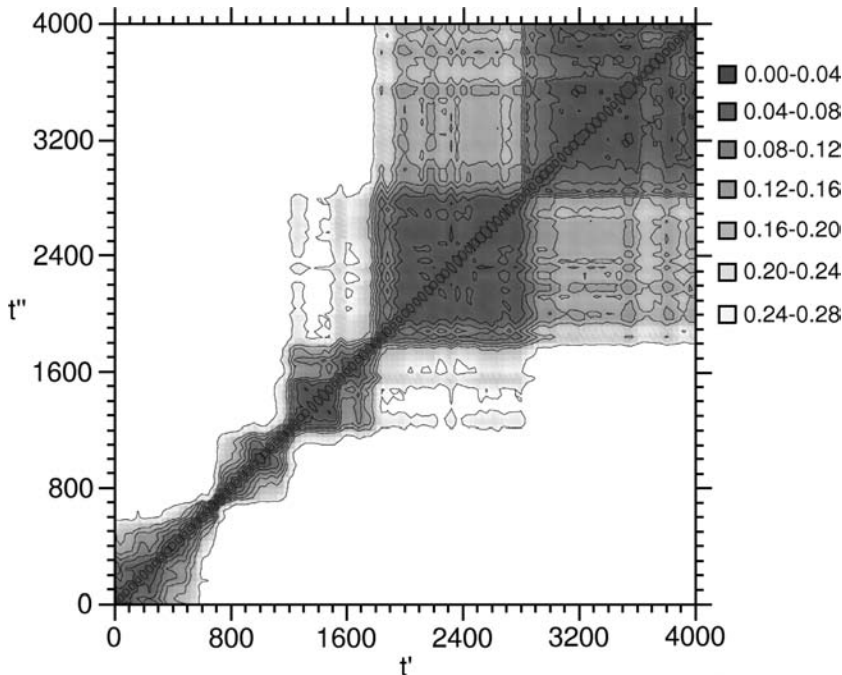


Figure 12.7 Contour plot of the distance matrix $\Delta^2(t', t'')$ for $T = 0.5$.

The gray levels correspond to the values that are given to the right.

From Ref. [36].

In order to discuss the physical content of Figure 12.7 in more detail, it is useful to recall some notions on the so-called energy landscape of glass-forming systems (see, e.g., Refs. [37–39] for a more extensive discussion). Long time ago Goldstein pointed out that at sufficiently low temperatures the dynamics of a glass-forming system can be viewed as an exploration of the free energy landscape that must have features that are particular to glass formers [40]. Since at low temperatures the time-correlation functions of such systems show a two-step decay (see Figures 12.2 and 12.3), their motion in configuration space can be viewed as an exploration of a local minimum in the free energy (which corresponds to the vibrational/rattling motion) and a subsequent hopping to another minimum (corresponding to the α -relaxation). Thus the dynamics of the system can be viewed as a motion in a landscape that has many (in fact exponentially many in the number of particles) local minima and the dynamical properties of the system (dependence of relaxation time on temperature, vibrational spectrum, etc.) are encoded in this landscape (dis-

tribution of the height of the local minima, distribution of the barrier heights, properties of the quasinormal modes around the local minima, etc.). At the time of Goldstein, it was not really possible to determine the properties of this landscape in a direct way. Only much later Stillinger and coworkers realized that using computer simulations it was possible to investigate at least some of the features of the landscape [41–44]. For this they associated to each configuration of particles the so-called inherent structure which is the local minimum in the potential energy that is found if the configuration of interest is used as a starting point of a steepest descent procedure. Thus this procedure allows to decompose configuration space in a (unique!) way into inherent structures (the location of the local minima) and their basin of attraction (all the configurations that lead to a given inherent structure). Hence the dynamics of the system can be viewed as jumps from one basin to a neighboring one, followed by a quasiharmonic motion within a basin. Computer simulations make it thus possible to investigate how these basins are organized (Is there a hierarchy? What are the barrier heights between adjacent basins? ...) and thus to understand better the relaxation dynamics of the glass former. See Refs. [37–39] for a discussion of these results.

We now return to the discussion of Figure 12.7. The fact that $\Delta^2(t', t'')$ shows the square-like regions seen in the figure is evidence that the (free) energy landscape of the system is a collection of local basins that are organized in a hierarchical way, i.e., that there exist so-called meta-basins (MB). To see this, one has to recognize that for this system size the average sojourn time of the system in a *local* minimum is very short [45], i.e., much shorter than the time scales for which we see the dark regions in Δ^2 , i.e., the time for which the system is basically stuck in configuration space. (Typical sojourn times of the system in a MB are 300–800 times units, which corresponds to about 10% of the α -relaxation time τ which is around 4000 time units [36].) This implies that within such a region the system makes many jumps between local minima but, since the distance matrix is not increasing, these jumps do not really help to propagate the system in configurations space. Thus the sum of these basins form the mentioned meta-basin that is a collection of configurations that are relatively near and not separated by a high barrier. (We note that qualitatively similar results have also been obtained by a direct investigation of the inherent structures, an approach which is, however, much more costly in terms of computer resources [45–47]). In summary, we thus can conclude from Figure 12.7 that the dynamics of the system is very heterogeneous in time, that the landscape of the system must have meta-basins, and that the motion of the system that is relevant for the relaxation dynamics is the one between two adjacent MB.

In order to enforce the evidence for the existence of MB it is useful to look at $\delta^2(t, \theta)$, the so-called averaged-squared displacement (ASD) of the particles,

which is defined as follows:

$$\delta^2(t, \theta) = \Delta^2(t - \theta/2, t + \theta/2) = \frac{1}{N} \sum_{i=1}^N |\mathbf{r}_i(t - \theta/2) - \mathbf{r}_i(t + \theta/2)|^2. \quad (12.7)$$

Thus $\delta^2(t, \theta)$ is just the displacement of the system within a time span θ , centered around time t . Note that the average of $\delta^2(t, \theta)$ over t is just the usual MSD from Eq. (12.1), i.e., $\langle r^2(\theta) \rangle$. In Figure 12.8, solid line and right-hand abscissa, we present the t -dependence of $\delta^2(t, \theta)$ for the same run shown in Figure 12.7. The value of θ is 160 time units, i.e., a time that is significantly shorter than the α -relaxation time. From this figure we recognize that $\delta^2(t, \theta)$ shows many well-defined peaks separated by time intervals in which the ASD is relatively small. A comparison of this figure with Figure 12.7 shows that these peaks occur exactly at the times at which the boundaries of the dark regions are found, i.e., when the system leaves a MB. In agreement with this the ASD is small when the system stays within a MB. Thus Figure 12.8 gives indeed evidence that the landscape of the system is organized in MB and that the MB-MB transitions are rather quick (a few hundred time units) and thus much shorter than the time scale for the α -relaxation.

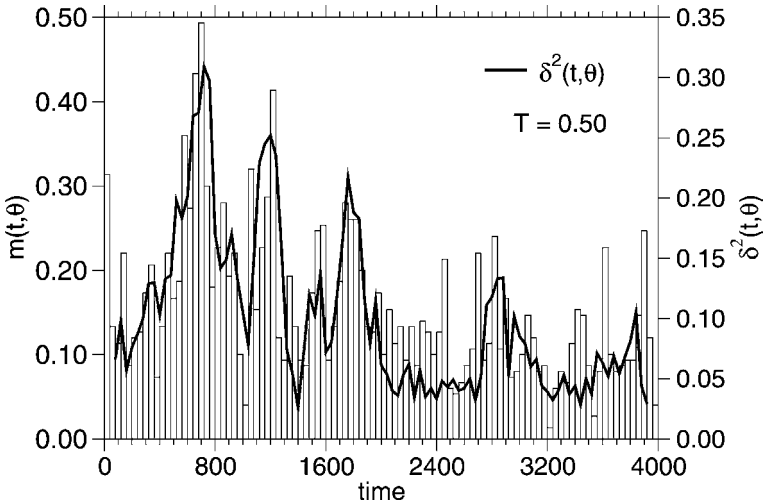


Figure 12.8 Solid line (right-hand abscissa): Averaged squared displacement $\delta^2(t, \theta)$ for the trajectory given in Figure 12.7. The value of θ is 160. Vertical bars (left-hand abscissa): The function $m(t, \theta)$ which gives the fraction of democratic particles, i.e., particles that moved more than the threshold value $r_{th} = 0.3$ in the time interval $[t, t + \theta]$, using $\theta = 40$. From Ref. [36].

Having established that the propagation of the system in configuration space is very heterogeneous in time we can now investigate what type of motion of the particles is responsible for the fast propagation of the system during

a MB–MB transition. For this it is useful to look first at the *average* dynamics in order to be able to quantify “fast” and “slow.” One observable that allows to characterize the (average) relaxation dynamics is the self-part of the van Hove function $G_s(r, \theta)$ which was defined in Eq. (12.5) and which gives the probability that a particles has made within a time span θ a displacement of size r . In order to see whether at a given time the dynamics of the system is faster or slower than the average we have to generalize the definition of $G_s(r, \theta)$ to a correlation function that takes into account the heterogeneous dynamics. We therefore define the function

$$\hat{G}_s(r, t, t + \theta) = N^{-1} \sum_{i=1}^N \delta(r - |\mathbf{r}_i(t + \theta) - \mathbf{r}_i(t)|). \quad (12.8)$$

Note that the t -average of this function gives $G_s(r, \theta)$ (if the system is ergodic).

In Figure 12.9, we show this distribution for the present system for different starting times t . The time lag is $\theta = 40$, thus a time that is much shorter than the α -relaxation time τ or the time scale t^* , the location of the maximum in $\alpha_2(t)$. Also included in the two panels are $G_s(r, \theta)$, which allows us to compare the function $\hat{G}_s(r, t, t + \theta)$ with its long time average.

In Figure 12.9(a) the values for t have been chosen such that they fall into a time regime in which the distance matrix has small values, i.e., when the system stays within one MB (the values of t and $t + \theta$ are given in the figure). From this figure we recognize that for these values of t the function $\hat{G}_s(r, t, t + \theta)$ is within the noise of the data identical to $G_s(r, \theta)$. Only at large r one sees a small difference in that the former function seems to be systematically below the latter one. Thus we can conclude that during the exploration of a MB the relaxation dynamics of the system is very similar to its long time average. This is in strong contrast to the situation in which t is chosen at the beginning of a MB–MB transition (Figure 12.9(b)). We see that in this case $\hat{G}_s(r, t, t + \theta)$ differs significantly from $G_s(r, \theta)$ in that the former distribution has much more weight at large r . Note that the *whole* distribution is shifted to larger distances, i.e., it is not only a small fraction of particles that lead to the fast increase of the distance matrix and the ASD seen in Figures 12.7 and 12.8, but an appreciable number. Thus this behavior is very different from the one that one would expect if a MB–MB transition would correspond to the string-like motion shown in Figure 12.6 since in the latter only a few percent of the particles participate whereas we find here a much higher percentage (see below).

Note that the increased weight that we find in $\hat{G}_s(r, t, t + \theta)$ at large r (with a t just before a MB–MB transition) is also the explanation for the observation discussed in the context of Figure 12.9(a) that *within* a MB $\hat{G}_s(r, t, t + \theta)$ is smaller than $G_s(r, \theta)$ at large r . This can be seen by recalling that the latter function is the *weighted* average of the function \hat{G}_s shown in panels (a) and (b).

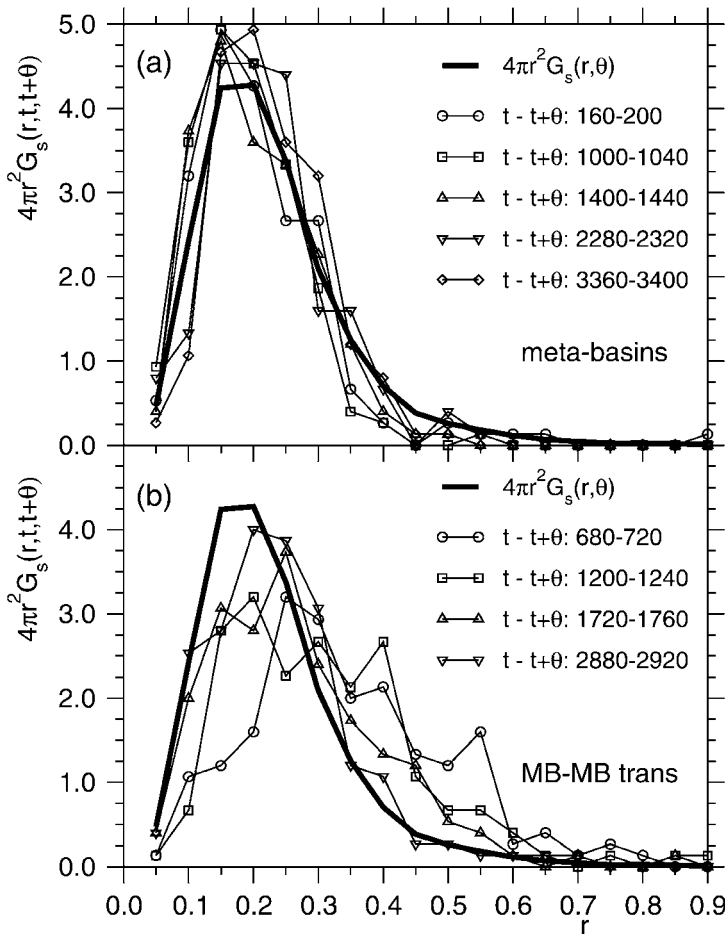


Figure 12.9 Curves with symbols: r -dependence of the distribution function $\hat{G}_s(r, t, t + \theta)$ for a time lag $\theta = 40$ and different values of t . Bold solid line: $G_s(r, \theta)$. (a): Values of t in which the system is exploring a MB. (b): Values of t in which the system is making a MB-MB transition. From Ref. [36].

Since MB-MB transitions occur only rarely, the weight of the functions \hat{G}_s from panel (b) is much smaller than the one from panel (a) and therefore the difference between $G_s(r, t)$ and \hat{G}_s as measured within a MB is small even at large r .

Figure 12.9 gives evidence that during a MB-MB transition a substantial number of particles participate in the relaxation dynamics. In order to quantify this “democratic motion” somewhat better we define as “democratic particles” all those particles that have moved within the time lag θ more than a distance r_{th} which we fix to be 0.3. Although this choice is somewhat arbitrary,

it is a reasonable one (see Figure 12.9(b)) and furthermore we have found that the results that we will discuss in the following do not depend significantly on this choice. (We also point out that the definition of a *democratic* particle has nothing to do with the one of a *mobile* particle, defined in the context of Figure 12.5 and the string-like relaxation discussed above. As we will discuss below these two classes of particles are quite different.)

Equipped with this definition we can immediately study how the concentration of democratic particles depends on time t and lag θ . This function $m(t, \theta)$, obtained as the r -integral of $\hat{G}_s(r, t, t + \theta)$ from r_{th} to infinity divided by N , is shown in Figure 12.8 (vertical bars, left abscissa). This graph shows that $m(t, \theta)$ shows the same peak and valley structure as we have already found in the ASD. Furthermore, we see that these two functions are strongly correlated from which we can conclude that when the system moves quickly through configuration space, *many* particles participate in this motion. By looking at the peak values of $m(t, \theta)$ we see that during a MB–MB transition between 30–40% of the particles participate in this democratic motion, which, recalling the system size $N = 150$, corresponds to about 40–60 particles. Thus we see that the motion that takes place during a MB–MB is indeed very collective. This behavior is in strong contrast to the one found for string-like motions of the mobile particles for which we find that a few percent of the particles make a *large* displacement, on the order of 1, and hence can also give rise to a relatively large ASD.

So far we have not made any statement about the relative position of the democratic particles: Are they randomly dispersed within the sample or are they forming a cluster? Within a computer simulation it is of course easy to answer this question and it is found that they indeed do form clusters that are relatively *compact*. A typical example is shown in Figure 12.10. Thus these clusters are very different from the ones found for the mobile particles which form sting-like objects (see Figure 12.6). Although we have so far not been able to obtain a good understanding how the particles move within these democratic clusters, one can say that, at least from a phenomenological point of view, they resemble strongly the cooperatively rearranging regions that have been postulated long time ago by Adam and Gibbs [33]. Whether this similarity is purely coincidental or whether the democratic clusters can indeed be taken as a proof for the existence of the CRRs, remains presently still unclear. Certainly more work is needed in order to see how the properties of the democratic clusters depend on temperature, the nature of the system, etc. But at least one can say that for the moment these clusters are excellent candidates to be the CRRs.

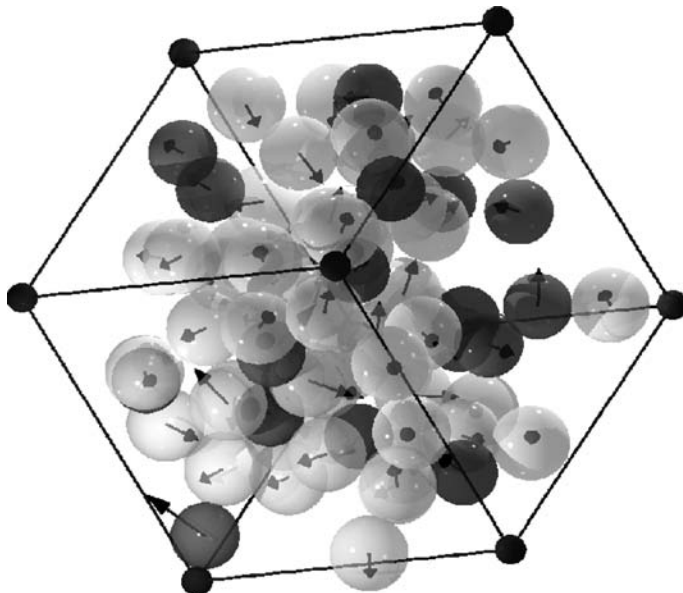


Figure 12.10 Snapshot of the democratic particles during the MB–MB transition $t = 680 \rightarrow t = 720$. The light and dark spheres show the location of the A and B particles, respectively, at $t = 680$. The arrows point to the location of the particles after the MB–MB transition. From Ref. [36].

12.4 Summary

The relaxation dynamics of glass-forming liquids is highly complex and shows features on several time scales. Obtaining a good understanding of this dynamics is therefore a difficult problem that has so far not been solved [1]. Underlying to this relaxation dynamics is the *microscopic* dynamics of the individual particles which seems to be complex as well. In fact, it is found that this dynamics is very cooperative and that the degree of cooperativity increases with decreasing temperature. Although many details of the nature of this cooperative dynamics are presently still not understood (What makes one region in configuration space “mobile?” How long does a “mobile region” live? To what extent does a “mobile region” affect the dynamics of the local neighborhood?) one can be optimistic that with some effort answers to these questions will be found in the near future. Furthermore, it has recently been shown that some aspects of the relaxation dynamics of glass-forming systems can be described very well by a continuous time random walk [48–51]. Thus this makes us hope that the anomalous transport found in glassy systems can be analyzed and understood (at least partially) by some of the approaches discussed in this book.

Acknowledgment

GAA is research fellow of CONICET and RAM is research fellow of CIC. Financial support from Fundación Antorchas, CONICET, UNS, SeCyT, and ECOS is gratefully acknowledged.

References

- 1 K. Binder and W. Kob, *Glassy Materials and Disordered Solids: An Introduction to Their Statistical Mechanics* World Scientific, Singapore, 2005
- 2 C. A. Angell, P. H. Poole, and J. Shao, *Nuovo Cimento D* 16, (1994), p. 993
- 3 W. Götze, in *Liquids, Freezing and the Glass Transition, Les Houches. Session LI, 1989* (J.P. Hansen, D. Levesque and J. Zinn-Justin, eds.) North-Holland, Amsterdam, 1991, p. 287
- 4 W. Götze, *J. Phys.: Condens. Matter* 10, (1999), p. A1
- 5 S. P. Das, *Rev. Mod. Phys.* 76, (2004), p. 785
- 6 L. F. Cugliandolo, in *Lecture Notes for "Slow relaxations and nonequilibrium dynamics in condensed matter"*, Les Houches July, 1–25, 2002; Les Houches Session LXXVII (J.-L. Barrat, M. Feigelman, J. Kurchan, and J. Dalibard, eds.) Springer, Berlin, 2003, p. 367
- 7 W. Kob and H. C. Andersen, *Phys. Rev. E* 51 (1995), p. 4626
- 8 J.-P. Hansen and I. R. McDonald, *Theory of Simple Liquids* Academic, London, 1986
- 9 R. Kohlrausch, *Ann. Phys. (Leipzig)* 12, (1847), p. 393
- 10 G. Williams and D. C. Watts, *Trans. Faraday Soc.* 66, (1980), p. 80
- 11 R. Richert, *J. Non-Cryst. Solids* 172–174, (1994), p. 209
- 12 M. F. Shlesinger, *J. Stat. Phys.* 10, (1974), p. 421
- 13 J. Klafter and R. Silbey, *Phys. Rev. Lett.* 44, (1980), p. 55
- 14 M. F. Shlesinger and E. W. Montroll, *Proc. Natl. Acad. Sci.* 81, (1984), p. 1280
- 15 W. Kob, C. Donati, S. J. Plimpton, S. C. Glotzer, and P. H. Poole, *Phys. Rev. Lett.* 79, (1997), p. 2827
- 16 C. Donati, J. F. Douglas, W. Kob, S. J. Plimpton, P. H. Poole, and S. C. Glotzer, *Phys. Rev. Lett.* 80, (1998), p. 2338
- 17 H. Sillescu, *J. Non-Cryst. Solids* 243, (1999), p. 81
- 18 S. C. Glotzer, *J. Non-Cryst. Solids* 274, (2000), p. 342
- 19 R. Richert, *J. Phys.: Condens. Matter* 14, (2002), p. R703
- 20 M. P. Allen and D. J. Tildesley, *Computer Simulation of Liquids*, Oxford University Press, New York, 1990
- 21 W. Kob and H. C. Andersen, *Phys. Rev. Lett.* 73, (1994), p. 1376
- 22 W. Kob and H. C. Andersen, *Phys. Rev. E* 52, (1995), p. 4134
- 23 A. Rahman, *Phys. Rev.* 136, (1964), p. A405
- 24 C. Donati, S. C. Glotzer, P. H. Poole, W. Kob, and S. J. Plimpton, *Phys. Rev. E* 60, (1999), p. 3107
- 25 G. A. Appignanesi, M. A. Frechero, and R. A. Montani, *Physica A* 329, (2003), p. 41
- 26 G. A. Appignanesi, M. A. Frechero, L. M. Alarcón, J. A. Rodríguez Fris, and R.A. Montani, *Physica A* 339, (2004), p. 469
- 27 E. R. Weeks, J. C. Crocker, A. C. Levitt, A. Schofield, and D. A. Weitz, *Science* 287, (2000), p. 627
- 28 W. K. Kegel and A. van Blaaderen, *Science* 287, (2000), p. 290
- 29 P. N. Pusey and W. van Megen, *Phys. Rev. Lett.* 59, (1987), p. 2083
- 30 W. van Megen, S. M. Underwood, and P. N. Pusey, *Phys. Rev. Lett.* 67, (1991), p. 1586
- 31 W. van Megen and S. M. Underwood, *Phys. Rev. E* 47, (1993), p. 248
- 32 W. van Megen and S. M. Underwood, *Phys. Rev. E* 49, (1994), p. 4206
- 33 G. Adam and J. H. Gibbs, *J. Chem. Phys.* 43, (1965), p. 139

- 34** L. Berthier, *Phys. Rev. E* 69, (2004), p. 020201
- 35** I. Ohmine, *J. Phys. Chem.* 99, (1995), p. 6765
- 36** G. A. Appignanesi, J. A. Rodríguez Fris, R. A. Montani, and W. Kob, *Phys. Rev. Lett.* 96, (2006), p. 057801
- 37** P. G. Debenedetti, T. M. Truskett, and C. P. Lewis, *Adv. Chem. Engin.* 28, (2001), p. 21
- 38** D. J. Wales, *Energy Landscapes*, Cambridge University Press, Cambridge, 2003
- 39** F. Sciortino, *J. Stat. Mech.* (2005), p. P05015
- 40** M. Goldstein, *J. Chem. Phys.* 51, (1969), p. 3728
- 41** F. H. Stillinger and T. A. Weber, *Phys. Rev. A* 25, (1982), p. 978
- 42** F. H. Stillinger and T. A. Weber, *Science* 225, (1984), p. 983
- 43** F. H. Stillinger, *Science* 267, (1995), p. 1935
- 44** S. Sastry, P. G. Debenedetti, and F. H. Stillinger, *Nature* 393, (1998), p. 554
- 45** B. Doliwa and A. Heuer, *Phys. Rev. E* 67, (2003), p. 031506
- 46** A. Heuer, *Phys. Rev. Lett.* 78, (1997), p. 4051
- 47** M. Vogel, B. Doliwa, A. Heuer, and S. C. Glotzer, *J. Chem. Phys.* 120, (2004), p. 4404
- 48** T. Odagaki and Y. Hiwatari, *Phys. Rev. A* 41, (1990), p. 929
- 49** L. Berthier, D. Chandler, and J. Garrahan, *Europhys. Lett.* 69 (2005), p. 320
- 50** J. S. Langer and S. Mukhopadhyay, arXiv:0704.1508.
- 51** P. Chaudhuri, L. Berthier, and W. Kob, *Phys. Rev. Lett.* 99 (2007), 060604

13

Subdiffusion-Limited Reactions

Santos Bravo Yuste, Katja Lindenberg, and Juan Jesús Ruiz-Lorenzo

13.1 Introduction

Anomalous diffusion processes are ubiquitous in nature [1–6]. Their occurrence is usually associated with complex systems that induce spatial and/or temporal correlations in the diffusion process. The signature of normal diffusion is the linear asymptotic dependence of the mean-square displacement of the diffusing entity (hereafter called “the particle”) on time, $\langle r^2 \rangle \sim t$, $t \rightarrow \infty$. The signature of anomalous diffusion is a nonlinear dependence on time. In particular, if the growth with time is sublinear, so that

$$\langle r^2 \rangle / t \rightarrow 0, \quad t \rightarrow \infty, \tag{13.1}$$

the particle is said to be subdiffusive. (The process is superdiffusive when the limit goes to infinity.) In this chapter, we focus on the important class of subdiffusive processes for which

$$\langle r^2 \rangle \sim t^\gamma, \quad t \rightarrow \infty \tag{13.2}$$

and where the (anomalous) diffusion exponent γ satisfies $0 < \gamma < 1$.

An interesting class of diffusive processes are so-called diffusion-limited reactions. These are processes in which diffusion is the dominant mixing mechanism and, furthermore, where the time for reactants to find one another is much longer than the time it takes for a reaction to occur following such an encounter. Therefore, in these systems diffusion is the key factor that determines the spatial distribution of reactants and the resultant reaction rate. Since diffusion is not a particularly effective mixing mechanism, diffusion-limited reactions often present extremely interesting spatial as well as temporal characteristics. In this context, it is especially appropriate to point to the pioneering work of Turing on pattern formation in reaction-diffusion systems [7]. Diffusion-limited reactions show up in a vast number of applications including not only chemical (see, e.g., [8]) but also biological (e.g., [9]), ecological (e.g., [10]) and economic processes (e.g., [11]) that have been studied over many decades.

The question that drives this chapter is the following: what happens if the reaction partners are subdiffusive instead of diffusive? How is the spatial distribution and, specifically, the reaction kinetics, affected by the subdiffusive nature of the reactants? Even more, what happens if the diffusive properties of different reactant species are qualitatively different, for example, if one species diffuses normally but the other is subdiffusive? We will see that the answers to these questions will take us to very diverse scenarios. Some will be answered via straightforward procedures related to the subordination of random processes (see Section 13.3.1), while others are unexpectedly complex and essentially unpredictable on any simple grounds [12–14]. Some will involve an almost automatic extension of normal diffusion results to the subdiffusive regime, while others involve profound qualitative changes (akin to critical phenomena) in the reaction kinetics as one reaches certain critical values of the anomalous diffusion exponents [15–17].

In Section 13.2, we introduce a number of physical scenarios that lead to subdiffusive motion as well as some of the mathematical language used to describe particle motion and chemical reactions in such environments. In Section 13.3, we review two classic reaction–(sub)diffusion problems, namely, the target problem (which involves a static particle in a sea of mobile traps), and the trapping problem (where the traps are static and the particle is mobile). The situation becomes more complicated when all reaction partners are mobile. In Section 13.4, we consider the reaction–(sub)diffusion problems $A + A \rightarrow \text{Products}$ and $A + B \rightarrow \text{Products}$ when all reactants are mobile and are initially randomly distributed. Sections 13.2–13.4 focus on the time dependence of global concentrations of reactants, $c(t)$, and on results that can be obtained by scaling arguments. There are situations involving nonhomogeneous distributions of reactants in which one wishes to focus not only on the global concentrations but on the local (space-dependent) concentrations $c(\mathbf{r}, t)$. An example, is the evolution of reaction fronts between initially separated reactants. In Section 13.5, we discuss the various ways in which the evolution of local concentrations has been modeled using reaction–subdiffusion equation approaches, and we illustrate some of these on the analysis of a reaction front. A special challenge presents itself when reacting particles that are all mobile are described by different subdiffusive exponents. Section 13.6 discusses some such reactions and arrives at results for global concentrations on the basis of mutually convergent bounding arguments. Finally, in Section 13.7 we present a brief concluding summary and mention a number of open problems in the reaction–subdiffusion arena.

13.2

Subdiffusion Contexts and Modeling Approaches

Subdiffusive processes arise in diverse contexts, of which we mention only the most ubiquitous.

Subdiffusion describes the way a particle moves through spatially disordered or fractal media [1, 5, 18, 19] (see the contribution by Hoffmann and Prehl, Chapter 14, in this volume). In such media, there are structural irregularities, bottlenecks, and dead ends, that is, impairments to normal diffusion that lead to a mean-square displacement given by [5, 20]

$$\langle r^2 \rangle \sim t^{2/d_w}, \quad t \rightarrow \infty. \quad (13.3)$$

Here, $d_w = 2d_f/\tilde{d}$ is the random walk dimension, d_f and \tilde{d} being, respectively, the fractal and spectral dimension of the substrate. This result describes the mean-square displacement on both random fractal structures such as percolation clusters and diffusion-limited aggregates, and regular fractals such as Sierpinski gaskets. For d -dimensional Euclidean media, $d = d_f = \tilde{d}$ and therefore $d_w = 2$ for all d .

Subdiffusion also describes the motion of a particle in a regular lattice with quenched (frozen) disorder [1–5, 19] or with dynamical disorder due to correlated (slow) temporal fluctuations of the medium [19, 21, 22]. Here, although the sites and connectivity are those of a regular lattice, the transition rates from one site to another vary from site to site due to random energy barriers, or potential wells of random depths or, more generally, the presence of a spatially random quenched force field (the Sinai problem) or a time-dependent random force field. Certain distributions of transition rates lead to subdiffusive motion (see Bouchaud's contribution, Chapter 11, in this volume). For example, suppose that at every node of a d -dimensional lattice there is a potential well of a fixed depth λ drawn from a distribution $p(\lambda)$. Suppose that this distribution behaves as $p(\lambda) \sim \lambda^{-1-\alpha}$ for large λ . If one assumes that the waiting-time distribution for exiting the well of depth λ follows the Arrhenius law, $\psi(t|\lambda) = \lambda^{-1} \exp(-t/\lambda)$, then one finds that

$$\langle r^2 \rangle \sim t^\gamma, \quad t \rightarrow \infty, \quad (13.4)$$

with $\gamma = 2\alpha/(1+\alpha)$ for a one-dimensional lattice. For d -dimensional lattices with $d \geq 2$ the anomalous diffusion exponent γ is simply α [1, 5]. In Figure 13.1, we show simulation results for $\langle r^2 \rangle$ for one-, two-, and three-dimensional lattices when $\alpha = 1/2$. The anomalous character of the diffusion process in this system is evident.

We note that the contexts mentioned above arise in vastly different physical situations. For instance, fractal media or quenched disorder is invoked in porous glasses, micelle systems, actin networks, intracellular transport, and

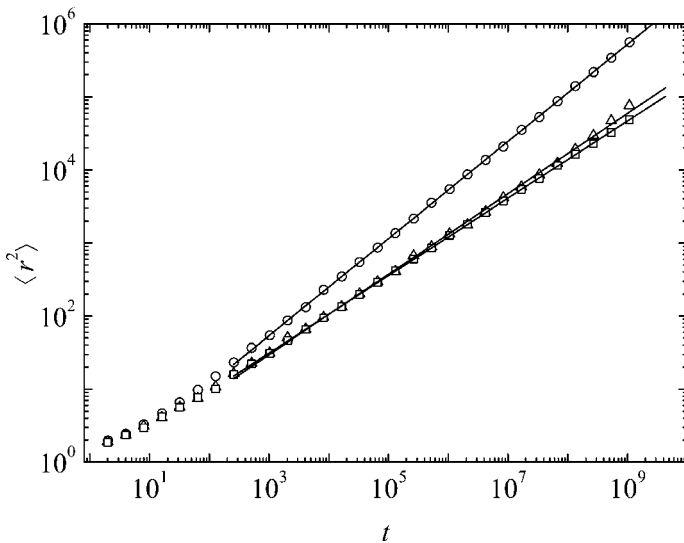


Figure 13.1 Mean-square displacement in one-, two-, and three-dimensional media with quenched disorder as described in the text for $\alpha = 1/2$. The points correspond to times $t = 2^1, 2^2, \dots, 2^{30}$ for $d = 1$ (circles), $d = 2$ (squares), and $d = 3$ (triangles). The lines

are fit to the simulation data from $t = 2^{10}$ to $t = 2^{30}$. The slopes are 0.66 for $d = 1$, 0.53 for $d = 2$, and 0.54 for $d = 3$, in good agreement with the corresponding theoretical anomalous diffusion exponent ($\gamma = 2/3$ for $d = 1$, $\gamma = 1/2$ for $d = 2, 3$).

geophysical phenomena such as subsurface hydrology or force distributions in static granular media (see the contributions by Kob et al., Chapter 12, and Kimmich et al., Chapter 17, in this volume). Dynamical disorder is invoked in relaxation processes in polymers and in viscoelastic materials, diffusion of particles in certain turbulent media, electron transfer processes in proteins and, more generally, in the relaxation of any system coupled to a complex (fractal) heat bath. In these systems, subdiffusion arises from fluctuations that are not much faster than the transfer rates associated with the transport process of interest. As a result, these dynamical fluctuations may give rise to a distribution of rates that in turn leads to anomalous transport properties.

Since each of these varied processes may be characterized by a subdiffusive mean-square displacement, it is clear that this quantity alone cannot distinguish between the vastly different underlying mechanisms all of which give rise to the same anomalous behavior in this single measure.

The theoretical and mathematical approaches to the subdiffusion problem, particularly those that lead to results beyond the mean-square displacement, are also varied. In fact, the distinctions invoked above do not necessarily lead to different models; in other words, essentially the same model (but with suitably interpreted parameter definitions) may be invoked in situations that are fundamentally different [2–4, 19]. For example, it is often assumed that motion

in a fractal medium can, in some sense, be represented by motion in a regular medium with quenched disorder. While this is often the case, there are instances where it is not [23]. Here, we briefly mention a few approaches, some of which we develop in more detail as needed in later sections. But here we also hasten to add that since subdiffusion is often associated with disorder of some sort, analytic work is difficult, and a great deal of work in this arena has been numerical. This, too, presents difficulties because a subdiffusive process is, by definition, slow, and in many cases it is beyond even current numerical capabilities to arrive at reliable statistics, especially when one is interested in asymptotic behavior, or when the subdiffusive process occurs amidst faster time scale processes. For example, simulations involving reactions between diffusive and subdiffusive particles are notoriously strenuous. This is a typical numerical quandary in problems involving very disparate time scales.

A frequent theoretical starting model for subdiffusive processes is the continuous time random walk (CTRW) [3, 24] (see the contribution by Gorenflo and Mainardi, Chapter 4, in this volume). Suppose a walker starts at $t = 0$ at the origin, waits a random time T_1 to make a jump of length X_1 , waits a random time T_2 to jump again over distance X_2 , etc., with the waiting times between jumps and the lengths of the jumps drawn from a probability distribution function (pdf) $\phi(x, t)$. This defines a CTRW. If the waiting times and jump lengths are independent random variables, then the pdf is a product, $\phi(x, t) = w(x)\psi(t)$, and the probability density $P(x, t)$ that the particle is at x at time t obeys the integral equation

$$P(x, t) = \delta(x)\Psi(t) + \int_0^t dt' \psi(t - t') \int_{-\infty}^{\infty} dx' w(x - x') P(x', t'), \quad (13.5)$$

where $\Psi(t) = \int_t^{\infty} dt' \psi(t')$ is the probability that at time t the particle is still at the origin. Ordinary random walks or ordinary diffusion arise if $w(x)$ has finite variance and $\psi(t)$ has a finite first moment. (Superdiffusion is associated with a $w(x)$ with infinite variance.) Subdiffusion arises if $w(x)$ has finite variance but the time density between jumps decays as a power law at long times [3, 25–27],

$$\psi(t) \sim t^{-1-\gamma}, \quad t \rightarrow \infty, \quad (13.6)$$

with $\gamma < 1$ so that the mean time between jumps diverges. Most often the CTRW is assumed to take place on a regular lattice or a Euclidean continuum, and it is then straightforward to deduce that

$$\langle r^2 \rangle \sim \frac{2dK}{\Gamma(1+\gamma)} t^\gamma, \quad t \rightarrow \infty. \quad (13.7)$$

Here, K is the (generalized) diffusion coefficient. One can generalize the discussion to the case where the time at which the observation begins ($t = 0$)

does not coincide with the time at which the walker makes a jump, thus introducing the notion of “aging” [28].

While CTRW models have been applied broadly, they can quickly become analytically onerous. They are then used as a point of departure for the formulation of more tractable coarse-grained models. These latter approaches also facilitate the consideration of force fields and of spatial boundaries, which are difficult to incorporate in the CTRW context. A favorite path to simplify the situation is to follow the route often taken for ordinary random walks, namely, to take a scaling limit in which the variance of the jump lengths and the mean time between jumps vanish in a particular way to arrive at the diffusion equation. The fractional diffusion equation for the probability density associated with a CTRW with an asymptotic power-law jump time distribution has been derived in various ways in the literature [3, 4, 29] (see Part I of this volume). A particularly illuminating recent discussion of a scaling approach appears in Ref. [30]. One arrives at the equation

$$\frac{\partial}{\partial t} P(x, t) = {}_0 D_t^{1-\gamma} K \frac{\partial^2}{\partial x^2} P(x, t), \quad (13.8)$$

where ${}_0 D_t^{1-\gamma}$ is the Riemann–Liouville operator (see Hilfer’s contribution, Chapter 2, in this volume for more information on this operator)

$${}_0 D_t^{1-\gamma} P(x, t) = \frac{1}{\Gamma(\gamma)} \frac{\partial}{\partial t} \int_0^t d\tau \frac{P(x, \tau)}{(t - \tau)^{1-\gamma}} \quad (13.9)$$

and K is the generalized diffusion coefficient that appears in Eq. (13.7). Solutions to this equation are well studied, and we will have occasion to invoke the equation in later sections.

A second starting point for subdiffusive processes has been invoked mainly for systems with dynamical disorder. This approach, called fractional Brownian motion [31], starts with a generalized Langevin equation with fluctuations that are, as usual, Gaussian, but whose correlation function includes a slow power-law time decay contribution [19, 21, 22]. Just as the ordinary Langevin equation with Gaussian δ -correlated noise can be recast in the form of the diffusion equation, so the generalized Langevin equation with fractional Gaussian noise can be recast as a fractional diffusion equation, but now with a time-dependent diffusion coefficient [22],

$$\frac{\partial}{\partial t} P(x, t) = \gamma D t^{\gamma-1} \frac{\partial^2}{\partial x^2} P(x, t), \quad (13.10)$$

which also leads to a sublinear mean-square displacement. We have mentioned this approach for completeness but do not apply it in our studies.

While we have thus briefly outlined a number of possible approaches to subdiffusion, the problem becomes much more complicated if subdiffusive

particles can also *react*. How to build reactions into any subdiffusive model is as yet far from clear, and different approaches have even produced mutually inconsistent results. In the reaction–diffusion problems one is accustomed to simply add a local law of mass action (product) reaction term to the diffusion or random walk equation, which clearly relies on the assumption that these processes are simply additive. Thus, for example, if one considers a bimolecular reaction of the form $A + B \rightarrow C$ in a normal diffusive system one would not hesitate to write the mean field equation for the local concentration $a(x, t)$ of A particles (or, equivalently, the probability density of finding an A particle at x at time t) as

$$\frac{\partial}{\partial t}a(x, t) = D \frac{\partial^2}{\partial x^2}a(x, t) - ka(x, t)b(x, t). \quad (13.11)$$

However, if the motion of one or both reactants is subdiffusive, it is not at all clear that the reaction contribution can simply be added to a subdiffusion equation this way. In fact, it is now known on the basis of theoretical arguments and numerical simulation results that simple addition of a product term is, in general, not correct [12, 13, 32–34]. Fortunately, there are some exact results as well as approximate results that have been supported by numerical simulations that point to more appropriate ways to model reaction–subdiffusion processes [1, 5, 6, 12, 13, 15, 16, 32–37]. In the following sections, we describe this scenario in more detail.

13.3

Target and Trapping Problem

The target problem and the trapping problem are the two classic reaction–diffusion scenarios on which rests the broader theory of diffusion-limited reactions. In the *target* (or scavenger) problem, a *static particle* A is surrounded by a distribution of *mobile traps* B [6, 38–40] (see Figure 13.2(a)), whereas in the traditional version of the *trapping* problem, a *diffusive (Brownian) particle* A wanders in a medium doped at random with *static traps* B [1, 5, 24, 25] (see Figure 13.2(b)). When a particle and a trap meet, the particle disappears. The trapping problem dates back to Smoluchowski's theory of reaction rates at the beginning of last century [41]. Both are among the most widely investigated and applied problems of nonequilibrium statistical mechanics. The principal quantity of interest is the survival probability $P(t)$ of the A particle as a function of time t . From this survival probability one is able to calculate essentially all other quantities of practical interest. The subdiffusive versions of these two problems, that is, the target problem with subdiffusive traps, and the trapping problem with subdiffusive particles, have also been studied extensively [6, 38–40, 42–50].

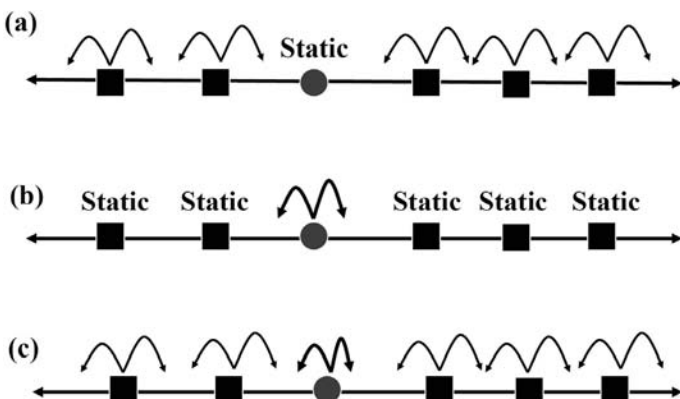


Figure 13.2 (a) Sketch of the target problem: a static particle (circle) in a sea of diffusive traps (squares). (b) Sketch of the trapping problem: a diffusive particle (circle) in a sea of static traps (squares). (c) Sketch of the generalized problem discussed in 13.6: a diffusive particle (circle) surrounded by a sea of diffusive traps (squares).

13.3.1

Target Problem

Whether the traps move diffusively or subdiffusively on a lattice, it can be proved that [38, 50]

$$P(t) = \exp[-cS(t)], \quad (13.12)$$

where c is the concentration of traps and $S(t) \equiv \langle \mathbf{S}(t) \rangle$ is the *mean* number of distinct sites that a random walker visits in time t . In a continuum “number of distinct sites visited” must be understood as the volume that has been generated by a randomly moving spherical particle, that is, the volume of the “Wiener sausage” generated by the spherical particle [51, 52]. For the case of ordinary diffusion one can think of the traps as random walkers taking steps of unit length per unit time in a d -dimensional lattice, and then one has, for large t [24–26],

$$S(t) \sim \begin{cases} \sqrt{\frac{8}{\pi}} t^{1/2}, & d = 1, \\ \omega t / \ln t, & d = 2, \\ \omega t, & d \geq 3. \end{cases} \quad (13.13)$$

The value of the constant ω in each dimension depends on the lattice geometry. For example, for a two-dimensional square lattice one has $\omega = \pi$, whereas for a simple cubic lattice $\omega = 1 - R$, where $R = 0.340537\dots$ is the probability of a random walker ever returning to his starting point [24, 50]. The expressions are, in general, valid with modified constant prefactors for walks with

a distribution of step lengths and stepping times if the variance of the jump lengths and the mean time between jumps remain finite.

In the subdiffusive case, one can think of traps that jump over distances of finite variance but with the jump times governed by a waiting time distribution whose long-time behavior is a power law as in (13.6) (CTRW model). The time dependences of the $S(t)$ are now different [6, 15, 38, 45, 49, 53, 54]:

$$S(t) \sim \begin{cases} \Omega t^{\gamma/2}, & d = 1, \\ \Omega t^\gamma / \ln t^\gamma, & d = 2, \\ \Omega t^\gamma, & d \geq 3, \end{cases} \quad (13.14)$$

where the Ω are constants that depend on the geometry of the substrate, the generalized diffusion coefficient, and the anomalous diffusion exponent γ . Note that one can obtain the correct time dependence of the subdiffusive formulas ($\gamma < 1$) from the normal diffusive counterparts by means of the substitution $t \rightarrow t^\gamma$. This is a manifestation of the “subordination” of the subdiffusive process to the normal diffusive one (the *parent process*) in the sense that the subdiffusive process $X(t)$ can be obtained from a Brownian process $B(n)$ in which its time n (the *operational time*) is conveniently randomized by a stochastic process (the directing process) $n = T(t)$ with nonnegative independent increments, i.e., $X(t) = B[n(t)]$ (see more details in [55, 56]). Therefore, the subdiffusive process can be fully described from its Brownian counterpart. However, in some cases, a rough but easier description of the subdiffusive process can be obtained by means of the simple substitution of $t \rightarrow t^\gamma$ into the normal diffusive quantities [6, 42]. This subordination procedure (or trick) can be understood taking into account that subdiffusion is due to the fact that the number of steps $n(t)$ within a given time interval t typically grows sublinearly with time, $n(t) \sim t^\gamma$, as opposed to the normal linear growth typical of ordinary diffusion [55]. Therefore, all properties that depend on time only through the number of steps taken by the random walker behave as they would in ordinary diffusion but with the replacement $t \rightarrow t^\gamma$. In our case, it is clear that the determining factor in the growth of $S(t)$, and hence in the decay of $P(t)$, is the number of steps $n(t)$ taken by the traps up to time t . Finally, for the CTRW model on a fractal one has $S(t) \sim t^{\gamma\tilde{d}/2}$ for $\tilde{d} < 2$, and $S(t) \sim t^\gamma$ for $\tilde{d} > 2$ [39].

Many interesting variations and applications of the target problem can be found in the literature. Some recent ones include stochastically gated [50] or evanescent [46] traps, and the target problem on scale-free networks and on small world networks [47].

13.3.2

Trapping Problem

The probability that any given site is *not* occupied by a trap is $1 - c$. From the definition of $\mathbf{S}(t)$ one then immediately concludes that the survival probability in the trapping problem is

$$P(t) = \langle (1 - c)^{\mathbf{S}(t)} \rangle \equiv \langle e^{-\lambda \mathbf{S}(t)} \rangle, \quad (13.15)$$

where $\lambda \equiv -\ln(1 - c)$. The average in this equation is performed over all realizations of the random walk from time $t = 0$ to time t . This average cannot be calculated exactly, and therefore to deal with the trapping problem one typically has to resort to short-time and long-time asymptotic approximations.

The extended Rosenstock approximation or truncated cumulant expansion is the standard approach for estimating the short-time asymptotics of the trapping problem [24, 25, 40, 57, 58]. The cumulant expansion technique allows an alternative expression for the survival probability as an infinite series,

$$P(t) = \exp \left[\sum_{n=1}^{\infty} \frac{(-\lambda)^n \kappa_n}{n!} \right], \quad (13.16)$$

where κ_n , $n = 1, 2, \dots$, denote the cumulants of $\mathbf{S}(t)$. The first two cumulants are $\kappa_1 = \langle \mathbf{S}(t) \rangle \equiv S(t)$ and $\kappa_2 = \langle \mathbf{S}^2(t) \rangle - \langle \mathbf{S}(t) \rangle^2 \equiv \sigma^2(t)$. If only the first term of the sum in Eq. (13.16) is retained, we get the zeroth order Rosenstock approximation

$$P(t) = e^{-\lambda S(t)}. \quad (13.17)$$

The error made in this truncation can be estimated by considering the next term in the exponent in Eq. (13.16). One finds that the zeroth order Rosenstock approximation is reasonable for concentrations and times sufficiently small to satisfy the condition $\lambda^2 \sigma^2 \ll 1$. A shortcoming of this approach is that the first moments of $\mathbf{S}(t)$ are known only for a few simple cases [24, 59].

The long-time behavior of the survival probability of the particle in a sea of stationary traps has been studied for diffusive particles in Euclidean media [24, 25, 60] and on fractal substrates [42, 43, 48]. It has also been studied for particles performing a long-tailed CTRW in Euclidean and fractal media [39, 40, 42, 49]. The mathematics leading to the results is too elaborate to reproduce in any abbreviated version, so we simply state the results. For diffusive particles on a Euclidean or fractal medium one finds

$$P(t) \sim \exp \left[-\alpha \lambda^{2/(\tilde{d}+2)} t^{\tilde{d}/(\tilde{d}+2)} \right], \quad (13.18)$$

where α is a substrate-dependent constant and \tilde{d} is the spectral dimension of the substrate. The difficulties in verifying this result numerically because of

the long times it takes to reach this asymptotic behavior are well known [61]. On the other hand, for a particle that performs a long-tailed CTRW the survival probability is given by $P(t) \sim t^{-\gamma}$ [39]. Note that now, at odds with what we founded for the target problem, one cannot arrive at the long-time behavior of $P(t)$ via the simple subordination substitution $t \rightarrow t^\gamma$ in the normal diffusive result. This is because the survival probability here is not determined mainly by the number of steps taken by the particle. In fact, the survival probability of the particle is greatest if it takes no steps at all, and the probability that it remains at its initial location up to time t is precisely $\int_t^\infty \psi(\tau)d\tau \sim t^{-\gamma}$.

In Figure 13.3, we show simulation results for the survival probability in a one-dimensional subdiffusive trapping problem where the particle motion is a long-tailed CTRW. We also show the long-time, $P(t) \sim 1 / [2\Gamma(1 - \gamma)\xi^2]$, and short-time, $P(t) \sim \exp[-2\xi/\Gamma(1 + \gamma/2)]$, asymptotic results [49]. Here, $\xi = \lambda\sqrt{Kt^\gamma}$.

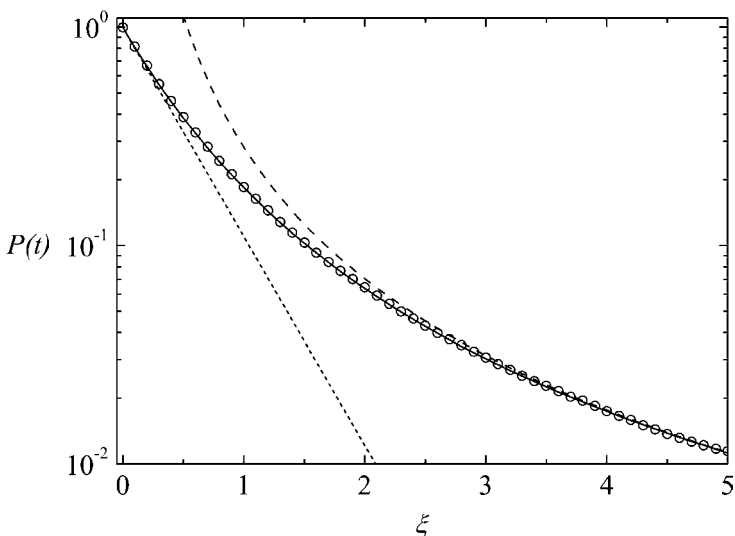


Figure 13.3 Survival probability $P(t)$ versus $\xi \equiv \lambda\sqrt{Kt^\gamma}$ for the one-dimensional CTRW trapping problem with $\gamma = 1/2$. The symbols are simulation results for $c = 0.01$ and 10^6 realizations. The dashed and dotted lines correspond to the long- and short-time asymptotic approximations, and the solid line represents the numerical estimation of an exact integral representation of $P(t)$ [49].

13.4

Two Basic Reactions

In both the target and the trapping problems discussed in Section 13.3, one of the two particles involved in the reaction (either the one that disappears or the one that survives) was *static*. As a result, the solution of these problems is relatively simple. The problem turns out to be much more difficult when all the reacting particles are mobile. In this section, we consider two basic reactions of this type. The first is a single-component reaction, $A + A \rightarrow \{A, 0\}$, and the second is a two-component reaction, $A + B \rightarrow 0$.

13.4.1

Annihilation and Coalescence Reactions

Consider a reactive system in which subdiffusive A particles merge when they meet, $A + A \rightarrow A$ (coalescence reaction). Although, we explicitly discuss only the coalescence reaction, all the results of this section are also valid for the annihilation reaction, where both particles disappear upon encounter, $A + A \rightarrow 0$.

For well-stirred systems, the concentration $c(t)$ of particles A follows the classical kinetics equation $dc/dt \sim -c^2$, so that $c(t) \sim 1/t$ independently of the initial concentration $c(0)$. However, when the particles are mixed only by diffusion, a system in low dimensions is not well-stirred and the kinetics is different [1,5]:

$$c(t) \sim \begin{cases} 1/t^{d/2}, & d < 2, \\ 1/t, & d > 2. \end{cases} \quad (13.19)$$

When the particles A are subdiffusive with anomalous diffusion exponent γ , the corresponding result is [6]

$$c(t) \sim \begin{cases} 1/t^{\gamma d/2}, & d < 2, \\ 1/t^\gamma, & d > 2. \end{cases} \quad (13.20)$$

Note that this result follows from Eq. (13.19) via the subordination replacement $t \rightarrow t^\gamma$.

In Figure 13.4, we show simulation results for the concentration $c(t)$ of A particles that react by annihilation or by coalescence, and that diffuse in one- and three-dimensional quenched-disorder lattices as described above Eq. (13.4) with $\alpha = 1/2$ (i.e., $\gamma = 2/3$ for $d = 1$ and $\gamma = 1/2$ for $d = 3$). The fitted lines for $d = 1$ [$d = 3$] correspond to the expression $c(t) = 0.88/t^{0.33}$ [$c(t)=1.44/t^{0.49}$] for the coalescence reaction, and to $c(t) = 0.44/t^{0.33}$ [$c(t)=0.74/t^{0.49}$] for the annihilation reaction. Note that, as one would expect, $c_{\text{annihilation}} \simeq c_{\text{coalescence}}/2$.

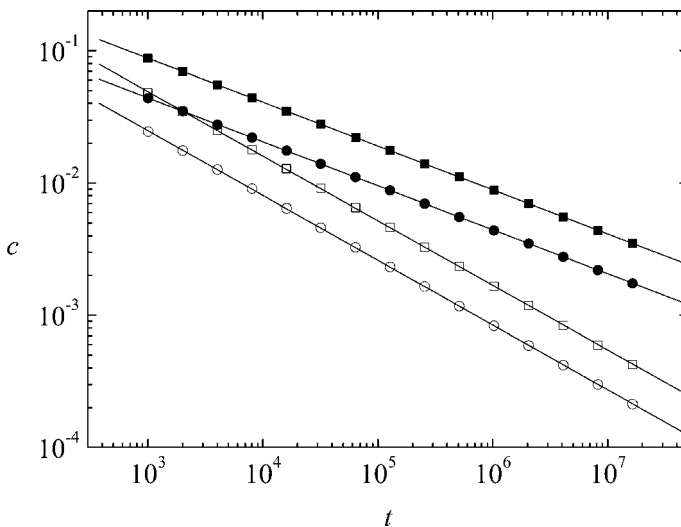


Figure 13.4 Simulation results for the concentration $c(t)$ of subdiffusive particles in a one-dimensional (open symbols) and three-dimensional (filled symbols) quenched-disorder lattice with $\alpha = 1/2$ where they react by coalescence ($A + A \rightarrow A$, squares) and annihilation ($A + A \rightarrow 0$, circles). The fitted lines have a slope of 0.33 for $d = 1$ [0.49 for $d = 3$] in good agreement with the theoretical exponents $\gamma/2 = 1/3$ [$\gamma = 1/2$].

Equation (13.20) can be justified by means of scaling arguments [1, 5] that involve $S(t)$, the volume swept out by a randomly moving particle (cf. Eq. (13.13)). One assumes that the number of particles that a given particle A destroys during time Δt is given approximately by the number of particles inside the volume swept by A during this time, namely, $c(dS/dt)\Delta t$. Recognizing that there is not just a single A in this volume but that there are in fact $c(t)V$ of them, the cV particles inside the volume V will destroy $cV \times c(dS/dt)\Delta t$ particles. Thus, as $\Delta t \rightarrow 0$ we have $dc/dt \sim c^2 V dS/dt$, which upon integration immediately leads to $c \sim 1/S$. For $d > 2$ this argument is clear because the random walk is not recurrent, that is, each step essentially brings the particle to a new previously unexplored location. However, for $d \leq 2$ the random walk is recurrent and the argument is less evident. Nevertheless, the same result holds precisely because the exploration of a particle is compact for $d \leq 2$, and thus only the (surviving) sweeping particle remains inside the swept volume $S(t)$, which means that again $c \sim 1/S$. It turns out that this result is valid for normally diffusive as well as subdiffusive particles in Euclidean and fractal substrates [6]. This formula, together with (13.14), explains (13.19) and (13.20). It is worth noting that for the one-dimensional case there are more precise and detailed results obtained by special methods for normal diffusive particles (see, e.g., [5, 62]) and also for subdiffusive particles (see, e.g., [63, 64]).

In this section, we have only explicitly considered reactions in Euclidean media. For fractal media the results (13.19) and (13.20) are also valid with the replacement of the dimension d by the spectral dimension \tilde{d} [6].

13.4.2

Annihilation of Two Species, $A + B \rightarrow 0$

Consider now the two-component annihilation reaction $A + B \rightarrow 0$ and let us assume that the initial concentration of both species of particles, arranged at random in a d -dimensional substrate, are equal, $c_A(0) = c_B(0)$. (Some two species reactions with different initial concentrations will be studied in Section 13.6.) It is well known that when the particles are normally diffusive, the concentration of either species decays as [5, 6, 65, 66]

$$c(t) \sim \begin{cases} 1/t^{d/4}, & d < 4, \\ 1/t, & d > 4, \end{cases} \quad (13.21)$$

where c stands for c_A or c_B . Thus, the law of mass action result $c(t) \sim t^{-1}$ obtained from the usual macroscopic rate law $dc/dt = -kc^2$ holds only above four dimensions (and with logarithmic corrections at the critical dimension $d = 4$). To understand the $d < 4$ behavior one notes that in an initially random distribution of reactants there are local density fluctuations which lead to a local surplus of one species over the other. In a region of volume r^d this surplus is of order $[c(0)r^d]^{1/2}$. The fluctuations decay by diffusion even while at the same time the concentrations of both species decay because of the reaction. For $d < 4$ the decay due to the occurrence of fluctuations and the attendant diffusion is slower than the rate equation decay. Thus, as time passes the particles inside this volume will diffuse and cover the entire volume in a time of order $t \sim r^2$ during which $A - B$ pairs will have annihilated. The concentration of the surviving majority species is then roughly the initial surplus divided by the volume r^d , that is, $c(t) \sim [c(0)r^d]^{1/2}/r^d = [c(0)/r^d]^{1/2} \sim t^{-d/4}$. This gives rise to increasing segregation of species, producing growing regions rich in one species or the other. The reaction occurs only at the interfaces and is hence slower than predicted by the macroscopic law of mass action rate equation. At the critical dimension $d = 4$ the rates of the two decay mechanisms coincide, and when $d > 4$ diffusion is able to mix the particles effectively and consequently the law of mass action applies.

For subdiffusive particles described by a CTRW the results in Eq. (13.21) generalize to

$$c(t) \sim \begin{cases} 1/t^{\gamma d/4}, & d < 4, \\ 1/t^\gamma, & d > 4. \end{cases} \quad (13.22)$$

The $d < 4$ result, which follows from the subordination trick $t \rightarrow t^\gamma$, can be found in Ref. [6] and can be obtained following the arguments laid out above generalized to the subdiffusive case (see Refs. [1, 5, 65, 66]). The initial surplus of one species over the other in a volume r^d is still $\sim [c(0)r^d]^{1/2}$. Now, however, the particles inside the volume will cover it in a time of order $t \sim r^{2/\gamma}$, so that reactions inside the volume will leave the majority species with concentration $c(t) \sim [c(0)/r^d]^{1/2} \sim t^{-\gamma d/4}$. That the concentration above the critical dimension decays as $c(t) \sim t^{-\gamma}$, and that the critical dimension for the above behavior is still $d = 4$, has, to our knowledge, not been proven and must rely for now on the subordination argument, which we repeat in this context for the sake of clarity. In the law of mass action regime (or its analog for subdiffusive particles), the change Δc in the density $c(t)$ when particles make Δn jumps is proportional to the number of encounters between opposite species during these jumps. For $d > 4$ we assume that, as in the case of normal diffusion, the subdiffusive process mixes the particles effectively so that the number of encounters is proportional to c^2 . Therefore, $dc/dn \sim c^2$ and it follows that $c \sim 1/n$. For diffusive particles $n \sim t$, and consequently one recovers the classical result $c \sim 1/t$. For subdiffusive particles $n \sim t^\gamma$, and consequently $c \sim 1/t^\gamma$.

Finally, for fractal media the results in (13.21) and (13.22) for $d < 4$ are also valid with the replacement of d by the spectral dimension \tilde{d} [6]. It would seem reasonable to conjecture, on the basis of the subordination procedure, that the results for $d > 4$ are also valid with this replacement.

13.5

Reactions with Nonhomogeneous Distribution of Reactants

In the preceding sections, we focused on the global reaction kinetics of different reactive systems, our main objective being the estimation of the time dependence of the global concentration $c_i(t)$ of the reactants. However, in some cases, specifically for systems where the spatial arrangement of reactants is inhomogeneous, it might be more convenient or even necessary to consider a mesoscopic description, and to study how the concentrations of the species vary in space as well as time. In this case, the quantities of interest will be the $c_i(\mathbf{r}, t)$.

Of course, as a first proviso this study requires knowledge of how the concentrations of species evolve in the absence of reactions. For normal diffusive particles, the evolution of $c_i(\mathbf{r}, t)$ is given by the diffusion equation. On the other hand, for the long-tailed CTRW model the concentration of particles

evolves according to the fractional diffusion equation (13.8):

$$\frac{\partial c_i}{\partial t} = K_i {}_0D_t^{1-\gamma} \nabla^2 c_i(\mathbf{r}, t). \quad (13.23)$$

For N -component reactive systems with normal diffusive species, the reaction-diffusion equations for the local concentrations are

$$\frac{\partial c_i}{\partial t} = K_i \nabla^2 c_i(\mathbf{r}, t) + f_i(c_1, \dots, c_N). \quad (13.24)$$

The reaction terms f_i are typically those corresponding to the law of mass action, $f_i = \pm \kappa_i \prod_{j=1}^N c_j^{n_j}$, where the n_j are the stoichiometric coefficients.

What are the analogous equations when the reactants are subdiffusive? In the previous sections, specially in Section 13.4, we have appealed to subordination arguments to obtain the reaction kinetics for subdiffusive systems from their diffusive counterparts by means of the change $t \rightarrow t^\gamma$. This might lead us to think that a similarly simple substitution could be true for reaction-diffusion equations. Looking at (13.8) and (13.24), one might be tempted to conjecture that the change equivalent to the subordination $t \rightarrow t^\gamma$ is perhaps $\nabla^2 \rightarrow {}_0D_t^{1-\gamma} \nabla^2$, so that the subdiffusion-limited reactions would be described by

$$\frac{\partial}{\partial t} c_i(\mathbf{r}, t) = K_i {}_0D_t^{1-\gamma} \nabla^2 c_i(\mathbf{r}, t) + f_i(c_1, \dots, c_N). \quad (13.25)$$

Although, this may seem natural, it is, in general, false!. For example, $\partial c / \partial t = K \partial^2 c / \partial x^2 - \kappa c(x, t)$ is a well-behaved equation describing the change in the concentration because the particles disappear with rate coefficient κ (we assume $\kappa > 0$) and also because of diffusion. However, the equation

$$\frac{\partial c}{\partial t} = K {}_0D_t^{1-\gamma} \frac{\partial^2 c}{\partial x^2} - \kappa c(x, t) \quad (13.26)$$

leads to the unphysical prediction of negative concentrations [13] (see Figure 13.5). This example should serve as a strong indicator that the subject of subdiffusion-limited reactions is tricky and should be approached with caution.

13.5.1

Reaction–Subdiffusion Equations

The above example prompts a less naive, less ad hoc, more fundamental construction of the reaction–subdiffusion equations . Indeed, it calls for building reaction–subdiffusion equations (equations that are a mesoscopic description of the reactive system) from a microscopic approach. Some work along

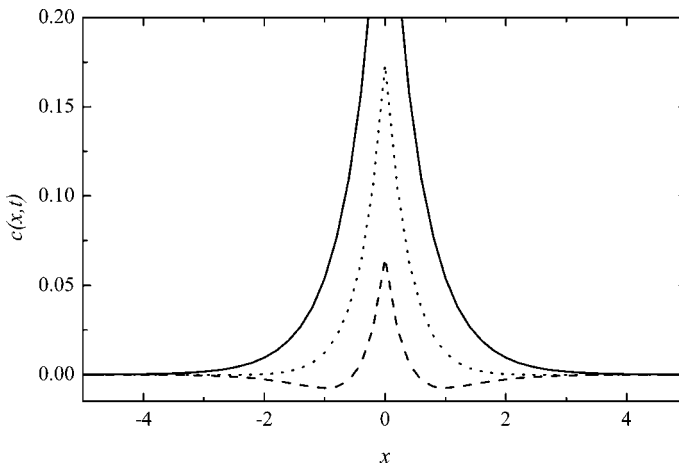


Figure 13.5 Concentration $c(x, t)$ for $t = 0.2$ (solid line), $t = 0.4$ (dotted line), and $t = 1$ (dashed line) obtained by solving Eq. (13.26) by means of the numerical methods for integrating fractional diffusion equations described in [67]. Here, $\gamma = 1/2$, $K = 1$, $\kappa = 5$, the initial condition is $c(x, 0) = \delta(x)$, and free boundary conditions are used.

these lines has recently been published [12, 13, 32–35, 37, 68–72]. In Ref. [32], Seki et al. consider geminate recombination (that is, recombination of particles produced from a common precursor) of subdiffusive particles. Their analysis is based on the CTRW scheme. In their model, one particle migrates subdiffusively back toward the other, the reaction taking place when the particles are separated by a distance between R (the reaction radius) and $R + dr$. If the reaction occurs at a rate comparable with the transport kinetics, two types of waiting time distributions at the encounter distance are relevant: the waiting time distribution for making a jump to a neighboring lattice site, $\psi_{\text{out}}(t) = \psi(t)\exp(-t/\tau_{\text{rc}})$, and the waiting time distribution of reaction defined as the probability that the particle which is initially at a site within the encounter distance will undergo reaction without making a jump at time t , $\psi_{\text{rc}}(t) = \tau_{\text{rc}}^{-1}\exp(-t/\tau_{\text{rc}})\int_0^\infty dt_1\psi(t_1)$, τ_{rc}^{-1} being the reaction rate constant.¹ In Ref. [32], it is shown that this model leads to the reaction–subdiffusion equation

$$\frac{\partial c}{\partial t} = {}_0D_t^{1-\gamma} \left[K\nabla^2 c(r, t) - \kappa\delta(r - R)c(r, t) \right], \quad (13.27)$$

1) When the jump waiting time distribution $\psi(t)$ is long-tailed, we see that the reaction has memory in the sense that the probability of not reacting during a given time affects the probability of reaction after this time; this is not the case when the jump waiting time distribution is exponential, that is, for normal diffusive particles.

where K and κ are constants. For $\gamma = 1$, the Riemann–Liouville derivative is the identity operator and the conventional equation is recovered. As discussed earlier, the substitution $\nabla^2 \rightarrow {}_0D_t^{1-\gamma}\nabla^2$ in the normal reaction–diffusion equation does not lead to the correct subdiffusive counterpart. Equation (13.27) is remarkable: it shows that the exit from the encounter distance described by a long-tailed waiting time distribution of jumps interferes with the reaction at the encounter distance. This leads to a memory in the reaction term like the one that describes subdiffusive motion [32].

Another interesting problem that leads to a reaction–subdiffusion equation where, as in Eq. (13.27), a fractional (subdiffusive) operator affects both the diffusion and the reaction terms is that proposed by Henry et al. [13] (see also Ref. [73]). In this problem, a constant proportion of subdiffusive particles in a one-component system is removed instantaneously at the start (or end) of each jump. It turns out that this CTRW model leads to the reaction–subdiffusion equation [13]

$$\frac{\partial c}{\partial t} = \mathcal{D}_t^{1-\gamma} \left[K \frac{\partial^2 c}{\partial x^2} - \kappa c(x, t) \right], \quad (13.28)$$

where K and κ are constants, and where $\mathcal{D}_t^{1-\gamma}$ is an integro-differential operator (closely related to the Riemann–Liouville derivative²⁾, defined by the relation $\mathcal{L}\mathcal{D}_t^{1-\gamma}y(t) = u^{1-\gamma}\tilde{y}(u)$. Here, \mathcal{L} is the Laplace operator, u the Laplace variable, and $\tilde{y}(u)$ the Laplace transform of $y(t)$. Once again the subdiffusive character of the reactants modifies the classical reaction term $-\kappa c(x, t)$ through the same fractional operator $\mathcal{D}_t^{1-\gamma}$ that modifies the classical diffusion term $K\partial^2 c/\partial x^2$.

In the models leading to Eqs. (13.27) and (13.28), the reactions at small scales are subdiffusion controlled, that is, in these models the (subdiffusive) movement of the particles leads to encounters among them which eventually lead to reactions. A different scenario occurs when the reaction at small scales is decoupled from the (subdiffusive) movement of the particles. Such models have also been proposed recently [12, 13, 33, 74]. For example, in Refs. [12, 13, 33] a model in which the subdiffusive particles disappear at a constant rate independent of their position and movement is considered. In this case, the reaction–subdiffusion equation is

$$\frac{\partial c}{\partial t} = K e^{-\kappa t} \mathcal{D}_t^{1-\gamma} \left[e^{\kappa t} \frac{\partial^2 c}{\partial x^2} \right] - \kappa c(x, t). \quad (13.29)$$

2) In fact, both operators $\mathcal{D}_t^{1-\gamma}$ and ${}_0D_t^{1-\gamma}$ are the same when applied to sufficiently regular functions $f(t)$ as determined by the condition $\lim_{t \rightarrow 0} \int_0^t d\tau (t - \tau)^{\gamma-1} f(\tau) = 0$.

Thus, in a form different from Eqs. (13.27) and (13.28), this equation again shows that the contributions of subdiffusion and reaction to the time evolution of the density are not separable.

The reaction–subdiffusion systems discussed in this section are monomolecular.³ Some attempts to arrive at mesoscopic descriptions of multicomponent reaction–subdiffusion systems where the subdiffusion is described by the CTRW formalism and the reaction is modeled locally by means of the law of mass action have recently begun to appear in the literature [33, 34]. However, on the whole, a microscopic approach to multicomponent subdiffusion controlled systems such as that considered below in Section 13.5.2, is still lacking, and the subdiffusion–reaction equations employed for these systems are for now mostly of an ad hoc nature.

13.5.2

Reaction Fronts

In many reaction–diffusion and reaction–subdiffusion systems, either by design or by natural evolution of the system, the spatial distribution of reactants is spatially inhomogeneous. This occurs, for instance, when initially the reactants are separated by a physical boundary that is then removed, or when there are inhomogeneous sources of reactants that feed the system through its boundaries, or even in constrained geometries where random fluctuations of initially mixed reactants can grow in time as the local majority species overwhelms the minority. In these cases, the system may consist of essentially single-component domains so that the reactions between different components occur only (or mainly) at the interphases or boundaries of the domains.

The quintessential front problem is a d -dimensional systems where two reacting species, A and B , that form product C , are initially separated by a $(d - 1)$ -dimensional planar wall situated at $x = 0$. The concentrations of the species are denoted by a , b , and c , and the problem is to determine a number of measures such as the concentration profiles $a(x, t)$ and $b(x, t)$ of the reactants, the rate of production of C particles $R(x, t) \equiv \partial c(x, t)/\partial t$ (often called the reaction profile), the global reaction rate $R(t) = \int_{-\infty}^{\infty} R(x, t)dx$, and the position of the front $x_f(t)$ defined as the position where $c(x, t)$ is maximum. This system, in contrast with those of Section 13.5.1, is a truly multicomponent reaction problem. Reaction fronts involving diffusive particles have been extensively studied. The standard analytic starting point in this case is the set

- 3) The geminate recombination reaction is analyzed by Seki et al. [32] as an effective monomolecular reaction where particles of a given species are absorbed at a boundary.

of mean-field reaction–diffusion equations

$$\begin{aligned}\frac{\partial}{\partial t}a(x,t) &= D_A \frac{\partial^2 a(x,t)}{\partial x^2} - ka(x,t)b(x,t), \\ \frac{\partial}{\partial t}b(x,t) &= D_B \frac{\partial^2 b(x,t)}{\partial x^2} - ka(x,t)b(x,t),\end{aligned}\tag{13.30}$$

where the choice $R(x,t) = ka(x,t)b(x,t)$ corresponding to the law of mass action has been made. Initially, the A particles are uniformly distributed with concentration a_0 in the region $x < 0$, and the B particles are uniformly distributed with concentration b_0 in the region $x > 0$. A variety of interesting analytic results are known for this system, obtained mainly from scaling approaches grounded on adiabatic time-scale separation arguments [5, 75, 76]. For example, for $d \geq 2$ the mean-field description (13.30) is valid, and when $D_A = D_B$ the width w of the reaction front (the region where $R(x,t)$ is appreciable) scales as $t^{1/6}$, its height $h = R(x_f, t)$ as $t^{-2/3}$, the global reaction rate $R(t)$ as $t^{-1/2}$, and, provided that $a_0 \neq b_0$, the position of the front x_f as $t^{1/2}$ (if $a_0 = b_0$ then clearly $x_f = 0$ at all times). Note that for the critical dimension $d = 2$ for this behavior there are logarithmic corrections to these results [77, 78]. Another version of the problem deals with a steady-state situation, where A and B particles are injected at equal rates J at opposite boundaries. Again there are scaling arguments that lead to steady state predictions for a number of quantities [79, 80]. For example, for $d \geq 2$ the width of the reaction front scales as $w \sim (kJ/D^2)^{-1/3}$ when $D_A = D_B \equiv D$. Here, too, $d = 2$ is the critical dimension for this behavior. These results break down below the critical dimension, that is, for systems such as one-dimensional lattices or two-dimensional percolation clusters. When $d < 2$, microscopic density fluctuations become important and the mean field reaction–diffusion formalism is no longer valid (see [5, 23, 81] and references in [82]). The exponents in this case are entirely different. For instance, in one dimension in the time-dependent scenario the width of the reaction front grows as $t^{1/4}$ (with perhaps a logarithmic correction [80]) instead of $t^{1/6}$ [78, 83, 84].

How do these results change when the particles are subdiffusive? First, it is commonly agreed that the critical dimension for the importance or negligibility of microscopic fluctuations is in any case still $d = 2$. Beyond this, the answers have been sought in two contexts. In one [81], numerical simulations are carried out in a system with a form of quenched disorder in which the mean-square displacement of the particles is sublinear in time, $\langle x^2 \rangle \sim t^\gamma$, as in Eq. (13.4). Araujo in [81] found empirically that for $d > 2$, $w \sim t^\alpha$ and $h \sim t^\beta$ with $\alpha = \gamma/6$ and $\beta = 1 - \gamma/3$. These exponents are thus associated with mean field behavior. For $d < 2$ the empirical results $\alpha = \gamma/(2 + 2\gamma)$ and $\beta = 1 - \gamma/2 + \alpha$ differ from mean field behavior, presumably due to the importance of microscopic fluctuations. Hecht et al. [23] simulated the reaction

on a two-dimensional percolation cluster, and found an exponent $\alpha \simeq 0.246$ very close to the one-dimensional normal-diffusive result $\alpha = 1/4$ and, again, $\beta = 1 - \gamma/2 + \alpha$.

The second context in which subdiffusive species in the quintessential front problem have been investigated is that of a regular lattice in which the particle motion is governed by a long-tailed CTRW model [82]. Computer simulations for $d = 2$ confirm the mean field exponents $\alpha = \gamma/6$, $\beta = 1 - \gamma/3$. The system was also studied analytically by postulating a set of fractional mean-field reaction–diffusion equations,

$$\begin{aligned}\frac{\partial}{\partial t}a(x,t) &= {}_0D_t^{1-\gamma} \left[K \frac{\partial^2 a(x,t)}{\partial x^2} - ka(x,t)b(x,t) \right], \\ \frac{\partial}{\partial t}b(x,t) &= {}_0D_t^{1-\gamma} \left[K \frac{\partial^2 b(x,t)}{\partial x^2} - ka(x,t)b(x,t) \right],\end{aligned}\tag{13.31}$$

which was inspired by the work of Seki et al. [32, 69, 70] in the geminate recombination problem. Note that Eqs. (13.31), like Eqs. (13.27) and (13.28), involve a fractional diffusion operator working simultaneously on the classical normal diffusion and reaction terms. Also, an entirely similar set of equations has recently been used by Langlands et al. [72] in a study of Turing patterns in subdiffusion–reaction systems. For simplicity the coefficients K in front of the second derivative terms have been set equal for the two species. While the validity of this form bears further discussion [33, 34], the predictions that emerge from this model agree with those obtained from the CTRW simulations, including the behaviors $w \sim t^{\gamma/6}$, $h \sim t^{1-\gamma/3}$, and $R(t) \sim t^{\gamma/2}$. From Eqs. (13.31) it is not difficult to prove that the position of the front is given by $x_f = S_f \sqrt{Kt^\gamma}$, where S_f is determined by the equation

$$\frac{2q}{1+q} = H_{11}^{10} \left[S_f \left| \begin{array}{c} (1, \frac{\gamma}{2}) \\ (0, 1) \end{array} \right. \right],\tag{13.32}$$

with $q = b_0/a_0 \leq 1$ [82]. Here, H_{11}^{10} is the Fox H -function [85]. An alternative analysis of Eqs. (13.31) that includes the case where one of the species is static is discussed in Ref. [86].

Clearly, the problem of fronts involving reactions of subdiffusive species is a field in its infancy in which much work remains to be done.

13.6

Reactants with Different (Sub)diffusion Exponents

The classic target and trapping problems discussed in Section 13.3 are both subsumed under the reaction $A + B \rightarrow B$. In the target problem, the particle A is stationary and the traps B move, while in the trapping problem the traps B

are stationary and A moves. A more difficult $A + B \rightarrow B$ problem occurs when both A and B move, especially if their motion is characterized by different exponents (see a sketch of this problem in Figure 13.2).

Even in the case of normally diffusive particles, the $A + B \rightarrow B$ problem is notoriously difficult and has only recently been fully solved asymptotically. The first rigorous results for this problem were actually derived from an analysis of the $A + B \rightarrow 0$ reaction. In Section 13.4.2, we reported results for this reaction when the initial concentrations $c_A(0)$ and $c_B(0)$ are equal. When the initial concentrations are not equal the decay laws are entirely different from the power laws reported in Eq. (13.21). Instead, the decay law for the minority species, say A , takes on an exponential form, shown by Bramson and Lebowitz [87] to be given by

$$c_A(t) \sim \begin{cases} \exp(-\lambda_d t^{d/2}), & d < 2, \\ \exp(-\lambda_2 \ln t/t), & d = 2, \\ \exp(-\lambda_d t), & d > 2. \end{cases} \quad (13.33)$$

The connection with the $A + B \rightarrow B$ problem arises because at the late times when these asymptotic laws apply one has a few isolated A particles diffusing in a background or sea of B particles whose density remains essentially fixed. While these exponential forms were posited, contradicted, and argued by a number of authors preceding Bramson and Lebowitz, theirs was the first rigorous proof that this is indeed the asymptotic behavior [8]. Note that because the A particles move independently, the evaluation of c_A is equivalent to that of the survival probability $P(t)$ of a single A particle moving in a sea of B traps, $c_A(t) \propto P(t)$.

The dimension-dependent constants λ_d remained undetermined for almost 15 years, until Bray and Blythe [88] applied an ingenious bounding procedure leading to lower and upper bounds that converge asymptotically to yield the explicit constant for $1 \leq d \leq 2$. Some of these bounding results were extended by Oshanin et al. [52] to systems where the traps perform a compact exploration of the space, that is, where the random walk dimension d_w of the traps is greater than the dimension d of the space. The upper bound for the survival probability was based on the so-called Pascal principle, which states that the best strategy for survival is for an A particle surrounded by moving traps not to move. Thus, the upper bound is the target problem of Section 13.3.1. That this is an upper bound was assumed without proof by Bray and Blythe and later proved by Moreau [89] and by Bray et al. [90], although it had been proved earlier [91] in the context of incoherent exciton quenching. The lower bound for the survival probability of the A particle was found by calculating the probability that A is surrounded by a trap-free region of size \mathcal{L} from which it does not move out as it diffuses and into which no B particle diffuses in. Optimization of this lower bound with respect to \mathcal{L} leads to the same leading contribution as the upper bound, and this procedure thus

led to explicit results for the λ_d . In one dimension they found the asymptotic survival probability (or, equivalently, the concentration of A particles)

$$c_A(t) \sim \exp[-4\rho(Dt/\pi)^{1/2}], \quad (13.34)$$

where ρ is the density of the sea of traps B [that is, $\rho \simeq c_B(0) - c_A(0)$] and D is the diffusion constant of the traps. Note that this is exactly the survival probability for a particle that remains still, but it is only the leading term of the lower bound and hence it is an asymptotic result. The asymptotic survival probability is thus independent of the diffusion coefficient of the particle A , which is consistent with the fact that the Pascal principle provides an upper bound that is ultimately hugged by the lower bound.

We now pose the question: What is the survival probability of a subdiffusive particle A in a sea of subdiffusive traps B ? To add to the complexity, what happens when the subdiffusive exponents for the particle and the traps are different? In particular, if a subordination procedure was to hold, how might it involve such different exponents? This is not just a theoretical scenario, see for example, [92].

An upper and lower bounds that meet asymptotically can be calculated for subdiffusive particles and traps in one dimension following the procedures of Bray and Blythe [88], but not for arbitrary subdiffusive exponents [15, 16]. The upper bound of the survival probability is found from the Pascal principle and can again be calculated exactly,

$$P_U(t) = \exp \left[-2\rho(Kt^\gamma)^{1/2} / \Gamma \left(1 + \frac{\gamma}{2} \right) \right], \quad (13.35)$$

where K and γ are the generalized diffusion coefficient and the subdiffusion exponent, respectively, for the traps. When $\gamma = 1$ this reduces to the result (13.34). The lower bound is again obtained by calculating the probability that A is surrounded by a trap-free region of size \mathcal{L} from which it does not move out as it diffuses and into which no B particle diffuses in. Interestingly, when the particle A is subdiffusive, optimization of the lower bound leads to a time independent size \mathcal{L} whereas for a diffusive A the optimal size is time dependent (regardless of the way the traps move). In any case, these two bounds do not converge asymptotically for all values of the exponents γ (traps) and γ' (particle). In particular, the bounds do meet for diffusive or subdiffusive traps as long as the particle is subdiffusive, that is, for $0 < \gamma' < 1$ and $0 < \gamma \leq 1$:

$$c_A(t) \sim \exp \left[-2\rho(Kt^\gamma)^{1/2} / \Gamma \left(1 + \frac{\gamma}{2} \right) \right]. \quad (13.36)$$

Thus, comparing this result with Eq. (13.34) we see that the subordination procedure works *as determined by the traps*, regardless of the particle's subdiffusive exponent (provided that the particle is subdiffusive). This is again reasonable

in view of the fact that the Pascal principle leads to an upper bound for the survival probability to which the lower bound eventually converges, so that it does not matter whether or not the particle moves at all. If the particle is diffusive, $\gamma' = 1$, then the result (13.36) is still asymptotically valid provided $2/3 < \gamma \leq 1$, that is, *provided the traps are not too slow*. Again, in this regime asymptotically it does not matter whether or not the particle moves.

The uncertainties about the survival probability remain when the particle is diffusive ($\gamma' = 1$) and the traps move too slowly ($0 < \gamma \leq 2/3$). The bounds now no longer converge [15]. We interpret this to mean that it is no longer unimportant that in fact the particle does move. In the marginal case $\gamma = 2/3$ the bounds provide sufficient information to determine that

$$c_A(t) \sim \exp(-\lambda t^{1/3}), \quad (13.37)$$

but not sufficient to determine the value of the constant λ . It is interesting to note that this particular time dependence is the same as the classic result for the survival probability of a diffusive particle in a sea of immobile traps, see Eq. (13.18) with $\tilde{d} = 1$. For even slower traps, $0 < \gamma < 2/3$, this procedure does not even provide converging bounds for the time dependence. One might postulate that the form (13.37) holds in this regime, but proof of this conjecture is still under investigation [17].

The asymptotic results obtained for subdiffusive particles and traps do not provide an estimate of the time of validity of these results, nor of the way in which the survival probability approaches the asymptotic regime. Exten-

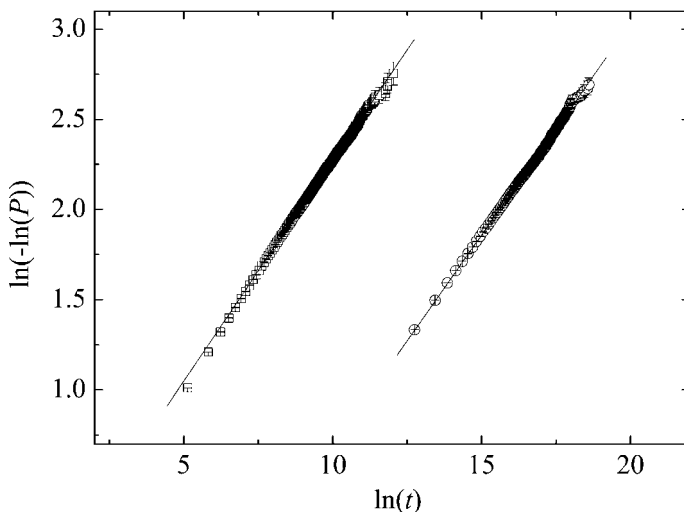


Figure 13.6 Simulation results for the survival probability for $\gamma = \gamma' = 0.5$. The left set of data (squares) corresponds to a trap density of $\rho = 0.5$ and a slope of 0.24, the right set (circles) to $\rho = 0.1$, and a slope of 0.23. The asymptotic prediction for the slope is $\gamma/2 = 0.25$.

sive computer simulations show that in some parameter regimes the asymptotic theory describes the simulation results very well even for relatively short times, while in others it is not even possible to arrive at asymptotes within ordinary computational means [16]. In particular, when $\gamma \geq \gamma'$ the asymptotic behavior is reached rather quickly: when the survival probability is of $O(10^{-1}) - O(10^{-2})$ the agreement of simulations with the asymptotic results is already very good. On the other hand, when $\gamma < \gamma'$ the asymptotic behavior is reached much more slowly, especially as the difference between the exponents increases. In some cases, we have been unable to reach the asymptotic regime even when the survival probability is as small as 10^{-6} . Representative results for the exponent of t in Eq. (13.36) are shown in Figure 13.6. Equation (13.36) can be rewritten in terms of the dimensionless quantities $\chi = \rho \langle x^2 \rangle^{1/2}$ and $\tilde{\lambda} = [2\Gamma(1 + \gamma)]^{1/2}/\Gamma(1 + \gamma/2)$ as

$$P(t) \sim \exp(-\tilde{\lambda}\chi). \quad (13.38)$$

In Figure 13.7, simulation results for $-\ln P/\chi$ together with the upper bound (and long-time asymptotic prediction) $\tilde{\lambda}$ are shown and also the theoretical lower bound (cf. Eq. (45) of Ref. [15]). The agreement between simulation results and theoretical predictions in this stringent test is excellent. In both the Figures 13.6 and 13.7, the anomalous diffusion exponents are $\gamma = \gamma' = 0.5$.

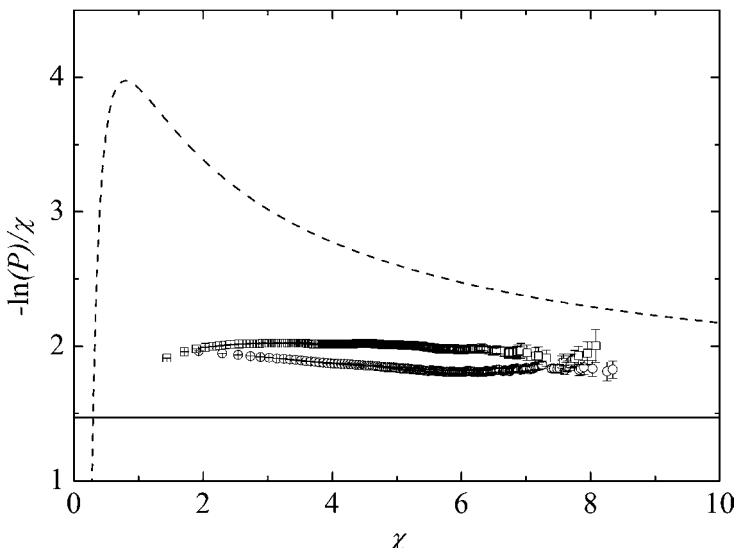


Figure 13.7 Simulation results for the exponential prefactor $\tilde{\lambda}$ in Eq. (13.38) for $\gamma = \gamma' = 0.5$. Solid line at $1.4688\dots$: upper bound; dashed curve: lower bound. Data points are for $\rho = 0.5$ (squares) and $\rho = 0.1$ (circles).

13.7

Finale

In this chapter, we have presented an overview of the current state of the literature on reaction–subdiffusion problems. Reactions that have been discussed include $A \rightarrow 0$, $A + A \rightarrow A$, $A + A \rightarrow 0$, $A + B \rightarrow B$, and $A + B \rightarrow 0$. Depending on the spatial distribution of reactants (homogeneous, nonhomogeneous) and on the way in which reactants move (diffusively, subdiffusively, or not at all), different methods have been brought to bear on this discussion, including scaling arguments and bounding arguments that lead to global concentrations $c(t)$, and reaction–subdiffusion equation approaches that provide information on local concentrations $c(\mathbf{r}, t)$. These theories are often asymptotic, and must be accompanied by extensive numerical simulations to ascertain when the asymptotic results are valid. While some results in the subdiffusion case follow from a subordination argument whereby one simply replaces t in the appropriate diffusion problem by t^γ , this is by no means always the case, nor is it always obvious when the subordination procedure may apply and when it does not.

The concentration of species (global or local) is of course not the only interesting measure of a reaction–subdiffusion process, and a fuller understanding requires that one go beyond, at least to the level of pair correlation functions, to understand the spatial structure of these systems. While there is work in the literature at this deeper level which length constraints did not permit us to review here, results are few and far between and are based mostly on numerical simulations.

We have highlighted some of the areas that are way open for further investigation. Very little is known about the behavior of subdiffusive systems with reactants characterized by different subdiffusive exponents, the only exception being the $A + B \rightarrow B$ system when the concentration of A is much smaller than that of B , and even then only in some parameter regimes. There is very little known about how to even construct reaction–subdiffusion equations at the mesoscopic level involving local concentrations; existing ones are either ad hoc or peculiar to very particular conditions. Effects of aging associated with processes that have been ongoing before the start of the observation have essentially not been addressed in the context of reactions. The structure and time dependence of two-particle (or higher) correlation functions is essentially unknown. This is a field that still requires the development of numerical simulation methods able to cover the long time scales and the presence of multiple time scales that arise in these problems. While such methods have been developed for reaction–diffusion problems, much work needs to be done to design and optimize numerical methods when the motion of reactants is subdiffusive. The list could go on, but we simply close by hoping to have aroused curiosity and engendered new ideas in our readership.

References

- 1 S. Havlin and D. ben-Avraham, *Adv. Phys.* **36** (1987) 695.
- 2 J.-P. Bouchaud and A. Georges, *Phys. Rep.* **195** (1990) 127.
- 3 R. Metzler and J. Klafter, *Phys. Rep.* **339** (2000) 1.
- 4 R. Metzler and J. Klafter, *J. Phys. A: Math. Gen.* **37** (2004) R161.
- 5 D. ben-Avraham and S. Havlin, *Diffusion and Reactions in Fractals and Disordered Systems*, (Cambridge University Press, Cambridge, 2000).
- 6 A. Blumen, J. Klafter and G. Zumofen, in *Optical Spectroscopy of Glasses*, edited by I. Zschokke (Reidel, Dordrecht, 1986).
- 7 A.M. Turing, *Philos. Trans. Roy. Soc. London Ser. B* **237** (1952) 37.
- 8 E. Kotomin and V. Kuzovkov, *Modern Aspects of Diffusion-Controlled Reactions* (Elsevier, Amsterdam, 1996).
- 9 J.D. Murray, *Mathematical Biology I: An Introduction*, 3rd edition (Springer, New York, 2002). J.D. Murray, *Mathematical Biology II: Spatial Models and Biomedical Applications*, 3rd edition (Springer, New York, 2003).
- 10 M.G. Clerc, D. Escaff and V.M. Kenkre, *Phys. Rev. E* **72** (2005) 056217. C. Escudero, J. Buceta, F.J. de la Rubia and K. Lindenberg, *Phys. Rev. E* **69** (2004) 021908. T.J. Case, *An Illustrated Guide to Theoretical Ecology* (Oxford University Press, Oxford, 2000).
- 11 J. Fort and V. Méndez, *Phys. Rev. E* **60** (1999) 5894; D. Becherer and M. Schweizer, *Ann. Appl. Probab.* **15** (2005) 1111.
- 12 I.M. Sokolov, M.G.W. Schmidt and F. Sagués, *Phys. Rev. E* **73** (2006) 031102.
- 13 B.I. Henry, T.A.M. Langlands and S.L. Wearne, *Phys. Rev. E* **74** (2006) 031116.
- 14 S.B. Yuste, J.J. Ruiz-Lorenzo and K. Lindenberg, in preparation.
- 15 S.B. Yuste and K. Lindenberg, *Phys. Rev. E* **72** (2005) 061103.
- 16 J.J. Ruiz-Lorenzo, S.B. Yuste, K. Lindenberg, *J. Phys.: Condens. Matter*, **19** (2007) 065120.
- 17 G. Oshanin, K. Lindenberg, O. Benichou, J. Klafter, and S.B. Yuste, in preparation.
- 18 P.G. de Gennes, *La Recherche* **7** (1976) 919.
- 19 B.J. West, M. Bologna and P. Grigolini, *Physics of Fractal Operators* (Springer, New York, 2003).
- 20 S. Alexander and R. Orbach, *J. Phys. (Paris) Lett.* **43** (1982) L623. in *Fractals and Disordered Systems*, edited by A. Bunde and S. Havlin, Eds. (Springer, Berlin, 1991). Y. Gefen, A. Aharony and S. Alexander, *Phys. Rev. Lett.* **50** (1983) 77. R. Rammal, *J. Stat. Phys.* **36** (1984) 547.
- 21 G.M. Zaslavsky, *Chaos* **4** (1994) 25.
- 22 E. Lutz, *Phys. Rev. E* **64** (2001) 051106.
- 23 I. Hecht, Y. Moran and H. Taitelbaum, *Phys. Rev. E* **73** (2006) 051109.
- 24 B.H. Hughes, *Random Walks and Random Environments, Volume 1: Random Walks* (Clarendon Press, Oxford, 1995).
- 25 G.H. Weiss, *Aspects and Applications of the Random Walk* (North-Holland, Amsterdam, 1994).
- 26 E.W. Montroll and G.H. Weiss, *J. Math. Phys.* **6** (1965) 167.
- 27 E.W. Montroll and B.J. West, in *Fluctuation Phenomena*, edited by E.W. Montroll and J.L. Lebowitz (North-Holland, Amsterdam, 1987).
- 28 E. Barkai and Y-C. Cheng, *J. Chem. Phys.* **118** (2003) 6167.
- 29 R. Hilfer and L. Anton, *Phys. Rev. E* **51** (1995) R848. R. Metzler, J. Klafter and I.M. Sokolov, *Phys. Rev. E* **58** (1998) 1621. E. Barkai, R. Metzler and J. Klafter, *Phys. Rev. E* **61** (2000) 132. I.M. Sokolov, J. Klafter and A. Blumen, *Physica A* **302** (2001) 268. E. Barkai, *Chem. Phys.* **284**, (2002) 13. I.M. Sokolov, J. Klafter and A. Blumen, *Phys. Today* **55** (2002) 48.
- 30 E. Scalas, R. Gorenflo and F. Mainardi *Phys. Rev. E* **69** (2004) 011107.
- 31 B.B. Mandelbrot and J.W. Van Ness, *SIAM Rev.* **10** (1968) 422.
- 32 K. Seki, M. Wojcik and M. Tachiya, *J. Chem. Phys.* **119** (2003) 2165.
- 33 A. Yadav and W. Horsthemke, *Phys. Rev. E* **74** (2006) 066118.
- 34 D. Froemberg and I.M. Sokolov, *arXiv:cond-mat/0703212v1*.
- 35 M.O. Vlad and J. Ross, *Phys. Rev. E* **66** (2002) 061908.

- 36** A.I. Shushin, New J. Phys. **7** (2005) 21.
- 37** M.G.W. Schmidt, F. Sagués and I.M. Sokolov, J. Phys.: Condens. Matter **19** (2007) 065118.
- 38** A. Blumen, G. Zumofen and J. Klafter, Phys. Rev. B **30** (1984) 5379.
- 39** J. Klafter, A. Blumen and G. Zumofen, J. Stat. Phys. **36** (1984) 561.
- 40** G. Zumofen, A. Blumen and J. Klafter, J. Chem. Phys. **79** (1983) 5131.
- 41** M. Smoluchowski, Ann. Physic. **21** (1906) 756.
- 42** A. Blumen, J. Klafter, B.S. White and G. Zumofen, Phys. Rev. Lett. **53** (1984) 1301.
- 43** G. Zumofen, A. Blumen and J. Klafter, J. Phys. A **17** (1984) L479.
- 44** A. Blumen, J. Klafter and G. Zumofen, Phys. Rev. B **28** (1983) 6112.
- 45** A.V. Barzykin and M. Tachiya, Phys. Rev. Lett. **73** (1994) 3479.
- 46** S.B. Yuste, J.J. Ruiz-Lorenzo and K. Lindenberg, Phys. Rev. E **74** (2006) 046119.
- 47** M. Galiceanu and A. Blumen, J. Phys.: Condens. Matter **19** (2007) 065122.
- 48** J. Klafter, G. Zumofen and A. Blumen, J. Physique Lett. **45** (1984) L49.
- 49** S.B. Yuste and L. Acedo, Physica A **336** (2004) 334.
- 50** O. Bénichou, M. Moreau and G. Oshanin, Phys. Rev. E **61** (2000) 3388.
- 51** M. Kac, Rocky Mt. J. Math. **4** (1974) 511. M.A. Leontovich and A.N. Kolmogorov, Phys. Z. Sowjetunion **4** (1933) 1. D.-Y. Yang, Yu. A. Makhnovskii, S.-Y. Sheu and S.H. Lin, Phys. Rev. E **62** (2000) 3116.
- 52** G. Oshanin, O. Bénichou, M. Coppey and M. Moreau, Phys. Rev. E **66** (2002) 060101R.
- 53** J. Sung, E. Barkai, R.J. Silbey and S. Lee, J. Chem. Phys. **116**, (2002) 2338.
- 54** S.B. Yuste, J. Klafter and K. Lindenberg, Phys. Rev. E **77** (2008) 032101.
- 55** I.M. Sokolov and J. Klafter, Chaos **15** (2005) 026103.
- 56** M.M. Meerschaert, D.A. Benson, H.-P. Scheffler and B. Baeumer, Phys. Rev. E, **65** (2002) 041103. A.A. Satinislavsky, Physica A **318** (2003) 469. R. Gorenflo, F. Mainardi and A. Vivoli, Chaos, Solitons Fractals **34** (2007) 89.
- 57** F. den Hollander, G.H. Weiss, in *Contemporary Problems in Statistical Physics*, edited by G.H. Weiss (SIAM, Philadelphia, 1994).
- 58** L. Acedo, S.B. Yuste, in *Recent Research Developments in Statistical Mechanics 2* (Transworld Research Network, Kerala, 2002).
- 59** S.B. Yuste and L. Acedo, Physica A **297** (2001) 323.
- 60** D.V. Donsker and S.R.S. Varadhan, Commun. Pure Appl. Math. **28** (1975) 525. A.A. Ovchinnikov and Y.B. Zeldovich, Chem. Phys. **28** (1978) 215. P. Grassberger and I. Procaccia, J. Chem. Phys. **77** (1982) 6281. R.F. Kayser and J.B. Hubbard, Phys. Rev. Lett. **51** (1983) 79. B. Ya. Balagurov and V.G. Vaks, Sov. Phys.-JETP **38** (1974) 968. J.K. Anlauf, Phys. Rev. Lett. **52** (1984) 1845.
- 61** V. Mehra and P. Grassberger, Phys. Rev. Lett. **65** (2002) 050101(R).
- 62** D.C. Torney and H. McConnell, J. Phys. Chem. **87** (1983) 1941. J.L. Spouge, Phys. Rev. Lett. **60** (1988) 871. C.R. Doering and D. ben-Avraham, Phys. Rev. A **38** (1988) 3035.
- 63** S.B. Yuste and K. Lindenberg, Phys. Rev. Lett. **87** (2001) 118301. S.B. Yuste and K. Lindenberg, Chem. Phys. **284** (2002) 169.
- 64** P.A. Alemany, J. Phys. A **30** (1997) 6587.
- 65** K. Kang and S. Redner, Phys. Rev. A **32** (1985) 435.
- 66** D. Toussaint and F. Wilczek, J. Chem. Phys. **78** (1983) 2642.
- 67** S.B. Yuste and L. Acedo, SIAM J. Numer. Anal. **42** (2005) 186. S.B. Yuste, J. Comput. Phys. **216** (2006) 264.
- 68** K. Seki, A.I. Shushin, M. Wojcik and M. Tachiya, J. Phys.: Condens. Matter **19** (2007) 065117.
- 69** K. Seki, M. Wojcik and M. Tachiya, J. Chem. Phys. **119** (2003) 7525.
- 70** K. Seki, K. Murayama and M. Tachiya, Phys. Rev. B **71** (2005) 235212.
- 71** J. Sung, E. Barkai, R.J. Silbey and S. Lee, J. Chem. Phys. **116** (2002) 2338; J.-H. Kim, D. Huh, J. Lee, S. Lee, J. Sung, K. Seki and M. Tachiya, J. Phys.: Condens. Matter **19** (2007) 065116.
- 72** T.A.M. Langlands, B.I. Henry and S.L. Wearne, J. Phys.: Condens. Matter **19** (2007) 065115.

- 73** G. Hornung, B. Berkowitz and N. Barkai, Phys. Rev. E **72** (2005) 041916.
- 74** M.A. Lomholt, I.M. Zaid and R. Metzler, Phys. Rev. Lett. **98** (2007) 200603.
- 75** L. Gárfi and Z. Rácz, Phys. Rev. A, **38** (1988) 3151.
- 76** I.M. Sokolov, JETP Lett. **44** (1986) 67.
- 77** S.J. Cornell, M. Droz and B. Chopard, Phys. Rev. A **44** (1991) 4826.
- 78** P.L. Krapivsky, Phys. Rev. E **51** (1995) 4774.
- 79** B.P. Lee and J. Cardy, Phys. Rev. E **50** (1994) R3287.
- 80** G.T. Barkema, M.J. Howard and J.L. Cardy, Phys. Rev. E **53** (1996) R2017.
- 81** M. Araujo, Physica A **219** (1995) 239.
- 82** S.B. Yuste, L. Acedo, K. Lindenberg, Phys. Rev. E **69** (2004) 036126.
- 83** S.J. Cornell, Phys. Rev. E **51** (1995) 4055.
- 84** H. Larralde, M. Araujo, S. Havlin and H.E. Stanley, Phys. Rev. A **46** (1992) 855.
- 85** W.E. Schneider and W. Wyss, J. Math. Phys. **30** (1989) 132. A.M. Mathai and R.K. Saxena, *The H-function with Applications in Statistics and Other Disciplines* (Wiley, New York, 1978).
- 86** T. Kosztolowicz and K. D. Lewandowska, arXiv:cond-mat/0603139v2.
- 87** M. Bramson and J.L. Lebowitz, Phys. Rev. Lett. **61** (1988) 2397. M. Bramson and J. L. Lebowitz, J. Stat. Phys. **62** (1991) 297.
- 88** A.J. Bray and R.A. Blythe, Phys. Rev. Lett. **89** (2002) 150601. R.A. Blythe and A.J. Bray, Phys. Rev E **67** (2003) 041101.
- 89** M. Moreau, G. Oshanin, O. Bénichou and M. Coppey, Phys. Rev. E **67** (2003) 045104(R).
- 90** A.J. Bray, S.N. Majumdar and R.A. Blythe, Phys. Rev. E **67** (2003) 060102(R).
- 91** S.F. Burlatsky, G.S. Oshanin and A.A. Ovchinnikov, Phys. Lett. A **139** (1989) 241.
- 92** T. Kues, R. Peters and U. Kubitscheck, Biophys. J. **80** (2001) 2954.

14

Anomalous Transport on Disordered Fractals

Karl Heinz Hoffmann and Janett Prehl

14.1

Motivation

In this chapter, we will give an introduction to anomalous diffusion and transport in disordered media modeled by disordered fractals. Anomalous diffusion processes are of great interest in the natural sciences as well as in many applications. Important examples are for instance diffusion in living cells [1, 2], submonolayer growth with repulsive impurities [3], turbulence diffusion [4], or diffusion in disordered media [5–7], such as porous rocks, cements, or different substrates like NaX zeolite crystallites or polystyrene, or as discussed in Chapter 17 by R. Kimmich, N. Fatkullin, M. Kehr, and Y. Li in the book.

Diffusion phenomena in disordered media can be simulated by performing many random walks on an appropriate lattice. In order to characterize the process we can determine the time development of the mean square displacement $\langle r^2(t) \rangle$, where r is the distance of a particle from its origin after time t . If this time development is linear in time the diffusive process is referred to as normal diffusion. However in many experimental realizations, as mentioned above, the diffusive process is anomalous, that means $\langle r^2(t) \rangle$ is not linear, but nevertheless it also satisfies a power law

$$\langle r^2(t) \rangle \sim t^\gamma, \quad (14.1)$$

where $0 < \gamma < 2$ is the (anomalous) diffusion exponent. If $\gamma = 1$ we obtain normal diffusion, otherwise the diffusion is called anomalous diffusion. It can be distinguished between subdiffusive behavior, if $0 < \gamma < 1$ and superdiffusive behavior for $1 < \gamma < 2$. In the following we discuss only subdiffusion, which means that the diffusive process is slower than normal diffusion, a situation which is often encountered in disordered materials.

Describing diffusive phenomena in porous materials the complex structure of these media has to be taken into account. As it is often quite complicated

to model disordered structures with classical geometries [8], we apply disordered fractals, which seems to be a more appropriate way. We use a special kind of disordered fractals, the disordered Sierpinski carpets [9], that are based on regular Sierpinski carpets [10, 11]. The disordered and regular carpets are two-dimensional models but may be generalized to three dimensions as variations of the Menger sponge [11].

We will use these fractal structures in order to construct lattices where random walkers representing diffusing particles can move on. Characterizing the dynamical behavior on such carpets the random-walk dimension d_w is defined as [5]

$$d_w = \frac{2}{\gamma}. \quad (14.2)$$

On Sierpinski carpets d_w is greater than 2. This indicates that random walkers are on average slower on these structures compared to a walk on a regular lattice.

Besides random-walk simulation [12] we also utilize the exact enumeration method [5, 13, 14] using the master equation for these random walks. Here, we obtain the whole time-dependent probability density distribution $P(\underline{r}, t)$ for each time step t . Due to this probability density distribution we are able to determine the mean square displacement $\langle r^2(t) \rangle$, the random-walk dimension d_w , and further important quantities [14–16].

In order to understand diffusion in disordered materials we start to investigate regular Sierpinski carpets. Learning about anomalous diffusion on these more self-similar structures we can comprehend diffusive processes in disordered media more easily.

Below, all this will be discussed in more detail. In Section 14.2, we establish anomalous transport and diffusion in regular fractals, more precisely in regular Sierpinski carpets. Therefore, we expose different structural and dynamical characteristics of fractal walks and their efficient implementations. In Section 14.3, we crossover to disordered fractals in order to model real materials and explain some new emerging and interesting features of them. In the last Section 14.4, we go back to regular fractals. But in contrast to the two previous sections, we try to derive differential equations that describe the whole diffusive process on fractals.

14.2

Anomalous Diffusion on Regular Sierpinski Carpets

It is known that real materials exhibit self-similar structures over a certain range of length scales [15, 17]. Although, we want to use disordered fractals later, already regular fractals, as the Sierpinski carpets, exhibit the property

of self-similarity. Due to that fact we can use regular Sierpinski carpets as a simple model for real materials.

In the following section, we first explain different structural and dynamical properties of regular Sierpinski carpets. Describing dynamical properties we present three efficient approaches to simulate diffusion on these structures and to determine the random-walk dimension d_w . Finally, we compare the virtues of these approaches.

14.2.1

Regular Sierpinski Carpets

Sierpinski carpets are determined by a generator. A generator is a square, divided in $n \times n$ congruent subsquares ($n > 1$ is a natural number), where m of these subsquares are labeled black and the other $(n^2 - m)$ are white, that means they will be removed. Figure 14.1(a) shows an example of a generator for a Sierpinski carpet.

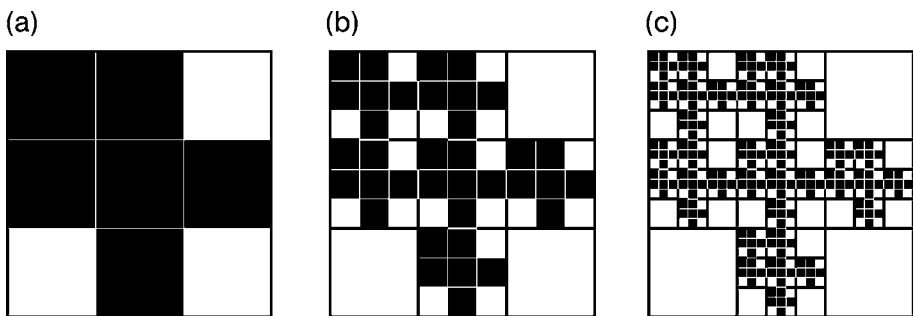


Figure 14.1 One example of a Sierpinski carpet generator (a) and the result of the second (b) and third (c) iteration step of the final carpet are shown.

Constructing a Sierpinski carpet we start with the generator and we replace each black subsquare with a scaled down version of the generator. If this construction procedure or iteration is repeated ad infinitum the limit object is a regular Sierpinski carpet. Figures 14.1(b) and (c) show the second and third iteration step of the Sierpinski carpet described by the generator shown in Figure 14.1(a).

To characterize the structural property of fractals, for example Sierpinski carpets, we can introduce the so-called Hausdorff–Besicovitch or fractal dimension d_f . The fractal dimension is given by

$$M \sim L^{d_f}, \quad (14.3)$$

which expresses the scaling of the mass of the fractal pattern by a factor of M when its linear length scales by a factor of L . In the case of the Sierpinski

carpet we identify the mass factor M with the numbers of black squares m and L with the length of one side of the fractal pattern n . So we can define d_f as

$$d_f = \frac{\ln m}{\ln n}. \quad (14.4)$$

For the generator in Figure 14.1(a), we can observe that $n = 3$ and $m = 6$, thus the fractal dimension is $d_f = \frac{\ln 6}{\ln 3} \approx 1.63$.

So far we considered fractals as objects of infinite depth. That means, if we enlarge a subset of the fractal we find the fractal pattern at each length scale. As we want to describe porous materials our model has to reproduce properties of disordered media. We said that real structures are self-similar over a certain range of length scale [15, 17]. They exhibit a smallest length scale which is given by the material and they have a largest length scale of self-similarity. For larger length scales the material is rather homogeneous.

According to the smallest length scale we stop the above mentioned construction procedure of fractals after s iteration steps. We call the obtained structure prefractal or iterator of depth s and thus we have the smallest length scale of self-similarity. Such an iterator could also be used as a generator of size $n^s \times n^s$, however we only call the smallest possible generator a generator. The homogeneity of real materials is obtained by combining such iterators to one carpet. These carpets are the discrete state space for our simulations.

Sierpinski carpets may be finitely or infinitely ramified. We call a carpet finitely ramified if we can separate any subset from the rest by cutting a finite number of connections, otherwise it is called infinitely ramified. Since a Sierpinski carpet is fully described by the generator, the ramification can be directly seen there: In the generator of a finitely ramified carpet the first and the last row coincide in exactly one black subsquare, and the same holds true for the first and the last column. If the first and last row or the first and last column of the generator coincide in more than one black subsquare, then the corresponding carpet is infinitely ramified. According to the example generator in Figure 14.1, we obtain a finitely ramified Sierpinski carpet. In Figure 14.3, the dark squares represent the coinciding squares in the first and the last row or column.

In this section, we only apply finitely ramified Sierpinski carpets. For these carpets we call a subsquare in the first column of the generator critical to the left, if this is the black subsquare in which this column coincides with the last column. In analogy we define critical squares in the last column and the first and last row, that is in the directions right, up and down. Due to our definition of finitely ramified carpets these generators have exactly one critical square in each direction. In some cases two of these squares may coincide, so there may be three or four critical squares, which can be seen in Figure 14.4(d).

14.2.2

Random Walks on Fractals

The diffusive process in real materials can be modeled by random walks on such iterators of depth s . A random walker is at every time step on a black subsquare and can move with a certain probability to one of the neighboring black subsquares in the next time step. Subsquares are called neighbors if they coincide in one edge. Equivalently, we can assign a graph to the iterator by putting the vertices at the midpoints of the black squares and connecting vertices by an edge if the corresponding subsquares are neighbors, and perform a random walk on this graph.

In the case of a regular lattice a random walker can move in each time step to one of its 4 neighbors j with a transition probability of Γ_{ji} or it stays on its current position i with Γ_{ii} . Thereby the sum of the transition probabilities over all neighbors is $\sum_j \Gamma_{ji} = 1 - \Gamma_{ii}$. Here, $\Gamma_{ji} = \frac{1}{4}$ is often used as transition probability and thus $\Gamma_{ii} = 0$.

However, on fractal lattices the walker can only move on allowed neighboring sites. So, what happens if the random walker cannot walk in a certain direction? In the literature, there are basically two different walking rules. They are known as the model of “the blind ant (Figure 14.2(a)) and the myopic ant (Figure 14.2(b)) in a labyrinth,” introduced by de Gennes in 1976 [5, 18, 19]. He imagined a random walker on structured lattices as a little ant in a labyrinth. In the first mentioned model, the ant is blind. That means each neighboring site j of site i will be selected with the same transition probability of $\Gamma_{ji} = \frac{1}{4}$. If the chosen site belongs to the black ones in the underlying generator the walker moves to this site. Otherwise it would stay at its current position (Figure 14.2(a)). In the model of the myopic ant, the walker can look (only) one step ahead. He chooses the next direction only among the allowed neighbors. For example, if a site has three neighbors, as shown in Figure 14.2(b), the transition probability to move in one of these three directions is $\Gamma_{ji} = \frac{1}{3}$. Therefore, the transition probability to stay equals zero, as again $\sum_j \Gamma_{ji} = 1$ is given.

As introduced in Section 14.1, the random-walk dimension d_w is defined via Eq. (14.2) and for Sierpinski carpets $d_w > 2$. In order to determine d_w , we discuss below different methods which can be applied. The simplest way to calculate d_w is simulating a lot of random walks and to estimate the mean square displacement $\langle r^2(t) \rangle$ as a function of time. In the corresponding log–log plot we observe a straight line. So we find a power-law behavior of $\langle r^2(t) \rangle$ over time. Fitting the slope of the straight line gives the diffusion exponent γ , and hence via Eq. (14.2) we obtain the random-walk dimension d_w .

Performing random walks on fractals normally long times have to be considered until a linear behavior in the log–log plot of $\langle r^2(t) \rangle$ over time can be observed. But long walks require large graphs. If sufficiently large iterators have to be stored in the computer, the amount of available memory restricts

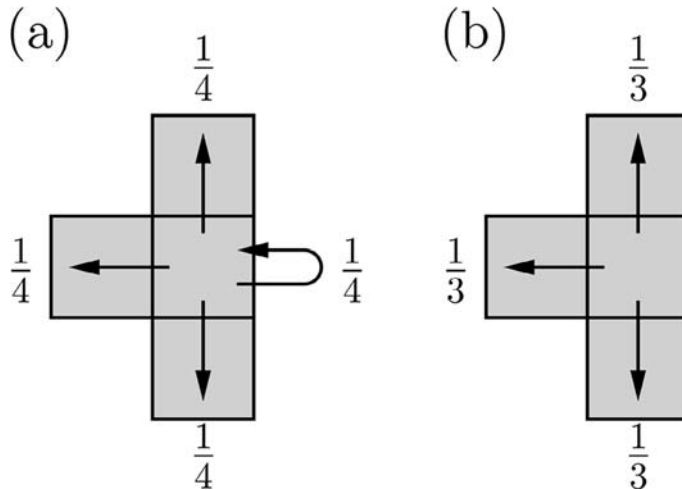


Figure 14.2 Here, two different models for the random walker are shown. (a) We see the model of the blind ant and (b) the model of the myopic ant is depicted.

the size of the iterator, and thus the number of possible steps until a walker may reach the boundary. Due to this restriction it can happen that the iterator is too small, so that the walkers reach the boundary after a few time steps. If we discarded them in the averaging process this will result in undesirable “surface effects.” So we would not observe the linear behavior in the log–log plot of $\langle r^2(t) \rangle$.

The memory problem is addressed by Dasgupta et al. [20]. There an algorithm is presented which stores only the generator but requires a lot of computations to decide for a given point whether it belongs to the fractal or not.

We improved an algorithm [12, 21] that also uses only the generator as input. We reduced the necessary computations per time step by employing a hierarchical coordinate notation and precomputed tables to determine neighborhood relations. Let us consider the iterator of depth i as a combination of m copies of the iterator of depth $(i - 1)$, ..., and the second iterator as a combination of m copies of the first iterator, where the first iterator coincides with the generator. Furthermore, we enumerate the black squares as $p^1 \in \{0, 1, \dots, m - 1\}$. The position $p^i \in \{0, 1, \dots, m - 1\}^i$ within the iterator of depth i of a walker can then be given as an i -tuple (the position vector) $p^i = (p_1, \dots, p_i)$, as is depicted in Figure 14.3 for the example carpet shown in Figure 14.1.

Using these hierarchical coordinates we can simulate our random-walk approach. If the walkers reach the boundary of the known fractal, we just expand the position vector p^i by one further element p_{i+1} so that $p^{i+1} = (p_1, \dots, p_{i+1})$. The number p_{i+1} is chosen randomly and defines the position of the known

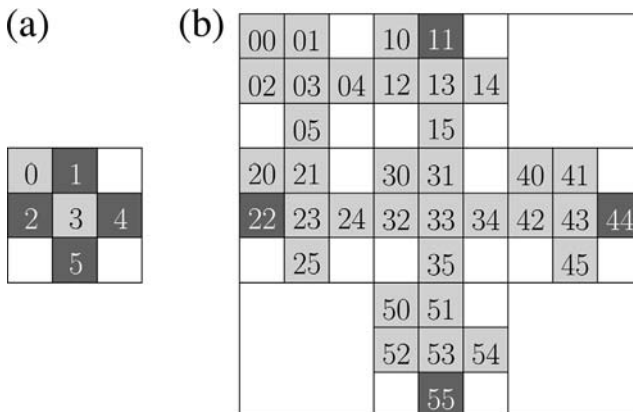


Figure 14.3 The enumeration of the squares of the generator in Figure 14.1 is shown in (a) and for the second iteration step all position vectors p^2 are depicted in (b). The dark squares are critical, there a walker might cross the iterator boundaries.

fractal in the next higher iteration level. Thus, the random walkers do not reach the boundary and we observe the linear time dependence in the log–log plot of $\langle r^2(t) \rangle$.

The resulting program benefits from high data locality, a very small inner loop and few “unexpected” jumps. A performance study and further details of the algorithm are given in [12, 21].

Two further possibilities will be introduced in the next two sections. On the one hand, we can use analogies between random walks on graphs and resistor networks in form of the Einstein relation connecting a resistance scaling exponent [21, 22] and the random-walk dimension, that will be mentioned in Section 14.2.3 shortly. The other possibility, explained in Section 14.2.4, is to iterate the master equation [13, 21]. Here, we get the whole probability density distribution to find a walker at a certain position after a certain time. From this distribution different important quantities can be extracted, as for instance the mean square displacement.

14.2.3

Resistance Scaling Method

Diffusion processes and the current flow through an adequate resistor network are strongly connected [23]. Assigning a unit resistance to every edge of the graph representation of a Sierpinski iterator (see Section 14.1) we get the corresponding resistor network. From analogy considerations between random walks and resistor networks [23, 24] the well-known Einstein rela-

tion [6, 25–27] for finitely ramified Sierpinski carpets follows:

$$d_w = d_f + \zeta, \quad (14.5)$$

where ζ is the scaling exponent of the resistance R with the linear length L of the network: $R \sim L^\zeta$. Since the fractal dimension d_f of the Sierpinski carpet is known (Eq. (14.4)) it remains to determine the resistance scaling exponent ζ in order to get the random-walk dimension d_w via Eq. (14.5).

The critical squares mentioned in Section 14.2.1 of a generator correspond to contact points in the resistor network, where one generator network may be connected to neighboring ones. By the use of Kirchhoff's laws we can convert every resistor network with four (three) contact points into a rhomboid (triangular) network (see Figure 14.4). In these networks, we use the effective resistances between two points which are calculated with the assumption that the other points are isolated.

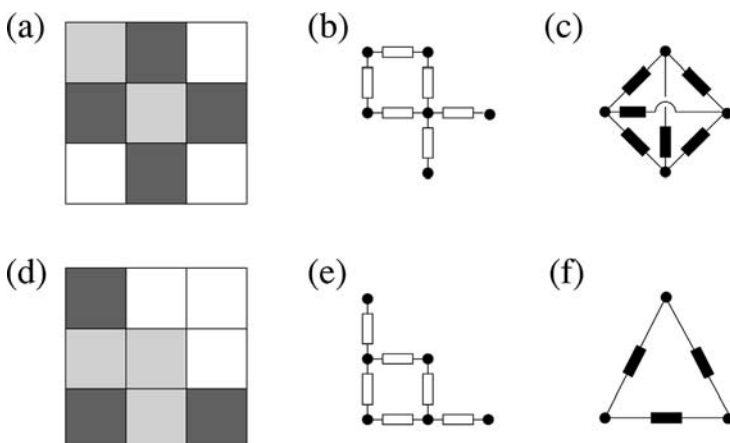


Figure 14.4 Generators of finitely ramified Sierpinski carpets for four (a) and three contact points (d), their interpretation as a generator network (b + e) and the transformation into a rhomboid (c) or triangular network (f). The dark squares are the contact points.

In order to create an iterated resistor network we

1. convert the resistor network corresponding to the Sierpinski carpet generator in a triangular or rhomboid network (see Figures 14.4(c) and (f)),
2. replace the nodes of the generator network with these triangles or rhombi (Figure 14.5),
3. convert the resulting network again into a triangle or rhombus (Figure 14.5),

4. repeat steps 2 and 3, until convergence is reached, that is successive networks differ by a constant scaling factor.

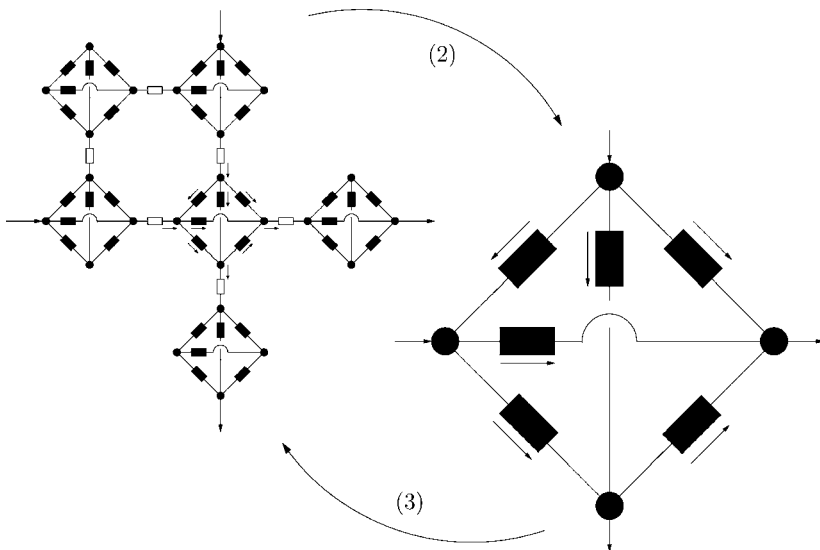


Figure 14.5 Illustration of the iteration scheme for a rhomboid network: (2) The generator network (with nodes replaced by rhombi) is transformed into a rhombus. (3) The nodes of the generator network (Figure 14.4 (b)) are replaced by the rhombus network.

Further details of this algorithm and its implementation using computer algebra methods can be found in [21, 22]. The resistance scaling algorithm determines the random-walk dimension d_w with arbitrary accuracy. So this algorithm is a powerful tool to investigate d_w of finitely ramified fractals.

14.2.4

Master Equation Approach

The random walk investigated in Section 14.2.2 can be characterized by a master equation

$$P(i, t+1) = P(i, t) + \sum_{j \neq i} [\Gamma_{ij} P(j, t) - \Gamma_{ji} P(i, t)], \quad (14.6)$$

where $P(i, t)$ denotes the probability that a walker is at a certain position i at time t and Γ_{ji} is the transition probability to move from i to j . The random walk is a stationary discrete Markov process. Compared to performing random walks iterating the master equation (14.6) has the advantage that a statistical average over a lot of walkers is no longer necessary. But of course now

memory is needed to store every position covered by a positive probability. In order to keep the needed memory as small as possible we use a dynamical storing scheme [13, 21].

The advantage of this efficient algorithm is that we can iterate the master equation until no memory is left on the used computer. The reason is that the size of the fractal and thus the number of possible time steps need not to be given in advance. It depends on the memory available. Of course the computation time per time step increases with ongoing time, since the list of generators which has to be processed becomes longer and longer. Furthermore, the communication requirement increases with increasing time, thus the connectivity between parts of the prefractal has to be carefully associated with communication between the computing nodes in order to ensure efficiency.

14.2.5

Diffusion Simulation

All three methods explained in the previous sections were applied in order to get estimates for the random-walk dimension d_w of the four 4×4 carpets shown in Figure 14.6 [20]. The (blind and myopic) random walks and the iteration of the master equation for the myopic ant model are done for 10,000 time steps, furthermore we averaged over 10,000,000 walkers. In Figure 14.7, there are shown two log–log plots of the mean square displacement over time for the carpet pattern given in Figure 14.6(a). In Figure 14.7(a), we can see

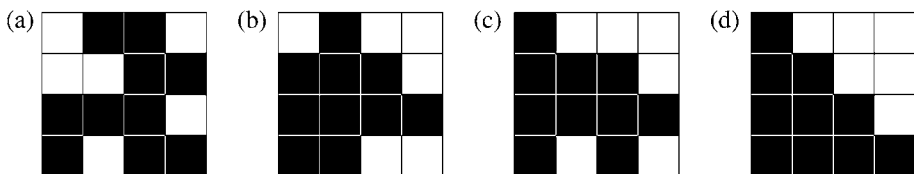


Figure 14.6 Four examples of Sierpinski carpet generators.

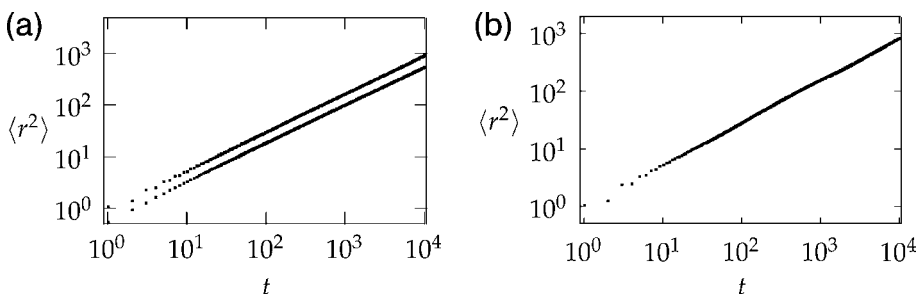


Figure 14.7 Log–log plots of $\langle r^2 \rangle$ over t for (i) the blind (lower line) and myopic (upper line) random-walk algorithm and (ii) the myopic ant master equation iteration for carpet pattern shown in Figure 14.6(a).

$\langle r^2(t) \rangle$ over time t for the blind and myopic random walk. Apart from the beginning these data points form obviously straight lines, the lower line for the blind ant and the upper line for the myopic ant. In the second plot (Figure 14.7(b)) the iteration of the myopic ant via the master equation is given.

We approximate the random-walk dimension by linear regression. Therefore, we choose the points with times 16, 32, 64, 128, 256, 512, 1024, 2048, 4096, and 8192, since these points are equidistant on the logarithmic scale. The values of d_w resulting from the regression together with confidence intervals of 95% are shown in Table 14.1, as well as the values resulting from the resistance scaling method. For comparison the values of [20] are cited in the last column of Table 14.1.

Table 14.1 Estimates for d_w for the four carpet patterns of Figure 14.6 resulting from our different methods and from [20].

	$d_{w,\text{blind}}$	$d_{w,\text{myopic}}$	$d_{w,\text{mastereq.}}$	$d_{w,\text{resistance}}$	$d_{w,\text{Dasgupta}}$
a	2.71 ± 0.01	2.68 ± 0.02	2.71 ± 0.05	2.670	2.538 ± 0.002
b	2.54 ± 0.01	2.52 ± 0.02	2.52 ± 0.06	2.576	2.528 ± 0.002
c	2.48 ± 0.01	2.47 ± 0.02	2.49 ± 0.05	2.492	2.524 ± 0.002
d	2.47 ± 0.01	2.47 ± 0.02	2.50 ± 0.09	2.509	2.514 ± 0.002

Since the resistance scaling method allows to compute the random-walk dimension up to arbitrary accuracy, these values can be taken as reference values. It can be seen from Table 14.1 that the values for d_w can be really different although all four example carpets have the same fractal dimension d_f .

While the resistance scaling algorithm is the most accurate one presented here to get an estimate of the random-walk dimension, the random-walk algorithm, and the master equation method yield additional information about the probability distribution of the walkers after a certain time. Thus these algorithms may be used to get more insight in the scaling behavior of the probability distribution for random walks on fractals.

14.3

Anomalous Diffusion on Disordered Sierpinski Carpets

Above we used regular fractals, like Sierpinski carpets [11] or prefractals for modeling fractal structures. However, the deterministic model does not capture the randomness of the local fractal structure present in real materials. A more appropriate model is based on disordered fractal structures. Recently Reis [28] studied properties of such structures. He used disordered Sierpinski carpets and investigated the characteristic exponents d_w , and concluded that the exponents are not changed significantly. We performed a similar investiga-

tion [9], but our construction of the disordered Sierpinski carpets is somewhat different and the results are quite different from Reis.

We found new and surprising features of such disordered fractal structures. We consider several Sierpinski carpets of different generators, whose diffusion properties have already been studied [14, 15, 21]. We disordered the carpets by mixing two generators during the construction procedure of the fractal. Surprisingly the exponents obtained did not depend monotonically on the concentration of one of the generators, but showed a clear extremum.

While in regular structures, like crystals, added disorder usually leads to a decrease in diffusion or transport properties, we find here that disorder can enhance diffusion on fractals. This is also observed for ionic conduction in solid electrolytes [29].

14.3.1

Disordered Sierpinski Carpets

In Section 14.2.1, we described the construction procedure of regular Sierpinski carpets. Disordered Sierpinski carpets are little different from regular ones. In the case of regular Sierpinski carpets we iterate only one generator pattern. However for disordered Sierpinski carpets at least two different generators are applied. Furthermore, we have to introduce some new structures in order to understand the observed phenomena easier.

Generating a disordered Sierpinski carpet the first black square is replaced by one generator chosen at random from the given set. As we use different generators, the obtained structure is called cell and all black squares inside a cell are referred to as active sites . In the next iteration step, each black subsquare of the cell is again replaced by a randomly chosen generator. As a result of applying the generators the subsquares of the cell become cells on their part. This procedure is repeated ad infinitum or up to a desired iteration depth s . For disordered Sierpinski carpets, prediction of the ramification of the resulting carpet and its relation to the diffusion behavior is a nontrivial problem.

For a finite iteration depth we note that the actual fractions of a generator in a particular realization of a disordered fractal might deviate from the probability with which it is chosen due to fluctuations. In the following fractions of generators always refer to probabilities with which they are chosen.

All new values which we introduce according to the disordered structures are shown in Figure 14.8 for the iterator of depth one in the middle of each graphic. First we start with some special sites in the cell: the connection points. A connection point is a black square at the border of each cell that has neighboring sites on different cells indicated by white arrows in Figure 14.8. It can be seen, that the corresponding neighboring site is also a connection point of

its or double. That means either they have only one connection to another cell (single) or two different connections to two different cells (double). The more connection points and thus the more connections a cell has, the higher the probability to contact with other cells. The double connection point can only be in the corner of a cell.

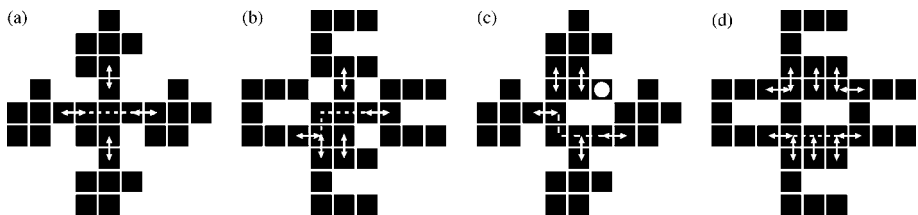


Figure 14.8 For several circumstances, the active sites (black squares), the connections between different cells (white arrows), the shortest path (dashed line), and dead ends (white dot) of the inner generator are shown here.

We define C_p as the total number of connections from one cell to all of its neighbors. If a connection point has no neighboring site on another cell, it is called dead end indicated by a white dot in Figure 14.8(c). Furthermore, we can determine the shortest path through a cell represented by the dotted lines in Figure 14.8.

14.3.2

Modeling Carpets and Calculating Diffusion Exponents

In order to analyze different diffusive phenomena which occur on disordered Sierpinski carpets we took eight different generators in total, which are represented in Figure 14.9. They are named A, B, ..., H, and mixed in pairs to create disordered fractals.

Generators A, B, and C contain 5×5 subsquares and they have different fractal dimensions d_f and different random-walk dimensions d_w . The other five patterns have 3×3 subsquares. Generator E is obtained by rotating D 180° clockwise, generator G is the result of a 90° rotation of D, so they exhibit same d_f and same d_w . Generator H is obtained by rotating generator F counterclockwise 90° , so again, these two generators have the same d_f and the same d_w .

For each of the following six pairs of generators we constructed at least 11 combinations: A_xC_{100-x} , B_xC_{100-x} , D_xE_{100-x} , D_xG_{100-x} , F_xD_{100-x} , and F_xH_{100-x} with $x = \{0, 10, 20, \dots, 100\}$. The disordered carpets containing 5×5 generators are iterated up to level $s = 6$ and the carpets corresponding to 3×3 generators have the iteration depth $s = 8$. In Section 14.2.1, we mentioned that real materials are rather homogeneous at large length scales.

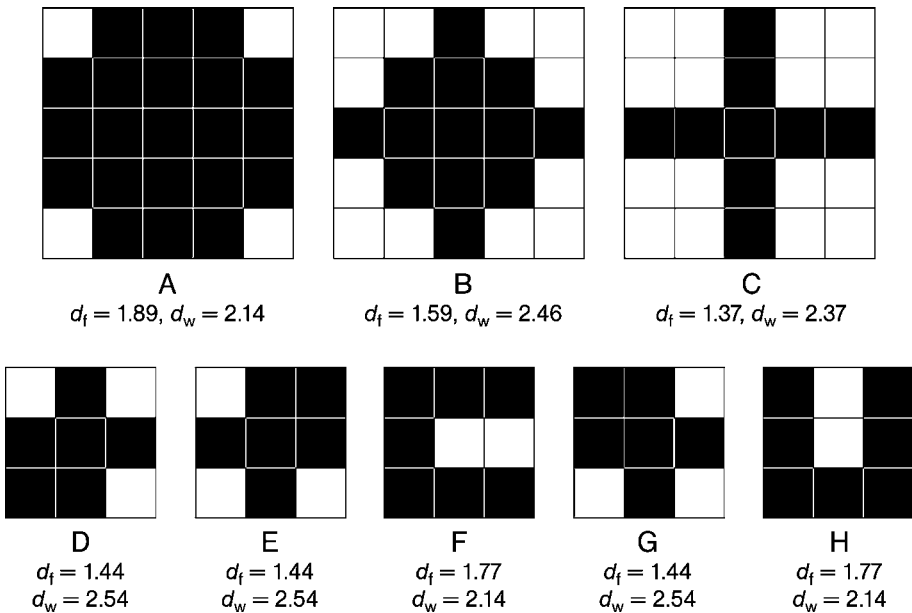


Figure 14.9 The generators A, ..., H used for constructing carpets.

Due to this we combine each iterator with identical copies of itself in all space directions. To receive a good average value of $\langle d_w \rangle$ for the random-walk simulation we created $v = 100$ different carpets for each fraction of the six combinations.

On these structures we performed random walks using the blind ant algorithm, with 20,000 walkers each. The initial site of the walker was selected randomly. For each walker we recorded the squared distance from its initial site and determined the average $\langle r^2(t) \rangle$ over all walkers as a function of time. Of course there is also a small deviation of $\langle r(t) \rangle^2$ over time, but this term is negligible in comparison with $\langle r^2(t) \rangle$ for long times.

As we now analyze disordered fractals a first question arises: Do we also observe a power-law behavior of the mean square displacement for disordered Sierpinski carpets? Figure 14.10 shows typical $\langle r^2(t) \rangle$ versus time plots for three different disordered Sierpinski carpets. In these cases the generators A and C are combined to one carpet for different fractions. For comparison we also plotted $\langle r^2(t) \rangle$ for the regular Sierpinski carpet of generator A. We can see that the figure shows rather straight lines for all four cases. Thus the randomness of the fractals does not alter the anomalous diffusion behavior showing a power-law-time behavior.

In order to obtain the random-walk dimension we performed runs with $t_{\max} = 262,144 = \sqrt[8]{2}^{144}$. We used times $t_i = \sqrt[8]{2}^i, i = 16 \dots 144$, which are

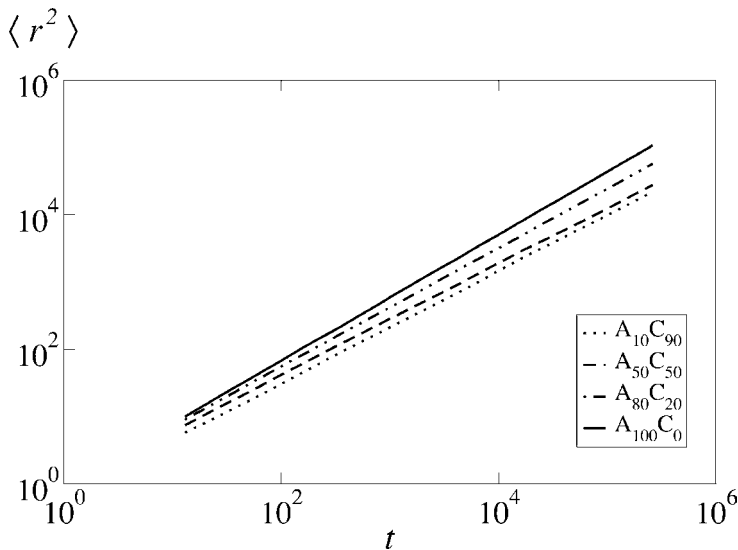


Figure 14.10 Log–log plot of the mean squared displacement, solid line: regular Sierpinski carpet of generator A, and three examples of disordered Sierpinski carpets.

equally spaced on a logarithmic scale so that there are 8 points for an increase in time by a factor of 2. The corresponding data points were used to fit a line for $\langle r^2(t) \rangle$ from which we calculated the corresponding d_w^k for the k th carpet realization. Using these data points we have $\langle r^2(t) \rangle_{\max} < 10,000$ and thus a typical distance r on the order of $r \approx 100$. With these values of r we see that the walkers are still walking inside the first iterator, and thus $\langle r^2(t) \rangle$ is not seriously affected by boundaries.

For each of the $\nu = 100$ realizations of the disordered carpets we determined d_w^k from the slope of the log–log plot of the mean square displacement over time. Thus we obtain the average value of d_w as

$$\langle d_w \rangle = \frac{1}{\nu} \sum_{k=1}^{\nu} d_w^k. \quad (14.7)$$

Furthermore, we determine the standard error of $\langle d_w \rangle$ with

$$\sigma_{\langle d_w \rangle} = \sqrt{\frac{\sum_{k=1}^{\nu} (d_w^k - \langle d_w \rangle)^2}{\nu(\nu - 1)}}. \quad (14.8)$$

In the following the standard deviations $\sigma_{\langle d_w \rangle}$ are indicated by error bars, which are so small that they cannot be resolved in the graphs shown.

14.3.3

Results and Discussion

14.3.3.1 Enhanced Disorder – Reduced Diffusion

In this section, we investigate two cases, where all used generators (A, C, D, and F) have different fractal dimension d_f and different random-walk dimensions d_w . In Figures 14.11 and 14.12, the resulting average $\langle d_w \rangle$ is shown as a function of the percentage x of generator A in combinations $A_x C_{100-x}$ (Figure 14.11) and generator F in combinations $F_x D_{100-x}$ (Figure 14.12). We can see, that both combinations exhibit a peak for $\langle d_w \rangle$. To locate the maximum to a higher degree of precision, we additionally analyzed further fractions x around the peak.

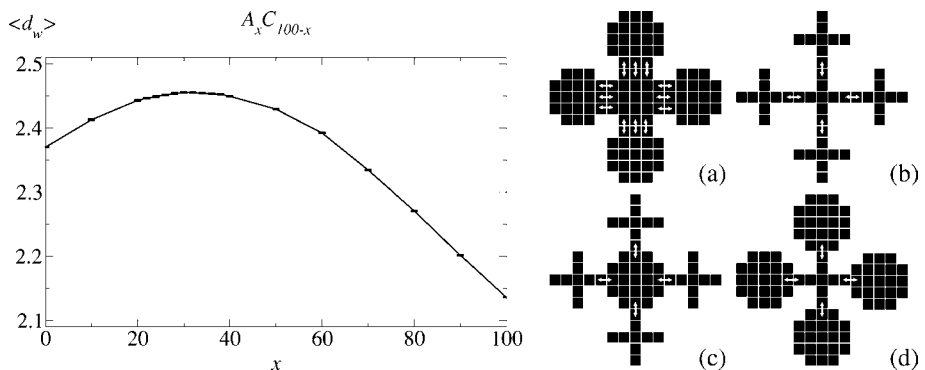


Figure 14.11 Result for mixture A–C. Left: $\langle d_w(x) \rangle$ (standard deviations are illustrated by error bars) and right: original carpets and mixtures with changed connecting points (marked by arrows).

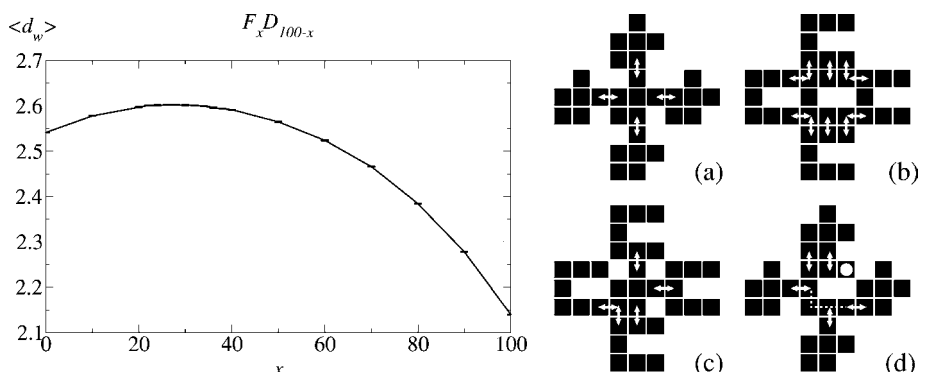


Figure 14.12 Result for mixture F–D. Left: $\langle d_w(x) \rangle$ (standard deviations are illustrated by error bars) and right: original carpets and mixtures with changed connecting points (marked by arrows).

First, we consider the combinations of $A_x C_{100-x}$. Starting at $x = 0$ we can observe an increase of $\langle d_w \rangle$ from 2.3702 to 2.4558 for $x = 30$, followed by a decrease to 2.1356 at $x = 100$. This behavior can be explained as follows: When $x = 0$, we have a regular Sierpinski carpet based on generator C, that means all cells are labeled according to generator C, with $C_p = 4$ and 9 active sites (Figure 14.11(a)). With increasing x , some cells labeled according to generator C are replaced by generator A. If a cell A is put among four cells C, its C_p still equals 4, but the number of active sites increases from 9 to 21, as shown in Figure 14.11(c). In this range of x , the number of cells A surrounded by cells C is much larger than the number of cells C surrounded by cells A. Consequently the walkers move more often inside a cell before they escape through one connection point. Therefore, the velocity of the diffusion drops to the slowest value at $x \approx 30$. But, as x goes up to 100, the C_p increases from 4 to 12, thus a walker has more opportunities to escape from one cell to another. So, diffusion increases and $\langle d_w \rangle$ decreases.

A similar curve was obtained for the combinations $F_x D_{100-x}$ shown in Figure 14.12. For $x = 0$ all cells of the carpet are marked by generator D (Figure 14.12(a)). Therefore, each cell has six active sites and $C_p = 4$. With increasing x , some cells F replaces cells D and they are surrounded by a number of cells D. If a cell F is put among four cells D, we can observe that C_p increases to 5. However we have more active sites on average (Figure 14.12(c)), due to the shape of generator F, the shortest path through the cell also increases from 3 to 4 and a dead end site appears created by the randomness, shown in Figure 14.12(d). Hence, $\langle d_w \rangle$ increases from 2.5416 to 2.6021, while x reaches 26. As x continues to go up, more and more cell F appears and the probability to find a cell D amid 4 cells F is higher. Then C_p still equals 5, but the dead end site disappears. Although, the shortest path along the horizontal direction is still 4, the shortest path traveling along the vertical direction falls to 3, thus $\langle d_w \rangle$ decreases. For $x = 100$, we obtain a pure carpet with cells F, so the shortest path along each direction is again 3 and C_p rises to 10. So $\langle d_w \rangle$ decreases, that means diffusion increases.

14.3.3.2 Enhanced Disorder–Enhanced Diffusion

In Figures 14.13 and 14.14, we present the average $\langle d_w \rangle$ over the fraction x for the combinations $F_x H_{100-x}$ and $D_x G_{100-x}$. These two cases are different in comparison to the previous section. As mentioned in Section 14.3.2, generator F and H and generator D and G have same d_f and same d_w , respectively. Nevertheless, in both plots a clear extremum of $\langle d_w \rangle$ at $x = 50$ can be observed. In contrast to all previous cases the combinations of $D_x G_{100-x}$ exhibit a minimum, which implies that diffusion on this mixture is faster than it is on the pure Sierpinski carpets.

The symmetry of both curves results from the choice of the generators. As we introduced in Section 14.3.2, generator H is generator F rotated by 90° . The same holds for generator G, which is the 90° rotated generator D. Therefore, $F_u H_{100-u}$ and $F_{100-u} H_u$ with $0 \leq u \leq 100$ are equivalent to each other.

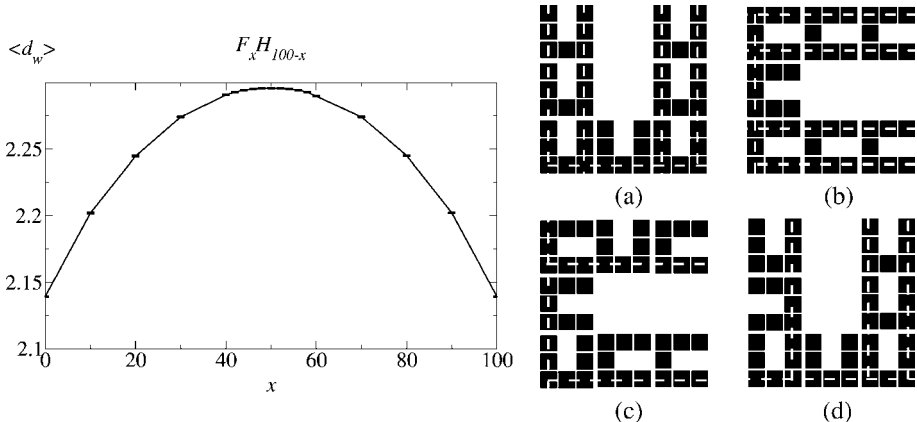


Figure 14.13 Result for mixture F–H. Left: $\langle d_w(x) \rangle$ (standard deviations are illustrated by error bars) and right: original carpets and mixtures with changed number of shortest paths (marked by dotted line).

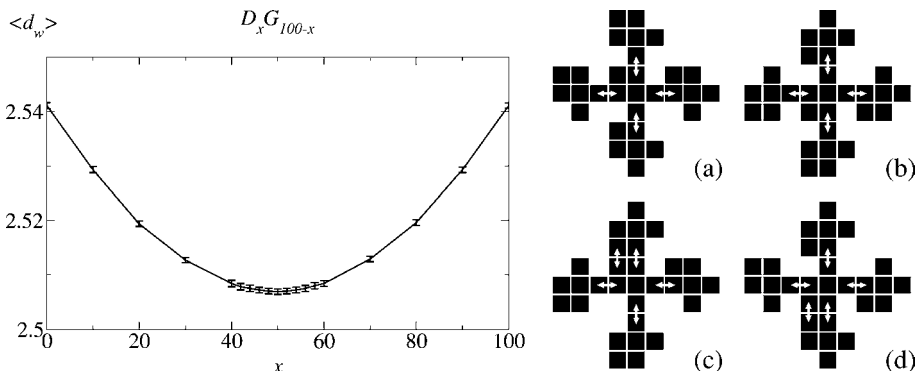


Figure 14.14 Result for mixture D–G. Left: $\langle d_w(x) \rangle$ (standard deviations are illustrated by error bars) and right: original carpets and mixtures with changed connecting points (marked by arrows).

We observe that for the $F_{50} H_{50}$ mixture the diffusion is slowed down compared to the regular carpets. This slow down can be understood on the basis of the following reasoning: Both generators have $C_p = 10$ and the shortest path to cross the cell is 3. If we place a cell F or H among four other cells with the other generator (Figures 14.13(c) and (d)), C_p and the shortest path

through one cell do not change, nevertheless $\langle d_w \rangle$ varies. So we have to analyze the cell according to the iterator of depth two (Figure 14.13). In the case of the regular Sierpinski carpets, we can see 5 possible shortest paths through the cells (Figures 14.13(a) and (b)). For $F_0 H_{100}$, there are four vertical and one horizontal shortest path and for $F_{100} H_0$ we can observe four horizontal paths and one vertical one. Starting with $x = 0$, when we now replace cells H by generator F, we obtain defects in the self-similar structure and several shortest paths break down. In the case of $F_{50} H_{50}$, the number of total shortest paths decreases to 3 (Figure 14.13(c)). Therefore, it takes more time for the walkers to travel through a cell, thus the velocity of the diffusion decreases. Due to symmetry reasons, if x increases the number of dashed lines increase and thus $\langle d_w \rangle$ decreases.

A completely different behavior is shown by the mixture of generator D and G. This can be seen from the plot in Figure 14.14: $\langle d_w \rangle$ goes down till the ratio of D to G is equal to one. The very surprising result is that diffusion is enhanced rather than slowed down. Again, the above reasoning helps in understanding the behavior: In the cases of the pure carpets $C_p = 4$. But if we place cells with generator D between cells with generator G, and this cell D is above one G cell (see Figures 14.14(c) and (d)), we will have five instead of four connection points. This can be observed most often for $D_{50} G_{50}$. Due to this for $x = 50$ $\langle d_w \rangle$ has its smallest value. Thus diffusion is enhanced.

14.3.3.3 Mixing Generators – Further Cases

Finally, we present two further cases that exhibit different behaviors than the previous cases. Again we have plotted the average value of $\langle d_w \rangle$ over the percentage x of generator B in combinations $B_x C_{100-x}$ on the left and of generator D combinations $D_x E_{100-x}$ on the right in Figure 14.15.

Mixing the patterns B and C, we do not observe an extremal value for $\langle d_w \rangle$, but it increases monotonically from $\langle d_w \rangle = 2.3702$ to 2.4563 . The reason for that is that both generators have $C_p = 4$ and a shortest path of length 5. However, the number of active sites changes from 9 to 13, while x increases and this results in increasing of $\langle d_w \rangle$, thus a slowing down of diffusion.

In the last case we mix generator D and E. These two patterns have the same number of connection points, same length of the shortest path and equal numbers of active sites, even when they are mixed together to one carpet (see Figure 14.15). As expected, we can recognize that the curve is a horizontal line within the statistical fluctuation.

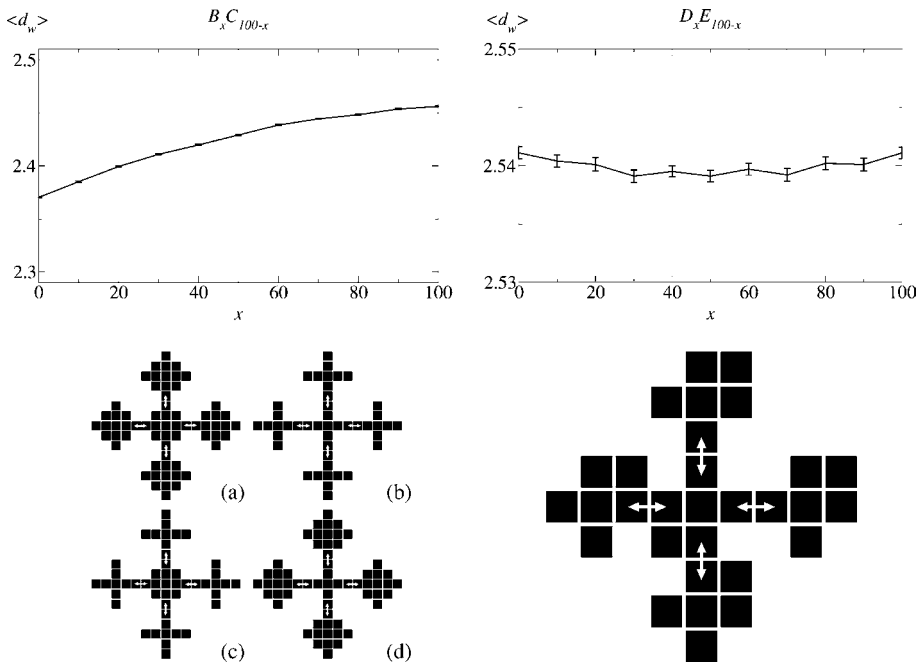


Figure 14.15 Results for mixtures B-C and D-E. Top: $\langle d_w(x) \rangle$ (standard deviations are illustrated by error bars) and bottom: mixtures with connecting points (marked by arrows).

14.4 Fractional Differential Equation

As shown in the previous sections random walks on fractal structures are frequently used to model anomalous diffusive behavior in disordered media [5]. We also explained that all these processes are characterized microscopically by a time-dependent distribution of particles $P(r, t)$, the probability density function (PDF), where the mean square distance $\langle r^2(t) \rangle$ is given by Eq. (14.1)

In the literature, there are many suggestions [30–37] to generalize the well-known Fickian diffusion equation

$$\frac{\partial}{\partial t} P(r, t) = \frac{\partial^2}{\partial r^2} P(r, t) \quad (14.9)$$

to anomalous diffusion. In Chapter 2 by R. Hilfer in the book an introduction to different generalized diffusion equations is given and further applications of fractional calculus to anomalous diffusion are discussed in Chapter 6 by D. del-Castillo-Negrete.

In [38], we compared four generalized diffusion equations. It was difficult to establish a criterion to compare the relative merits and weaknesses of the solutions of these different equations. However, all these models share the

same implicit scaling relationship between space and time, as given in (14.1) regardless whether the underlying mechanism is diffusion on a fractal or not. Due to this it is possible to compare probabilities in terms of a function of only one variable η . This auxiliary density function $G(\eta)$ is one factor, invariant under a similarity group [39], of the PDF and can be written in the form

$$P(r, t) = t^{-\frac{d_f}{d_w}} G(\eta), \quad (14.10)$$

where

$$\eta = rt^{-\frac{1}{d_w}} \quad (14.11)$$

is the similarity variable. We found that all information about the random walk is given by this $G(\eta)$ density function (GDF). Therefore, we can reconstruct the original density $P(r, t)$ using just the information from these functions.

Due to this comparison we observed that all these approaches, which include nonlinearities [36] or fractional derivatives [32, 33, 35], were at best partially successful [38]. It seems that a detailed and comprehensive physical theory for generalized diffusion equations, in terms of the underlying fractal dynamics, is still missing. Such a theory has proven to be much more difficult to construct than that for the regular case. However, this law is needed to convert a simple balance equation into a differential equation.

The main reason for these complications is that fractals are, by definition, spiky or rough. So random walks on fractals are not naturally described by differential or integral equations, as they require a certain degree of smoothness.

As shown in the last two sections, a common way around this obvious difficulty is to look at averaged quantities (see Figure 14.16, upper branch). But the type of angle averaging implied by $P(r, t)$ does not impart enough smoothness [30, 31, 38], so in consequence, the probability density $P(r, t)$ is a fractal

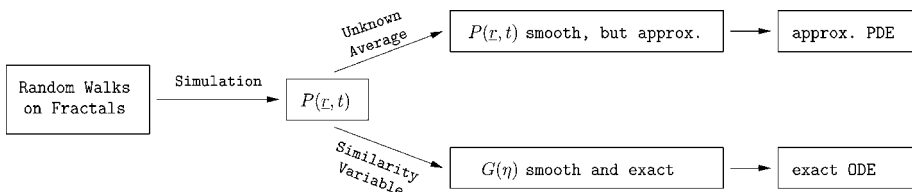


Figure 14.16 This figure underlines the difference of our similarity variable approach, where a ordinary differential equation (ODE) can be obtained, to previous discussions of diffusion on fractals in this chapter and in the literature, where only approximated partial differential equations (PDE) can be determined. Instead of averaging the data after the simulation we impose the similarity transformation (14.10).

itself. As we do not know the dynamics of random walks on fractals well enough it is complicated to do a kind of physically meaningful averaging needed for smoothness. So far, averaging must still be considered as a hypothetical solution for this problem. However, the attempt to find a partial differential equation for diffusion on fractals using any kind of average has not succeeded.

A more promising starting point to describe random walks on fractals is the use of the natural similarity group of such a walk (see Figure 14.16, lower branch). Therefore, we started with relatively simple fractals, as the Sierpinski gasket and the Koch curve. We determined the probability density functions $P(r, t)$ by random walks on these structures and estimate due to Eqs. (14.10) and (14.11) the auxiliary functions $G(\eta)$. In further steps, we try to find an ordinary differential equation for these GDFs, which would completely describe the diffusion process on the considered fractal.

14.4.1

Sierpinski Gasket

First we apply the similarity approach mentioned above (see [38, 39]) to the Sierpinski gasket [40]. We construct finitely iterated Sierpinski gaskets of depth 10–12 and then we inject walkers into each of them at the center of the bottom face of the biggest triangle (see Figure 14.17(a)).

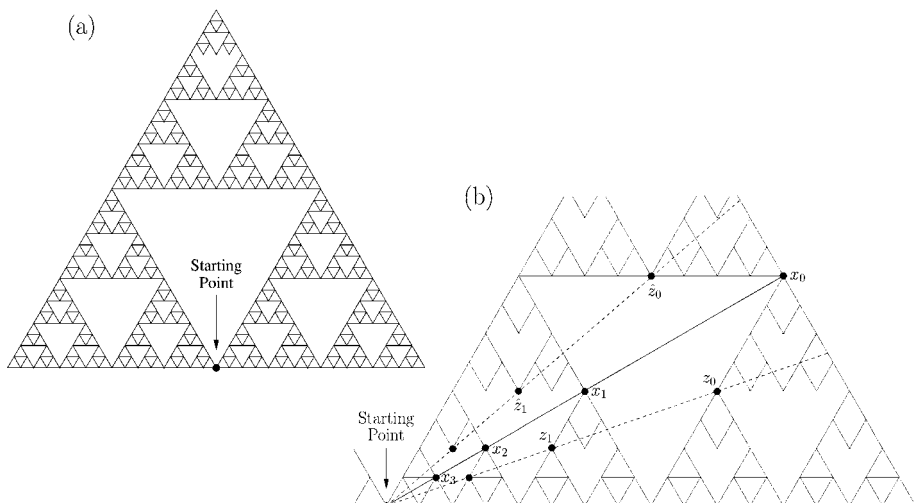


Figure 14.17 (a) Fifth iteration of the Sierpinski gasket. (b) A few members of three different classes of echo points $\{x_k\}$, $\{z_k\}$, $\{\hat{z}_k\}$ are represented on a gasket schematic. The x_k 's are situated along a symmetry line, while the points z_k and \hat{z}_k are reflections of each other about that line.

We determined the probability density $P(r, t)$ for several distinct times t . These distributions turn out to be multivalued and even self-similar. They all can be plotted against the similarity variable η in one graph by applying Eq. (14.10). Figure 14.18 is the resulting GDF plot from all points computed on the fractal, which is in effect the plotting of data along all rays. The data points do not fall onto a simple curve, but on a muscle-like cloud, as shown in Figure 14.18. This muscle-like cloud appears to be the assembly of a number of curves on which data fall. We name these curves fibers, in keeping with our muscle analogy.

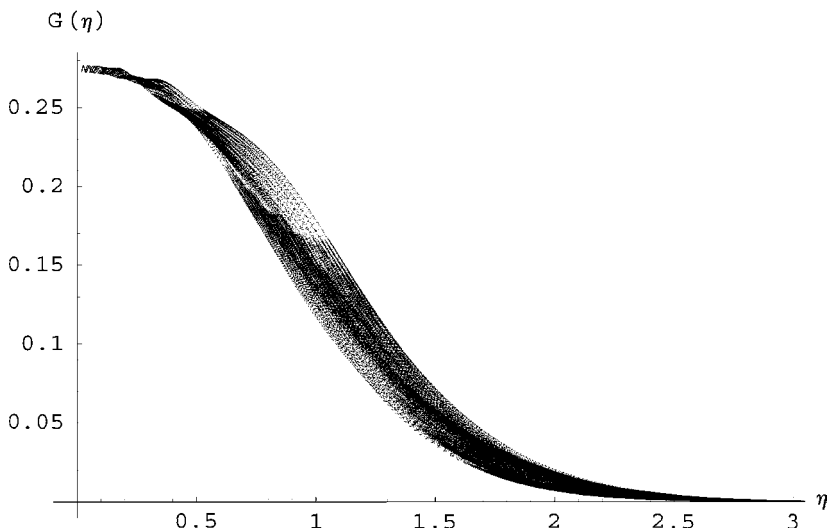


Figure 14.18 The muscle shaped cloud $G(\eta)$ for the diffusion on a Sierpinski gasket. It is generated by taking the data $P(r, t)$ for many different times t and transforming them using Eq. (14.10). Note the fibers within the cloud, which can be shown to be continuous functions of η . This figure is taken from [40].

The fibers can be explained in terms of sets of echo points introduced below. Echo points are induced by the similarity group described in (14.11). In Figure 14.17(b), there are shown a few members of the three different echo point classes $(x_k)_{k=0}^{\infty}$, $(z_k)_{k=0}^{\infty}$ and $(\hat{z}_k)_{k=0}^{\infty}$. In order to explain these echo points we focus attention, for example, on the pair of points x_1 and x_2 . We can recognize that all distances between the points and the triangles in their neighborhood are just scaled by a factor of 2. With $d_w = \frac{\ln 5}{\ln 2}$ and Eq. (14.11) we can see, that

$$\eta(x_1, 5t) = \eta(x_2, t). \quad (14.12)$$

This tells us that every point in the η space induced by x_2 also shows up in the η space induced by x_1 . Furthermore, the fact that x_1 and x_2 play identical

roles, up to a change of scale, in the gasket implies that the similarity scaling argument for the PDFs evaluated at those points also applies, so that

$$P(x_1, 5t) = t^{\frac{d_f}{d_w}} P(x_2, t). \quad (14.13)$$

Because of this,

$$G(\eta_{1,5t}) = G(\eta_{2,t}), \quad (14.14)$$

where $\eta_{k,t} = x_k t^{-\frac{1}{d_w}}$.

Therefore, the GDF created by waiting at the point x_1 and monitoring the PDF is identical to that created by waiting at point x_2 . Using the same arguments, we can show that the point x_3 and all the other implied sequential points, x_k , which are suppressed in the Figure 14.17(b) schematic for clarity, generate the same GDF.

It can be shown easily, that for symmetry reasons different echo point classes yield the same fiber, but in general different echo point classes induces different GDF curves. So by introducing the echo point classes, we are able to produce smooth GDF curves whose physical interpretation is unambiguous.

These fibers, that are continuous functions, and the muscles defining a family of functions, are natural objects to investigate differential equations, in contrast to the fractal PDFs, which have been unsuccessfully treated previously with them. In further steps, we will examine the possibility to describe these fibers by ordinary or extraordinary (that is fractional) differential equations, and we will attempt to retrieve the evolution equation for the GDF of random walkers on a fractal in that way.

After establishing the nature of the fibers as continuous single valued functions that are invariant across an echo point class, we can return to Figure 14.18 to analyze the envelope defining the muscle due to the behavior of the fibers. Careful examination shows that not a single fiber corresponds to the envelope, but that the envelope is instead formed by segments of successive fibers. Furthermore, wiggles evidently cause some fibers to touch the envelope on both sides of the muscle. These wiggles for small η turn out to be intrinsic to individual fibers and they appear to be log-periodic in η . Similar sorts of behavior have been noticed in [41–43].

Finding a differential equation for these fibers, which turn out to be continuous functions of η , would completely describe the diffusion process on the considered fractal. This approach is much more promising than trying to construct a partial differential equation for a somehow averaged or even fractal probability density $P(r, t)$.

14.4.2

Koch Curve

In this section, we apply the similarity solution method and our approach of clouds, fibers and echo points to the much easier case of the Koch curve [44]. The Koch curve is constructed by dividing a line of length 2 into three equal segments and replacing the part in the middle by two sides of an equilateral triangle of the same length as the removed segment. The number of segments is referred to as mass m [6]. In the second iteration stage this procedure is repeated with each of the four segments of length $2/3$. If this iteration process is repeated ad infinitum, the limiting object is the Koch curve [45]. With the relation (14.3) the fractal dimension of the Koch curve is $d_f = \frac{\ln 4}{\ln 3}$.

For our investigations we consider a Koch curve of finite iteration depth, like the one depicted in Figure 14.19. The coordinate origin is set at the apex of the center triangle. Topologically, the s -times iterated Koch curve is just a one-dimensional lattice. The chemical distance l to the origin of an arbitrary point x of the Koch curve is defined as the number of sites this point is away from the origin times Δx , where Δx is the Euclidean distance between two neighboring points with $\Delta x = 2/3^s$ [6].

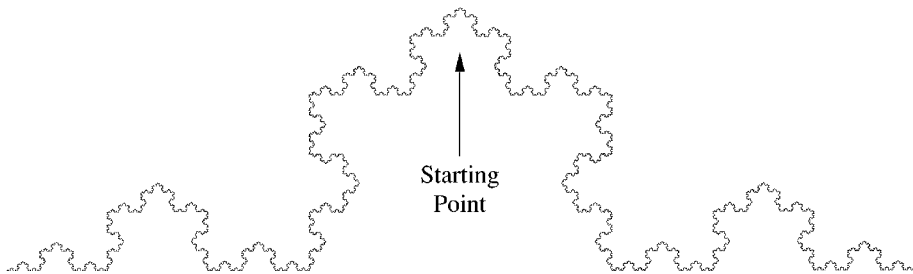


Figure 14.19 The 6-times generated Koch curve.

Considering random walks on the Koch curve in terms of the chemical distance l , which start at the origin, we can apply the well-known results for normal diffusion in one dimension. For small Δx and long times the resulting binomial distribution converges to a normal distribution and thus the probability density function for the walk is given by:

$$P(l, t) = \frac{1}{2\sqrt{Dt}} \exp\left(-\frac{l^2}{4Dt}\right), \quad (14.15)$$

where D is the diffusion constant. With (14.15) we obtain a smooth distribution, which tells us the probability to find a particle at a point of the Koch curve which has a certain chemical distance to the origin. But we want to know the probability in terms of the Euclidean distance r (analog to the linear length L

of the Sierpinski carpet) which this point has from the origin. Therefore, we need the relation $l(r)$ for all points of the Koch curve.

Due to the relations $m \sim l^{d_l}$ [6], where the chemical dimension $d_l = 1$ and $m \sim r^{d_f}$ (14.3), we find $l \sim r^{d_{min}}$, with $d_{min} = d_f/d_l = d_f$ and therefore,

$$l(r) = \alpha r^{d_f}, \quad (14.16)$$

with a constant α . It can be shown, that on average this power-law behavior is valid, but there are deviations from this power law which reveals the fractal nature of the Koch curve. The analysis of the deviations for different iteration depths exhibit, that α values for corresponding points in different iteration depths are equal, as a result of the self-similarity of the Koch curve. Furthermore we found that the values for α are bounded and we observe $\alpha_{\min} = 0.823$ and $\alpha_{\max} = 1.07$. Because of the described scaling property the extreme values of α converge for increasing iteration depths.

In the case of the Koch curve we are able to determine our classes of echo points according to same values of α . As an example we start with the solid circle denoted by x_1 in Figure 14.20, that has the Euclidean and chemical distance $r_1 = l_1 = \Delta x$. Thus, we get $\alpha_1 = l_1/r_1^{d_f} = (\Delta x)^{1-d_f}$. For the next filled circle x_2 along this ray we obtain $r_2 = 3\Delta x$ and $l_2 = 4\Delta x$ and so $\alpha_2 = 4/3^{d_f}\alpha_1 = \alpha_1$. For all successive filled circles, x_3, x_4, \dots along this ray the Euclidean and chemical distances are multiplied each time by the factors 3 and 4, respectively. All these points have the same value $\alpha = \alpha_1$. Due to the symmetry of the rays the points x_1, x_2, \dots and y_1, y_2, \dots belong to the same echo point class. In Figure 14.20 the line of symmetry is denoted by dashes.

According to Eq. (14.16), the relation between l and r is given. So we can now express the probability density $P(r, t)$ in terms of its scaling properties (14.10) in the following form:

$$P(l, t) = t^{-1/2} G_\alpha(\eta), \quad (14.17)$$

with

$$G_\alpha(\eta) = \frac{1}{2\sqrt{D\pi}} \exp\left(-\frac{1}{4D} \frac{l^2}{r^{d_w}} \eta^{d_w}\right) = \frac{1}{2\sqrt{D\pi}} \exp\left(-\frac{\alpha^2}{4D} \eta^{d_w}\right), \quad (14.18)$$

with $d_w = 2d_f$ as a special property of the Koch curve. As Eq. (14.18) just depends on α and no longer on the distinct values of r or l , each member of an echo points class produces the same fiber $G_\alpha(\eta)$. These functions are stretched exponentials with the parameter α . We mentioned that α has an upper and lower boundary. Plotting $G_\alpha(\eta)$ for different echo point classes α , we obtain a muscle-like cloud, where the top and bottom fibers are given by α_{\min} and α_{\max} .

In Figure 14.21, the fibers for the first eight echo point classes (denoted by the symbols from Figure 14.20) are shown. Introducing more values of

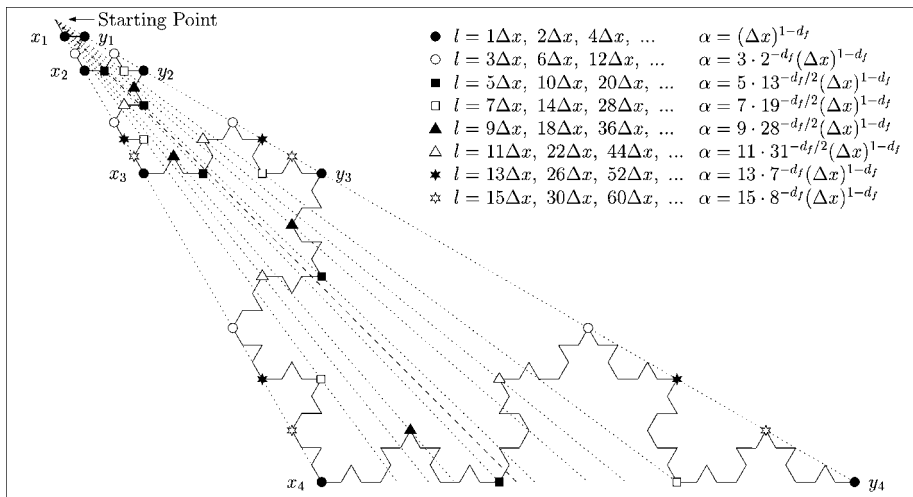


Figure 14.20 Echo point classes of the Koch curve. All points denoted by the same symbol have the same value for α . Note that the rays are symmetric with respect to the dashed line. This figure is taken from [44].

α makes the cloud denser and the extremal values are represented more exactly. Nevertheless, Figure 14.21 gives a reasonable impression of the thickness of the cloud. Here, the values for the chemical distances l and thus for α have been rescaled so that l to the endpoints of the Koch curve in Figure 14.19 equals 1.

Comparing Figure 14.18 for the Sierpinski gasket (compare [40]) and Figure 14.21 for the Koch curve we find that both muscle-like clouds $G(\eta)$ are very similar, but they have two major differences: First, we do not encounter any wiggles for the Koch curve. We conjecture that these wiggles are a consequence of the lacunarity of the gasket. For a nonlacunar fractal, like the Koch curve, the topological equivalence to a straight line implies the use of (14.15) which has no wiggles. Secondly, in the simple case of the Koch curve we are able to write down a closed form for $G_\alpha(\eta)$. That is still an open problem for random walks on other fractals.

With the closed form for the smooth fibers (14.18) it is straightforward to find an ordinary differential equation for them, which describes the diffusive behavior on the Koch curve.

An obvious choice is to seek a first order differential equation because its solutions have one arbitrary integration constant. In our case we can identify this constant with the parameter α . From this viewpoint $G(\eta)$ represents a one-parameter family of functions, one for each α . In order to find the equation which yields this family of functions we calculate the logarithmic deriva-

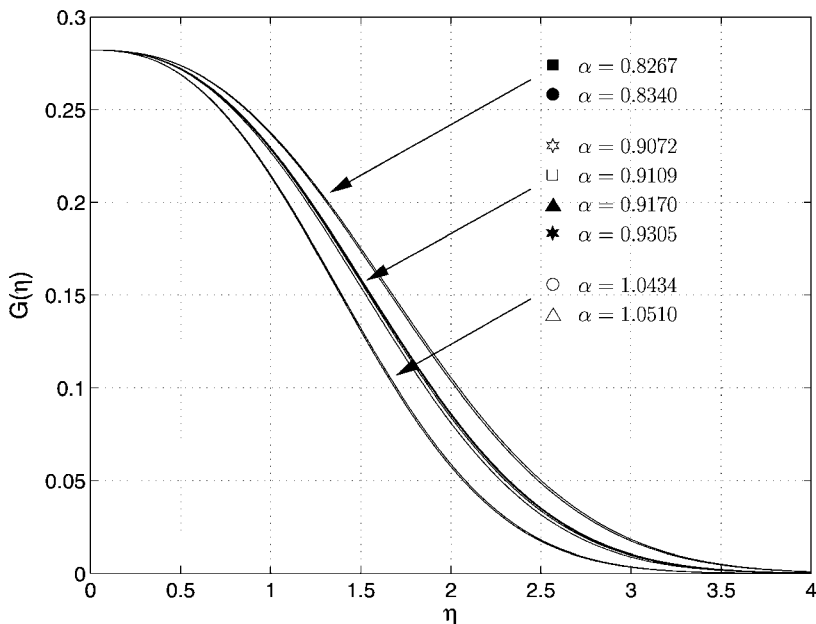


Figure 14.21 The fibers $G_\alpha(\eta)$ for all the echo point classes in Figure 14.20 form a muscle shaped cloud $G(\eta)$. Introducing more and more fibers will make the cloud denser. For this figure, we used $D = 1$ in Eq. (14.18). This figure is taken from [44].

tive of $G(\eta)$

$$\frac{G'(\eta)}{G(\eta)} = \frac{d}{d\eta} \ln(G(\eta)) = -d_w \frac{\alpha^2}{4D} \eta^{d_w-1} = \frac{d_w}{\eta} \ln\left(2\sqrt{D\pi} \cdot G(\eta)\right), \quad (14.19)$$

for eliminating the free parameter α . It follows that the ordinary differential equation

$$\eta G'(\eta) - d_w G(\eta) \ln\left(2\sqrt{D\pi} \cdot G(\eta)\right) = 0 \quad (14.20)$$

has the desired family of solutions (14.18). From (14.19) it is clear that no other first order ordinary differential equation will have this particular family of solutions.

14.5 Summary

In this chapter we investigated anomalous diffusion and transport in disordered materials represented by disordered fractals. We started to analyze the

diffusive process in regular Sierpinski carpets, which we extended to disordered fractals afterwards. In contrast to uniform media, we showed that the mean square displacement $\langle r^2(t) \rangle$ of diffusive particles in such structured media, modeled by random walkers, does not scale linearly with time t , but with t^{2/d_w} . The random-walk dimension d_w is usually greater than 2 and thus diffusion is called anomalous diffusion. Next to random-walk simulations we also implemented the master equation approach and the resistance scale method in order to determine d_w .

Analyzing disordered Sierpinski carpets we also obtained a power-law behavior of $\langle r^2(t) \rangle$ over time t . But we found for mixing pairs of different fractal patterns, that the average $\langle d_w \rangle$ depends on the number of connection points C_p , the number of active sites and on the length and the number of shortest paths through the structure.

Some of the methods additionally yield the whole probability distribution for every time step, containing much more information than just the scaling behavior of the mean square displacement. Going to a time-continuous description, the time evolution of the probability distribution can be described by differential equations. In order to investigate ordinary differential equation, which describes the diffusion property of random walks on fractals, we applied a new approach of clouds, fibers and echo points.

For all cases we determined the scaling exponent of the mean square displacement of the walkers with time as an important quantity to characterize diffusion properties. Furthermore, we developed techniques to calculate further properties of diffusion on fractals, that is the resistance scaling exponent, chemical dimension or the pore structure.

Acknowledgment

We want to thank D.H.N. Anh, P. Blaudeck, M. Davison, C. Essex, A. Franz, C. Schulzky, S. Seeger, and S. Tarafdar for helpful discussions during our extended collaborations.

References

- 1 M. Weiss, M. Elsner, F. Kartberg, and T. Nilsson. Anomalous subdiffusion is a measure for cytoplasmic crowding in living cells. *Biophys. J.*, 87:3518–3524, 2004.
- 2 D. S. Banks and C. Fradin. Anomalous diffusion of proteins due to molecular crowding. *Biophys. J.*, 89:2960–2971, 2005.
- 3 S. Liu, L. Bönig, J. Detch, and H. Metiu. Submonolayer growth with repulsive impurities: Island density scaling with anomalous diffusion. *Phys. Rev. Lett.*, 74(22):4495–4498, 1995.
- 4 A. E. Hansen, M. C. Jullien, J. Paret, and P. Tabeling. Dispersion in freely decaying and forced 2D turbulence. In A. Pekalski and R. Kutner, editors, *Anomalous Diffusion from Basics to Application*, Lecture Notes in Physics; 519, pages XVIII, 378 S. Springer, Berlin, Heidelberg, 1999.
- 5 S. Havlin and D. Ben-Avraham. Diffusion in disordered media. *Adv. Phys.*, 36(6):695–798, 1987.
- 6 A. Bunde and S. Havlin, editors. *Fractals and Disordered Systems*. Springer, Berlin, Heidelberg, New York, 2nd edition, 1996.
- 7 J. Kärger, G. Fleischer, and U. Roland. PFG NMR studies of anomalous diffusion. In J. Kärger, editor, *Diffusion in Condensed Matter*, pages XIII, 391 S. Vieweg-Verlag, Braunschweig, 1998.
- 8 B. B. Mandelbrot. *The Fractal Geometry of Nature*. W. H. Freeman and Company, New York, 3rd edition, 1983.
- 9 D. H. N. Anh, K. H. Hoffmann, S. Seeger, and S. Tarafdar. Diffusion in disordered fractals. *Europhys. Lett.*, 70(1):109–115, 2005.
- 10 Richard F. Bass. Diffusions on the Sierpinski carpet. In N. Kono, editor, *Trends in Probability and Related Analysis, Proceedings of SAP '96*, pp. 1–34. World Scientific, Singapore, 1997.
- 11 B. B. Mandelbrot. *Fractals – Form, Chance and Dimension*. Freeman, San Francisco, 1977.
- 12 S. Seeger, A. Franz, C. Schulzky, and K. H. Hoffmann. Random walks on finitely ramified Sierpinski carpets. *Comp. Phys. Comm.*, 134(3):307–316, 2001.
- 13 A. Franz, C. Schulzky, S. Seeger, and K. H. Hoffmann. An efficient implementation of the exact enumeration method for random walks on Sierpinski carpets. *Fractals*, 8(2):155–161, 2000.
- 14 A. Franz, C. Schulzky, S. Tarafdar, and K. H. Hoffmann. The pore structure of Sierpinski carpets. *J. Phys. A: Math. Gen.*, 34(42):8751–8765, 2001.
- 15 S. Tarafdar, A. Franz, S. Schulzky, and K. H. Hoffmann. Modelling porous structures by repeated Sierpinski carpets. *Physica A*, 292(1-4):1–8, 2001.
- 16 P. Blaudeck, S. Seeger, C. Schulzky, K. H. Hoffmann, T. Dutta, and S. Tarafdar. The coastline and lake shores of a fractal island. *J. Phys. A: Math. Gen.*, 39:1609–1618, 2006.
- 17 D. ben Avraham and S. Havlin. *Diffusion and Reactions in Fractals and Disordered Systems*. Cambridge University Press, Cambridge, UK, 2000.
- 18 Pierre Gilles de Gennes. La percolation: Un concept unificateur. *La Recherche*, 7(72):919–927, 1976.
- 19 J. P. Bouchaud and A. Georges. Anomalous diffusion in disordered media: Statistical mechanisms, models and physical applications. *Phys. Rep.*, 195:127–293, 1990.
- 20 R. Dasgupta, T. K. Ballabh, and S. Tarafdar. Scaling exponents for random walks on Sierpinski carpets and number of distinct sites visited: A new algorithm for infinite fractal lattices. *J. Phys. A: Math. Gen.*, 32(37):6503–6516, 1999.
- 21 A. Franz, C. Schulzky, S. Seeger, and K. H. Hoffmann. Diffusion on fractals – efficient algorithms to compute the random walk dimension. In J. M. Blackledge, A. K. Evans, and M. J. Turner, editors, *Fractal Geometry: Mathematical Methods, Algorithms, Applications, IMA Conference Proceedings*, pp. 52–67. Horwood Publishing, Chichester, West Sussex, 2002.
- 22 C. Schulzky, A. Franz, and K. H. Hoffmann. Resistance scaling and random walk dimensions for finitely ramified Sierpinski carpets. *SIGSAM Bulletin*, 34(3):1–8, 2000.
- 23 P. Tetali. Random walks and the effective resistance of networks. *J. Theor. Prob.*, 4(1):101–109, 1991.

- 24** José Luis Palacios and Prasad Tetali. A note on expected hitting times for birth and death chains. *Statistics & Prob. Lett.*, 30:119–125, 1996.
- 25** J. A. Given and B. B. Mandelbrot. Diffusion on fractal lattices and the fractal Einstein relation. *J. Phys. B: At. Mol. Opt. Phys.*, 16:L565–L569, 1983.
- 26** M. T. Barlow, R. F. Bass, and J. D. Sherwood. Resistance and spectral dimension of Sierpinski carpets. *J. Phys. A: Math. Gen.*, 23(6):L253–L238, 1990.
- 27** A. Franz, C. Schulzky, and K. H. Hoffmann. The Einstein relation for finitely ramified Sierpinski carpets. *Nonlinearity*, 14(5):1411–1418, 2001.
- 28** F. D. A. Araúo Reis. Diffusion on regular random fractals. *J. Phys. A: Math. Gen.*, 29(24):7803–7810, 1996.
- 29** S. Chandra. *Superionic Solids: Principles and Applications*. North-Holland, Amsterdam, 1981.
- 30** B. O’Shaughnessy and I. Procaccia. Analytical solutions for diffusion on fractal objects. *Phys. Rev. Lett.*, 54(5):455–458, 1985.
- 31** B. O’Shaughnessy and I. Procaccia. Diffusion on fractals. *Phys. Rev. A*, 32(5):3073–3083, 1985.
- 32** M. Giona and H. E. Roman. Fractional diffusion equation for transport phenomena in random media. *Physica A*, 185:87–97, 1992.
- 33** Massimiliano Giona and H. Eduardo Roman. Fractional diffusion equation on fractals: One-dimensional case and asymptotic behaviour. *J. Phys. A: Math. Gen.*, 25(8):2093–2105, 1992.
- 34** H. Eduardo Roman and Massimiliano Giona. Fractional diffusion equation on fractals: Three-dimensional case and scattering function. *J. Phys. A: Math. Gen.*, 25(8):2107–2117, 1992.
- 35** R. Metzler, W. G. Glockle, and T. F. Nonnenmacher. Fractional model equation for anomalous diffusion. *Physica A*, 211(1):13–24, 1994.
- 36** Albert Compte and David Jou. Non-equilibrium thermodynamics and anomalous diffusion. *J. Phys. A: Math. Gen.*, 29:4321–4329, 1996.
- 37** W. R. Schneider and W. Wyss. Fractional diffusion and wave equation. *J. Math. Phys.*, 30(1):134–144, 1989.
- 38** C. Schulzky, C. Essex, M. Davison, A. Franz, and K. H. Hoffmann. The similarity group and anomalous diffusion equations. *J. Phys. A: Math. Gen.*, 33(31):5501–5511, 2000.
- 39** K. H. Hoffmann, C. Essex, and C. Schulzky. Fractional diffusion and entropy production. *J. Non-Equilib. Thermodyn.*, 23(2):166–175, 1998.
- 40** M. Davison, C. Essex, C. Schulzky, A. Franz, and K. H. Hoffmann. Clouds, fibres and echoes: a new approach to studying random walks on fractals. *J. Phys. A: Math. Gen.*, 34(20):L289–L296, 2001.
- 41** J. Klafter, G. Zumofen, and A. Blumen. On the propagator of Sierpinski gaskets. *J. Phys. A: Math. Gen.*, 24(20):4835–4842, 1991.
- 42** Didier Sornette. Discrete-scale invariance and complex dimensions. *Phys. Rep.*, 297(5):239–270, 1998.
- 43** C. Schulzky. *Anomalous Diffusion and Random Walks on Fractals*. PhD thesis, University of Technology Chemnitz, Chemnitz, August 2000. <http://archiv.tu-chemnitz.de/pub/2000/0070>.
- 44** C. Essex, M. Davison, C. Schulzky, A. Franz, and K. H. Hoffmann. The differential equation describing random walks on the Koch curve. *J. Phys. A: Math. Gen.*, 34(41):8397–8406, 2001.
- 45** Helge von Koch. Sur une courbe continue sans tangente obtenue par une construction géométrique élémentaire. *Arkiv för Matematik, Astronomi och Fysik*, 1:681–704, 1904.

Part IV Applications to Complex Systems and Experimental Results

Introduction to Part IV

The previous three parts of this book introduced to fundamentals of anomalous transport from theoretical points of view. The final Part IV now connects these theoretical concepts with *Applications to complex systems and experimental results*. All systems studied in the following are complex in the sense that their overall properties cannot be deduced by simply taking the sum of the single parts. In terms of dynamics, here the complex interplay between the different ingredients leads to anomalous transport on large scales.

The first two chapters approach this theme still within a theoretical framework: *Superstatistics: Theoretical concepts and physical applications* by Christian Beck proposes a description of complex dynamics by a superposition of two different statistics, which models the situation where complexity emerges from the coupling of spatio-temporal inhomogeneous dynamics on different time scales. Applications of this theory identify anomalous transport in various real world data, from the dynamics of Lagrangian and defect turbulence over the statistics of cosmic rays to a superstatistical analysis of train delays. *Money circulation science – fractional dynamics in human mobility* by Dirk Brockmann samples human travel in the modern world by tracing the circulation of individual bank notes. Statistical analysis shows that human dispersal is an ambivalent, effectively superdiffusive process taking place on different spatiotemporal scales. This can be understood in terms of Lévy flights and continuous time random walk theory as introduced in Part I of this book. The last three contributions report anomalous transport properties directly observed in experiments: *Anomalous molecular displacement laws in porous media and polymers probed by nuclear magnetic resonance techniques* by Rainer Kimmich and coworkers reviews a set of NMR techniques, whose combined application covers an impressive range of about 15 decades in time. These experimental methods reveal anomalous molecular diffusion in a variety of complex systems such as bulk polymer melts, porous glasses and percolation model clusters. NMR methods are also used by Rustem Valiullin and Jörg Kärger for their study of *Anomalous molecular dynamics in confined spaces*. Probing molecular diffusion in crystalline zeolite nanopores reveals anomalous properties

of single-file diffusion, where the mutual passage of guest molecules is prevented by small pore diameters. In randomly structured mesoporous glasses and silica a variety of phase transitions is studied such as freezing and melting, evaporation and condensation pointing towards diffusive anomalies in a wider sense. The book concludes with an exposition of anomalous molecular diffusion in cell biology: *Paradigm shift of the molecular dynamics concept in the cell membrane: high-speed single-molecule tracking revealed the partitioning of the cell membrane* by Akihiro Kusumi and coworkers shows that there is anomalous transport in the plasma membrane of living biological cells. Results obtained by high-speed single-molecule tracking techniques demonstrate that the plasma membrane exhibits a complex structure being parceled up into different domains, which leads to non-Brownian diffusion between different compartments.

15

Superstatistics: Theoretical Concepts and Physical Applications

Christian Beck

15.1

Introduction

Complex systems often exhibit a dynamics that can be regarded as a superposition of several dynamics on different time scales. As a very simple example consider a Brownian particle moving through a changing environment. Assume that the environment exhibits temperature fluctuations on a large scale. Then there is a relatively fast dynamics given by the velocity of the Brownian particle and a slow one given by the temperature changes of the environment, which is spatiotemporally inhomogeneous. The two effects produce a superposition of two statistics, or in a short, a “superstatistics” [1–8]. The result is a mixture of distributions. The concept of a superstatistics was introduced in [1], in the meantime many applications for a variety of complex systems have been pointed out [9–24]. The stationary probability distributions of superstatistical systems typically exhibit non-Gaussian behavior with fat tails, which can decay, for example, with a power law, or as a stretched exponential, or in an even more complicated way.

Essential for the superstatistical approach is the existence of an intensive parameter β which fluctuates on a large spatiotemporal scale. For the above simple example of a superstatistical Brownian particle, β is the fluctuating inverse temperature of the environment, but in general β can also be an effective friction constant, a changing mass parameter, a changing amplitude of Gaussian white noise, the fluctuating energy dissipation in turbulent flows, a fluctuating volatility in finance, an environmental parameter for biological systems, or simply a local variance parameter extracted from a signal. Some superstatistical models exhibit anomalous transport, others do not. Most superstatistical models are somewhat “less anomalous” than Lévy-type models, in the sense that usually more of the higher moments exist as compared to Lévy processes. The tails of the distributions exhibit “fat” tails, but usually these are less pronounced than for a Lévy distribution.

The superstatistics concept is very general and has been applied to a variety of complex systems. Recent successful applications include hydrodynamic

turbulence [2,9–12], pattern-forming systems [14], cosmic rays [15], solar flares [13], mathematical finance [17–19], random matrix theory [20], networks [21], quantum systems at low temperatures [23], wind velocity fluctuations [16,25], hydro-climatic fluctuations [22], and delay statistics in traffic models [24]. The aim in the following is to explain the basic concepts and applications in an easy-going way.

15.2

The Basic Idea

Consider a complex system in a stationary nonequilibrium state that is driven by some external forces. Usually here we think of a physical system (e.g., a turbulent flow) but we may easily apply similar techniques to economic, biological, social systems, where the meaning of the mathematical variables will be different, though the mathematical structure is similar. Generally, a complex system will be inhomogeneous in space and in time. Effectively, it may consist of many spatial cells (or, the measured time series may consist of many time slices) where there are different values of some relevant system parameter β . The cell size is effectively determined by the correlation length of the continuously varying β -field. Superstatistical systems are characterized by a simplifying effect, namely the fact that the relaxation time is short so that each cell can be assumed to be in local equilibrium (in a certain approximation at least). Sometimes this property will be satisfied for a given complex system and sometimes it will not.

In the long term, the stationary distributions of the superstatistical inhomogeneous system arise as a superposition of Boltzmann factors $e^{-\beta E}$ (or analogs of Boltzmann factors describing the local behavior of the system under consideration) weighted with the probability density $f(\beta)$ to observe some value β in a randomly chosen cell:

$$p(E) = \int_0^\infty f(\beta) \frac{1}{Z(\beta)} \rho(E) e^{-\beta E} d\beta. \quad (15.1)$$

Here E is an effective energy for each cell, $Z(\beta)$ is the normalization constant of $\rho(E)e^{-\beta E}$ for a given β , and $\rho(E)$ is the density of states.

A typical example is a Brownian particle of mass m moving through a changing environment in d dimensions. Such a Langevin model has applications in many different areas of science. In the simplest case we may write down a linear local Langevin equation for the velocity \vec{v}

$$\dot{\vec{v}} = -\gamma \vec{v} + \sigma \vec{L}(t), \quad (15.2)$$

($\vec{L}(t)$: d -dimensional Gaussian white noise) which becomes superstatistical due to the fact that for a fluctuating environment the parameter $\beta := \frac{2}{m} \frac{\gamma}{\sigma^2}$ be-

comes a random variable as well: It varies from cell to cell on a rather large spatiotemporal scale T (this time scale T should not be confused with the temperature, which is denoted as β^{-1}). Of course, for this example $E = \frac{1}{2}mv^2$, and while the local stationary distribution in each cell is Gaussian

$$p(\vec{v}|\beta) = \left(\frac{\beta}{2\pi}\right)^{d/2} e^{-\frac{1}{2}\beta mv^2}, \quad (15.3)$$

the marginal distribution describing the long-time behavior of the particle

$$p(\vec{v}) = \int_0^\infty f(\beta) p(\vec{v}|\beta) d\beta \quad (15.4)$$

exhibits nontrivial behavior. The large $|v|$ tails of this distribution depend on the behavior of $f(\beta)$ for $\beta \rightarrow 0$ [4]. As a result of the integration over β , the probability distribution $p(\vec{v})$ will typically have fat tails. These can be e.g., power-law tails, stretched exponentials, or whatever.

One of the most important example for practical application is a χ^2 -distribution for $f(\beta)$ (see the next section for concrete formulas) and a Gaussian distribution for $p(\vec{v}|\beta)$. In this case one obtains from Eq. (15.4)

$$p(\vec{v}) \sim \frac{1}{(1 + (q-1)\frac{1}{2}bv^2)^{\frac{1}{q-1}}}, \quad (15.5)$$

where q and b are suitable parameters, and $v = |\vec{v}|$. The function on the right-hand side of Eq. (15.5) is called a q -Gaussian [34] and denoted by $e_q^{-\frac{1}{2}bv^2}$. Note that q -Gaussians decay asymptotically with a power law for $v \rightarrow \infty$. They reduce to ordinary Gaussians for $q \rightarrow 1$. But power laws are not the only possibility one can get for superstatistical systems. Many examples will be discussed in the following sections.

A generalized thermodynamics for superstatistical systems has been recently developed in [8] (see also [5] for early attempts). Here one starts from a Boltzmann–Gibbs–Shannon entropy function that also includes contributions from the fluctuations in β . Given that entropy, one can do formally thermodynamics. Ordinary thermodynamics (no fluctuations in β) is contained as a special case in this more general formalism.

15.3

Typical Distributions $f(\beta)$

The distribution $f(\beta)$ is determined by the spatiotemporal dynamics of the driven nonequilibrium system under consideration. By construction, β is positive, so $f(\beta)$ cannot be a Gaussian. Let us here consider important examples

of what to expect in typical experimental situations for driven nonequilibrium systems.

(a) There may be many (nearly) independent microscopic random variables $\xi_j, j = 1, \dots, J$ contributing to β in an additive way. For large J their rescaled sum $\frac{1}{\sqrt{J}} \sum_{j=1}^J \xi_j$ will approach a Gaussian random variable X_1 due to the Central Limit Theorem (CLT). In total, there can be many subsystems consisting of such microscopic random variables, leading to n Gaussian random variables X_1, \dots, X_n due to various degrees of freedom in the system. As mentioned before, β needs to be positive and a positive β is obtained by squaring these Gaussian random variables. The resulting $\beta = \sum_{i=1}^N X_i^2$ is χ^2 -distributed with degree n , i.e.,

$$f(\beta) = \frac{1}{\Gamma(\frac{n}{2})} \left(\frac{n}{2\beta_0} \right)^{n/2} \beta^{n/2-1} e^{-\frac{n\beta}{2\beta_0}}. \quad (15.6)$$

The marginal distributions obtained by integrating over all β exhibit power-law tails for large energies E . They are q -exponentials, $p(E) \sim e_q^{-bE} = (1 + (q - 1)bE)^{-1/(q-1)}$, where q and b can be related to n and β_0 [26, 27]. Note that this statistics arises as a universal limit dynamics, i.e., the details of the microscopic random variables ξ_j (e.g., their probability densities) are irrelevant.

(b) The same consideration as above may apply to the “temperature” β^{-1} rather than β itself. β^{-1} may be the sum of several squared Gaussian random variables arising out of many microscopic degrees of freedom ξ_j . The resulting $f(\beta)$ is the inverse χ^2 -distribution given by

$$f(\beta) = \frac{\beta_0}{\Gamma(\frac{n}{2})} \left(\frac{n\beta_0}{2} \right)^{n/2} \beta^{-n/2-2} e^{-\frac{n\beta_0}{2\beta}}. \quad (15.7)$$

It generates distributions that have exponential decays in \sqrt{E} [4, 28, 29]. Again this superstatistics is universal: details of the ξ_j are irrelevant.

(c) Instead of β being a sum of many contributions, for other systems (in particular turbulent ones) the random variable β may be generated by multiplicative random processes. We may have a local cascade random variable $X_1 = \prod_{j=1}^J \xi_j$, where J is the number of cascade steps and the ξ_i are positive microscopic random variables. Due to the CLT, $\log X_1 = \sum_{j=1}^J \log \xi_j$ becomes Gaussian for large J if it is properly rescaled. Hence X_1 is lognormally distributed. In general there may be n such product contributions to the superstatistical variable β , $\beta = \prod_{i=1}^n X_i$. Then $\log \beta = \sum_{i=1}^n \log X_i$ is a sum of Gaussian random variables, hence it is Gaussian as well. Thus β is lognormally distributed, i.e.,

$$f(\beta) = \frac{a}{\beta} \exp \left[-c(\ln \beta - b)^2 \right], \quad (15.8)$$

where a, b, c are suitable constants. The result is independent of the details of the microscopic cascade random variables ξ_j , hence there is universality again. This type of lognormal superstatistics is particularly relevant for turbulent flows [9–12, 30].

15.4

Asymptotic Behavior for Large Energies

Superstatistical probability densities, as given by Eq. (15.1) or (15.4), typically exhibit “fat tails” for large E , but what is the precise functional form of this large energy behavior? The answer depends on the distribution $f(\beta)$ and can be obtained from a variational principle. Details are described in [4]; here we just summarize some results. For simplicity, let us put $\rho(E) = 1$ in Eq. (15.1). We may define a new probability density \tilde{f} by

$$\tilde{f}(\beta) := c \frac{f(\beta)}{Z(\beta)}, \quad (15.9)$$

where c is a suitable normalization constant. The new density \tilde{f} absorbs the β -dependence of the local partition function $Z(\beta)$. With this notation, $p(E)$ can now be regarded as the Laplace transform of \tilde{f} . Renaming $\tilde{f} \rightarrow f$ we obtain

$$\begin{aligned} p(E) &\sim \int_0^\infty f(\beta) e^{-\beta E} d\beta \\ &= \int_0^\infty e^{-\beta E + \ln f(\beta)} d\beta \\ &\sim e^{\sup_\beta \{-\beta E + \ln f(\beta)\}} \\ &= e^{-\beta_E E + \ln f(\beta_E)} \\ &= f(\beta_E) e^{-\beta_E E}. \end{aligned} \quad (15.10)$$

Here we used the saddle point approximation. β_E is the value of β where the function $-\beta E + \ln f(\beta)$ has a maximum. The expression

$$\sup_\beta \{-\beta E + \ln f(\beta)\} \quad (15.11)$$

corresponds to a Legendre transform of $\ln f(\beta)$.

For the case where $f(\beta)$ is smooth and has only a single maximum we can obtain the supremum by differentiating, i.e.,

$$\sup_\beta \{-\beta E + \ln f(\beta)\} = -\beta_E E + \ln f(\beta_E) \quad (15.12)$$

where β_E satisfies the differential equation

$$0 = -E + (\ln f(\beta))' = -E + \frac{f'(\beta)}{f(\beta)}. \quad (15.13)$$

By taking into account the next-order contributions around the maximum, Eq. (15.10) can be improved to

$$p(E) \sim \frac{f(\beta_E)e^{-\beta_E E}}{\sqrt{-(\ln f(\beta_E))''}}. \quad (15.14)$$

Let us consider a few examples. Consider an $f(\beta)$ which for small β is of the power-law form $f(\beta) \sim \beta^\gamma$, $\gamma > 0$. An example is the χ^2 -distribution of n degrees of freedom, which was mentioned previously:

$$f(\beta) = \frac{1}{\Gamma(\frac{n}{2})} \left(\frac{n}{2\beta_0} \right)^{n/2} \beta^{n/2-1} e^{-\frac{n\beta}{2\beta_0}}, \quad (15.15)$$

($\beta_0 \geq 0$, $n > 1$). This behaves for $\beta \rightarrow 0$ as

$$f(\beta) \sim \beta^{n/2-1}, \quad (15.16)$$

i.e.,

$$\gamma = \frac{n}{2} - 1. \quad (15.17)$$

Other examples exhibiting this power-law form are the so-called F -distributions [1,29]. With the above formalism one obtains from Eq. (15.13)

$$\beta_E = \frac{\gamma}{E} \quad (15.18)$$

and

$$p(E) \sim E^{-\gamma-1}. \quad (15.19)$$

These types of $f(\beta)$ form the basis for power-law generalized Boltzmann factors (q -exponentials) used in generalized versions of statistical mechanics, so-called nonextensive statistical mechanics [31–34]. These depend on an entropic index q coming from a more general entropy functional, and the relation between γ and q is

$$\gamma + 1 = \frac{1}{q - 1}. \quad (15.20)$$

Another example would be an $f(\beta)$ which for small β behaves as $f(\beta) \sim e^{-c/\beta}$, $c > 0$. In this case one obtains

$$\beta_E = \sqrt{\frac{c}{E}} \quad (15.21)$$

and

$$p(E) \sim E^{-3/4} e^{-2\sqrt{cE}}. \quad (15.22)$$

The above example can be generalized to stretched exponentials. For $f(\beta)$ of the form $f(\beta) \sim e^{-c\beta^\delta}$ one obtains after a short calculation

$$\beta_E = \left(\frac{E}{c|\delta|} \right)^{1/(\delta-1)} \quad (15.23)$$

and

$$p(E) \sim E^{(2-\delta)/(2\delta-2)} e^{aE^{\delta/(\delta-1)}}, \quad (15.24)$$

where a is some factor depending on δ and c . In this case the superstatistical complex system exhibits stretched exponential tails.

15.5

Anomalous Diffusion in Superstatistical Systems

We now illustrate that superstatistical systems can exhibit normal as well as anomalous transport. This depends on the dynamical properties of the model considered.

For simplicity, we restrict ourselves to a one-dimensional model. Let us again consider locally a one-dimensional Brownian particle of mass m and a Langevin equation of the form

$$\dot{v} = -\gamma v + \sigma L(t), \quad (15.25)$$

where v denotes the velocity of the particle, and $L(t)$ is normalized Gaussian white noise with the following expectations:

$$\langle L(t) \rangle = 0 \quad (15.26)$$

$$\langle L(t)L(t') \rangle = \delta(t-t'). \quad (15.27)$$

We assume that the parameters σ and γ are constant for a sufficiently long time scale T , and then change to new values either by an explicit time dependence or by a change of the environment through which the Brownian particle moves. Formal identification with local equilibrium states in the spatial cells where β is approximately constant (ordinary statistical mechanics at temperature β^{-1}) yields during the time scale T the relation [35]

$$\langle v^2 \rangle = \frac{\sigma^2}{2\gamma} = \frac{1}{\beta m} \quad (15.28)$$

or

$$\beta = \frac{2}{m} \frac{\gamma}{\sigma^2}. \quad (15.29)$$

Again, we emphasize that after the time T , γ and σ will take on new values in a stochastic way. During a time interval of the order of T , the probability density $P(v, t)$ obeys the Fokker–Planck equation

$$\frac{\partial P}{\partial t} = \gamma \frac{\partial(vP)}{\partial v} + \frac{1}{2}\sigma^2 \frac{\partial^2 P}{\partial v^2} \quad (15.30)$$

with the local stationary solution

$$P(v|\beta) = \sqrt{\frac{m\beta}{2\pi}} \exp\left\{-\frac{1}{2}\beta mv^2\right\}. \quad (15.31)$$

In the adiabatic approximation, valid for large T , one assumes that the local equilibrium state is reached very fast so that relaxation processes can be neglected. Within a cell in local equilibrium the correlation function is given by [35]

$$C(t - t'|\beta) = \langle v(t)v(t') \rangle = \frac{1}{m\beta} e^{-\gamma|t-t'|}. \quad (15.32)$$

It is now interesting to see that the long-term invariant distribution $P(v)$, given by

$$P(v) = \int_0^\infty f(\beta)P(v|\beta) d\beta \quad (15.33)$$

depends only on the probability distribution of $\beta = \frac{2}{m} \frac{\gamma}{\sigma^2}$ and not on that of the single quantities γ and σ^2 . This means, one can obtain the same stationary distribution (15.33) from different dynamical models based on a Langevin equation with fluctuating parameters. Either γ may fluctuate, and σ^2 is constant, or the other way round. On the other hand, the superstatistical correlation function

$$C(t - t') = \int_0^\infty f(\beta)C(t - t'|\beta) d\beta = \frac{1}{m} \int_0^\infty f(\beta)\beta^{-1}e^{-\gamma|t-t'|} d\beta \quad (15.34)$$

can distinguish between these two cases. The study of correlation functions thus yields more information for any superstatistical model.

Let us illustrate this with a simple example. Assume that σ fluctuates and γ is constant and that $\beta = \frac{2}{m} \frac{\gamma}{\sigma^2}$ is χ^2 -distributed. Since γ is constant, we can move the exponential $e^{-\gamma|t-t'|}$ out of the integral in Eq. (15.34), meaning that the superstatistical correlation function still decays in an exponential way:

$$C(t - t') \sim e^{-\gamma|t-t'|}. \quad (15.35)$$

On the other hand, if σ is constant and γ fluctuates and β is still χ^2 -distributed with degree n , we get a completely different answer. In this case, in the adiabatic approximation, the integration over β yields a power-law decay of $C(t - t')$:

$$C(t - t') \sim |t - t'|^{-\eta}, \quad (15.36)$$

where

$$\eta = \frac{n}{2} - 1 \quad (15.37)$$

Note that this decay rate is different from the asymptotic power-law decay rate of the invariant density $P(v)$, which, using (15.31) and (15.33), is given by $P(v) \sim v^{-2/(q-1)}$, with

$$\frac{1}{q-1} = \frac{n}{2} + \frac{1}{2}. \quad (15.38)$$

Now let us proceed to the position

$$x(t) = \int_0^t v(t') dt' \quad (15.39)$$

of the test particle. One has

$$\langle x^2(t) \rangle = \int_0^t \int_0^t \langle v(t') v(t'') \rangle dt' dt''. \quad (15.40)$$

Asymptotic power-law velocity correlations with an exponent $\eta < 1$ are expected to imply asymptotically anomalous diffusion of the form

$$\langle x^2(t) \rangle \sim t^\alpha \quad (15.41)$$

with

$$\alpha = 2 - \eta. \quad (15.42)$$

This relation simply results from the two time integrations.

It is interesting to compare our superstatistical model with other dynamical models generating anomalous diffusion. Plastino and Plastino [36] and Tsallis and Bukmann [37] study a generalized Fokker–Planck equation of the form

$$\frac{\partial P(x, t)}{\partial t} = -\frac{\partial}{\partial x}(F(x)P(x, t)) + D \frac{\partial^2}{\partial x^2} P(x, t)^\nu \quad (15.43)$$

with a linear force $F(x) = k_1 - k_2 x$ and $\nu \neq 1$. Basically this model means that the diffusion constant becomes dependent on the probability density P .

The probability densities generated by Eq. (15.43) are q -Gaussians with the exponent

$$q = 2 - \nu. \quad (15.44)$$

The model generates anomalous diffusion with $\alpha = 2/(3-q)$. Assuming the validity of $\alpha = 2 - \hat{\eta}$, i.e., the generation of anomalous diffusion by slowly decaying velocity correlations with exponent $\hat{\eta}$, one obtains

$$\hat{\eta} = \frac{4-2q}{3-q}. \quad (15.45)$$

On the other hand, for the χ^2 -superstatistical Langevin model one obtains by combining Eqs. (15.37) and (15.38) the different relation

$$\eta = \frac{5-3q}{2q-2}. \quad (15.46)$$

Interesting enough, there is a distinguished q -value where both models yield the same answer:

$$q = 1.453 \Rightarrow \hat{\eta} = \eta = 0.707. \quad (15.47)$$

These values of q and η correspond to realistic, experimentally observed numbers, for example in defect turbulence (see Section 15.9).

15.6

From Time Series to Superstatistics

We now want to be more practically oriented and apply superstatistical techniques to some complex systems (of whatever kind) where we do not know the equations of motion, and neither the distribution $f(\beta)$, but do have some information in the form of a measured time series. Suppose an experimentally measured scalar time series $u(t)$ is given. Our goal is to test the hypothesis that it is due to a superstatistics and if yes, to extract $f(\beta)$. First we have to determine the superstatistical time scale T . For this we divide the time series into N equal time intervals of size Δt . The total length of the signal is $t_{max} = N\Delta t$. We then define a function $\kappa(\Delta t)$ by

$$\kappa(\Delta t) = \frac{1}{t_{max} - \Delta t} \int_0^{t_{max} - \Delta t} dt_0 \frac{\langle (u - \bar{u})^4 \rangle_{t_0, \Delta t}}{\langle (u - \bar{u})^2 \rangle_{t_0, \Delta t}^2}. \quad (15.48)$$

Here $\langle \dots \rangle_{t_0, \Delta t} = \frac{1}{\Delta t} \int_{t_0}^{t_0 + \Delta t} \dots dt$ denotes an average over an interval of length Δt starting at t_0 . The integration result fluctuates for each value of t_0 and is averaged by the integral over t_0 . \bar{u} denotes the average of u . $\kappa(\Delta t)$ measures the

mean kurtosis (mean standardized 4th moment) of the signal. Now assume the simplest case that our complex system dynamics basically arises out of a superposition of local Gaussians on some unknown time scale T . How can we extract T ? We should be looking for the special value $\Delta t = T$ where

$$\kappa(T) = 3. \quad (15.49)$$

Clearly this condition defining the superstatistical time scale T simply reflects the fact that we are looking for locally Gaussian behavior in the time series, which implies a local kurtosis of 3. If Δt is so small that only one constant value of u is observed in this interval, then of course $\kappa(\Delta t) = 1$. On the other hand, if Δt is so large that it includes the entire time series, then we obtain the kurtosis of the distribution of the entire signal, which is larger than 3, since superstatistical distributions are generically fat-tailed. Inbetween, there should be a distinguished time scale where $\kappa = 3$.

Figure 15.1 shows the function $\kappa(\Delta t)$ for an example of a time series that has been studied in [2], the longitudinal velocity difference $u(t) = v(t + \delta) - v(t)$ in a turbulent Taylor–Couette flow on a scale δ . For each scale δ the relevant superstatistical time scale T leading to locally Gaussian behavior can be extracted as the intersection with the line $\kappa = 3$. These time scales T are to be compared with the relaxation times γ^{-1} of the dynamics, which can be estimated from the short-time exponential decay of the correlation function $C(t - t') = \langle u(t)u(t') \rangle$. One obtains the result that the ratio T/γ^{-1} is pretty large and increases with Reynolds number [2]. This time scale separation is indeed the deeper reason why superstatistical models of turbulence work quite well [2, 11, 12].

Next, given a general signal $u(t)$ we are interested in the analysis of the slowly varying stochastic process $\beta(t)$. Since the variance of local Gaussians $\sim e^{-\frac{1}{2}\beta u^2}$ is given by β^{-1} , we can determine the process $\beta(t)$ from the time series as

$$\beta(t_0) = \frac{1}{\langle u^2 \rangle_{t_0, T} - \langle u \rangle_{t_0, T}^2} \quad (15.50)$$

We can then easily make a histogram of $\beta(t_0)$ for all values of t_0 , thus obtaining the probability density $f(\beta)$.

Figure 15.2 shows this probability density for our example of turbulent time series. Motivated by our consideration in Section 15.3, the data are compared with a χ^2 -distribution, inverse χ^2 -distribution and lognormal distribution, all having the same mean $\langle \beta \rangle$ and variance $\langle \beta^2 \rangle - \langle \beta \rangle^2$ as the experimental data. Clearly the lognormal distribution yields the best fit. Indeed, the cascade picture of energy dissipation in turbulent flow strongly suggests that lognormal superstatistics should be relevant, with β being related to a suitable power of

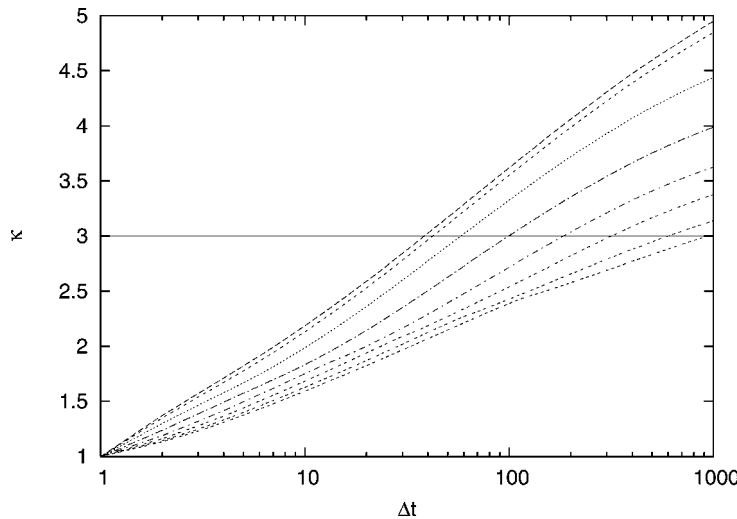


Figure 15.1 Determination of the superstatistical time scale T from the intersection with the line $\kappa = 3$ for turbulent Taylor–Couette flow, $\delta = 2^j, j = 0, 1, 2, \dots, 7$ (from top to bottom).

the fluctuating energy dissipation rate [11, 27]. However, again let us mention that other complex systems can generate a completely different type of superstatistics. Still the same methods apply.

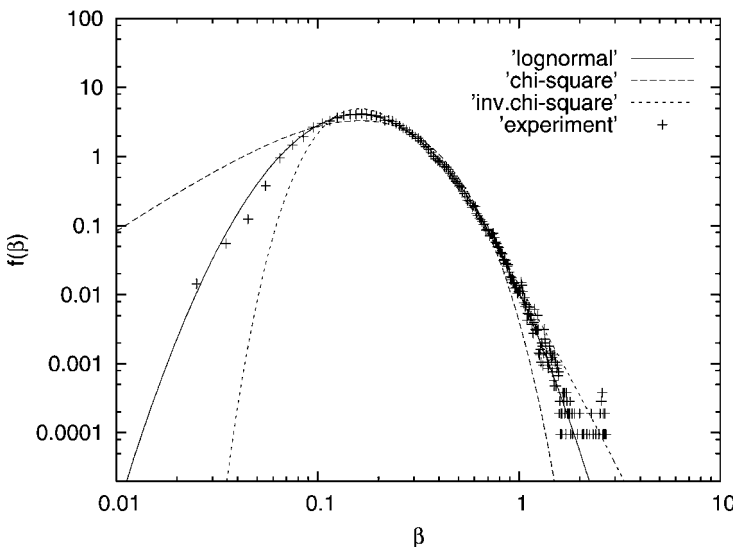


Figure 15.2 Probability distribution $f(\beta)$ as extracted from the measured turbulent time series in [2].

For superstatistics to be a good approximation we need the variable $\beta(t)$ to change very slowly as compared to $u(t)$. This is indeed the case for our turbulence example, as can be seen in Figure 15.3.

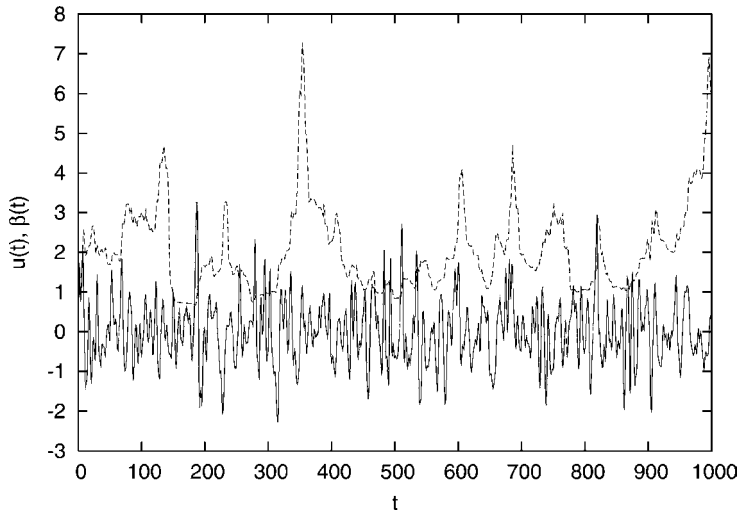


Figure 15.3 Typical evolution of $u(t)$ (solid line) and $\beta(t)$ (dashed line) for the turbulent Taylor–Couette flow.

15.7 Overview of Applications

The superstatistics concept has been applied to many different complex systems. Let us first give a short overview of applications, after that we will treat four examples in more detail. Rizzo and Rapisarda [16, 25] study experimental data of wind velocities at Florence airport and find that superstatistics does a good job. Swinney et al. [2, 38] extract lognormal superstatistics for turbulent flow between counterrotating disks. Paczuski et al. [13] study data of solar flares on various time scales and embed this into a superstatistical model based on χ^2 -superstatistics. Human behavior when sending off print jobs might also stand in connection to such a superstatistics [39]. Bodenschatz et al. [40–42] and Pinton et al. [43, 44] have detailed experimental data on the accelerations of single test particles in a turbulent flow, which are well described by lognormal superstatistics [9–11]. The statistics of cosmic rays is well described by χ^2 -superstatistics, with $n = 3$ due to the three spatial dimensions [15]. In mathematical finance superstatistical techniques are well known and come under the heading “volatility fluctuations,” see e.g., [17–19]. Possible applications also include granular media, which could be described by

different types of superstatistics, depending on the boundary conditions [45]. The observed fat tails of solar wind speed fluctuations [46] could also be related to a superstatistical model. Hydroclimatic fluctuations have been analyzed using the superstatistics concept [22]. Briggs and Beck [24] apply a superstatistical model to observed train delays on the British rail network. On the theoretical side, Chavanis [6] points out analogies between superstatistics and the theory of violent relaxation for collisionless stellar systems. Abul-Magd [20] applies superstatistics to random matrix theory. Luczka and Zaborek [47] have studied a simple model of dichotomous fluctuations of β on different time scales where everything can be calculated analytically. Mathai and Haubold [48] investigate a link between superstatistics and fractional reaction equations.

15.8 Lagrangian Turbulence

We now treat some examples of applications in more detail. We start with the recent Lagrangian turbulence applications [11]. Over the past few years there has been experimental progress [40–44] in tracking single test particles advected by a turbulent flow. This area of research is called “Lagrangian turbulence.” To theoretically model Lagrangian turbulence, one may first start from a Gaussian turbulence model, the Sawford model [49, 50]. This model considers the joint stochastic process $(a(t), v(t), x(t))$ of an arbitrary component of acceleration, velocity and position of a Lagrangian test particle embedded in the turbulent flow, and assumes that they obey the stochastic differential equation

$$\dot{a} = -(T_L^{-1} + t_\eta^{-1})a - T_L^{-1}t_\eta^{-1}v + \sqrt{2\sigma_v^2(T_L^{-1} + t_\eta^{-1})T_L^{-1}t_\eta^{-1}} L(t) \quad (15.51)$$

$$\dot{v} = a \quad (15.52)$$

$$\dot{x} = v, \quad (15.53)$$

where

$L(t)$: Gaussian white noise

T_L and t_η : two time scales, with $T_L \gg t_\eta$,

$$T_L = 2\sigma_v^2 / (C_0 \bar{\epsilon})$$

$$t_\eta = 2a_0 v^{1/2} / (C_0 \bar{\epsilon}^{1/2})$$

$\bar{\epsilon}$: average energy dissipation

C_0, a_0 : Lagrangian structure function constants

σ_v^2 : variance of the velocity distribution

$R_\lambda = \sqrt{15}\sigma_v^2 / \sqrt{\nu \bar{\epsilon}}$ Taylor scale Reynolds number.

For our purposes it is sufficient to consider the limit $T_L \rightarrow \infty$, which is a good approximation for large Reynolds numbers. In that limit the Sawford model reduces to just a linear Langevin equation for the acceleration

$$\dot{a} = -\gamma a + \sigma L(t) \quad (15.54)$$

with

$$\gamma = \frac{C_0}{2a_0} \nu^{-1/2} \bar{\epsilon}^{1/2} \quad (15.55)$$

$$\sigma = \frac{C_0^{3/2}}{2a_0} \nu^{-1/2} \bar{\epsilon}. \quad (15.56)$$

Note that this is a Langevin equation for the acceleration, so the meaning of the variables is slightly different as compared to the case of an ordinary Brownian particle, where the Langevin equation describes the velocity. In practice, the acceleration is measured as a velocity difference on a very small time scale.

Unfortunately, the Sawford model predicts Gaussian stationary distributions for a and v , and is thus at variance with the recent measurements [41, 43], which provide evidence for distributions with fat tails. So how can we extend the Sawford model to make it physically realistic?

As said before, the idea is to generalize the Sawford model with constant parameters to a superstatistical Sawford model with fluctuating ones. To construct a superstatistical extension of Sawford model, one replaces the constant

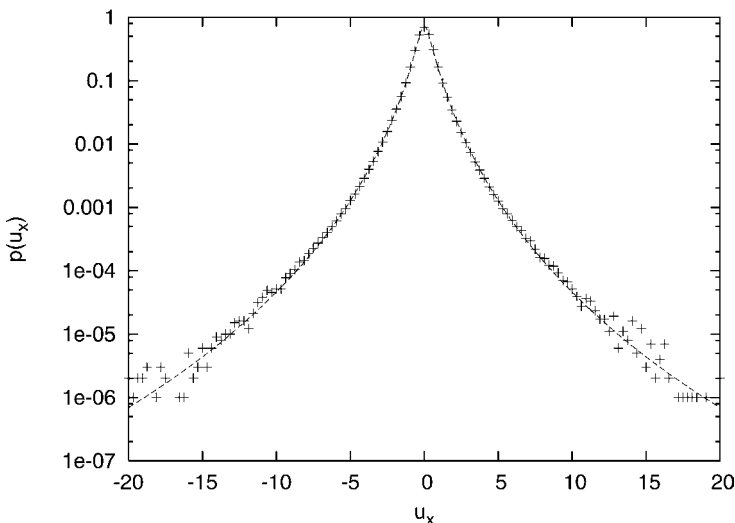


Figure 15.4 Predicted and measured probability density of a component of the small-scale velocity difference of a Lagrangian test particle in a turbulent flow. The dashed line is based on lognormal superstatistics [11]. The experimental data are from [43].

energy dissipation $\bar{\epsilon}$ by a fluctuating one. It is assumed to be lognormally distributed. Moreover, one extends the model to include all three components of the velocity and acceleration, as well as contributions from a fluctuating enstrophy (rotational energy) surrounding the test particle. From this new theory [11] excellent agreement with the experimental data is obtained, see Figure 15.4 for an example. One obtains not only the correct one-point probability distributions, but also good agreement for the decay of correlation functions, the observed statistical dependencies between acceleration components, and scaling exponents.

15.9

Defect Turbulence

Let us now consider another physically relevant example, so-called defect turbulence. Defect turbulence shares with ordinary turbulence only the name, otherwise it is very different. It is a phenomenon related to convection and has nothing to do with fully developed hydrodynamic turbulence. Consider a Raleigh–Benard convection experiment: a liquid is heated from below and cooled from above. For large enough temperature differences, interesting convection patterns start to evolve. An inclined layer convection experiment [14,51,52] is a kind of Raleigh–Benard experiment where the apparatus is tilted by an angle (say 30°), moreover the liquid is confined between two very narrow plates. For large temperature differences, the convection rolls evolve chaotically. Of particular interest are the defects in this pattern, i.e., points where two convection rolls merge into one (see Figure 15.5). These defects behave very much like particles. They have a well-defined position and velocity, they are created and annihilated in pairs, and one can even formally attribute a “charge” to them: There are positive and negative defects, as indicated by the black and white boxes in Figure 15.5.

The probability density of defect velocities has been quite precisely measured [14]. As shown in Figure 15.6, it quite precisely coincides with a q -Gaussian with $q \approx 1.46$. The defects are also observed to exhibit anomalous diffusion. Their position $X(t)$ roughly obeys an anomalous diffusion law of the type

$$\langle X^2(t) \rangle \sim t^\alpha, \quad (15.57)$$

where $\alpha \approx 1.33$ (see Figure 15.7).

The simple superstatistical model of Section 15.5 with fluctuating effective friction γ makes sense as a very simple model for the defect velocity v . While ordinary Brownian particles have constant damping due to Stokes’ law $\gamma = \frac{6\pi\nu\rho a}{m}$, where ν is the kinematic viscosity of the liquid, ρ is its density, m is the mass of the particle and a is the radius of the particle, defects are

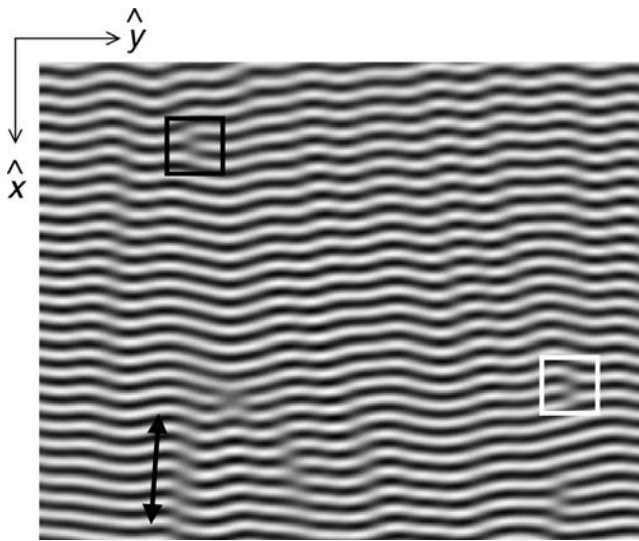


Figure 15.5 Convection rolls and defects (black and white boxes) as observed in the experiment of Daniels et al. [14].

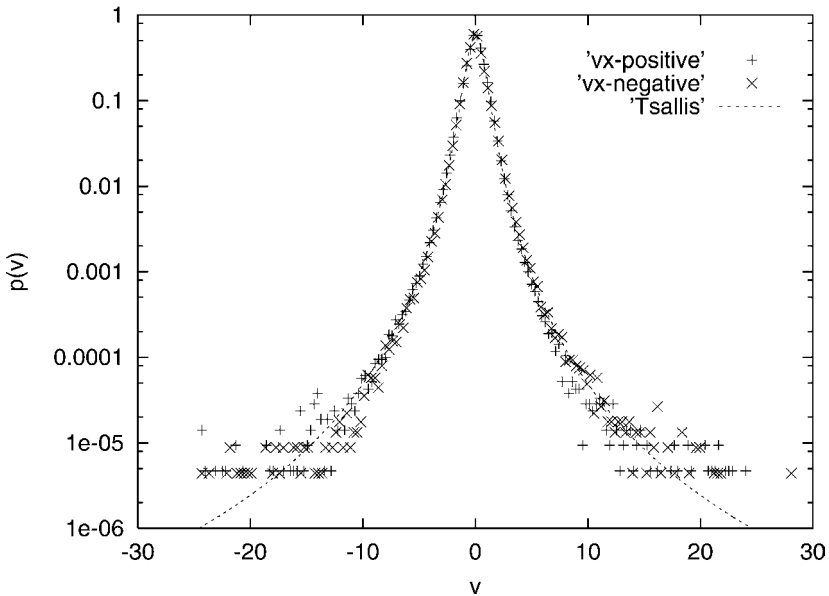


Figure 15.6 Measured probability density of defect velocities and fit with a q -Gaussian with $q = 1.46$.

no ordinary particles: they are nonlinear excitations and have neither a well-defined mass m nor a well-defined radius a . Thus one expects that there is an ensemble of damping constants γ which depend on the topology of the de-

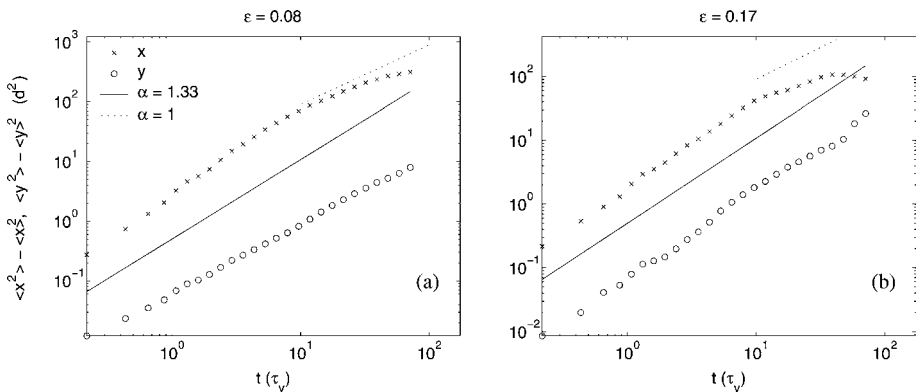


Figure 15.7 Measured anomalous diffusion of defects for two different values of the nondimensional temperature differences ϵ between upper and lower plate.

fect and its fluctuating environment. In particular, the fastest velocities result from circumstances in which the defect is moving in a local environment with only a very small effective local damping γ acting. The driving forces $L(t)$ are hardly damped during such a time interval, and lead to very large velocities for a limited amount of time, until another region with another γ is reached. The results are q -Gaussians, as shown in Figure 15.6, and anomalous diffusion. In good approximation this system is described by χ^2 -superstatistics.

15.10

Statistics of Cosmic Rays

Our third example is from high-energy physics. We will proceed to extremely high temperatures, where (similar as in defect turbulence) particles are created and annihilated in pairs. We will apply superstatistical techniques to high-energy collision processes on astrophysical scales, leading to the creation of cosmic ray particles that are ultimately observed on the earth. The idea to apply superstatistical techniques to the measured cosmic ray spectrum was first presented in [15], based on some earlier work in [53].

Experimental data of the measured cosmic ray energy spectrum are shown in Figure 15.8. Also shown is a curve that corresponds to a prediction of a superstatistical model. Up to energies of 10^{16} eV, the measured flux rate of cosmic ray particles with a given energy E is well fitted by a distribution of the form

$$p(E) = C \cdot \frac{E^2}{(1 + b(q-1)E)^{1/(q-1)}}. \quad (15.58)$$

E is the energy of the particles,

$$E = \sqrt{c^2 p_x^2 + c^2 p_y^2 + c^2 p_z^2 + m^2 c^4}, \quad (15.59)$$

$b = (k\tilde{T})^{-1}$ is an effective inverse temperature variable, and C is a constant representing the total flux rate. For relativistic particles the rest mass m can be neglected and one has $E \approx c|\vec{p}|$. The distribution (15.58) is a q -generalized relativistic Maxwell–Boltzmann distribution in the formalism of nonextensive statistical mechanics [31]. The factor E^2 takes into account the available phase space volume. As seen in Figure 15.8, the cosmic ray spectrum is very well fitted by the distribution (15.58) if the entropic index q is chosen as $q = 1.215$ and if the effective temperature parameter is given by $k\tilde{T} = b^{-1} = 107$ MeV.

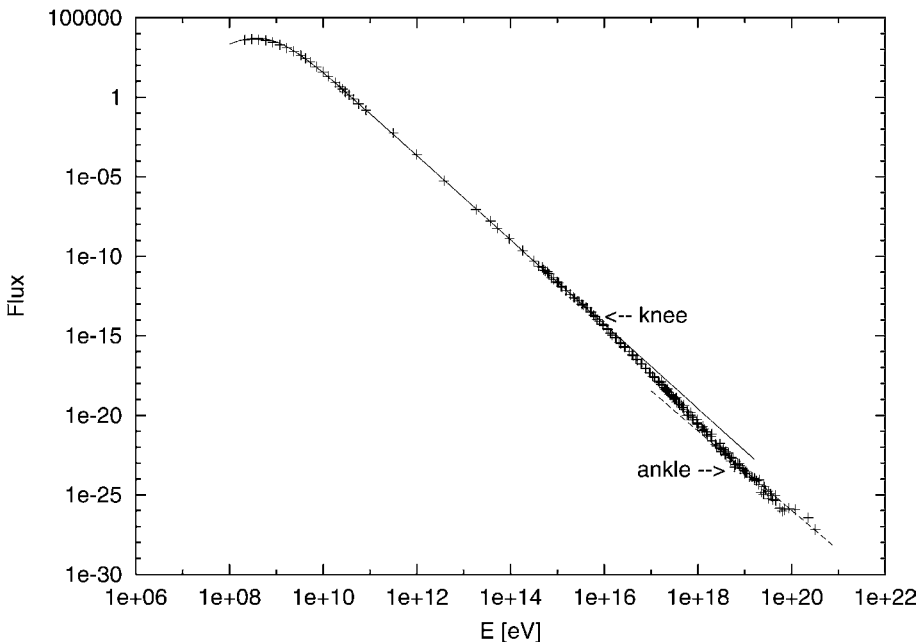


Figure 15.8 Observed energy spectrum of cosmic rays and a fit by Eq. (15.58) with $q = 1.215$ (solid line).

The above effective temperature is of the same order of magnitude as the so-called Hagedorn temperature T_H [54,55], an effective temperature well known from collider experiments. The Hagedorn temperature is much smaller than the center-of-mass energy E_{CMS} of a typical collision process and represents a kind of “boiling temperature” of nuclear matter at the confinement phase transition. It is a kind of maximum temperature that can be reached in a collision experiment. Even largest E_{CMS} cannot produce a larger average temper-

ature than T_H due to the fact that the number of possible particle states grows exponentially.

Let us now work out the assumption that the power law of the measured cosmic ray spectrum is due to fluctuations of temperature. Assume that locally, in the creation process of some cosmic ray particle, some value of the fluctuating inverse temperature β is given. We then expect the momentum of a randomly picked particle in this region to be distributed according to the relativistic Maxwell–Boltzmann distribution

$$p(E|\beta) = \frac{1}{Z(\beta)} E^2 e^{-\beta E}. \quad (15.60)$$

Here $p(E|\beta)$ denotes the conditional probability of E given some value of β . We neglect the rest mass m so that $E = c|\vec{p}|$. The normalization constant is given by

$$Z(\beta) = \int_0^\infty E^2 e^{-\beta E} dE = \frac{2}{\beta^3}. \quad (15.61)$$

Now assume that β is χ^2 -distributed. The observed cosmic ray distribution at the earth does not contain any information on the local temperature at which the various particles were produced. Hence we have to average over all possible fluctuating temperatures, obtaining the measured energy spectrum as the marginal distribution

$$p(E) = \int_0^\infty p(E|\beta) f(\beta) d\beta. \quad (15.62)$$

The integral (15.62) with $f(\beta)$ given by (15.6) and $p(E|\beta)$ given by (15.60) is easily evaluated and one obtains Eq. (15.58) with

$$q = 1 + \frac{2}{n+6} \quad (15.63)$$

and

$$b = \frac{\beta_0}{4-3q}, \quad (15.64)$$

where β_0 is the average inverse temperature.

The variables X_i in Section 15.3 describe the independent degrees of freedom contributing to the fluctuating temperature. At very large center-of-mass energies, due to the uncertainty relation, the probed volume r^3 is very small, and all relevant degrees of freedom in this small volume are basically represented by the 3 spatial dimensions into which heat can flow, leading to a fluctuating effective temperature in each creation process of cosmic ray particles. The 3 spatial degrees of freedom yield $n = 3$ or, according to Eq. (15.63),

$$q = \frac{11}{9} = 1.222. \quad (15.65)$$

For cosmic rays E_{CMS} is very large; hence we expect a q -value that is close to this asymptotic value. The fit in Figure 15.8 in fact uses $q = 1.215$, which agrees with the predicted value in Eq. (15.65) to about three digits. Assuming the existence of two different sources of cosmic rays, one can also reproduce the “knee” and the “ankle” structures seen in Figure 15.8 for energies $E > 10^{16}$ eV, see [15, 53] for more details.

15.11 Statistics of Train Delays

Our final example leaves the classical area of physics and turns to a more practical problem that almost everybody has experienced in the past. Trains, buses, planes, etc. are often delayed! A statistical analysis of train delay data in the UK was recently performed in [24]. One observes probability densities of delays that are q -exponentials, i.e., that have power-law tails (see Figure 15.9 for an example).

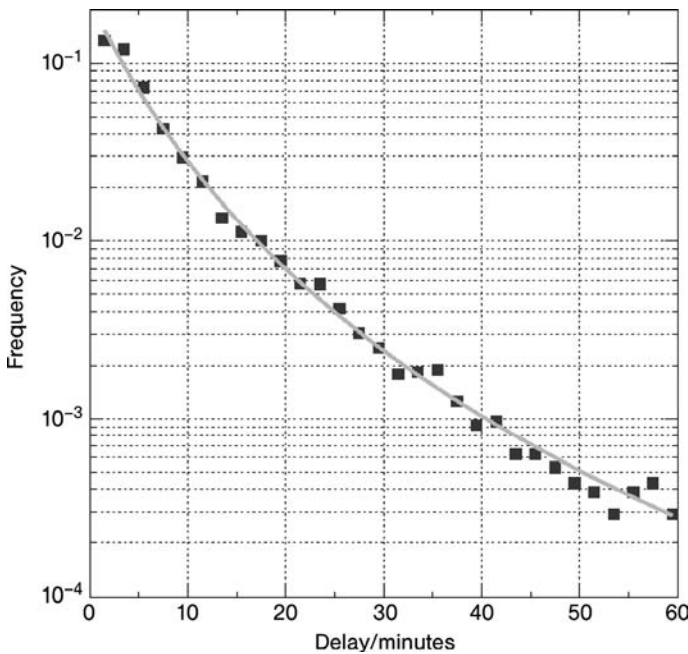


Figure 15.9 Delay statistics of train departures at Swindon station.
The trains are heading for London Paddington.

We start with a very simple theoretical model for the local departure statistics of trains. The waiting time distribution until departure takes place is

simply given by that of a Poisson process [35]

$$P(t|\beta) = \beta e^{-\beta t}. \quad (15.66)$$

Here t is the time delay from the scheduled departure time, and β is a positive parameter. The symbol $P(t|\beta)$ denotes the conditional probability density to observe the delay t provided the parameter β has a certain given value. Clearly, the above probability density is normalized. Large values of β mean that most trains depart very well in time, whereas small β describes a situation where long delays are rather frequent.

The above simple exponential model becomes superstatistical by making the parameter β a fluctuating random variable as well. These fluctuations describe large-scale temporal variations of the British rail network environment. For example, during the start of the holiday season, when there are many passengers, we expect that β is smaller than usual for a while, resulting in frequent delays. Similarly, if there is a problem with the track or if bad weather conditions exist, we also expect smaller values of β on average. The value of β is also influenced by extreme events such as derailments, industrial action, terror alerts, etc.

The observed long-term distribution of train delays is then a mixture of exponential distributions where the parameter β fluctuates. If β is distributed with probability density $f(\beta)$, and fluctuates on a large time scale, then one obtains the marginal distributions of train delays as

$$p(t) = \int_0^\infty f(\beta) p(t|\beta) d\beta = \int_0^\infty f(\beta) \beta e^{-\beta t} d\beta. \quad (15.67)$$

Again, a χ^2 -distribution of n degrees of freedom makes sense for β , leading to q -exponential waiting time distributions of the form

$$p(t) \sim (1 + b(q-1)t)^{\frac{1}{1-q}} \quad (15.68)$$

where $q = 1 + 2/(n+2)$ and $b = 2\beta_0/(2-q)$. Our model generates q -exponential distributions of train delays by a simple mechanism, namely a χ^2 -distributed parameter β of the local Poisson process. This is in good agreement with the recorded delay data of the British rail network [24].

Typical q -values obtained from our fits for various stations are in the region $q = 1.15 \dots 1.35$ (see Table 15.1). Hence

$$n = \frac{2}{q-1} - 2 \quad (15.69)$$

is in the region $4 \dots 11$. This means that the number of degrees of freedom influencing the value of β is just of the order we expected it to be: A few

large-scale phenomena such as weather, seasonal effects, passenger fluctuations, signal failures, repairs of track, etc. seem to be relevant. In general, it makes sense to compare stations with the same q (the same number of external degrees of freedom of the network environment): The larger the value of b , the better the performance of this station under the given environmental conditions.

Table 15.1 The fitted parameters q and b for the departure statistics of 23 UK stations.

Station	q	b	Code
Bath Spa	1.195	0.209	BTH
Birmingham	1.257	0.271	BHM
Cambridge	1.270	0.396	CBG
Canterbury East	1.298	0.400	CBE
Canterbury West	1.267	0.402	CBW
City Thameslink	1.124	0.277	CTK
Colchester	1.222	0.272	COL
Coventry	1.291	0.330	COV
Doncaster	1.289	0.332	DON
Edinburgh	1.228	0.401	EDB
Ely	1.316	0.393	ELY
Ipswich	1.291	0.333	IPS
Leeds	1.247	0.273	LDS
Leicester	1.231	0.337	LEI
Manchester Piccadilly	1.231	0.332	MAN
Newcastle	1.378	0.330	NCL
Nottingham	1.166	0.209	NOT
Oxford	1.046	0.141	OXF
Peterborough	1.232	0.201	PBO
Reading	1.251	0.268	RDG
Sheffield	1.316	0.335	SHF
Swindon	1.226	0.253	SWI
York	1.311	0.259	YRK

15.12 Conclusion and Outlook

The superstatistics concept is a general principle for the description of complex systems which possess large-scale fluctuations of a suitable intensive system parameter. This parameter can, for example, be the inverse temperature in a driven nonequilibrium system but a much broader interpretation is pos-

sible. For example, in turbulent flows the fluctuating parameter is related to the fluctuating energy dissipation rate, and more generally it can be any parameter describing a fluctuating environment. If there is suitable time scale separation, then the result is a “statistics of a statistics,” effectively described by a mixture of distributions. The marginal probability densities of superstatistical systems typically exhibit fat tails, which can be power laws, stretched exponentials, or more complicated functions. For superstatistical systems both normal and anomalous transport is possible.

We have shown that there are interesting applications of the superstatistics concept for a large variety of complex systems. We started with examples from physics (Lagrangian turbulence, defect turbulence, statistics of cosmic rays), and then went on to examples from a broader context, such as the delay statistics on the British train network. It should be clear that one can think of further applications for many other complex systems. These may include human travel behavior as mirrored by money circulation dynamics [56] or even applications in medicine, such as a superstatistical model for the progression statistics of malignant cancer cells [57].

References

- 1** C. Beck and E.G.D. Cohen, Physica A **322**, 267 (2003)
- 2** C. Beck, E.G.D. Cohen, and H.L. Swinney, Phys. Rev. E **72**, 026304 (2005)
- 3** C. Beck and E.G.D. Cohen, Physica A **344**, 393 (2004)
- 4** H. Touchette and C. Beck, Phys. Rev. E **71**, 016131 (2005)
- 5** C. Tsallis and A.M.C. Souza, Phys. Rev. E **67**, 026106 (2003)
- 6** P.-H. Chavanis, Physica A **359**, 177 (2006)
- 7** C. Vignat, A. Plastino, and A.R. Plastino, cond-mat/0505580
- 8** S. Abe, C. Beck, and E.G.D. Cohen, Phys. Rev. E **76**, 031102 (2007)
- 9** C. Beck, Europhys. Lett. **64**, 151 (2003)
- 10** A. Reynolds, Phys. Rev. Lett. **91**, 084503 (2003)
- 11** C. Beck, Phys. Rev. Lett. **98**, 064502 (2007)
- 12** C. Beck, Physica D **193**, 195 (2004)
- 13** M. Baiesi, M. Paczuski and A.L. Stella, Phys. Rev. Lett. **96**, 051103 (2006)
- 14** K. E. Daniels, C. Beck, and E. Bodenschatz, Physica D **193**, 208 (2004)
- 15** C. Beck, Physica A **331**, 173 (2004)
- 16** S. Rizzo and A. Rapisarda, *Environmental atmospheric at Florence airport*, Proceedings of the 8th Experimental Chaos Conference, Florence, AIP Conf. Proc. **742**, 176 (2004) (cond-mat/0406684)
- 17** J.-P. Bouchard and M. Potters, *Theory of Financial Risk and Derivative Pricing*, Cambridge University Press, Cambridge (2003)
- 18** M. Ausloos and K. Ivanova, Phys. Rev. E **68**, 046122 (2003)
- 19** Y. Ohtaki and H.H. Hasegawa, cond-mat/0312568
- 20** A.Y. Abul-Magd, Physica A **361**, 41 (2006)
- 21** S. Abe and S. Thurner, Phys. Rev. E **72**, 036102 (2005)
- 22** A. Porporato, G. Vico, and P.A. Fay, Geophys. Res. Lett. **33**, L15402 (2006)
- 23** A.K. Rajagopal, cond-mat/0608679
- 24** K. Briggs and C. Beck, Physica A **278**, 498 (2007)
- 25** S. Rizzo and A. Rapisarda, Application of superstatistics to atmospheric turbulence,

- in *Complexity, Metastability and Nonextensivity*, eds. C. Beck, G. Benedek, A. Rapisarda, C. Tsallis, World Scientific, Singapore (2005) [cond-mat/0502305]
- 26** G. Wilk and Z. Włodarczyk, Phys. Rev. Lett. **84**, 2770 (2000)
- 27** C. Beck, Phys. Rev. Lett. **87**, 180601 (2001)
- 28** H. Touchette, Temperature fluctuations and mixtures of equilibrium states in the canonical ensemble, in *Nonextensive Entropy – Interdisciplinary Applications*, M. Gell-Mann, C. Tsallis (eds.) Oxford University Press, Oxford (2004)
- 29** F. Sattin and L. Salasnich, Phys. Rev. E **65**, 035106(R) (2002)
- 30** B. Castaing, Y. Gagne, and E.J. Hopfinger, Physica D **46**, 177 (1990)
- 31** C. Tsallis, J. Stat. Phys. **52**, 479 (1988)
- 32** C. Tsallis, R.S. Mendes, and A.R. Plastino, Physica A **261**, 534 (1998).
- 33** C. Tsallis, Braz. J. Phys. **29**, 1 (1999)
- 34** S. Abe, Y. Okamoto (eds.), *Nonextensive Statistical Mechanics and Its Applications*, Springer, Berlin (2001)
- 35** N.G. van Kampen, *Stochastic Processes in Physics and Chemistry*, North Holland, Amsterdam (1981)
- 36** A.R. Plastino and A. Plastino, Physica A **222**, 347 (1995)
- 37** C. Tsallis and D.J. Bukmann, Phys. Rev. E **54**, R2197 (1996)
- 38** S. Jung and H.L. Swinney, Phys. Rev. E **72**, 026304 (2005)
- 39** U. Harder and M. Paczuski, cs/PF/0412027
- 40** A. La Porta, G.A. Voth, A.M. Crawford, J. Alexander, and E. Bodenschatz, Nature **409**, 1017 (2001)
- 41** N. Mordant, A.M. Crawford, and E. Bodenschatz, Phys. Rev. Lett. **93**, 214501 (2004)
- 42** A.M. Reynolds, N. Mordant, A.M. Crawford, and E. Bodenschatz, New J. Phys. **7**, 58 (2005)
- 43** N. Mordant, P. Metz, O. Michel, and J.-F. Pinton, Phys. Rev. Lett. **87**, 214501 (2001)
- 44** N. Mordant, E. Leveque, and J.-F. Pinton, New J. Phys. **6**, 116 (2004)
- 45** J.S. van Zon et al., cond-mat/0405044
- 46** L.F. Burlaga and A.F. Vinas, J. Geophys. Res. **109**, A12107 (2004)
- 47** J. Luczka and B. Zaborek, Acta Phys. Polon. B **35**, 2151 (2004)
- 48** A.M. Mathai and H.J. Haubold, Physica A **375**, 110 (2007)
- 49** B.L. Sawford, Phys. Fluids **A3**, 1577 (1991)
- 50** S.B. Pope, Phys. Fluids **14**, 2360 (2002)
- 51** K.E. Daniels, E. Bodenschatz, Phys. Rev. Lett. **88**, 034501 (2002)
- 52** K.E. Daniels, E. Bodenschatz, Chaos **13**, 55 (2003)
- 53** C. Tsallis, J.C. Anjos, E.P. Borges, Phys. Lett. A **310**, 372 (2003)
- 54** R. Hagedorn, Nuovo Cimento **3**, 147 (1965)
- 55** C. Beck, Physica A **286**, 164 (2000)
- 56** D. Brockmann, this volume.
- 57** L. Leon Chen, C. Beck, Physica A **387**, 3162 (2008)

16**Money Circulation Science – Fractional Dynamics in Human Mobility***Dirk Brockmann*

The dispersal of individuals of a species is the key driving force of various spatiotemporal phenomena which occur on geographical scales. It can synchronize populations of interacting species, stabilize them, and diversify gene pools [1–3]. The geographic spread of human infectious diseases such as influenza, measles, and the recent severe acute respiratory syndrome (SARS) is essentially promoted by human travel which occurs on many length scales and is sustained by a variety of means of transportation [4–8]. In the light of increasing international trade, intensified human traffic, and an imminent influenza A pandemic the knowledge of dynamic and statistical properties of human dispersal is of fundamental importance and acute [7, 9, 10]. A quantitative statistical theory for human travel and concomitant reliable forecasts would substantially improve and extend existing prevention strategies. Despite its crucial role, a quantitative assessment of human dispersal remains elusive and the opinion that humans disperse diffusively still prevails in many models [11]. In this chapter I will present a report on a recently developed technique which permits a solid and quantitative assessment of human dispersal on geographical scales [12]. The key idea is to infer the statistical properties of human travel by analyzing the geographic circulation of individual bank notes for which comprehensive datasets are collected at the online bill-tracking website www.wheresgeorge.com. The analysis shows that the distribution of traveling distances decays as a power law, indicating that the movement of bank notes is reminiscent of superdiffusive, scale-free random walks known as Lévy flights [13]. Secondly, the probability of remaining in a small, spatially confined region for a time T is dominated by heavy tails which attenuate superdiffusive dispersal. I will show that the dispersal of bank notes can be described on many spatiotemporal scales by a two parameter continuous time random walk (CTRW) (CTRW) model to a surprising accuracy. To this end, I will provide a brief introduction to CTRW theory [14] and will show that human dispersal is an ambivalent, effectively superdiffusive process.

16.1

Dispersal Ecology

The notion of dispersal in ecology usually refers to the movement of individuals of a species in their natural environment [1, 3]. The statistical properties of dispersal can be quantified by the dispersal curve $p_{\Delta t}(\Delta x)$. The dispersal curve reflects the relative frequency of geographical displacements Δx which are traversed within a given period of time Δt . In the ecological literature, the term “dispersal” is commonly used in the context of the spatial displacement of individuals of a species between their geographical origin of birth and the location of their first breeding place, a process which occurs on time scales of the lifespan of the individuals. Here we make use of the notion of dispersal somewhat differently, referring to geographical displacements that occur on much shorter timescales of the order of days. A large class of dispersal curves (for example, exponential, Gaussian, stretched exponential, etc.) exhibit a characteristic length scale [15]. That is, when interpreted as the probability of finding a displacement of length Δx , a length scale can be defined by the square root of second moment, i.e., $\sigma = \sqrt{\langle \Delta x^2 \rangle}$. The existence of a typical length scale often justifies the description of dispersal in terms of diffusion equations on spatiotemporal scales larger than Δt and σ [16]. Because, if single displacements are sufficiently uncorrelated the probability density $W(x, t)$ of having traversed a total displacement $X(t)$ after time t is a Gaussian which obeys Fick’s second law:

$$\partial_t W = D \partial_x^2 W, \quad (16.1)$$

where $D = \sigma^2 / \Delta t$ is the diffusion coefficient. This result is a consequence of the central limit theorem [17] and does not depend on the precise form of the short time dispersal curve as long as the variance $\langle \Delta x^2 \rangle$ is finite.

16.2

Diffusive Dispersal and Reaction Kinetics

In population dynamical systems this type of diffusive dispersal is quite frequently combined with a reaction kinetic scheme which accounts for local interactions between various types of reacting agents, for example, various species in predator-pray systems. Sometimes groups of individuals of a single species which interact are classified according to some criterion. For instance in the context of epidemiology a population is often classified according to their infective status.

In an approximation which neglects the intrinsic fluctuations of the underlying reaction kinetics one obtains for these systems mean field reaction-diffusion equations, the most prominent example of which is the Fisher equa-

tion¹ [18],

$$\partial_t u = \lambda u(1 - u) + D\partial_x^2 u, \quad (16.2)$$

for the concentration $u(x, t)$ of a certain class of individuals, a species etc.

16.2.1

SIS Dynamics

A paradigmatic system which naturally yields a description in terms of Eq. (16.2) and has been used to describe geographic spread of infectious diseases is the SIS model in which a local population of N individuals segregates into the two classes of a) susceptibles S who may catch a disease and b) infecteds I who transmit it. Transmission is quantified by the rate α and recovery by the rate β [11]. The reaction scheme could not be simpler:



In the limit of large population size N the dynamics can be approximated by the set of differential equations

$$\partial_t S = -\alpha IS/N, \quad \partial_t I = \alpha IS/N - \beta I. \quad (16.4)$$

Assuming that the number of individuals is conserved (i.e., $I(t) + S(t) = N$) and that disease transmission is more frequent than recovery ($\alpha > \beta$) one obtains for the rescaled relative number of infecteds $u(t) = \alpha I(t)/N(\alpha - \beta)$ a single ordinary differential equation (ODE):

$$\partial_t u = \lambda u(1 - u), \quad (16.5)$$

where $\lambda = \alpha - \beta$. If, additionally reactants are free to move diffusively one obtains Eq. (16.2) for the dynamics of the relative number of infecteds $u(x, t)$ as a function of position and time.

16.2.2

A Word of Caution

The popularity and success of the Fisher equation and similar equations in the field of theoretical biology can be ascribed to some extend to the fact that they possess propagating front solutions and that qualitatively similar patterns were observed in historic pandemics, the most prominent example of which is the bubonic plague pandemic of the 14th century which crossed the

1) Also referred to as the Fisher–Kolmogorov–Petrovsky–Piscounov equation.

European continent as a wave within 3s years at an approximate speed of a few kilometers per day. Aside from factors which are known to play a role, such as social contact networks, age structure, inhomogeneities in local populations and inhomogeneities in the geographic distribution of the population, there is something fundamentally wrong with the diffusion assumption on which this class of equations is based. Humans (with the exception maybe of nomads) do not and never did diffuse on timescales much shorter than their lifespan. A simple argument can be given why this cannot be so. For a diffusion process the expected time for returning to the point of origin is infinite [19] (despite the fact that in spatial dimensions $d \leq 2$ the probability of returning is unity). It would not make much sense to have a home if the expected time to return to it is infinite. However, in the context of the geographic spread of infectious diseases it does at times make sense to employ reaction-diffusion equations. That is because the position of what is passed from human to human, i.e., the pathogens, is what matters and not the position of single host individuals. Unlike humans, pathogens are passed from human to human and compared to humans pathogens have no inclination of returning. They disperse diffusively and a description in terms of reaction-diffusion dynamics is justified, see Figure (16.1).

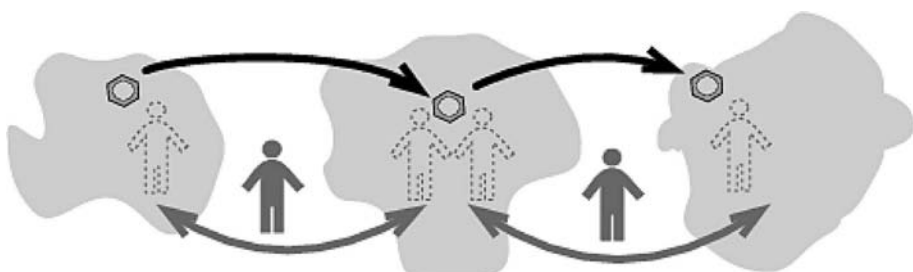


Figure 16.1 Human travel and the dispersal of pathogens. The gray areas depict home ranges of individuals. By virtue of overlapping home ranges and inter-home range travel an infectious disease spreads in space. Although humans travel back and forth between home ranges, pathogens spread continuously in space.

16.3 Long Distance Dispersal and Lévy Flights

Recently the notion of long-distance dispersal (LDD) has been established in dispersal ecology [20], taking into account the observations that a number of dispersal curves exhibit long, algebraic tails which forbid the identification of a typical scale and thus a description of dispersal phenomena based on

diffusion equations. If, for instance, the probability density of traversing a distance r in a given period of time Δt decreases according to

$$p_{\Delta t}(r) \sim \frac{1}{r^{1+\beta}} \quad (16.6)$$

with a tail exponent $\beta < 2$, the variance of the displacement magnitude is infinite and consequently no typical length scale can be identified. Power-law distributions are abundant in nature. Meteorite sizes, city sizes, income, and the number of species per genus follow power-law distributions [21]. In the context of animal movements such power laws have been observed in foraging movements of an increasing number of species, bumble bees and deer [22], microzooplankton [23], reindeer [24], albatrosses [25], spider monkeys [26] and jakaals [27], to name a few.

16.3.1

Lévy Flights

In physics, random walk processes with a power-law single-step distribution are known as Lévy flights [14, 28–30]. Due to the lack of scale in the single steps, Lévy flights are qualitatively different from ordinary random walks. Unlike ordinary random walks the position $\mathbf{X}_N = \sum_n^N \Delta \mathbf{x}_n$ after N steps $\Delta \mathbf{x}_n$ scales with the number of steps according to

$$\mathbf{X}_N \sim N^{1/\beta} \quad (16.7)$$

with $\beta < 2$. Thus, Lévy flights disperse “faster” than the ordinary $N^{1/2}$ behavior exhibited by ordinary random walks; Lévy flights are superdiffusive. Furthermore, the probability density for the position $p(\mathbf{x}, N)$ for Lévy flights behaves asymptotically as

$$p(\mathbf{x}, N) \sim N^{-D/\beta} L_\beta \left(\mathbf{x}/N^{1/\beta} \right) \quad (16.8)$$

where D is the spatial dimension and the function L_β is known as the symmetric Lévy-stable law of index β . This limiting function is a generalization of the ordinary Gaussian and can be expressed by its Fourier-transform

$$L_\beta(\mathbf{z}) = \frac{1}{(2\pi)^{D/2}} \int d\mathbf{k} e^{-i\mathbf{z}\cdot\mathbf{k}} \exp \left(-|\mathbf{k}|^\beta \right). \quad (16.9)$$

The limiting value $\beta = 2$ corresponds to the Gaussian, the limiting function for ordinary random walks. The lack of scale in a Lévy flight, its superdiffusive nature and the geometrical difference between Lévy flights and ordinary random walks are illustrated in Figure 16.2. Lévy flights and superdiffusive random motion were observed in a variety of physical and biological systems,

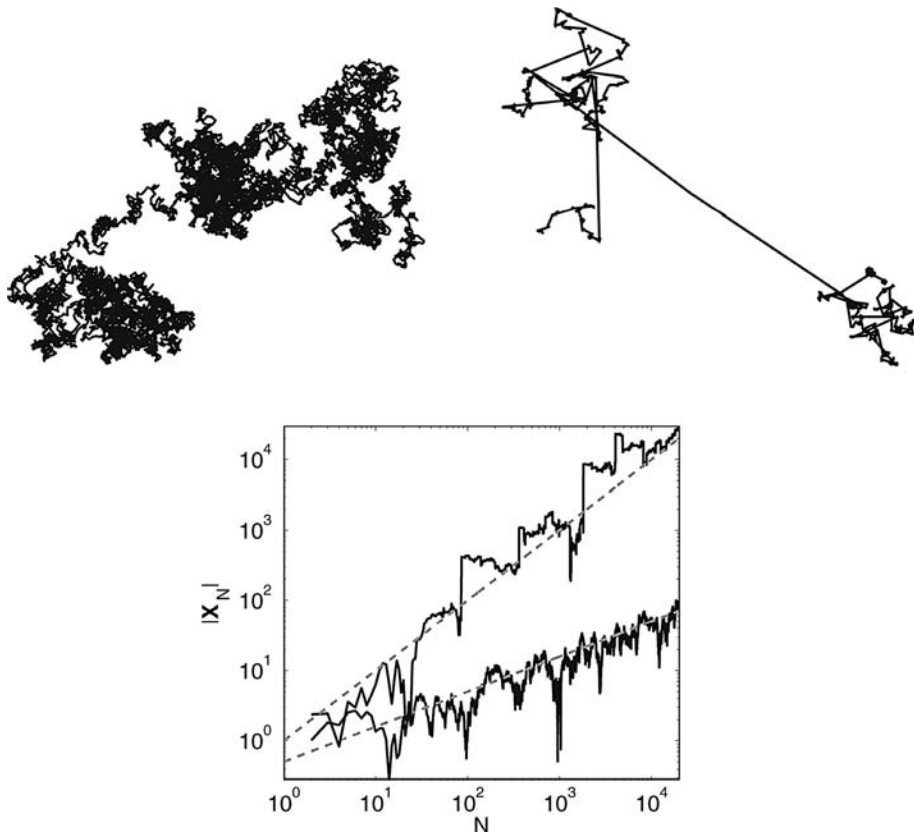


Figure 16.2 Ordinary random walks and Lévy flights. *Left:* The trajectory of an ordinary random walk in two dimensions, equivalent to Brownian motion on large spatiotemporal scales. *Middle:* Unlike Brownian motion, the trajectory of the two-dimensional Cauchy-process, i.e., a Lévy flight with Lévy exponent $\beta = 1$ exhibits local clustering interspersed

with long-distance jumps. *Right:* The distance $|X_N|$ from the starting point $X_0 = 0$ of an ordinary random walk (lower trajectory) and a Lévy flight ($\beta = 1$, upper trajectory) as a function of step number N . The dashed lines indicate the scaling $N^{1/2}$ and $N^{1/\beta}$ respectively. Clearly, the Lévy flight is superdiffusive.

ranging from transport in chaotic systems [31] to foraging patterns of wandering albatrosses [25] and spider monkeys [26].

16.4

Human Travel in the 21st Century

Nowadays, humans travel on many spatial scales, ranging from a few to thousands of kilometers over short periods of time. A person in the 21st century can reach virtually any point on the globe in a matter of days. The intensity of



Figure 16.3 Worldwide air traffic network. Links represent routes between the 500 most frequented airports. Brightness indicates the intensity of traffic between nodes.

modern human travel is convincingly illustrated in Figure 16.3 which depicts nearly the entire international air traffic network.

The direct quantitative assessment of human movements, however, is difficult, and a statistically reliable estimate of human dispersal comprising all spatial scales does not exist. Contemporary models for the spread of infectious diseases across large geographical regions have to make assumptions on human travel. The notion that humans travel short distances more frequently than long ones is typically taken into account. Yet, the precise ratio of the frequency of short trips and the frequency of long trips is not known and must be assumed. Furthermore, it is generally agreed upon that human travel, being a complex phenomenon, adheres to complex mathematical rules with a lot of detail.

Recently, it was shown that the global spread of SARS in 2003 can be reproduced by a model which takes into account nearly the entire civil aviation network [7, 10]. Despite the high degree of complexity of aviation traffic, the strong heterogeneity of the network yields an unexpectedly narrow range of fluctuations, supporting the idea that reliable forecasts of the geographic spread of disease is possible. Although the model successfully accounts for the geographic spread on global scales, it cannot account for the spread on small and intermediate spatial scales. To this end a comprehensive knowledge of human travel on scales ranging from a few to a few thousand kilometers is necessary. However, collecting comprehensive traffic data for all means of human transportation involved is difficult if not impossible.

16.5

Money as a Proxy for Human Travel

In a recent study [12,32], the problem of measuring human travel was directly resolved by a trick. Instead of measuring individual human travel paths directly, the geographic dispersal of bank notes in the United States was investigated instead. The key idea of the project was to use bank note dispersal as a proxy for human travel on all geographical length scales. The data was collected from the online bill-tracking website, www.wheresgeorge.com. The idea of this Internet game, which was initiated in 1998 by Hank Eskin, is simple. Individual bank notes are marked by registered users and brought into circulation. When people come into possession of such marked bank notes, they can register at the website and report their current location and return the bank note into circulation. Thus, registered users can monitor the geographical dispersal of their money. Meanwhile, over 80 millions dollar bills have been registered and over 3 million users participate in the game. As bank notes are primarily transported by traveling humans, the statistical properties of human travel can be inferred from the dispersal of bank notes with high spatiotemporal precision.

The original study of human movements was based on the trajectories of a subset of 464 670 dollar bills obtained from the website and the dispersal of bank notes in the United States, excluding Alaska and Hawaii, was analyzed. The core data consisted of 1,033,095 reports to the website. From these reports the geographical displacements $r = |\mathbf{x}_2 - \mathbf{x}_1|$ between a first (\mathbf{x}_1) and secondary (\mathbf{x}_2) report location of a bank note and the elapsed time T between successive reports was computed. The pairs of datapoints $\{r_i, T_i\}$ represented the core dataset, from which the probability density function (pdf) $W(r, t)$ of having traveled a distance r after a time t was estimated.

In order to illustrate qualitative features of bank note trajectories, Figure 16.4 depicts short-time trajectories ($T < 14$ days) originating from three major cities (Seattle, WA, New York, NY, Jacksonville, FL). Succeeding their initial entry, the majority of bank notes are reported next in the vicinity of the initial entry location, i.e., $r < 10$ km (Seattle 52.7%, New York 57.7% Jacksonville 71.4%). However, a small yet considerable fraction is reported beyond a distance of 800 km (Seattle 7.8%, New York 7.4%, Jacksonville 2.9%).

16.5.1

The Lack of Scale in Money Movements

From a total of $N = 20,540$ short-time displacements one can measure the probability density $p(r)$ of traversing a distance r in a time interval δT between one and four days. The result is depicted in Figure 16.5. A total of 14,730 (i.e., a fraction $Q = 0.71$) secondary reports occur outside a short range

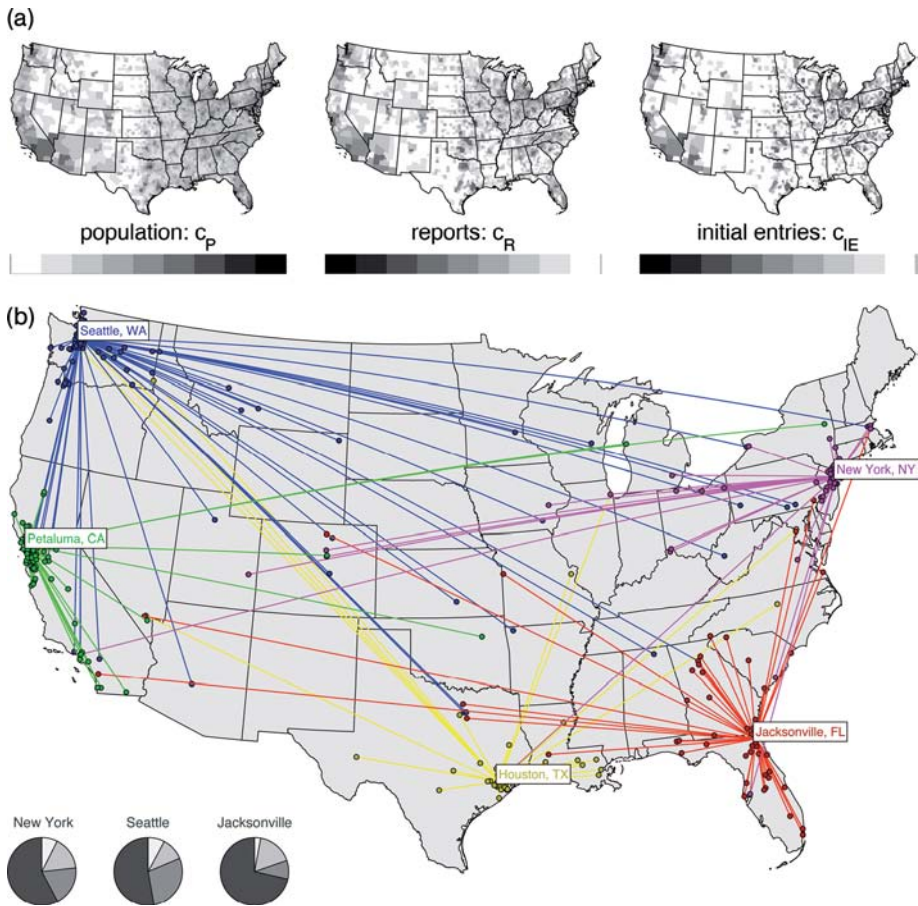


Figure 16.4 Dispersal of bank notes on geographical scales. **a:** Relative logarithmic densities of population ($c_P = \log_{10} \rho_P / \langle \rho_P \rangle$), reports ($c_R = \log_{10} \rho_R / \langle \rho_R \rangle$) and initial entry ($c_{IE} = \log_{10} \rho_{IE} / \langle \rho_{IE} \rangle$) as functions of geographical coordinates. The shades of gray encode the densities relative to the nationwide averages (3,109 counties) of $\langle \rho_P \rangle = 95.15$, $\langle \rho_R \rangle = 0.34$ and $\langle \rho_{IE} \rangle = 0.15$ individuals, reports, and initial entries per km^2 , respectively. **b:** Short-time trajectories of bank notes originating from three different places. Tags indicate initial, symbols secondary report locations. Lines rep-

resent short-time trajectories with traveling time $T < 14$ days. The inset depicts a close-up of the New York area. Pie charts indicate the relative number of secondary reports coarsely sorted by distance. The fractions of secondary reports that occurred at the initial entry location (dark), at short ($0 < r < 50$ km), intermediate ($50 < r < 800$ km), and long ($r > 800$ km) distances are ordered by increasing brightness. The total number of initial entries are $N = 524$ (Seattle), $N = 231$ (New York), $N = 381$ (Jacksonville).

radius $L_{\min} = 10$ km. Between L_{\min} and the approximate average east–west extension of the United States $L_{\max} \approx 3200$ km $p(r)$ exhibits power law behavior $p(r) \sim r^{-(1+\beta)}$ with an exponent $\beta = 0.59 \pm 0.02$. For $r < L_{\min}$, $p(r)$

increases linearly with r which implies that displacements are distributed uniformly inside the disk $|\mathbf{x}_2 - \mathbf{x}_1| < L_{\min}$.

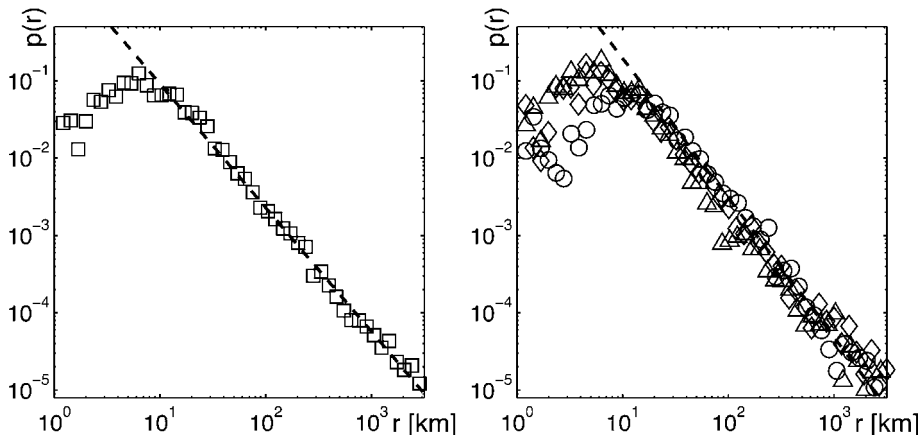


Figure 16.5 Quantitative analysis of bank note dispersal. *Left:* The short-time dispersal kernel. The measured probability density function $p(r)$ of traversing a distance r in less than $T = 4$ days is depicted by squares. It is computed from an ensemble of 20,540 short-time displacements. The dashed black

line indicates a power law $p(r) \sim r^{-(1+\beta)}$ with an exponent of $\beta = 0.59$. *Right:* $p(r)$ for three classes of initial entry locations (black triangles for metropolitan areas, diamonds for cities of intermediate size, and circles for small towns).

One might speculate whether the observed lack of scale in $p(r)$ is not a dynamic property of dispersal but rather imposed by the substantial spatial inhomogeneity of the United States. For instance, the probability of traveling a distance r might depend strongly on static properties such as the local population density. In order to test this hypothesis, $p(r)$ was measured for three classes of initial entry locations: highly populated metropolitan areas (191 locations, local population $N_{\text{loc}} > 120,000$), cities of intermediate size (1544 locations, local population $120,000 > N_{\text{loc}} > 22,000$), and small towns (23,640 locations, local population $N_{\text{loc}} < 22,000$) comprising 35.7%, 29.1%, and 25.2% of the entire population of the United States, respectively. Figure 16.5 also depicts $p(r)$ for these classes. Despite systematic deviations for short distances, all distributions exhibit an algebraic tail with the same exponent $\beta \approx 0.6$. This confirms that the observed power law is an intrinsic and universal property of dispersal, the first experimental evidence that bank note trajectories are reminiscent of Lévy flights and that their geographic dispersal is superdiffusive.

16.6

Is That All?

However, the situation is more complex. If one assumes that the dispersal of bank notes can be described by a Lévy flight with a short-time probability distribution $p(r)$ as depicted in Figure 16.5, one can estimate the time T_{eq} for an initially localized ensemble of bank notes to reach the stationary distribution (maps in Figure 16.4). Assume that the Lévy flight evolves in a two-dimensional region of linear extent L . Furthermore, assume that the single step distribution for a vectorial displacement \mathbf{x} of the random walk can be approximated by

$$p_{\Delta t}(\mathbf{x}) = (1 - Q)\delta(\mathbf{x}) + Q f_{\delta L}(\mathbf{x}). \quad (16.10)$$

Here Δt denotes the typical time between single steps, Q the fraction of walkers which jump a distance $d > \delta L$ and $(1 - Q)$ the fraction which remains in a disk defined by $|\mathbf{x}| \leq \delta L$. The function $f_{\delta L}(\mathbf{x})$ comprises the power law in the single steps, characteristic for Lévy flights:

$$f_{\delta L}(\mathbf{x}) = C \delta L^\beta |\mathbf{x}|^{-(2+\beta)} \quad |\mathbf{x}| \geq \delta L. \quad (16.11)$$

Inserting this into Eq. (16.10) one obtains that $f_{\delta L}(\mathbf{x})$ is normalized to unity and that the normalization constant C is independent of the microscopic length δL . The Fourier transform of $p(\mathbf{x})$ is given by $\tilde{p}(\mathbf{k}) = (1 - Q) + Q \tilde{f}_{\delta L}(\mathbf{k})$. The Fourier transform of the probability density function $W_N(\mathbf{x})$ of the walker being located at a position \mathbf{x} after N steps can be computed in terms of $\tilde{p}(\mathbf{k})$ according to

$$\tilde{W}_N(\mathbf{k}) = \tilde{p}(\mathbf{k})^N \approx \left(1 - Q \delta L^\beta |\mathbf{k}|^\beta\right)^N \approx e^{-QN|\delta L \mathbf{k}|^\beta}. \quad (16.12)$$

The relaxation time in a confined region is provided by the lowest mode $k_{\min} = L/2\pi$. Inserted into (16.12) with $N = t/\Delta t$ one obtains

$$T_{\text{eq}} \approx \delta T/Q (L/2\pi\delta L)^\beta = 68 \text{ days}. \quad (16.13)$$

Thus, after 2–3 months bank notes should have reached the equilibrium distribution. Surprisingly, the long-time dispersal data do not reflect a relaxation within this time.

Figure 16.6 shows secondary reports of bank notes with initial entry at Omaha, NE which have dispersed for times $T > 100$ days (with an average time $\langle T \rangle = 289$ days). Only 23.6% of the bank notes traveled more than 800 km, the majority of 57.3% traveled an intermediate distance $50 < r < 800$ km and a relatively large fraction of 19.1% remained within a radius of 50 km even after an average time of nearly one year. From Eq. (16.13) a much higher fraction of bills is expected to reach the metropolitan areas of the West Coast and

the New England states after this time. This indicates that the simple Lévy flight picture for dispersal is incomplete. What causes this attenuation of the dispersal?

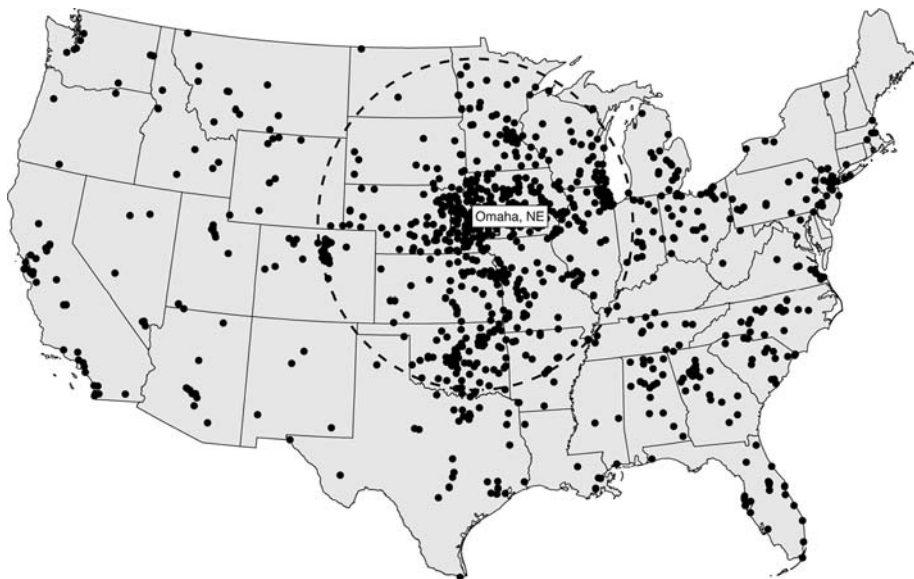


Figure 16.6 Long-time dispersal of bank notes with an initial entry in Omaha, NE. Points denote the location of the second report. Each bill traveled for a time greater than 100 days, with an average of 289 days. The dashed circle indicates the distance of 800 km from Omaha.

16.7 Scaling Analysis

In order to understand the underlying cause of attenuated dispersal a useful theoretical tool is a spatiotemporal scaling analysis. The ordinary Lévy flight pictures suggest that the process of money dispersal obeys a scaling relation $X(t) \sim t^{1/\beta}$ with an exponent $\beta \approx 0.6$. According to the empirical evidence of Figure 16.6 the process is slowed down. Thus, a valid question would be: does the dispersal exhibit a scaling relation

$$X(t) \sim t^{1/\mu} \quad (16.14)$$

with a somewhat larger exponent $\mu > \beta$? If so, in what time window can one observe such a scaling and what is the exponent? Various methods for detecting a spatiotemporal scaling exist. One method is as follows: For a potential candidate of an exponent μ one computes the distances divided by time of

flights traveled raised to the power of $1/\mu$, i.e., the quantity

$$Z(t) = \frac{|\mathbf{X}(t)|}{t^{1/\mu}}. \quad (16.15)$$

The scalar $Z(t)$ is a stochastic time-dependent quantity and in general with a time-dependent associated pdf $p(z, t)$. If the process $\mathbf{X}(t)$ is scaling and for the right choice of exponent μ , $p(z, t)$ is time-independent

$$p(z, t) = p(z). \quad (16.16)$$

As the pdfs $p(\mathbf{x}, t)$ and $p(z, t)$ of the processes $\mathbf{X}(t)$ and $Z(t)$, respectively, are related by

$$p(z, t) = \left\langle \delta \left(z - |\mathbf{X}(t)| / t^{1/\mu} \right) \right\rangle, \quad (16.17)$$

one can deduce that $p(\mathbf{x}, t)$ must fulfill

$$p(\mathbf{x}, t) = t^{-D/\mu} f_{\mathbf{x}} \left(\mathbf{x} / t^{1/\mu} \right), \quad (16.18)$$

where the function $f_{\mathbf{x}}$ is a scaling function. Likewise, one obtains for the pdf $p(r, t)$ of the distance $R = |\mathbf{X}|$ traveled the relation

$$p(r, t) = t^{-1/\mu} f_r \left(r / t^{1/\mu} \right). \quad (16.19)$$

The quantity on the left-hand side can be estimated from the data. Multiplied by the temporal factor on the right one obtains a quantity that depends on the ratio $r / t^{1/\mu}$ only. The results of the scaling analysis of the money dispersal data are depicted in Figure 16.7. For an exponent

$$\mu \approx 1$$

and in a time window of $50 < T < 365$ days one finds that the data collapse on one curve which reflects the empirical scaling function f_r . Consequently, in a time window of approximately 2 months up to a year, money dispersal exhibits spatiotemporal scaling. Furthermore, the empirical exponent μ is greater than the exponent β promoted by the short-time dispersal kernel

$$1 \approx \mu > \beta \approx 0.6,$$

reflecting the qualitative observation that the process is slowed down. Interestingly, the process is still superdiffusive as $\mu < 2$. What could be a possible reason for this attenuation?

16.8

Scale Free Waiting Times

A possible, conceptually straightforward explanation of this effect is a strong impact of the spatial inhomogeneity of the system. For instance, the typical

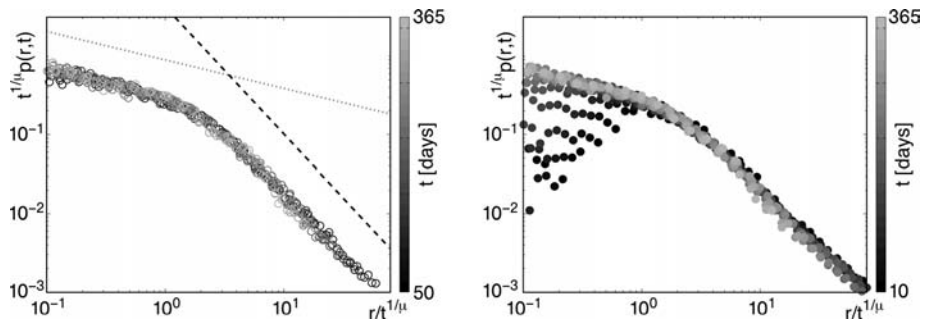


Figure 16.7 Scaling analysis of money dispersal. *Left:* For times in the range of 50 to 365 days (indicated by the shade of gray) the quantity $t^{1/\mu} p(r,t)$ is plotted against the ratio $r/t^{1/\mu}$ for a scaling exponent $\mu \approx 1$. As all data point collapse on a single curve, the underlying process $X(t)$ exhibits spatiotemporal

scaling. The emergent function f_r is the empirical scaling function of Eq. (16.19). Notice two regimes with power-law behavior. *Right:* Deviation (dark gray) from the scaling function are observed, if short times are included ($10 < t < 50$), consistent with the short-time dispersal kernel of Figure 16.5.

time of rest in a geographical region might depend on local properties such as the population density. People might be less likely to leave large cities than e.g. suburban areas.

In order to address this issue one can investigated the relative proportion $P_0^i(t)$ of bank notes which is reported again in a small (20 km) radius of the initial entry location i as a function of time (Figure 16.8). The quantity $P_0^i(t)$ is a local quantity that estimates the probability for a bank note of being reported at the initial location at time t a second time. In order to obtain reliable estimates this quantity is averaged over the above classes of initial entry locations (e.g. metropolitan areas, cities of intermediate size,s and small towns): For all classes one finds the asymptotic behavior $P_0(t) \sim A t^{-\eta}$ with an exponent $\eta \approx 0.60 \pm 0.03$ and a coefficient A . The observed difference in values of the coefficient A reflect the impact of the spatial inhomogeneity of the system, i.e., bank notes are more likely to remain in highly populated areas. The exponent η , however, is approximately the same for all classes which indicates that waiting time and dispersal characteristics are universal and do not depend significantly on external factors such as the population density. Notice that for a pure two dimensional Lévy flight with index β the function $P_0(t)$ scales as $t^{-\eta}$ with $\eta = 2/\beta$. For $\beta \approx 0.6$ (as put forth by Figure 16.5) this implies $\eta \approx 3.33$ [19], i.e., a fivefold steeper decrease than observed, which clearly shows that dispersal cannot be described by a pure Lévy flight model. The measured decay is even slower than the decay exhibited by ordinary two-dimensional diffusion ($\eta = 1$ [19]). This is very puzzling.

One way of slowing down dispersal are long periods of rest. In as much as an algebraic tail in the spatial displacements yields superdiffusive behavior, a tail in the probability density $\psi(\Delta t)$ for times Δt between successive spatial

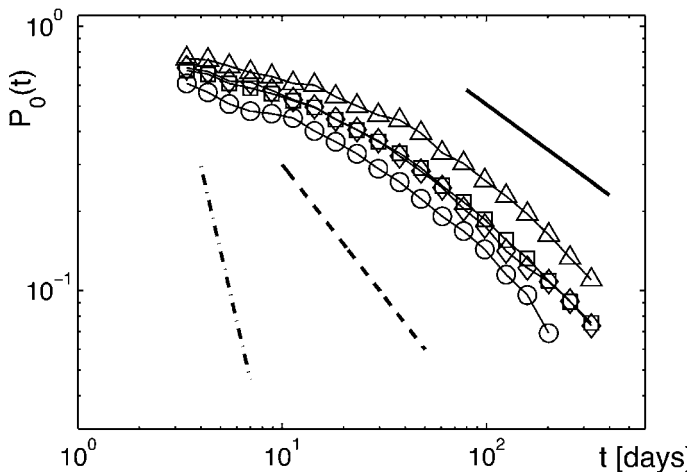


Figure 16.8 The relative proportion $P_0(t)$ of secondary reports within a short radius ($r_0 = 20$ km) of the initial entry location as a function of time. Squares depict $P_0(t)$ averaged over 25,375 initial entry locations. Triangles, diamonds, and circles show $P_0(t)$ for the same classes as in Fig 16.5. All curves decrease asymptotically as $t^{-\xi}$ with an expo-

nent $\xi = 0.6 \pm 0.03$ indicated by the solid line. Ordinary diffusion in two dimensions predicts an exponent $\xi = 1$ (black dashed line). Lévy flight dispersal with an exponent $\beta = 0.6$ as suggested by the short-time dispersal kernel (Figure 16.5) predicts an even steeper decrease, $\xi = 3.33$ (dot-dashed line).

displacements of an ordinary random walk can lead to subdiffusion. For instance, if $\psi(\Delta t) \sim \Delta t^{-(1+\alpha)}$ with $\alpha < 1$, the position of an ordinary random walker scales according to $X(t) \sim t^{2/\alpha}$ [14]. In combination with a power law in the spatial displacements this ambivalence yields a competition between long jumps and long rests and can be responsible for the attenuation of dispersal [33].

16.9 Ambivalent Processes

The idea of an antagonistic interplay between scale-free displacements and waiting times can be explored within the framework of CTRW introduced by Montroll and Weiss [34]. A CTRW consists of a succession of random displacements Δx_n and random waiting times Δt_n each of which is drawn from a corresponding probability density function $p(\Delta x)$ and $\psi(\Delta t)$. Spatial and temporal increments are assumed to be statistically independent. Furthermore, we assume that the spatial distribution is symmetric, i.e., $p(\Delta x) = p(|\Delta x|)$, and since the temporal increments are all positive $\psi(\Delta t)$ is single sided. After

N iterations the position of the walker and the elapsed time is given by

$$\mathbf{X}_N = \sum_n \Delta \mathbf{x}_n \quad \text{and} \quad T_N = \sum_n \Delta t_n,$$

respectively.

16.9.1

Scaling Relation

These two equations relate position and time to step number. However, one is interested in the functional relationship of position and time. For instance, if the pdfs $p(\Delta \mathbf{x})$ and $\psi(\Delta t)$ possess a steep enough decrease for large arguments, i.e., existing moments, the central limit theorem implies that position scales with step number according to

$$\mathbf{X}_N \sim N^{1/2},$$

and time increases linearly with step number:

$$T_N \sim N.$$

Combining both the scaling relationships one finds that in this case the process $\mathbf{X}(t)$ exhibits ordinary diffusive scaling

$$\mathbf{X}(t) \sim t^{1/2}. \tag{16.20}$$

If, however both, spatial increments and waiting time possess an algebraic tail asymptotically, i.e.,

$$p(\Delta \mathbf{x}) \sim \frac{1}{|\Delta \mathbf{x}|^{2+\beta}} \quad \text{and} \quad \psi(\Delta t) \sim \frac{1}{\Delta t^{1+\alpha}}, \tag{16.21}$$

with spatial and temporal exponents $0 < \beta < 2$ and $0 < \alpha < 1$, respectively, the second moment of $\Delta \mathbf{x}$ as well as the first moment of Δt are divergent. This implies a scaling of position of the form

$$\mathbf{X}_N \sim N^{1/\beta}, \tag{16.22}$$

as observed for ordinary Lévy flights but a superlinear scaling of time with step number as well:

$$T_N \sim N^{1/\alpha}. \tag{16.23}$$

The combination of these two scaling relations gives a heuristic scaling of position with time which depends on the ratio of both exponents α and β

$$\mathbf{X}(t) \sim t^{\alpha/\beta}. \tag{16.24}$$

Comparing with the scaling relation of superdiffusive ordinary Lévy processes, $X(t) \sim t^{1/\beta}$, Eq. (16.37) ones sees that long waiting times slow down the process as the temporal exponent is less than unity. This is easily demonstrated by a numerical realization of an ambivalent process as depicted in Figure 16.9. Clearly long waiting times slow down the process and the scaling relation (16.24) is valid.

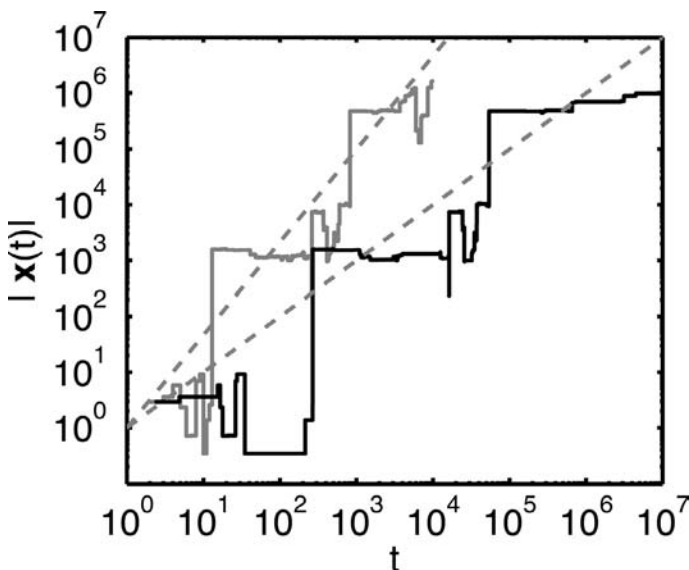


Figure 16.9 Dispersal characteristics of an ordinary Lévy (gray) flight in comparison to an ambivalent process (black). The distance $|X(t)|$ from the origin as a function of time is depicted. The choice of exponents is $\beta = 0.6$ for the Lévy process and $\alpha = \beta = 0.6$ for the ambivalent process. The dashed lines indicate the heuristic scaling relations $|X(t)| = t^{1/\beta}$ and $|X(t)| = t^{\alpha/\beta}$, respectively.

The scaling relation (16.24) implies that by choosing waiting time and jump length exponents in their valid ranges one can generate processes with any type of spatiotemporal scaling. The phase diagram (Figure 16.10) illustrates the various processes one can generate by varying the exponents α and β and show the limiting processes. For instance when $2\alpha > \beta$ the process is superdiffusive and when $2\alpha < \beta$ the process is subdiffusive. The limiting processes of ordinary Lévy flights, fractional Brownian motion (regular subdiffusion) and ordinary diffusion are attained by choosing $(\alpha = 1, 0 < \beta < 2)$, $(0 < \alpha < 1, \beta = 2)$ and $(\alpha = 1, \beta = 2)$, respectively. Note that the family of processes for which the ratio of exponents is $\alpha/\beta = \text{const.}$ exhibit the same spatiotemporal scaling. This does not imply however, that these processes are identical and will become clear below. This is best illustrated for a choice of

processes which fulfill $2\alpha = \beta$. These exhibit ordinary diffusive scaling but nevertheless are not diffusion processes.

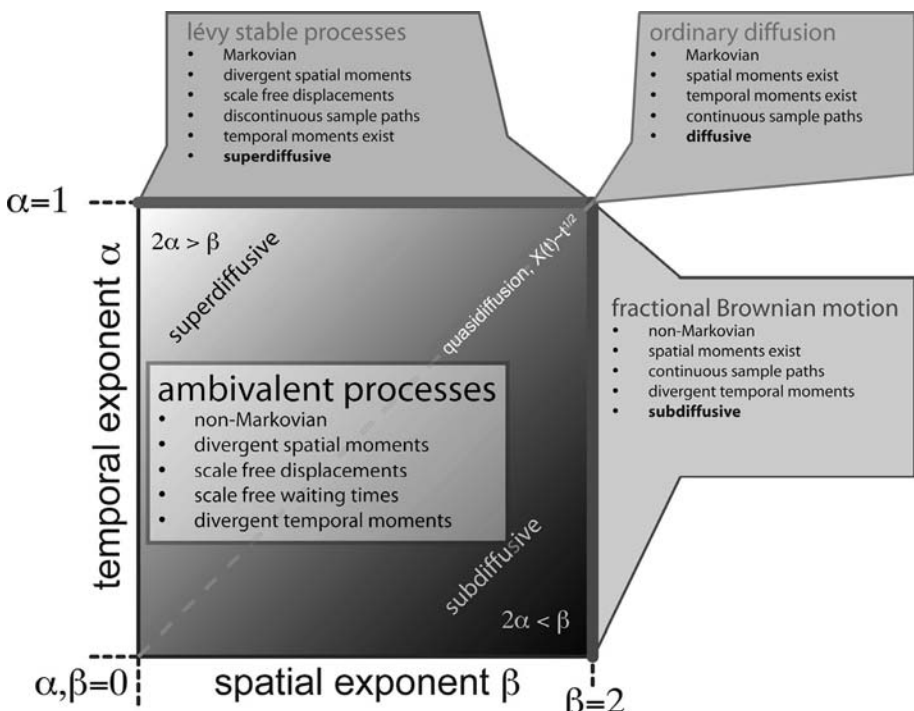


Figure 16.10 Phase diagram for ambivalent anomalous diffusion processes with scale-free waiting times and scale-free spatial displacements and their limiting processes. The valid ranges for temporal and spatial exponents α and β are $(0, 1]$ and $(0, 2]$, respectively.

In Figure 16.11 such a quasidiffusive process is compared with an ordinary diffusion process. This example illustrates that processes with identical ratio α/β are geometrically quite different but also that in order to fully comprehend the properties of ambivalent anomalous diffusion processes one is required to compute the pdf $W(x, t)$ for the process $X(t)$ or a dynamical equation for it.

16.9.2

The Limiting Function for Ambivalent Processes

The quantity of interest is the position $X(t)$ after time t . The probability density $W(x, t)$ for this process can be computed in a straightforward fashion [14] and can be expressed in terms of the spatial distribution $p(\Delta x)$ and the temporal distribution $\psi(\Delta t)$. The Fourier–Laplace transform of $W(x, t)$ is given

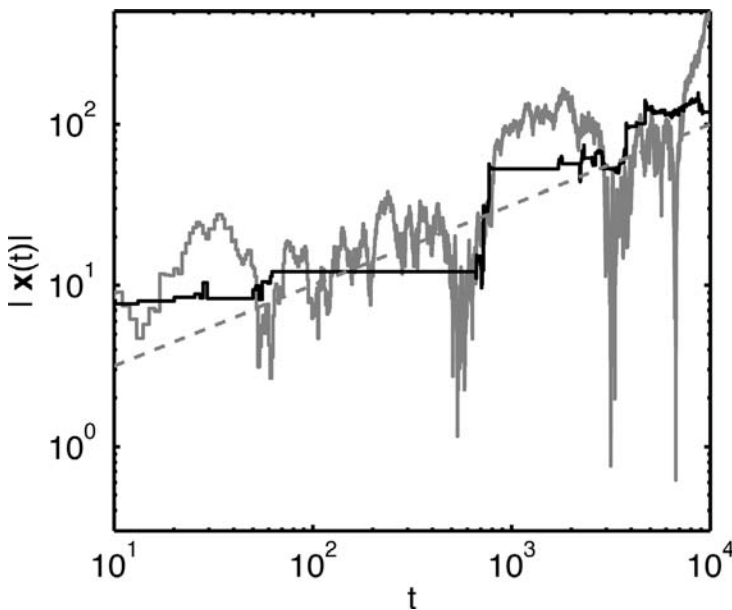


Figure 16.11 Two processes that exhibit diffusive scaling, i.e., $|X(t)| \sim t^{1/2}$ (dashed line). The gray process is ordinary diffusion, and the black one is ambivalent anomalous diffusion process with exponents $\alpha = 3/4$ and $\beta = 3/2$ which implies diffusive scaling. Note that the geometry of both the processes are remarkably different.

by

$$\tilde{W}(\mathbf{k}, u) = \frac{1 - \tilde{\psi}(u)}{u (1 - \tilde{\psi}(u) \tilde{p}(\mathbf{k}))}, \quad (16.25)$$

which can be computed within the CTRW framework, for details see [14, 35]. In Eq. (16.25) $\tilde{\psi}(u)$ and $\tilde{p}(\mathbf{k})$ denote the Laplace–Fourier transform of $\psi(\Delta t)$ and $p(\Delta \mathbf{x})$, respectively. The probability density $W(\mathbf{x}, t)$ is then obtained by inverse Laplace–Fourier transform

$$W(\mathbf{x}, t) = \frac{1}{(2\pi)^3 i} \int_{c-i\infty}^{c+i\infty} du \int d\mathbf{k} e^{ut - ikx} \tilde{W}(\mathbf{k}, u). \quad (16.26)$$

When both the variance of the spatial steps $\langle (\Delta \mathbf{x})^2 \rangle = \sigma^2$ and the expectation value $\langle \Delta t \rangle = \tau$ of the temporal increments exist the Fourier–Laplace transform of $p(\Delta \mathbf{x})$ and $\psi(\Delta t)$ are given by

$$\tilde{p}(\mathbf{k}) = 1 - \sigma^2 \mathbf{k}^2 + \mathcal{O}(\mathbf{k}^4) \quad (16.27)$$

$$\tilde{\psi}(u) = 1 - \tau u + \mathcal{O}(u^2), \quad (16.28)$$

for small arguments, which yield the asymptotics of the process. Inserted into Eq. (16.25) and employing inversion (16.26) one obtains

$$W(\mathbf{x}, t) = (2\pi D t)^{-1} e^{-\mathbf{x}^2/2Dt} \quad (16.29)$$

in this limit with $D = \sigma^2/\tau$. Thus, whenever $\langle (\Delta\mathbf{x})^2 \rangle$ and $\langle \Delta t \rangle$ are finite a CTRW is asymptotically equivalent to ordinary Brownian motion as expected.

The situation is drastically different, when both, $p(\Delta\mathbf{x})$ and $\psi(\Delta t)$ exhibit algebraic tails of the form

$$p(\Delta\mathbf{x}) \sim \frac{1}{|\Delta\mathbf{x}|^{2+\beta}} \quad 0 < \beta < 2 \quad \text{and} \quad \psi(\Delta t) \sim \frac{1}{\Delta t^{1+\alpha}} \quad 0 < \alpha < 1. \quad (16.30)$$

In this case one obtains for the asymptotics of $\tilde{p}(\mathbf{k})$ and $\tilde{\psi}(u)$:

$$\tilde{p}(\mathbf{k}) = 1 - D_\beta |\mathbf{k}|^\beta + \mathcal{O}(k^2) \quad (16.31)$$

$$\tilde{\psi}(u) = 1 - D_\alpha u^\alpha + \mathcal{O}(u). \quad (16.32)$$

Inserted into (16.25) yields the solution for the process in Fourier–Laplace space:

$$\tilde{W}_{\alpha,\beta}(\mathbf{k}, u) = \frac{u^{-1}}{1 + D_{\alpha,\beta} |\mathbf{k}|^\beta / u^\alpha}, \quad (16.33)$$

where the constant $D_{\alpha,\beta} = D_\beta / D_\alpha$ is a generalized diffusion coefficient. After inverse Laplace transform the solution in (\mathbf{x}, t) coordinates reads

$$W(\mathbf{x}, t) = \frac{1}{2\pi} \int d\mathbf{k} e^{-i\mathbf{k}\mathbf{x}} E_\alpha(-D_{\alpha,\beta} |\mathbf{k}|^\beta t^\alpha). \quad (16.34)$$

Here, E_α is the Mittag-Leffler function defined by

$$E_\alpha(z) = \sum_{n=0}^{\infty} \frac{z^n}{\Gamma(1+\alpha n)}, \quad (16.35)$$

which is a generalization of the exponential function to which it is identical for $\alpha = 1$. The integrand $E_\alpha(-D_{\alpha,\beta} |\mathbf{k}|^\beta t^\alpha)$ is the characteristic function of the process. As it is a function of $\mathbf{k}t^{\alpha/\beta}$, the probability density $W(\mathbf{x}, t)$ can be expressed as

$$W(\mathbf{x}, t) = t^{-2\alpha/\beta} L_{\alpha,\beta} \left(\mathbf{x}/t^{\alpha/\beta} \right) \quad (16.36)$$

in which the function $L_{\alpha,\beta}(\mathbf{z}) = (2\pi)^{-1} \int d\mathbf{k} E_\alpha(-|\mathbf{k}|^\beta - i\mathbf{k}\mathbf{z})$ is a universal scaling function which is characteristic for the process and depends on the two

exponents α and β only. Most importantly, one can extract the spatiotemporal scaling of the ambivalent process from (16.34)

$$X(t) \sim t^{\alpha/\beta}, \quad (16.37)$$

identical to the relation derived heuristically above. The ratio of the exponents α/β resembles the interplay between sub- and superdiffusion. For $\beta = 2\alpha$ the process exhibits the same scaling as ordinary Brownian motion, despite the crucial difference of infinite moments and a non-Gaussian shape of the probability density $W(x, t)$. The function $W(x, t)$ is a probability density for the vectorial displacements x . From Eqs. (16.34) and (16.36) we can compute the probability density $W_r(r, t)$ for having traveled the scalar distance $r = |x|$ by integration over all angles:

$$W_r(r, t) = t^{-\alpha/\beta} \tilde{L}_{\alpha, \beta} \left(r/t^{\alpha/\beta} \right), \quad (16.38)$$

with a universal scaling function $\tilde{L}_{\alpha, \beta}$ which can be expressed in terms of $L_{\alpha, \beta}$.

Finally, the validity of the ambivalent CTRW model can be tested against the dollar bill dispersal data by estimating the empirical $W_r(r, t)$ from the entire dataset of a little over half a million displacements and elapse times and compared to Eq. (16.38). The results of this analysis are compiled in Figure 16.12. Comparing with the spatiotemporal scaling promoted by the CTRW model $r(t) \sim t^{\alpha/\beta}$ a value of $\mu = 1$ would imply that temporal and spatial exponents are the same

$$\alpha = \beta. \quad (16.39)$$

Combining with the results obtained from the short-time analysis yields

$$\alpha = \beta = 0.6. \quad (16.40)$$

A final test of the CTRW model is the comparison of the empirically observed scaling function F with the predicted scaling function $\tilde{L}_{\alpha, \beta}$ for the values of the exponents in Eq. (16.40). As depicted in Figure 16.12 the asymptotics of the empirical curve is given by $y^{-(1-\xi_1)}$ and $y^{-(1+\xi_2)}$ for small and large arguments $y = r/t^{1/\mu}$, respectively. Both the exponents fulfill $\xi_1 \approx \xi_2 \approx 0.6$. By series expansions one can compute the asymptotics of the CTRW scaling function $\tilde{L}_{\alpha, \beta}(y)$ which gives $y^{-(1-\beta)}$ and $y^{-(1+\beta)}$ for small and large arguments, respectively. Consequently, as $\beta \approx 0.6$ the theory agrees well with the observed exponents. For the entire range of y one can compute $L_{\alpha, \beta}(y)$ by numeric integration for $\beta = \alpha = 0.6$ and superimpose the theoretical curve on the empirical one. The agreement is very good and supports the CTRW model. In summary, this is a solid evidence that the dispersal of bank notes can be accounted for by a simple random walk process with scale-free jumps and scale-free waiting times.

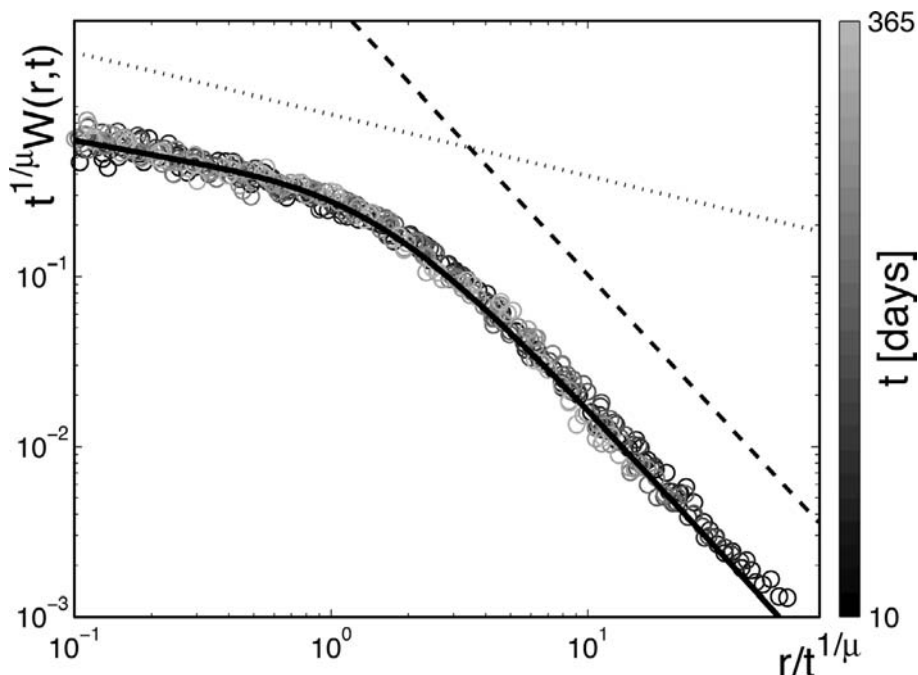


Figure 16.12 The empirical radial probability density function $W_r(r, t)$ and theoretical scaling function $\tilde{L}_{\alpha, \beta}$. In order to extract scaling the function $W(r, t)$ is shown for various but fixed values of time t between 10 and 365 days as a function of $r/t^{1/\mu}$. For $\mu \approx 1.0$ the measured (circles) curves collapse on a single curve and the process exhibits universal scaling. The scaling curve represents the empirical limiting density F of the process. The asymptotic behavior for small

(dotted line) and large (dashed line) arguments $y = r/t^{1/\mu}$ is given by $y^{-(1-\xi_1)}$ and $y^{-(1+\xi_2)}$, respectively, with estimated exponents $\xi_1 = 0.63 \pm 0.04$ and $\xi_2 = 0.62 \pm 0.02$. According to our model these exponents must fulfill $\xi_1 = \xi_2 = \beta$ where β is the exponent of the asymptotic short-time dispersal kernel (Figure 16.5), i.e., $\beta \approx 0.6$. The superimposed solid line represents the scaling function predicted by our theory with spatial and temporal exponents $\beta = 0.6$ and $\alpha = 0.6$.

The question remains how the dispersal characteristics of bank notes carry over to the dispersal of humans and more importantly to the spread of human-transmitted diseases. In this context one can safely assume that the power law with exponent $\beta = 0.6$ of the short-time dispersal kernel for bank notes reflects the human dispersal kernel as only short times are considered. However, as opposed to bank notes humans tend to return from distant places they traveled to. This however, has no impact on the dispersal of pathogens which, much like bank notes, are passed from person to person and have no tendency to return.

The issue of long waiting times is more subtle. One might speculate that the observed algebraic tail in waiting times of bank notes is a property of bank note dispersal alone. Long waiting times may be caused by bank notes

which exit the money-tracking system for a long time, for instance in banks. However, if this were the case the inter-report time statistics would exhibit a fat tail. Analyzing the interreport time distribution one finds an exponential decay which suggests that bank notes are passed from person to person at a constant rate. Furthermore, if one assumes that humans exit small areas at a constant rate which is equivalent to exponentially distributed waiting times and that bank notes pass from person to person at a constant rate, the distribution of bank note waiting times would also be exponential in contrast to the observed power law.

Based on this analysis one can conclude that the dispersal of bank notes and human-transmitted diseases can be accounted for by a CTRW process incorporating scale-free jumps as well as long waiting time in between displacements.

However, a word of caution is necessary at this point. The above model for the dispersal of bank notes is only an initial step toward a better understanding of human mobility and universal features of human transportation networks on global scales. One obvious reason is that the CTRW model, despite its wonderful agreement with the data, is a heuristic model and represents a population-averaged model. As alluded to above, spatial heterogeneities do impact on the dispersal characteristics quantitatively although they do not change the qualitative features of the dispersal process. This is analogous to a situation in which a Brownian particle diffuses on a two-dimensional liquid layer which in turn is heterogeneously heated from below. A position-dependent temperature profile would introduce a position-dependent diffusion coefficient for the particle which changes the local diffusion properties. Despite the fact that such a particle performs ordinary diffusion at every location one would have to incorporate a position-dependent diffusion coefficient in a quantitative description of the particle's motion in the corresponding Fokker–Planck equation. Replacing the position-dependent diffusion coefficient by a spatially averaged quantity only gives an incomplete description of the system. A promising line of investigation could then be provided by the concept of superstatistics introduced by Beck and Cohen [36] that is introduced and explained in detail in Chapter 15 in this book.

In the context of human travel behavior, one would have to determine position dependences in the generalized diffusion coefficient for which the originally explored wheresgeorge dataset is insufficient. Alternatively, one could investigate these processes within the framework of complex embedded networks in which places in the United States are nodes of the network and the flux of bills weighted, nonnegative links between them. This approach introduces a number of powerful analytic and numeric technique which in my view could complete our understanding of human travel in our globalized world.

References

- 1 J.M. Bullock, R.E. Kenward, and R.S. Hails, editors. *Dispersal Ecology*. Blackwell, Malden, Massachusetts, 2002.
- 2 J. D. Murray. *Mathematical Biology*. Springer), Address =Berlin, Heidelberg, New York, Year = 1993.
- 3 J. Clobert. *Dispersal*. Oxford University Press, Oxford, 2001.
- 4 K. Nicholson and R. G. Webster. *Textbook of Influenza*. Blackwell Publishing, Malden, MA, USA, 1998.
- 5 B. T. Grenfell, O. N. Bjornstadt, and J. Kappey. Travelling waves and spatial hierarchies in measles epidemics. *Nature*, 414:716, 2001.
- 6 M. J. Keeling, M. E. J. Woolhouse, D. J. Shaw, L. Matthews, M. Chase-Topping, D. T. Haydon, S. J. Cornell, J. Kappey, J. Wilesmith, and B. T. Grenfell. Dynamics of the 2001 uk foot and mouth epidemic: Stochastic dispersal in a heterogeneous landscape. *Science*, 294:813–817, 2001.
- 7 L. Hufnagel, D. Brockmann, and T. Geisel. Forecast and control of epidemics in a globalized world. *Proceedings of the National Academy of Sciences of the United States of America*, 101(42):15124–15129, 2004.
- 8 Nicholas C. Grassly, Christophe Fraser, and Geoffrey P. Garnett. Host immunity and synchronized epidemics of syphilis across the united states. *Nature*, 433(27):417–421, 2005.
- 9 R. J. Webby and R. G. Webster. Are we ready for pandemic influenza? *Science*, 302:1519–1522, 2003.
- 10 D. Brockmann, L. Hufnagel, and T. Geisel. Dynamics of modern epidemics. In A. McLean, R. May, J. Pattison, and R. Weiss, editors, *SARS: A Case Study in Emerging Infections*, pages 81–92. Oxford University Press, Oxford, 2005.
- 11 Roy M. Anderson, Robert M. May, and B. Anderson. *Infectious Diseases of Humans : Dynamics and Control*. Oxford University Press, USA, 1992.
- 12 D. Brockmann, L. Hufnagel, and T. Geisel. The scaling laws of human travel. *Nature*, 439(7075):462–465, 2006.
- 13 M.F. Shlesinger. *Lévy Flights and Related Topics in Physics*. Springer, Berlin, 1995.
- 14 R. Metzler and J. Klafter. The random walk's guide to anomalous diffusion: a fractional dynamics approach. *Physics Reports – Review Section of Physics Letters*, 339(1):1–77, 2000.
- 15 M. Kot, M. A. Lewis, and P. vandenDriessche. Dispersal data and the spread of invading organisms. *Ecology*, 77(7):2027–2042, 1996.
- 16 C. W. Gardiner. *Handbook of Stochastic Methods*. Springer, Berlin, 1985.
- 17 W. Feller. *An Introduction to Probability Theory and Its Application*, volume I. Wiley, New York, 1968.
- 18 R. A. Fisher. The wave of advance of advantageous genes. *Ann. Eugen.*, vol. 7, 355–369, 1937.
- 19 W. Feller. *An Introduction to Probability Theory and Its Application*, volume II. Wiley, New York, 1971.
- 20 R. Nathan, G. G. Katul, H. S. Horn, S. M. Thomas, R. Oren, R. Avissar, S. W. Pacala, and S. A. Levin. Mechanisms of long-distance dispersal of seeds by wind. *Nature*, 418(6896):409–413, 2002.
- 21 M. Schoeder. *Fractals, Chaos, Power Laws. Minutes from an Infinite Paradise*. W. H. Freeman and Company, New York, 1991.
- 22 G. M. Viswanathan, S. V. Buldyrev, S. Havlin, M. G. E. da Luz, E. P. Raposo, and H. E. Stanley. Optimizing the success of random searches. *Nature*, 401(6756):911–914, 1999.
- 23 F. Bartumeus, F. Peters, S. Pueyo, C. Marzá, and J. Catalan. Helical Lévy walks: Adjusting searching statistics to resource availability in microzooplankton. *Proceedings of the National Academy of Sciences of the United States of America*, 100(22):12771–12775, 2003.
- 24 A. Marell, J. P. Ball, and A. Hofgaard. Foraging and movement paths of female reindeer: insights from fractal analysis, correlated random walks, and levy flights. *Canadian Journal of Zoology-Revue Canadienne De Zoologie*, 80(5):854–865, 2002.

- 25** G. M. Viswanathan, V. Afanasyev, S. V. Buldyrev, E. J. Murphy, P. A. Prince, and H. E. Stanley. Lévy flight search patterns of wandering albatrosses. *Nature*, 381(6581):413–415, 1996.
- 26** G. Ramos-Fernandez, J. L. Mateos, O. Miramontes, G. Cocho, H. Larralde, and B. Ayala-Orozco. Lévy walk patterns in the foraging movements of spider monkeys (*ateles geoffroyi*). *Behavioral Ecology and Sociobiology*, 55(3):223–230, 2004.
- 27** R. P. D. Atkinson, C. J. Rhodes, D. W. Macdonald, and R. M. Anderson. Scale-free dynamics in the movement patterns of jackals. *Oikos*, 98(1):134–140, 2002.
- 28** M. F. Shlesinger, G. M. Zaslavsky, and U. Frisch, editors. *Lévy flights and related topics in physics*. Springer, Berlin, 1995.
- 29** D. Brockmann and T. Geisel. Lévy flights in inhomogeneous media. *Physical Review Letters*, 90(17):170601, 2003.
- 30** D. Brockmann and I. M. Sokolov. Lévy flights in external force fields: from models to equations. *Chemical Physics*, 284(1–2):409–421, 2002.
- 31** T. Geisel, J. Nierwetberg, and A. Zacherl. Accelerated diffusion in Josephson junctions and related chaotic systems. *Physical Review Letters*, 54(7):616–619, 1985.
- 32** M. F. Shlesinger. Follow the money. *Nature Physics*, 2(2):69–70, 2006.
- 33** M. F. Shlesinger, J. Klafter, and Y. M. Wong. Random-walks with infinite spatial and temporal moments. *Journal of Statistical Physics*, 27(3):499–512, 1982.
- 34** E. W. Montroll and G. H. Weiss. Random walks on lattices 2. *Journal of Mathematical Physics*, 6(2):167, 1965.
- 35** A. I. Saichev and G. M. Zaslavsky. Fractional kinetic equations: solutions and applications. *Chaos*, 7(4):753–764, 1997.
- 36** C. Beck and E. G. D. Cohen. Superstatistics. *Physica A – Statistical Mechanics and Its Applications*, 322(1–4):267–275, 2003.

17

Anomalous Molecular Displacement Laws in Porous Media and Polymers Probed by Nuclear Magnetic Resonance Techniques

Rainer Kimmich, Nail Fatkullin, Markus Kehr, and Yujie Li

17.1

General Introduction

Molecular transport by flow and Brownian motions in fluidic systems of sufficient complexity and randomness can often be described by power laws for the mean-squared displacement as a function of time given by [1]

$$\langle r^2 \rangle \sim t^\kappa. \quad (17.1)$$

One distinguishes the cases $\kappa = 0$, “localized”; $0 < \kappa < 1$, “subdiffusive”; $\kappa = 1$, “normal”; $\kappa > 1$, “superdiffusive”; $\kappa = 2$, “ballistic”; $\kappa = 3$, “turbulent”. Quite a few situations are known where this sort of power-law anomaly is expected to apply. In the context of the present chapter, we focus on two typical examples where sub- and superdiffusive displacement laws have been observed. This is segment diffusion in polymer liquids [2] and diffusion and hydrodynamic dispersion of fluids in random porous systems [3], respectively.

Apart from the above, power-law-exponent-based classification, two principally different categories of anomalous particle transport must be distinguished according to the origin of the anomalies: “trapping” and “obstruction” [4]. Anomalies of the first category, “trapping,” originate from “traps” holding the diffusing particle temporarily back. An example is diffusion of particles on fractals [5] (for an introduction see Chapter 14 by Hoffmann and Prehl [6]). Another situation where trapping matters is reptation of polymers along a randomly coiled tube [2, 7]. Dead ends of fractal percolation clusters as well as loops of the randomly coiled tube confining a polymer chain act as structural “traps” in a sense leading to some waiting-time delays in the displacement process of the diffusing particle. The result is a non-Gaussian propagator. Another example, Lévy walks [8] as they occur in the frame of “bulk mediated surface diffusion” [9–11] for instance, can also be attributed to this class of diffusion phenomena.

On the other hand, a Gaussian shape of the propagator resulting as a solution of Fick’s diffusion equation for a homogeneous medium is not necessarily

indicative for ordinary transport characterized by a linear time dependence of the mean-squared displacement. There are situations where the propagator is Gaussian while the mean-squared behavior nevertheless is subdiffusive. This occurs if the second category, “obstruction,” applies. The anomaly is then due to a time-dependent diffusion coefficient defined by $D(t) \equiv \langle r^2(t) \rangle / (6t)$, while the propagator may still be Gaussian. Examples for such a scenario are the so-called single-file diffusion in straight tight cylindrical pores [12–14] and diffusion of Rouse polymer chains [2, 15–17]. On a certain length scale, these are systems homogeneous with respect to diffusion. The sole source of anomalies is the mutual obstruction of molecules or segments which leads to a subdiffusive behavior.

Tests of the power-law behavior given in Eq. (17.1) should be based on a time scale of several orders of magnitude to allow for reliable statements and conclusions. This is not much of a problem in theoretical treatments and computer simulations where merely the analytical tractability and the available computer power may limit the time range probed. In experiments, however, one faces severe technical restrictions that often do not permit measurements over more than a single decade of time. This is often not enough to permit the identification of the “scaling window” intrinsic to the system under investigation where the anomalous mean squared displacement behavior according to Eq. (17.1) occurs.

The purpose of the following treatise is to demonstrate that certain nuclear magnetic resonance (NMR) techniques or the combined application of several such methods offer an extremely wide time range on which diffusive molecular displacements can be studied. NMR techniques are particularly suited for probing anomalous displacement behavior in a noninvasive manner. Emphasis will be laid on the description of the methodological background of a choice of NMR techniques appropriate in this context. It should be mentioned that a part of these methods may be considered to be standard in NMR diffusometry. Others are novel and have not yet been exploited very often.

As application examples permitting the demonstration of the techniques and their experimental time ranges, on the one hand we focus on molecular diffusion in polymer melts and on diffusive displacements in liquids confined in percolation clusters on the other. In both cases subdiffusive displacement behavior has been detected. Hydrodynamic dispersion of fluids in porous materials moreover leads to superdiffusive mean-squared displacement laws. Diffusion in porous materials is also considered in Chapter 18 by Valliulin and Kärger [18].

The standard NMR technique for measuring molecular displacements is pulsed or steady field-gradient NMR diffusometry [19–21]. The diffusion time scale probed by this class of methods is $10^{-4} \text{ s} < t < 10^0 \text{ s}$ [22]. In suitable cases, much shorter times can be probed by examining spin-lattice

relaxation due to fluctuations of intermolecular dipolar coupling as recently demonstrated for polymer melts [23]. The relevant diffusion time scale is $10^{-9} \text{ s} < t < 10^{-4} \text{ s}$. The longest, in principle unlimited diffusion time scale, $t > 10^0 \text{ s}$, can be covered using an isotope interdiffusion NMR technique [24] in analogy to radiotracer methods.

Taking all these methods together, the total time scale covers the enormous range from nanoseconds to periods as long as tolerable in the frame of a laboratory study, that is 15 decades of time and more. The total diffusion time range that can be practically covered by NMR experiments delineated in the following is $10^{-9} \text{ s} < t < 1.44 \times 10^6 \text{ s} = 400 \text{ h}$.

17.2

From Nano- to Milliseconds: Segment Diffusion in Polymer Melts

Most polymer dynamics models predict power laws for the time dependence of the mean-squared displacement of chain segments on a time scale shorter than the so-called terminal relaxation time [2, 25]. The analytical form may generally be represented by the subdiffusive power law

$$\langle r^2 \rangle = b^2 \left(\frac{t}{\tau_s} \right)^\kappa \quad (0 < \kappa < 1), \quad (17.2)$$

where b is the Kuhn segment length, and τ_s is the local segment fluctuation time.

Anticipating that such a power law applies, a NMR relaxometry measuring protocol for mean-squared displacements can be established for a time scale from nanoseconds to hundreds of microseconds. This time scale is conjugated to the frequency range probed by field-cycling NMR relaxometry which ranges from kHz up to several 100 MHz of conventional NMR spectrometers [26].

The principle of the technique is to evaluate the mean-squared displacement from the spin-lattice relaxation rate caused by intermolecular dipolar interactions, which fluctuate due to *translational displacements* of the molecules relative to each other. The intermolecular spin-lattice relaxation rate can be determined with the aid of a series of isotopic dilution experiments where one assumes that there is no other isotopic effect than the modification of dipolar couplings among spins. With proton resonance, this refers to undeuterated molecules dispersed in a matrix of deuterated molecules of the same chemical species.

The spin-lattice relaxation rate of protons in diamagnetic liquids is usually governed by fluctuating dipole–dipole interactions. It is consequently composed of inter- and intramolecular contributions. The Hamiltonian of dipolar interaction between protons (“H”) and deuterons (“D”) is lowered by the

quotient of the gyromagnetic ratios, $\gamma_D/\gamma_H \approx 0.15$, relative to proton–proton couplings. The intermolecular dipolar spin-lattice relaxation rate of proton–deuteron pairs is diminished by the square of this factor, i.e., by a factor of about 0.023.

17.2.1

Evaluation Theory for the Field-Cycling NMR Relaxometry Technique

In the following, we consider mixtures of undeuterated and deuterated molecules. Let φ_H be the fraction of undeuterated hydrogen atoms so that $\varphi_D = 1 - \varphi_H$ is the fraction of the deuterated counterparts. The total proton spin-lattice relaxation rate, $1/T_1^{\text{tot}}(\omega_H, \varphi_H)$, can be split into two terms [26]:

$$\frac{1}{T_1^{\text{tot}}(\omega_H, \varphi_H)} = \frac{1}{T_1^{\text{intra}}(\omega_H, \varphi_H)} + \frac{1}{T_1^{\text{inter}}(\omega_H, \varphi_H)}, \quad (17.3)$$

where ω_H is the proton resonance angular frequency, and $1/T_1^{\text{intra}}(\omega_H, \varphi_H)$ and $1/T_1^{\text{inter}}(\omega_H, \varphi_H)$ are the spin-lattice relaxation rates caused by intra- and intermolecular dipolar interactions, respectively (see Figure 17.1(a)). Isotopic dilution is expected to have no perceptible effect on molecular dynamics. The intramolecular proton spin-lattice relaxation rate therefore is independent of the value of φ_H ,

$$\frac{1}{T_1^{\text{intra}}(\omega_H)} = \frac{1}{T_1^{\text{intra}}(\omega_H, \varphi_H)}. \quad (17.4)$$

More precisely, in the case of polymers, this refers to a time scale longer than the segmental relaxation time τ_s , that is $t > \tau_s \approx 10^{-11} \text{ s}$ – 10^{-9} s .

The intermolecular proton spin-lattice relaxation rate is composed of contributions from proton–proton (HH) and proton–deuteron (HD) dipolar couplings. The latter are much weaker but anyway finite. The intermolecular contribution is then

$$\frac{1}{T_1^{\text{inter}}(\omega_H, \varphi_H)} = \frac{1}{T_1^{\text{inter}}(\omega_H, \varphi_H)} + \frac{1}{T_1^{\text{inter}}(\omega_H, \varphi_H)}, \quad (17.5)$$

where $1/T_1^{\text{inter}}(\omega_H, \varphi_H = 1) = 0$ and $1/T_1^{\text{inter}}(\omega_H, \varphi_H \rightarrow 0) \rightarrow 0$.

Inserting Eqs. (17.4) and (17.5) in Eq. (17.3) gives

$$\frac{1}{T_1^{\text{tot}}(\omega_H, \varphi_H)} = \frac{1}{T_1^{\text{intra}}(\omega_H)} + \frac{1}{T_1^{\text{inter}}(\omega_H, \varphi_H)} + \frac{1}{T_1^{\text{inter}}(\omega_H, \varphi_H)}. \quad (17.6)$$

The total relaxation rate for $\varphi_H = 1$ (undeuterated system) minus the total

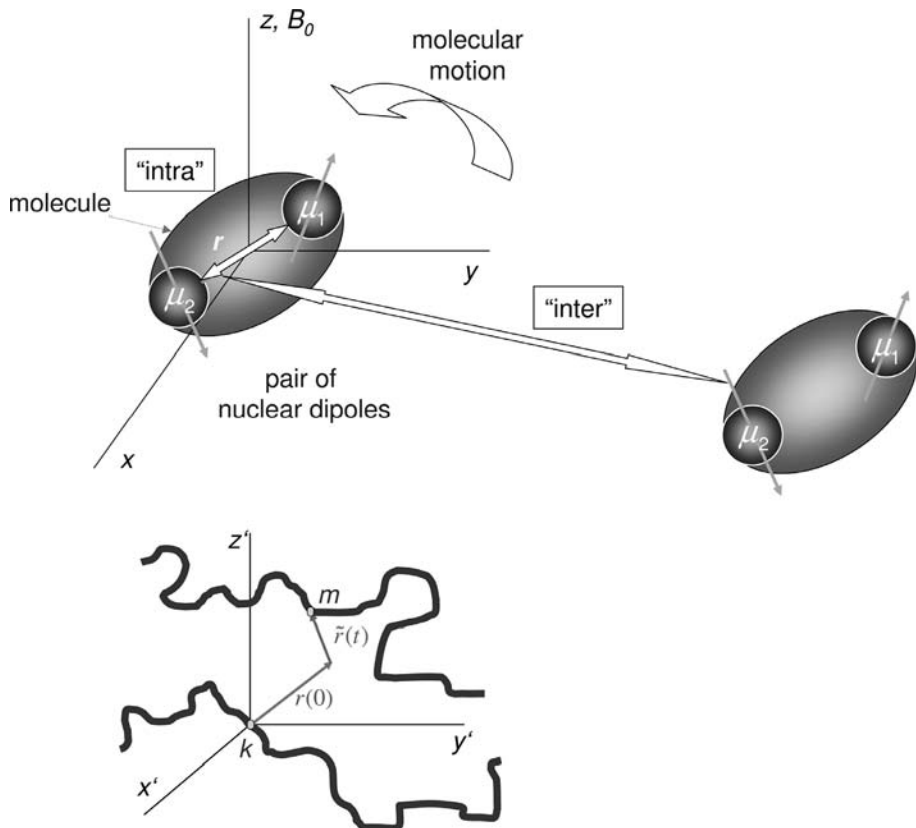


Figure 17.1 Schematic representation of intra- and intermolecular dipolar couplings of spin pairs. Top: Intramolecular interactions are modulated by rotational diffusion. Intermolecular couplings fluctuate due to translational displacements of molecules relative to each other. Bottom: In polymer liquids, intermolecular interactions refer to spins on

different macromolecules. The interchain nuclear distance vector between spins with the numbers k and m , for instance, is changed from an initial value $\vec{r}(0)$ to $\vec{r}(0) + \Delta\vec{r}(t)$ in a time interval t by translational diffusion. The frame of reference is assumed to be fixed on segment k .

relaxation rate for $\varphi_H \ll 1$ (optimally diluted system) is

$$\frac{1}{T_1^{\text{tot}}(\omega_H, \varphi_H = 1)} - \frac{1}{T_1^{\text{tot}}(\omega_H; \varphi_H \ll 1)} = \frac{1}{T_{1\text{HH}}^{\text{inter}}(\omega_H, \varphi_H = 1)} - \frac{1}{T_{1\text{HH}}^{\text{inter}}(\omega_H; \varphi_H \ll 1)} - \frac{1}{T_{1\text{HD}}^{\text{inter}}(\omega_H; \varphi_H \ll 1)}. \quad (17.7)$$

That is, the intramolecular contribution has been eliminated, and the right-hand side of Eq. (17.7) is merely composed of intermolecular relaxation rates. Corresponding expressions have been published in Ref. [23]. For power laws

as given in Eq. (17.2), the result for undeuterated systems is for $\kappa < 2/3$

$$\frac{1}{T_{1\text{HH}}^{\text{inter}}(\omega_{\text{H}}, \varphi_{\text{H}} = 1)} = \left(\frac{\mu_0}{4\pi} \right)^2 \frac{16\sqrt{\pi}}{5\sqrt{6}} f_1(\kappa) \frac{\gamma_{\text{H}}^4 \hbar^2 I(I+1)\rho}{\omega_{\text{H}} \langle \tilde{r}^2(1/\omega_{\text{H}}) \rangle^{3/2}}, \quad (17.8)$$

where

$$f_1(\kappa) = \frac{\pi (1 + 2 \times 2^{3\kappa/2})}{2\cos(3\pi\kappa/4)\Gamma(3\kappa/2)}. \quad (17.9)$$

ρ is the number density of protons in the undiluted system, $\Gamma(x)$ is the gamma function, $I = 1/2$ is the proton spin quantum number, κ is the subdiffusive exponent of the mean-squared displacement law given in Eq. (17.2). $\langle \tilde{r}^2(1/\omega_{\text{H}}) \rangle$ is the mean-squared displacement of molecules relative to each other in a time interval $t = 1/\omega_{\text{H}}$ determined by the angular frequency of proton resonance.

In isotopically diluted systems, $\varphi_{\text{H}} \ll 1$, the contribution to the proton relaxation rate by proton–proton interactions differs from the expression in Eq. (17.8) only by a factor φ_{H} :

$$\frac{1}{T_{1\text{HH}}^{\text{inter}}(\omega_{\text{H}}; \varphi_{\text{H}} \ll 1)} = \underbrace{\left(\frac{\mu_0}{4\pi} \right)^2 \frac{16\sqrt{\pi}}{5\sqrt{6}} f_1(\kappa) \frac{\gamma_{\text{H}}^4 \hbar^2 I(I+1)\rho}{\omega_{\text{H}} \langle \tilde{r}^2(1/\omega_{\text{H}}) \rangle^{3/2}}}_{1/T_{1\text{HH}}^{\text{inter}}(\omega_{\text{H}}; \varphi_{\text{H}}=1)} \varphi_{\text{H}}. \quad (17.10)$$

Analogously we find for the contribution by deuteron–proton dipolar interactions

$$\begin{aligned} \frac{1}{T_{1\text{HD}}^{\text{inter}}(\omega_{\text{H}}; \varphi_{\text{H}} \ll 1)} \\ = (1 - \varphi_{\text{H}}) \left(\frac{\gamma_{\text{D}}}{\gamma_{\text{H}}} \right)^2 \frac{S(S+1)}{I(I+1)} f_2(\kappa) \frac{1}{T_{1\text{HH}}^{\text{inter}}(\omega_{\text{H}}, \varphi_{\text{H}} = 1)}, \end{aligned} \quad (17.11)$$

where

$$f_2(\kappa) = \frac{1 + 2 (1 + \gamma_{\text{D}}/\gamma_{\text{H}})^{(3\kappa-2)/2} + (1 - \gamma_{\text{D}}/\gamma_{\text{H}})^{(3\kappa-2)/2}}{1 + 2 \times 2^{3\kappa/2}/3}. \quad (17.12)$$

$S = 1$ is the deuteron spin quantum number. The factor $1 - \varphi_{\text{H}} = \varphi_{\text{D}}$ corresponds to the factor φ_{H} in Eq. (17.10). The ratio $\frac{\gamma_{\text{D}}}{\gamma_{\text{H}}}$ reflects the reduced dipolar magnetic field of deuterons relative to protons.

Using Eqs. (17.8), (17.10), and (17.11), relation (17.7) can be rewritten as

$$\begin{aligned} \frac{1}{T_1^{\text{tot}}(\omega_{\text{H}}, \varphi_{\text{H}} = 1)} - \frac{1}{T_1^{\text{tot}}(\omega_{\text{H}}; \varphi_{\text{H}} \ll 1)} \\ = \frac{1}{T_{1\text{HH}}^{\text{inter}}(\omega_{\text{H}}, \varphi_{\text{H}} = 1)} (1 - \varphi_{\text{H}}) \left\{ 1 - \left(\frac{\gamma_{\text{D}}}{\gamma_{\text{H}}} \right)^2 \frac{S(S+1)}{I(I+1)} f_2(\kappa) \right\}. \end{aligned} \quad (17.13)$$

Rearranging Eq. (17.13) leads to the final expression of the intermolecular spin-lattice relaxation rate of an undeuterated system,

$$\frac{1}{T_{1\text{HH}}^{\text{inter}}(\omega_{\text{H}}, \varphi_{\text{H}} = 1)} = \frac{\frac{1}{T_1^{\text{tot}}(\omega_{\text{H}}, \varphi_{\text{H}} = 1)} - \frac{1}{T_1^{\text{tot}}(\omega_{\text{H}}, \varphi_{\text{H}} \ll 1)}}{(1 - \varphi_{\text{H}}) \left\{ 1 - \left(\frac{\gamma_{\text{D}}}{\gamma_{\text{H}}} \right)^2 \frac{S(S+1)}{I(I+1)} f_2(\kappa) \right\}}. \quad (17.14)$$

The only parameter in Eq. (17.14), which is not directly determined by experimental data, is the exponent κ in the anticipated range (for a discussion see Ref. [23]).

Determining $1/T_{1\text{HH}}^{\text{inter}}(\omega_{\text{H}}, \varphi_{\text{H}} = 1)$ from experimental data according to Eq. (17.14) permits one to evaluate the mean-squared displacement of molecules relative to each other in a time interval $t = 1/\omega_{\text{H}}$ from Eq. (17.8) as

$$\begin{aligned} & \langle \tilde{r}^2(t = 1/\omega_{\text{H}}) \rangle \\ &= \left(\left(\frac{\mu_0}{4\pi} \right)^2 \frac{16\sqrt{\pi}}{5\sqrt{6}} f_1(\kappa) \frac{\gamma_{\text{H}}^4 \hbar^2 I(I+1) \rho}{\omega_{\text{H}}} T_{1\text{HH}}^{\text{inter}}(\omega_{\text{H}}, \varphi_{\text{H}} = 1) \right)^{2/3}. \end{aligned} \quad (17.15)$$

If the molecules move independently of each other, the mean-squared displacement relative to the laboratory frame is just half the relative mean-squared displacement,

$$\langle R^2(t) \rangle = \frac{1}{2} \langle \tilde{r}^2(t) \rangle. \quad (17.16)$$

Note that the only condition which Eq. (17.15) anticipates is a subdiffusive mean-squared displacement law according to Eq. (17.2) with $\kappa < 2/3$. This can be relevant for very different, but usually relatively complex systems. Typical examples where subdiffusive mean-squared displacement laws apply are polymer liquids. The situation is illustrated in Figure 17.1(b). In the following, we will focus on melts of so-called entangled polymers.

17.2.2

Results for Polymer Melts

Starting from a data set of proton spin-lattice relaxation times T_1^{tot} in polybutadiene melts at various mixture ratios φ_{H} with the perdeuterated species, data point by data point was extrapolated to “infinite” dilution, i.e., $\varphi_{\text{H}} \rightarrow 0$. This provides the proton spin-lattice relaxation time $T_1^{\text{tot}}(\omega_{\text{H}}; \varphi_{\text{H}} \rightarrow 0)$ for intramolecular dipolar proton–proton interactions plus intermolecular proton–deuteron dipolar interactions [23]. Note that this extrapolation is not really necessary but is recommendable if appropriate samples are available, since

it ensures that any imperfections by incomplete molecular mixing are eliminated. From these data one can determine the pure intermolecular contribution represented by the spin-lattice relaxation time $T_{1\text{HH}}^{\text{inter}}(\omega_H, \varphi_H = 1)$ according to Eq. (17.14), and from this the relative mean-squared segment displacement as defined by Eq. (17.15). Figure 17.2 shows a corresponding plot.

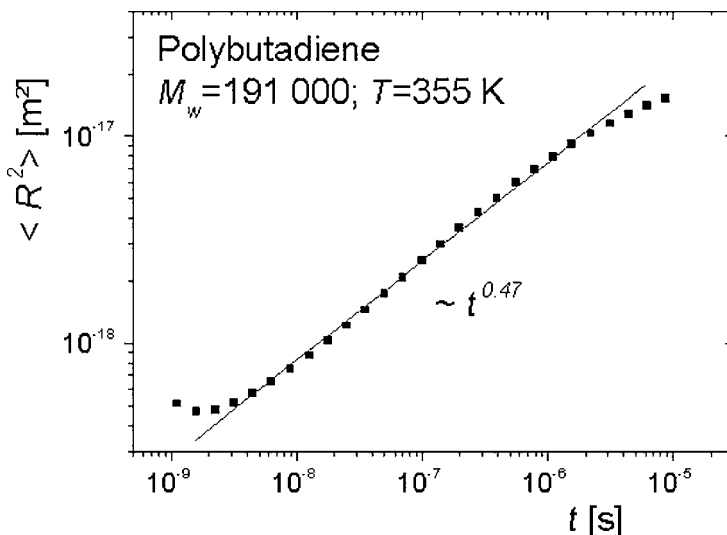


Figure 17.2 Mean-squared segment displacement versus diffusion time $t = 1/\omega_H$ in polybutadiene melts according to Eqs. (17.14)–(17.16). The crossover to a plateau at short times indicates the measuring limit of the technique. The power law given in the plot represents the dispersion in the middle of the experimental time range corresponding to the straight line. A flatter slope appears at times $t > 1\text{ }\mu\text{s}$. For a detailed discussion see Ref. [23].

Analogous experiments have been carried out with polyethyleneoxide melts [23]. The mean-squared segment displacement versus time is shown in Figure 17.3 in comparison to data measured with fringe field-gradient NMR diffusometry to be described below. The range of the root-mean-squared displacements probed by the technique ranges from roughly 0.5 nm to 50 nm, i.e., two orders of magnitude.

17.2.3

Discussion of the Results for Polymer Melts

The experiments described above were performed with polymer melts, although the method may be suitable for any other system with subdiffusive mean-squared displacement laws. Polymer liquids are particularly suited for this sort of investigation since there is a strong tendency for anomalous seg-

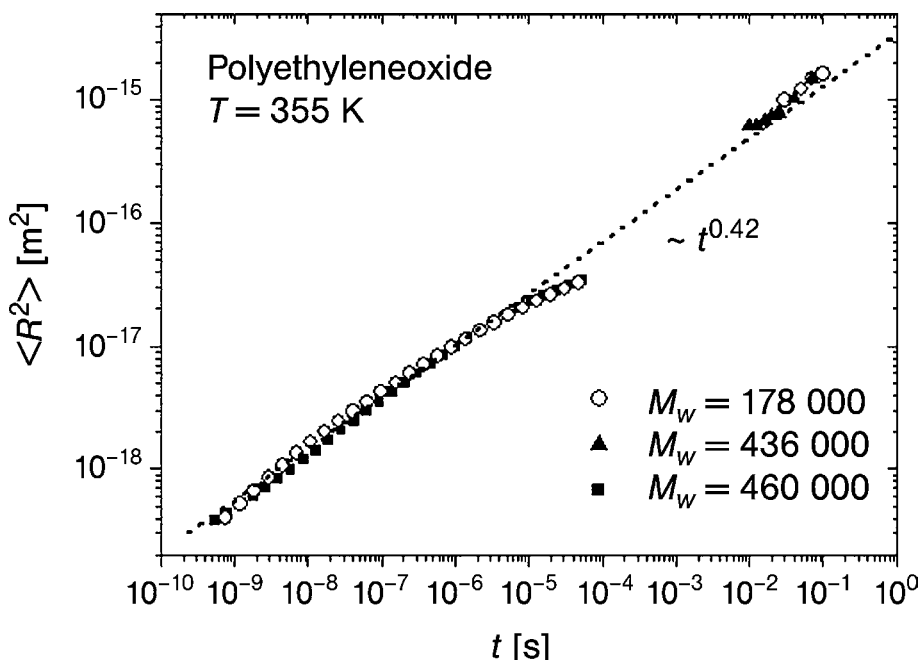


Figure 17.3 Mean-squared segment displacement versus diffusion time in polyethyleneoxide melts with different molecular weights [23]. The short-time data refer to the relaxometry technique, while those for $t > 10 \text{ ms}$ have been measured with fringe field gradient NMR diffusometry. The data in the nanosecond range and below indicate the

increasing influence of local segment fluctuations, which are not affected by intermolecular interactions. The dotted line and its slope tentatively anticipate the validity of a power law in the total range. Note, however, that a crossover to a flatter slope appears at about $10 \text{ }\mu\text{s}$ and above which is not described by the power law shown in the plot.

ment diffusion properties on a time scale where center-of-mass diffusion does not yet dominate. Under such conditions, a theory has been developed directly providing the mean-squared segment displacement as a function of time (Eq. (17.15)).

Qualitatively, this relation can also be obtained on the basis of scaling arguments. In our previous work [27], it was shown that the autocorrelation function of the Hamiltonian of intermolecular dipolar interaction in an undeuterated system varies as

$$G(t) \propto \frac{\rho}{\langle \vec{r}^2(t) \rangle^{3/2}}. \quad (17.17)$$

We now assume the subdiffusive mean-squared displacement law given in Eq. (17.2) in the time range $\tau_s < t < \tau_l$ relevant for segment diffusion in polymer liquids, where τ_s and τ_l are the shortest and longest chain-mode relaxation times. The frequency dependence of the intermolecular contribution

to the proton spin-lattice relaxation rate scales according to the Fourier transform of Eq. (17.17), i.e.,

$$\begin{aligned} \frac{1}{T_{1\text{HH}}^{\text{inter}}(\omega_{\text{H}}, \varphi_{\text{H}} = 1)} &\propto \int_0^{\infty} \frac{\rho}{\langle \tilde{r}^2(t) \rangle^{3/2}} \cos(\omega_{\text{H}} t) dt \\ &\propto \frac{\rho}{\omega \langle \tilde{r}^2(1/\omega_{\text{H}}) \rangle^{3/2}}, \end{aligned} \quad (17.18)$$

where we have anticipated $\kappa < 2/3$. The diffusion time can be set $t = 1/\omega_{\text{H}}$ since at angular frequencies $\omega_{\text{H}} \gg 1/\tau_t$, the main contribution to the right-hand side of Eq. (17.18) comes from times of the order $t \approx 1/\omega_{\text{H}}$ (and from spins with initial distances from each other in the order of $\langle \tilde{r}^2(t \sim 1/\omega_{\text{H}}) \rangle^{1/2}$). The simple scaling relation given in Eq. (17.18) thus permits one to extract the time dependence of the relative mean-squared segment displacement from the frequency dependence of the intermolecular contribution to spin-lattice relaxation rate according to

$$\langle \tilde{r}^2(t = 1/\omega_{\text{H}}) \rangle \propto \left(\frac{\rho T_{1\text{HH}}^{\text{inter}}(\omega_{\text{H}}, \varphi_{\text{H}} = 1)}{\omega_{\text{H}}} \right)^{2/3} \quad (17.19)$$

in accordance with Eq. (17.15).

In principle, the time limits of the isotopic dilution experiments under consideration are determined by the field-cycling NMR relaxometry technique [28]. The low-frequency limit, which is the extent of the application range at long times, is determined either by local fields or by the spin-lattice relaxation dispersion cutoff at $\omega_{\text{H}} \approx 1/\tau_t$. For polymers with large enough molecular weights as in the present case, this limitation can be ruled out. It can therefore be concluded that the low-field limitation is given by local fields starting to dominate the external magnetic field. This is a system-dependent effect that may be influenced by the choice of the sample material. With polymer melts, the limit $\omega_{\text{H}} \gg 1/\tau_t$ on the one hand, and the empirical inequality for the weight average molecular mass, $M_w > 60\,000$, on the other will provide the best compromise in the sense of the application range at long times. A time range up to milliseconds thus becomes realistic.

The short-time limit is again determined by two factors. The highest switchable magnetic field achievable with field-cycling magnets restrict the technique to about $v_{\text{H}} \equiv \omega_{\text{H}}/2\pi \leq 4 \times 10^7$ Hz [28]. The experimental accuracy becomes worse when approaching this limit, while conventional NMR spectrometers are often only available for much higher frequencies. Then another condition may be violated, namely the limit $\omega_{\text{H}} \ll 1/\tau_s$. That is, local intramolecular motions start to dominate spin-lattice relaxation, and intermolecular interactions become irrelevant. In the case of the polymer species

considered above, a short-time limit of nanoseconds appears to be typical. In this time range, the evaluated time dependence of the mean-squared displacement consequently begins to disappear (see Figure 17.2) as a manifestation of the experimental measuring limit.

The above analysis of spin-lattice relaxation in polymers in a wide frequency range directly reveals that the intermolecular contribution to dipolar interactions becomes dominant below several MHz for molecular masses of about 100 000. This finding is important since it is often intuitively anticipated for the interpretation of low-frequency NMR experiments such as free-induction decays or double-quantum NMR evaluations.

17.3

From 100 Microseconds to Seconds

17.3.1

The Measuring Principles of Field-Gradient NMR Diffusometry

The most popular principle of diffusion measurements by NMR is to dephase spin coherences with the aid of magnetic field gradients and to refocus them in the form of a spin echo after some diffusion time. The Larmor frequency is given by $\omega = \gamma B$, where γ is the gyromagnetic ratio of the spin-bearing nuclei and B is the local magnetic flux density. The Larmor precession of spins at different positions will be dephased by a gradient of B . Refocusing of the precession phases is possible with the aid of a variety of different sequences of radio frequency (RF) and field gradient pulses. The result of refocusing is the formation of spin-echo signals. Spin echoes can be of a very different nature. Well-known versions are the Hahn spin echo and the stimulated echo [26].

For diffusometry purposes, the RF pulse sequence is combined with field gradients in pulsed or steady form. Apart from relaxation effects, the spin-echo amplitude to be measured in this sort of experiment is attenuated by incomplete refocusing of the spin coherences as a consequence of incoherent molecular displacements in the diffusion interval of the pulse sequence. This phenomenon can be evaluated in terms of a diffusion coefficient or a mean-squared displacement.

Most variants of NMR diffusometry techniques are based on gradients of the main magnetic flux density B_0 combined with Hahn or stimulated echo RF pulse sequences ("laboratory frame NMR diffusometry") [19, 20, 26]. In principle, even the simplest form of a spin echo, the so-called gradient spin echo can be used as well. A schematic representation of such a pulse sequence is shown in Figure 17.4 together with an illustration of winding up and unwinding the so-called helix of the local transverse magnetization vectors during the two gradient pulses.

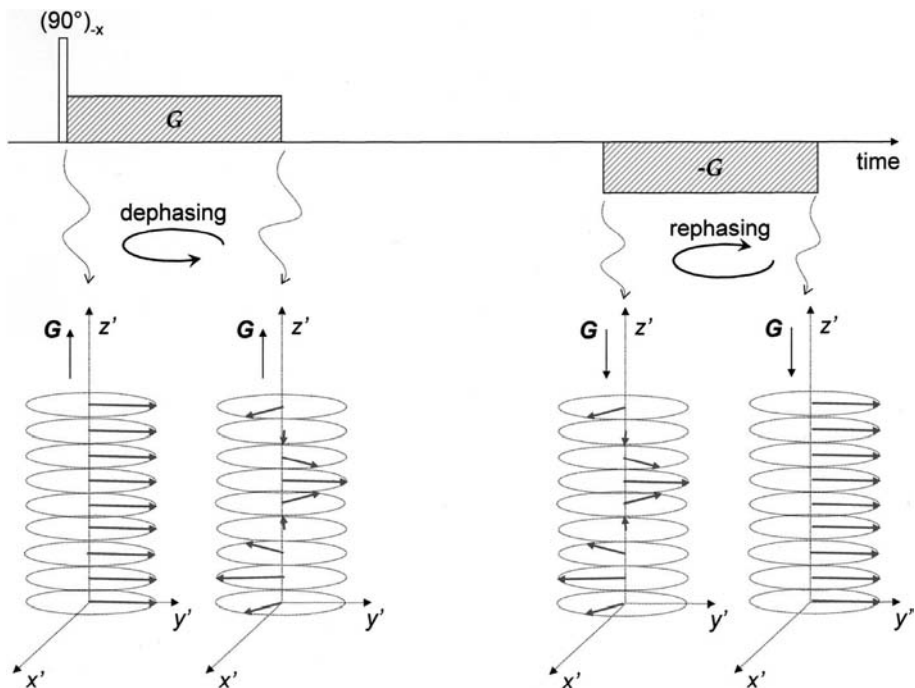


Figure 17.4 Schematic representation of the pulse sequence for a gradient spin echo [26] (top), and of the spatial distribution of the transverse magnetization vectors at different times (bottom). As usual, a frame of reference, x' , y' , z' , is chosen rotating with the Larmor frequency in the absence of the field gradient around the external magnetic field which is assumed to be aligned along the z' -axis. The field gradient is also assumed to be aligned along the z' -axis. The sequence consists of a 90° RF pulse (with a \mathbf{B}_1 vector aligned along the $-x'$ -axis of the rotating frame of reference) and a pair of pulses of

gradients of the external magnetic flux density, \mathbf{B}_0 (hatched). The 90° pulse produces transverse magnetization aligned along the y' direction. A positive gradient pulse \mathbf{G} along the z' -axis dephases the transverse magnetization leading to a “helix” distribution. The local magnetization vectors are represented by arrows in the lower part of the figure. After a diffusion interval, a negative gradient pulse of the same magnitude and length rephases the transverse magnetization leading to a gradient spin echo. The amplitude of this signal is attenuated by diffusive displacements during the pulse sequence.

Instead of field gradients in pulsed form, it can sometimes be favorable to employ steady gradients. This is of interest if very short diffusion times are to be probed and if diffusion is relatively slow as in systems with strong obstruction or trapping effects. The point is that the dephasing/rephasing efficiency is optimized in this way due to the absence of any switching intervals.

Figure 17.5(a) schematically shows a sequence consisting of three RF pulses in the presence of a steady gradient of the main magnetic field. A particularly strong and stable field gradient is available in the fringe field of superconducting magnets (see Figure 17.5(b)) as they are ubiquitous in typical NMR labs. The signals to be acquired are the stimulated echo and, for auxiliary purposes,

the primary echo [26]. Note that the stimulated echo is merely affected by the gradient sections during the free coherence evolution intervals, that is the first and the second τ_1 interval. During τ_2 , the moiety of the magnetization contributing to the stimulated echo is “stored” along the z direction and is not subject to Larmor precession. Therefore, the gradient is irrelevant during τ_2 . The first two RF pulses together with the gradient produce a so-called grating of the z magnetization illustrated in Figure 17.5(c). The effect of diffusion is then leveling of this grid-like distribution of the magnetization. The third RF pulse converts the z magnetization to transverse magnetization again, which then evolves in the field gradient leading to the stimulated echo.

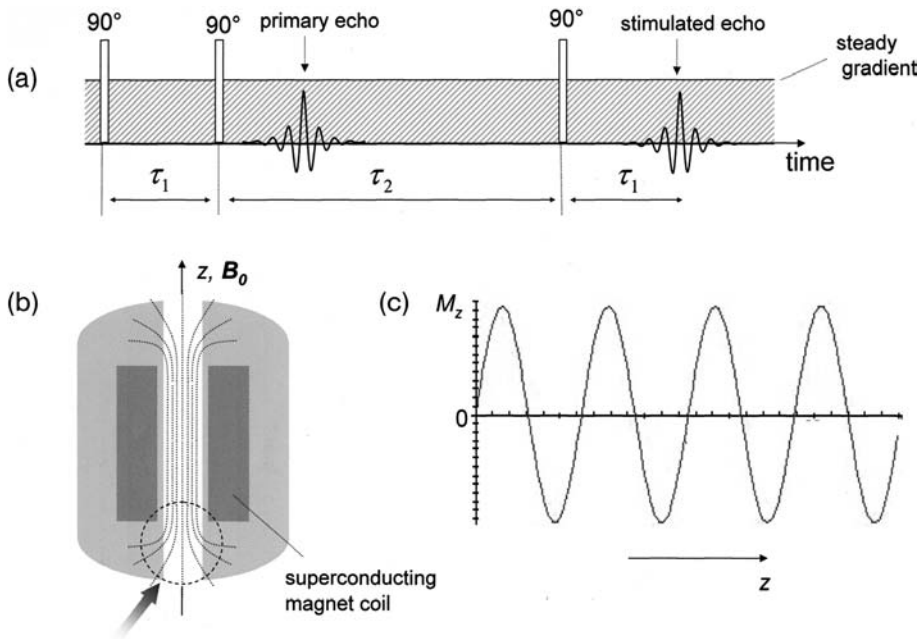


Figure 17.5 Schematic representation of the steady fringe field gradient NMR diffusometry technique. (a) The pulse sequence consists of three 90° RF pulses applied in the presence of a steady gradient (hatched) of the main magnetic field. The signal of interest is the stimulated echo arising after the third pulse. Its amplitude can be divided by

that of the primary echo in order to eliminate relaxation factors [26]. (b) Schematic cross section of a superconducting magnet indicating the area where fringe-field measurements are carried out. (c) Grating (or grid) of the z -magnetization in the τ_2 interval after the second 90° pulse.

Apart from the laboratory frame techniques, there is a number of analogous “rotating-frame” methods employing gradients of the amplitude of the RF flux density B_1 . Such an alternative protocol for diffusion measurements was successfully demonstrated with rotating-frame echo phenomena [22, 29].

The principle common to all laboratory and rotating-frame methods mentioned so far is to first produce a nonequilibrium magnetization distribution in the form of a helix (for an illustration see Figure 17.4, bottom). The projection of the helix on the gradient axis, forms the so-called magnetization grating or grid (for an illustration see Figure 17.5(c)). Translational diffusion then tends to level the magnetization distribution along the gradient direction during the diffusion time. This leveling process can be probed indirectly via the acquisition of echo amplitudes attenuated by diffusion in the diffusion interval.

A second, entirely different principle is to record the leveling of the grating directly by imaging the magnetization profile across the sample after a diffusion interval. Depending on this diffusion delay, the grating will be more or less leveled. A method of this type is the "magnetization grid rotating-frame imaging technique" (MAGROFI) [22, 30].

Figure 17.6 shows a schematic representation of the MAGROFI pulse sequence. All RF pulses are understood to be subject to a (constant) gradient of the RF amplitude. This gradient is produced by a suitably shaped RF transmitter and pick-up coil. In rotating-frame diffusometry variants, the direction of the gradient is preferably perpendicular to the main magnetic field for practical reasons. Again a grating of the z magnetization is produced along the gradient direction by a preparation pulse. The magnetization grid surviving the diffusion time is imaged with the aid of the rotating frame technique. The diffusion coefficient is then evaluated from the local leveling effect.

In the context of diffusion in liquids in unsaturated porous glasses, one faces strong internal field gradients due to inhomogeneities of the magnetic susceptibility and a substantial spatial distribution of the transverse relaxation time. Both phenomena can lead to artifacts in conventional pulsed gradient spin echo diffusometry. It turned out that a combination of two special field-gradient NMR diffusometry techniques is useful to overcome this problem. The steady fringe-field gradients of superconducting magnets are normally so strong that internal field gradients can be neglected. Moreover, diffusion times as short as $100 \mu\text{s}$ or even less can be probed with this technique.

On the other hand, the MAGROFI method which inherently uses much weaker gradients is suitable for long diffusion times merely limited by spin-lattice relaxation. Due to its rotating-frame nature, this technique is insensitive to internal B_0 gradients as well. As a unique feature, it is also insensitive to any distribution of transverse relaxation times. The total range of the diffusion time that can be probed by the combination of both methods ranges from $100 \mu\text{s}$ up to seconds [22, 31].

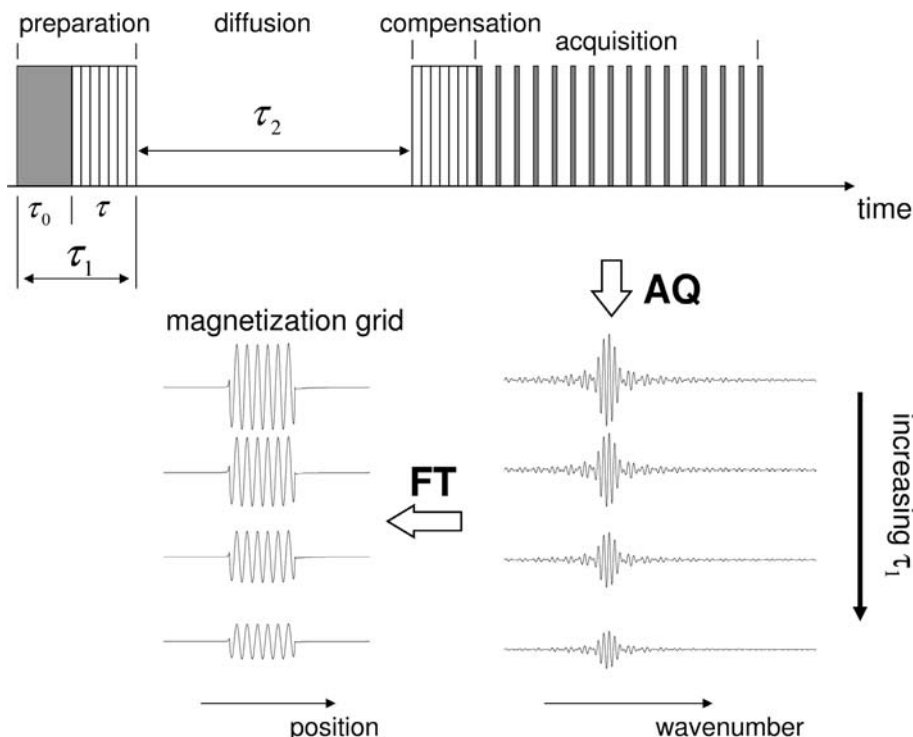


Figure 17.6 Schematic representation of the MAGROFI technique for the measurement of diffusion coefficients with the aid of gradients of the amplitude of the RF field, g . The preparation pulse of variable length produces the magnetization grid along the gradient direction. After the diffusion time, the magnetization grid is imaged with the aid of the rotating frame technique. The purpose of the compensation pulse is to keep the wavelength of the grating to be rendered as an image

constant. This facilitates the evaluation of a diffusion coefficient at a certain position. The primary data set stroboscopically acquired in the acquisition (AQ) interval is the signal as a function of a wavenumber defined by $k = \gamma g \tau_1$. The magnetization grid more or less leveled by diffusion is then directly obtained by Fourier transformation (FT). The diffusion time is defined by $t_{\text{diff}} = \frac{1}{3}\tau_1 + \tau_2 + \frac{1}{3}\tau_3$, where τ_3 is the width of the compensation pulse. Details can be found in Ref. [22].

17.3.2

Sub- and Superdiffusive Transport in Porous Glasses

Transport phenomena mediated by simultaneous laminar flow and diffusion is called “hydrodynamic dispersion” [32]. Coherent and incoherent transport are superimposed. “Coherent” means here that the velocity vector of each particle is stationary during the experimental time in contrast to “incoherent” processes, where these vectors are randomized with respect to magnitude and/or direction.

In porous media, the tortuosity of flow streamlines comes into play in addition. At large Péclet numbers, $\text{Pe} \gg 1$, that is for displacements by flow larger

than displacements by Brownian diffusion, the dominating source of the dispersion of the particle trajectories is the tortuosity determined by the pore space geometry. Incoherent displacements by tortuous flow dominate then over Brownian displacements, and particle transport tends to be superdiffusive according to the definition given in Section 17.1. Corresponding computer simulations [33, 34] and NMR experiments [3, 35] have been reported in the literature.

The coherent and incoherent displacement contributions can easily be distinguished in pulsed gradient spin-echo experiments. All phase shifts of the Larmor precession arising from velocities constant in the measuring interval can be eliminated by appropriate choice of the field gradient pulses [26]: Echo attenuation by coherent transport components can be compensated by using gradient sequels $G(t)$ (including all B_0 gradients present during the RF pulse sequence) with vanishing zeroth, first and, possibly, higher moments. Assuming spatially constant gradient pulses along the z -axis for example, and expanding the z component of the particle trajectory, $z = z(t')$, according to $z_0 + v_z t' + \dots$, the z gradient pulses occurring in the experimental time t can be adjusted in such a way that

$$\int_0^t G_z(t') (z_0 + v_z t' + \dots) dt' = 0. \quad (17.20)$$

Then there will be no Larmor precession phase shift effect for particle trajectories starting at an initial position component z_0 with a velocity component v_z stationary during the gradient pulse sequence. What remains is spin echo attenuation by motions incoherent on this time scale.

The instantaneous velocity field \vec{v} can be analyzed in two terms according to

$$\vec{v}(t) = \vec{u}(t) + \vec{V}, \quad (17.21)$$

where $\vec{V} \equiv \lim_{t \rightarrow \infty} < \vec{v} >$ is the average velocity, and $\vec{u}(t)$ is the fluctuation of the Lagrangian velocity. The idea of the pulse sequence shown in Figure 17.7 is to compensate phase shifts caused by \vec{V} while examining the echo attenuation by $\vec{u}(t)$. The trajectory of a nucleus (i.e., the component along the experimental field gradient direction) can be expressed as

$$r(t) = r_0 + \int_0^t v(t') dt' = r_0 + \int_0^t [V + u(t')] dt' = r_0 + Vt + \int_0^t u(t') dt', \quad (17.22)$$

where r_0 is the initial position. A field gradient pulse of an arbitrary shape,

$$G = \begin{cases} G(t) & \text{for } 0 \leq t \leq T \\ 0 & \text{otherwise} \end{cases} \quad (17.23)$$

produces the accumulative phase shift

$$\begin{aligned}
 \phi(T) &= \gamma \int_0^T G(t)r(t) dt \\
 &= \gamma \left[r_0 \int_0^T G(t) dt + V \int_0^T G(t)t dt + \int_0^T dt G(t) \int_0^t dt' u(t') \right] \quad (17.24) \\
 &= \phi_0(T) + \phi_1(T) + \phi_2(T)
 \end{aligned}$$

The phase shifts by the position dependent term $\phi_0(T)$ and the coherent-velocity dependent term $\phi_1(T)$ can be compensated by using a bipolar gradient pulse of the form [26]:

$$G_z(t) = \begin{cases} G_0 & \text{for } 0 \leq t \leq \tau \\ -G_0 & \text{for } \tau \leq t \leq 3\tau \\ G_0 & \text{for } 3\tau \leq t \leq 4\tau \\ 0 & \text{otherwise} \end{cases} \quad (17.25)$$

That is, $\phi_0(4\tau) = 0$ as well as $\phi_1(4\tau) = 0$ after this bipolar gradient pulse. Merely the fluctuation term

$$\phi_2(4\tau) = \gamma G_0 \left[\int_0^\tau \int_0^t u_z(t') dt' dt - \int_\tau^{3\tau} \int_0^t u_z(t') dt' dt + \int_{3\tau}^{4\tau} \int_0^t u_z(t') dt' dt \right]$$

still contributes. Instead of the bipolar scheme, a combination of 180° RF pulses and unipolar gradient pulses of width δ can be used. Practically it is moreover more convenient to split the 180° pulses into two 90° pulses each, and to compose the gradient pulses of identical pulses of unit length τ [3]. Figure 17.7 shows such a pulse sequence. Note that a combination of two 90° radio frequency pulses effectively inverts the effect of the gradient pulses with respect to the sign. The spoiling gradient pulse spoils all spin coherences in the interval Δ . The use of 90° pulse pairs instead of 180° pulses reduces the echo amplitude by a factor of $1/4$ on the one hand, but avoids excessive transverse relaxation losses on the other. The dispersion time is given by the combined interval $t = 2\Delta$.

With tortuous flow through a porous medium, the question whether the velocity of a particle is constant depends on the length of the displacement sensitive interval. In the limit of small measuring intervals, that is, for root-mean-squared displacements shorter than the elementary length scale, a , of the pore network, $\sqrt{\langle z^2 \rangle} < a$, flow is not hindered and velocities tend to be constant so that the only incoherent displacement contribution can arise from Brownian

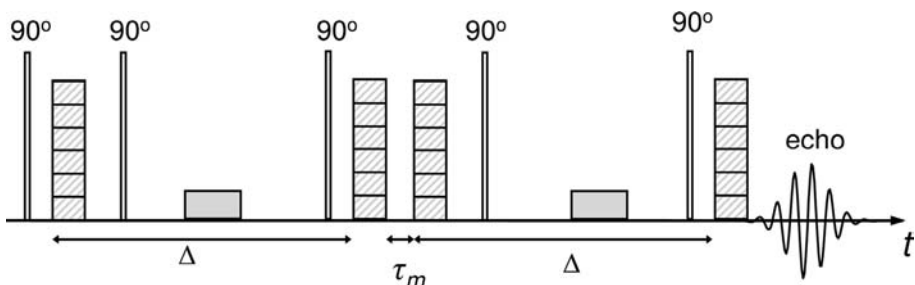


Figure 17.7 Schematic RF and field gradient pulse sequence for the acquisition of echo amplitudes attenuated by hydrodynamic dispersion. This is a version optimized to avoid excessive transverse relaxation losses. The hatched gradient pulses are chosen and arranged in such a manner that phase shifts due to coherent motions are suppressed. They are incremented in subsequent echo

acquisition scans as indicated by the horizontal lines in the gradient pulses. In this way, a data set for the echo-attenuation curve is recorded while all intervals are kept constant. The gray shaded gradient pulses in the middle of the Δ intervals serve the spoiling of undesired spin coherences. The effective dispersion time is 2Δ . Details of the experimental protocol can be found in Ref. [3].

diffusion. Intervals permitting displacements in the range $a < \sqrt{\langle z^2 \rangle} < \xi$, where ξ is the correlation(s) length of the pore space, are connected with more or less random velocity changes so that the compensation for flow becomes incomplete. In this case, random phase shifts by tortuous flow lead to the attenuation of the echo amplitude indicating incoherent displacements. The influence of such motions will be the larger the longer the sensitive interval is, that is, the more randomly the particle trajectories develop.

Finally, for displacements $\sqrt{\langle z^2 \rangle} \gg \xi$ reached in the sensitive interval, we have a superposition of a constant drift velocity and randomized displacements due to the tortuosity of the percolation cluster. In coherent-velocity compensation experiments, the drift contribution can completely be eliminated so that attenuation by incoherent tortuous flow governs the echo amplitude.

From the echo attenuation curves, the mean-squared displacement can be evaluated in principle according to

$$\langle z^2 \rangle = 2D_{\text{disp}}(t)t, \quad (17.26)$$

where t is the relevant gradient pulse interval, and D_{disp} is the dispersion coefficient. In the limit $\sqrt{\langle z^2 \rangle} < a$, the dispersion coefficient approaches the ordinary Brownian diffusion coefficient,

$$D_{\text{disp}} \approx D_{\text{Brown}} = \text{const.} \quad (17.27)$$

For $\sqrt{\langle z^2 \rangle} \gg \xi$, the dispersion coefficient is again stationary and adopts a value,

$$D_{\text{disp}} \approx \text{const.} \gg D_{\text{Brown}}. \quad (17.28)$$

However, in the scaling window $a < \sqrt{\langle z^2 \rangle} < \xi$, a time-dependent diffusion coefficient is expected for flow through random media at large Péclet numbers, $\text{Pe} \gg 1$,

$$D_{\text{disp}} = D_{\text{disp}}(t) \propto t^f \text{ with } 0 < f < 1 \text{ and } D_{\text{Brown}} < D_{\text{disp}}(t) < D_{\text{eff}}. \quad (17.29)$$

Figure 17.8 schematically shows an experimental setup for hydrodynamic dispersion NMR studies in porous samples. The spin-echo attenuation curves measured in fluids in porous media tend to be nonexponential. For an evaluation, one therefore uses the proportionality

$$E(q, t)_{q \rightarrow 0} \propto \exp(-q^2 D_{\text{eff}} t) \quad (17.30)$$

typical for diffusive echo attenuation experiments under ordinary conditions as an approach [26]. The wavenumber is defined by $q = \gamma \delta G$ for a gradient pulse width δ . The coefficient determined in this way will be called “effective dispersion coefficient,” D_{eff} , and tends to be a function of the dispersion time, $t = 2\Delta$. Furthermore, anticipating that the displacement propagator can be approached by a Gaussian function, the mean-squared displacement along the gradient direction can be determined according to

$$\langle z^2 \rangle \approx 2D_{\text{eff}}(t)t \quad (17.31)$$

Figure 17.9 shows typical plots of the $\langle z^2 \rangle$ data obtained in this way for different flow rates as a function of the dispersion time [3]. A power law of the form $\langle z^2 \rangle \propto (2\Delta)^\kappa$ can be stated in the frame of the experimental accuracy for low and high flow rates. This applies in particular to the flow rates 0, 0.7, and 0.8 ml/min. Obviously, a crossover between the subdiffusive limit in the absence of flow to a superdiffusive limit in the presence of strong enough flow occurs. The fitted exponents are $\kappa \approx 0.84$ and $\kappa \approx 1.95$, respectively.

The root-mean-squared displacements probed experimentally ranges from 10 to 130 μm . This is the length scale of the pore-space topology of the examined porous glass. That is, the transport properties refer to the scaling window where a power-law behavior can be expected. In the absence of flow, transport is governed by molecular diffusion which is obstructed by the confining geometry. The consequence is the subdiffusive mean-squared displacement law. Above a flow rate of about 0.7 ml/min, the exponent $\kappa \approx 1.95$ indicates a superdiffusive law even approaching the “ballistic” case $\kappa = 2$. In this limit, particles are displaced in all directions with the same mean velocity. For hydrodynamic dispersion in disordered porous media, this is the case when pure mechanical mixing under the influence of the local geometry is relevant as demonstrated with computer simulations by Duplay and Sen [36].

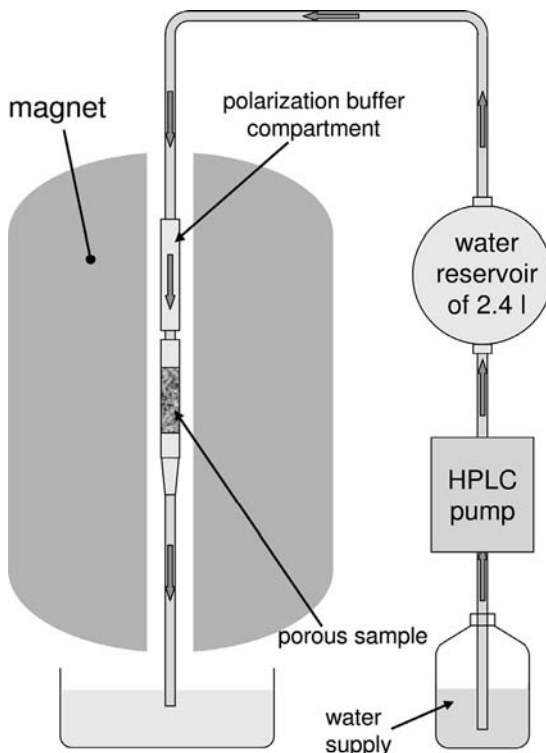


Figure 17.8 Schematic representation of the setup of a typical hydrodynamic dispersion experiment in a superconducting NMR magnet [3]. Before entering the proper sample, the water passes a buffer compartment in the magnet, where the nuclear spins spend enough time to become polarized prior to the application of the RF and field gradient pulse sequence (see Figure 17.7).

17.3.3

Discussion of the Results for Porous Glasses

In the scaling window, $a < \sqrt{\langle z^2 \rangle} < \xi$, anomalous power laws for the time dependence occur as expected for random media. In a previous work [24] (see below), diffusion in a quasi-two-dimensional random-site percolation model object was simulated by solving the ordinary diffusion equation numerically for the corresponding initial and boundary conditions given by spin density mapping experiments. An anomalous time dependence of the mean-square displacement $\langle z^2 \rangle \propto t^\kappa$ was obtained with $\kappa \approx 0.8$, while for the present work the experimental value is $\kappa \approx 0.84$. The mean-squared displacement can be expressed as $\langle z^2 \rangle \propto t^{2/d_w}$, where d_w is the fractal dimension of the random walk [5]. The value obtained from the data shown in Figure 17.9, $d_w = 2.38$, is lower than the one reported in Ref. [24], $d_w = 2.87$. The difference is attributed

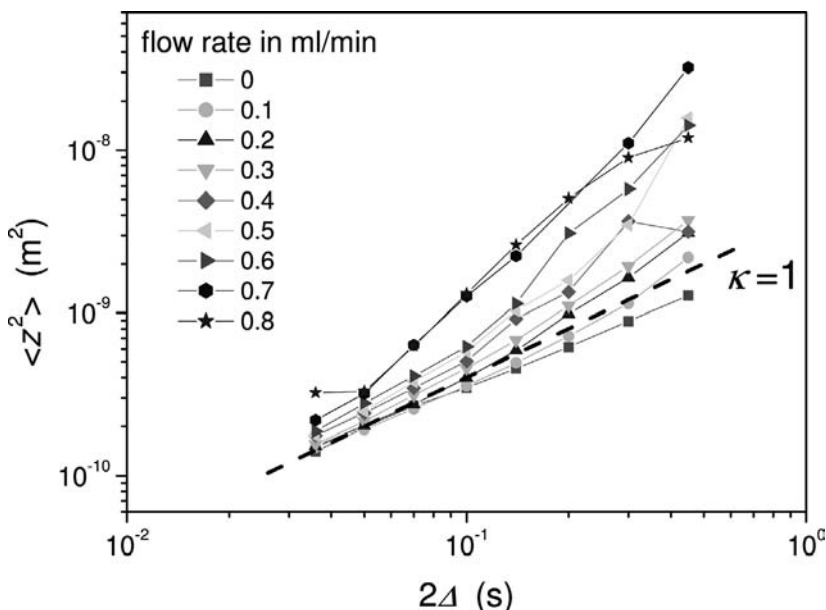


Figure 17.9 Hydrodynamic dispersion in a porous silica glass (VitraPor #1; nominal pore size 100–160 µm) [3]. The sample diameter was 6 mm. The mean-squared displacement along the field gradient direction, $\langle Z^2 \rangle$, is plotted as a function of the effective dispersion time, 2Δ , at different flow rates. The dashed line represents $\langle Z^2 \rangle \propto 2\Delta$. The crossover from subdiffusive (in the absence of flow) to superdiffusive behavior for superimposed flow is obvious.

to different structures. The porous glass to which the data in Figure 17.9 refer is a more or less random porous glass, whereas the percolation cluster in Ref. [24] is designed to have true fractal properties in the scaling window (see the results delineated in the next section below). According to the Alexander–Orbach conjecture [37], the value of d_w is related to the fractal dimension of the structure d_f by $d_w = 1.5d_f$ for Euclidean dimensions $d_E \geq 2$. Anticipating fractal properties for the porous glass under consideration, a value $d_f = 1.6$ follows.

17.4 The Time Scale Beyond Seconds

17.4.1 NMR Microscopy Diffusometry Techniques

Much longer time scales than discussed so far can be probed with the aid of NMR microimaging [26] of isotope interdiffusion between two chemically

identical compartments having initially a different isotope composition. Detecting selectively one of the isotopes permits one to image the concentration profile as a function of time. The spatial resolution of such experiments is typically 100 μm in two or three dimensions. Isotopes of interest in this context are ¹³C in a ¹²C environment, and ¹H in a deuterated (²H) matrix or – less favorable – the other way round.

The main difficulty of experiments of this sort is not so much the experiment itself but the preparation of the initial isotope distribution. Ideally one would like to have a step-like concentration profile at the beginning of the experiment. The flattening of the concentration distribution can then be probed by repeated NMR imaging of the system as a function of time. Examples will be described below. The initial interface between the two isotope compartments should be as planar as possible, and the two moieties of the system should be in close contact on a molecular length scale. These conditions must be established in a relatively short time before the measurements in order to avoid premature interdiffusion.

The proton/deuteron interdiffusion scenario can be examined with any of the standard NMR imaging techniques [26]. For a good diffusion time resolution, a fast imaging variant may be preferable [26]. Due to the much better detection sensitivity, this also means generally that the detection of proton signals is preferable to the direct measurement of deuterons or ¹³C nuclei.

Figure 17.10 shows an example of proton/deuteron interdiffusion between two aqueous gel compartments (see inset) [24]. Since no obstruction or trapping effect can be expected in diluted aqueous gels on a length scale short compared with the sample dimension, the known spatiotemporal solution of the ordinary Fickian diffusion equation of the proton concentration $C(\vec{r}, t)$ should apply. This diffusion equation reads

$$\frac{\partial C(\vec{r}, t)}{\partial t} = D \nabla^2 C(\vec{r}, t), \quad (17.32)$$

where D is the ordinary diffusion coefficient. Ideally, the bulk H₂O and D₂O two-compartment setup shown in the inset of Figure 17.10 can be represented by the one-dimensional initial condition

$$C(x, 0) = \begin{cases} C_0 & \text{for } x \leq 0 \\ 0 & \text{for } x > 0 \end{cases} \quad (17.33)$$

For a diffusion time range where the root-mean-squared displacement is much less than the actual sample extension, we may approximate the system by infinite boundary conditions. For the initial condition (17.33), the solution of Eq. (17.32) is then [38]

$$C(x, t) = \frac{1}{2} C_0 \operatorname{erfc} \left\{ \frac{x}{2\sqrt{Dt}} \right\} \quad (17.34)$$

in perfect agreement with the experimental data shown in Figure 17.10. $\text{erfc}\{\dots\}$ is the complementary error function.

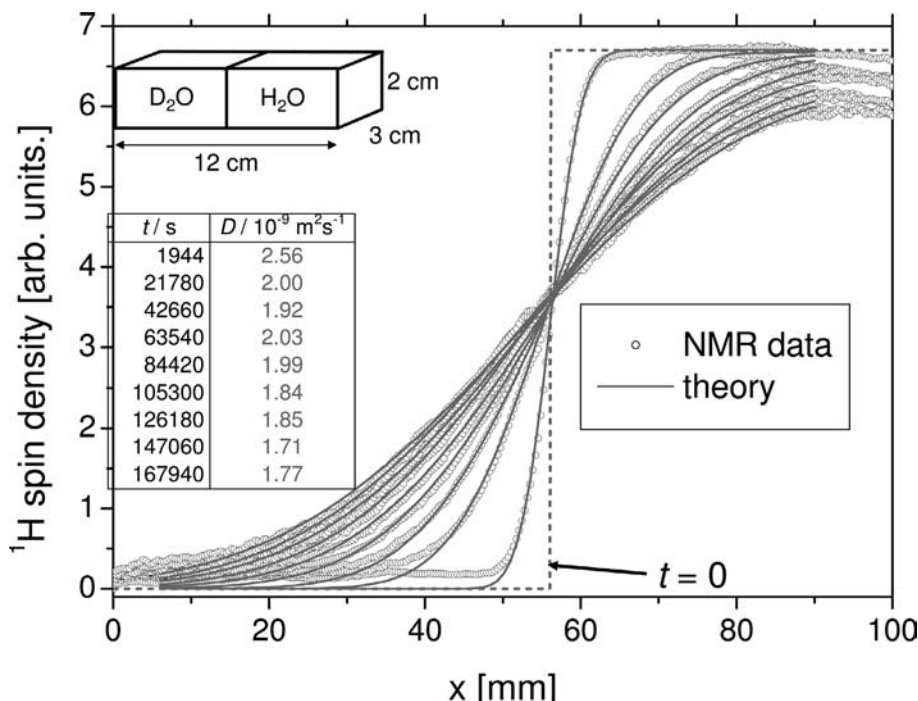


Figure 17.10 Comparison of theoretical and experimental interdiffusion profiles between bulk H_2O and D_2O gels. The dotted line represents the idealized initial distribution of ${}^1\text{H}$ nuclei. The solid lines represent fits of Eq. (17.34) to the experimental data for different diffusion times. The fitted diffusion coeffi-

cients are given in the inset table. Deviations at the shortest and longest diffusion times from the room temperature water diffusion coefficient ($D \approx 2 \times 10^{-9} \text{ m}^2/\text{s}$) are due to imperfections of the initial concentration profile and the finite size of the object, respectively.

In systems of hydrocarbons, it is favorable to detect ${}^{13}\text{C}$ indirectly in the ${}^1\text{H}$ channel by first cross-polarizing the ${}^{13}\text{C}$ spins at the expense of the ${}^1\text{H}$ spins with the aid of the Hartmann/Hahn method, and then repolarizing the ${}^1\text{H}$ spins to be detected [26]. This cyclic cross-polarization technique (CYCLCROP) ensures both optimal sensitivity and selectivity with respect to different chemical species.

Figure 17.11 shows a typical CYCLCROP pulse sequence [39–42] for one-dimensional mapping of ${}^{13}\text{C}$ concentrations along the z direction. The sequence starts with the unselective excitation of proton coherences by a $\pi/2$ RF pulse. In the first section, cross-polarization is performed chemical-shift selectively to ${}^{13}\text{C}$ spins J -coupled to the protons of the respective chemical group (J is the spin–spin coupling constant). The polarization of ${}^{13}\text{C}$ spins

is enhanced by cross-polarization from the initially excited proton spins [43]. The so-called Hartmann/Hahn condition for optimal (on-resonance) polarization transfer is

$$\gamma_H B_{1,H} = \gamma_C B_{1,C}, \quad (17.35)$$

where γ_H and γ_C are the gyromagnetic ratios of proton and ^{13}C nuclei, respectively, and $B_{1,H}$ and $B_{1,C}$ are the amplitudes of the radio frequency fields in the ^1H and ^{13}C channels, respectively.

The cross-polarization method employed in this pulse sequence is the PRAWN variant described in Ref. [44]. This variant has the advantage of being particularly tolerant against Hartmann/Hahn mismatch, i.e., against violation of Eq. (17.35). It also keeps the RF power deposit in the sample moderate, so that temperature variations on these grounds should be of no problem. This cross-polarization technique consists of two combs of RF pulses of width τ_w and spacing τ_s in either radio frequency channels (see Figure 17.11). The flip angle of these pulses is θ for both spin species. The conditions for the time intervals are

$$\begin{aligned} n\theta &= 2m\pi(n, m = 1, 2, 3, \dots) \\ n(\tau_s + \tau_w) &= C/J. \end{aligned} \quad (17.36)$$

The second condition refers to the total length of the PRAWN sequence. The optimal value of the constant C is theoretically equal to 1 for CH groups, equal to $1/\sqrt{2}$ for CH_2 groups, and ≈ 0.61 for CH_3 groups [44].

After the cross-polarization process, the resulting transverse ^{13}C magnetization of the hydrocarbon group selected is then aligned along the z direction by a $\pi/2$ “storage pulse.” The following interval serves spoiling any remaining proton coherences. In addition to the coherence crusher gradient pulse shown in Figure 17.11, one or more adiabatic 90° pulses followed by spoil gradients can be inserted in this interval if needed in critical cases [39]. The ^{13}C magnetization is then flipped to the transverse plane again and transferred to proton coherences via a reverse cross-polarization process complying with the same conditions as given above. The proton coherences produced in this way refer to protons that are J -coupled to the spins of the selected ^{13}C resonance line. These proton coherences are detected as a Hahn spin echo in the presence of a readout gradient for spatial frequency encoding along the gradient direction. The profile of the ^{13}C distribution is thus indirectly obtained as the Fourier transformed proton signal. Optionally a ^{13}C decoupling pulse can be applied while acquiring the proton signal in order to suppress the occurrence of any doublet signals.

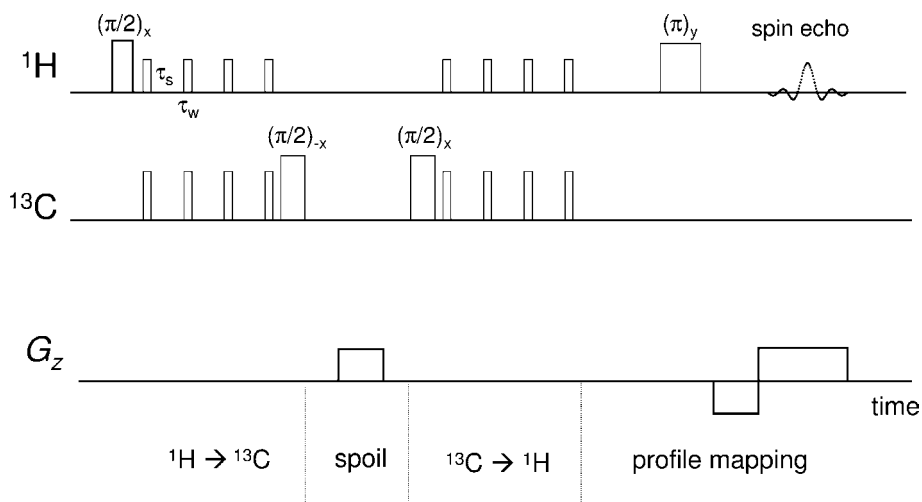


Figure 17.11 Typical CYCLCROP RF and field gradient pulse sequence for one-dimensional mapping of ^{13}C concentrations. The pulse sequence can easily be extended for the record of two- or three-dimensional maps [47].

17.4.2

Diffusion of Solvents in Swollen Polymers

The CYCLCROP NMR diffusometry method can be applied for studies of any hydrocarbon system. Organic solvent diffusion in swollen polymers is a typical example. This sort of system is of interest, since anomalous transport features may arise in the frame of the so-called case II diffusion limit when the host material is microstructurally modified by the diffusant [45, 46]. In the frame of the present overview, we restrict ourselves to the demonstration of ordinary diffusion in a scenario equivalent to the aqueous gel system described above (see Figure 17.10).

A schematic cross section of the sample system is shown in Figure 17.12. It consists of two swollen polymethylmethacrylate (PMMA) rods tightly pressed on each other. One of the compartments was initially swollen with ^{13}C enriched methanol ($> 90\%$), the other one with methanol with ^{13}C in natural abundance (ca. 1%). The swelling degree was the same in both cases. Note that neither the enrichment nor the single-line ^{13}C spectrum of the solvent are prerequisites of the technique. The ^{13}C lines of the swollen PMMA are suppressed by the CYCLCROP technique. After bringing the two separately swollen PMMA rods into contact with each other and sealing them in a polyethylene container, the ^{13}C concentration profile measurements were started.

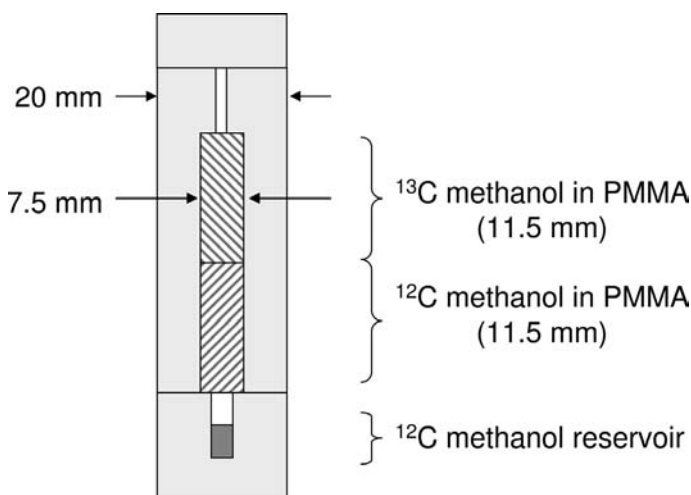


Figure 17.12 Cross section through the cylindrical sample used for CYCLCROP interdiffusion experiments: two PMMA rods (hatched areas) are embedded in a polyethylene container. One of the rods is initially saturated with ^{13}C enriched methanol, the other one with ordinary methanol. The ^{12}C methanol reservoir at the bottom serves the compensation of volatilization losses during sealing the sample system.

Figure 17.13 shows typical concentration profiles of ^{13}C methanol measured with the CYCLCROP method after diffusion times of 2 h, 7 h, and 18 h [47]. Since the ^{13}C content in natural abundance as well as after enrichment does not change the chemical and physical properties of methanol perceptibly, and since both PMMA rods were saturated with the solvent, we are actually dealing with self-diffusion rather than interdiffusion. That is, the long-time self-diffusion coefficient can be determined in this way and can be compared with the value for the bulk solvent.

The initial distribution of the ^{13}C methanol is of the type given in Eq. (17.33), so that the solution of Fick's diffusion equation, Eq. (17.34), can be used again under the same restrictions for the root-mean-squared displacements. Typical data sets are shown in Figure 17.13 for different diffusion times in good agreement with the prediction. Merely for the longest diffusion times a slight finite-size effect shows up, and the description of the data becomes somewhat worse. The fitted value for the self-diffusion coefficient of methanol in PMMA is $D = 3 \times 10^{-10} \text{ m}^2 \text{ s}^{-1}$. This compares to the bulk value $D = 2.4 \times 10^{-9} \text{ m}^2 \text{ s}^{-1}$. That is, methanol diffusion in PMMA is considerably hindered and slowed down due to the tortuous diffusion pathways imposed by the host material, and because of solvent/polymer interactions.

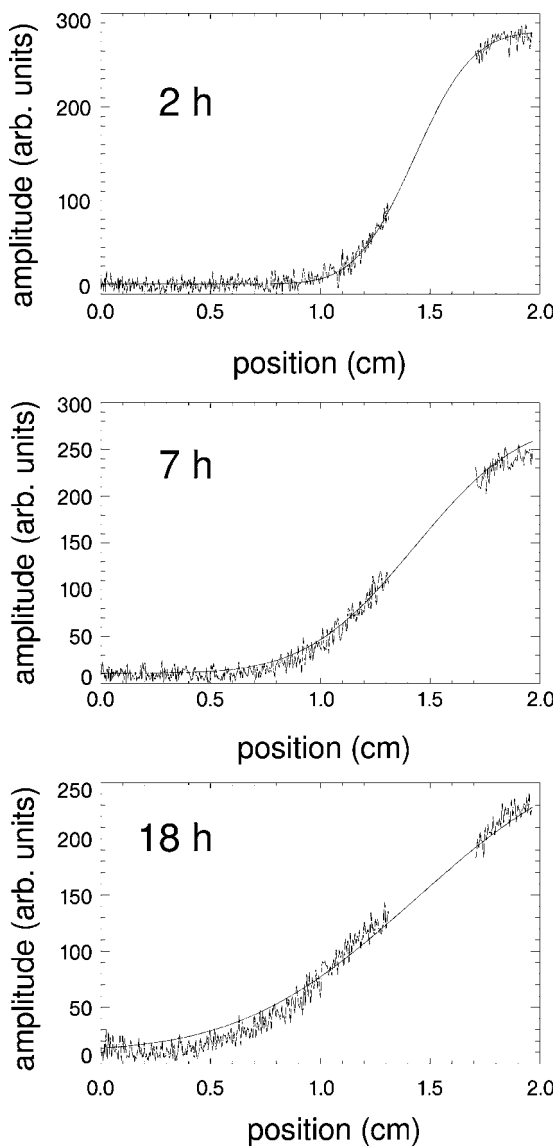


Figure 17.13 Typical profiles of the ^{13}C methanol concentration across the sample shown in Figure 17.12. The diffusion times were 2 h, 7 h, and 18 h (from the top to the bottom) after initially bringing the two PMMA rods into contact with each other. The data have been measured with the CYCLCROP pulse sequence shown in Figure 17.11 with the following parameters: $\tau_w = 22.3 \mu\text{s}$; $\tau_s = 100 \mu\text{s}$; $n = 40$; relaxation delay 5 s;

gradient strength 0.65 T/m; number of scans 256; dwell time 0.68 μs ; data points per profile 2048. The signal data at the interface between the two rods are somewhat distorted because of the experimentally imperfect contact, and are omitted for fitting purposes. The theoretical lines represent fits of Eq. (17.34). The room temperature self-diffusion coefficient of methanol in swollen PMMA was found to be $D = 3 \times 10^{-10} \text{ m}^2 \text{ s}^{-1}$.

17.4.3

Diffusion on Random-Site Percolation Clusters

Random-site percolation clusters [48] are textbook examples for structures showing fractal properties and correspondingly anomalous diffusion properties for random walkers on the cluster [5]. The length scale of fractal properties is $a < r < \xi$, where a is now the base lattice constant and ξ is the correlation length. The consequence of the tortuous structure of the percolation cluster is that a random walker in the pore space formed on this basis is frequently and temporarily trapped in dead end pores and bottlenecks or even "red sites" [49], so that diffusion is slowed down and becomes anomalous (subdiffusive).

The mean-squared displacement of a random walker on a percolation cluster is predicted to obey [50]

$$\langle r_d^2 \rangle \propto \begin{cases} t^{2/d_w} & \text{for } t \ll t_\xi \\ \tilde{D}t & \text{for } t \gg t_\xi, \end{cases} \quad (17.37)$$

where $t_\xi \propto \xi^{d_w}$ is the time a random walker needs to explore the correlation length ξ , and d_w is the fractal dimension of the random walk. As discussed before, anomalous diffusion is only expected in the scaling range $a < \sqrt{\langle r_d^2 \rangle} < \xi$. The diffusion coefficient becoming effective in the long-time limit, $t \gg t_\xi$, is denoted by \tilde{D} . According to the Alexander–Orbach conjecture [37], the quantity d_w is assumed to be related to the fractal dimension by $d_w \approx 1.5d_f$ in two or three Euclidean dimensions. That is, the structural parameter d_f characteristic for the volume-averaged porosity is linked to the dynamic parameter d_w specifying anomalous diffusion.

Apart from computer simulations [51], experimental tests using model objects of percolation clusters have been reported [24]. The cluster was first generated as a template on a computer and then milled into polystyrene sheets. For an example see the photograph in Figure 17.14. The fabrication resolution of the objects under consideration here was 400 μm . It should be mentioned that a better resolution of about 20 μm can be achieved with a lithography technique [52]. The preparation process is however very time consuming.

After filling the pore space with water, diffusion of the water molecules was examined on a time scale up to 400 h using the proton/deuteron interdiffusion method described above. Coherent flow by convection was prevented by stabilizing the water with a gel (Klcogel) of a concentration low enough not to affect molecular diffusion. The initial light/heavy water distribution is shown in the inset of Figure 17.15. The displacement of the isotopic interdiffusion front was then measured as a function of time in the form of repeatedly recorded proton spin density maps [24].

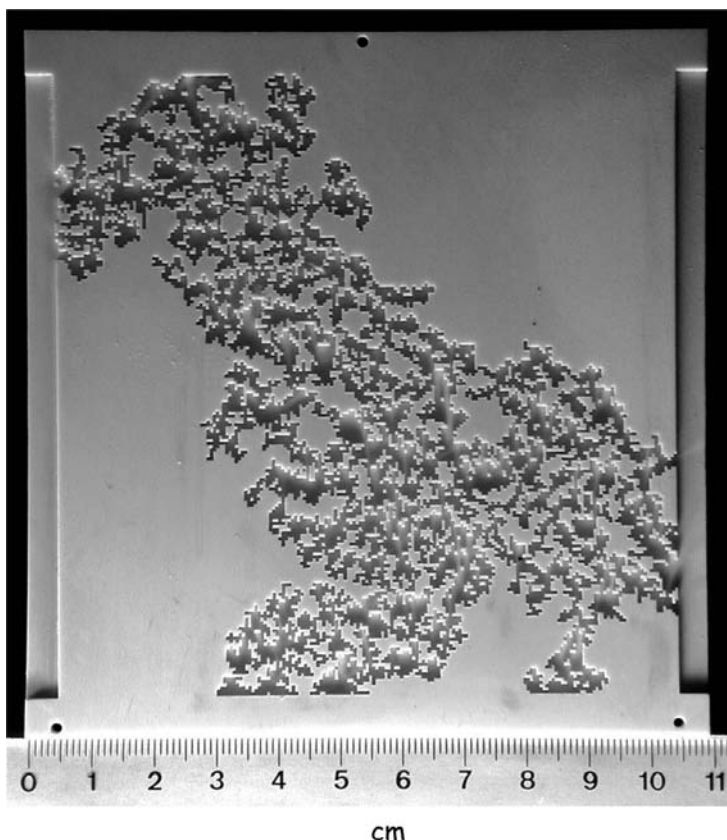


Figure 17.14 Photograph of a typical percolation cluster milled into a polystyrene sheet. Note that this is the “infinite” cluster whereas all “finite” clusters have been omitted.

At long times when the imperfections of the initial isotope distribution, the finite lateral size of the compartment interface, and the finite time resolution of $26'$ do not matter anymore, the data can be described by a power law as suggested by Eq. (17.37) for $t \ll t_\zeta$. Fitting the exponent of this equation to the long-time data leads to a value $d_w = 2.86$. According to the Alexander-Orbach conjecture [37] this suggests a fractal dimension of $d_f = 1.87$. This result is close to the fractal dimension directly evaluated from the volume averaged porosity separately determined on the basis of a proton spin density map of an object completely filled with light water [53]. Likewise this parameter can be evaluated from the template structure generated on a computer. The two values coincide in the frame of the experimental accuracy. The anomalous diffusion data are thus in accordance with the Alexander-Orbach conjecture, which is of particular interest as an example linking geometrical with dynamical parameters.

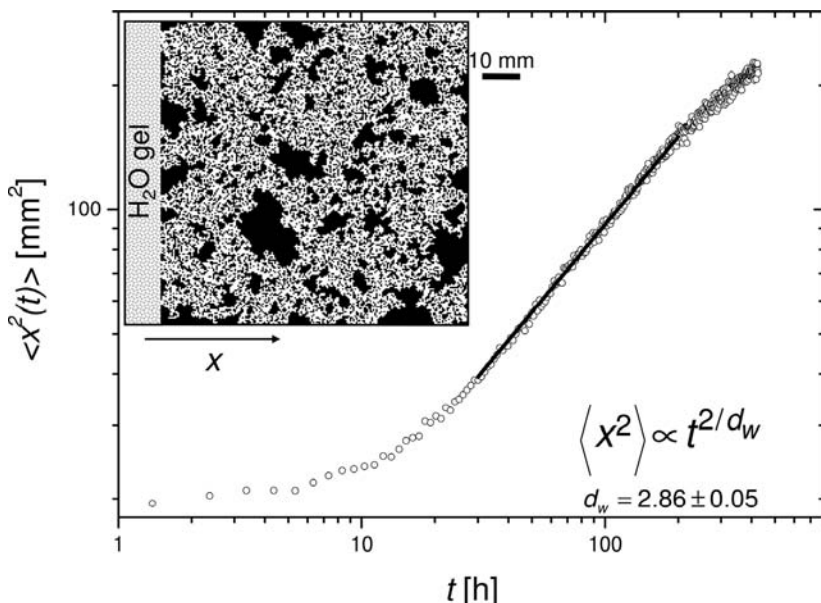


Figure 17.15 Mean-squared proton displacement as a function of diffusion time in a two-dimensional random site percolation object. The inset shows the experimental setup (cross section). The characteristic data of the percolation cluster are: matrix size 200×200 ; occupation probability relative to the threshold value $p - p_c = 0.030$; fractal dimension $d_f = 1.87$; porosity of the percolating cluster $\rho = 0.4845$. The mean-squared

displacement data were evaluated from proton concentration profiles recorded in the form of one-dimensional NMR images along the x -axis. The proton concentration profiles were used to calculate the mean-squared proton displacement in the percolation cluster moiety. The solid line represents a fit of Eq. (17.37) for $t \ll t_\xi$. The fitted exponent parameter is $d_w = 2.86$.

17.4.4

Discussion of the Results for Percolation Clusters

Interestingly, anomalous diffusion was found even for displacements considerably exceeding the correlation length contrary to the expectation according to Eq. (17.37). That is, the crossover to normal diffusion occurs only for times much longer than t_ξ or for root mean-squared displacements much larger than ξ . This finding is in accordance with recent Monte-Carlo simulations [51], where the same conclusion was drawn.

The origin and nature of the anomaly discussed above can be elucidated by treating the problem of diffusion in the pore space of a percolation cluster with Fick's diffusion equation, Eq. ((17.32)), by considering the boundary conditions imposed by the solid matrix. The numerical solution shows good coincidence with the experimental results [4]. The fact that the Fickian diffusion equation, that is microscopically ordinary diffusion, macroscopically leads to an anomalous time dependence of the mean-squared displacement

shows that the origin of the anomaly is due to dead ends and bottlenecks of the percolation cluster where the particles are intermittently trapped. As a consequence, one expects a *non-Gaussian propagator*. An analytical expression can be obtained by solving the fractional diffusion equation [1],

$$\frac{\partial P(x,t)}{\partial t} = {}_0R_t^{1-\kappa} D_\kappa \frac{\partial^2}{\partial x^2} P(x,t), \quad (17.38)$$

where ${}_0R_t^{1-\kappa}$ is the Riemann–Liouville operator and D_κ is the generalized diffusion coefficient which is of dimension $\text{m}^2/\text{s}^\kappa$. Anticipating a given value for the diffusion exponent κ defined in Eq. (17.1), the propagator can analytically be expressed as

$$P(x,t) = \frac{1}{\sqrt{4\pi D_\kappa t^\kappa}} H_{1,2}^{2,0} \left[\frac{x^2}{4D_\kappa t^\kappa} \middle| \begin{array}{c} (1-\frac{\kappa}{2}, \kappa) \\ (0, 1), (\frac{1}{2}, 1) \end{array} \right], \quad (17.39)$$

where $H_{1,2}^{2,0}$ represents the Fox function [1]. In the limit $|x| \gg \sqrt{D_\kappa t^\kappa}$, this expression is approached by the stretched Gaussian

$$P(x,t) \propto \frac{1}{\sqrt{4\pi D_\kappa t^\kappa}} \left(\frac{|x|}{\sqrt{D_\kappa t^\kappa}} \right)^{-(\frac{1-\kappa}{2-\kappa})} \exp \left[-\frac{2-\kappa}{2} \left(\frac{\kappa}{2} \right)^{\frac{\kappa}{2-\kappa}} \left(\frac{|x|}{\sqrt{D_\kappa t^\kappa}} \right)^{\frac{1}{1-\kappa/2}} \right]. \quad (17.40)$$

This is to be compared with the ordinary Gaussian propagator for ordinary, i.e., unrestricted and unobstructed one-dimensional diffusion with the ordinary diffusion coefficient D ,

$$P(x,t) = \frac{1}{\sqrt{4\pi Dt}} \exp \left[\frac{-x^2}{\sqrt{4Dt}} \right]. \quad (17.41)$$

The fractal nature of the confining matrix is expressed by the exponent κ , so that the propagator given in Eq. (17.40) links a structural parameter, κ , with a dynamic one, D_κ . Diffusion on a percolation cluster may be considered as a textbook example for the interrelation between structure and dynamics. The effective propagator must contain elements of both categories.

17.5

General Discussion and Outlook

The molecular diffusometry techniques presented here cover at least 15 decades of the diffusion time. The time scales of the individual methods are schematically shown in Figure 17.16. They were demonstrated with application examples in the range $10^{-9} \text{ s} < t < 1.44 \times 10^6 \text{ s}$. This appears to be

a perfect basis for studies of anomalous transport laws such as the one given in Eq. (17.1). The experimental basis is not a single method but a combination of different protocols derived from a common physical phenomenon, namely nuclear magnetic resonance. The measuring principles are entirely different. At the shortest times from nano- to 100 μ s, it is the intermolecular contribution to spin-lattice relaxation that is exploited for the detection of subdiffusive transport laws. The intermediate time scale from 100 μ s up to seconds, diverse field-gradient methods are suitable. The longest diffusion times beyond seconds can be probed with microimaging techniques rendering the temporal evolution of spatial isotopic distributions.

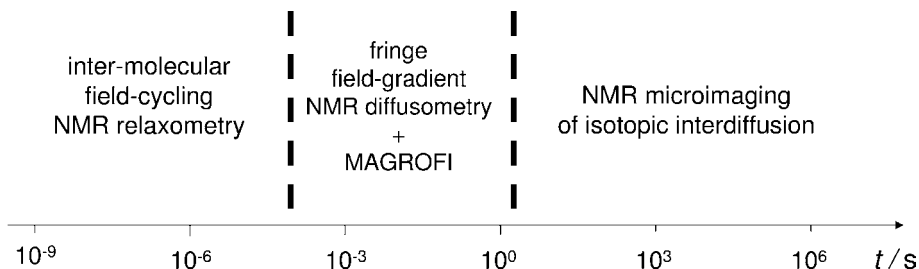


Figure 17.16 Schematic representation of the time scales of the NMR diffusometry techniques considered in this chapter.

The applicability of the diverse methods partially depends on certain conditions the system to be studied must fulfill. The practical examples discussed above therefore refer to different systems and experimental setups. This is a collection of typical data sets as far as they are available in the literature. They refer to bulk polymer melts, liquids in porous glasses, and percolation model clusters. Numerous other systems suitable for this sort of investigation are known and have been studied on a limited time scale predominantly using field-gradient NMR diffusometry [19].

Although not a single study has been reported so far, where the whole time range of molecular diffusion considered here was examined with the same system, there are cases that would be suitable for such investigations. An example is bulk polymer liquids. Apart from the spin-lattice relaxation and field gradient diffusometry studies discussed above, microimaging experiments should be feasible as well. All methodological restrictions mentioned above in the description of the techniques would not matter with polymers or could easily be overcome. This is a perspective promising insight in fundamental aspects of such a complex field as polymer dynamics.

References

- 1 R. Metzler, J. Klafter, Phys. Rep. 339 (2000) 1.
- 2 M. Doi, S. F. Edwards, *The Theory of Polymer Dynamics*, Oxford University Press, Oxford, 1986.
- 3 Y. Li, G. Farrher, and R. Kimmich, Phys. Rev. E 74 (2006) 066309.
- 4 R. Kimmich, Chem. Phys. 284 (2002) 253.
- 5 R. Orbach, Science 231 (1986) 814.
- 6 K. H. Hoffmann, J. Prehl in R. Klages, G. Radons, I. M. Sokolov (Eds.), *Anomalous Transport: Foundations and Applications*, Wiley-VCH, Weinheim, 2007.
- 7 N. Fatkullin, R. Kimmich, Phys. Rev. E 52 (1995) 3273.
- 8 J. Klafter, M. F. Shlesinger, and G. Zumofen, Phys. Today 49 (1996) 33.
- 9 O. V. Bychuk, B. O'Shaughnessy, J. Phys. II 4 (1994) 1135.
- 10 T. Zavada, R. Kimmich, J. Chem. Phys. 109 (1998) 6929.
- 11 R. Valiullin, R. Kimmich, and N. Fatkullin, Phys. Rev. E 56 (1997) 4371.
- 12 K. Hahn, J. Kärger, and V. Kukla, Phys. Rev. Lett. 76 (1996) 2762.
- 13 M. Ylihautala, J. Jokisaari, E. Fischer, and R. Kimmich, Phys. Rev. E 57 (1998) 6844.
- 14 R. Kimmich, W. Doster, J. Polym. Sci., Polym. Phys. Ed. 14 (1976) 1671.
- 15 T. N. Khazanovich, Polym. Sci. USSR 4 (1963) 727.
- 16 P. E. Rouse, J. Chem. Phys. 21 (1953) 1272.
- 17 N. Fatkullin, R. Kimmich, J. Chem. Phys. 101 (1994) 822.
- 18 R. Valiullin, J. Kärger, in: R. Klages, G. Radons, I. M. Sokolov (Eds.), *Anomalous Transport: Foundations and Applications*, Wiley-VCH, Weinheim, 2007.
- 19 J. Kärger, P. Heijmans, and R. Haberlandt (Eds.), *Diffusion in condensed matter*, Vieweg, Berlin, 1998.
- 20 I. Ardelean, R. Kimmich, Ann. Rep. NMR Spectroscopy 49 (2003) 43.
- 21 I. Ardelean, R. Kimmich, Isr. J. Chem. 43 (2003) 9.
- 22 G. Farrher, I. Ardelean, and R. Kimmich, J. Magn. Reson. 182 (2006) 215.
- 23 M. Kehr, N. Fatkullin, and R. Kimmich, J. Chem. Phys. 126 (2007) 094903.
- 24 A. Klemm, R. Metzler, and R. Kimmich, Phys. Rev. E 65 (2002) 021112.
- 25 R. Kimmich, N. Fatkullin, Advan. Polym. Sci. 170 (2004) 1.
- 26 R. Kimmich, *NMR Tomography, Diffusometry, Relaxometry*, Springer, Berlin, 1997.
- 27 R. Kimmich, N. Fatkullin, R.-O. Seitter, and K. Gille, J. Chem. Phys. 108, 2173 (1998).
- 28 R. Kimmich, E. Aneroado, Progr. Nucl. Magn. Reson. Spectr. 44, 257 (2004).
- 29 D. Canet, Progr. Nucl. Magn. Reson. Spectr. 30 (1997) 101.
- 30 B. Simon, R. Kimmich, and H. Köstler, J. Magn. Reson. A 118 (1996) 78.
- 31 G. Farrher, I. Ardelean, and R. Kimmich, submitted for publication.
- 32 M. Sahimi, *Flow and Transport in Porous Media and Fractured Rock*, VCH, Weinheim, 1995.
- 33 J. Koplik, S. Redner, and D. Wilkenson, Phys. Rev. A 37 (1988) 2619.
- 34 H. A. Makse, J. S. Andrade, and H. E. Stanley, Phys. Rev. E 61 (2000) 583.
- 35 R. Kimmich, A. Klemm, M. Weber, and J. Seymour, Mat. Res. Soc. Symp. Proc. 951 (2001) T2.7.1.
- 36 R. Duplay, P. N. Sen, Phys. Rev. E 70 (2004) 066309.
- 37 S. Alexander, R. Orbach, J. Phys. (Paris), Lett. 43 (1982) L625.
- 38 J. Crank, *The Mathematics of Diffusion*, Clarendon Press, Oxford, 1975.
- 39 M. Heidenreich, W. Köckenberger, R. Kimmich, N. Chandrakumar, and R. Bowtell, J. Magn. Reson. 132 (1998) 109.
- 40 A. Spyros, N. Chandrakumar, M. Heidenreich, and R. Kimmich, Macromolecules 31 (1998) 3021.
- 41 C. Kunze, R. Kimmich, Magn. Reson. Imag. 12 (1994) 805.
- 42 A. M. J. Hudson, W. Köckenberger, M. Heidenreich, N. Chandrakumar, R. Kimmich, and R. Bowtell, J. Magn. Reson. 155 (2002) 64.

- 43** R. R. Ernst, G. Bodenhausen, and A. Wokaun, *Principles of nuclear magnetic resonance in one and two dimensions*, Oxford University Press, Oxford, 1987.
- 44** N. Chandrasekharan, R. Kimmich, J. Magn. Reson. 137 (1999) 100.
- 45** C.-Y. Hui, K.-C. Wu, R. C. Lasky, and E. J. Kramer, J. Appl. Phys. 61 (1987) 5129.
- 46** J. Kowalcuk, J. Tritt-Goc, and N. Pislewski, Solid State NMR 25 (2004) 35.
- 47** E. Kossel, R. Kimmich, Solid State NMR 28 (2005) 233.
- 48** D. Stauffer, A. Aharony, *Introduction to Percolation Theory*, Taylor and Francis, London, 1992.
- 49** A. Bunde, S. Havlin (Eds), *Fractals and disordered systems*, Springer, Berlin, 1996.
- 50** Y. Gefen, A. Aharony, and S. Alexander, Phys. Rev. Lett. 50 (1983) 77.
- 51** O. J. Poole, D. W. Salt, J. Phys. A 29 (1996) 7959.
- 52** E. Kossel, M. Weber, and R. Kimmich, Solid State NMR 25 (2004) 28.
- 53** A. Klemm, R. Kimmich, and M. Weber, Phys. Rev. E 63, 041514 (2001).

18

Anomalous Molecular Dynamics in Confined Spaces

Rustem Valiullin and Jörg Kärger

18.1

Introduction

Modern technologies which have decisively contributed to the development of novel, environment friendly routes to value-added products (i.e., products that have increased in value due to processing, here in particular by catalytic reaction or mass separation) are, to a large extent, based on the application of nanoporous materials [1]. These substances are traversed by an internal system of holes and channels with diameters comparable to molecular dimensions. They are key to mass separation [2] by selective adsorption and to mass conversion by heterogeneous catalysis [3,4]. In all these industrial applications, overall performance notably depends on the transport properties of the guest molecules within these materials since the output of the value-added products cannot be faster than allowed by the respective diffusion processes [5,6]. It is due to this reason that modern nanoporous materials often comprise networks of “micro-” (less than 2 nm) and “mesopores” (from 2 to 50 nm) [7]. Similarity between molecular and pore dimensions makes the micropores the preferred locations for molecular conversion and separation. Due to the same reason the rate of molecular propagation within the micropores is dramatically reduced in comparison with the bulk fluid. With pore diameters of the order of several molecular diameters, such a transport inhibition does not occur in the mesopores so that their presence ensures the desired fast transport of the value-added products generated inside the material to the surroundings.

Among the techniques applied to the experimental exploration of molecular transport in nanoporous materials, the pulsed field gradient technique of nuclear magnetic resonance (PFG NMR, also referred to as pulsed field gradient spin echo (PGSE) NMR) has attained an outstanding position [8,9]. The application of PFG NMR notably contributed to our present understanding of the transport phenomena in nanoporous host–guest systems. In parallel to many discoveries of basic relevance for their industrial application, the application of PFG NMR to diffusion studies in nanoporous materials has also

stimulated the research of quite fundamental aspects of molecular diffusion in porous networks.

We are going to highlight some of these transport properties and to illustrate their correlation with the architecture of the confining pore system. Sections 18.2 and 18.3 introduce the various porous materials considered in this chapter and the NMR techniques used in our experiments. Section 18.4 deals with the transport mechanisms in micropores, consisting of sets of either parallel or mutually intersecting channels. The concluding Section 18.5 illustrates the variety of phenomena occurring with molecular ensembles in mesopores. We shall again consider pore networks and pore systems consisting of tailor-made channels. In addition to quite general phenomena of molecular transport in such systems, we shall in particular highlight the influence of phase transitions, considering both freezing and melting, and evaporation and condensation.

18.2

The Materials Under Study

18.2.1

Zeolites

Zeolites are nanoporous crystalline aluminosilicates. As typical examples, Figure 18.1 displays the structure of zeolites of the so-called structure types MFI and AFI. The vertices indicate the positions of the silicon or aluminium atoms, which are connected by oxygen atoms, as schematically represented by the connecting rods. Today, approximately 200 different zeolite structure types are known [10]. Their number increases essentially into an uncountable number if one considers the variations brought about by varying the content of cations and by replacing the silicon or aluminium atoms by other lattice atoms like phosphorous, boron, titanium, and gallium. As an example, Figure 18.2 illustrates the effect of such structures, namely that of MFI-type zeolites, on the propagation properties of guest molecules. Since the smaller (five- and six-membered) rings are impenetrable for most of the molecules under consideration, the zeolite structure may be represented by an array of mutually intersecting straight and sinusoidal channels. By contrast, already from Figure 18.1(b) zeolites of the type AFI are found to represent arrays of parallel (i.e., nonintersecting) channels.

The great industrial relevance of zeolites results from the coincidence of a number of remarkable features. They include their well-defined pore size being of the order of typical molecular dimensions, their internal reactivity, their thermal and chemical durability and their cation content. Today, owing to these properties, zeolites find widespread application as catalysts [3, 4], deter-

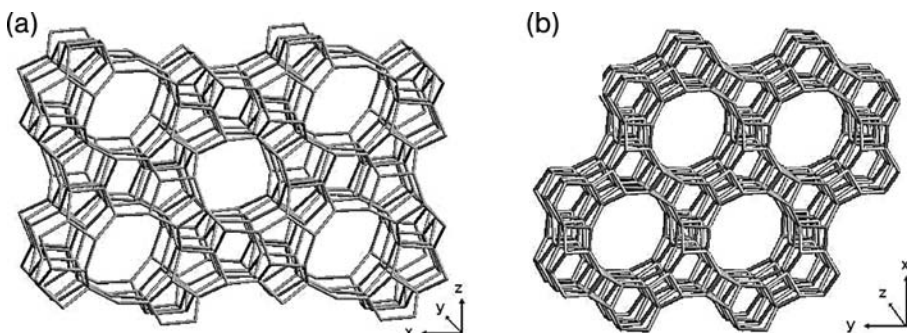


Figure 18.1 Crystallographic structure of (a) MFI- and (b) AFI-type zeolites viewed along [010] and [001] directions, respectively.

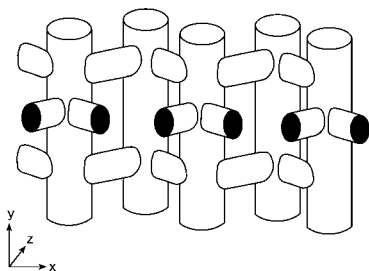


Figure 18.2 Schematic representation of the MFI-type zeolite structure in Figure 18.1(a).

gent additives [11], selective adsorbents (“molecular sieves”) [1, 2], hosts for optoelectronic devices [12, 13], and in many other areas of the economy. Estimates about the benefit provided by the use of zeolites attain the order of hundreds of billions Euro per year. Impressive kaleidoscopes of the multifarious use of zeolites are provided by the International Zeolite conferences which regularly unite a thousand users and researchers in the field [14, 15].

18.2.2

Mesoporous Glass and Silica

Vycor porous glass [16], which is a typical representative of porous glasses with random pore structure, is among the materials most commonly applied for fundamental research [17, 18]. It is produced using a spinodal phase separation with subsequent removing of one of the phases. Intrinsic properties of the spinodal decomposition process result in an interconnected network of pores characterized by a narrow pore size distribution. Structural characterization of this material has been a subject of numerous studies, and relevant information may be found elsewhere [19–21]. Here we only note that a typical pore size is of about 5 nm, with about 96% of the pores within an interval

of ± 0.3 nm around the average radius [16] and the porous network is often referred to as being random, e.g., exhibiting topological and morphological disorder.

In contrast to porous glasses and their relatives, which accommodate a pore network of random architecture, the recently introduced method of electrochemical etching (anodizing) of single crystalline (100) oriented p-type silicon wafers provides us with porous materials traversed by channel-like mesopores [22, 23]. By an appropriate choice of the dopant concentration (i.e., the resistivity) in the starting material (the silicon wafers), the electrolyte composition, and the anodization current, mesoporous silicon with the desired channel diameter may be produced. Moreover, a periodic variation of one of these properties, usually an appropriate time variation of the anodization current, allows modulation of the porosity or, associated with it, channel diameter along the channel axis [24, 25]. These materials are often referred to as silicon superlattices [26]. As an example, Figure 18.3 provides a typical example of the pore profile attainable in this way (top panel) and an SEM micrograph perpendicular to the wafer surface (bottom panel). It reveals a well-defined periodic structure with layers, characterized by specific channel diameters.

18.3 NMR Fundamentals

18.3.1

The Phenomenon and Measurement of Concentration

Nuclear magnetic resonance (NMR) provides direct access to the key data of fluid dynamics in porous space: it is able to simultaneously record the number of molecules in the different states of mobility and their translational mobility. The way in which this crucial information becomes accessible may be rationalized using the classical interpretation of nuclear magnetism [5, 8, 9, 27], which is based on the fact that a nucleus (nuclear “spin”) combines the properties of a magnetic dipole (i.e., an elementary magnet) and a gyroscope.

Hence, under the influence of a magnetic field of intensity B_0 , each nucleus performs a precessional motion about the direction of B_0 , with the frequency

$$f = \frac{\omega}{2\pi} = \frac{\gamma B_0}{2\pi}, \quad (18.1)$$

where γ ($= 2.675 \times 10^8 \text{ T}^{-1}\text{s}^{-1}$ for protons) is known as the gyromagnetic ratio and represents a fundamental quantity for the particular nucleus.

By the application of an intense radiofrequency field of this frequency over a well-defined short interval of time (a so-called $\pi/2$ pulse), each of these elementary magnets, and hence also their vector sum, is turned from the direc-

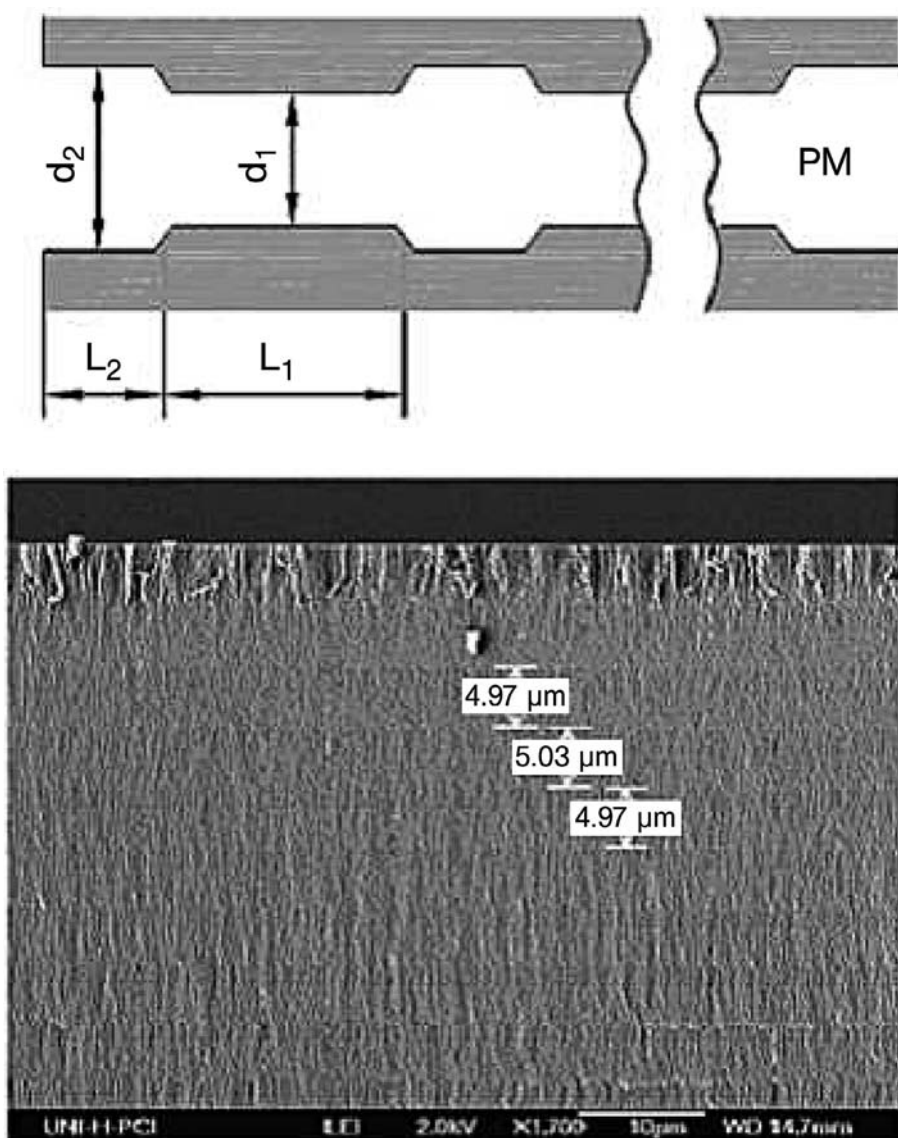


Figure 18.3 (Top figure) 2D representation of the pore section in the porous silicon obtained by modulation of the anodization current density. For highly doped silicon crystals we are working with, the pore diameters d_1 and d_2 could be varied in a range from about 5 to 10 nm. The channel lengths L_1 and L_2 have a lower limit of about 100 nm and an

upper limit given by the initial silicon wafer thickness, which is typically of about 500 μm . (Lower figure) SEM micrograph parallel to the wafer surface displaying a well-defined periodic structure due to the different porosities in the layers. The regions with different porosities consist of pores with different channel diameters.

tion of the magnetic field (the equilibrium position) into the plane perpendicular to it, giving rise to a macroscopic, rotating magnetization. In the receiver coil, surrounding the sample under consideration, this varying magnetization generates an radiofrequency voltage which is monitored as the NMR signal. Obviously, the intensity of this signal is proportional to the number of spins and thus to the number of molecules in the sample.

Information on the state of the molecules under consideration may be deduced from the speed of the relaxation process by which the observed NMR signal disappears, i.e., by the time constant of the decay of the magnetization perpendicular to the external magnetic field toward its equilibrium value, namely to zero. This phenomenon is referred to as the free induction decay. In solids, the time constant of the free induction decay (the transverse nuclear magnetic relaxation time) is typically on the order of a couple of microseconds, while the averaging of the mutual interaction in fluids leads to a notable enhancement of the relaxation times into the range of milliseconds and above. Thus, just by measuring the respective signal intensities, both the absolute number of molecules (from the signal intensity) and their state of mobility (namely fluidity for large and rigidness for short decay constants) becomes directly accessible.

18.3.2

Diffusion Measurement

For rationalizing the way in which the translational mobility of the fluid molecules may even be quantified, we consider the influence of field inhomogeneities on the “resonance frequencies” f of the nuclear spin system under study. Applying, e.g., a magnetic field linearly increasing in the z -direction, $B = B_0 + gz$, with Eq. (18.1) the resonance frequency becomes a function of the z -coordinate

$$2\pi f(z) = \gamma B_0 + \gamma g z. \quad (18.2)$$

Let us recollect that the intensity of a signal is proportional to the contributing spins. In view of Eq. (18.2), this statement means that the number (density) of spins at position z is proportional to the intensity of the NMR signal observed at the resonance frequency $f = \gamma(B_0 + gz)/(2\pi)$. This direct correlation between the intensity of the signal (the “NMR spectrum”) at frequency f and the number density of spins (in general protons; considering human tissues, e.g., water molecules) at that position z which, via Eq. (18.2), corresponds to the considered frequency, is the basis of NMR imaging [8, 9, 27]. Generally referred to as MR tomography, it is currently among the most powerful tools of medical diagnosis.

Information about molecular dynamics within the system under study becomes accessible by the twofold application of an additional magnetic field

with a large gradient. In a simplistic way one might argue that in this way one may become sensitive to the difference of the locations of the individual molecules at the instants of the gradient pulses rather than to the locations themselves. In the basic version of pulsed field gradient NMR the sample is subjected to two “pulsed field gradients” of duration δ at separation t in addition to the constant magnetic field. Implementing these field gradient pulses into an appropriate sequence of radiofrequency pulses, one is able to determine an NMR signal (the so-called spin echo). It may be shown that the attenuation $\psi(g\delta, t)$ of the signal intensity under the influence of the field gradient pulses [28],

$$\psi(g\delta, t) = \int P(z, t) \cos(\gamma\delta z) dz, \quad (18.3)$$

is nothing else than the Fourier transform of the so-called mean propagator $P(z, t)$, one of the key functions describing the internal dynamics in complex systems [29]. $P(z, t)$ denotes the probability density that, during time t , an arbitrarily selected molecule (with a nuclear spin contributing to the observed NMR signal) is shifted over a distance z , i.e., in the direction of the applied field gradient. In principle, the direction of the field gradient (and hence of the z -axis) may be arbitrarily chosen. In most cases, however, it is parallel to the axis of the NMR sample tube (in general, cylinders of typically 5–10 mm diameter and with a filling height of 10 mm), since in this way largest gradient amplitudes (and, correspondingly, largest spatial resolutions) are attained. The observation times t are of the order of milliseconds up to seconds. Typical molecular displacements observable by PFG NMR are on the order of a few micrometers, with minimum values below 100 nm [30–32]. As a disadvantage in comparison with other spectroscopic techniques, NMR has to operate with relatively high concentrations. Typical lower values are on the order of one hydrogen nucleus per 10 nm^3 which corresponds to about 0.1 moles per liter. Current research tries to counteract these deficiencies by either the use of hyperpolarized nuclei [33, 34] or by the application of ultra-high magnetic fields [35].

For unrestricted, normal diffusion, by assuming an initial concentration given by Dirac's δ function, the propagator results as the solution of Fick's second law:

$$P(z, t) = \frac{1}{\sqrt{4\pi Dt}} \exp \left\{ -\frac{z^2}{4Dt} \right\}, \quad (18.4)$$

with D denoting the self-diffusivity. Completely equivalently [36], D may be considered to be defined by Fick's first law as the factor of proportionality between the flux density of labeled molecules and their concentration gradient or by Einstein's relation

$$\langle z^2(t) \rangle = 2Dt \quad (18.5)$$

indicating proportionality between the molecular mean square displacement and the observation time. With this relation, Eq. (18.4) may also be noted as

$$P(z, t) = \frac{1}{\sqrt{2\pi \langle z^2(t) \rangle}} \exp \left\{ -\frac{z^2}{2 \langle z^2(t) \rangle} \right\}. \quad (18.6)$$

Inserting Eq. (18.4) into (18.3) yields

$$\psi(g\delta, t) = \exp \left(-\gamma^2 \delta^2 g^2 D t \right) = \exp \left(-\gamma^2 \delta^2 g^2 \langle z^2(t) \rangle / 2 \right), \quad (18.7)$$

where, with the second equation, we have used Eq. (18.5). Thus, the diffusivity (and the mean square displacement, respectively) may be easily determined from the slope of the semilogarithmic representation of the intensity of the NMR signal (the spin echo) versus the squared pulse gradient “intensity” (δg).

Often, as a useful approximation, Eq. (18.7) may be assumed to hold when molecular propagation deviates from normal, unrestricted diffusion. In such cases, the second equality of Eq. (18.7) is the essential one and the quantity D has to be interpreted as an “effective” diffusivity defined by Eq. (18.5) (which clearly coincides with the real diffusivity as soon as the prerequisites of normal diffusion are fulfilled).

18.4

Diffusion in Channel Micropores

18.4.1

Single-File Diffusion

Molecular ensembles confined to channels with diameters small enough to prevent the mutual passage of guest molecules have been recognized as ideal host systems for investigating a special type of anomalous molecular dynamics referred to as single-file diffusion [37,38]. One may easily rationalize that, in contrast to the dependence represented by Eq. (18.5), in such systems the molecular mean square displacement increases less than linearly with increasing observation time. As a mean prerequisite, normal diffusion and hence Eq. (18.5) imply that at least for sufficiently large observation times, subsequent molecular displacements are uncorrelated. In sufficiently largely extended single-file systems, however, this is not the case anymore. Since molecular displacements into a given direction are only possible if all the other molecules “in front” of the given diffusant are as well shifted into this direction, any molecular shift implies that, in general, the molecular density “in front” of this diffusant is larger than “behind.” As a consequence, displacements in a given direction are more likely to be followed by displacements

into the opposite direction than into the same direction. Assuming, e.g., that molecular propagation proceeds by jumps of length λ with a mean time τ between subsequent jump attempts and that jump attempts are only successful if they are directed to a vacant site, one may derive [37–39]

$$\langle x^2(t) \rangle = 2F\sqrt{t} \quad (18.8)$$

with

$$F = \lambda^2 \frac{1-\theta}{\theta} \frac{1}{\sqrt{2\pi\tau}}, \quad (18.9)$$

where θ is the mean occupation probability of the channel sites (i.e., the mean pore-filling factor). It may be shown [40] that under single-file conditions the propagator is exactly given by the same relation, Eq. (18.6), which also holds for normal diffusion. The difference between the two modes of propagation appears in the different time dependencies as indicated by Eqs. (18.5) and (18.8), respectively.

In view of the pore architecture displayed by Figure 18.1(b) it was not unexpected, therefore, that for sufficiently large molecules (e.g., CF₄) PFG NMR diffusion studies with AlPO₄-5 as a host system revealed mean square displacements increasing linearly with the square root of the observation time rather than with the observation time itself [41–43]. In the meantime, however, real zeolite crystals have been repeatedly found to deviate notably from their ideal textbook structure. This turned out to be particularly true for zeolites of type AFI (like the just considered AlPO₄-5) [44, 45] so that, in addition to the influence of single-file restriction, deviations from normal diffusion are most likely also caused by transport resistances (either on the external surface or in the intracrystalline space) acting in addition to the drag exerted by the genuine pore network [46]. This problem has been found to hold quite generally for numerous zeolite specimens where a minute observation of the internal transport processes, in particular by means of the recently introduced interference microscopy [47, 48], revealed quite dramatic deviations from the patterns to be expected for defect-free solids. Thus, one of the most pressing challenges of current diffusion research in microporous materials is to obtain the zeolite specimen of perfect crystal structure.

18.4.2

Molecular Transport in Intersecting Channels

18.4.2.1 Correlated Diffusion Anisotropy

The by far largest fraction of zeolite structure types exhibit three-dimensional pore networks [10]. In many cases, the topology of the pore space may be characterized as an array of mutually intersecting channels. A most important

representative of this structure type is zeolites of type MFI. Figure 18.2 illustrates that their pore space is formed by mutually intersecting straight (in crystallographic y -direction) and sinusoidal (in the crystallographic x -direction) channels. Although there is no corresponding third channel system, molecular propagation is also clearly possible in the z -direction. Obviously, displacements in the z -direction imply subsequent shifts along segments of the straight and sinusoidal channels. Since the latter shifts, simultaneously, effect displacements into the x - and y -directions, the rate of propagation into different directions may be expected to be not independent from each other. In fact, in [49,50] this effect of correlated diffusion anisotropy has been shown to lead to the simple relation

$$\frac{c^2}{D_z} = \frac{a^2}{D_x} + \frac{b^2}{D_x} \quad (18.10)$$

between the principal elements of the diffusion tensor. a , b and c denote the unit cell extensions in the x -, y - and z -direction. Equation (18.10) holds exactly under the supposition that molecular propagation from one channel intersection to another may be considered as an ideal random walk. This means that molecular displacements from a given intersection to the subsequent one are independent from the direction, along which this intersection has been entered. In other words, the molecular "memory" is shorter than the mean traveling time from intersection to intersection. Considering small molecules like methane and CF_4 as diffusants, Eq. (18.10) has been found to be nicely reflected by the results of both MD simulations [51–53] and experimental measurement [54,55]. For longer molecules, like 1-butene, molecular trajectories are more appropriately described by a sequence of displacements from one channel segment to another [56]. In this case, simple correlation rules of diffusion anisotropy of the type of Eq. (18.10) cannot be derived anymore.

With the advent of MFI-type zeolites, researchers are fascinated by the option that the existence of different channel types within one and the same material may be used for an enhancement of the performance of chemical reactions. Obviously, the output of the desired components in heterogeneous catalysis can never be faster than allowed by the speed of transportation of the involved components within the catalyst particles. Since the diffusion streams of the reactant and product molecules are opposite to each other, they mutually reduce their rate of propagation. Hence, their direction to different channels may notably reduce this effect of mutual impediment and may notably contribute to performance enhancement. Thus, the idea of reactivity enhancement by "molecular traffic control" [57, 58] has meanwhile also become an interesting subject of fundamental physical research [59–62].

18.4.2.2 Anomalous Diffusion due to Deviation from Ideal Crystallinity

With Figure 18.4 we once again refer to the divergence between the textbook structure of zeolites and their real habit [63,64]. The figure displays the results of PFG NMR diffusion measurements with *n*-butane in silicalite-1 at different temperatures. The diffusivities resulting, via Eq. (18.7), from the measured spin echo attenuations are plotted as a function of the mean displacements over which these diffusivities have been measured. These displacements are correlated with the diffusivities as plotted in Figure 18.4 and the diffusion time via Eq. (18.5). The decrease in the diffusivities with increasing displacements indicates the existence of internal transport resistances (intracrystalline barriers, e.g., due to stacking faults) which act in addition to the transport resistance exerted by the genuine zeolite pore system. The full lines in Figure 18.4 indicate that the observed dependence may be generated by means of a quite simple model. It is based on the assumption that the crystal is traversed by equidistant barriers with a mutual separation of 3 μm. In comparison with Monte-Carlo jumps for generating genuine intracrystalline diffusion, the activation energy for jumps across these barriers has been enhanced by 21.5 kJ/mol. In this way, the simulation exactly reproduces the main features of these experimental studies, namely the approach of the true diffusivities

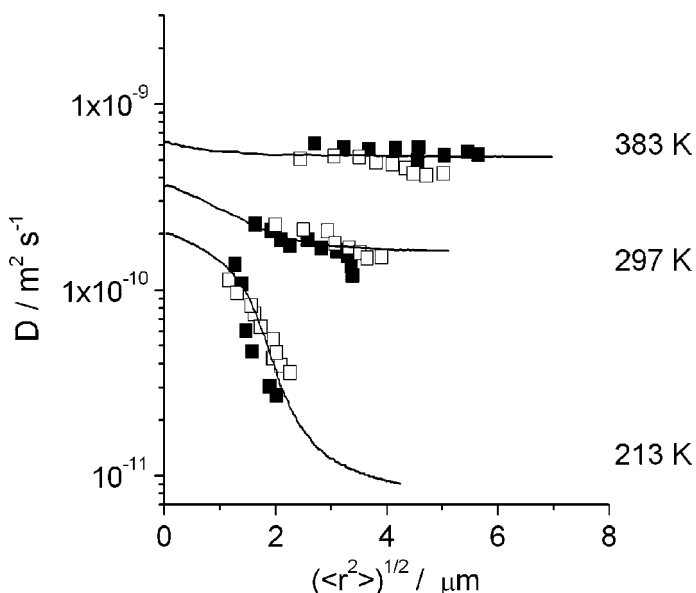


Figure 18.4 Dependencies of the diffusion coefficients on the root mean square displacements at different temperatures measured by using PFG NMR (points, two series of experiment) and determined in dynamic MC simulations (lines) for *n*-butane in silicalite-1.

for both sufficiently small displacements (i.e., correspondingly small observation times) and sufficiently high temperatures (when – owing to their thermal energy – the diffusants may easily overcome the assumed energy barrier).

18.5

Molecular Dynamics in Mesopores

18.5.1

Dynamics in Random Pore Spaces

18.5.1.1 Hysteresis Dynamics

Though known since a century [65], the phenomenon of adsorption hysteresis is still a subject of controversial discussion [66–69]. Only very recently, NMR has been recollected and applied as a powerful tool to contribute to an eventual clarification of the underlying phenomena. This potential is particularly based on the ability of NMR to simultaneously measure both the molecular concentrations and diffusivities.

As an example, Figure 18.5 displays the results of such combined NMR measurements with cyclohexane in a Vycor porous glass [69]. The amount adsorbed in Figure 18.5(a) exhibits the typical pattern of adsorption hysteresis: following the “adsorption branch,” i.e., by gradually enhancing the cyclohexane pressure P in the surrounding atmosphere, the amount adsorbed is also found to gradually increase until (already below saturation pressure) the whole pore space is filled by “capillary condensation.” Following the desorp-

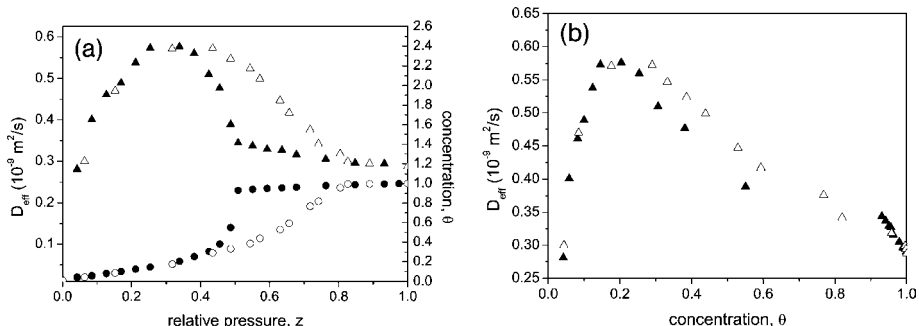


Figure 18.5 (a) The adsorption and desorption isotherms (circles, right axis) and the effective diffusivities D_{eff} (triangles, left axis) for cyclohexane in Vycor porous glass as a function of the relative pressure $z = P/P_s$ (P_s is the saturated vapor pressure) on the adsorption (open symbols) and the desorption (filled symbols) branches. (b) D_{eff} plotted as a function of the amount adsorbed θ measured during adsorption (open symbols) and desorption (filled symbols).

tion branch one observes that capillary condensation is preserved even after a notable reduction of the gas phase pressure, until, eventually, desorption and adsorption follow the same dependence. From this pressure, down to zero, molecular ad- and desorption will be completely reversible. Within the loop formed by the ad- and desorption branches, however, in addition to the given pressure, the actual state is also found to depend on the "past". In analogy to magnetism, this phenomenon is therefore referred to as hysteresis.

Obviously, in the hysteresis loop, for one and the same pressure, two different states (characterized by vastly differing concentrations) may be maintained over extended intervals of time. Hence, they have to represent local minima in the free energy of the system [70]. By the application of pulsed field gradients, the NMR technique is also able to monitor the mobility of the molecules in the pores. The resulting diffusivities are also shown in Figure 18.5(a). Not unexpectedly, at a given pressure, the diffusivities on the adsorption branch notably exceed those on the desorption branch [71]. This is a simple consequence of the fact that, on the desorption branch, all channels are blocked while, during adsorption, they are still open and accessible by fast molecular movement in the gas phase.

The most remarkable information, however, is provided by combining the data in Figure 18.5(a) to the presentation of the diffusivity as a function of the total amount adsorbed (concentration or pore-filling factor θ) as provided by Figure 18.5(b). It turns out that, for one and the same total loading, the diffusivity, i.e., the rates of molecular propagation through the pore space, may notably differ from each other. Thus, the molecular diffusivity within the system appears as a valuable indicator of the given state. Note that, irrespective of fast molecular movement within the system, the two states are preserved over appreciable intervals of time. Though the two states are formed with identical numbers of molecules, their diffusivities are found to be different. This, clearly, has to be attributed to the different arrangement in space. Thus, in turn, the diffusivity may serve as an indicator of the given state of molecular arrangement.

In immediate correlation with this consideration are the experimental results shown in Figure 18.6. The experimental points indicate the molecular uptake (in fractions of total pore filling) by a well-shaped body of Vycor porous glass initiated by an enhancement of the pressure in the surrounding atmosphere of cyclohexane from 40 to 45 mbar (Figure 18.6(a)) and from 70 to 75 mbar (Figure 18.6(b)), respectively. Comparison with Figure 18.5(a) reveals that the first uptake process covers a pressure range far below the range of hysteresis, while the uptake shown in Figure 18.6(b) occurs under hysteresis conditions. The full lines in Figure 18.6 represent the theoretical uptake curves calculated on the basis of the measured diffusivities (Figure 18.5, adsorption branch) from the analytical expression of molecular uptake for the cylindrical

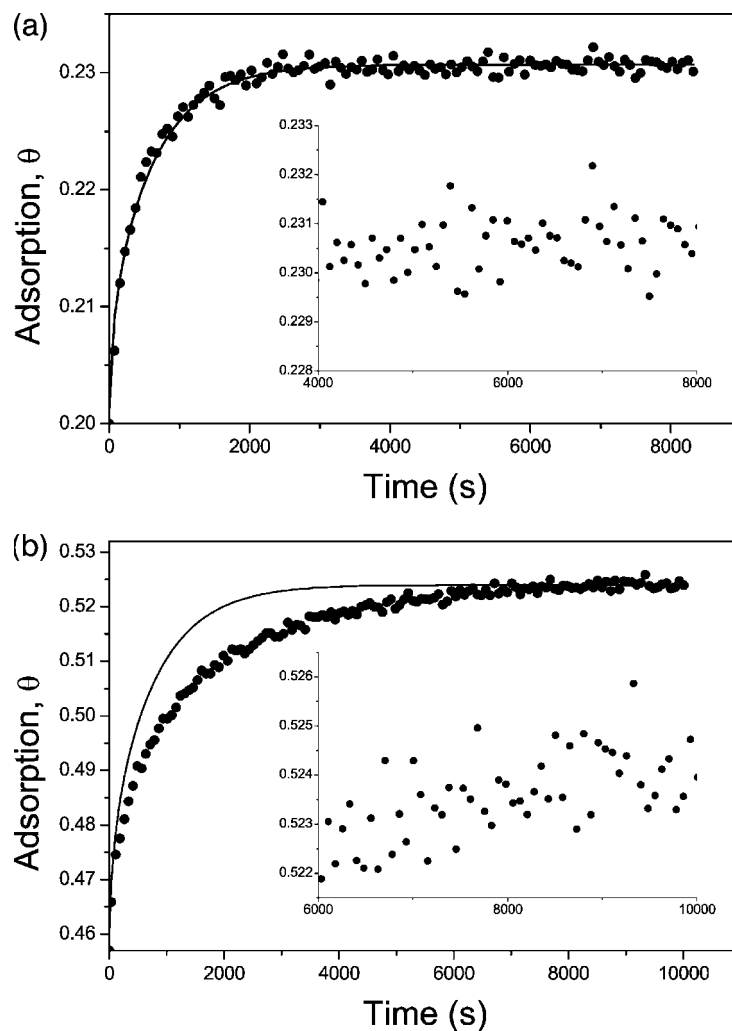


Figure 18.6 Adsorption kinetics data (points) obtained upon step-wise change of the external vapor pressure from (a) 40 mbar to 45 mbar (out of hysteresis regime) and (b) 70 mbar to 75 mbar (hysteresis regime). In the insets the long-time part of the same data are shown. The solid lines show the calculated kinetics curve assuming that the uptake is solely controlled by diffusion.

geometry of the monolithic Vycor particle [69,72]

$$\theta(t) = \left(1 - \frac{4}{a^2} \sum_{n=1}^{\infty} \frac{1}{\alpha_n^2} \exp\{-\alpha_n^2 D t\} \right) \quad (18.11)$$

with a representing the radius of the cylindrical particle, α_n the positive roots of the equation $J_0(\alpha_n(a)) = 0$, and J_0 the Bessel function of the first kind. The

excellent agreement between the measured uptake curve and the theoretical prediction in the reversible region of the adsorption isotherm (Figure 18.6) nicely reflects the self-consistency of the experiments. Following this line of argument, also the striking discrepancy between the measured molecular uptake and its prediction on the basis of the molecular diffusivities is in complete agreement with the above discussion of diffusion hysteresis in Figure 18.5(b). The stable existence of states, traversed on the hysteresis loop, is only possible if there is some ordering effect in the system. In the systems under consideration such effects typically result as a consequence of the competing interaction of the molecules with each other and with the pore walls. Thus, depending on the history, quite different molecular configurations may remain stable over long time intervals, irrespective of the fast movement of individual guest molecules within these configurations. With the present study, for the first time direct experimental evidence on the transport phenomena in the metastable states during sorption hysteresis could be provided. It turns out that the thus prepared quasiequilibrium molecular configurations exhibit very slow relaxation toward equilibrium [69]. This provides a novel random-field system whose dynamical features may be probed by using NMR and further mapped onto existing theoretical approaches [73–75].

18.5.1.2 Deviations from the Arrhenius Dependence

A rather special effect of anomalous diffusion in mesoporous materials is associated with the fact that, depending on temperature and external vapor pressure, diffusion within the pore network may occur via different mechanisms, including diffusion in the liquid bulk phase, surface diffusion, and Knudsen diffusion [76] through the free pore space. In addition, all these mechanisms are subject to some retardation which is referred to as the effect of tortuosity and takes into account that, in general, the solid matrix of the material leads to a prolongation of the diffusion paths in comparison with the bulk phase [17, 77, 78]. We are going to demonstrate that this situation may lead to quite irregular temperature dependencies of the measured diffusivities and hence to completely wrong interpretations if the resulting “energies of activation” are correlated with some real activation mechanism.

Figure 18.7 displays the diffusivities measured with two samples of Vycor porous glass, loaded with *n*-pentane [79]. The samples were sealed. In one sample the amount of *n*-pentane was just sufficient to fill the pore space at the starting temperature of the experiments ($T = 234\text{ K}$), while the other sample contained *n*-pentane in excess, guaranteeing that the pore space remained filled with liquid *n*-pentane up to the largest temperatures considered. The data shown in Figure 18.7 refer only to the pore space. Not unexpectedly, in the overloaded sample the diffusivities nicely follow the Arrhenius behavior indicating that, in the considered temperature range, the system does not

undergo any disruption in the course of the experiment. By contrast, starting from a temperature of about 295 K, the diffusivities in the other sample notably deviate from the Arrhenius dependence toward larger values. The broken line in Figure 18.7 is the result of a model calculation. It is implied that the molecules, on their diffusion paths as observed in the PFG NMR experiments, undergo all modes of propagation. Recollecting that the observable displacements are typically on the order of micrometers, this assumption is clearly fulfilled. Most interestingly, the simulations may exclusively be based on experimentally accessible data (temperature dependence of fluid density, total pore space volume, mean pore diameter). Thus, with neither the need nor the option for any fitting, the model calculations are in perfect agreement with the experimental data. The increasing slope in the Arrhenius plot of Figure 18.7 with increasing temperature (which might erroneously be attributed to some emerging, novel activation mechanism) is thus found to be a simple consequence of the progressive formation of free space in the pore system leading to a promotion of molecular transport due to the increasing mean free paths.

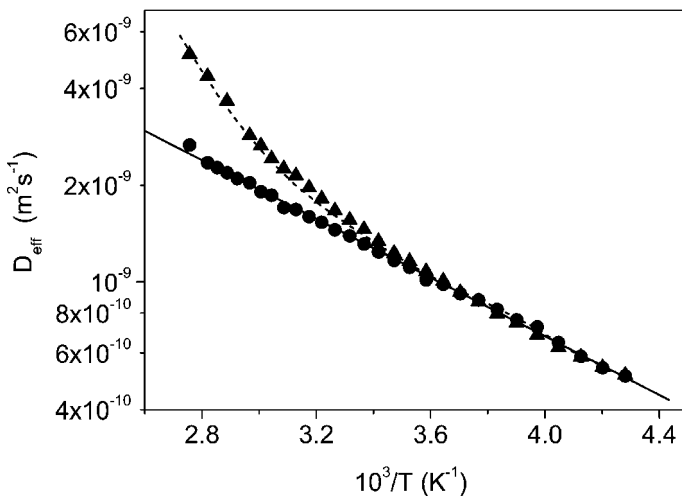


Figure 18.7 Effective intrapore diffusion coefficients of *n*-pentane in Vycor porous glass for the sample with excess bulk liquid (filled circles) and for the sample without excess liquid phase (filled triangles). The solid line shows fit of the Arrhenius equation $D = D_0 \exp\{-E/RT\}$ to the data shown by circles. The broken line shows the result of a model calculation (free of any fitting parameters).

It is noteworthy to add that this perfect agreement did only result by implying that, under the given situation, the effect of tortuosity on Knudsen diffusion may be neglected. One may rationalize this assumption by recollecting that a molecule passing the free space within a channel from wall to wall will,

most likely, continue its diffusion path within the layer of guest molecules on the pore wall. Hence, as in unrestricted space, subsequent molecular displacements through the gas phase will be uncorrelated.

With further increasing temperatures the experimentalist will be rewarded with the occurrence of two further phenomena. Operating with closed samples, the temperature increase will continuously enhance the number of molecules in the gas phase, at the expense of the molecules within the pore system. Obviously, this lack of molecules may lead to a distinction of regions of high and low concentration within the pore space which appears in the observation of restricted-diffusion phenomena. Finally, the fluid phase within the sample attains the supercritical state. Most interestingly, the transition into this state occurs at notably smaller temperatures in the pores than in the bulk. The effect of this transition on the observed mobilities, however, is much more pronounced in the bulk phase than in the pore space, as a simple consequence of the confinement of the molecular mean free path by the pore walls. Both phenomena are in the focus of our present activities.

18.5.2

Molecular Dynamics in Channel Pores

18.5.2.1 Molecular Diffusion on Surfaces

The advent of porous silicon wafers with a well-defined cylindrical pore structure (see Figure 18.3 and consider pores with a uniform radius) opened a novel field of diffusion research, namely the option to measure molecular diffusion on silicon surfaces. It is true that also PFG NMR diffusion studies of guest molecules in zeolites, as presented in Section 18.4, focus on the study of molecular propagation under the perpetual influence of a pore wall. However, during this type of propagation (referred to as zeolithic or configurational diffusion) the diffusants experience the force field of the pore walls from essentially all directions. In mesoporous silicon, however, the pore sizes notably exceed the diameters of the typical diffusants (such as acetone and cyclohexane) used in our studies, so that – at loading below one monolayer and for sufficiently low temperatures – the diffusing molecules are attached to an essentially infinitely extended surface. As a consequence of the relatively poor sensitivity of NMR spectroscopy, this type of measurement would be impossible on plain surfaces. The large internal surface of the porous silicon samples, however, allows the application of diffusants at sufficiently high sample densities so that these measurements become possible.

As an example of this type of measurement, Figure 18.8 displays the diffusivity data of *n*-heptane on the internal surface of silicon wafers with straight channel pores. The increase of the diffusivities with increasing loading (Figure 18.8(a)) is in total agreement with the fact that the activation energy of

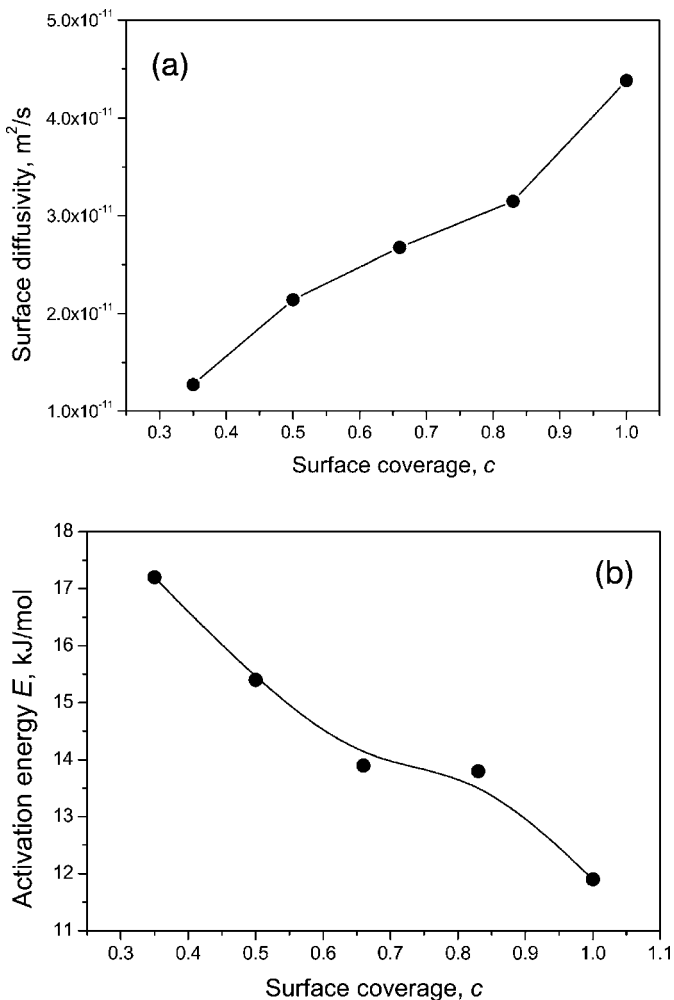


Figure 18.8 Surface diffusivity at 200 K (a) and activation energies for diffusion (b) of *n*-heptane in porous silicon as a function of the surface coverage. Lines are shown to guide the eye.

diffusion decreases with increasing loading (Figure 18.8(b)). At small loadings, molecules will preferentially reside on surface positions with the lowest potential energy, which corresponds to low diffusivities and high energies of activation. With increasing loading, also the positions with higher potential energies will be occupied, leading to increasing diffusivities and decreasing activation energies. Conceptually, molecular diffusion on the silicon surface is thus understood as a random walk through an irregular potential landscape [38]. In contrast to the situation considered in the context of the high-temperature region of the diffusivity data shown in Figure 18.7, it is now

justified to correlate the observed activation energy with the height of the energy barrier which the molecules have to overcome on their diffusion path. Reconstructing energy landscapes [80] on the basis of complete sets of the temperature and loading dependence of the surface diffusivities is among the challenging tasks for the future.

18.5.2.2 Freezing and Melting

The very special channel architecture attainable with porous silicon has opened up a novel route of exploring the dynamics of melting and freezing under confinement. Figure 18.9 provides an example of such studies with porous silicon of different channel geometry, namely straight channels with diameters of 5.6 nm (Figure 18.9(b)) and of 7.5 nm (Figure 18.9(c)), and channels with diameters alternating between 5.6 and 7.5 nm (Figure 18.9(a)). The material with the straight channels is the same which has been considered in Section 18.5.2.1. The material with alternating channel diameters is illustrated by Figure 18.3. The channels have been saturated with nitrobenzene. Figure 18.9 displays the relative amount of liquid molecules upon cooling down (i.e., freezing, open symbols) and warming up (i.e., melting, filled symbols) of the system [25]. As described in Section 18.3.1, this type of information is directly provided by the NMR signal intensity. The data reflect the well-known fact that, under confinement, the temperatures of freezing and melting (5.6 °C for the bulk) are shifted to lower values [66]. Correspondingly, for the smaller channels (Figure 18.9(b)) this shift is found to be more pronounced than for the larger channels (Figure 18.9(c)). As a most prominent feature, a significant difference between the melting and freezing curves is observed, indicating that, upon temperature reduction, the system remains in the liquid state even at those temperatures where, upon heating, the fluid was frozen. Freezing is said to be inhibited. In the literature two mechanisms are considered which may initiate the phase transition from the liquid to the frozen state on cooling, namely the propagation of a solid front into the pore or a nucleation process within the pore [81].

In freezing/melting experiments with channels of the geometry shown in Figure 18.3 we may decide, which freezing mechanism dominates in the given pore system. The porous silicon under consideration (Figure 18.9(a)) is traversed by channels with varying diameters. They are chosen to alternate between the two channel diameters considered in Figures 18.9(b) and 18.9(c). The full line shown in Figure 18.9(a) indicates the temperature dependence of the relative amount of fluid molecules determined from the data of Figures 18.9(b) and 18.9(c) under the assumption that the freezing behavior in the channel segments would coincide with the freezing behavior of the straight channels considered for Figures 18.9(b) and 18.9(c). The observed freezing curve, however, is in striking contrast to this prediction. As a consequence,

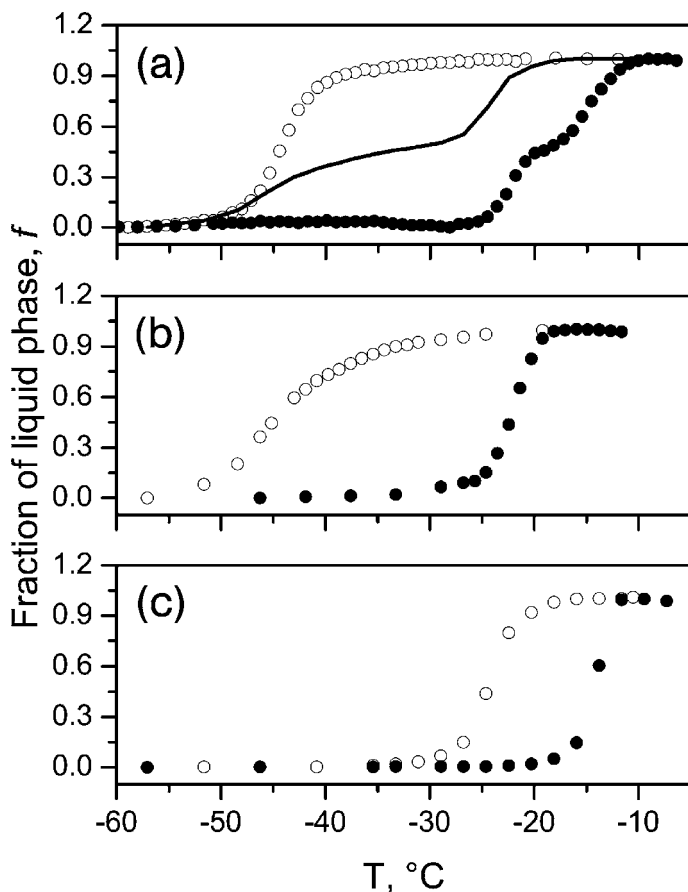


Figure 18.9 Freezing (open symbols) and melting (filled symbols) transition of nitrobenzene in the porous silicon samples with channel-like pores with (i) uniform diameters of 5.6 nm (b) and 7.5 nm (c) and with (ii) diameters alternating between 5.6 nm and 7.5 nm (a).

freezing within the systems under study cannot be considered as a nucleation process since in this case the accessibility of the different channel sections should remain without any influence.

The stringency of this conclusion is confirmed by the experimental findings displayed in Figure 18.10, which have been attained with a fourth, specially prepared specimen of porous silicon which, in addition, has been totally immersed in the liquid. However, the porous silicon considered in these experiments is of the type as indicated by Figure 18.3 with the difference that the diameter of the wider channel segments has been notably enhanced, namely up to 10.4 nm. With increasing diameters, also the nucleation probability in the wider channel segments increases (which eventually would affect that

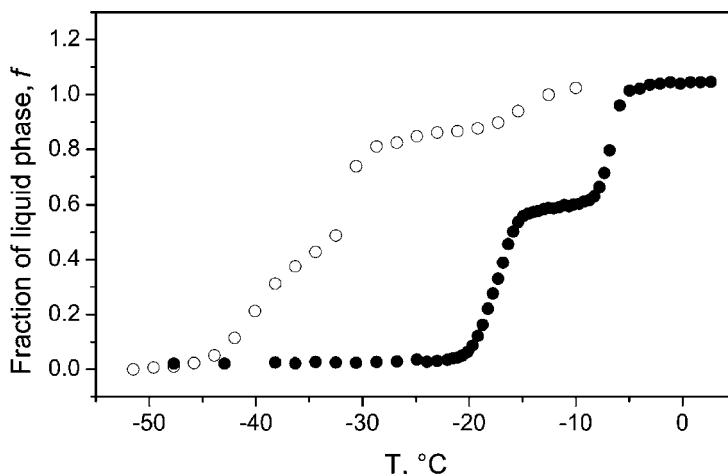


Figure 18.10 Freezing (open symbols) and melting (filled symbols) transition of nitrobenzene in the porous silicon with channel-like pores with diameters alternating between 6.2 nm and 10.4 nm.

freezing occurs at the bulk freezing point, with completely released confinement). In complete agreement with our consideration, the freezing curve of Figure 18.10 shows three steps. The first one, between $-10\text{ }^{\circ}\text{C}$ and $-15\text{ }^{\circ}\text{C}$, reflects freezing in the two wide channel sections reaching the wafer surface. It is caused by the ingress of a solid front from the bulk frozen phase. Thereafter, the pore-blocking mechanism due to the narrow channels (necks) prevents further ingress. However, already at a temperature of about $-30\text{ }^{\circ}\text{C}$ the second step appears. This indicates that wing to the larger pore size freezing is now initiated by homogeneous nucleation, i.e., without the need of ingress through the pore mouths (which would only occur at about $-40\text{ }^{\circ}\text{C}$ as seen in Figure 18.9(a)). With further decreasing temperature, a gradual freezing in the narrow-channel sections is observed.

Combination of the present studies with PFG NMR measurement of the diffusivity in the various liquid domains emerging and disappearing during the different stages of melting and freezing and the option of their use for “dynamic imaging” is among the fascinating plans for our future activities in this field.

18.6 Conclusions

Molecular transport in confined spaces is known to reveal numerous effects of anomalous dynamics. We have focused on some options of NMR spectroscopy to reveal such anomalies. They are related to the ability of NMR to

directly measure the probability distribution of molecular displacements (including the root mean square displacement as its most robust measure) during typical diffusion times of milliseconds till seconds and to provide direct information about the absolute numbers of molecules in different states of mobility. Our examples include microporous materials, in particular zeolites. Being able to concentrate on intrinsic dynamics, application of NMR has revolutionized our understanding of molecular diffusion in such systems. Simultaneously, in many cases the real structure of zeolites turned out to notably deviate from their textbook structure.

While molecular dynamics in microporous materials is dominated by the guest interaction with the host matrix, in mesoporous materials the guest-guest interaction may become the dominating mechanism. This leads to a further enhancement of the variety of the phenomena accessible by direct information. Our examples included the observation of transport anomalies under the conditions of sorption hysteresis as well as the melting and freezing behavior and the information accessible from the observation of temperature-dependent diffusivities. Further activities in the field will be devoted to the observation of percolation phenomena by phase separation in the pore space and, eventually, to the transition into the supercritical state. We are aware of the situation that most of the phenomena communicated in this contribution are not yet fully understood. The more we would be pleased if, with the given examples of anomaly of diffusion under confinement, we succeeded in generating some more appetite for cooperation between theory and experiment.

References

- 1** F. Schüth, K. S. W. Sing, and J. Weitkamp, editors. *Handbook of Porous Solids*. Wiley-VCH, Wienheim, 2002.
- 2** D. M. Ruthven, S. Farooq, and K. S. Knaebel. *Pressure Swing Adsorption*. VCH, New York, 1994.
- 3** G. Ertl, H. Knötzinger, and J. Weitkamp. *Handbook of Heterogeneous Catalysis*. Wiley-VCH, Chichester, 1997.
- 4** J. Weitkamp and L. Piuppe. *Catalysis and Zeolites*. Springer, Berlin, Heidelberg, 1999.
- 5** J. Kärger and D.M. Ruthven. *Diffusion in Zeolites and Other Microporous Solids*. Wiley, New York, 1992.
- 6** N. Y. Chen, T. F. Degnan, and C. M. Smith. *Molecular Transport and Reaction in Zeolites*. VCH, New York, 1994.
- 7** R. Pitchumani, W. J. Li, and M. O. Coppen. Tuning the morphology of sba-15 by stirring in the presence of phosphoric acid: films, cakes, fibers and bundles of threads. *Nanoporous Materials Iv*, 156:83–88, 2005.
- 8** P. T. Callaghan. *Principles of Nuclear Magnetic Resonance Microscopy*. Clarendon Press, Oxford, 1991.
- 9** R. Kimmich. *NMR: Tomography, Diffusometry, Relaxometry*. Springer, Berlin, Heidelberg, 1997.
- 10** C. Baerlocher, L. B. McCusker, and D. H. Olson. *Atlas of Zeolite Framework Types*. Elsevier, Amsterdam, 2007.
- 11** A. Dyer and A. M. Yusof. Diffusion in heteroionic analcimes .1. sodium-potassium water-system. *Zeolites*, 7:191–196, 1987.

- 12** M. E. Davis. Ordered porous materials for emerging applications. *Nature*, 417:813–821, 2002.
- 13** F. Laeri, F. Schüth, U. Simon, and M. Wark. *Host-Guest Systems Based on Porous Crystals*. Wiley-VCH, Weinheim, 2003.
- 14** J. Weitkamp, H. G. Karge, H. Pfeifer, and W. Hölderlich, editors. *Zeolites and Related Microporous Materials: State of Art*. Elsevier, Amsterdam, 1994.
- 15** E. van Steen, M. Clayes, and L. H. Callanan. *Recent Advances in the Science and Technology of Zeolites and Related Materials*. Elsevier, Amsterdam, 2004.
- 16** T. H. Elmer. Porous and reconstructed glasses. In *Engineered Materials Handbook*, Vol. 4, pages 427–432. ASM, 1992.
- 17** W. D. Dozier, J. M. Drake, and J. Klafter. Self-diffusion of a molecule in porous vycor glass. *Phys. Rev. Lett.*, 56:197–200, 1986.
- 18** J. H. Page, J. Liu, B. Abeles, H. W. Deckman, and D. A. Weitz. Pore-space correlations in capillary condensation in vycor. *Phys. Rev. Lett.*, 71:1216–1219, 1993.
- 19** P. Wiltzius, F. S. Bates, S. B. Dierker, and G. D. Wignall. Structure of porous vycor glass. *Phys. Rev. A*, 36:2991–2994, 1987.
- 20** E. S. Kikkinides, M. E. Kainourgiakis, K. L. Stefanopoulos, A. Ch. Mitropoulos, A. K. Stubos, and N. K. Kanellopoulos. Combination of small angle scattering and three-dimensional stochastic reconstruction for the study of adsorption-desorption processes in vycor porous glass. *J. Chem. Phys.*, 112:9881–9887, 2000.
- 21** R. J. M. Pellenq, B. Rousseau, and P. E. Levitz. A grand canonical monte carlo study of argon adsorption/condensation in mesoporous silica glasses. *Phys. Chem. Chem. Phys.*, 3:1207–1212, 2001.
- 22** R. Herino, G. Bomchil, K. Barla, C. Bertrand, and J. L. Ginoux. Porosity and pore-size distributions of porous silicon layers. *J. Electrochem. Soc.*, 134:1994–2000, 1987.
- 23** V. Lehmann, R. Stengl, and A. Luigart. On the morphology and the electrochemical formation mechanism of mesoporous silicon. *Mater. Sci. Eng. B*, 69:11–22, 2000.
- 24** M. G. Berger, C. Dieker, M. Thonissen, L. Vescan, H. Luth, H. Munder, W. Theiss, M. Wernke, and P. Grosse. Porosity superlattices: a new class of si heterostructures. *J. Phys. D: Appl. Phys.*, 27:1333–1336, 1994.
- 25** A. Khokhlov, R. Valiullin, and J. Kärger. Freezing and melting transitions of liquids in mesopores with ink-bottle geometry. *New J. Phys.*, 9:272, 2007.
- 26** A. G. Cullis, L. T. Canham, and P. D. J. Calcott. The structural and luminescence properties of porous silicon. *J. Appl. Phys.*, 82:909–965, 1997.
- 27** B. Blümich. *Essential NMR*. Springer, Berlin, Heidelberg, 2005.
- 28** E. O. Stejskal and J. E. Tanner. Spin diffusion measurements – spin echoes in presence of a time-dependent field gradient. *J. Chem. Phys.*, 42:288–292, 1965.
- 29** J. Kärger and W. Heink. The propagator representation of molecular-transport in microporous crystallites. *J. Magn. Reson.*, 51:1–7, 1983.
- 30** P. Galvosas, F. Stallmach, G. Seiffert, J. Kärger, U. Kaess, and G. Majer. Generation and application of ultra-high-intensity magnetic field gradient pulses for NMR spectroscopy. *J. Magn. Reson.*, 151:260–268, 2001.
- 31** M. E. Komlosh and P. T. Callaghan. Segmental motion of entangled random coil polymers studied by pulsed gradient spin echo nuclear magnetic resonance. *J. Chem. Phys.*, 109:10053–10067, 1998.
- 32** F. Stallmach and P. Galvosas. Spin echo NMR diffusion studies (Annual reports on NMR spectroscopy), Academic Press, New York.
- 33** D. Raftery, H. Long, T. Meersmann, P. J. Grandinetti, L. Reven, and A. Pines. High-field NMR of adsorbed xenon polarized by laser pumping. *Phys. Rev. Lett.*, 66:584–587, 1991.
- 34** G. Navon, Y. Q. Song, T. Room, S. Appelt, R. E. Taylor, and A. Pines. Enhancement of solution NMR and mri with laser-polarized xenon. *Science*, 271:1848–1851, 1996.
- 35** M. B. Kozlov, J. Haase, C. Baumann, and A. G. Webb. ^{56}Fe NMR at 2.4 ghz in a pulsed high-field magnet. *Solid State Nucl. Magn. Reson.*, 28:64–67, 2005.

- 36** J. Kärger. *Leipzig, Einstein, Diffusion.* Leipziger Universitätsverlag, Leipzig, 2007.
- 37** P. A. Fedders. 2-point correlation-functions for a distinguishable particle hopping on a uniform one-dimensional chain. *Phys. Rev. B*, 17:40–46, 1978.
- 38** K.W. Kehr, K. Mussawisade, M.G. Schütz, and T. Wichmann. Diffusion of particles on lattices. In P. Heitjans and J. Kärger, editors, *Diffusion in Condensed Matter*. Springer, Berlin/Heidelberg, 2nd edition, 2005.
- 39** J. Kärger. Straightforward derivation of the long-time limit of the mean-square displacement in one-dimensional diffusion. *Phys. Rev. A*, 45:4173–4174, 1992.
- 40** J. Kärger. Long-time limit of the self-correlation-function of one-dimensional diffusion. *Phys. Rev. E*, 47:1427–1428, 1993.
- 41** V. Gupta, S. S. Nivarthi, A. V. McCormick, and H. T. Davis. Evidence for single file diffusion of ethane in the molecular sieve alpo4-5. *Chem. Phys. Lett.*, 247:596–600, 1995.
- 42** K. Hahn, J. Kärger, and V. Kukla. Single-file diffusion observation. *Phys. Rev. Lett.*, 76:2762–2765, 1996.
- 43** V. Kukla, J. Kornatowski, D. Demuth, I. Gimus, H. Pfeifer, L. V. C. Rees, S. Schunk, K. K. Unger, and J. Kärger. Nmr studies of single-file diffusion in unidimensional channel zeolites. *Science*, 272:702–704, 1996.
- 44** E. Lehmann, C. Chmelik, H. Scheidt, S. Vasenkov, B. Staudte, J. Kärger, F. Kremer, G. Zadrozna, and J. Kornatowski. Regular inter-growth in the afi-type crystals: Influence on the intracrystalline adsorbate distribution as observed by interference and ftir-microscopy. *J. Am. Chem. Soc.*, 124:8690–8692, 2002.
- 45** E. Lehmann, S. Vasenkov, J. Kärger, G. Zadrozna, and J. Kornatowski. Intracrystalline monitoring of molecular uptake into the one-dimensional channels of the afi-type crystals using interference microscopy. *J. Chem. Phys.*, 118:6129–6132, 2003.
- 46** J. Kärger, R. Valiullin, and S. Vasenkov. Molecular dynamics under confinement to one-dimension: options of measurement and accessible information. *New J. Phys.*, 7:15, 2005.
- 47** U. Schemmert, J. Kärger, C. Krause, R. A. Rakoczy, and J. Weitkamp. Monitoring the evolution of intracrystalline concentration. *Europhys. Lett.*, 46:204–210, 1999.
- 48** J. Kärger, P. Kortunov, S. Vasenkov, L. Heinke, D. R. Shah, R. A. Rakoczy, Y. Traa, and J. Weitkamp. Unprecedented insight into diffusion by monitoring the concentration of guest molecules in nanoporous host materials. *Angewandte Chemie – International Edition*, 45:7846–7849, 2006.
- 49** J. Kärger. Random-walk through 2-channel networks – a simple means to correlate the coefficients of anisotropic diffusion in ZSM-5 type zeolites. *J. Phys. Chem.*, 95:5558–5560, 1991.
- 50** D. Fenzke and J. Kärger. On the correlation between the step rates and the diffusivities of guest molecules in microporous crystals. *Z Phys. D Atom. Mol. Cl.*, 25:345–350, 1993.
- 51** R. Haberlandt and J. Kärger. Molecular dynamics under the confinement by the host lattice in zeolitic adsorbate-adsorbent systems. *Chem. Eng. J.*, 74:15–24, 1999.
- 52** S. Jost, N. K. Bar, S. Fritzsche, R. Haberlandt, and J. Kärger. Diffusion of a mixture of methane and xenon in silicalite: A molecular dynamics study and pulsed field gradient nuclear magnetic resonance experiments. *J. Phys. Chem. B*, 102:6375–6381, 1998.
- 53** D. N. Theodorou, R. Q. Snurr, and A. T. Bell. Molecular dynamics and diffusion in microporous materials. In G. Alberti and T. Bein, editors, *Comprehensive Macromolecular Chemistry*. Oxford, Oxford, 1996.
- 54** U. Hong, J. Kärger, H. Pfeifer, U. Muller, and K. K. Unger. Observing diffusion anisotropy in zeolites by pulsed field gradient NMR. *Z. Phys. Chem.*, 173:225–234, 1991.
- 55** J. Caro, M. Noack, P. Kolsch, and R. Schafer. Zeolite membranes – state of their development and perspective. *Microporous Mesoporous Mat.*, 38:3–24, 2000.

- 56** A. Schuring, S. Fritzsche, R. Haberlandt, S. Vasenkov, and J. Kärger. Modeling molecular diffusion in channel networks via displacements between the channel segments. *Phys. Chem. Chem. Phys.*, 6:3676–3679, 2004.
- 57** E. G. Derouane and Z. Gabelica. A novel effect of shape selectivity – molecular traffic control in zeolite ZSM-5. *J. Catal.*, 65:486–489, 1980.
- 58** N. Neugebauer, P. Bräuer, and J. Kärger. Reactivity enhancement by molecular traffic control. *J. Catal.*, 194:1–3, 2000.
- 59** P. Bräuer, A. Brzank, and J. Kärger. Two-component desorption from anisotropic pore networks. *J. Chem. Phys.*, 124:034713, 2006.
- 60** A. Brzank, G. M. Schütz, P. Bräuer, and J. Kärger. Molecular traffic control in single-file networks with fast catalysts. *Phys. Rev. E*, 69:031102, 2004.
- 61** A. Brzank and G. Schütz. Molecular traffic control in porous nanoparticles. *Appl. Catal. A -Gen.*, 288:194–202, 2005.
- 62** A. Brzank and G. M. Schütz. Amplification of molecular traffic control in catalytic grains with novel channel topology design. *J. Chem. Phys.*, 124:214701, 2006.
- 63** S. Vasenkov and J. Kärger. Evidence for the existence of intracrystalline transport barriers in mfi-type zeolites: a model consistency check using mc simulations. *Microporous Mesoporous Mat.*, 55:139–145, 2002.
- 64** S. Vasenkov, W. Böhlmann, P. Galvosas, O. Geier, H. Liu, and J. Kärger. Pfg NMR study of diffusion in mfi-type zeolites: Evidence of the existence of intracrystalline transport barriers. *J. Phys. Chem. B*, 105:5922–5927, 2001.
- 65** J. M. van Bemmelen. Die Absorption. Das Wasser in den Kolloiden, besonders in dem Gel der Kieselsäure. *Z. Anorg. Allg. Chem.*, 13:233–356, 1897.
- 66** L. D. Gelb, K. E. Gubbins, R. Radhakrishnan, and M. Sliwinska-Bartkowiak. Phase separation in confined systems. *Rep. Prog. Phys.*, 62:1573–1659, 1999.
- 67** E. Kierlik, P. A. Monson, M. L. Rosinberg, L. Sarkisov, and G. Tarjus. Capillary condensation in disordered porous materials: Hysteresis versus equilibrium behavior. *Phys. Rev. Lett.*, 87:055701, 2001.
- 68** A. V. Neimark, P. I. Ravikovitch, and A. Vishnyakov. Inside the hysteresis loop: Multiplicity of internal states in confined fluids. *Phys. Rev. E*, 65:031505, 2002.
- 69** R. Valiullin, S. Naumov, P. Galvosas, J. Kärger, H. J. Woo, F. Porcheron, and P. A. Monson. Exploration of molecular dynamics during transient sorption of fluids in mesoporous materials. *Nature*, 443:965–968, 2006.
- 70** H. J. Woo and P. A. Monson. Phase behavior and dynamics of fluids in mesoporous glasses. *Phys. Rev. E*, 67:041207, 2003.
- 71** S. Naumov, R. Valiullin, P. Galvosas, J. Kärger, and P. A. Monson. Diffusion hysteresis in mesoporous materials. *Eur. Phys. J. Special Topics*, 141:107–112, 2007.
- 72** H. S. Carslaw and J. C. Jaeger. *Conduction of Heat in Solids*. Clarendon Press, Oxford, 1946.
- 73** J. Klafter and M. F. Shlesinger. On the relationship among 3 theories of relaxation in disordered-systems. *Proc. Natl. Acad. Sci. U.S.A.*, 83:848–851, 1986.
- 74** J. P. Bouchaud and A. Georges. Anomalous diffusion in disordered media – statistical mechanisms, models and physical applications. *Phys. Rep.*, 195:127–293, 1990.
- 75** F. Iglói and C. Monthus. Strong disorder approach of random systems. *Phys. Rep.*, 412:277–431, 2005.
- 76** W. G. Pollard and R. D. Present. On gaseous self-diffusion in long capillary tubes. *Phys. Rev.*, 73:762–774, 1948.
- 77** S. Vasenkov, O. Geier, and J. Kärger. Gas diffusion in zeolite beds: Pfg NMR evidence for different tortuosity factors in the knudsen and bulk regimes. *Eur. Phys. J. E*, 12:S35–S38, 2003.
- 78** J. M. Zalc, S. C. Reyes, and E. Iglesia. The effects of diffusion mechanism and void structure on transport rates and tortuosity factors in complex porous structures. *Chem. Eng. Sci.*, 59:2947–2960, 2004.
- 79** M. Dvoyashkin, R. Valiullin, and J. Kärger. Temperature effects on phase equilibrium and diffusion in mesopores. *Phys. Rev. E*, 75:041202, 2007.

- 80** J. L. Riccardo, M. A. Chade, V. D. Pereyra, and G. Zgrablich. Adsorption and surface-diffusion on generalized heterogeneous surfaces. *Langmuir*, 8:1518–1531, 1992.
- 81** K. Morishige, H. Yasunaga, R. Denoyel, and V. Wernert. Pore-blocking-controlled freezing of water in cagelike pores of kit-5. *J. Phys. Chem. C*, 111:9488–9495, 2007.

19

Paradigm Shift of the Molecular Dynamics Concept in the Cell Membrane: High-Speed Single-Molecule Tracking Revealed the Partitioning of the Cell Membrane

Akihiro Kusumi, Yasuhiro Umemura, Nobuhiro Morone, and Takahiro Fujiwara

19.1

Introduction

The plasma membrane is the outermost membrane of the cell, surrounding the entire cell and determining the boundaries between the cell and the outside world. All of the living organisms on the earth share essentially the same fundamental plasma membrane structure. The plasma membrane has, like all of the other membranes in the cell, a quasi-two-dimensional liquid-like structure, but it is not a simple liquid. Rather, it is a nonideal mixture of various molecules with differing miscibilities in the fluid state. Therefore, the plasma membrane contains dynamic structures, like molecular complexes and domains, functioning on various time scales and space scales, and forming and dispersing continually within the plasma membrane. These molecular complexes and domains range from small protein clusters with short lifetimes, like transient dimers of rhodopsin [21], to large micron-sized stable domains, like cell-to-cell or cell-to-substrate adhesion structures (see Figure 19.1 for various membrane domains).

Another interesting feature of the plasma membrane, which makes it different from a simple two-dimensional ideal liquid, is its association with the cellular filamentous protein meshwork that consists of actin filaments, called the cytoskeleton. The actin cytoskeleton is a three-dimensional structure present throughout the cell, for the creation, modification, and maintenance of the cellular morphology. On the cytoplasmic surface of the plasma membrane, the actin filament interacts with many plasma-membrane-integrated proteins and lipids, indirectly, but specifically, via connecting molecules, and also directly, but with lower affinities (but at many sites). At the interface between the actin-based cytoskeleton and the plasma membrane, the cytoskeleton uses various protein components different from those of the bulk cytoskeleton to interact with the plasma membrane molecules, and as a result, its structure at the interface differs from the bulk structure of the cytoskeleton. Furthermore, the part of the cytoskeleton that associates with the plasma membrane is, both structurally and functionally, an integrated part of the plasma mem-

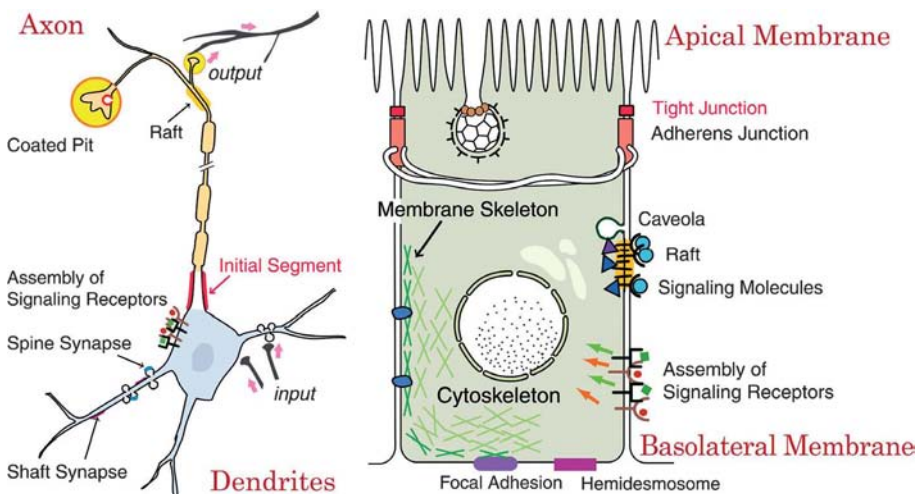


Figure 19.1 The plasma membranes are full of transient molecular complexes, domains, and compartments. Shown here are a plethora of specialized domains, key to a cell's function, which must be continually formed and dissolved during the life of a cell. Their lifetimes range between microseconds

and hours. Understanding the basic mechanisms and principles for organizing these molecules is a key objective of biophysical studies of biological membranes. Schematic figures of the plasma membranes of a neuron (left) and an epithelial cell (right) are shown.

brane. Therefore, this part of the cytoskeleton is often called the membrane skeleton (Figure 19.2). Recent research has revealed that this close association of the membrane skeleton with the plasma membrane profoundly affects the dynamics and functions of membrane molecules and their interactions [22,24].

Since the plasma membrane is likely to have complex dynamic domain structures, many of which are smaller than the optical spatial resolution of 300 nm or so, unlike those in artificial membranes, the use of normal optical microscopy and electron microscopy for the studies of these complex dynamic domain structures has turned out to be difficult. The experimental results could be explained by various completely different models, and allow different interpretations, i.e., the experimental results are often unable to reveal which models better represent the dynamic membrane structure and molecular dynamics in the membrane. To clarify these complex spatiotemporal organizations and molecular dynamics, one of the best approaches appears to be high-definition single-molecule tracking, with enhanced time and spatial resolutions.

The recent advent of single-molecule techniques now allows researchers to track single molecules or small groups of molecules in the plasma membrane, even in living cells. These methods include single-fluorescent molecule tracking (SFMT) with the use of fluorescent probes, and single-particle tracking (SPT) using colloidal gold probes with a diameter of 20 or 40 nm

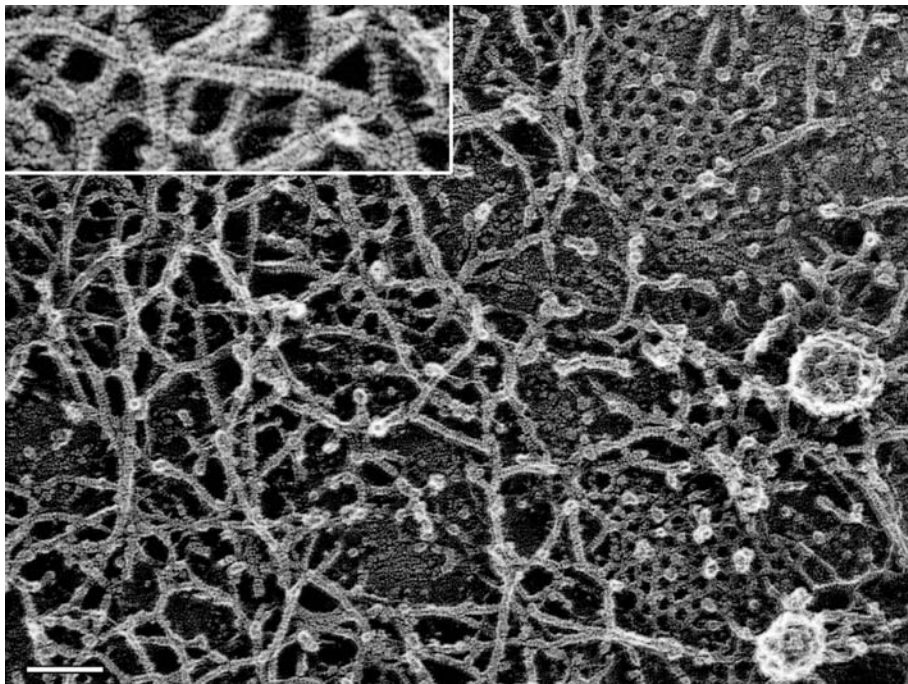


Figure 19.2 The cytoplasmic surface of the upper membrane, observed by electron microscopy. The plasma membrane specimen was rapidly frozen on a copper block precooled in liquid helium, deeply etched to remove excess ice, and platinum-carbon replicated. The presence of clathrin-coated structures (structures that look like a honeycomb or a soccer ball) shows that this image represents that of the cytoplasmic surface of the plasma membrane. The striped band-

ing patterns with the 5.5-nm periodicity on individual filaments (see the inset) are characteristic of actin filaments. This banding pattern can be found in every filament, showing that the membrane skeleton is made of actin filaments and their associated proteins. This image also reveals the close links of the actin filaments of the membrane skeleton with the clathrin-coated structures. Bar = 100 nm (50 nm for the inset).

[1,6–8,14,16,18,25,29,34,36,50,59,61,65,67–69]. SFMT is advantageous in that the researcher can be sure that s/he is following a single molecule, whereas SPT gives better image contrast, allowing her/him to observe at faster frame rates or higher spatial precisions. By using both of these techniques for the same target molecule, the problems of each method can be compensated for each other. Therefore, they together have given researchers the unprecedented ability to directly observe the movement, assembly, and localization of individual, single molecules in the plasma membrane of living cells in culture [24,57,61,68,69]. Furthermore, not only the movement of single molecules, but also the *activation* of cellular signaling molecules, including the small GTP binding proteins (G proteins) H- and K-Ras, has been tracked at the level of single molecules in the living cell membrane [36].

The next important step in the development of single-molecule techniques has been the great improvement of the frame rate in SFMT and SPT. In particular, with SPT, a frame rate of 40 000 frames per second (fps), or a time resolution of 25 μ s, has been achieved in the tracking of single phospholipid molecules in the plasma membrane of living cells, with a relatively small loss of the spatial precision in the determination of the positions of gold particles in the two-dimensional plane (24 nm in two-dimensional space [12]).

The ability to track single molecules at high frame rates with sufficient spatial accuracies has fostered a new fundamental understanding of molecular diffusion in the cell membrane. High-speed SPT and SFMT are revealing that the plasma membranes of virtually all mammalian cells in culture are parcelled up into apposed domains, with regard to the translational diffusion of practically all of the membrane molecules. In addition, virtually all of these molecules undergo non-Brownian diffusion in the plasma membrane, i.e., short-term confined diffusion in a compartment and long-term hop diffusion between the compartments in the cell membrane (Figure 19.3; details will be given later; Fujiwara et al. [12], Kusumi and Sako [24], Murase et al. [37]).

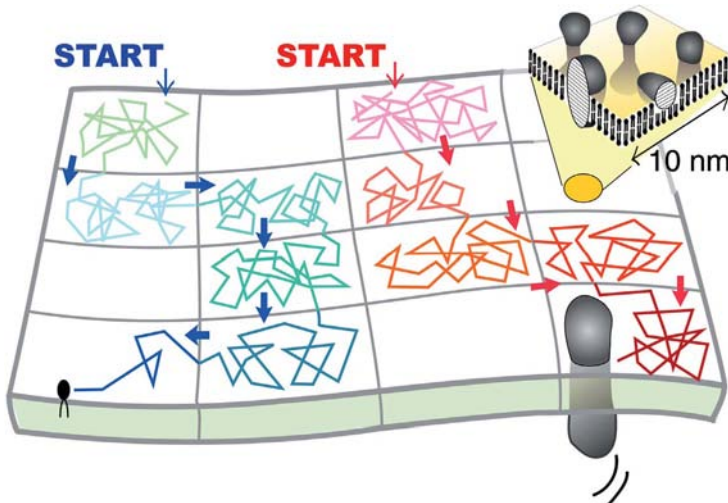


Figure 19.3 A paradigm shift for the plasma membrane concept is required from the (two-dimensional) continuum model to the compartmentalized fluid model, in which the membrane constituent molecules undergo short-term confined diffusion within a compartment and long-term hop diffusion between the compartments. The plasma membrane is partitioned into many compartments with regard to the translational diffusion of membrane-incorporated molecules,

and practically all of the molecules undergo macroscopic diffusion, by repeating their confinement within a compartment and hopping to an adjacent one. The two-dimensional fluid model of Singer and Nicolson is perfectly suitable if the scale is limited within 10 nm (inset), as shown in the cartoon of their original article, but it cannot be over-extended to a cell membrane structure over several 10s of nanometers.

This entails a paradigm shift of the structure of the plasma membrane from the fluid-mosaic model, proposed by Singer and Nicolson [66], and widely accepted for over 30 years: the plasma membrane in space scales greater than several 10s of nanometers should not be considered as a two-dimensional continuum fluid, but rather that partitioned into closely apposed compartments (*compartmentalized fluid model*, Figure 19.3).

In this chapter, we will first summarize the various observations that led to the concept of the partitioned plasma membrane, which induces hop diffusion of practically all of the molecules in the cell membrane. The membrane-skeleton fence model and the anchored-protein picket model will be described. We will critically compare these models with other observations and models, and evaluate them. Finally, we will discuss the important consequences of plasma membrane compartmentalization in signal transduction in the plasma membrane.

19.2

Thirty-Year Old Enigma about the Diffusion Rate of Membrane Molecules in the Plasma Membrane

For many years, physicists interested in biological membranes have struggled to understand two enigmas. First, for over 30 years, they have wondered why the diffusion coefficients for both proteins and lipids in the plasma membrane are smaller than those found in artificially reconstituted membranes and liposomes, by factors of 5 to 50, with a factor of 20 being a good round number to keep in mind (see Table 1 in Murase et al. [37] and Table 1 in Kusumi et al. [22]). Since a factor of 20 is large, this could not be explained by the crowding of membrane proteins [43] or by the presence of cholesterol [9, 31]. Note that here the diffusion coefficients are those measured at length scales greater than 300 nm, using methods like fluorescence recovery after photobleaching (FRAP) or fluorescence correlation spectroscopy (FCS), or those observed by SFMT or SPT at the normal video rate (time window of about 100 ms). In this chapter, we call these *macroscopic* diffusion coefficients. In a classical view of diffusion, one might think it strange to talk about microscopic diffusion and macroscopic diffusion, because, whatever the time scale is, the diffusion should be self-similar. However, in the case of a nonideal fluid where various membrane domains with different solubilities with the probe molecule exist, and which interacts with the associated membrane-skeleton meshwork, the diffusion depends on the time scales and the length scales over which the measurements are taken.

The second enigma for membrane biophysicists is the following. When membrane molecules, including receptor molecules and other signaling molecules in the membrane, form oligomers or molecular complexes, either

their macroscopic diffusion rates drop dramatically or they may be temporarily immobilized [17, 18, 40]. This is completely opposite from the general view of membrane biophysicists. Based on the fluid-mosaic model of Singer and Nicolson [66], Saffman and Delbrück (1975) [47] derived an equation that relates the diffusant size to the translational diffusion coefficient in a two-dimensional continuum fluid. For a cylinder (a transmembrane protein) of radius a and height h , floating in a two-dimensional fluid of viscosity μ with a matched thickness (h) immersed in an aqueous medium of viscosity μ' (Figure 19.4), the translational and rotational diffusion coefficients, D_T and D_R , respectively, for the cylinder can be expressed as,

$$D_T = \frac{k_B T}{4\pi\mu h} \left(\log \frac{\mu h}{\mu' a} - \gamma \right) \quad (19.1)$$

$$D_R = \frac{k_B T}{4\pi\mu a^2 h'} \quad (19.2)$$

where γ is the Euler constant (≈ 0.5772). This equation predicts that translational diffusion is very *insensitive* to the diffusant size: tetramer formation from monomers (an increase in radius by a factor of 2) will decrease the diffusion rate by only a factor of 1.1, and even 100mers (an increase in radius by a factor of 10) will have their diffusion rate reduced by only a factor of 1.4 from monomers, assuming a 0.5 nm monomer radius of the membrane-spanning domain. (One should be aware that, at variance with the translational diffusion coefficient (Eq. (19.1)), the rotational diffusion rate is quite sensitive to changes in the oligomer size (Eq. (19.2)). It is inversely proportional to a^2 , i.e., to the number of proteins in a complex in larger oligomers.) Furthermore, Peters and Cherry [43] found that the Saffman-Delbrück theory worked well in the reconstituted membranes of bacteriorhodopsin, which was further supported later [75]. Therefore, the considerable decreases in the diffusion coefficients of membrane receptors upon ligand binding could not be explained by ligand-induced receptor oligomerization. Alternatively, the formation of very large aggregates of thousands of receptor molecules has to be assumed to explain the reduction of the diffusion coefficient upon receptor engagement.

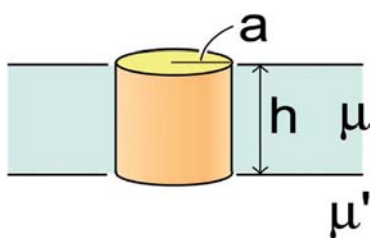


Figure 19.4 A cylinder floating in the two-dimensional fluid continuum in water.

However, the induction of such large aggregates of receptors upon liganding has never been found.

Recently, the Saffman–Delbrück theory was challenged by Gambin et al. [13]. These authors asserted that the dependence of the diffusion coefficient on the diffusant size is much stronger, based on the data by Lee and Petersen (2003) [28]. However, in their presentation, they omitted the diffusion data for the largest diffusant in the Lee and Petersen paper, which are rather consistent with the Saffman–Delbrück theory, and inconsistent with their theory. Steeper changes with an increase in the diffusant radius than those expected from the Saffman–Delbrück theory did take place around the radius of the phospholipid (the basic membrane constituent molecular species, which form the fluid membrane matrix; ~ 0.45 nm in radius) and that of an α -helix (~ 0.55 nm in radius), with the dependence on radius being $1/\text{[radius]}$ (based on the free area theory). If we adopt this model, then when a transmembrane α -helix forms a dimer, the diffusion coefficient will decrease by a factor of 1.4. The breakdown of the Saffman–Delbrück theory in this scale regime, where the diffusant size becomes comparable to the size of the phospholipid, which forms the membrane matrix, has been expected because the Saffman–Delbrück theory assumes the diffusion in a two-dimensional continuum fluid [76]. This was also implied in 1982, when the collision rates of molecular oxygen with lipid membrane probes were measured [26].

Therefore, a convenient rule of thumb with regard to the relationship between the size of the transmembrane α -helix of an integral membrane protein and its diffusion coefficient may be that the diffusion coefficient would decrease by a factor of about 1.4, following the $1/\text{[radius]}$ law, when the protein forms a dimer, and then any oligomers greater than dimers may follow the Saffman–Delbrück relationship, i.e., very slight dependence of the diffusion coefficient on protein oligomerization.

19.3

Macroscopic Diffusion Coefficients for Transmembrane Proteins are Suppressed by the Presence of the Membrane Skeleton

We will deal with the first enigma, i.e., why the macroscopic diffusion coefficients for both proteins and lipids in the plasma membrane are smaller than those found in artificially reconstituted membranes and liposomes, by a factor of ≈ 20 . To clarify the idea, we will initially limit our argument to the diffusional motion of transmembrane proteins.

Even before the single-molecule era, there were quite a few FRAP reports indicating that the reduction of the macroscopic diffusion coefficient in the plasma membrane from that found in artificial membranes may be caused by

the actin-based membrane skeleton [42, 52, 63, 64, 71, 73, 74, 81]. Sheetz and colleagues found that the transmembrane protein band 3 (the majority of the ConA receptor observed in this study is known to be band 3) diffuses about 10 times faster [64] in spectrin-deficient mutant mouse erythrocytes than in normal cells. In mammalian red blood cells, the spectrin meshwork, instead of the f-actin network, forms the membrane skeleton. Furthermore, a number of reports have shown that the lateral diffusion coefficients of transmembrane proteins were increased in blebbled membranes or after partial depolymerization of actin filaments (for example, see Paller [42], Tank et al. [71], Wu et al. [81]).

Tsuji and Ohnishi [74] and Tsuji et al. [73] carried out *both translational and rotational diffusion measurements* for the transmembrane protein band 3 in human red blood cell ghost membranes, and showed that the translational diffusion coefficient of band 3 was increased (decreased) when the spectrin network was stabilized (destabilized, i.e., the tetramer–dimer equilibrium of spectrin was shifted toward the tetramer [dimer]), whereas the rotational diffusion coefficient of band 3 was unaffected. These results clearly indicate that (1) the spectrin meshwork partitions the membrane into small compartments, (2) the non-specific collision of band 3 with the spectrin tetramer, which forms the compartment boundary, is responsible for the reduction of the translational diffusion coefficient in the erythrocyte membrane, and (3) the spectrin tetramer is the effective barrier, and when it temporarily dissociates into dimers, band 3 molecules can cross the compartment boundary. Based on these observations, Tsuji et al. [73] proposed a “spectrin dimer–tetramer equilibrium” gate model (SPEQ gate model).

As such, data showing the involvement of the membrane skeleton in the reduction of the translational diffusion rate were abundant in the era before single molecule observations, particularly in human red blood cells, but direct observations of molecules undergoing short-term confined diffusion within a compartment (made of the membrane skeleton) and long-term hop diffusion between the compartments had to wait until the single-molecule technologies became available. The percolation threshold idea advanced by Saxton played an important role in these studies [53].

19.4

Single-Molecule Tracking Revealed That Transmembrane Proteins Undergo Hop Diffusion

SPT was developed in the late 1980s [6–8, 14, 20, 25, 60, 65]. Using SPT, Sako and Kusumi [48] were the first to directly observe the “hop diffusion” of membrane molecules: transferrin receptor, a transmembrane protein, is temporarily confined in a compartment of about 700 nm in diameter in the membrane,

and then it hops to an adjacent apposed compartment, where it again becomes trapped temporarily (we later found that NRK cells have nested compartments of 230 nm within 700 nm compartments. However, in earlier techniques, only the larger compartments of 700 nm could be detected). By repeating such confinement and hop movements between the compartments, a phenomenon termed hop diffusion, the receptor covers macroscopic areas (Figure 19.5). Since virtually all of the examined transferrin receptor molecules and α 2-macroglobulin receptor molecules were found to undergo hop diffusion, it was proposed that the entire plasma membrane is parceled up into small, apposed domains (except for specialized membrane domains, such as clathrin-coated pits, cell–cell and cell–substrate junctions, and microvilli).

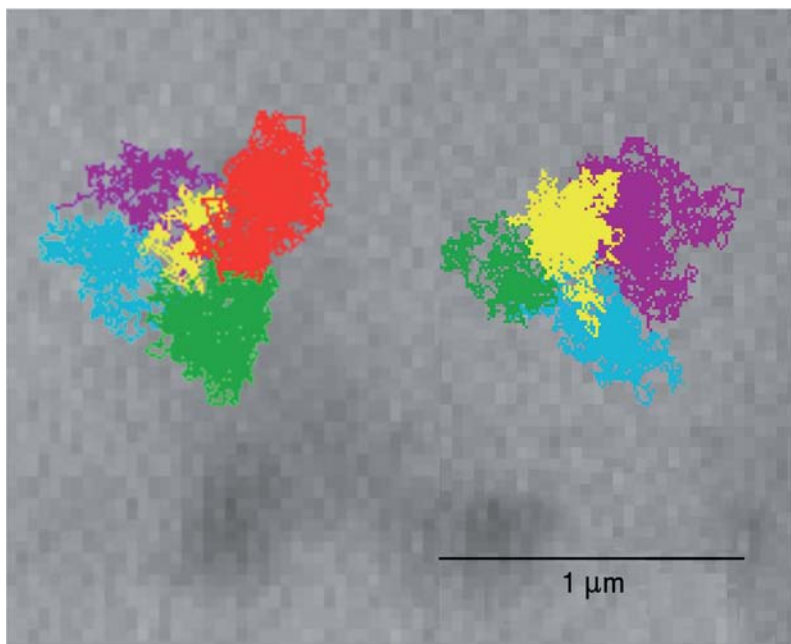


Figure 19.5 Typical trajectories of 40-nm gold probes bound to transferrin receptor, recorded at a time resolution of 25 μ s for a duration of 250 ms (10 000 frames). The background is the actual image of a single frame. Different colors represent various plausible compartments, detected by computer software developed in our laboratory

(in a time sequence of purple, blue, green, yellow, and red). These trajectories suggest that transferrin receptor molecules undergo short-term confined diffusion in a compartment and long-term hop diffusion between the compartments. This was confirmed by the statistical analysis method developed by Fujiwara et al. [12].

The detection of such hop diffusion or temporary confinement within a compartment requires statistical analysis, because such trajectories might occur as a consequence of thermal diffusion [12, 25]. Here, we briefly explain how such an analysis is carried out.

For each molecule's trajectory, the mean-square displacement (MSD), $\langle (\Delta r(\Delta t))^2 \rangle$, for every time interval is calculated according to the formula [25, 45, 65]:

$$\begin{aligned} MSD(\Delta t) &= MSD(n\delta t) \\ &= \frac{1}{N-1-n} \sum_{j=1}^{N-1-n} \left\{ \left[x(j\delta t + n\delta t) - x(j\delta t) \right]^2 \right. \\ &\quad \left. + \left[y(j\delta t + n\delta t) - y(j\delta t) \right]^2 \right\}, \end{aligned} \quad (19.3)$$

where δt is the frame time and $(x(j\delta t + n\delta t), y(j\delta t + n\delta t))$ describes the molecule's position following a time interval $\Delta t = n\delta t$ after starting at position $(x(j\delta t), y(j\delta t))$, N is the total number of frames in a recording sequence, n and j are positive integers, and n determines the time increment.

We have developed a statistical method to classify each trajectory into the following three modes of motion (Figure 19.6): (1) simple Brownian diffusion mode, in which $MSD(\Delta t) = 4D\Delta t$, (2) directed diffusion mode, in which a molecule moves in a direction at a constant drift velocity (v_x, v_y), with superimposed random diffusion, $MSD(\Delta t) = 4D\Delta t + v^2(\Delta t)^2$, where $v^2 = v_x^2 + v_y^2$, and (3) confined diffusion mode, in which a molecule undergoes Brownian diffusion while totally confined within a limited area (compartment; $0 \leq x \leq L_x, 0 \leq y \leq L_y$) during the observation period. The $MSD(\Delta t)$ plot levels off and asymptotically approaches a constant value, as expressed by

$$\begin{aligned} MSD_x(\Delta t) &= \frac{L_x^2}{6} - \frac{16L_x^2}{\pi^4} \sum_{n=1(odd)}^{\infty} \frac{1}{n^4} \exp \left\{ -\frac{1}{2} \left(\frac{n\pi\sigma_x}{L_x} \right)^2 \Delta t \right\} \\ MSD_y(\Delta t) &= \frac{L_y^2}{6} - \frac{16L_y^2}{\pi^4} \sum_{n=1(odd)}^{\infty} \frac{1}{n^4} \exp \left\{ -\frac{1}{2} \left(\frac{n\pi\sigma_y}{L_y} \right)^2 \Delta t \right\} \\ \sigma_x^2 &= 2D_x, \quad \sigma_y^2 = 2D_y, \quad 4D = 2D_x + 2D_y \\ L_r^2 &= L_x^2 + L_y^2. \end{aligned} \quad (19.4)$$

To describe a molecule undergoing intercompartmental jumps during the observation period, an equation for the $MSD(\Delta t) - \Delta t$ plot has been derived by Powles et al. [44], based on the model in which a Brownian particle (diffusion coefficient in the absence of barriers, D_{micro}) is placed in an infinite array of evenly spaced (L), semipermeable (with a permeability, P) barriers. At long times, relative to the average residency time in a compartment, the transitions over many compartments will look like simple Brownian diffusion with a constant diffusion coefficient, defined as D_{MACRO} , which has the relationship,

$D_{\text{MACRO}}/D_{\text{micro}} = [1 + (PL)^{-1}]^{-1}$. The average residency time within each compartment, τ , is often a useful parameter, and can be determined through the average compartment size and the average long-term diffusion coefficient as $\tau = L^2/4D_{\text{MACRO}}$ (see Kusumi et al. [25], Sako and Kusumi [48], Fujiwara et al. [12] and Suzuki et al. [67] for the details).

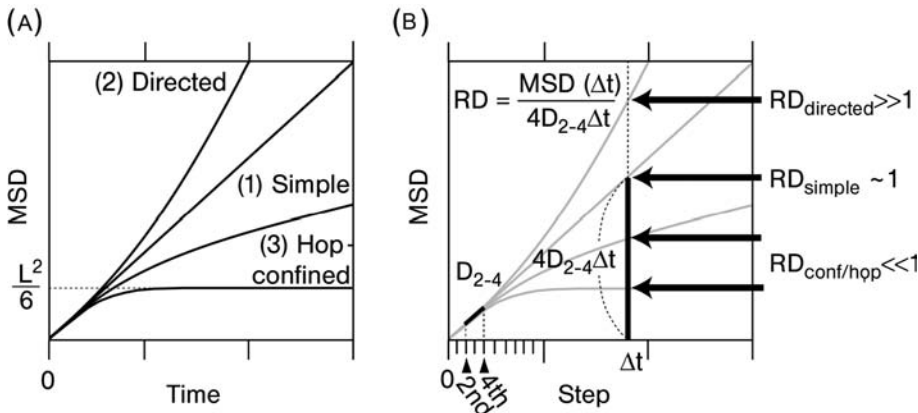


Figure 19.6 Analysis of single-molecule trajectories based on the $MSD(\Delta t) - \Delta t$ plot, and their statistical classification into the three modes of motion. (A) Theoretical $MSD(\Delta t) - \Delta t$ curves representing (1) simple Brownian diffusion, (2) directed diffusion, and (3) confined/hop diffusion. See the text for their equations. The graphs are drawn assuming that the short-term diffusion coefficients that are proportional to the slope near time 0 are identical for all of the cases. (B) The definition of the relative deviation (RD).

RD is defined as the ratio of an experimental $MSD(\Delta t)$ to the fictitious MSD at time $\Delta t(4D_{2-4}\Delta t)$, assuming that the molecule undergoes simple Brownian diffusion without confinement or directed diffusion with a diffusion coefficient determined from the initial slope ($4D_{2-4}$, determined from a linear fit to the MSD values at the second, third, and fourth frames of elapsed time). The more or less that the RD deviates from 1 reflects the chances that the molecule undergoes directed or confined/hop diffusion, respectively.

In essence, the shape of the $MSD(\Delta t)$ curve is characterized based on the relative deviation (RD) from ideal Brownian diffusion (Figure 19.6). RD is defined as $MSD(\Delta t)/4D_{\text{micro}}\Delta t$, where D_{micro} is the two-dimensional short-term diffusion coefficient that is proportional to the slope of the $MSD(\Delta t) - \Delta t$ plot near time 0, which is practically determined from a linear fit to the $MSD(\Delta t) - \Delta t$ plot at the second, third, and fourth frames of elapsed time (D_{2-4} as described in Kusumi et al. [25]; one has to be careful about the accuracy of these values. See Saxton [56] and Martin et al. [33]). This diffusion coefficient only reflects the viscosity properties in the space scale of tens of nanometers, and therefore can be determined independently of the motional modes (one must consider classifying molecules with very small D_{2-4} into the immobile mode, but its value has to be decided for each set of experiments, depending on the noise level and the overall distribution of the diffusion coefficient). The theoretical distribution of RD for free diffusion (which should

have an average value of 1) is obtained by a computer simulation of Brownian molecules, and RD values that give 2.5 (or 5; these are typical values and could be adjusted for the individual studies) percentile of the molecules from both ends of the distribution, referred to as RD_{\min} and RD_{\max} , are determined (Figure 19.7). When the trajectory of an experimental molecule shows an RD value between RD_{\min} and RD_{\max} , it is classified into the simple Brownian diffusion mode, and when $RD > RD_{\max}$ or $RD < RD_{\min}$, it is classified into the directed or confined/hop diffusion mode, respectively.

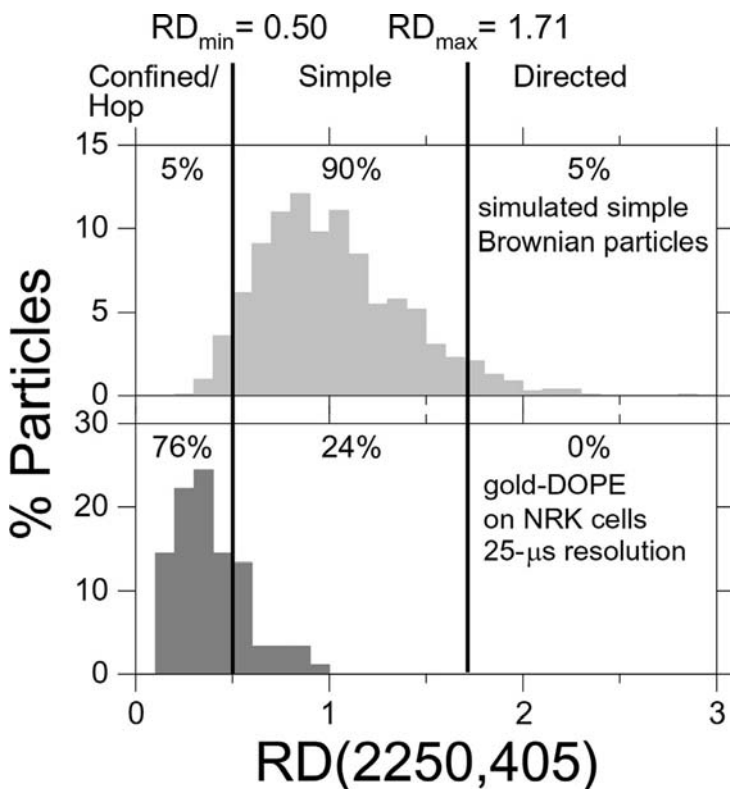


Figure 19.7 The distribution of RD for gold-tagged DOPE molecules observed in the plasma membrane of NRK cells at a 25- μ s resolution (bottom) is quite different from that expected from simulated simple Brownian particles (top). In this example, the total number of frames in each trajectory is 2250 steps (56 ms) and the analysis window (Δt) is 405 steps (10 ms). For the classification of the trajectories into the three modes of motion, 1 000 simple Brownian trajectories were generated by Monte Carlo simulations, and the

RD values that give 5% of the particles from both ends of the distribution were determined (RD_{\min} of 0.50 and RD_{\max} of 1.71, shown by bold vertical lines). When an experimental trajectory exhibited an RD value smaller than RD_{\min} or greater than RD_{\max} , it was classified into the confined/hop or directed diffusion mode, respectively. The majority (76%) of the DOPE trajectories ($N = 90$) were classified into the confined/hop mode at a time resolution of 25 μ s.

This is a simplified, but practical approach to anomalous diffusion discussed throughout this book, although there may be finer or more elegant ways of describing anomalous diffusion (see the Chapters by Kimmich et al., Shlesinger, and Chechkin et al. in this book). Furthermore, the diffusion data have to be analyzed and interpreted, based on or in the way consistent with the data on the membrane-associated part of the actin cytoskeleton meshwork observed by electron tomography with subnanometer precisions [35] as well as single-molecule force measurements on membrane molecules [49, 51, 72]. Interpretations simply based on the analysis of the diffusion measurements, particularly done at low-time resolutions or for a collection of molecules, have to be re-examined based on these other important observations.

Therefore, the goal of analyzing results obtained by single-molecule tracking in the plasma membrane is to classify each experimental trajectory into one of these motional modes and to obtain the distribution or the histogram of the parameters characterizing each motional mode. Fitting the above theoretical $MSD(\Delta t) - \Delta t$ equation to the experimental $MSD(\Delta t) - \Delta t$ plot, independently in two orthogonal directions, quantitatively provides estimates for various diffusion parameters. Furthermore, for hop diffusion, individual compartments in each trajectory can be detected automatically by a computer program (see the methods section of Suzuki et al. [67] for details). Briefly, a variable size window in time is moved through the trajectory, and the local diffusivity is recorded. Intercompartmental jumps are seen as sharp increases in the diffusivity of the molecule as it extends its motion into a neighboring compartment.

The hop rates of transferrin receptor for the smaller and greater compartments in NRK cells (NRK cells have a plasma membrane with nested double compartments with sizes of 230 and 710 nm, Fujiwara et al. [12]) were recently found to be an average of every 55 and 570 ms (direct SPT measurements gave 55 and 1800 ms, respectively, but the latter value needed to be corrected for the crosslinking effect of gold probes, using a macroscopic diffusion coefficient determined by SFMT with fluorescently labeled transferrin (a time window of 3 s, giving $0.22 \mu\text{m}^2/\text{s}$) and the compartment size determined by SPT (710 nm)) [12]. Furthermore, all of the transmembrane proteins examined thus far, including E-cadherin [51], transferrin receptor [48], $\alpha 2$ -macroglobulin receptor [48], CD44 (Ritchie and Kusumi, unpublished observations), band 3 [72], stem cell factor receptor (Kobayashi, Murakami, and Kusumi, unpublished observations), and various GPCRs (Suzuki et al. [67], Kasai, Prossnitz, and Kusumi, unpublished observations), undergo hop diffusion. The macroscopic diffusion coefficients for these molecules, determined by SPT (reflecting hop diffusion rate over many compartments), are basically consistent with the SFMT and FRAP data, although due to the crosslinking effects of gold probes, the macroscopic diffusion coefficients may be smaller by a factor of 1–5. Since,

even in the presence of crosslinking effects, the compartment sizes determined by SPT are likely to be correct, a good strategy to evaluate the correct average hop frequency across the compartment boundaries (inverse the average residency time within a compartment) is to use the macroscopic diffusion coefficient determined by SFMT with fluorescent probes and the compartment size obtained by SPT, using the equation,

$$\text{Residency time} = \frac{(\text{Average compartment size from SPT})^2}{(4 \times D_{\text{MACRO}} \text{ from SFMT})}. \quad (19.5)$$

With this equation, one assumes a stylized model of hop diffusion (for the purpose of simple calculation), in which the molecule undergoes diffusion in the presence of an equally spaced, infinite array of barriers of the same height, and the hops occur between the central points in the compartments. Murase et al. [37] successfully employed this strategy to obtain the residency time as well as the permeability of the barriers in the plasma membranes for a phospholipid molecule, in a variety of cultured mammalian cells.

19.5

Corralling Effects of the Membrane Skeleton for Transmembrane Proteins (the Membrane-Skeleton Fence Model)

What makes the boundaries between these compartments for transmembrane proteins? We proposed the “membrane-skeleton fence” or “membrane-skeleton corralling” model (Figure 19.8, left). Transmembrane proteins protrude into the cytoplasm, and, in this model, their cytoplasmic domains collide with the membrane skeleton, which induces temporary confinement

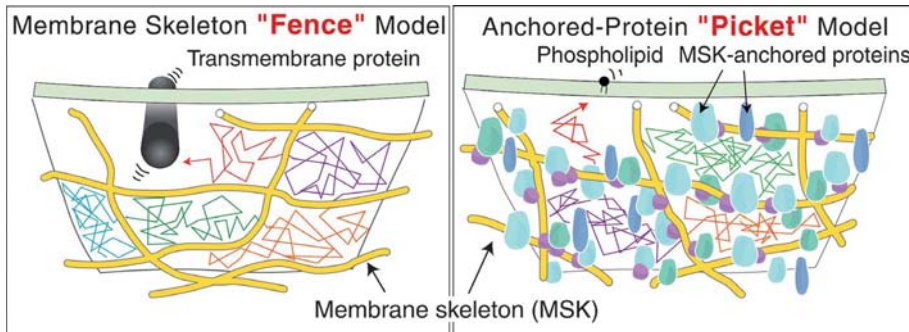


Figure 19.8 The effects of the membrane-skeleton “fence” (left) and the anchored-protein “pickets” (right) that together partition the entire plasma membrane into small compartments. See the text for further details. The hydrodynamic-friction-like effect was first described by Bussell et al. [2, 3].

or corraling of the transmembrane proteins in the membrane skeleton mesh. Transmembrane proteins may hop between the compartments when a space that allows the passage of the cytoplasmic domain of the transmembrane protein is formed between the membrane and the membrane skeleton. This space may be created as a consequence of the thermal fluctuation of these structures, when the actin filament that forms the compartment boundary temporarily dissociates, and/or when the transmembrane protein incidentally has sufficient kinetic energy to overcome the confining potential energy of the compartment barrier when it is in the boundary region.

Here is a summary for the evidence supporting the membrane skeleton fence model for the partitioning of the cell membrane with respect to transmembrane proteins. The problems with other models, including raft-induced compartmentalization of the plasma membrane, crowding of the extracellular surface by the extracellular domains of membrane molecules, protrusions and dips throughout the membrane, and/or a two-dimensional continuum fluid, are that they can explain one or several of these observations, but not *all* of these observations.

- (1) The hop rate of band 3 in the red-cell ghost membrane and that for E-cadherin in cultured L cells (both are transmembrane proteins) were increased with a decrease in the cytoplasmic domain size [51, 72]. This clearly indicates that the cytoplasmic domain of the transmembrane protein is involved in temporarily trapping the transmembrane protein.
- (2) When each individual transmembrane protein molecule was dragged by an optical trap (transferrin receptor and E-cadherin), the compartment size estimated by the free dragging length in optical trap experiments employing very weak trapping forces agrees with that detected by single-molecule diffusion measurements [49, 51], indicating the presence of actual force barriers between the compartments.
- (3) The experiments in which each individual molecule of transferrin receptor, E-cadherin, and band 3 was dragged using an optical trap revealed that the compartment boundaries are elastic, consistent with the model in which the basis for the compartment barrier is the membrane skeleton meshwork [49, 51, 72].
- (4) When the membrane skeleton is dragged, by moving the optical trap that grabbed a polystyrene bead bound to the membrane skeleton, transmembrane proteins (band 3) that are not bound to the membrane skeleton and undergo diffusion were also moved, along with the movement of the membrane skeleton [72].

(5) Hop diffusion of transmembrane proteins depends on the integrity of the membrane skeleton [48, 67, 72]. Very mild latrunculin or cytochalasin D treatments increased the average compartment size. Note that since harsher treatments tend to induce membrane protein aggregation and overall changes in the cell shape, making the interpretation of diffusion data virtually impossible, only very mild treatments are useful. Under these conditions, one should note that the effects of these drugs are complex, depending on the treatment duration (because cells start compensating for the initial changes in the actin filaments), the cell type (the overall amounts of actin and the ratio of the amounts of actin molecules in stress fibers vs. single filaments), the action mechanisms of the drugs, and the drug concentrations. Furthermore, the effects of latrunculin or cytochalasin D are difficult to find if one measures the macroscopic diffusion coefficients by FRAP or slow-rate (like video-rate) single-molecule tracking, because, after cells are treated with these drugs, the compartment size slightly increases, whereas the hop rate tends to decrease slightly, resulting in only minor increases in the macroscopic diffusion coefficient (between a factor of 1 and 2). In fact, several reports have noted the absence of the effects of latrunculin, cytochalasin, gelsolin, and siRNA of spectrin on the movement of various membrane molecules [11, 32, 41, 58, 77], whereas Lenne et al. [30], using fluorescence correlation spectroscopy, found that the diffusion of transferrin receptor is affected by drugs that target the actin-based membrane skeleton.

Furthermore, hop diffusion could not be found in liposomes and in membrane blebs, where the membrane skeleton is essentially absent (Suzuki et al. [67]; in some cell types, considerable fractions of the actin skeleton remain in the blebbled membrane, and if this happens, the membrane has to be further treated with latrunculin or cytochalasin D to remove the remaining actin skeleton, for the elimination of hop diffusion). In these membranes, the membrane molecules undergo rapid, simple Brownian diffusion that can be characterized by a single diffusion coefficient in the range of 5–10 $\mu\text{m}^2/\text{s}$ for DOPE or 3 $\mu\text{m}^2/\text{s}$ for transmembrane proteins in all of the observation time scales (0.025 ms–1 s, i.e., by a factor of 40 000).

(6) Electron microscopy results, in particular those with rapidly frozen, deeply etched specimens of the plasma membranes [35] or those obtained with a scanning electron microscope (Morone and Kusumi, unpublished observations), showed that, except for the specific locations where internalization apparati, cell adhesion structures, microvilli, or filopodia are located, the plasma membrane exhibits a gently undulating surface, which generally lacks sharp protrusions or dips. In fact, in our previous observations of high-speed single-particle tracking, the candidate

cell lines were first examined by scanning electron microscopy, and only those without too many microvilli were selected for our observations. The presence of membrane protrusions and dips has been thought to cause apparent confinement. However, this cannot be true. First, to reduce the macroscopic diffusion coefficient by a factor of 10, the protrusions or dips must be as large as 100–300 nm for a compartment size of 200 nm, and they must be present throughout the cell membrane. This is clearly inconsistent with the electron microscope observations (possibly except for the brush-border membranes of epithelial cells) [35, 46]. Furthermore, the idea of membrane protrusions and/or dips for the apparent confinement is inconsistent with the observations (1), (2), and (3) described above.

- (7) The instances of hops are clearly visible and also are detectable with a computer program in the analysis of single-molecule trajectories with sufficient time resolutions [67].
- (8) Oligomerization of transmembrane proteins reduces the macroscopic diffusion coefficient by decreasing the intercompartmental hop rate (without affecting the compartment size), a phenomenon termed oligomerization-induced trapping by [18]. This can be easily explained by the membrane skeleton fence model, but cannot be naturally explained by the two-dimensional continuum fluid model, the viscoelastic model, the general anomalous diffusion model, or the model of long membrane protrusions and deep dips throughout the membrane.

The other aspect of this result is that it indicates a need for control experiments for the crosslinking effect of the gold probes using SFMT or FRAP, when SPT with gold particles is employed. To circumvent such a nuisance, in our lab, we always begin our studies using SFMT with a fluorescent tag, and only when we need high-speed single molecule tracking or when we wish to carry out optical trapping experiments, we develop colloidal gold probes. The crosslinking effect could become very extensive, so that it could cause the long-term trapping of the target protein within a compartment, when the probes were attached to cells at lower temperatures for over several 10s of minutes [4, 5, 67].

19.6

Phospholipids Also Undergo Hop Diffusion in the Plasma Membrane

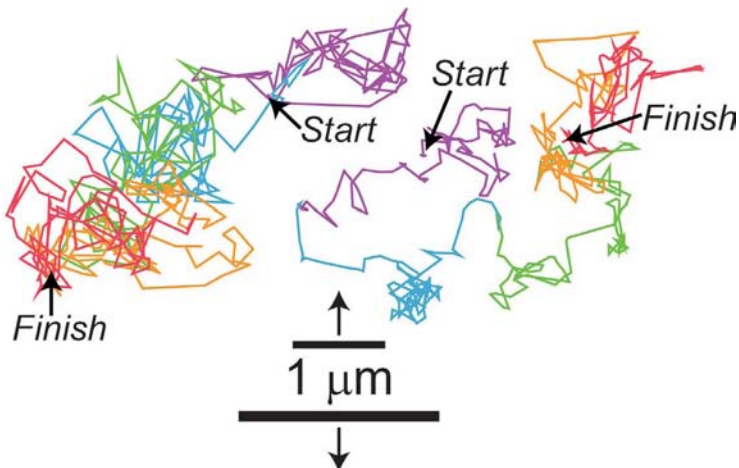
The next natural question is “What about lipids?” Fujiwara et al. [12] and Murase et al. [37] indeed addressed this question, by observing an unsaturated phospholipid, L- α -dioleoylphosphatidylethanolamine (DOPE), which is considered to be one of the most difficult molecules to immobilize in the

plasma membrane, due to its unsaturation and low-levels of headgroup interactions. To observe the movement of single DOPE molecules, the DOPE was tagged with the fluorescent dye Cy3 or with a 40-nm diameter colloidal gold particle, and was observed by SFMT and SPT, respectively. The colloidal gold probes were necessary to observe DOPE diffusion at frame rates much higher than video rate (30 Hz). Due to low sensitivity, SFMT would not accommodate observations at frame rates much faster than 200 Hz. In video-rate observations (30 Hz) and in NRK cells, both methods yielded about the same diffusion coefficients, as long as they remained in time windows shorter than 100 ms. This result justifies the use of such a large colloidal gold particle as a probe for a small molecule, like DOPE. In longer time scales, the diffusion coefficient of gold-tagged DOPE was smaller than that of Cy3-tagged DOPE by a factor of 3, due to the crosslinking effect of gold probes (Fujiwara et al. [12], which, by the way, in itself shows that the plasma membrane cannot be considered as a two-dimensional continuum fluid).

Using high-speed SPT with a time resolution of 25 μ s (a frame rate of 40 kHz, about 1300-fold faster than normal video rate), Fujiwara et al. [12] and Murase et al. [37] found that an unsaturated phospholipid, DOPE, undergoes hop diffusion. Representative trajectories of DOPE in the plasma membrane of NRK cells, recorded at time resolutions of 33 ms and 25 μ s, are shown in Figure 19.9. At a 33-ms resolution (normal video rate), practically all of the DOPE trajectories were classified into the simple Brownian diffusion mode. However, when the time resolution was enhanced to 25 μ s, it became clear that the simple Brownian nature found at the 33-ms resolution is only an apparent one. The hop diffusion is clearly visible (individual compartments were detected by the computer program we developed), and the statistical analysis method described above indeed showed that over 85% of the DOPE trajectories were classified into the hop-confined diffusion mode, rather than the simple Brownian diffusion mode.

Quantitative analysis of the trajectories, such as those displayed in Figure 19.6, revealed that the average compartment size was 230 nm in the case of NRK cells. The average residency time within each 230-nm compartment was 11 ms. No wonder we did not see hop movement at video rate, with a time resolution of only 33 ms. In fact, all of these trajectories shown in Figure 19.9 (bottom) are 62-milliseconds long, and if we had used video rate observations, there would have been only 2 or 3 points in the whole trajectory, and there would have been no way of detecting the hop diffusion of DOPE molecules. The diffusion rate within the 230-nm compartment, which is $5.4 \mu\text{m}^2/\text{s}$ on average, is interesting. It is almost as large as that of DOPE molecules observed in artificial membranes, such as giant liposomes. Therefore, lipid diffusion in the cell membrane is slow, not because the diffusion per se is slow,

33-ms Resolution (16.7-s Observation)



25-μs Resolution (62-ms Observation)

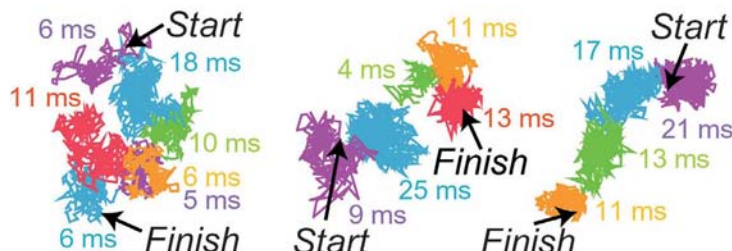


Figure 19.9 Representative trajectories of single or small groups of DOPE molecules recorded at time resolutions of 33 ms and 25 μ s (see the text for details). The different colors of the trajectories obtained at a 33-ms resolution simply represent a time sequence of every 3.3 s. The different colors in the bottom trajectories obtained at a 25- μ s resolution represent various plausible compartments, detected by computer software developed in our laboratory (in a time sequence of purple,

blue, green, orange, and red for both time resolutions). These results show that the simple Brownian nature of diffusion observed at a video rate (33 ms/frame) is only superficial, and that it is due to the low-time resolution of the observation: the confined + hop movement of each DOPE molecule is totally smeared out at video rate. To resolve such movement, the time resolution must be considerably shorter than the average residency time within a compartment.

but because (1) the plasma membrane is compartmentalized with regard to the translational diffusion of phospholipids, (2) the lipid molecules undergo hop diffusion over these compartments, and (3) it takes time to hop from a compartment to an adjacent one (Figure 19.3). These observations solved the 30-year old enigma in the fluid mosaic model: the mechanism underlying the reduction of the diffusion rate in the plasma membrane by a factor of ~ 20 from that found in artificial membranes.

What makes the boundaries between these compartments, which even work for phospholipids located in the outer leaflet of the membrane? Fujiwara et al. [12] observed DOPE diffusion in membrane blebs (balloon-like structures of the plasma membranes, where the membrane skeleton is largely lost, and Fujiwara et al. further reduced the actin-based membrane skeleton by treating the cells with latrunculin) as well as in liposomes, and found that DOPE molecules undergo rapid, simple Brownian diffusion with a diffusion coefficient of $\approx 9 \mu\text{m}^2/\text{s}$ in these membranes. Furthermore, Fujiwara et al. [12] and Murase et al. [37] examined the involvement of the membrane skeleton, as well as the effects of the extracellular matrices, the extracellular domains of membrane proteins, and the cholesterol-rich raft domains, in phospholipid hop diffusion. They found that the phospholipid movement was only affected when they modulated the membrane skeleton with actin drugs. This is consistent with the previous FRAP observations, in the sense that the modulation of the membrane skeleton influences the lipid movement (although FRAP did not allow researchers to observe such detailed motion; see Paller [42]). All of these results point to the involvement of the membrane skeleton in both the temporal corralling and hop diffusion of phospholipids.

However, this is a very strange and surprising result! Since the DOPE molecules they observed were located in the extracellular leaflet of the membrane (unlabeled DOPE may flip, but the large DOPE molecule tagged with a gold particle cannot flip to enter the cytoplasmic leaflet), whereas the membrane skeleton is located on the cytoplasmic surface of the membrane, the DOPE and the membrane skeleton cannot interact directly. To explain this apparent discrepancy, the “anchored transmembrane-protein picket model” was proposed (Figure 19.8, right). In this model, various transmembrane proteins anchored to and lined up along the membrane skeleton (fence) effectively act as rows of pickets (these transmembrane proteins act like posts for the fence, and are thus termed pickets) against the free diffusion of phospholipids, due to steric hindrance as well as the hydrodynamic-friction-like effects of immobilized anchored membrane protein pickets. The latter effect, first proposed by Hammer’s group [2,3], propagates over about several nanometers, and is prominent in the membrane because the membrane viscosity is much greater than that of water, by a factor of ≈ 100 , and is particularly marked when immobile pickets are aligned along the membrane-skeleton fence. When the number density of these transmembrane picket proteins exceeds a certain threshold (20–30% coverage of the intercompartmental boundary to reproduce the experimentally observed residency time of 11 ms in a 230-nm compartment in NRK cells, as determined by a series of Monte Carlo simulations by Fujiwara et al. [12]), the rows of pickets on the membrane-skeleton fences become effective diffusion barriers that confine the phospholipids for some time. Note that these transmembrane picket proteins do not have to be stably

bound to the membrane skeleton for a long time. Assuming that the boundary region between the compartments is 10 nm wide, it takes about 10 μ s for a molecule to traverse this region. Therefore, the zeroth approximation is that if a transmembrane protein is bound to the membrane skeleton for at least 10 μ s, then it becomes an effective picket to participate in the formation of the diffusion barrier. Note that, in this model, the transmembrane proteins anchored to the membrane skeleton are coupling the membrane skeleton, which is located on the cytoplasmic surface of the membrane, with the phospholipids that are located in the outer leaflet of the membrane.

Here, the evidence supporting the anchored-protein picket model (and membrane-skeleton fence model) is summarized.

- (1) As described in point 5 for the membrane-skeleton fence model, the hop diffusion of DOPE depends on the integrity of the membrane skeleton [12, 37, 39]. Similar cautionary remarks can be applied to DOPE diffusion. Furthermore, hop diffusion cannot be found in liposomes and in membrane blebs, where the membrane skeleton is largely absent [12]. In these membranes, the membrane molecules undergo rapid, simple Brownian diffusion that can be characterized by a single diffusion coefficient, in the range of 5–10 $\mu\text{m}^2/\text{s}$ for DOPE, in all of the observation time scales (0.025 ms–1 s, i.e., by a factor of 40 000).
- (2) Using electron tomography of rapidly frozen, deeply etched specimens of plasma membranes, Morone et al. [35] determined the distribution of the mesh size of the actin-based membrane skeleton right on the cytoplasmic surface of the plasma membrane, and found that it agrees well with that for the compartment size determined from the DOPE diffusion data (Figure 19.10). Good agreements between the electron tomography data and the DOPE diffusion results were observed for two cell types, NRK and FRSK cells, which exhibited quite different compartment sizes for DOPE diffusion, 230 nm and 42 nm, respectively, further supporting the anchored-protein picket model. In addition, their results showed that the cytoplasmic surface of the entire plasma membrane is coated with the actin-based membrane skeleton, except for the locations of the internalization apparatus and cell adhesion structures.
- (3) In the case of the human erythrocyte ghost, the compartment size determined from the diffusion measurements of transmembrane proteins and lipids is consistent with the mesh size of the spectrin-based membrane skeleton on the cytoplasmic surface of the ghost membrane, determined by AFM [70, 72].

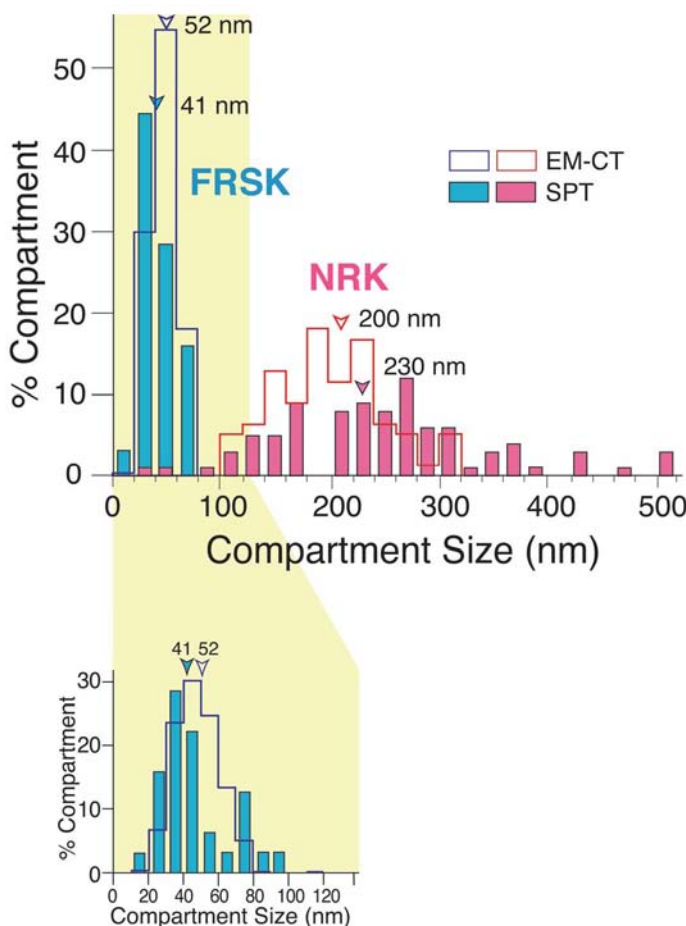


Figure 19.10 Comparison of the distributions of the membrane-skeleton mesh size on the cytoplasmic surface of the plasma membrane estimated by electron tomography (open bars), with that of the compartment size determined from the phospholipid diffusion data (closed bars, adapted from Fujiwara et al. [12] and Murase et al. [37]), for NRK (magenta)

and FRSK (blue) cells. Within the same cell type, the MSK mesh size and the diffusion compartment size exhibited similar distributions (compare the open and closed bars with the same color). The actual sizes are quite different between NRK and FRSK cells. The bottom figure shows the histograms for FRSK in more detail.

- (4) Mild treatments with jasplakinolide, which stabilizes the actin filaments, reduced the macroscopic diffusion coefficient, without strongly affecting the compartment size, by decreasing the hop frequency [12, 37, 39].
- (5) As mentioned in point 8 for the membrane-skeleton fence model (oligomerization-induced trapping found for E-cadherin), the oligomerization of DOPE by crosslinking gold probes considerably reduced the inter-

compartmental hop rate, without affecting the compartment size, which thus decreased the macroscopic diffusion coefficient [37]. This entails the oligomerization-induced trapping of a phospholipid. This dependence of the diffusion coefficient on the diffusant size can easily be explained by the anchored-protein picket model, due to the steric effects, but not by other models.

- (6) The hop diffusion is not affected by removing the major fraction of the extracellular domains of transmembrane proteins and the extracellular matrix [12,37], indicating that these are not the major causes for the induction of hop diffusion.
- (7) The removal of cholesterol has no major effects on the hop diffusion [12, 37], suggesting that lipid rafts are not the primary causes for membrane compartmentalization or hop diffusion.
- (8) The compartment sizes detected by transmembrane proteins (transferrin receptor, α_2 -macroglobulin receptor) and the phospholipid DOPE are the same in all of the cell types examined thus far ([12, 48], Fujiwara, Iwasawa, and Kusumi, unpublished observations, Murase and Kusumi, unpublished observations), supporting the membrane-skeleton fence and anchored-protein picket models.
- (9) Monte Carlo simulations reproduced the experimentally observed residency times when only 20–30% of the compartment boundaries were occupied by the anchored transmembrane protein pickets [12, 37, 39]. This represents the anchoring of only about 15% of the total transmembrane proteins in the plasma membrane.
- (10) The instances of hops are clearly visible and also are detectable with a computer program in the analysis of single-molecule observations with sufficient time resolution [12, 37].

The anchored transmembrane protein pickets would be operative on any molecules incorporated in the membrane, including transmembrane proteins. Therefore, the diffusion of transmembrane proteins will be doubly suppressed in the membrane. Both the fence and picket will act on transmembrane proteins.

The oligomerization-induced trapping described above in point (5) indicates that the intercompartmental hop rate, or the residency time within a compartment, strongly depends on the oligomer size. Therefore, the correct residency time for monomeric DOPE (or other molecules) within a compartment was estimated, using the macroscopic diffusion coefficient obtained from single fluorescent-molecule tracking (SFMT) at a video rate and the compartment size obtained from the high-speed SPT (this should not be affected

by oligomerization) with the use of the equation $[\text{compartment size}]^2 / 4D$. In the slow frame-rate regime, the diffusing molecule can be modeled as that hopping between the centers of adjacent compartments. This was necessary because, with single fluorophore observations, obtaining trajectories with both a sufficient length and time resolution is difficult, due to poor signal-to-noise ratios and photobleaching.

How universal is this plasma membrane compartmentalization? Using the unsaturated phospholipid DOPE, Murase et al. [37] found such plasma membrane compartmentalization in all of the nine mammalian cells they examined. This list has slightly expanded since then, and in the 11 types of cultured mammalian cells we have analyzed, we detected the hop diffusion of DOPE incorporated in the plasma membrane. Among the different cell types, the compartment size varies greatly, from 30 nm up to 230 nm, and the residency time of DOPE varies between 1 and 17 ms.

Several recent studies reported the failure to detect such hop diffusion, but the experimental methods employed in these studies appear to be suboptimal, with unsuitable spatial resolutions, low frame rates, short overall observation durations for a single molecule, and wrong time scales for tracking etc [30, 78, 79].

19.7

The Biological Significance of Oligomerization-Induced Trapping Based on the Membrane-Skeleton Fences and Pickets

In the earlier part of this review, it was stated that one of the two long-standing problems for biophysicists studying molecular diffusion in the plasma membrane is that we do not understand why the macroscopic diffusion coefficients considerably decrease when membrane molecules, including receptor molecules and other signaling molecules in the membrane, form oligomers or molecular complexes [17, 18, 40]. These observations are completely opposite from the general view of membrane biophysicists. The theory by Saffman and Delbrück (1975) and experiments by Peters and Cherry [43] and Vaz et al. [75] consistently showed that translational diffusion is very *insensitive* to the diffusant size.

The partitioning of the plasma membrane into many small compartments could explain why the diffusion in the plasma membrane is very sensitive to oligomerization or the formation of molecular complexes (Figure 19.11, left), in contrast to the prediction from the two-dimensional continuum fluid model (Figure 19.11, right). These points have been already touched upon as evidence to support the fence and picket models, but they are more comprehensively described here. Monomers of membrane molecules may hop across the

picket-fence with relative ease, but upon oligomerization or molecular complex formation, the oligomers or the complexes as a whole, rather than single molecules, have to hop across the picket-fence all at once, and therefore, much more free space that lasts longer is required for the passage of these oligomers across the picket-fence of the intercompartmental boundary. Hence, these complexes are likely to have a much slower rate of hopping between the compartments, as found with oligomers of DOPE [37]. In addition, molecular complexes are more likely to be bound or tethered to the membrane skeleton, perhaps temporarily, which also induces (temporary) immobilization or trapping of molecular complexes. Such enhanced confinement and binding effects induced by oligomerization or molecular complex formation were collectively termed “oligomerization-induced trapping” [18, 24].

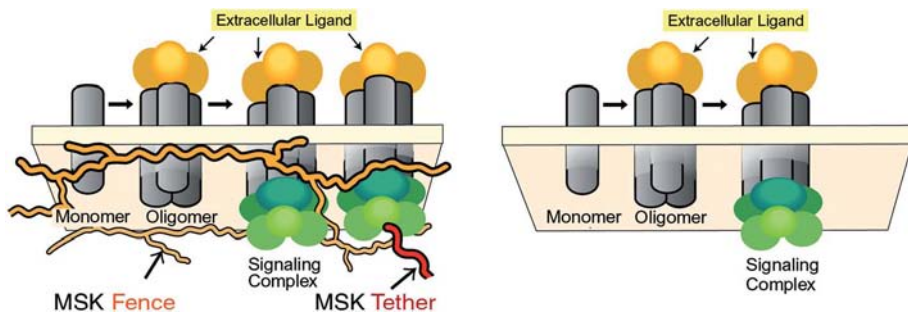


Figure 19.11 Oligomerization-induced trapping model, indicating how slowing or immobilization of membrane molecules may be induced upon oligomerization or the formation of greater molecular complexes. Upon oligomerization or molecular complex formation (left), the hop rate across the intercompartmental barrier would be reduced greatly, because, in contrast to monomers, in the case of molecular complexes, all of the molecules that form the complex have to hop across the picket-fence simultaneously, which re-

quires greater and longer openings in the intercompartmental boundaries. In addition, due to the avidity effect, molecular complexes are more likely to be tethered to the membrane skeleton, perhaps temporarily, which also reduces their overall diffusion rate. This enhanced confinement and the binding effects induced by oligomerization or molecular complex formation are collectively termed “oligomerization-induced trapping” [18]. This would not occur in the absence of membrane skeleton fences and pickets (right).

This oligomerization-induced trapping might play very important roles in the temporary localization of signal transduction complexes (Figure 19.11, left). When an extracellular signal is received by a receptor molecule, the receptor often forms oligomers and signaling complexes by recruiting cytoplasmic signaling molecules. Due to the “oligomerization-induced trapping”, these oligomeric complexes tend to be trapped in the same membrane skeleton compartment as that where the extracellular signal was initially received. Therefore, the membrane skeleton fence and the anchored transmembrane-protein pickets help to temporarily localize the initiation of the cytoplasmic signal to the place where the extracellular signal was received. Such spatial

confinement is particularly important for signals that induce local or polarized reorganization of the cytoskeleton or chemotactic events.

This would not occur in the absence of membrane skeleton fences and pickets (Figure 19.11). If there were no such structures, then even when the signalling complex is formed, the diffusion rate of such a complex would be almost the same as that of the single receptor molecules, as diffusion theory teaches us (Saffman and Delbrück, 1975).

Therefore, in the plasma membrane, oligomerization or molecular complex formation is tied to immobilization by the membrane skeleton fence and anchored-protein pickets.

19.8

A Paradigm Shift of the Plasma Membrane Structure Concept is Necessary: From the Simple Two-dimensional Continuum Fluid Model to the Compartmentalized Fluid Model

As described above, the membrane-skeleton “fence” and the anchored-protein “picket” together solved the two long-standing problems of molecular diffusion in the plasma membrane: (1) the oligomerization-induced slowing of diffusion and (2) the reduced diffusion coefficients of membrane molecules in the plasma membrane, relative to those found in artificial membranes, by a factor of ~ 20 . These results could not be explained by the two-dimensional continuum fluid model. The two-dimensional continuum fluid model is just fine, as long as the spatial scale is limited to the size of the original cartoon depicted by Singer and Nicolson ([66], although at the smaller limit of the molecular scale, the continuum model would also fail), which is about $10\text{ nm} \times 10\text{ nm}$, based on the number of lipid molecules in the cartoon (Figure 19.3 inset). However, in spatial scales over several 10s of nm in the plasma membrane, simple-minded extensions of the fluid-mosaic model of Singer and Nicolson and the theory by Saffman–Delbrück fail. The cell seems to have developed (during evolution) means to control the long-range diffusion of membrane molecules and to make this control sensitive to the diffusant size. The long-range control of diffusion appears to be carried out by the actin-based membrane skeleton, as indicated by the partitioning (corralling) effect of the membrane skeleton and the rows of anchored-protein pickets.

Furthermore, when the cell needs to build a macroscopic diffusion barrier that blocks the diffusion of even phospholipids over the barrier region, like that found in the initial segment region of the neuronal cell membrane, the cell achieves this task by forming very dense picket-fences in the barrier region, effectively blocking the diffusion of membrane molecules across this region [19, 39, 80].

As such, a paradigm shift for the concept of plasma membrane structures in the space scales greater than 10 nm is required, from the two-dimensional continuum fluid to the compartmentalized fluid, in which its constituent molecules undergo hop diffusion over the compartments.

An important corollary of these results is that all of the diffusion coefficients obtained by FRAP, single-molecule techniques at slow rates (like a video rate), or fluorescence correlation spectroscopy (FCS) must be considered as “*the effective diffusion coefficients*”, which may be useful only when the involved time-space window is specified [10, 12, 15, 38, 54, 55, 62, 67]. One should be clearly aware that membrane molecules do *not* undergo simple Brownian diffusion, although they may undergo “*effective simple Brownian diffusion*” in limited time-space windows, generally in time scales longer than several 10s of milliseconds and in spatial scales greater than 0.3 μm .

We emphasized the importance of tracking single molecules at enhanced frame rates. Thus far, the frame rate has been up to 40 000 frames per second (fps, 25 $\mu\text{s}/\text{frame}$) for single-particle tracking and 300 fps for single fluorescent-molecule tracking. The improvements have been continued in our laboratory, and currently, the frame rates are 250 000 fps (4 $\mu\text{s}/\text{frame}$) for single-particle tracking and 20 000 fps (50 $\mu\text{s}/\text{frame}$) for single fluorescent-molecule tracking. Since the rotational (reorientational) correlation times for monomeric proteins in the membrane (monomeric rhodopsin in reconstituted membranes, Kusumi and Hyde [21], Kusumi et al. [23] and for 40-nm colloidal gold particles in water are both about a few microseconds, further improvements in the frame rate would make the tracking too sensitive to rotational diffusion, and obscure the true displacement of molecules in space. Therefore, this time resolution of 4 μs is just about the useful limitation of the frame rate in studying molecular diffusion in the cell membrane using single-particle tracking. In the present article, we pay special attention to the short-range regulation mechanisms. However, the cell might also use some means for long-range regulations, perhaps combining the corralling and dragging effects of the cytoskeleton [24, 27]. For the detection of such long-range mechanisms, slower rate of observations would be required.

Acknowledgments

This research was supported in part by Health and Labour Sciences Research Grant nano-001 to N. Morone, and Grants-in-Aid for Scientific Research from the MEXT to N. Morone and A. Kusumi, and that on Priority Areas from the MEXT to A. Kusumi.

References

- 1** Borgdorff, A.J., and Choquet, D. *Nature* 2002, 417, 649–53.
- 2** Bussell, S.J., Hammer, D.A., and Koch, D.L. *J. Fluid Mech.* 1994, 258, 167–190.
- 3** Bussell, S.J., Koch, D.L., and Hammer, D.A. *Bioophys. J.* 1995, 68, 1836–49.
- 4** Daumas, F., Destainville, N., Millot, C., Lopez, A., Dean, D., and Salome, L. *Bioophys. J.* 2003a, 84, 356–66.
- 5** Daumas, F., Destainville, N., Millot, C., Lopez, A., Dean, D., and Salome, L. *Biochem. Soc. Trans.* 2003b, 31, 1001–5.
- 6** De Brabander, M., Geuens, G., Nuydens, R., Moeremans, M., and De Mey, J. *Cytobios*. 1985, 43, 273–83.
- 7** De Brabander, M., Nuydens, R., Geerts, H., and Hopkins, C.R. *Cell Motil. Cytoskelet.* 1988, 9, 30–47.
- 8** De Brabander, M., Nuydens, R., Ishihara, A., Holifield, B., Jacobson, K., and Geerts, H. *J. Cell Biol.* 1991, 112, 111–24.
- 9** Dietrich, C., Volovyk, Z.N., Levi, M., Thompson, N.L., and Jacobson, K. *Proc. Natl. Acad. Sci. U.S.A.* 2001, 98, 10642–7.
- 10** Feder, T.J., Brust-Mascher, I., Slattery, J.P., Baird, B., and Webb, W.W. *Bioophys. J.* 1996, 70, 2767–73.
- 11** Frick, M., Schmidt, K., and Nichols, B.J. *Curr. Biol.* 2007, 17, 462–7.
- 12** Fujiwara, T., Ritchie, K., Murakoshi, H., Jacobson, K., and Kusumi, A. *J. Cell Biol.* 2002, 157, 1071–81.
- 13** Gambin, Y., Lopez-Esparza, R., Reffay, M., Sierecki, E., Gov, N.S., Genest, M., Hodges, R.S., and Urbach, W. *Proc. Natl. Acad. Sci. U.S.A.* 2006, 103, 2098–102.
- 14** Gelles, J., Schnapp, B.J., and Sheetz, M.P. *Nature* 1988, 331, 450–3.
- 15** Ghosh, R.N., and Webb, W.W. *Bioophys. J.* 1994, 66, 1301–18.
- 16** Harms, G.S., Cognet, L., Lommerse, P.H., Blab, G.A., Kahr, H., Gamsjager, R., Spaink, H.P., Soldatov, N.M., Romanin, C., and Schmidt, T. *Bioophys. J.* 2001, 81, 2639–46.
- 17** Hegener, O., Prenner, L., Runkel, F., Baader, S.L., Kappler, J., and Haberlein, H. *Biochemistry* 2004, 43, 6190–9.
- 18** Iino, R., Koyama, I., and Kusumi, A. *Bioophys. J.* 2001, 80, 2667–77.
- 19** Kobayashi, T., Storrie, B., Simons, K., and Dotti, C.G. *Nature* 1992, 359, 647–50.
- 20** Kucik, D.F., Elson, E.L., and Sheetz, M.P. *Nature* 1989, 340, 315–7.
- 21** Kusumi, A., and Hyde, J.S. *Biochemistry* 1982, 21, 5978–83.
- 22** Kusumi, A., Nakada, C., Ritchie, K., Murase, K., Suzuki, K., Murakoshi, H., Kasai, R.S., Kondo, J., and Fujiwara, T. *Annu. Rev. Biophys. Biomol. Struct.* 2005, 34, 351–78.
- 23** Kusumi, A., Sakaki, T., Yoshizawa, T., and Ohnishi, S. *J. Biochem. (Tokyo)* 1980, 88, 1103–11.
- 24** Kusumi, A., and Sako, Y. *Curr. Opin. Cell Biol.* 1996, 8, 566–74.
- 25** Kusumi, A., Sako, Y., and Yamamoto, M. *Bioophys. J.* 1993, 65, 2021–40.
- 26** Kusumi, A., Subczynski, W.K., and Hyde, J.S. *Proc. Natl. Acad. Sci. U.S.A.* 1982, 79, 1854–58.
- 27** Kusumi, A., Suzuki, K., and Koyasako, K. *Curr. Opin. Cell Biol.* 1999, 11, 582–90.
- 28** Lee, C.C., and Petersen, N.O. *Bioophys. J.* 2003, 84, 1756–64.
- 29** Lee, G.M., Zhang, F., Ishihara, A., McNeil, C.L., and Jacobson, K.A. *J. Cell Biol.* 1993, 120, 25–35.
- 30** Lenne, P.F., Wawrzynieck, L., Conchonaud, F., Wurtz, O., Boned, A., Guo, X.J., Rigneault, H., He, H.T., and Marguet, D. *EMBO J.* 2006, 25, 3245–56.
- 31** Lindblom, G., Johansson, L.B., and Arvidsson, G. *Biochemistry* 1981, 20, 2204–7.
- 32** Lommerse, P.H., Vastenhoud, K., Pirinen, N.J., Magee, A.I., Spaink, H.P., and Schmidt, T. *Bioophys. J.* 2006, 91, 1090–7.
- 33** Martin, D. S., Forstner, M. B., and Käs, J. A. *Bioophys. J.* 2002, 83, 2109–17.
- 34** Mashanov, G.I., Tacon, D., Peckham, M., and Molloy, J.E. *J. Biol. Chem.* 2004, 279, 15274–80.
- 35** Morone, N., Fujiwara, T., Murase, K., Kasai, R.S., Ike, H., Yuasa, S., Usukura, J., and Kusumi, A. *J. Cell Biol.* 2006, 174, 851–62.
- 36** Murakoshi, H., Iino, R., Kobayashi, T., Fujiwara, T., Ohshima, C., Yoshimura, A., and

- Kusumi, A. *Proc. Natl. Acad. Sci. U.S.A.* 2004, 101, 7317–22.
- 37** Murase, K., Fujiwara, T., Umemura, Y., Suzuki, K., Iino, R., Yamashita, H., Saito, M., Murakoshi, H., Ritchie, K., and Kusumi, A. *Biophys. J.* 2004, 86, 4075–93.
- 38** Nagle, J.F. *Biophys. J.* 1992, 63, 366–70.
- 39** Nakada, C., Ritchie, K., Oba, Y., Nakamura, M., Hotta, Y., Iino, R., Kasai, R.S., Yamaguchi, K., Fujiwara, T., and Kusumi, A. *Nat. Cell Biol.* 2003, 5, 626–32.
- 40** Nelson, S., Horvat, R.D., Malvey, J., Roess, D.A., Barisas, B.G., and Clay, C.M. *Endocrinology* 1999, 140, 950–957.
- 41** Nishimura, S.Y., Vrljic, M., Klein, L.O., McConnell, H.M., and Moerner, W.E. *Biophys. J.* 2006, 90, 927–38.
- 42** Paller, M.S. *J. Membr. Biol.* 1994, 142, 127–35.
- 43** Peters, R., and Cherry, R.J. *Proc. Natl. Acad. Sci. U.S.A.* 1982, 79, 4317–21.
- 44** Powles, G.J., Mallett, M.J.D., Rickayzen, G., and Evans, W.A.B. *Proc. R. Soc. Lond. A* 1992, 436, 391–403.
- 45** Qian, H., Sheetz, M.P., and Elson, E.L. *Biophys J* 1991, 60, 910–21.
- 46** Rothberg, K.G., Heuser, J.E., Donzell, W.C., Ying, Y.S., Glenney, J.R., and Anderson, R.G. *Cell* 1992, 68, 673–82.
- 47** Saffman, P.G. and Delbrück, M. *Proc. Natl. Acad. Sci. USA* 1975, 72, 3111–3.
- 48** Sako, Y., and Kusumi, A. *J. Cell Biol.* 1994, 125, 1251–64.
- 49** Sako, Y., and Kusumi, A. *J. Cell Biol.* 1995, 129, 1559–74.
- 50** Sako, Y., Minoghchi, S., and Yanagida, T. *Nat. Cell Biol.* 2000, 2, 168–72.
- 51** Sako, Y., Nagafuchi, A., Tsukita, S., Takeichi, M., and Kusumi, A. *J. Cell Biol.* 1998, 140, 1227–40.
- 52** Saxton, M.J. *Biophys. J.* 1989, 55, 21–8.
- 53** Saxton, M.J. *Biophys. J.* 1990, 57, 1167–77.
- 54** Saxton, M.J. *Biophys. J.* 1994, 67, 2110–9.
- 55** Saxton, M.J. *Biophys. J.* 1996, 70, 1250–62.
- 56** Saxton, M.J. *Biophys. J.* 1997, 72, 1744–53..
- 57** Saxton, M.J., and Jacobson, K. *Annu. Rev. Biophys. Biomol. Struct.* 1997, 26, 373–99.
- 58** Schmidt, K., and Nichols, B.J. *Curr. Biol.* 2004, 14, 1002–6.
- 59** Schmidt, T., Schutz, G.J., Baumgartner, W., Gruber, H.J., and Schindler, H. *J. Phys. Chem.* 1995, 99, 17662–17668.
- 60** Schnapp, B.J., Gelles, J., and Sheetz, M.P. *Cell Motil. Cytoskelet.* 1988, 10, 47–53.
- 61** Schutz, G.J., Kada, G., Pastushenko, V.P., and Schindler, H. *EMBO J.* 2000, 19, 892–901.
- 62** Sheets, E.D., Lee, G.M., Simson, R., and Jacobson, K. *Biochemistry* 1997, 36, 12449–58.
- 63** Sheetz, M.P. *Semin. Hematol.* 1983, 20, 175–188.
- 64** Sheetz, M.P., Schindler, M., and Koppel, D.E. *Nature* 1980, 285, 510–1.
- 65** Sheetz, M.P., Turney, S., Qian, H., and Elson, E.L. *Nature* 1989, 340, 284–8.
- 66** Singer, S.J., and Nicolson, G.L. *Science* 1972, 175, 720–31.
- 67** Suzuki, K., Ritchie, K., Kajikawa, E., Fujiwara, T., and Kusumi, A. *Biophys. J.* 2005, 88, 3659–80.
- 68** Suzuki, K.G., Fujiwara, T.K., Edidin, M., and Kusumi, A. *J. Cell Biol.* 2007a, 177, 731–42.
- 69** Suzuki, K.G., Fujiwara, T.K., Sanematsu, F., Iino, R., Edidin, M., and Kusumi, A. *J. Cell Biol.* 2007b, 177, 717–30.
- 70** Takeuchi, M., Miyamoto, H., Sako, Y., Komizu, H., and Kusumi, A. *Biophys. J.* 1998, 74, 2171–83.
- 71** Tank, D.W., Wu, E.S., and Webb, W.W. *J. Cell Biol.* 1982, 92, 207–12.
- 72** Tomishige, M., Sako, Y., and Kusumi, A. *J. Cell Biol.* 1998, 142, 989–1000.
- 73** Tsuji, A., Kawasaki, K., Ohnishi, S., Merkle, H., and Kusumi, A. *Biochemistry* 1988, 27, 7447–52.
- 74** Tsuji, A., and Ohnishi, S. *Biochemistry* 1986, 25, 6133–9.
- 75** Vaz, W.L., Criado, M., Madeira, V.M., Schoellmann, G., and Jovin, T.M. *Biochemistry* 1982, 21, 5608–12.
- 76** Vaz, W.L., Goodsaid-Zalduondo, F., and Jacobson, K. *FEBS Lett.* 1984, 174, 199–207.
- 77** Vrljic, M., Nishimura, S.Y., Brasselet, S., Moerner, W.E., and McConnell, H.M. *Biophys. J.* 2002, 83, 2681–92.
- 78** Wenger, J., Conchonaud, F., Dintinger, J., Wawrezinieck, L., Ebbesen, T.W., Rigneault,

- H., Marguet, D., and Lenne, P.F. *Biophys. J.* 2007, 92, 913–9.
- 79** Wieser, S., Moertelmaier, M., Fuertbauer, E., Stockinger, H., and Schutz, G.J. *Biophys. J.* 2007, 92, 3719–28.
- 80** Winckler, B., Forscher, P., and Mellman, I. *Nature* 1999, 397, 698–701.
- 81** Wu, E.S., Tank, D.W., and Webb, W.W. *Proc. Natl. Acad. Sci. USA* 1982, 79, 4962–6.

Index

α -relaxation 70, 351, 357
 χ^2 -distribution 443

a

acceleration 94, 102, 105, 106, 108, 110
actin filaments 545, 547, 552
additivity 31
adjoint operators 30
adsorption hysteresis 530
advection–diffusion equation 165, 167, 190
aging 230, 329, 331, 332, 336, 349, 372, 392
airports 465
Alexander–Orbach conjecture 505
ambivalent processes 473
anchored-protein picket model 549, 565, 567
anharmonic oscillators 294
annihilation 378–380
anomalous diffusion, *see* diffusion, anomalous
anomalous molecular displacement 485
anomalous transport, *see* transport, anomalous
arcsine law 215, 221
Arrhenius law 77, 369
asymptotic universality 94, 103
attraction property 104, 105
aviation network 465

b

Balakrishnan A.V. 94, 114
ballistic 276, 282, 286, 289
– motion 340, 343
– regime 349
– transport 294, 314
Banach space 38, 42, 49, 61
bank notes 466
Bateman Project 112
binomial formula 17, 38
black-body 297
Boltzmann factors 434

Boltzmann L. 293, 296
Boltzmann transport equation 296
Boltzmann–Gibbs theory 214
Borel measure 51
Brillouin zone 316
Brownian
– diffusion 500–502, 554, 555, 560, 562, 564, 565, 571
– motion 90, 133, 140, 145, 149, 150, 163, 213–216, 327, 338, 464, 478, 479
– – fractional 328, 475
– particle 131, 149–151, 215, 216, 337, 433, 434, 439, 447, 481, 554
bubonic plague 461
bulk mediated surface diffusion 485

c

cage effect 349
Caputo fractional derivative, *see* fractional derivative, Caputo
Caputo M. 117
carbon-13 concentration 507
Cauchy
– distribution 79
– principal value 113
– problem 48
causality 50
central limit theorem 131, 154, 181, 436, 460, 474
chaos 245, 250
– Hamiltonian 270, 273–276
– strong 243, 269, 312–313
– weak 269
chaotic advection 166, 191, 208
characteristic function 119, 120, 130, 134, 135, 142, 148, 150, 155, 156, 179, 182, 478
chemical distance 421
cholesterol 549, 567
Clausius R. 293, 295, 296
coalescence 378, 379
coarse-grained models 372
collective motion 343
compact exploration 388

- complete monotonicity 123
 compressed exponential relaxation 338,
 340, 343
 concentration profiles 385
 confinement time 202, 204
 conjugate Riesz potential 27
 contaminant 278, 281, 283
 continuity in time 49
 continuous time random walk (CTRW) 2,
 56–57, 85, 87, 94, 98–101, 108, 110, 113–
 115, 133, 135, 137, 159, 164, 165, 170–173,
 175–177, 179, 181, 182, 193, 206, 210, 270–
 272, 275–277, 286, 288, 352, 371, 372, 375–
 377, 380, 381, 383–385, 387, 459, 473
 – integral equation 105, 108, 109
 – time fractional 48, 56, 57, 94, 114
 convection rolls 448
 convergence in distribution 95
 convolution
 – distributions 28
 – functions 26
 – integral 23
 – kernel 26, 28, 37, 67
 – operators 26, 28, 43, 50
 – periodic functions 25
 – product 26, 29
 – semigroup 51
 cooperatively relaxing clusters 356
 correlation(s)
 – function 265, 328–335, 340, 341, 357,
 372, 440, 443
 – length 502
 – long-term 275, 289
 cosmic rays 450
 counting function 94, 99, 110, 115
 counting number 115
 coupled memory 86, 87, 89
 Cox D.R. 98
 critical phenomena 41
 CTRW, *see* continuous time random walk
 curvature terms 251
 CYCLCROP 507
 cycle expansions 250
 cytoskeleton 545, 557, 570, 571
- d**
- Debye P. 293, 294, 297, 298
 deceleration 102, 107, 108
 defect turbulence 448
 defects 448
 – turbulence 448–450
 density of states 305
 deterministic map 79
 difference quotient 20, 21, 37, 38
 diffusion
 – anisotropy 528
 – anomalous XV, 7, 15, 46, 93, 150, 167,
 192, 204, 214, 221–222, 227–228, 230, 234,
 248, 253, 256, 257, 270, 294, 317–320, 327–
 329, 343, 367–370, 375, 378, 391, 397–399,
 407–408, 416, 424, 439–442, 448, 450, 476,
 477, 512–514, 529–530, 533, 557, 561
 – Bochner–Lévy 42, 53
 – case II 509
 – coefficient, *see* diffusion, constant
 – confined 548, 552–556, 563
 – constant 6, 163, 177, 221, 237, 248, 252–
 254, 256, 257, 270, 277, 278, 282, 285, 286,
 288, 289, 371, 372, 375, 389, 421, 460, 478,
 481, 495, 498, 499, 503, 506, 507, 515, 550–
 552, 554, 555, 558, 560–562, 564–568
 – – effective, *see* effective diffusion coefficient
 – deterministic 243
 – directed 555, 556
 – equation 42, 54, 56, 57, 86, 88, 108, 109,
 114, 134, 140, 163–165, 171–173, 181, 185,
 214, 221, 295, 372, 381, 504, 506
 – exponent 397, 401
 – fractional 42, 47, 53–57
 – hysteresis 531
 – limit 95, 104–107, 110, 114
 – normal 397, 421
 – relativistic 90
 – space fractional 46, 109
 – – with memory 108
 – space–time fractional 94, 105–109, 114
 – subdiffusion 46, 397
 – superdiffusion 397
 – time fractional 53–57, 94
 diffusive regime 349
 diffusivity 296
 dimension
 – fractal, *see* fractal dimension
 – Hausdorff–Besicovitch 399
 – random walk 398, 401
 Dirac δ function 26, 28, 66, 67
 Dirac-measure 51
 disorder 229, 246, 304, 369–372, 378, 386
 disordered fractal 398, 408, 409
 dispersal curve 460
 dispersion coefficient 502
 distance matrix 357
 distribution(s) 65
 – binomial 421
 – convolution 28, 68
 – differentiation 66
 – Dirac δ , *see* Dirac δ function
 – direct product 68
 – homogeneous 67
 – regular 28, 65
 – singular 28, 65

- tempered 66
- with compact support 67
- dynamical
 - heterogeneities 343, 352, 357, 361
 - ultrametricity 332
 - zeta functions 250, 254
- e**
 - echo points 419
 - class 419, 422
 - Edwards–Anderson parameter 334
 - Edwards–Wilkinson equation 318
 - effective diffusion coefficient 165, 167–169, 187–189, 571
 - Ehrenfest classification 41
 - Einstein relation 221, 282, 403, 404, 525
 - electron tomography 557, 565, 566
 - energy dissipation 444
 - equilibrium, thermodynamic 300
 - equipartition 312
 - ergodicity 214, 275
 - breaking 48
 - – weak 213, 214, 225–226, 230, 231, 234
 - Eskin H. 466
 - essential range 62
 - Euclidean distance 421
 - Euler 18, 19
 - Beta function 31
 - exponential
 - relaxation 335, 336, 338
 - series 18, 20
 - extremal unilateral stable density 111, 113
- f**
 - Faà di Bruno formula 252, 261
 - Feller–Takayasu diamond 120, 121
 - Fermi E. 293, 298–300
 - fibers 419, 422
 - wiggles 420
 - Fick’s law
 - first 525
 - second 460, 525
 - Fickian diffusion equation 416, 485, 506, 514
 - first passage
 - leapover 137
 - time 131, 137, 138, 215, 216, 218, 223
 - Fisher equation 460
 - flight 277, 282, 283, 285, 288
 - fluid 269, 278, 283
 - fluid-mosaic model 549, 550, 570
 - Fokker–Planck equation 53, 237, 238, 269, 302, 304, 440, 441, 481
 - backward 216
 - fractional 159, 221
 - space-fractional 135–137, 141
 - standard 137, 141
 - time-fractional 134
 - force dipole 340, 341
 - Fourier 21, 293, 295
 - integral 113
 - law 293, 296, 297, 303, 311, 312
 - modes 317
 - representation 119
 - series 24
 - transform 29, 37, 95, 99, 106, 109, 111, 113
 - Fourier–Fick’s law 163, 164, 177, 186, 187, 202, 204, 205
 - Fourier–Laplace
 - domain 99–101
 - representation 101, 102, 105, 108
 - transform 111
 - Fox H -function 52, 55, 387
 - FPU experiment 298–301, 310
 - fractal 369, 371, 375, 376, 380, 381
 - dimension 129, 369, 399, 400, 404, 407, 412, 421, 504, 505, 512–514
 - fractional derivative 17–57, 100, 118, 120, 136, 164, 165, 173–176, 179, 183, 187, 196–198, 201, 234
 - at lower limit 41
 - Caputo 101, 117, 118, 175, 176, 194
 - Caputo–Dzerbashyan 118
 - eigenfunction 44
 - generalized Riemann–Liouville 34
 - Grünwald–Letnikov 37–39, 196, 197
 - history 17
 - – Euler 18
 - – Fourier 21
 - – Grünwald 21
 - – Leibniz 18
 - – Liouville 18, 20
 - – paradoxa 17, 18
 - – Riemann 22
 - interpolation 34
 - Liouville(–Caputo) 34
 - local 41
 - lower limit 31
 - Marchaud–Hadamard 34, 40, 52
 - notation 32
 - of distributions 39
 - order 31, 34, 36–39
 - Riemann–Liouville 31, 34, 100, 117, 118
 - Riesz 37, 106, 119, 120
 - Riesz–Feller 120
 - symbols 32
 - type 34
 - upper limit 31
 - Weyl–Liouville 36
 - Weyl–Marchaud 36

- fractional difference quotient 38
- fractional differential equation 44–46, 416
- fractional diffusion 53, 54, 56
 - Bochner–Lévy 42, 53
 - Montroll–Weiss 54
- fractional diffusion equation 54, 106, 107, 164, 177, 181, 182, 184, 185, 194, 210, 372, 375, 382, 383, 389, 515
- fractional Fokker–Planck equation 214
- fractional Gaussian noise 372
- fractional integral 20, 22, 30, 111, 117, 120, 173, 176, 237
 - by parts 30
 - common symbols 24
 - composition law 31
 - domain of definition 24
 - interpolation 27
 - inverse 33
 - lower limit 23
 - of distributions 28, 29
 - Riemann 22
 - Riemann–Liouville 23, 24, 111, 117, 118
 - Riesz 26, 27
 - Riesz–Feller 27
 - upper limit 23
 - Weyl 24, 25
- fractional master equation 56
- fractional powers 42
- fractional stationarity 53
- fractional time 48
- fractional time evolution 50
- Frenkel–Kontorova model 313
- fringe field-gradient NMR diffusometry 492
- function(s)
 - p -integrable 61
 - Bernstein 51
 - Bessel 55
 - Beta 31
 - Bose 261
 - continuous differentiable 61
 - essential range 62
 - Gamma 18, 23
 - generalized 65
 - Hölder continuous 62
 - locally integrable 22, 61
 - Mittag-Leffler 44
 - periodic 24, 25, 36
 - regularly varying 41
 - slowly varying 42
 - smooth 61
- fundamental term 251

- g**
- Gamma function 23
- Gaussian

- process 349, 352, 353, 355
- random variables 436
- statistics 351
- geminate recombination 383, 387
- generalized diffusion coefficient 515
- generalized function 96, 98
- generating function 247, 248, 261, 279
- Goldstone modes 313
- Green–Kubo formula 169, 265, 314
- Greer W.L. 304
- Grünwald A.K. 21

- h**
- H -function 52, 55
- Hagedorn temperature 451
- Hahn spin echo 495
- Hamiltonian chaos 270
- Hamiltonian system 269, 270, 272, 273, 275–277, 281, 284, 288, 289
- Hardy–Littlewood theorem 30, 31
- harmonic
 - chain 293
 - crystal 297, 301, 314
 - oscillators 301
- heat
 - bath 302, 309
 - capacity 297
 - flux 202, 296, 301, 303, 307–308, 311, 316
 - insulator 293
 - reservoir 301
 - superconductor 293
 - transport 165, 202, 243, 293–298, 318
- Helmholtz W. 295
- heterogeneous dynamics 351
- hierarchical coordinate 402
- Hilbert space 42, 61
- Holtsmark distribution 76
- homogeneity 400
 - of time 49
- homogeneous dynamics 351
- homogenous divisibility 50–52
- hop diffusion 548, 552, 553, 555–565, 567, 568, 571
- human travel 462
- hydrodynamic dispersion 485
- hydrodynamic friction-like effect 558, 564
- Hölder space 62
- Hörmander symbol class 43

- i**
- infectious diseases 462
- infinite ergodic theory 228
- infinitesimal generator 43, 52
- inherent structure 359
- instabilities 249
- integrable models 314

- integral transforms 29
- integration
 - fractional 23, 24, 26, 28
 - by parts 30
 - Riemann–Liouville 23
 - Riesz 26
 - Weyl 24
 - iterated 22
- integro-differential equation 114
- integro-pseudodifferential equation 106
- integroderivatives 21
- intermediate scattering function 349, 350
- intermittency 169, 229, 245, 257, 259, 269, 275, 276, 288
- intermolecular dipolar interactions 487
- internal field gradients 498
- inverse χ^2 -distribution 436, 443
- irreversibility problem
 - normal 48
 - reversed 48
- Ishii K. 306
- isotope interdiffusion 505
- isotopic dilution 487
- iterated integrals 22

- j**
- Jackson E.A. 310
- jump
 - length 371, 372, 375
 - time 371, 372, 375
 - width 94, 108
 - density 110
 - distribution 98
- jumping numbers 249

- k**
- KAM
 - island 273–275, 279, 281, 285, 288
 - theory 273
- Karamata theorem 104
- Kardar–Parisi–Zhang equation 317
- kinetic theory 295–297, 300
- Kirchhoff's law 404
- Klein–Gordon chain 313
- Klein–Kramers equation 151
 - standard 148
 - velocity-fractional 147, 148, 152
- kneading determinant 253, 256
- kneading matrix 255
- Koch curve 418, 421
- Kochubei A.N. 118
- Kohlrausch–Williams–Watts function 351
- Kohn–Nirenberg pseudodifferential operator 43
- Kolmogorov–Feller equation
 - classical 100, 106
- generalized 99, 109
- time fractional 100, 106, 109
- Krönig A.K. 293, 296
- Kramers problem 145–146
- Kruskal M.D. 301
- kurtosis 443

- I**
- Lévy
 - distribution 155, 157, 186, 339, 433
 - flights 15, 42, 53, 82, 129, 130, 135, 137, 138, 140–146, 151–155, 157–159, 170, 173, 338, 339, 343, 344, 459, 463, 464, 469, 470, 472–475
 - confined 141
 - damped 152
 - power-law truncated 153, 158
 - noise 129, 141, 142, 146, 147, 150
 - processes 42, 53, 130, 152, 154
 - stable distributions 129, 130, 148, 151, 179, 181, 186
 - stable law 338, 463
 - stable probability density function (LS PDF) 130, 131, 133, 135, 148
 - walks 43, 53, 82, 215, 318, 320, 485
- Lévy flights 129
- Lagrangian
 - turbulence 446–448
 - velocity autocorrelation 168, 169, 192
- Lamperti J. 214, 226–228
- Langevin
 - equation 135, 141, 147–149, 151, 152, 159, 302, 339, 372, 434, 439, 440, 447
 - heat baths 307
- Laplace
 - domain 96, 97, 99, 103, 111, 114
 - transform 30, 94, 95, 97, 99, 101, 103, 104, 109, 111–113, 118, 123, 124, 437
- Laplacian 42, 53
- lattice walk 80, 82
- law of mass action 373, 380–382, 385, 386
- LDD, *see* long-distance dispersal
- leading eigenvalue 248
- Lebesgue space 61
- Lebowitz J.L. 302
- Legendre transform 437
- Leibniz 17, 18
 - paradox 17, 18
 - product rule 17
- Lennard–Jones system 349, 352
- Lieb E. 302
- Liouville 20
- lipid rafts 567
- liquid 347
- Lizorkin space 29
- local rearrangement 340

locality 47, 54
 localization length 305, 308, 309
 locally integrable function 61
 lognormal distribution 443
 long-distance dispersal 462
 long-time tail 243, 269, 313, 315
 Lorentz gas 245, 246, 256, 257, 265, 278
 Lyapunov exponent 312

m

M-Wright function 112, 113, 140
 Mach E. 296
 magnetic field gradients 495
 MAGROFI 498
 MANIAC 1 299
 map 215, 228
 – implicit 280
 – one dimensional 277
 – standard 276
 – symplectic 273
 Marchaud A. 120
 marginal fixed point 258
 Markov process, stationary discrete 405
 master equation 56, 80, 81, 170, 171, 181, 182, 398, 405
 – approach 405, 406
 – fractional 56
 Matsuda H. 306
 Maxwell J.C. 293, 295, 296
 Maxwell–Boltzmann distribution 149, 451, 452
 Mazur P. 314
 mean field 373, 386, 387
 mean-square displacement 214, 234, 327, 349, 350, 367, 369, 370, 372, 386, 397, 485, 491, 504, 554
 Mellin transformation 52
 membrane skeleton 546, 547, 552, 558–560, 564, 565, 569, 570
 – fence model 549, 558, 565, 567
 memory function 109, 110
 Menger sponge 398
 mesopores 519
 meta-basin 359
 method of images 140, 141
 micropores 519
 Mittag-Leffler
 – function 44, 45, 93–95, 97, 113, 114, 123, 124, 134, 178, 319, 478
 – generalized function 44, 55, 94
 – memory function 101, 106
 – probability distribution 93–95, 97, 100, 101, 103, 104, 106, 107, 113–115
 – renewal process 93, 95, 110, 115
 mixed phase space 243, 270, 273–275, 289
 mode coupling theory 244, 315, 349

molecular diffusion 270, 278, 281, 282, 284, 286, 289, 431, 520, 535, 536, 540, 548, 570

molecular traffic control 528

money movements 466

Montroll E.W. 98

Montroll–Weiss diffusion 54

Montroll–Weiss equation 170

Mori–Zwanzig projection 315

muscle-like cloud 419, 422

n

Narayan O. 315

NMR, *see* nuclear magnetic resonance

noise 282, 284

non ergodicity (Edwards–Anderson) parameter 334

non-Gaussian

– parameter 353

– propagator 485

nonequilibrium 2, 4, 5, 48, 53, 151, 297, 301, 302, 310, 311, 313, 318, 434–436, 455, 498

nonextensive statistical mechanics 438

nonlocality 46–48, 164, 173, 185, 188

– space 46

– time 48

nonstationary dynamics 329

normal diffusion 56, 156, 157, 221, 222, 225, 238, 248, 249, 253, 272, 289, 325, 327–329, 339, 367–369, 381, 387, 397, 514, 525–527

nuclear magnetic resonance 485, 486, 522

– diffusometry 486, 495

– interdiffusion 487

– microimaging 505

– microscopy diffusometry 505

– PFG 524

– relaxometry 487

o

obstruction 485

occupation times 214–220, 222, 226, 228, 230–232, 234

oligomerization-induced trapping 567, 569

operator(s)

– adjoint 30

– closed 42

– convolution 26, 28, 43, 50

– fractional powers of 42

– identity 35, 37

– Kohn–Nirenberg 43

– pseudodifferential 43

– semigroup of 49

– spectral decomposition 42

- symbol 43
- translation 35, 37
- optical trapping of single molecules 559
- ordinary differential equation 423
- Ostwald W. 296

- p**
- p -integrable function 61
- pandemic 461
- partition function 247, 248
- Pascal principle 388–390
- passive tracer 281, 283
- Pasta J. 298–300, 310
- pathogens 462
- Payton D.N. 310
- PDF, *see* probability density function
- Péclet number 499
- Peierls R. 293, 298
- percolation clusters 485
- periodic orbit 249, 250, 253, 254, 256, 260, 263
- theory 249
- Perron–Frobenius operator 247, 252
- perturbative
- scheme 251
- transport 208, 209
- perturbative transport 206
- phase transition(s) 253, 262, 329, 537
- classification of 41
- phonon 297, 298
- phospholipids 561, 563–565, 570
- photon 297
- Planck M. 297
- plasma membrane 545–549, 551, 553, 556–560, 562, 563, 565, 566, 568, 570, 571
- Poincaré H. 297
- Poisson process 93, 97, 454
- polymers 485–489, 491–495, 509–510, 516
- population dynamical systems 460
- pore-blocking 539
- porous
- glasses 499
- media 485, 499, 503
- silicon 522
- potential energy landscape 358, 536
- power law 94, 95, 97, 102–105, 107, 108, 110, 114, 155, 157, 229, 331, 344, 371, 375, 435, 452, 459, 467–469, 473, 480, 487, 492, 493, 513
- tails 435, 453
- prefractal 400
- prime periodic orbits 249
- principal value 66
- probability density 98, 416, 419
- function 76, 214, 416, 418, 421, 468, 469, 473
- multivalued 419
- self-similar 419
- profile peaking 205
- propagator 525
- pruning rules 254
- pulsed gradient spin echo diffusometry 498

- q**
- q -exponentials 453
- q -Gaussian 435, 442, 448, 450
- quantum mechanics 295, 297, 298

- r**
- Raleigh–Benard convection 448
- Ramaswamy S. 315
- random
- advection 339, 344
- variables products 77
- walk 80, 82, 85, 86, 89, 398, 401, 418
- approach 402, 406
- continuous time 56
- dimension 369, 388
- random-site percolation 504
- rapidly decreasing function 62
- rarefaction 94–96
- Rayleigh equation
- velocity-fractional 148, 152
- reaction fronts 368, 385
- reaction-diffusion XV, 325, 462
- recurrence 273–275, 277
- recurrent random walk 379
- regular lattice 398
- regularly varying function 41
- relaxation
- dynamics 352
- time 300, 312
- distribution of 336
- renewal process 93–95, 98, 99, 108, 110, 114, 115, 223
- compound 98
- Mittag-Leffler 93, 95, 110, 115
- with reward 98
- renormalization group 315
- Rényi A. 97
- reptation 485
- rescaling 94, 95, 101, 102, 104, 105, 107, 108, 110, 114, 115
- factor 93, 101, 110, 114
- resistance
- effective 404
- scaling algorithm 405
- scaling exponent 404
- resistor network 403
- contact points 404

- respeeding 93, 94, 101, 102, 104, 105, 108,
 110, 114
 – factor 93, 102, 105, 108
 Rich M. 310
 Rieder Z. 302
 Riemann B. 21
 Riemann–Liouville
 – derivative 31, 372, 384
 – fractional derivative 100, 117, 118, 174–
 176, 194, 196
 – fractional integral 23, 111, 117, 118, 173
 Riesz
 – fractional derivative 37, 106, 119, 120
 – fractional integral 26
 – kernel 27
 – potential 26, 120
 – – conjugate 27
 Riesz M. 120
 Riesz–Feller
 – fractional derivative 120
 – kernel 27
 Rosenstock approximation 376
 rotating-frame diffusometry 498
 rotor chain 313
 Rubin R.J. 304
- s**
- SARS 465
 Sawford model 446
 scaling 368, 372, 379, 386
 – analysis 472
 – relation 97
 – window 486, 503
 Scher H. 98
 Schwartz space 63, 66
 segment diffusion 487
 self-similarity 104, 399, 422
 – variable 111
 semigroup 31, 42, 43, 48, 49, 51, 52
 – generator 49
 – of convolutions 51
 Sierpinski carpet
 – active sites 408
 – connection points 408
 – – single 409
 – critical squares 400
 – disordered 398, 407, 408
 – finitely ramified 400, 404
 – generator 399, 404
 – infinitely ramified 400
 – regular 398, 399
 Sierpinski gasket 418
 similarity group 417
 similarity solution method 421
 sinai problem 369
 single-file diffusion 486, 526
- single-particle tracking 546
 SIS-model 461
 slow relaxation 533
 slowly varying function 42, 93
 soliton 301, 314
 space
 – Banach 38, 42, 49, 61
 – continuous functions 61
 – Hilbert 42, 61
 – Hölder 62
 – Lebesgue 61
 – Lizorkin 29
 – Schwartz 63
 – Sobolev 62
 – test functions 65
 space-time fractional diffusion 48–57, 94,
 105–109, 114
 space-translation symmetry 246
 spectral determinant 250
 spectral dimension 369, 380, 381
 spectrum of transport moments 253, 262
 speed of sound 293, 311, 316
 spin-echo attenuation 525
 spin-lattice relaxation 487
 St. Petersburg paradox 75
 stable probability density 104, 105, 121
 – extremal 111, 113
 – symmetric 119
 stickiness 269, 270, 272, 274–279, 281–286,
 288, 289
 stimulated echo 495
 stochasticity threshold 312
 Stokes' law 448
 stretched exponential 134, 328, 331, 335–
 337, 344, 433, 435, 439, 460
 – relaxation 328, 335, 338, 344
 stretching parameter 351
 subaging 331
 subdiffusion XV, 46, 134, 167, 214, 270,
 272, 277, 327–330, 344, 367–373, 375, 378–
 385, 389, 392, 473, 475, 485
 subordination 98, 113, 158, 225, 238, 368,
 375, 377, 378, 381, 382, 389, 392
 superdiffusion 11, 135, 151, 156, 168, 270,
 272, 277, 286, 289, 327, 338, 339, 344, 367,
 371, 463, 485
 superstatistics 433, 445
 surface barriers 529
 surface diffusion 535
 survival probability 56, 94, 95, 98, 140,
 145, 217–219, 222, 227, 238, 337, 373, 376,
 377, 388–391
 swollen polymers 509
 synchronization 308
 Szántai T. 95

t

target problem 368, 373, 375–377, 387, 388
 Tauberian theory 97, 103, 104
 Taylor–Couette flow 443
 telegrapher's equation 86–89
 thermal conductivity 293, 296–298, 301,
 308–310
 thermal reservoir 302, 306, 307, 309
 thermodynamic formalism 243, 246
 thermodynamic limit 248, 293, 297, 306,
 309
 thermostat 304, 310
 thinning 94, 95, 114
 – infinite 97
 time
 – continuity 49
 – evolution 49
 – fractional 48
 – homogeneity 49
 – homogenous divisibility 50–52
 – infinitesimal generator 52
 – translation 48, 50
 time series 442
 time-dependent diffusion coefficient 486
 time-fractional
 – CTRW 56–57, 94, 108, 113, 114
 – derivative 48–57, 117
 – diffusion 94
 – diffusion-wave equation 111
 – drift 94, 110–115
 – Kolmogorov–Feller equation 100, 106,
 109
 time-space windows 571
 Toda lattice 294
 Toda M. 314
 tortuosity 500
 torus map 246
 traffic 465
 train delays 454
 transfer operator 247
 transition probability 401
 – blind ant 401
 – myopic ant 401
 translation invariance 48, 50
 translation operator 35, 37
 transmembrane proteins 551, 552, 559–
 561, 564, 565, 567
 transport
 – anomalous XV–XVII, 1, 2, 5, 8, 10, 15,
 16, 163–172, 194, 208, 210, 215, 243, 245,
 246, 253, 262, 266, 269, 270, 272, 276–279,
 282, 284–289, 294, 310–320, 325, 326, 364,
 370, 398, 431–433, 439, 456, 509, 516
 – coherent 499
 – deterministic XVII, 243, 245, 265
 – incoherent 499

– moments 246, 253

– velocity 167
 trap model 328, 332, 336, 344
 trapping 271, 281, 282, 285, 288, 368, 373,
 376–378, 387, 485
 traps
 – evanescent 375
 – stochastically gated 375
 truncated Lévy distribution 181, 182, 210
 turbulent transport 90, 164, 190–194, 210,
 339, 443
 Turing patterns 367, 387
 two-phase exchange model 534
 two-step relaxation 332–334

u

Ulam S. 298–300
 umklapp processes 298
 unit of measurement
 – change in space 94, 105, 108
 – change in time 93, 95, 101, 108
 uphill transport 164, 173, 187, 188, 202,
 205

v

van Hove function 354
 viscosity 283, 296, 316, 347–349, 448, 550,
 555, 564
 Visscher W.M. 310
 von Neumann J. 299
 vortices 90, 165–167, 170, 172, 191, 208
 Vycor porous glass 521

w

waiting time
 – density 56, 57, 80
 – distribution 56, 57, 85, 93–98, 100–106,
 108, 110, 133, 253, 369, 371, 375, 383, 384,
 453, 454
 Waters J.F. 310
 weak convergence 95
 weak ergodicity breaking 213, 214, 225–
 226, 230, 231, 233, 234
 Weierstrass walk 83
 Weiss G.H. 98
 well-scaled 107–110, 114
 Weyl fractional integrals 24
 wheresgeorge.com 466
 wiener process 302
 wiener sausage 374
 Wright function 112

y

Young's inequality 30

z

Zabusky N.J. 301

- Zaslavsky G.M. 120
zeolites 520
Zermelo E. 297
zonal flow 165–167, 169, 170, 172, 191,
 208
Zotos X. 314